

# Mining the Obscured OB Star Population in Carina

— Michael Smith —

Centre for Astrophysics Research  
Science and Technology Research Institute  
— University of Hertfordshire —

Submitted to the University of Hertfordshire in partial  
fulfilment of the requirements of the degree of Ph.D.

**Principal Supervisor:** Professor Janet Drew

— April 2016 —

# Acknowledgements

I would like to thank my supervisor Janet Drew for her dedicated guidance throughout my PhD and for providing me with the opportunity to work with such an exciting and impressive dataset. I would also like to thank the rest of my supervisory team, Nick Wright and Ralf Napiwotzki and the members of the EGAPS consortium for their feedback and the role that they played in making this project possible. Thanks goes to Geert Barentsen and Neil Cook who taught me (nearly) everything I know about programming in PYTHON. Thank you to my friends and family who have supported me throughout my education.

This project is based on data products from observations made with ESO Telescopes at the La Silla Paranal Observatory under programme ID 177.D-3023, as part of the VST Photometric H $\alpha$  Survey of the Southern Galactic Plane and Bulge (VPHAS+, [www.vphas.eu](http://www.vphas.eu)). Use is also made of data products from the Two Micron All Sky Survey, which is a joint project of the University of Massachusetts and the Infrared Processing and Analysis Center/California Institute of Technology, funded by the National Aeronautics and Space Administration and the National Science Foundation. This research made use of Astropy, a community-developed core Python package for Astronomy ([Astropy Collaboration et al., 2013](#)) and TopCat ([Taylor, 2005](#)).

# Abstract

Massive OB stars are very influential objects in the ecology of galaxies like our own. Current catalogues of Galactic OB stars are heavily biased towards bright ( $g < 13$ ) objects, only typically including fainter objects when found in prominent star clusters (Garmany et al., 1982; Reed, 2003; Maíz-Apellániz et al., 2004). Exploitation of the VST Photometric H $\alpha$  Survey (VPHAS+) allows us to build a robust catalogue of photometrically-selected OB stars across the entire Southern Galactic plane, both within clusters and in the field, down to  $\sim 20$ th magnitude in  $g$ . For the first time, a complete accounting of the OB star runaway phenomenon becomes possible.

Along with making the primary selection using VPHAS+ colours, I have performed Markov-Chain Monte Carlo fitting of the spectral energy distributions of the selected stars by combining VPHAS+  $u$ ,  $g$ ,  $r$ ,  $i$  with published  $J$ ,  $H$ ,  $K$  photometry. This gives rough constraints on effective temperature and distance, whilst delivering much more precise reddening parameters  $A_0$  and  $R_V$  - allowing us to build a much richer picture of how extinction and extinction laws vary across the Galactic Plane.

My thesis begins with a description of the method of photometric selection of OB star candidates and its validation across a 2 square degree field including the well-known young massive star cluster Westerlund 2 (Mohr-Smith et al., 2015)<sup>1</sup>. Following on from this I present spectroscopy with AAOmega of 283 candidates identified by our method, which confirms that  $\sim 94\%$  of the sample are the expected O and early B stars. I then develop this method further and apply it to a Galactic Plane strip of 42 square-degrees that runs from the Carina Arm tangent region to the much studied massive cluster in NGC 3603. A new aspect I attend to in this expansion of method is tightening up the uniform photometric calibration of the data, paying particular attention to the always-challenging  $u$  band. This leads to a new and reliable catalogue of 5915 OB stars.

As well as increasing the numbers of identified massive stars in this large region of the sky by nearly an order of magnitude, a more complete picture of massive star formation in the Carina Arm has emerged. I have found a broad over-density of O stars around the highly luminous cluster NGC 3603 and have uncovered two new candidate OB clusters/associations. I have also paired up the ionization sources of a number of HII regions catalogued by the RMS survey. It is also shown that the OB star scale-height can serve as a roughly standard ruler, leading to the result that the OB star layer shows the onset of warping at  $R_G \sim 10$ kpc. My results confirm that this entire region requires a non-standard ( $3.5 < R_V < 4.0$ ) reddening law for distances greater than  $\sim 2$ kpc.

The methods developed in this study are ready to roll out across the rest of the VPHAS+ footprint that has been observed to date. This extension will take in a strip  $\sim \pm 2$  degrees across the entire Southern Galactic mid-plane (a sky area of over 700 square degrees), within which we expect to find the majority of massive OB stars. This will result in the largest catalogue of Galactic OB stars to date.

---

<sup>1</sup>Due to confusion with other M. Smiths, I publish under the name M. Mohr-Smith

# Contents

	Page
Acknowledgements . . . . .	ii
Abstract . . . . .	iii
Table of Contents . . . . .	iv
List of Figures . . . . .	vi
List of Tables . . . . .	xi
<b>1 Introduction</b>	<b>1</b>
1.1 Classification and Evolution of OB stars . . . . .	1
1.2 Galactic structure and OB stars . . . . .	5
1.3 Massive Star Clusters and their evolution . . . . .	8
1.4 Interstellar dust and extinction . . . . .	11
1.5 Carina Arm . . . . .	15
1.6 The VPHAS+ survey . . . . .	19
1.7 Motivation and organisation of later chapters . . . . .	20
<b>2 Data, calibration, selection and SED fitting</b>	<b>24</b>
2.1 Data . . . . .	24
2.2 Synthetic Photometry and Reddening . . . . .	26
2.2.1 Updated Q method . . . . .	29
2.3 Calibration . . . . .	30
2.4 Probabilistic SED fitting . . . . .	38
<b>3 Test case: Westerlund 2</b>	<b>47</b>
3.1 Introduction . . . . .	47
3.2 Selection and fitting method . . . . .	49
3.2.1 Photometric selection and cross matching . . . . .	49
3.3 Validation of Method . . . . .	50
3.3.1 Photometric selection . . . . .	50
3.3.2 SED fitting . . . . .	53
3.4 Results . . . . .	58
3.4.1 Parameters of the candidate OB stars . . . . .	68
3.4.2 Inferences from the best-fit parameters and other aspects of the photometry . . . . .	69
3.4.3 Reddening . . . . .	73
3.5 Discussion . . . . .	77
3.5.1 The number and spatial distribution of the OB candidates . . . . .	77
3.5.2 Westerlund 2 . . . . .	80
3.5.3 Candidate blue supergiants and sub-luminous stars . . . . .	81
3.6 Conclusions . . . . .	82

<b>4</b>	<b>Spectroscopic confirmation</b>	<b>84</b>
4.1	Spectroscopic observations . . . . .	84
4.2	Broad classification of the spectra . . . . .	86
4.3	Model atmosphere fitting . . . . .	87
4.3.1	B star model fitting . . . . .	89
4.3.2	O star model fitting . . . . .	90
4.4	Results . . . . .	92
4.5	Comparison of the spectroscopic best-fit effective temperatures with photometric estimates . . . . .	94
<b>5</b>	<b>Carina Region</b>	<b>98</b>
5.1	Results of the photometric selection . . . . .	98
5.1.1	Subdwarfs and Over-luminous Stars . . . . .	103
5.1.2	Emission line stars . . . . .	106
5.2	Extinction properties and spatial distribution . . . . .	110
5.2.1	Extinction law . . . . .	110
5.2.2	The changing OB star distribution with increasing extinction . . . . .	114
5.2.3	Onset of the Galactic warp . . . . .	121
5.3	Clustering of O stars . . . . .	121
5.3.1	NGC 3603 . . . . .	125
5.3.2	New Clusters . . . . .	130
<b>6</b>	<b>Comparisons with selected catalogues</b>	<b>135</b>
6.1	OB star catalogues . . . . .	135
6.2	RMS HII regions . . . . .	138
<b>7</b>	<b>Conclusions and future work</b>	<b>143</b>
7.1	Conclusion . . . . .	143
7.2	Improvements . . . . .	145
7.3	Future work . . . . .	146
	<b>References</b>	<b>150</b>
<b>A</b>	<b>Reddening Tables and Figures</b>	<b>158</b>
<b>B</b>	<b>Table of OB candidates followed up with AAOmega spectroscopy</b>	<b>166</b>
<b>C</b>	<b>Table of Candidate O stars</b>	<b>172</b>

# List of Figures

1.1	A schematic side view of the Milky Way taken from <a href="#">Sparke &amp; Gallagher (2000)</a> . . . . .	6
1.2	The distribution of known OB associations over-plotted on a four spiral arm model for the Galaxy taken directly from <a href="#">Russeil (2003)</a> . . . . .	8
1.3	Family of UV through IR extinction curves normalized to $A(1\mu\text{m})$ . The uppermost curves have low values of $R_V$ while the bottom curves have high $R_V$ . Taken directly from <a href="#">Fitzpatrick &amp; Massa (2007)</a> . . . . .	14
1.4	Top: Integrated CO emission as a function of Galactic longitude and LSR radial velocity for the Carina Arm. Bottom: Corresponding heliocentric distances. Both plots are taken directly from <a href="#">Grabelsky et al. (1987)</a> . . . . .	16
1.5	Integrated CO emission as a function of Galactic longitude for the Carina Arm taken directly from <a href="#">Grabelsky et al. (1987)</a> . . . . .	18
1.6	VPHAS+ survey footprint in Galactic coordinates. With fields complete up to March 2016 . . . . .	19
1.7	The transmission profiles of the Sloan $u, g, r$ and $i$ and narrow band $\text{H}\alpha$ filters multiplied by CCD response curves and atmospheric transmission used in VPHAS+(from <a href="#">Drew et al., 2014</a> ). . . . .	21
1.8	An illustration of the VPHAS+ offset pattern for the $\text{H}\alpha$ and $g$ filters (taken directly from <a href="#">Drew et al., 2014</a> ). Both axis are marked off in pixel number. In the $u, r$ and $i$ bands just the outer positions are exposed	21
1.9	Apparent B magnitude and Galactic longitude distribution of O stars in GOSC from <a href="#">Maíz Apellániz et al. (2016)</a> . . . . .	22
2.1	Top panel: <a href="#">Fitzpatrick (2004)</a> extinction curves for $R_V = 2.7$ (top curve) to $R_V = 5.1$ (bottom curve) which have been normalised as $\lambda = 5500\text{\AA}$ . Bottom panel: VHPAS+ filter profiles, an O6V spectrum and the spectrum of Vega as a function of wavelength. . . . .	28
2.2	Example of $u$ band calibration . . . . .	31
2.3	Cumulative distributions of $\sigma_u$ (blue) and $\sigma_g$ (green) across the overlap regions for each photometric band in VPHAS+ before (dashed line) and after (solid line) calibration. The dotted lines show the upper quartile for each case (see Table. 2.3 for more details) . . . . .	34
2.4	Spatial plot of objects in the 42 square degree region with two or more detections, colour coded by the standard deviation of the measured $g$ band magnitudes. The left panel shows the objects before calibration and the right panel after calibration. . . . .	36
2.5	Colour-colour density plots showing the position of the main stellar locus with respect to the synthetic tracks before (left) and after (right) calibration. . . . .	37

2.6	Examples of how the SED of an OB star changes with each parameter. <b>Top:</b> increasing $A_0$ , <b>Second:</b> increasing $R_V$ , <b>Third:</b> increasing $T_{\text{eff}}$ , <b>Bottom:</b> Square markers indicate SED with $T_{\text{eff}} = 40$ kK at $\mu = 13.5$ while the circle markers are for a $T_{\text{eff}} = 20$ kK SED at $\mu = 10$ . Changes in effective temperature weakly effect the shape of the SED and are only noticeable in the $u$ band. This makes it difficult to discern a distant O star from a nearby B star. . . . .	41
2.7	PDFs of the fitting parameters as a result of the MCMC simulation for stars #913 an O4V (top) and #549 and B1V (bottom) using the numbering system from Vargas Álvarez et al. (2013) (see. Section 3.3.1).	45
2.8	Visualisation of the posterior distributions of objects #913 and #549 .	46
3.1	RGB image of the $\sim 2$ square degree region ( $H\alpha$ , g, i). This region falls within the star forming complex G283 identified by Rahman & Murray (2010) . . . . .	48
3.2	Selection of OB stars in and around Wd2 . . . . .	51
3.3	Inverse VPHAS+ $g$ band image of the central region of Wd 2 showing the objects with known spectral type from Vargas Álvarez et al. (2013)	52
3.4	Testing the selection process of OB stars associated with Wd2. . . . .	53
3.5	The difference between stellar parameters found in this study and those found by Vargas Álvarez et al. (2013). . . . .	57
3.6	$\chi^2$ distributions for the known objects (bottom) and the wider selection (top) . . . . .	59
3.7	$(u - g, g - r)$ diagram showing the stages of selection. . . . .	60
3.8	Positions of objects with $\chi^2 \leq 7.82$ (blue dots) and $\chi^2 > 7.82$ (grey crosses) in the $(r - i, g - r)$ plane. . . . .	67
3.9	Distribution of the best fit parameters for the selection of objects with $\chi^2 < 7.82$ . . . . .	70
3.10	Uncertainty on each parameter as a function of g band magnitude. Uncertainties are derived from the 16 <sup>th</sup> and 84 <sup>th</sup> percentiles of the posterior distributions. . . . .	71
3.11	2-D distribution of the best fit parameters for the final selection of OB candidates ( $\chi^2 \leq 7.82$ and $\log(T_{\text{eff}}) \geq 4.3$ ) and objects in the selection with known spectral type . . . . .	72
3.12	$(r - i, r - H\alpha)$ diagram showing emission line objctcs) . . . . .	75
3.13	$A_0$ vs. $R_V$ plot for the final selection with and without the objects within the 8 arcmin box surrounding Wd 2. . . . .	76
3.14	Known and candidate OB stars, in our selection, coloured according to their inferred reddening ( $A_0$ ) and over-plotted on the high-confidence inverse VPHAS+ $H\alpha$ image. . . . .	78
4.1	Positions of the 276 OB candidates coloured by their photometrically determined extinction. Triangles are candidate O stars and circles are candidate B stars. The large black circle represents the AAOmega 2dF field of view. . . . .	85
4.2	Distribution of spectral classes found for sample of stars with AAOmega spectra. . . . .	88

4.3	Example of spectra and best fit models. Top: ID #1374, $g = 15.5$ mag, $A_0 = 5.6$ , $T_{\text{eff}} = 38600$ K and $\log(g) = 4.19$ . Bottom: ID #2593 $g = 17.2$ mag, $A_0 = 4.5$ , $T_{\text{eff}} = 23100$ K and $\log(g) = 4.32$ . . . . .	93
4.4	Distribution of effective temperature, surface gravity and projected rotation speeds for spectroscopic fits. . . . .	95
4.5	Comparison of the derived effective temperature from the photometric SED fitting with those derived from spectroscopy. . . . .	96
4.6	Change in derived reddening parameters when using a temperature prior defined by the spectroscopic fits (free - fixed). . . . .	97
5.1	VPHAS+ $H\alpha$ image showing the footprint of the 42 square degrees in Carina that are studied here. . . . .	98
5.2	Distribution of the best fit parameters for the selection of objects with $\chi^2 < 7.82$ . Objects with $\log(T_{\text{eff}}) > 4.3$ (2 s.f) are coloured in grey. The remaining cooler objects are coloured red. . . . .	101
5.3	Distribution of O and early B star candidates across the 42 square degree region over-plotted on the VPHAS+ $H\alpha$ mosaic. Red circles are candidate B stars and blue triangles are candidate O stars . . . . .	102
5.4	Distribution in Galactic latitude and longitude of O and early B star candidates. The dashed marks $b = 0$ . . . . .	102
5.5	Top panel: $g$ and $K$ band magnitude distribution of $\chi^2 < 7.82$ $\log(T_{\text{eff}}) > 4.295$ objects. Bottom panel: $g - K$ distribution. . . . .	103
5.6	Objects coloured in red are likely sub-luminous compared to the rest of the population. Objects coloured in green are likely over-luminous when compared to the rest of the population. . . . .	104
5.7	Emission line stars selected using the VPHAS+ ( $r - i, r - H\alpha$ ) diagram with various stars of known spectral class. The top panel shows OB candidates with $\chi^2 < 7.82$ and the bottom panel shows OB candidates with $\chi^2 > 7.82$ . . . . .	108
5.8	CMD for Emission line stars selected using the VPHAS+ ( $r - i, r - H\alpha$ ) diagram shown in Fig. 5.7. . . . .	109
5.9	<b>Top:</b> Density plot showing the distribution in $A_0$ vs $R_V$ . The red dashed lines show least squared fits for $A_0 \leq 2$ and $A_0 > 2$ . The green circles show derived values for O stars from Fitzpatrick & Massa (2007). <b>Bottom:</b> Sensitivity of detecting OB stars in VPHAS+ for different combinations of $A_0$ and $R_V$ . An increase in extinction of 0.625 mag/kpc is adopted. . . . .	111
5.10	Detectability of OB stars in VPHAS+ for different combinations of $A_0$ and $R_V$ . Panels (a) and (b) separate B and O stars respectively and adopt an increase in extinction of 0.625 mag/kpc. Panels (c) and (d) separate B and O stars respectively for the case of a steeper increase in extinction of 1 mag/kpc. . . . .	112
5.11	Series of plots showing the positions of OB stars through windows increasing in $A_0$ . O stars and early B stars are represented as triangles and circles respectively. The large circle and rectangle represent the area covered by AAOmega follow up and the area covered in Mohr-Smith et al. (2015) respectively. The histogram to the right of the plot shows the distribution in $A_0$ . . . . .	115
5.12	Measuring extinction as a function of distance . . . . .	117

5.13	Comparison of the derived values of extinction as a function of distance between <a href="#">Marshall et al. (2006)</a> and this study for sight lines towards and away from the Carina tangent. . . . .	120
5.14	Galactic latitude distributions of OB stars with best fitting extinctions in the ranges $2.5 < A_0 < 4.0$ and $5.5 < A_0 < 7.0$ , drawn from the Galactic longitude range $287.6 < \ell < 293.2$ . . . . .	122
5.15	Spatial distribution of candidate O stars across the Carina region, coloured by the extinction. The histograms above and to the right of the plot show the Galactic longitude and latitude distribution respectively . . .	124
5.16	The G291 star forming complex ( <a href="#">Rahman &amp; Murray, 2010</a> ). Top panel: taken directly from <a href="#">Rahman &amp; Murray (2010)</a> . Bottom panel: VPHAS+ H $\alpha$ image with OB stars over-plotted. Triangles are candidate O stars and circles are candidate B stars. Objects are coloured by their extinction.	126
5.17	Top: A zoomed in view of the region containing both NGC 3603 (left of image) and NGC 3576 (right of image). NGC 3576 is situated in the foreground of G291 at $\sim 2.4$ kpc. Bottom: A zoomed in view of VPHAS+ $r$ band image of the core of NGC 3603. The coloured circles and triangles are candidate OB stars from this study. The black triangles are the O stars from <a href="#">Melena et al. (2008)</a> . . . . .	127
5.18	Top: Corresponding positions of OB stars over plotted on the VPHAS+ H $\alpha$ image, coloured by their extinction. Bottom: Extinction map in the form of a Voronoi tessellation diagram for the region surrounding NGC 3603. In both diagrams the circle drawn represents the location of the expanding shell ( <a href="#">Pang et al., 2011</a> ). The region shown spans $6 \times 6$ arcmin <sup>2</sup> , or a sky area of $12 \times 12$ pc <sup>2</sup> at $D = 6.9$ kpc . . . . .	129
5.19	Possible new clusters/OB associations over plotted on the associated warm dust emission from the WISE 12 micron image. . . . .	132
5.20	Possible new clusters/OB associations over plotted on the H $\alpha$ emission from the VPHAS+ image. . . . .	133
5.21	$A_0$ distributions of Cl 1 (left panel) and Cl 2 (right panel) . . . . .	134
6.1	Top: Comparison of the B band apparent magnitudes of OB stars in the <a href="#">Reed (2003)</a> catalogue (green) with the $g$ band apparent magnitudes of candidate OB stars in this study (grey). Bottom: Comparison of the B band apparent magnitudes of O stars only, from GOSC (green) with the $g$ band apparent magnitudes of candidate O stars in this study (grey). .	137
6.2	Cumulative distributions in cross match radius (in arcsec) between RMS HII regions and the VPHAS+ O star candidates (left) and B star candidates (right). . . . .	140
6.3	Selection of HII regions cross matched with OB star candidates from VPHAS+. Triangles are O stars, circles are B stars and diamonds are objects with poor $\chi^2$ values from their SED fits. . . . .	141
6.4	Selection of HII regions cross matched with OB star candidates from VPHAS+. Triangles are O stars, circles are B stars and diamonds are objects with poor $\chi^2$ values from their SED fits. . . . .	142
7.1	Candidate OB stars over plotted on the VPHAS+ H $\alpha$ image of Wd 2, coloured by their derived values of $R_V$ . . . . .	148

7.2	VPHAS+ survey footprint in Galactic coordinates. With completed fields up to April 2016. . . . .	148
A.1	VST/OmegaCam synthetic colours for main-sequence dwarfs in the $(u - g), (g - r)$ plane reddened with an $R_V = 2.5, 3.1$ and $3.8$ extinction law from top to bottom. The dashed red tracks are affected by the $u$ and $g$ filter red leaks. . . . .	161
A.2	VST/OmegaCam synthetic colours for main-sequence dwarfs in the $(r - i), (r - H\alpha)$ plane reddened with an $R_V = 2.5, 3.1$ and $3.8$ extinction law from top to bottom. . . . .	165

# List of Tables

2.1	Table showing the positions, dates, seeing and limiting magnitudes for each field. . . . .	25
2.2	Photometric calibration shifts applied to the VPHAS+ data . . . . .	33
2.3	Measure of uniformity: standard deviation of multiple detections in each band before and after calibration. . . . .	34
2.4	Sample values of the intrinsic SEDs with approximate spectral type equivalents. Magnitudes are in the Vega system. . . . .	39
3.1	Table comparing the derived stellar parameters of objects with known spectral type from <a href="#">Vargas Álvarez et al. (2013)</a> with the results in this study. The ID given corresponds to the numeration given by <a href="#">Vargas Álvarez et al. (2013)</a> . Most of the effective temperatures in the HST column were derived spectroscopically by <a href="#">Vargas Álvarez et al. (2013)</a> and uncertainties were given. The rest have no provided uncertainty as they were estimated from their spectral types using the temperature scales from <a href="#">Martins et al. (2005)</a> and <a href="#">Zorec &amp; Briot (1991)</a> . . . . .	55
3.2	Breakdown of the number of new OB candidates, previously identified OB candidates and objects with known spectral type according to effective temperature and fit quality. . . . .	61
3.3	Objects crossed matched with SIMBAD in the selection which have known spectral type. Derived parameters of highly evolved objects will be inaccurate due to the main-sequence assumption as shown by their large $\chi^2$ values. On further inspection of the literature the classification object #895 is much different from that in SIMBAD (see Section 3.4)	64
3.4	Sample table containing the positions and photometry of all 1073 objects. The first five columns are the objects IDs given in this study, VPHAS ID, <a href="#">Moffat et al. (1991)</a> , MSP ID, <a href="#">Vargas Álvarez et al. (2013)</a> , VA ID, <a href="#">Tsujimoto et al. (2007)</a> , TFT ID, and in SIMBAD, SIMBAD ID, where applicable. The full table can be found in the electronic version of <a href="#">Mohr-Smith et al. (2015)</a> . . . . .	65
3.5	Sample table containing the derived parameters of all 1073 objects. The 16 <sup>th</sup> , 50 <sup>th</sup> and 84 <sup>th</sup> percentiles are given for each parameter as well as the $\chi^2$ value at the 50 <sup>th</sup> percentile. The notes column indicates if the object shows emission (EM), is a sub-luminous candidate (SUB), is a blue supergiant candidate (BSG) or is a new O star candidate near Wd 2 (WD2) with similar reddening. The full table can be found in the electronic version of <a href="#">Mohr-Smith et al. (2015)</a> . . . . .	65
3.6	Table containing the derived stellar parameters of the sub-luminous and blue supergiant candidates in the $\chi^2 \leq 7.82$ and $\log(T_{\text{eff}}) \geq 4.3$ group. .	74

3.7	The reddening parameters and angular separation from the centre of Wd 2 ( RA 10 24 18.5 DEC -57 45 32.3 (J2000)) of new O star candidates with similar reddening to the cluster, outside the 8 arcmin box shown in figure 3.14. All objects have $\log(T_{\text{eff}}) > 4.477$ and $5.8 > A_0 > 7.2$ . See Tables 3.4 and 3.5 for the full set of data. . . . .	81
5.1	Breakdown of the number of OB candidates according to effective temperature and fit quality. . . . .	100
5.2	Breakdown of the number of selected OB candidates with spectroscopically confirmed types according to SIMBAD and those with spectroscopically confirmed types from AAOmega in Chapter 4. . . . .	100
A.1	VST/OmegaCam synthetic colours for main-sequence dwarfs in the $(u-g)$ , $(g-r)$ plane reddened with an $R_V = 2.5$ extinction law. Objects in <i>italics</i> are affected by the $u$ and $g$ filter red leaks. The top panel of Fig. A.1 plots these values. . . . .	158
A.2	VST/OmegaCam synthetic colours for main-sequence dwarfs in the $(u-g)$ , $(g-r)$ plane reddened with an $R_V = 3.1$ extinction law. Objects in <i>italics</i> are affected by the $u$ and $g$ filter red leaks. The middle panel of Fig. A.1 plots these values. . . . .	159
A.3	VST/OmegaCam synthetic colours for main-sequence dwarfs in the $(u-g)$ , $(g-r)$ plane reddened with an $R_V = 3.8$ extinction law. Objects in <i>italics</i> are affected by the $u$ and $g$ filter red leaks. The bottom panel of Fig. A.1 plots these values. . . . .	160
A.4	VST/OmegaCam synthetic colours for main-sequence dwarfs in the $(r-i)$ , $(r-H\alpha)$ plane reddened with an $R_V = 2.5$ extinction law. The top panel of Fig. A.2 plots these values. . . . .	162
A.5	VST/OmegaCam synthetic colours for main-sequence dwarfs in the $(r-i)$ , $(r-H\alpha)$ plane reddened with an $R_V = 3.1$ extinction law. The middle panel of Fig. A.2 plots these values. . . . .	163
A.6	VST/OmegaCam synthetic colours for main-sequence dwarfs in the $(r-i)$ , $(r-H\alpha)$ plane reddened with an $R_V = 3.8$ extinction law. The bottom panel of Fig. A.2 plots these values. . . . .	164
B.1	Table of OB candidates followed up with AAOmega spectroscopy. The table contains the positions of the objects, the photometrically derived extinctions and effective temperatures as well as the spectroscopically derived effective temperatures, surface gravities and rotational velocities.	166
C.1	Photometry and derived parameters from the SED fits for candidate O stars with $\chi^2 < 7.82$ and $\log(T_{\text{eff}}) > 4.477$ . The notes column indicates if an object has been selected as subluminoous (SUB), over luminous (LUM) or as an emission-line objects (EM). . . . .	172



---

# CHAPTER 1: INTRODUCTION

---

The aim of this study is to begin a deep and uniform census of the OB star population, to  $g = 20$ , in the plane of the Milky Way, using a focused investigation of the Carina Arm region to establish viable methods. By utilising optical and near-infrared photometry from VPHAS+ and 2MASS respectively, SED fitting allows for precise determinations of the amount of extinction and the extinction laws that govern the OB star sight lines as well as rough estimates of their effective temperature and distance. These quantities contribute towards tracing the structure of the Carina Arm and the distribution of dust within it. The first chapter is a summary of our current understanding of Galactic OB stars, and the role they have played in tracing the spiral arm structure within the Galactic disk and in probing extinction and extinction law variations within our Galaxy.

## 1.1 Classification and Evolution of OB stars

Stars of spectral type O and early B, more massive than  $\sim 8 - 12M_{\odot}$ , are massive enough to form collapsing cores at the end of their nuclear-burning lifetimes (see e.g. [Langer, 2012](#); [Smartt, 2009](#)). These objects also known as OB stars, roughly correspond to stars of spectral type B2 and earlier. With effective temperatures  $\gtrsim 20000\text{K}$  and luminosities  $\gtrsim 10^4L_{\odot}$ , main-sequence OB stars are the most luminous and hottest objects on the Hertzsprung-Russell diagram (HRD). At these extreme temperatures, OB stars produce ionising UV radiation that forms and shapes H II regions in the surrounding interstellar medium (ISM). The absolute magnitude of main-sequence OB stars ranges from  $V \sim -2$  at early B up to  $V \sim -6$  at very early O (see e.g. [Zorec & Briot, 1991](#); [Martins & Plez, 2006](#)). As a consequence of the initial mass function (IMF) these objects are extremely rare, making up just  $\sim 0.0001\%$  of the stellar population by number (see e.g. [Salpeter, 1955](#); [Kroupa, 2001](#)).

Despite their rarity, OB stars are an important source of kinetic energy, driving turbulence and the mixing of the interstellar medium, mediated by a range of phenomena

(stellar winds, wind-blown bubbles, expanding HII regions and supernova explosions). The alpha elements (He, C, O, Ne, Mg and Si) found in the interstellar medium are created via stellar nucleosynthesis in the layered cores of massive stars, via the process of addition of the He nuclei. They are then introduced into the interstellar medium when a star explodes as a Type II or Type Ib/c core-collapse supernova. A large majority of the extremely rare neutron capture elements are thought to form when a massive star ends its life as a core collapse supernova via the r-process mechanism (Wanajo et al., 2003). This last process is referred to as supernova nucleosynthesis. OB stars are the main source of ultraviolet radiation in galaxies and, being short-lived ( $\sim 1 - 40$  Myr), they are excellent tracers of recent star formation in galaxies.

Classically, the spectral sub-types of OB stars are classified by the ratios of the neutral helium (He I) and ionised helium (He II) absorption lines found in the blue optical range (4000-5000Å) of the electromagnetic spectrum. For B stars the strength of He I lines reaches a maximum at around B2 ( $\sim 20000$ K). For stars hotter than this the He I lines begin to shrink as the further ionisation of helium sets in. When spectral type O is reached at around 30000K the He II lines become more dominant than the He I lines, which all but disappear in very early O stars.

Despite the importance of massive stars in shaping the structure and evolution of the galaxy, their formation is still poorly understood. At present there is very little evidence that can inform the current models of the earliest stages of massive star formation ( $\lesssim 10^5$  yr). Due to their scarce numbers, relatively short life times and therefore rapid evolution, observations of key evolutionary stages of massive star formation are infrequent. Not only are these events rare, they are particularly difficult to observe. The early stages of massive star formation are usually distant, highly extinguished or indeed completely obscured by dust (see e.g. Zinnecker & Yorke, 2007, for a broad discussion). Not only are the empirical data limited and complex, the theory faces many problems. As massive stars may form in especially dense environments their formation can be influenced by gravitational interactions, multiplicity and supernovae. Modelling star-formation in these environments with so many variables becomes unreliable.

Our understanding of the evolution of OB stars beyond the main-sequence is some-

what clearer than that of their formation, but faces many of the same problems. As noted already, it is generally accepted that all stars beyond  $\sim 8 - 12M_{\odot}$  will end their lives as core collapse supernova (Poelarends et al., 2008). Our knowledge of how they reach this final stage in their evolution is largely based on models and observational evidence is scarce and often ambiguous (Langer, 2012). However, there are a number of known key evolutionary stages that an OB star will go through in its lifetime; it is the order in which they occur and the mass of the main-sequence progenitors that is difficult to disentangle.

OB stars in the initial mass range of  $\sim 8 - 45M_{\odot}$ , after core hydrogen exhaustion, are thought to evolve into red supergiants (RSGs) (see e.g. Maeder & Meynet, 2010; Sander et al., 2012). In the RSG phase, the core of the star collapses and rapidly heats up causing the outer layers of the star to expand and cool and therefore appear red. After burning a significant fraction of their helium in this stage, the most massive of this mass range, are thought to evolve into the blue supergiant (BSG) phase. Here, the rate of fusion has slowed causing the outer layers of the star to contract, heat up and appear bluer. It is thought that a star may oscillate back and forth between the RSG and BSG phase, in what is known as the ‘blue loop’ before moving onto the Wolf-Rayet (WR) phase or going supernova (Maeder & Meynet, 2010). However, the ‘blue loop’ phase is highly sensitive to assumptions made about internal mixing in evolutionary models and is therefore a subject of much debate (Langer, 2012). Stars above  $\sim 45M_{\odot}$  may skip the RSG and/or BSG phase to become luminous blue variables (LBVs) (Maeder & Meynet, 2010; Sander et al., 2012). Empirically, LBVs are luminous, hot and unstable supergiants that have periodic episodes of increased mass loss and luminosity.

After the RSG, BSG and/or LBV phase, O stars with an initial mass of around  $\geq 25M_{\odot}$  are thought to evolve into WR stars for the final stage of their pre-supernova evolution (Crowther, 2007). However, this mass limit is expected to be lower at a lower metallicity (Meynet & Maeder, 2005) or in close binary systems with stars of initial mass of around  $10M_{\odot}$  or less (Langer, 2012). WR type stars can be classified into 3 main types; WN, WC and WO with spectra characterized by broad emission lines in He and N (WN) and He, C and O (WC and WO). These emission lines originate

in a hot stellar wind with a terminal velocity in the range  $v_\infty \approx 400 - 5000 \text{ km s}^{-1}$ . Mass loss rates approaching  $10^{-4} M_\odot \text{ yr}^{-1}$  (van der Hucht, 2001) are achieved (Crowther, 2007). The exact evolution of massive stars from the main sequence to the WR phase is still not satisfactorily understood (see e.g. Hamann et al., 2006; Langer, 2012). Putting the observed WR types and those of their progenitors and descendants into an evolutionary sequence has been attempted many times (Langer, 2012). There are two main difficulties. The first is obtaining the bolometric luminosities of the WR stars. WR stars are extremely hot and therefore much of their radiation arises in the UV wavelength range. As most of this UV radiation is inaccessible due to telluric absorption, huge bolometric corrections are needed, making the luminosity unreliable (Crowther, 2007). The second is a lack of a statistically meaningful sample of observed evolved OB stars and WR stars (Langer, 2012). It is a further weakness of this sample that the majority of distances to stars remain unknown.

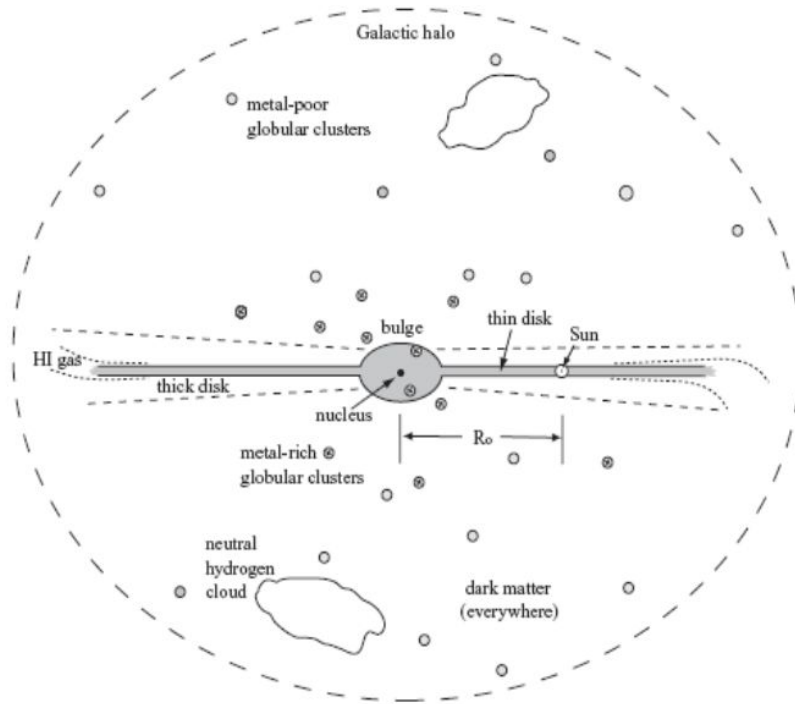
The VLT-FLAMES Tarantula Survey (VFTS) (Evans et al., 2011) is the most comprehensive spectroscopic and photometric study of massive stars in a single star forming region to date. The VFTS has collected multi-epoch optical spectroscopy of over 800 massive stars situated outside of the Milky Way in the 30 Doradus region of the Large Magellanic Cloud (LMC). The data obtained with this homogeneous study in the LMC and data from more heterogeneous samples of Galactic OB stars (Mason et al., 2009; Sana & Evans, 2011; Sana et al., 2012) have found that the binary fraction of OB stars is likely to be at least  $\sim 70\%$ . Sana et al. (2013) suggest that the fraction of O stars in VFTS that are in close interacting binaries may be as high as  $\sim 50\%$ . Similar studies of Massive stars in the Milky Way also suggest a high binary fraction of over 50% (Kobulnicky et al., 2014). This adds to the complexity of massive star evolution and suggests that binary interaction greatly affects the evolution of most massive stars and should be taken into account when modelling their evolution (Sana et al., 2013). The extensive work done in the LMC means that knowledge of the OB star content in the Magellanic Clouds is currently more complete compared to that of the Milky Way, as illustrated by the large compilations presented by Bonanos et al. (2010) and previous papers. Currently, the most comprehensive cataloguing effort in the Milky

Way is a product of the ‘Galactic O Star Survey’ (see [Maíz Apellániz et al., 2016](#), and previous papers) but is incomplete beyond  $g \sim 8$  mags. Given that the metallicity in the Milky Way,  $[Fe/H] \sim 0$ , is higher than that in the LMC,  $[Fe/H] \sim -0.34$ , and SMC,  $[Fe/H] \sim -0.68$  ([Luck et al., 1998](#)), improving the census of Galactic OB stars will assist the quest to understand the impact of metallicity on massive star evolution.

## 1.2 Galactic structure and OB stars

The Milky Way galaxy is believed to be a barred spiral Galaxy and broadly speaking consists of 3 main components; the halo, the bulge and the disk. Fig. 1.1 shows a schematic side view of the Milky Way taken from [Sparke & Gallagher \(2000\)](#). The halo and bulge contain the oldest stellar content in the Galaxy ( $\sim 10 - 13 \times 10^9$  yrs), known as ‘population II’ stars. Population II stars tend to have lower metallicities and follow a somewhat random and spherical orbit around the Galactic centre. However, in recent years large numbers of young massive stars have been found near the Galactic centre but their exact origins are still debated (see e.g. [Eisenhauer et al., 2005](#); [Mauerhan et al., 2010](#)). Conversely, the Galactic disk consists of the more recently formed ( $< 10 \times 10^9$  yrs), and higher metallicity, group of stars known as population I stars. Population I stars orbit the centre of the Milky Way in a more regular manner in the form of a disk, of very much larger radius than it is thick. It has been argued that the disk of the Milky Way is made of two components, the thick disk with a scale height of  $\sim 900$  pc and the thin disk with a scale height of  $\sim 350$  pc ([Jurić et al., 2008](#)). The latter is thought to be a younger population and contains the vast majority of the stars in the Milky Way extending out to a Galactocentric radius of  $R_G \sim 13$  kpc, where the radial stellar density gradient steepens ([Sale et al., 2010](#)).

Containing  $\sim 90\%$  of the H I content of the Milky Way ([Kalberla & Kerp \(2009\)](#)), the Galactic disk is the main site of ongoing star formation in the Milky Way. Current estimates for the star formation rate in the Milky Way are  $0.68 - 1.45 M_\odot$  per year (e.g. [Robitaille & Whitney, 2010](#)). Like many external star-forming galaxies that we see in the universe, the disk of the Milky Way contains spiral arms. According to density



Sparke and Gallagher 2007

**Figure 1.1:** A schematic side view of the Milky Way taken from Sparke & Gallagher (2000)

wave theory, spiral arms are over-densities in the distribution of gas and stars within Galaxies sweeping around at pattern speeds distinct from the rotation speeds of matter. The stars and gas orbiting within the Galactic disk are free to move in and out of the spiral arms over many disk orbits (Elmegreen, 2011). The over density of gas within spiral arms allows gravitational instabilities and cloud collisions to occur more readily, when compared to the inter-arm regions. This in turn encourages the formation of molecular clouds, and allows the star formation rate per unit area within spiral arms to be higher (Elmegreen, 2011).

As the Sun is situated in the disk of the Galaxy and the spiral arms are also embedded within it, it is difficult to assert the distribution and number of spiral arms that the Milky Way possesses. The large quantity of dust within the Galactic disk and spiral arms obscures our view, making it difficult to discern structure within the disk and determine accurate distances to any structures present. In the Galaxy, OB star clusters and OB associations have played an important role in tracing spiral arm

structure (Russeil, 2003; Vallée, 2005). As the brightest optical objects in the Galaxy, OB stars have allowed us to peer through the large amounts of extinction caused by the build up of dust within the spiral arms and disk of the Milky Way. Being short lived (on the order of  $\lesssim 10\text{Myr}$ ) their life times are shorter than the kinematic time scales associated with moving in and out of spiral arms ( $\gtrsim 10\text{Myr}$ , Sparke & Gallagher, 2000) and are therefore found near their birth sites within the spiral arms.

Currently, the majority view is that the Milky way consists of four major spiral arms. This assertion is largely based on tracing the distribution of radio-detected H II regions, CO and optical OB associations and clusters (see Vallée, 2005). This allows us to trace the positions of the stars themselves, the giant molecular clouds that they are formed from and the surrounding H II regions that they ionise throughout their lifetimes. The typical scale height for OB stars, forming in the Galactic disk, is estimated to be  $\sim 45 \pm 15$  pc (e.g. Reed, 2000; Garmany et al., 1982), in keeping with estimates of the scale height for giant molecular clouds ( $\sim 35\text{pc}$ ), their birth sites (e.g. Stark & Lee, 2005). Figure 1.2, taken directly from Russeil (2003), shows the estimated positions of known OB star complexes over-plotted on a four spiral arm model of the Galaxy. The four arms shown in the plot are 1: Sagittarius-Carina, 2: Scutum-Crux, 1': Norma-Cygnus and 2': Perseus. Figure 1.2 shows that while the star forming regions are not exclusively found in the spiral arms they do show a preference to trace the spiral arm structure. It is noted that the distances to OB stars, and therefore the spiral arms, are nevertheless still difficult to obtain due to uncertainties in the absolute magnitude calibration of OB stars.

Historically OB stars have been used to probe Galactic structure to large distances in the outer disk of the Milky Way. In particular they have been used to trace the chemical abundance gradient in the Galactic disk (see Chiappini et al., 2001, and references therein). As OB stars are short lived, and therefore relatively young, their stellar abundances give an accurate reflection of the abundances in the ISM in the present day. They can therefore been used to constrain chemical evolution models of galaxies. Smartt & Rolleston (1997) used spectroscopy of early B-type stars in the Galactic disk over Galactocentric distances of  $6 \lesssim R_g \lesssim 18\text{kpc}$  and found an oxygen

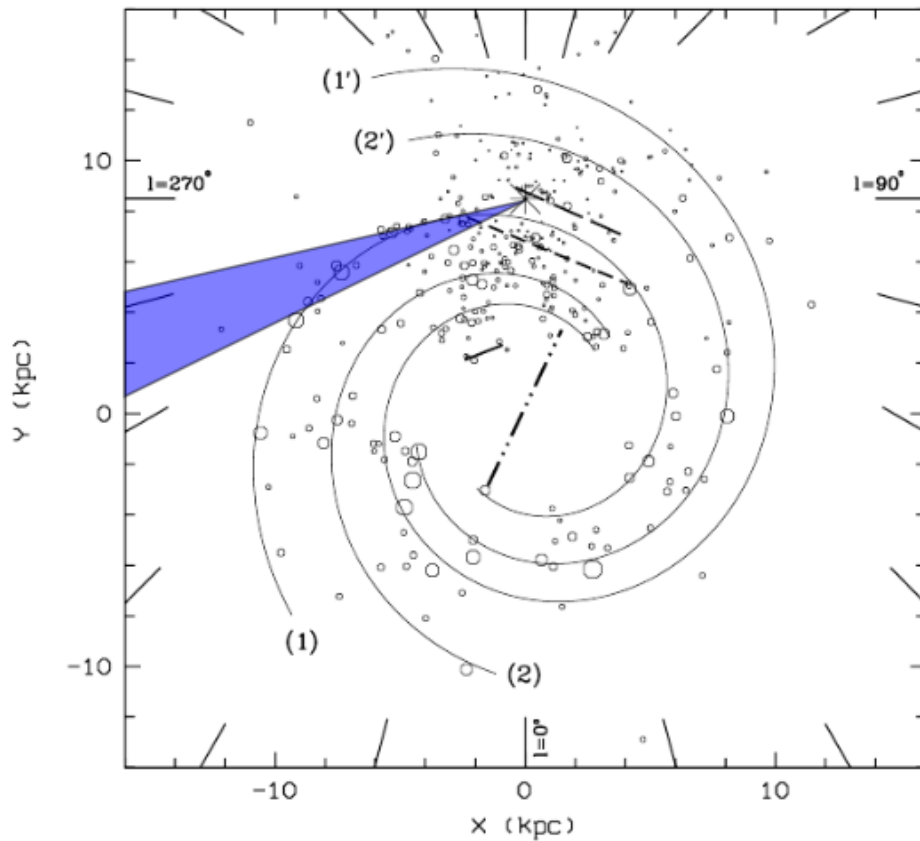


**Figure 1.2:** The distribution of known OB associations over-plotted on a four spiral arm model for the Galaxy taken directly from [Russeil \(2003\)](#). The Sun's position is shown by the star symbol. The four arms are: 1: Sagittarius-Carina, 2: Scutum-Crux, 1':Norma-Cygnus and 2': Perseus. The over-plotted blue triangle shows the field of view under consideration in this study

abundance gradient of  $-0.07 \pm 0.01 \text{dex kpc}^{-1}$ . This was the first study of early type stars to produce an oxygen abundance gradient consistent with that derived from abundances in H II regions ([Chiappini et al., 2001](#)). A more comprehensive study by [Rolleston et al. \(2000\)](#) traced the abundances of C, N, O, Mg, Al and Si in 80 early B stars out to a distance of  $R_g \sim 18 \text{kpc}$  and found the average abundance slope to be in agreement with previous results ( $-0.07 \pm 0.01 \text{dex kpc}^{-1}$ ).

### 1.3 Massive Star Clusters and their evolution

As summarised by [Portegies Zwart et al. \(2010\)](#), broadly speaking there are three types of star cluster found in the Milky Way; globular clusters (GCs), open clusters (OCs) and young massive clusters (YMCs). The fundamental differences between these

clusters are their age, mass, radius and location within the galaxy.

Globular clusters are more commonly found in the Galactic bulge and halo and are the most massive ( $M \gtrsim 10^5 M_\odot$ ), biggest ( $r \sim 10\text{pc}$ ), and oldest ( $\gtrsim 10\text{Gyr}$ ) clusters in the Galaxy. Conversely open clusters are much less massive ( $M \lesssim 10^3 M_\odot$ ), smaller ( $r \gtrsim 1\text{pc}$ ) and younger ( $\sim 0.3\text{Gyr}$ ) and are most commonly found in the Galactic disk. Somewhere between these two lie the Young Massive Clusters whose radii ( $r \gtrsim 1\text{pc}$ ), ages ( $\gtrsim 0.1\text{Gyr}$ ) and location in the galaxy (disk) are more in line with OCs but their mass and density are more similar to GCs ( $M \gtrsim 10^4 M_\odot$ ) (Portegies Zwart et al., 2010). This implies that the formation of clusters with masses close to GCs is not restricted to the early universe. This becomes even more apparent when we look at the Magellanic Clouds and starburst galaxies where the typical mass and interior stellar density of YMCs exceeds those of the Milky Way.

YMCs are dense populations of young OB stars that form the building blocks of galaxies. They are tracers of star formation and act as a probe for the study of massive stars and massive star evolution. There is overwhelming evidence that stars form in clustered groups. In the Milky Way  $\sim 96\%$  of O-type stars can be identified as members of young open clusters or OB associations or can be kinematically linked to clustered environments (de Wit et al., 2005). In the Galaxy there are also relatively sparse groupings of massive stars known as OB associations (such as Cygnus OB2 and the Perseus OB association) which can measure up to  $\sim 100\text{pc}$  across and span several degrees on the sky. These gravitationally unbound systems may have dispersed from dense star clusters (Portegies Zwart et al., 2010).

The evolution of young star clusters can be broadly divided into three main stages. During the first few megayears, stars are still forming and the cluster contains significant amounts of gas. Here the dynamics of the cluster are largely driven by gas dynamics, stellar evolution, stellar mass loss and radiation from OB stars. After an upper age limit of around  $\sim 3\text{Myr}$ , enough time has passed for the cluster to have its first supernova explosion, expelling most of the gas from the cluster. This allows gravitational interactions between the stars to begin to dominate the dynamical evolution of the cluster, with stellar winds still playing a significant role. Once nearly all of the

gas from the cluster has been expelled via continual SNe and stellar radiation, –taking anywhere between  $\sim 10\text{Myr}$  and  $\sim 1\text{Gyr}$ – the evolution of the cluster is purely dominated by gravitational interactions between the stars that remain (Portegies Zwart et al., 2010).

The early stages of cluster evolution rely on very complex gas dynamical interactions that are incompletely understood (Portegies Zwart et al., 2010). This affects our ability to model basic cluster properties such as star formation rate and efficiency and the origin of the stellar mass function. Our understanding of the latter stages of evolution of young star clusters, where gravitational dynamics are the dominant factor, can be modelled with relative ease and accurately via N-body simulations. However, as the initial conditions of these simulations are in reality provided by the early stages of cluster evolution, they must rely on assumptions.

OB stars are usually regarded as forming in clustered environments (Zinnecker & Yorke, 2007) and are less common in the field. However, examples of isolated field O stars are known and the question has arisen as to whether these high-mass stars have formed in situ, perhaps as the result of stochastic sampling of the initial mass function (IMF) as outlined by Parker & Goodwin (2007), or have been ejected from clusters as runaways (see e.g. Portegies Zwart et al., 2010; Bestenlehner et al., 2011). In the Milky Way, up to  $\sim 4\%$  of catalogued Galactic O-type stars possibly formed in isolation (de Wit et al., 2005). Deep comprehensive searches for OB stars away from clusters in the Milky Way have not yet been undertaken, unlike those in the Magellanic Clouds (e.g. Lamb et al., 2016). Known OB-runaway stars travel through interstellar space with an anomalously high velocity ( $\sim 40 - 200 \text{ kms}^{-1}$ , see e.g. Perets & Šubr, 2012; Napiwotzki & Silva, 2012). The trajectories of OB runaways can usually be traced back to origins in OB associations or clusters. There are two suggestions as to the mechanism behind the ejection of OB stars from their birth place. Both involve binarity or higher multiplicity. The first case is the binary ejection mechanism (BEM, Blaauw, 1961) whereby an OB star is ejected from its association when its binary companion explodes as a supernova. Evidence for this scenario has been found, for example, in the case of Vela X-1. The second case is the dynamical ejection method (DEM, Poveda et al., 1967) whereby

close dynamical interactions between stars in young clusters can result in one or more stars being ejected. In particular, interactions between two binary systems cause the largest ejection velocities. Most runaway stars can be explained by these two scenarios. However, there is a group of stars with velocities which exceed those predicted by the BEM and DEM that are known as hypervelocity stars. [Napiwotzki & Silva \(2012\)](#) suggest that hypervelocity stars can be explained by a variation of the BEM in which the massive companion explodes as a WR star following a common envelope phase. In the dispute over the stochastic or dense-cluster origins of massive stars, the runaway phenomenon can be invoked to ‘explain away’ apparent instances of isolated massive young stars. At present the statistical basis for apportioning the Milky Ways OB population between the field and clustered environments remains weak. A deeper, more complete Galactic census would help alleviate this problem.

## 1.4 Interstellar dust and extinction

Interstellar dust is responsible for the obscuration or ‘extinction’ of starlight in the interstellar medium (ISM) due to scattering and absorption. It is a commonly held view that the overall dust to gas mass ratio, sometimes expressed in terms of the more directly observable counterpart ratio  $N_H/E(B - V)$ , is more or less constant ( $\sim 4.5 \times 10^{-23} \text{ cm}^{-2} \text{ mag}^{-1}$ ) throughout the Milky Way ([Draine, 2003](#)). As a mass ratio this is approximately 1/100 in favour of gas. This implies that large quantities of gas correspond to large quantities of dust. Dust grains are created in stars and then redistributed by dynamic circumstellar and interstellar processes. They primarily consist of carbon rich compounds and oxygen rich compounds. The latter, including silicates, are more refractory and dominate the obscuration of light in the ISM ([Draine, 2003](#)). In cold dark clouds where the column density is very high, dust grains are often protected from being destroyed by radiation. Within cold dark clouds, ices can form around the dust grains increasing their effective size. Dust grains are typically sub-micron sized and are detected via extinction at wavelengths less than  $\sim 2\mu\text{m}$ . At wavelengths longer than this dust clouds emit radiation as modified black bodies.

The optical depth due to dust is given by:

$$\tau_{\lambda}^{dust} = N_{dust} Q_e(\lambda) \sigma_{dust} \quad (1.1)$$

where,  $N_{dust}$  is dust the column density,  $Q_e(\lambda)$  is the extinction efficiency and  $\sigma_{dust}$  is the geometric cross section of the dust grains. For simplicity we assume that they are spherical so,  $\sigma_{dust} = \pi a^2$ , where  $a$  is the radius of the dust grain. The efficiency of extinction,  $Q_e$ , is the sum of the absorption efficiency,  $Q_a$  and the scattering efficiency,  $Q_s$ . It is dependant on how the wavelength of the incident light,  $\lambda$ , compares with the size of the dust grain so that:

$$\begin{aligned} 2\pi a > \lambda &\Rightarrow Q_e = 2 \\ 2\pi a \sim \lambda &\Rightarrow Q_e \propto 1/\lambda \\ 2\pi a \ll \lambda &\Rightarrow Q_e \propto 1/\lambda^4 \end{aligned} \quad (1.2)$$

This means that the dust grains entirely absorb/reflect light at very short wavelengths and become increasingly ineffective at absorbing/reflecting light as wavelength increases. The intensity of light affected by the presence of dust grains is then given by:

$$I(\lambda) = I_0(\lambda) \exp[-\tau_{\lambda}^{dust}] \quad (1.3)$$

where,  $I_0(\lambda)$ , is the light intensity before passage through the dust column and  $I_{\lambda}$  is the intensity of the source after extinction. The extinction in magnitudes,  $A_{\lambda}$ , is defined by the reduction in intensity caused by the presence of dust:

$$A_{\lambda} = -2.5 \log_{10}[I(\lambda)/I_0(\lambda)] = 2.5 \log_{10}(e) \tau_{\lambda}^{dust} = 1.086 \tau_{\lambda}^{dust} \quad (1.4)$$

The amount of extinction,  $A_{\lambda}$  acting on light from a star may be expressed in terms of the absolute magnitude of the star,  $M_{\lambda}$ , its apparent magnitude,  $m_{\lambda}$ , and the distance modulus  $\mu$ :

$$A_\lambda = m_\lambda - M_\lambda - \mu \quad (1.5)$$

where  $\mu = 5 \log(D) - 5$ , and  $D$  is the distance to the star in parsecs.

As this requires knowledge of the distance and intrinsic luminosity of the source, we can use the distance-independent ‘selective extinction’ instead which compares the extinction of a source at wavelength  $\lambda$  to the extinction at a reference wavelength  $\lambda_{ref}$ . This is known as the colour excess,  $E(\lambda - \lambda_{ref})$ :

$$E(\lambda - \lambda_{ref}) = A(\lambda) - A(\lambda_{ref}) = (m_\lambda - m_{\lambda_{ref}}) - (m_\lambda - m_{\lambda_{ref}})_0 \quad (1.6)$$

where  $A(\lambda)$  and  $A(\lambda_{ref})$  are the total extinction in magnitudes at wavelengths  $\lambda$  and  $\lambda_{ref}$  respectively and  $(m_\lambda - m_{\lambda_{ref}})$  and  $(m_\lambda - m_{\lambda_{ref}})_0$  are the apparent and intrinsic,  $m_\lambda - m_{\lambda_{ref}}$ , colour of the source respectively. In order to remove the dependency on dust column, standard interstellar extinction curves are normalized in terms of  $E(B - V)$  so that:

$$\frac{A_\lambda - A_V}{E(B - V)} = \frac{E(\lambda - V)}{E(B - V)} \propto Q_e(\lambda) \sigma_{dust} \quad (1.7)$$

At very long wavelengths,  $A_\lambda \rightarrow 0$ , leading to a quantity,  $R_V$ , known as the ratio of total to selective extinction:

$$R_V = \frac{A_V}{E(B - V)} \quad (1.8)$$

The value of  $R_V$  is used to label the ‘slope’ of extinction laws in different sight lines. A low value of  $R_V$  indicates a steep reddening law with small dust grains on average and preferentially extinguishes short wavelengths of light. A large value of  $R_V$  is a flatter extinction law and indicates large dust grains on average. In the Galaxy values of  $R_V$  range from  $\sim 2.1$  to  $5.1$  and have been found to be  $3.1$  on average (see e.g. [Cardelli et al., 1989](#); [Fitzpatrick & Massa, 2007](#)). [Fig. 1.3](#) taken directly from [Fitzpatrick & Massa \(2007\)](#) shows a family of extinction laws for different values of  $R_V$ , with low to high values of  $R_V$  going from top to bottom.

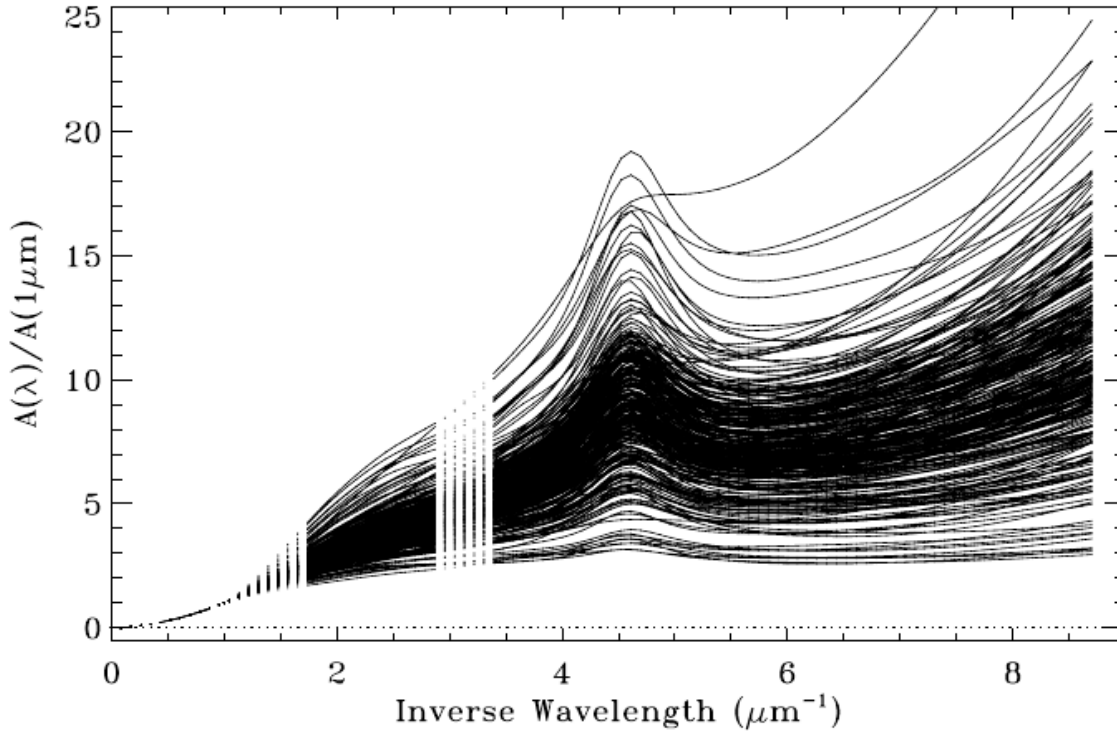


**Figure 1.3:** Family of UV through IR extinction curves normalized to  $A(1\mu\text{m})$ . The uppermost curves have low values of  $R_V$  while the bottom curves have high  $R_V$ . Taken directly from [Fitzpatrick & Massa \(2007\)](#)

More recently, many studies have adopted the monochromatic description of extinction  $A_0$ , which is usually the total extinction at a wavelength of  $5495\text{\AA}$  (see e.g. [Bailer-Jones, 2011](#); [Sale et al., 2014](#)). This is because the value of  $A_V$  depends on both the shape of the V band filter profile as well as the shape of the stellar SED within the band pass. In contrast,  $A_0$  measures the extinction at a single wavelength and is therefore independent of the temperature of the star in question. This approach is also adopted in this study.

As luminous objects detected to great distances across the Galactic disk and through substantial obscuration, OB stars have long been recognised as a highly-suitable means for characterising the spatial variation of interstellar extinction, in terms of both dust column and extinction law (e.g. [Cardelli et al., 1989](#); [Fitzpatrick & Massa, 2007](#)). This is greatly aided by their relatively simple optical near-infrared (OnIR) spectral energy distributions (SEDs) and their decreasing sensitivity to effective temperature passing from the early B types up through the O star range. It follows from this that the more densely we can map the positions and extinctions towards these luminous probes, the

more high-quality empirical constraints we can set on the 3-D distribution of dust and dust properties across the Galactic Plane.

## 1.5 Carina Arm

The Carina region of the Sagittarius-Carina Arm spans a Galactic longitude range of  $l \approx 270^\circ$  to  $330^\circ$ . Grabelsky et al. (1987) traced the structure of the Carina Arm in massive molecular clouds using CO line emission. The top panel of Fig. 1.4 taken directly from Grabelsky et al. (1987) shows the integrated CO emission as a function of Galactic longitude and LSR radial velocity. The negative velocity portion of the image indicates the near side of the spiral arm while the positive velocity portion indicates the far side. The zero velocity region of the map between  $l \approx 280^\circ - 284^\circ$  is the location of the Carina Arm tangent. The lower panel of Fig. 1.4 provides an interpretation of the longitude-velocity map with corresponding heliocentric distance and position of the spiral arm, also taken from Grabelsky et al. (1987). The sub-region of the Carina Arm which is the subject of study in this project spans the Galactic longitude range  $l \approx 281^\circ$  to  $293^\circ$  as approximately indicated by the blue triangle over-plotted on Fig. 1.2. In Fig. 1.4 it can be seen that the near side of the Carina Arm in this longitude range is located at a approximately  $\sim 2$  kpc away while the far side may be as far as  $\sim 10$  kpc away, although the uncertainties on the far side distance are much larger (Grabelsky et al., 1987). Around the tangent region, we see a sharp upturn in the intensity of CO emission when compared to the high longitude,  $l \approx 290^\circ$ , part of this region as shown in Fig. 1.5, also taken from Grabelsky et al. (1987). This location of the Carina Arm CO tangent has been upheld in more recent work by Dame et al. (2001) and Dame (2007) at higher resolution. Vallée (2014) compiled a catalogue of the distances and positions derived to the spiral arms based on different tracers from across the literature. The tracers include CO, H II complexes,  $60\mu\text{m}$  &  $240\mu\text{m}$  dust and far infrared C II and N II observations. Table 1 of Vallée (2014) shows that, based on these tracers, the tangent of the Carina Arm has been found to be between  $282^\circ < l < 287^\circ$  at distances of  $\sim 5 \pm 0.5$  kpc.

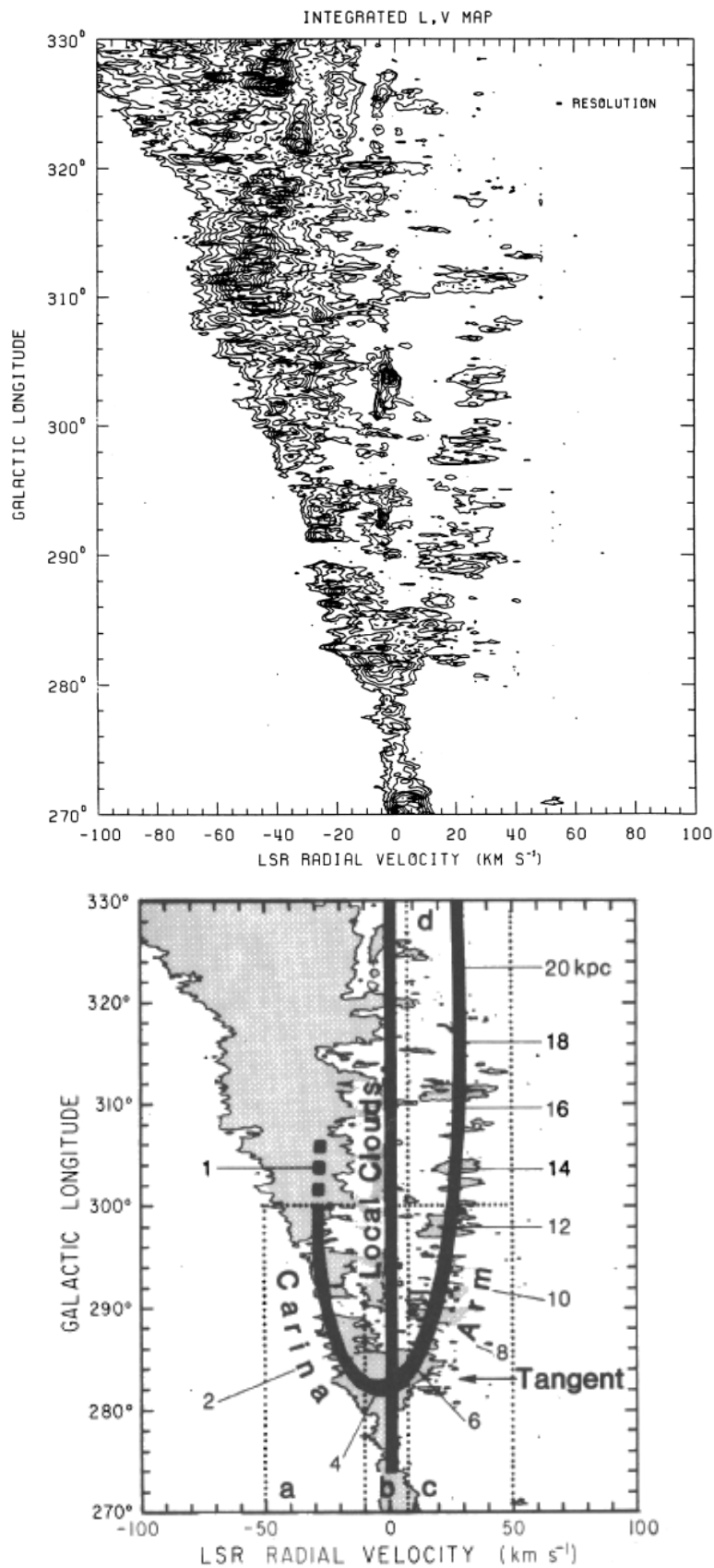


**Figure 1.4:** Top: Integrated CO emission as a function of Galactic longitude and LSR radial velocity for the Carina Arm. Bottom: Corresponding heliocentric distances. Both plots are taken directly from [Grabelsky et al. \(1987\)](#)

The most prominent feature of the Carina arm is the Carina Nebula (NGC 3372), a star forming region which hosts hundreds of known OB stars and is the largest collection of known massive stars within 3 kpc of the Sun (Povich et al., 2011). One of the most well studied and most massive stars in the Galaxy  $\eta$  Carina (Davidson & Humphreys, 1997), a luminous blue variable, is situated in the heart of the Carina Nebula at a distance of 2.3 kpc (Allen & Hillier, 1993; Smith, 2006b), a distance often adopted for the Carina Nebula itself.

The ionization of the Carina Nebula is largely sustained by two prominent massive star clusters Trumpler (Tr) 16 and Tr 14 thought to be at a similar distance to  $\eta$  Carina (Smith, 2006b), both with a relatively low dust extinction of  $A_V \sim 2.5$  mag (Ascenso et al., 2007b; Hur et al., 2012). It has been suggested in several works that the extinction law into the Carina Nebula region is represented by a higher than average total to selective extinction ratio with values ranging from  $R_V = 3.5$  to 5 (see e.g. Herbst, 1976; Walborn, 1995; Fitzpatrick & Massa, 2007; Hur et al., 2012). It has also been suggested that the extinction law in the foreground of Tr 14 and Tr 16 is represented by a normal  $R_V \sim 3.1$  law for foreground stars with  $A_V \lesssim 2.5$  (Fitzpatrick & Massa, 2007; Hur et al., 2012). This gives the impression that the average dust grain size increases significantly as the molecular clouds of the Carina Arm are entered, when compared to the inter-arm region in the foreground.

Being relatively close by with low extinction, the well studied massive star content of the Carina Nebula is largely too bright for photometric measurements by means of the survey data exploited in this study (see Chapter 5). At these distances and reddenings we are only able to detect later B stars. Here, the aim is to probe deeper beyond the Carina Nebula itself to many kpc along the Carina Arm. This will bring into consideration the young massive star cluster Westerlund 2 (Wd 2) situated  $\sim -4^\circ$  in Galactic longitude away towards the Carina Arm tangent and the young massive star cluster NGC 3603 situated  $\sim +4^\circ$  in Galactic longitude away towards the Galactic centre. These clusters are likely to be situated in the Carina arm as it curves around to cross the lines of sight a second time with distances in the region of  $\sim 6$  kpc for Wd 2 (Dame, 2007) and  $\sim 7$ kpc for NGC 3603 (Sung & Bessell, 2004), see Figs. 1.2

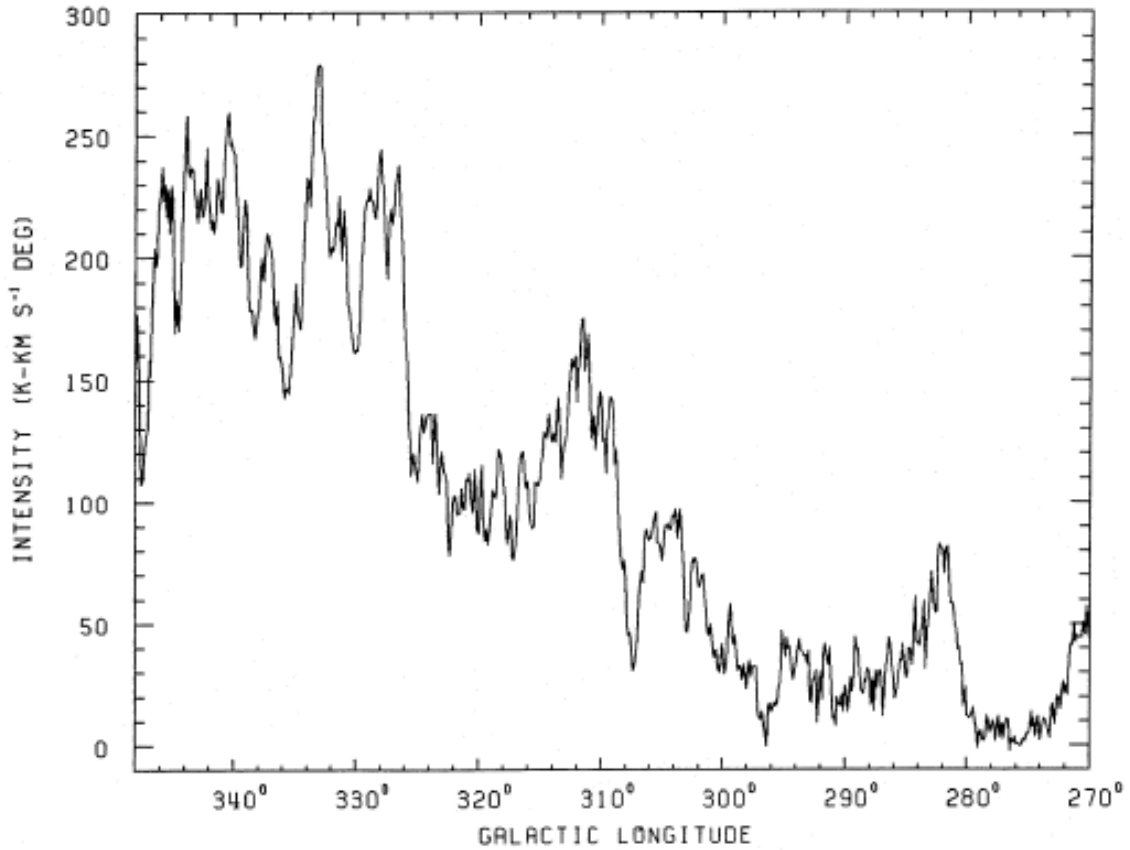


**Figure 1.5:** Integrated CO emission as a function of Galactic longitude for the Carina Arm taken directly from [Grabelsky et al. \(1987\)](#)

and 1.4. The OB star populations of NGC 3603 and Wd 2 have an average extinction of  $A_V \sim 5.4$  and  $A_V \sim 6.3$  respectively and both share raised values of  $R_V \gtrsim 3.8$  similar to that of the Carina Nebula ([Sung & Bessell, 2004](#); [Vargas Álvarez et al., 2013](#)). Although Wd 2 is thought to be closer than NGC 3603 its extinction is higher. This is due to the fact that Wd 2 is more closely aligned with the Carina Arm tangent region where the column density of dust can be expected to be higher, in keeping with the sharp rise in CO emission (as shown in Fig. 1.5). Further evidence for this is given and discussed in Chapter 5.

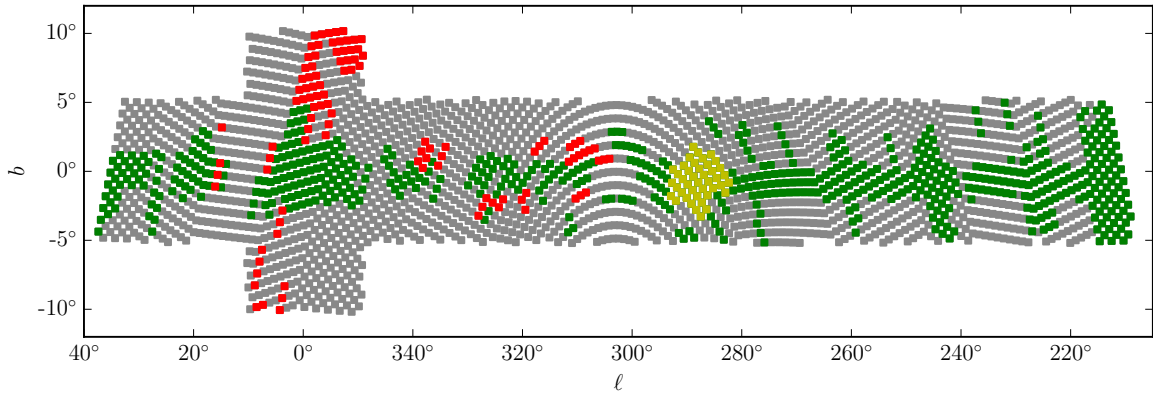


**Figure 1.6:** VPHAS+ survey footprint in Galactic coordinates. The coloured points show which fields have been completed only in the ‘red’ set (red points), and those that are complete in both sets (green points) and those yet to be observed (grey points) up to February 2015. The points coloured in yellow are the fields used in this study.

## 1.6 The VPHAS+ survey

The VST Photometric H $\alpha$  Survey (VPHAS+) (VPHAS+ [Drew et al., 2014](#)) is a deep, uniform, photometric survey of the entire Southern Galactic Plane and Bulge in broad-band  $u$ ,  $g$ ,  $r$ ,  $i$  and narrow-band H $\alpha$  filters on ESO’s VLT Survey Telescope (VST). The transmission profiles of each band are shown in [Fig. 1.7](#). The survey footprint includes the entire southern Galactic Plane within the Galactic latitude range of  $-5^\circ < |b| < 5^\circ$ . This is extended to  $-10^\circ < |b| < 10^\circ$  in the Galactic centre in order to capture the Bulge region. [Fig. 1.6](#) shows the positions of each field in Galactic coordinates and the completion status of each field up to February 2015 (the latest date of observations in this study). In total the survey covers  $\sim 2000$  square degrees. The VST’s OmegaCam imager provides a full square degree field of view and is made up of a 32 CCD mosaic with  $0.2''$  pixels sampling a median VPHAS+ seeing of 0.8-0.9 arcsec. To cover the survey footprint there are a total of 2269 field centres each made up of 2 offset exposures (3 in H $\alpha$  and  $g$ ) to cover the CCD gaps as shown in [Fig. 1.8](#). The median seeing across all bands is 0.8 – 1.0 arcsec. The target depth of the VPHAS+ survey observations is to reach  $\sim 20th$  magnitude with  $10\sigma$  detections in each band. The bright limit at which saturation sets in is 12–13 mag. The VPHAS+ observations of each field are split into two observing blocks. The ‘red’ set consists of exposures in the  $r$ ,  $i$  and H $\alpha$  bands while the ‘blue’ set consists of exposures in the  $u$ ,  $g$  and  $r$  bands.

Fig. 1.6 shows which fields have been only completed in the ‘red’ set (red points) and those that are complete in both sets (green points) and those yet to be observed (grey points) up to February 2015. The points coloured in yellow are the fields used in this study. The exposure times in seconds for the  $u, g, r, i$  and  $H\alpha$  bands is 150, 40, 25, 25 and 120 respectively. The VPHAS+ data is reduced and processed via the Cambridge Astronomical Survey Unit (CASU) pipeline. The CASU pipeline produces images and single-band source catalogues that are illumination corrected using the AAVSO Photometric All-Sky Survey (APASS), a process that results in a preliminary photometric calibration. The illumination correction takes care of photometric zero point variation across the 1 square degree field due to vignetting and scattered light. This is computed within the pipeline on a monthly basis i.e. not for individual fields. These catalogues are then bandmerged at the University of Hertfordshire.

## 1.7 Motivation and organisation of later chapters

O and early B stars are at the apex of galactic ecology, but in the Milky Way, only a minority of them may yet have been identified. There are an estimated  $\sim 60000$  OB stars in the Milky Way (Reed, 2000) which make up just  $\sim 0.0001\%$  of the stellar population. However, past cataloguing efforts have been limited to brighter, nearer objects (e.g Garmany et al., 1982; Reed, 2003; Maíz-Apellániz et al., 2004). Indeed the most comprehensive collection so far, ‘The Catalog of Galactic OB Stars’ (Reed, 2003) contains  $\sim 16000$  Galactic OB stars that are either spectroscopically confirmed or candidates selected via photometry taken from across the literature. However, around 95% of the entries are brighter than 13<sup>th</sup> magnitude in the visual bands. Other comprehensive spectroscopic catalogues include the ‘Instituto de Astrofísica de Canarias OB’ (IACOB) project (Simón-Díaz et al., 2011) and the ‘Galactic O star Catalogue’ (Maíz-Apellániz et al., 2004) (GOSC). GOSC is attempting to collect high resolution spectra of all known Galactic O stars. Fig. 1.9, taken from Maíz Apellániz et al. (2016) shows the B band magnitude distribution and Galactic longitude distribution of the current status of the project. Again we can see that there is a large deficit in the numbers

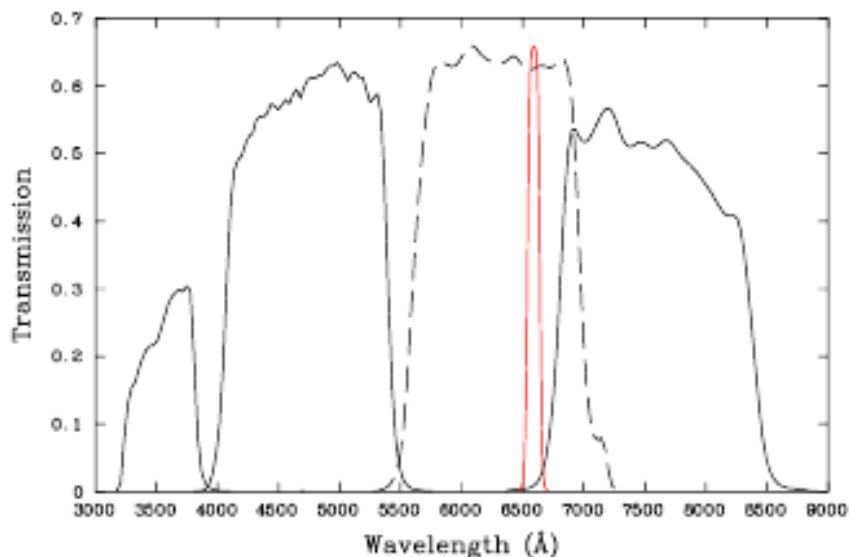


**Figure 1.7:** The transmission profiles of the Sloan  $u$ ,  $g$ ,  $r$  and  $i$  and narrow band  $H\alpha$  filters multiplied by CCD response curves and atmospheric transmission used in VPHAS+ (from [Drew et al., 2014](#)).

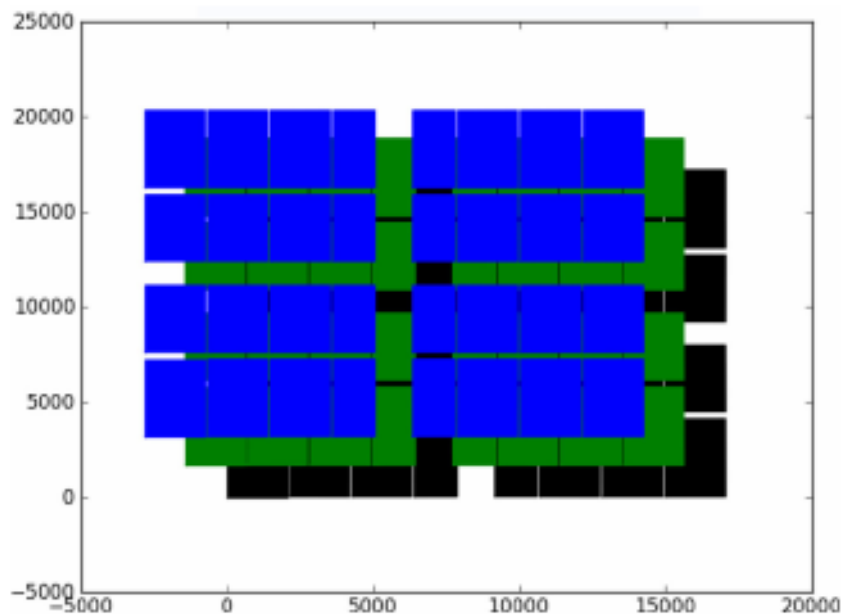


**Figure 1.8:** An illustration of the VPHAS+ offset pattern for the  $H\alpha$  and  $g$  filters (taken directly from [Drew et al., 2014](#)). Both axis are marked off in pixel number. In the  $u$ ,  $r$  and  $i$  bands just the outer positions are exposed

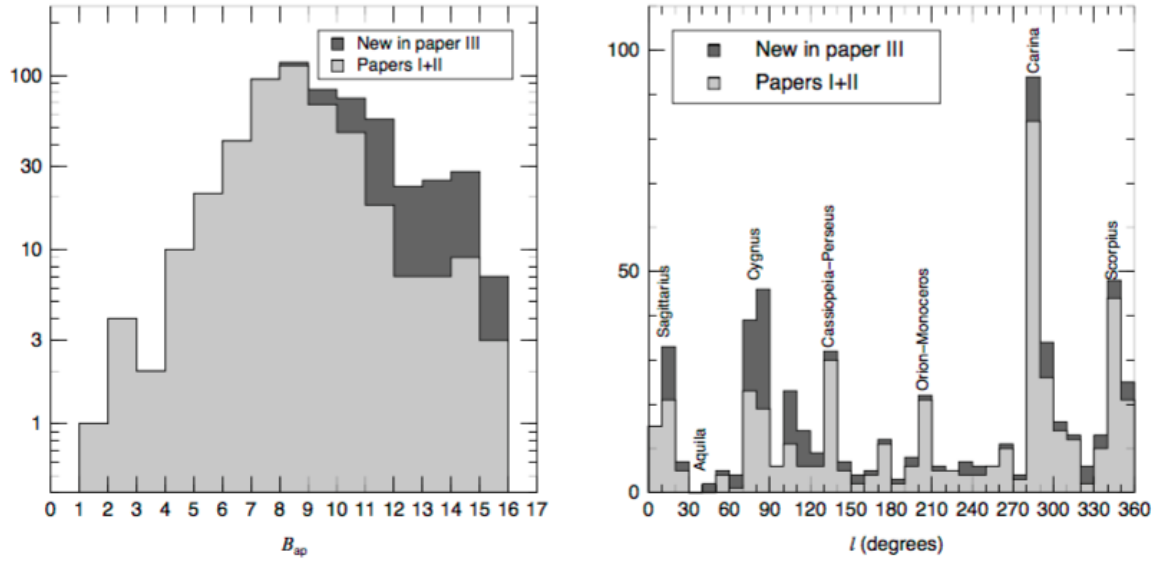


**Figure 1.9:** Apparent B magnitude and Galactic longitude distribution of O stars in GOSC from Maíz Apellániz et al. (2016)

of faint objects. Now is the right time to push the magnitude limit much fainter, to  $\sim 20^{\text{th}}$  magnitude in  $g$  given the likely delivery of astrometry to this depth by the Gaia mission from  $\sim 2017$ .

The practical motivation of this study is to establish and test a reliable method of photometric selection and analysis: this will form the basis for a new homogeneous census of Galactic OB stars as faint as  $g = 20$ . Efficient, purely photometric selection of OB stars in the field as well as in clusters continues to be best undertaken at blue optical wavelengths, where colour selection via the  $Q$  method (a photometric technique pioneered by Johnson & Morgan, 1953a) is proven to separate O and early B stars from later type stars. The  $u$ ,  $g$  and  $r$  filters of the VPHAS+ survey are ideal for achieving this goal. By combining the optical VPHAS+ data with near infrared data from 2MASS, the spectral energy distributions (SEDs) of the selected OB stars can be used to accurately constrain the amount of extinction and the extinction laws characterising their sight-lines. Presently, OB stars are notorious for the large uncertainties in their spectroscopic parallaxes – a situation that will transform as Gaia parallaxes become available from late 2017. More precise distances to these rare objects will reduce these uncertainties. This, along with the accurate extinction parameters derived in this study, will permit a much improved assessment of the structure of the star-forming

Galactic disk and the distribution of dust within it.

The layout of this study is as follows. In Chapter 2, I present the data and methods used to select and parametrise OB stars in the VPHAS+ survey. In Chapter 3, I represent the results from [Mohr-Smith et al. \(2015\)](#) in which the methods are established and tested on a  $\sim 2$  square degree area of the sky containing Wd 2 and are validated against results from the literature. In Chapter 4, I present spectroscopic follow up of a representative sample of candidate OB stars as further means of validating and testing my methods. In Chapter 5, I take my photometric selection and SED fitting methods and apply them to 42 square degrees of the Carina Arm and provide detailed analysis of the region. This results in a catalogue of nearly 6000 high-confidence OB stars, and provides a demonstration of how the new discoveries can yield insights into the properties of the Galactic disc – even before Gaia parallaxes become available. In Chapter 6, I compare my catalogue of OB stars with other catalogues in the literature. Finally in Chapter 7, I present the conclusions of this study and look ahead to further work that would naturally follow on from the work presented here.

---

# CHAPTER 2: DATA, CALIBRATION, SELECTION AND SED FITTING

---

## 2.1 Data

My analysis begins with band-merged catalogues created from the single-band catalogues created by the Cambridge Astronomical Unit (CASU) pipeline. We make use of the photometry from 42 VPHAS+ fields, each of these cover an area on the sky around  $\sim 1$  square degree.

Each field consists of two sets of observations; the blue set and the red set. The blue set consists of exposures in the  $u$ ,  $g$  and  $r$  filters while the red set consists of exposures in the  $H\alpha$ ,  $r$  and  $i$  filters. Within each set, the exposures in each band are taken in succession on the same night. For a given field the blue set and the red set are usually executed on separate nights, sometimes several months apart. Each field was observed in the blue filters on dates between January 2012 and February 2015 and in the red filters between February 2012 and February 2014. The central positions of each field and the dates in which the data were taken are listed in Table. 2.1.

The average seeing for each band, across all fields, as measured from the data point spread function is:  $u$ : 0.98",  $g$ : 0.86",  $r$ : 0.80",  $i$ : 0.74" and  $H\alpha$ : 0.80". The average  $5\sigma$  magnitude limits on the single exposures are  $u$ : 21.3,  $g$ : 22.3,  $r$ : 21.6,  $i$ : 20.8, and  $H\alpha$ : 20.6. Viewed in comparison to all the VPHAS+ data collected so far, these observations rank as 2<sup>nd</sup>-quartile on average (i.e. relatively high quality). The seeing and limiting magnitude for each field is listed in Table. 2.1. All magnitudes are in the Vega system. Full details on the survey strategy, the offsets, the exposure times, photometric quality and the data-processing pipeline used are given by [Drew et al. \(2014\)](#).

I select stars in the magnitude range  $13 < g < 20$  and require random photometric errors to be less than 0.1. I also require that each object has a ‘good’ detection in the  $u$ ,  $g$ ,  $r$  and  $i$  bands according to the CASU pipeline. Here, a ‘good’ detection means that

**Table 2.1:** Table showing the positions, dates, seeing and limiting magnitudes for each field.

Field	RA	DEC	<i>ugr</i> date	<i>H<math>\alpha</math></i> date	Seeing					Limiting magnitude				
					<i>u</i>	<i>g</i>	<i>r</i>	<i>i</i>	<i>H<math>\alpha</math></i>	<i>u</i>	<i>g</i>	<i>r</i>	<i>i</i>	<i>H<math>\alpha</math></i>
1632	10:10:02.96	-57:05:48.4	20130305	20120430	0.9	1.0	0.9	0.6	0.9	21.5	22.5	21.7	20.8	20.6
1633	10:17:08.57	-57:05:48.4	20130305	20120430	0.9	1.1	1.0	0.6	0.9	21.4	22.4	21.7	20.8	20.7
1634	10:24:14.19	-57:05:48.4	20140501	20130519	0.8	1.0	0.8	0.8	0.8	21.7	22.8	21.8	20.9	20.8
1635	10:31:19.80	-57:05:48.4	20140501	20130519	0.8	1.0	0.9	0.9	0.9	21.7	22.7	21.8	20.9	20.7
1636	10:38:25.42	-57:05:48.4	20140501	20130519	0.9	1.0	0.8	0.9	1.0	21.7	22.7	21.7	20.8	20.6
1677	10:10:54.55	-58:03:52.3	20120122	20120429	0.9	0.7	0.9	0.8	0.9	21.7	22.6	21.9	20.8	20.7
1678	10:18:10.91	-58:03:52.3	20120122	20120429	0.9	0.7	1.0	1.0	0.9	21.7	22.6	21.8	20.6	20.7
1679	10:25:27.27	-58:03:52.3	20120122	20120429	0.8	0.7	1.0	0.8	0.8	21.7	22.5	21.8	20.8	20.7
1680	10:32:43.64	-58:03:52.3	20130213	20120220	1.1	0.8	0.7	1.2	1.1	21.3	22.4	21.8	20.6	20.6
1681	10:40:00.00	-58:03:52.3	20130213	20120220	1.0	0.9	0.7	1.0	1.0	21.3	22.3	21.8	20.7	20.7
1682	10:47:16.36	-58:03:52.3	20150212	20140219	1.2	0.9	0.7	0.8	0.8	21.2	22.7	21.8	20.7	20.7
1683	10:54:32.73	-58:03:52.3	20150212	20140219	1.1	0.9	0.7	0.7	0.8	21.2	22.7	21.8	20.8	20.6
1684	11:01:49.09	-58:03:52.3	20150212	20140219	1.3	0.8	0.7	0.7	0.9	21.2	22.7	21.8	20.8	20.1
1734	10:26:44.15	-59:01:56.1	20120214	20120429	0.7	0.6	0.6	0.7	0.6	21.2	22.1	21.6	20.7	20.4
1735	10:34:11.81	-59:01:56.1	20120214	20120429	0.7	0.6	0.5	0.7	0.6	21.2	22.1	21.6	20.7	20.6
1736	10:41:39.48	-59:01:56.1	20120214	20120429	0.7	0.6	0.6	0.6	0.8	21.1	22.0	21.5	20.8	20.5
1737	10:49:07.15	-59:01:56.1	20120214	20120530	0.8	0.8	0.6	0.5	0.7	21.2	22.0	21.6	20.8	20.6
1738	10:56:34.82	-59:01:56.1	20120214	20120530	0.8	0.7	0.6	0.6	0.6	21.2	22.1	21.6	20.8	20.3
1739	11:04:02.49	-59:01:56.1	20120214	20120530	0.8	0.7	0.6	0.5	0.6	21.2	22.1	21.6	20.7	19.9
1786	10:31:26.63	-60:00:00.0	20120214	20130419	0.7	0.6	0.6	0.7	0.6	21.4	22.2	21.6	20.7	20.6
1787	10:39:08.66	-60:00:00.0	20120214	20130419	0.7	0.6	0.6	0.6	0.6	21.2	22.1	21.5	20.7	20.6
1788	10:46:50.70	-60:00:00.0	20120214	20130419	0.7	0.7	0.6	0.6	0.7	21.1	21.9	21.3	20.7	20.7
1789	10:54:32.73	-60:00:00.0	20130121	20130419	1.2	0.9	0.9	0.9	1.1	21.3	22.3	21.6	20.7	20.5
1790	11:02:14.76	-60:00:00.0	20130121	20130419	1.2	1.0	1.1	0.8	1.0	21.3	22.3	21.5	20.7	20.4
1791	11:09:56.79	-60:00:00.0	20130121	20130419	1.2	1.0	0.9	0.6	0.6	21.3	22.3	21.6	20.9	20.5
1833	10:28:30.50	-60:58:03.9	20150220	20130320	1.2	0.9	0.7	0.6	0.6	21.3	22.6	21.8	20.9	20.5
1834	10:36:27.85	-60:58:03.9	20150220	20130320	1.2	1.0	0.7	0.6	0.6	21.2	22.5	21.7	20.9	20.7
1835	10:44:25.19	-60:58:03.9	20130304	20120331	1.1	0.8	0.8	0.6	0.6	20.9	22.2	21.4	20.9	20.7
1836	10:52:22.54	-60:58:03.9	20130304	20120331	1.1	0.8	1.0	0.6	0.6	21.0	22.2	21.3	20.9	20.7
1837	11:00:19.89	-60:58:03.9	20130304	20120331	1.1	0.8	0.8	0.6	0.6	21.0	22.2	21.4	20.9	20.7
1838	11:08:17.24	-60:58:03.9	20120214	20130121	0.8	0.6	0.6	0.8	0.9	21.1	22.0	21.6	21.0	20.7
1839	11:16:14.59	-60:58:03.9	20120214	20130121	0.7	0.6	0.6	0.8	0.8	21.2	22.0	21.5	21.0	20.7
1840	11:24:11.93	-60:58:03.9	20120214	20130121	0.7	0.6	0.6	0.8	0.8	21.2	22.0	21.5	21.0	20.8
1877	10:33:36.00	-61:56:07.7	20150220	20130519	1.0	1.1	1.0	0.7	0.8	21.3	22.4	21.7	20.9	20.7
1878	10:41:49.71	-61:56:07.7	20150220	20130519	1.1	1.1	1.2	0.7	0.8	21.3	22.4	21.5	20.9	20.7
1879	10:50:03.43	-61:56:07.7	20150220	20130519	1.5	1.2	1.1	0.7	0.7	21.0	22.3	21.5	20.9	20.8
1880	10:58:17.14	-61:56:07.7	20150211	20130617	1.1	0.9	1.0	0.7	1.0	20.9	22.0	21.3	20.7	20.3
1881	11:06:30.86	-61:56:07.7	20150211	20130617	1.0	1.1	1.0	0.7	0.8	20.9	22.0	21.3	20.8	20.5
1882	11:14:44.57	-61:56:07.7	20150211	20130617	1.2	1.1	1.2	0.8	0.7	20.9	22.0	21.3	20.8	20.6
1883	11:22:58.29	-61:56:07.7	20120214	20120223	0.8	0.6	0.5	0.7	0.9	21.2	22.1	21.7	21.1	20.9
1921	11:13:08.17	-62:54:11.6	20130402	20130130	1.1	1.2	0.8	1.2	0.9	21.4	22.5	21.7	20.5	20.6
1922	11:21:39.41	-62:54:11.6	20130402	20130130	1.3	1.1	1.0	1.0	1.1	21.3	22.6	21.7	20.7	20.5
<b>Average:</b>					<b>0.98</b>	<b>0.86</b>	<b>0.80</b>	<b>0.74</b>	<b>0.80</b>	<b>21.27</b>	<b>22.32</b>	<b>21.61</b>	<b>20.81</b>	<b>20.59</b>

the photometry has a non zero morphological class to remove noise like sources and that the photometry has a confidence greater than 90%. Mean magnitudes were taken when repeat photometry was available from the offset fields. Objects were removed if the photometry in the offset field differed by  $> 0.2$  mags. This removes unreliable photometry due to objects that fall on a CCD edge. Each object is then cross matched to within a  $1''$  radius of the 2MASS point source catalogue to obtain NIR magnitudes in the  $J$ ,  $H$  and  $K$  bands. Here, we only require that each object has a detection in all three bands. Each star then has an Optical-NIR SED consisting of seven bands.

## 2.2 Synthetic Photometry and Reddening

This section describes the selection of young massive stars using VPHAS+ colour-colour diagrams. The positions of unreddened stars of different spectral type in any photometric colour-colour plane can be modelled by means of synthetic photometry. Here, I describe the calculations needed to produce these colours.

Given the flux calibrated spectrum of a star,  $F_{\lambda,*}$ , along with the transmission function of a relevant filter  $x$ ,  $T_x$ , the unreddened magnitude in  $x$ ,  $m_{x,0}$ , of the star can be expressed as:

$$m_{x,0} = -2.5 \log \int \lambda F_{\lambda,*} T_x d\lambda + c \quad (2.1)$$

where  $c$  is an arbitrary constant. In the system referred to Vega as the zero-magnitude and zero-colour object, this expression becomes:

$$m_x = -2.5 \log \left[ \frac{\int \lambda F_{\lambda,*} T_x d\lambda}{\int \lambda F_{\lambda,V} T_x d\lambda} \right] \quad (2.2)$$

where  $F_{\lambda,V}$  is the spectral energy distribution (SED) of Vega.

Therefore the intrinsic colour  $m_{x,0} - m_{y,0}$  of the given star can be expressed as:

$$m_{x,0} - m_{y,0} = -2.5 \log \left[ \frac{\int \lambda F_{\lambda,*} T_x d\lambda}{\int \lambda F_{\lambda,*} T_y d\lambda} \cdot \frac{\int \lambda F_{\lambda,V} T_y d\lambda}{\int \lambda F_{\lambda,V} T_x d\lambda} \right] \quad (2.3)$$

To account for attenuation due to interstellar extinction, a multiplicative reddening

term  $e^{-\tau_\lambda}$  is introduced, where  $\tau_\lambda$  is the optical depth as a function of wavelength associated with dust. Hence the observed flux from the reddened star can be written as  $F_{\lambda,\star}e^{-\tau_\lambda}$ . Substituting this into equation 2.2 we have the reddened magnitude of a star in band  $x$ :

$$m_x = -2.5 \log \left[ \frac{\int \lambda F_{\lambda,\star} e^{-\tau_\lambda} T_x d\lambda}{\int \lambda F_{\lambda,V} T_x d\lambda} \right] \quad (2.4)$$

This can be recast in terms of  $A_\lambda$ , the monochromatic extinction due to interstellar dust as a function of wavelength, where  $A_\lambda = 1.086\tau_\lambda$ . Substituting into equation 2.4 we have:

$$m_x = -2.5 \log \left[ \frac{\int \lambda F_{\lambda,\star} 10^{-0.4A_\lambda} T_x d\lambda}{\int \lambda F_{\lambda,V} T_x d\lambda} \right] \quad (2.5)$$

The form of extinction law used throughout this work, defining  $A_\lambda$  over the ultraviolet, optical and near-infrared regime, is due to [Fitzpatrick \(2004\)](#). It is well-known that the detailed form of the extinction law is liable to change from sightline to sightline. This variation is commonly parameterised in terms of  $R$ , the ratio of total to selective extinction, e.g.

$$R_V = \frac{A_V}{E_{B-V}} \quad (2.6)$$

where  $A_V$  is the total extinction in the  $V$  band, and  $E_{B-V}$  is the  $(B - V)$  colour excess. The typical value of  $R_V$  in the Galaxy is 3.1, and is seen to vary from 2.1 to  $\sim 5.1$  ([Cardelli et al., 1989](#)). Figure 2.1 shows the form of the  $A_\lambda/A_0$  for different values of  $R_V$  over a range of wavelengths.

The filters used in the VPHAS+ survey are  $u$ ,  $g$ ,  $r$ ,  $i$  and narrowband  $H\alpha$  (NB\_659 in ESO's naming convention). The transmission curves for these filters have to be corrected for the wavelength dependence of both the detector response and atmospheric transmission, before they are used in the above equations. The filter profiles shown in the bottom panel of figure 2.1 incorporate these corrections.

Finally to compute unreddened and reddened stellar colours as a function of spec-

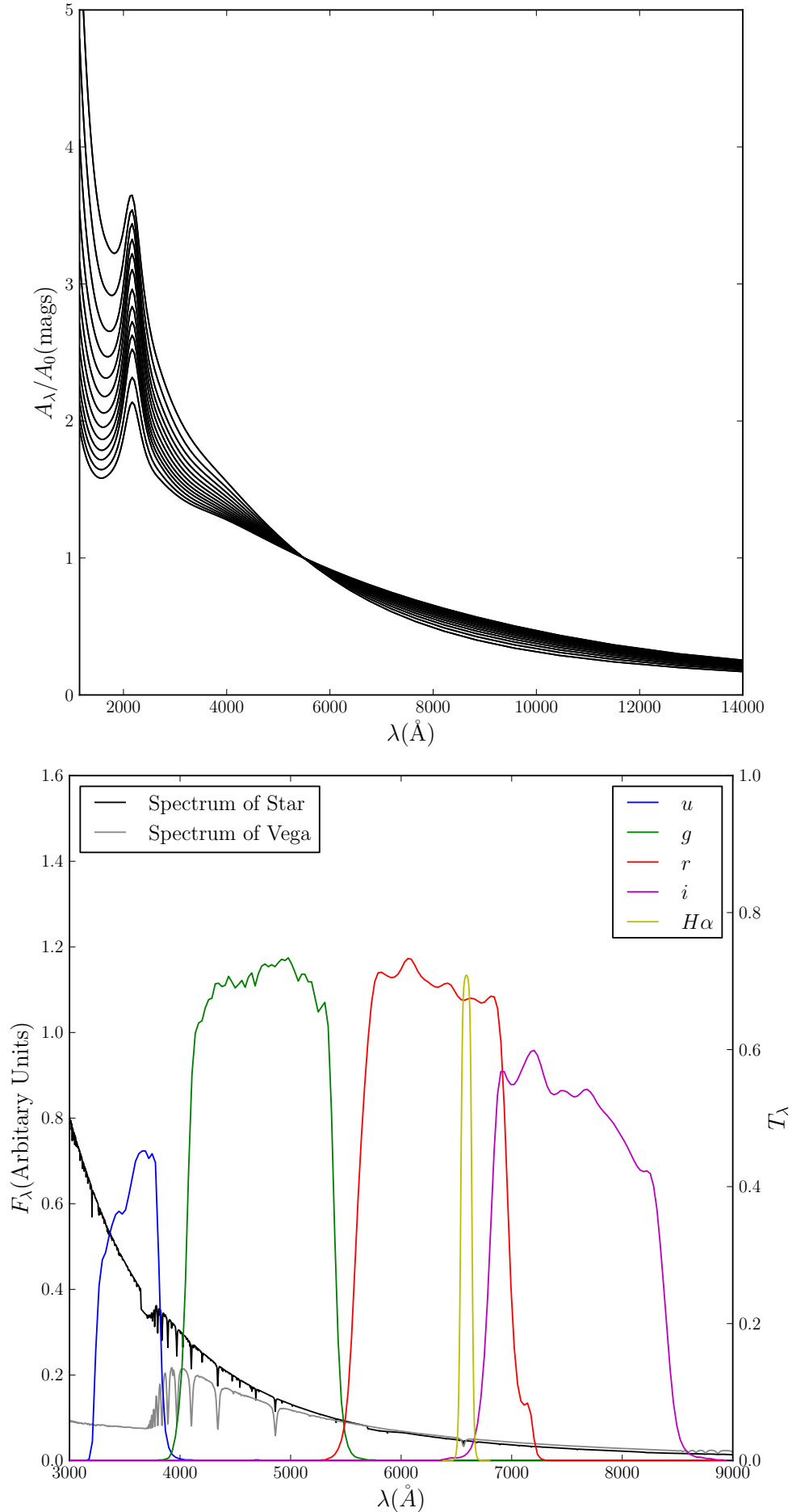


**Figure 2.1:** Top panel: Fitzpatrick (2004) extinction curves for  $R_V = 2.7$  (top curve) to  $R_V = 5.1$  (bottom curve) which have been normalised as  $\lambda = 5500\text{\AA}$ . Bottom panel: VHPAS+ filter profiles, an O6V spectrum and the spectrum of Vega as a function of wavelength.

tral type, I have used the stellar SEDs presented by Munari et al (2005). These are ATLAS9 LTE model atmospheres best-suited to stars of A type and later. For OB stars, non-LTE effects are important and can be better represented by model atmospheres obtained with e.g. CMFGEN (Hillier & Lanz, 2001). However, the effect that the non-LTE models have on the derived broad-band SEDs of main-sequence OB stars is negligible and therefore the LTE models have not adversely affected the derived synthetic tracks.

Appendix A contains tables and figures for reddened colours computed in the VPHAS+ ( $u - g$ ,  $g - r$ ) and ( $r - i$ ,  $r - H\alpha$ ) plane for  $R_V = 2.5$ , 3.1 and 3.8 reddening laws. Figure 2.2 shows the synthetic main-sequence intrinsic colours and includes the  $R = 3.1$  reddening lines of  $B3V$  and  $G0V$  stars on the VPHAS+ ( $u - g$ ,  $g - r$ ) colour-colour diagram over-plotted on a VPHAS+ data field. No reddening line, computed this way, is straight. The  $B3V$  line is picked out as it will be used in selecting candidate OB stars (see section 2.2.1) and the  $G0V$  line is picked out as it and the zero reddening main sequence are used for calibrating the  $u$  band (see section 2.3).

As the pipeline photometric calibration of VPHAS+ data is provisional, rather than final, there cannot be the expectation that real data will conform to the modelled colours. In order for the survey data to be matched to the models, it is presently necessary to ‘shift’ the data so that the  $G0V$  reddening line sits at the top of the main stellar locus in the ( $u - g$ ,  $g - r$ ) diagram, and the lower unreddened MS corresponds to that apparent from the data. The systematic offset between the model and observation arises mainly from the calibration of the  $u$  band as discussed in section 2.3.

### 2.2.1 Updated Q method

We select OB stars using a method that has its origins in the Q Method of Johnson & Morgan (1953b). On the ( $u - g$ ,  $g - r$ ) diagram, reddened OB stars of spectral type earlier than B3 are located above and away from the main stellar locus. We initially select our candidate objects above the reddening vector associated with a B3V star. In principle no single star can be bluer than the Rayleigh-Jeans (RJ) limit which sets

an upper bound on the likely location of OB stars in the diagram as shown in Fig. 2.2. The blue objects that lie above the RJ reddening vector were nevertheless included in the selection and their possible origins are discussed in section 3.4. I have used the spectroscopically-confirmed OB stars of the massive star cluster Westerlund 2 (Wd 2) as a basis for testing the integrity of the above synthetic photometry and the calibration technique shown in the next section. This is discussed in Section 3.3.1.

## 2.3 Calibration

In order to improve the initial calibration applied by the pipeline and achieve better uniformity, we have made comparisons with  $g$ ,  $r$  and  $i$  observations from the AAVSO Photometric All-Sky Survey (APASS) and then have used the main stellar locus in the  $(u-g, g-r)$  colour-colour (CC) diagram to calibrate the  $u$  band for which there is no external reference data.

The first step in the process adopted here is to cross match sources within each group of VPHAS+ fields with their counterparts in the APASS survey to within a 0.5 arcsec radius. Groups of fields in this instance should be understood to be either pairs or triplets of fields which were observed consecutively within minutes of each other. Each field consists of at least two pointings in  $g$ ,  $r$  and  $i$ . The VPHAS+  $g$ ,  $r$  and  $i$  band photometric scales were compared to APASS on a pointing-by-pointing basis, constructing a set of estimates for the corrections needed to place the VPHAS+ magnitudes on the APASS scale. The median of these corrections (6 for a group made of three fields) is taken to be the best estimate for the entire group's shift between VPHAS+ and APASS, per band. Each pointing is then brought onto a scale consistent with this adopted shift. The net effect of this procedure is to place the data onto a photometric scale that amounts to a two or three square-degree running median of the APASS scale. This approach also minimises the impact of localised non-uniformities in the APASS database that are known to exist. While the computed shifts for these bands were small (see Table 2.2), this has to be done first in order to ensure that the correction needed to align the main stellar locus in the  $(u-g, g-r)$  diagram with its

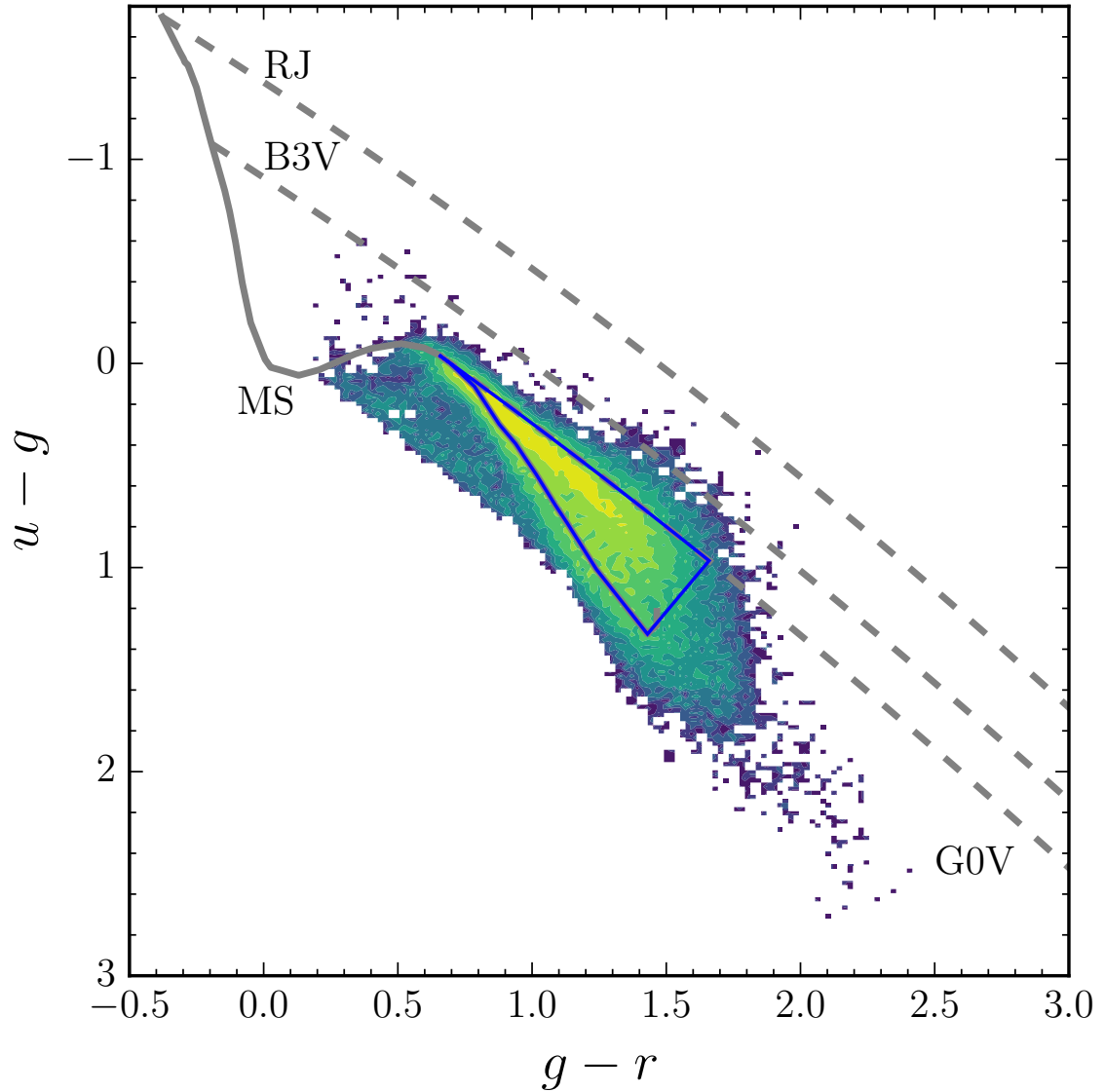


**Figure 2.2:** Synthetic reddening tracks of a B3V, G0V and a pure RJ spectrum are shown by the dashed grey lines. The zero reddening main sequence is shown by the solid grey line. Candidate OB stars are selected above the B3V line. The shift in the  $u$  magnitude scale maximising the number of stars falling within the blue triangle, defined by the unreddened main sequence and G0V reddening line, is the measure used to place the  $u$  band onto a scale that is astrophysically consistent with the APASS-verified  $g$  and  $r$  photometric scales. Bright yellow colour picks out the highest stellar densities in this CC diagram. The data shown are drawn from the 1 square degree field centered on RA 10:25:27.27 DEC -58.03:52.3.

predicted position measures the  $u$  band offset alone.

As the  $u$  band is the most effective-temperature-sensitive band in the selection and parametrization of OB stars, it is important to calibrate it consistently across the Carina region. In the ( $u-g$ ,  $g-r$ ) diagram, we require that the empirical main stellar locus, dominated by FGK stars within 1-2 kpc of the Sun, matches up with the position predicted by solar-metallicity synthetic tracks. This was achieved by finding the vertical shift maximising the number of objects between the G0V reddening vector and the zero reddening main sequence as represented by the blue triangle in Fig. 2.2. This procedure has revealed that the pipeline  $u$  band magnitude scale needs to be made brighter by anywhere between 0.28 and 0.52 mags (0.38 on average) as shown in Table 2.2. We use this technique, rather than one dependent on extrapolated colour relations involving  $g$  and  $r$  magnitudes, because it has been demonstrated by Patat et al. (2011) that variations in the atmosphere’s transmission at wavelengths below 4000 Å are effectively uncorrelated with changes at longer wavelengths. The significant  $u$  corrections obtained, relative to the pipeline which adopts an ATLAS high-Galactic latitude  $g, r$  extrapolation (see Shanks et al., 2015), illustrates the importance of a tailored approach to this challenging band.

We have exploited the field overlaps provided by the tiling pattern of VPHAS+ (see Drew et al., 2014) in order to check the final uniformity of the recalibration. Within the overlap regions, it is possible for a star to have up to 4 independently recalibrated detections in each band. Using these, we can evaluate the convergence to a common scale by comparing the standard deviation of multiple measurements before and after the APASS-dependent homogenization process. Fig. 2.3 shows the cumulative distribution of the standard deviation across multiple measurements before and after calibration for the  $u$  and  $g$  bands. Here we can see that there is a  $\sim 50\%$  increase in the uniformity of the  $g$  band after calibration, while the  $u$  band improves by 7%. The fact that we see an improvement in the uniformity of the  $u$  band data, despite a fairly large range (0.21 - 0.52 mags) in the calibration shifts, shows that the calibration method is consistent. Table 2.3 shows how the uniformity improves for all bands.

**Table 2.2:** Photometric calibration shifts applied to the VPHAS+ data

Field	$u$	$g$	$r$	$i$
1632	-0.37	-0.04	-0.06	-0.04
1633	-0.37	-0.04	-0.06	-0.04
1634	-0.45	-0.04	-0.07	-0.07
1635	-0.45	-0.04	-0.07	-0.07
1636	-0.45	-0.04	-0.07	-0.07
1677	-0.36	0.05	-0.01	-0.03
1678	-0.36	0.05	-0.01	-0.03
1679	-0.36	0.05	-0.01	-0.03
1680	-0.37	0.01	-0.07	0.03
1681	-0.37	0.01	-0.07	0.03
1682	-0.38	-0.12	-0.10	-0.06
1683	-0.38	-0.12	-0.10	-0.06
1684	-0.38	-0.12	-0.10	-0.06
1734	-0.43	-0.01	-0.07	-0.01
1735	-0.43	-0.01	-0.07	-0.01
1736	-0.43	-0.01	-0.07	-0.01
1737	-0.30	0.01	-0.08	-0.13
1738	-0.30	0.01	-0.08	-0.13
1739	-0.30	0.01	-0.08	-0.13
1786	-0.37	-0.00	-0.06	-0.01
1787	-0.37	-0.00	-0.06	-0.01
1788	-0.37	-0.00	-0.06	-0.01
1789	-0.29	0.01	-0.06	-0.03
1790	-0.29	0.01	-0.06	-0.03
1791	-0.29	0.01	-0.06	-0.03
1833	-0.44	-0.10	-0.23	-0.06
1834	-0.44	-0.10	-0.23	-0.06
1835	-0.28	0.02	-0.08	-0.10
1836	-0.28	0.02	-0.08	-0.10
1837	-0.28	0.02	-0.08	-0.10
1838	-0.41	-0.04	-0.12	-0.10
1839	-0.41	-0.04	-0.12	-0.10
1840	-0.41	-0.04	-0.12	-0.10
1877	-0.52	-0.14	-0.22	-0.16
1878	-0.52	-0.14	-0.22	-0.16
1879	-0.52	-0.14	-0.22	-0.16
1880	-0.41	-0.05	-0.12	-0.09
1881	-0.41	-0.05	-0.12	-0.09
1882	-0.41	-0.05	-0.12	-0.09
1883	-0.36	-0.00	-0.08	-0.15
1921	-0.41	-0.06	-0.07	-0.04
1922	-0.41	-0.06	-0.07	-0.04
Average	-0.38	-0.03	-0.09	-0.07

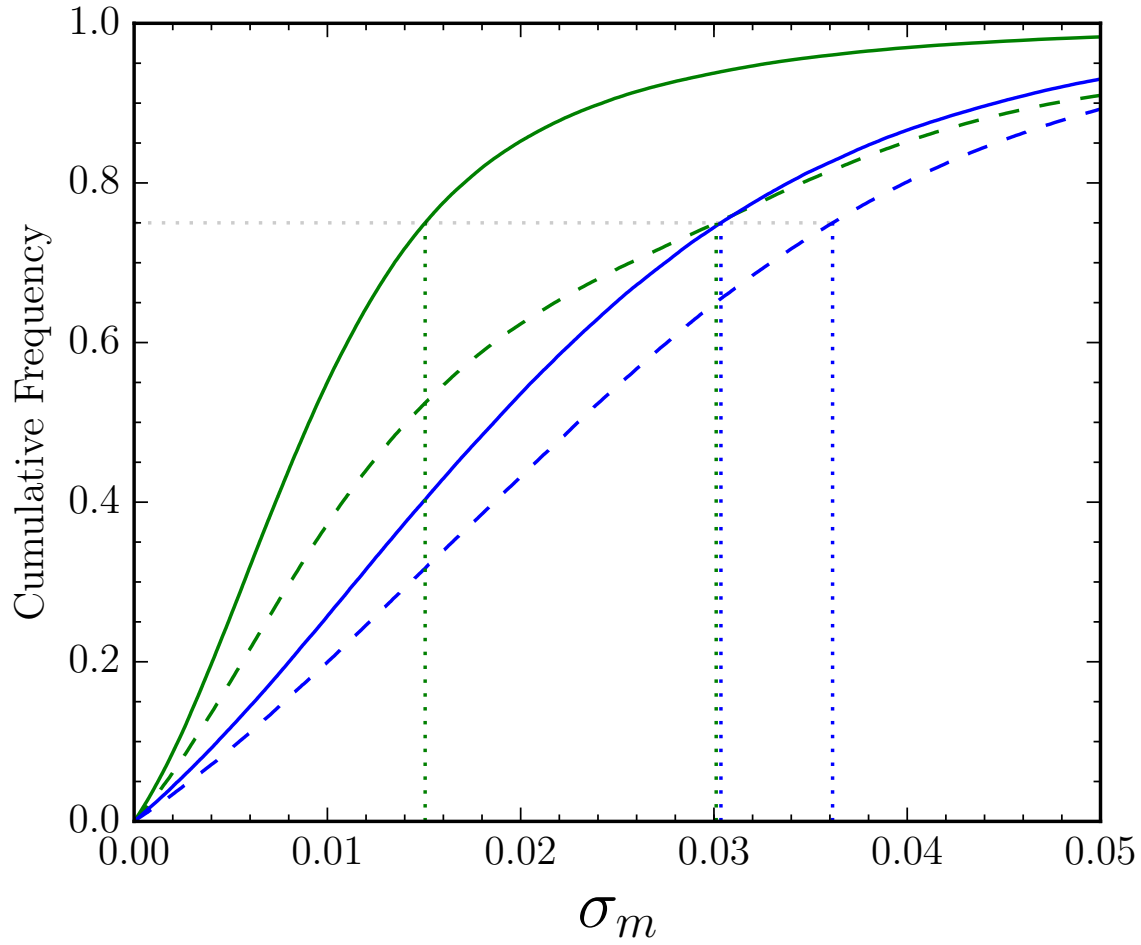


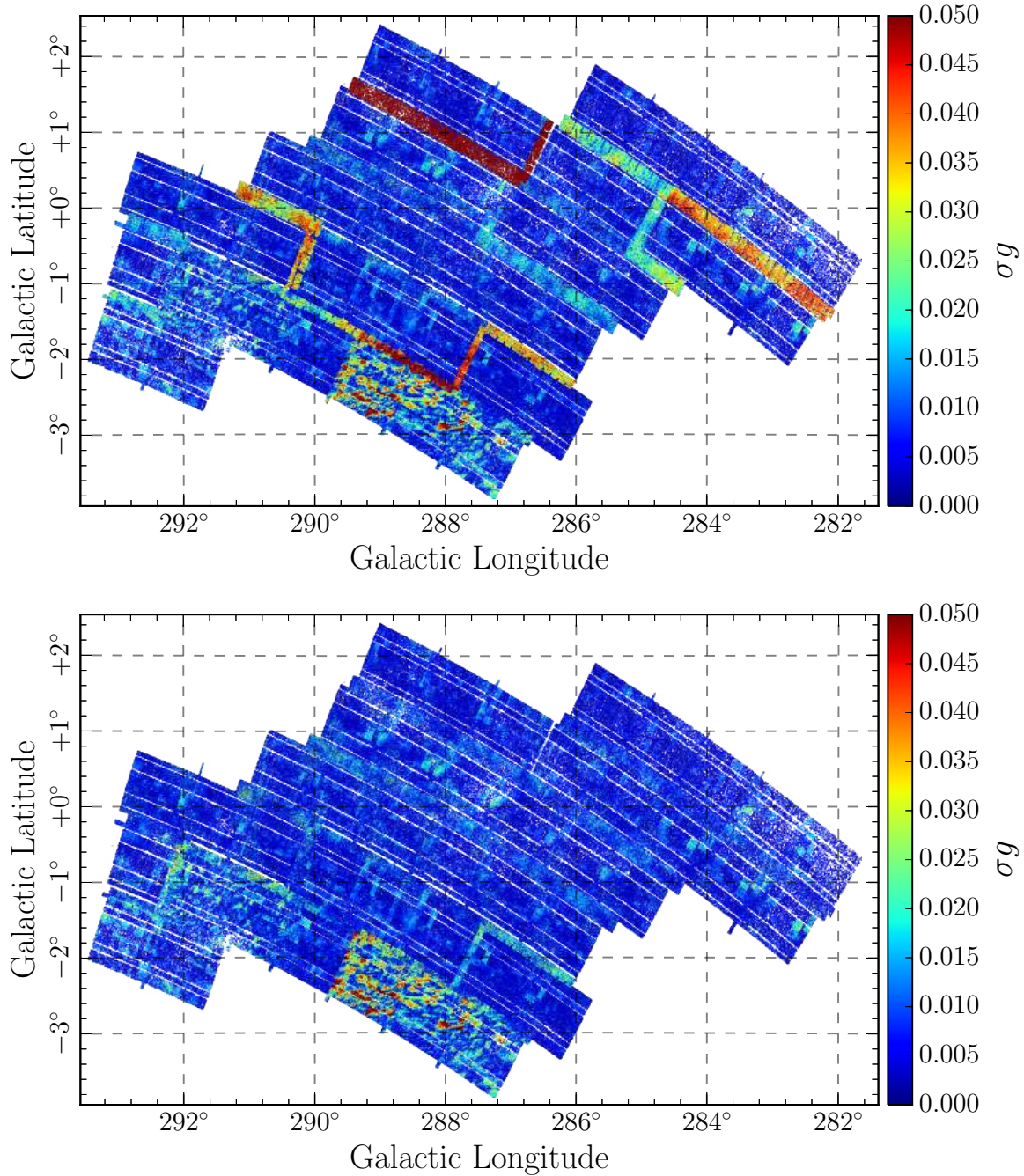
**Figure 2.3:** Cumulative distributions of  $\sigma_u$  (blue) and  $\sigma_g$  (green) across the overlap regions for each photometric band in VPHAS+ before (dashed line) and after (solid line) calibration. The dotted lines show the upper quartile for each case (see Table. 2.3 for more details)

**Table 2.3:** Measure of uniformity: standard deviation of multiple detections in each band before and after calibration.

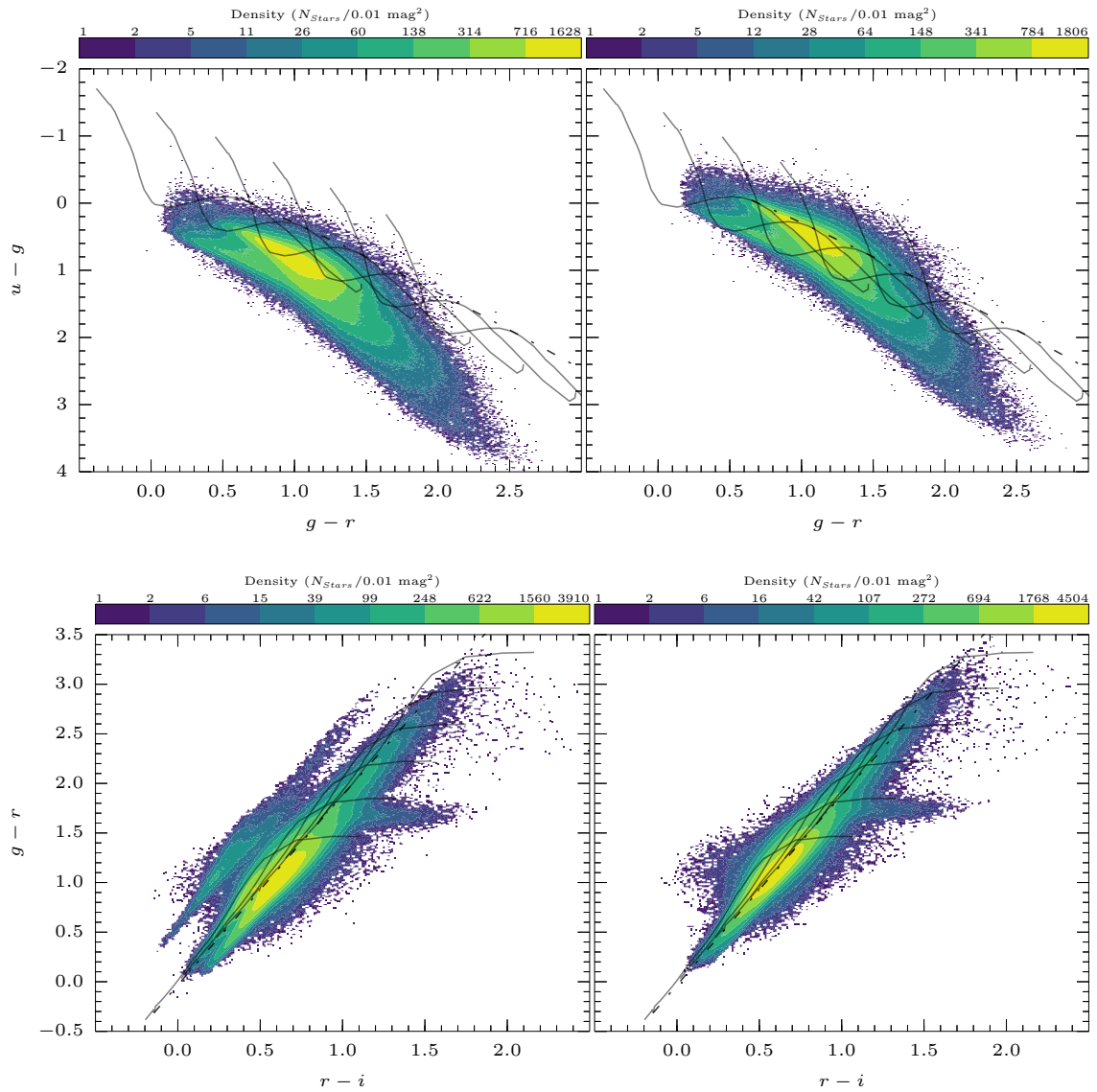
	$\sigma_m$ Before	$\sigma_m$ After	Improvement
<i>u</i>	0.029	0.027	7 %
<i>g</i>	0.030	0.015	50 %
<i>r</i>	0.027	0.019	30 %
<i>i</i>	0.028	0.024	14 %

Fig. 2.4 shows the spatial distribution of stars across the region with multiple detections coloured by the standard deviation of measurements in the  $g$  band, both before (top panel) and after (bottom panel) calibration. Here we can see that before calibration there is disagreement between overlapping sets of fields. Once the calibration procedure has been applied the disagreements at the field boundaries are largely solved. The two fields at the foot of the region plotted in Fig. 2.4 show that the definitive calibration may need to be conducted on the finer angular scale of the individual CCD ( $7.5 \times 15 \text{ arcmin}^2$ ) to better eliminate the effects of variable transmission due to thin cloud. The blotchy, colourful appearance of these two fields betrays calibration errors caused by localised cloud up to three times greater than the typical level of  $\sim 0.02$  magnitudes.

Fig. 2.5 shows density plots of the  $(u - g, g - r)$  and  $(r - i, g - r)$  CC diagrams for the entire region before (left) and after (right) calibration. We can see that the resulting diagrams have much tighter distributions with less scatter. The main-stellar locus (highest density region) is also placed in the correct position with respect to the synthetic tracks.



**Figure 2.4:** Spatial plot of objects in the 42 square degree region with two or more detections, colour coded by the standard deviation of the measured g band magnitudes. The left panel shows the objects before calibration and the right panel after calibration.



**Figure 2.5:** Colour-colour density plots showing the position of the main stellar locus with respect to the synthetic tracks before (left) and after (right) calibration.

## 2.4 Probabilistic SED fitting

We calculate the probability distribution of a range of model parameters corresponding to a set of empirical measurements, in a Bayesian scheme. This approach is chosen over a straight forward  $\chi^2$  minimisation scheme so that we may recover the full posterior probability distribution. This can reveal covariance between different parameters.

Given a set of empirical data,  $d = \{d_1, \dots, d_i\}$ , and a model, parametrised by a set of parameters,  $\theta = \{\theta_1, \dots, \theta_i\}$ , the *posterior* probability of the parameters can be calculated using Bayes' Theorem:

$$P(\theta | d) = \frac{P(d | \theta) \cdot P(\theta)}{P(d)} \quad (2.7)$$

In this expression,  $P(d | \theta)$ , the *likelihood* is the probability of the data being measured given a set of model parameters. The *posterior* and the *likelihood* are related by the *prior*,  $P(\theta)$ , which encodes any known constraints on the model parameters, including known physical bounds. Here  $P(d)$  can be treated as a normalising constant and ignored. Hence the *posterior* probability distribution can be found by the relation:

$$P(\theta | d) \propto P(d | \theta) \cdot P(\theta) \quad (2.8)$$

In this work, the empirical data are derived from the observed SED of each star and they consist of optical and near infrared apparent magnitudes:

$$SED_{obs} = \{u, g, r, i, J, H, K_S\}, \quad (2.9)$$

and their uncertainties:

$$\sigma(SED_{obs}) = \{\sigma_u, \sigma_g, \sigma_r, \sigma_i, \sigma_J, \sigma_H, \sigma_{K_S}\}. \quad (2.10)$$

Along with the random flux errors supplied by the surveys, we have included a systematic uncertainty to account for the independent absolute calibration errors in each band. The values adopted for the latter are 0.04 in the  $u$  band, 0.03 in  $g, r$  and  $i$ , 0.03

**Table 2.4:** Sample values of the intrinsic SEDs with approximate spectral type equivalents. Magnitudes are in the Vega system.

ST	$\log(T_{\text{eff}})$	$u$	$g$	$r$	$i$	$J$	$H$	$K_s$
O3V	4.65	-7.32	-5.78	-5.48	-5.33	-4.88	-4.73	-4.63
O9V	4.50	-5.28	-3.86	-3.60	-3.45	-3.03	-2.90	-2.80
B1V	4.40	-3.97	-2.70	-2.47	-2.34	-1.98	-1.85	-1.77
B3V	4.27	-2.31	-1.33	-1.16	-1.07	-0.80	-0.70	-0.65

in the  $J$  band and 0.02 in  $H$  and  $K_s$  (see [Drew et al., 2014](#); [Skrutskie et al., 2006](#)).

The model parameters that we are interested in estimating are:

$$\theta = \{\log(T_{\text{eff}}), A_0, R_V, \mu\} \quad (2.11)$$

where  $T_{\text{eff}}$  is the effective temperature,  $A_0$  is the monochromatic extinction at  $5495\text{\AA}$ ,  $R_V$  is the ratio of total to selective extinction and  $\mu$  is the distance modulus.

### Likelihood function

Defining the likelihood function requires us to define a forward model,  $SED_{\text{mod}}(\theta)$ , which predicts the apparent SED of OB stars based on the model parameters  $\theta$ . The intrinsic SEDs used in the model are taken from the Padova isochrone database (CMD v2.2<sup>1</sup>; [Bressan et al., 2012](#); [Bertelli et al., 1994](#)) and are supplied in the Vega system. Since the optical/NIR colours of OB stars do not vary significantly with luminosity class ([Martins et al., 2005](#)),  $\log(g)$  was fixed and only main-sequence models were used ( $\log(g) \sim 4.0$ ). Solar metallicity  $Z = 0.019$  has been adopted throughout, in view of the fact that the sight lines we explore do not sample a wide range of Galactic radii. Fixing these parameters provides a simple grid of absolute magnitude,  $M_\lambda$ , as a function of  $\log(T_{\text{eff}})$  in each of the seven bands.

To obtain a continuous grid, each  $M_\lambda - \log(T_{\text{eff}})$  relationship was fit with a 2<sup>nd</sup> order polynomial. It can be noted that a linear fit was also trialled but failed to characterize the distributions especially for the low-end values of  $\log(T_{\text{eff}})$ . [Table 2.4](#) provides sample SEDs.

<sup>1</sup><http://stev.oapd.inaf.it/cgi-bin/cmd>

The theoretical SEDs are then reddened using a [Fitzpatrick & Massa \(2007\)](#) reddening law, parametrised by  $A_0$  and  $R_V$ , and then shifted according to a distance modulus. As the SEDs in the Padova isochrones are supplied in magnitude form, a template spectrum of an O5V star from [Munari et al. \(2005\)](#) was used to calculate the extinction in each band as a function of  $A_0$  and  $R_V$ . The effect on the derived values of extinction in each band caused by the choice of template spectrum (B3V to O5V) was negligible to 3 significant figures. The shape of OnIR SEDs of O and early B stars are largely controlled by these reddening parameters because, in this wavelength range, their colours change very slowly as a function of effective temperature ([Martins et al., 2005](#)), as the Rayleigh-Jeans limit is approached. This means that  $\log(T_{\text{eff}})$  is only weakly constrained, albeit well enough to reach our goal of confirming OB status. As we have no handle on luminosity class, the distance modulus takes the role of a normalisation factor and will also be only weakly constrained. Fig. 2.6 demonstrates how the shape of the SED changes with the various parameters and visualises the points made above.

We can now use the forward model to construct a *likelihood* model  $P(SED_{obs} | \theta)$  that computes the probability of  $SED_{obs}$  given the set of physical parameters  $\theta$ . Assuming that the uncertainties on the measurements are normally distributed and uncorrelated, this can be described by a multi-variate Gaussian:

$$P(SED_{obs} | \theta) \propto \exp \left[ -\frac{1}{2} (SED_{obs} - SED_{mod})^T \Sigma^{-1} (SED_{obs} - SED_{mod}) \right] \quad (2.12)$$

where  $\Sigma$  is the covariance matrix containing the variance  $\sigma^2(SED_{obs})$  in the leading diagonal. In this case Equation 2.12 reduces to the familiar sum for  $\chi^2$ :

$$P(SED_{obs} | \theta) \propto \exp \left( -\frac{1}{2} \sum_i^n \frac{(m(obs)_i - m(mod)_i)^2}{\sigma_i^2} \right) \quad (2.13)$$

Where  $m(obs)_i$  and  $m(mod)_i$  are the observed and model magnitudes in the  $i^{th}$

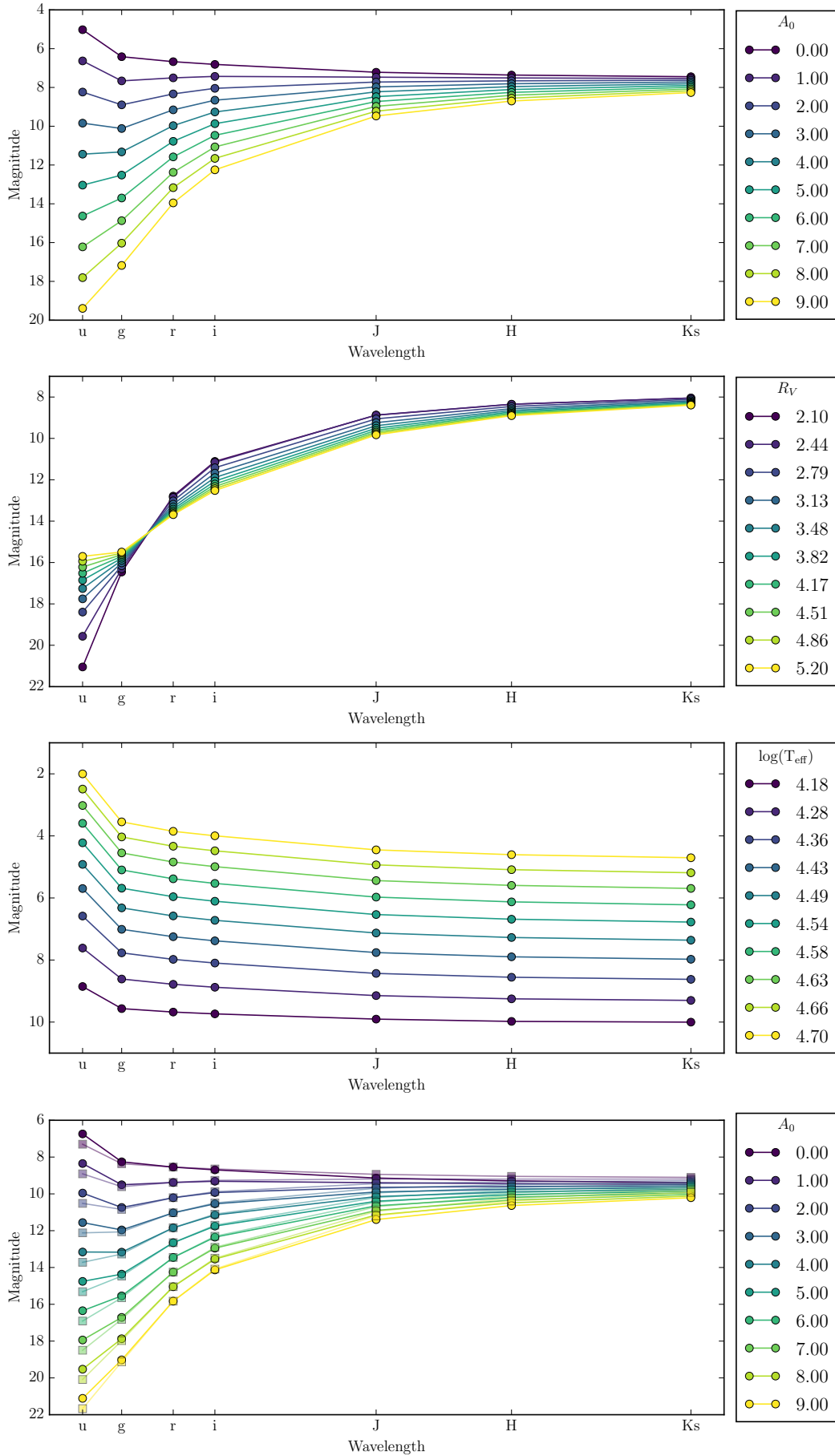


**Figure 2.6:** Examples of how the SED of an OB star changes with each parameter. **Top:** increasing  $A_0$ , **Second:** increasing  $R_V$ , **Third:** increasing  $T_{\text{eff}}$ , **Bottom:** Square markers indicate SED with  $T_{\text{eff}} = 40$  kK at  $\mu = 13.5$  while the circle markers are for a  $T_{\text{eff}} = 20$  kK SED at  $\mu = 10$ . Changes in effective temperature weakly effect the shape of the SED and are only noticeable in the  $u$  band. This makes it difficult to discern a distant O star from a nearby B star.

band.

## Priors

We adopt a uniform *prior* on each of the model parameters:

$$P(\theta) = \begin{cases} 1 & \text{if } \begin{cases} 4.2 \leq \log(T_{\text{eff}}) \leq 4.7 \\ 0 \leq A_0 \leq 15 \\ 2.1 \leq R_V \leq 5.1 \\ 0 \leq \mu \leq 20 \end{cases} \\ 0 & \text{else} \end{cases} \quad (2.14)$$

The upper bound on  $\log(T_{\text{eff}})$  is governed by the available models and the lower bound is somewhat less than the typical temperature of a B3V star (Zorec & Briot, 1991) in accordance with our selection in the  $(u - g, g - r)$  diagram. The constraints on  $R_V$  are the upper and lower limits measured in the Galaxy (Fitzpatrick & Massa, 2007). The upper limit on  $A_0$  is much larger than maximum extinction plausible for the detection of OB stars in VPHAS+ down to  $g = 20$ , assuming a typical rise in visual extinction of  $\sim 1$  magnitude per kpc. This makes the prior on  $A_0$  essentially unbound. The upper limit on the distance modulus  $\mu$  of 20 is well beyond the realms of the galaxy and so is also essentially unbound. Placing large but finite limits on  $A_0$  and  $\mu$  enables the MCMC algorithm to converge more quickly.

## Sampling the posterior distribution using MCMC

Characterising the *posterior* distribution by computing the probability at all values in the parameter space is computationally expensive. Instead one can sample the distribution using an MCMC algorithm.

In this study we use the Python package *emcee* developed by Foreman-Mackey et al. (2013). In brief, the software takes a set of parameters and supplies them to a group

of  $n$  *walkers*. The *walkers* then use a pseudo-random walk to sample the parameter space. At each sample the probability is calculated. By communicating their relative probabilities to one another the *walkers* are able to quickly find and sample the region of high probability without wasting computational time on the parameter combinations of very low probability. The software then returns what are known as *chains* which contain the values of the parameters at every step in the walk. The frequency at which each region in the parameter space is visited is proportional to its probability. The finer details on this technique can be found in [Foreman-Mackey et al. \(2013\)](#).

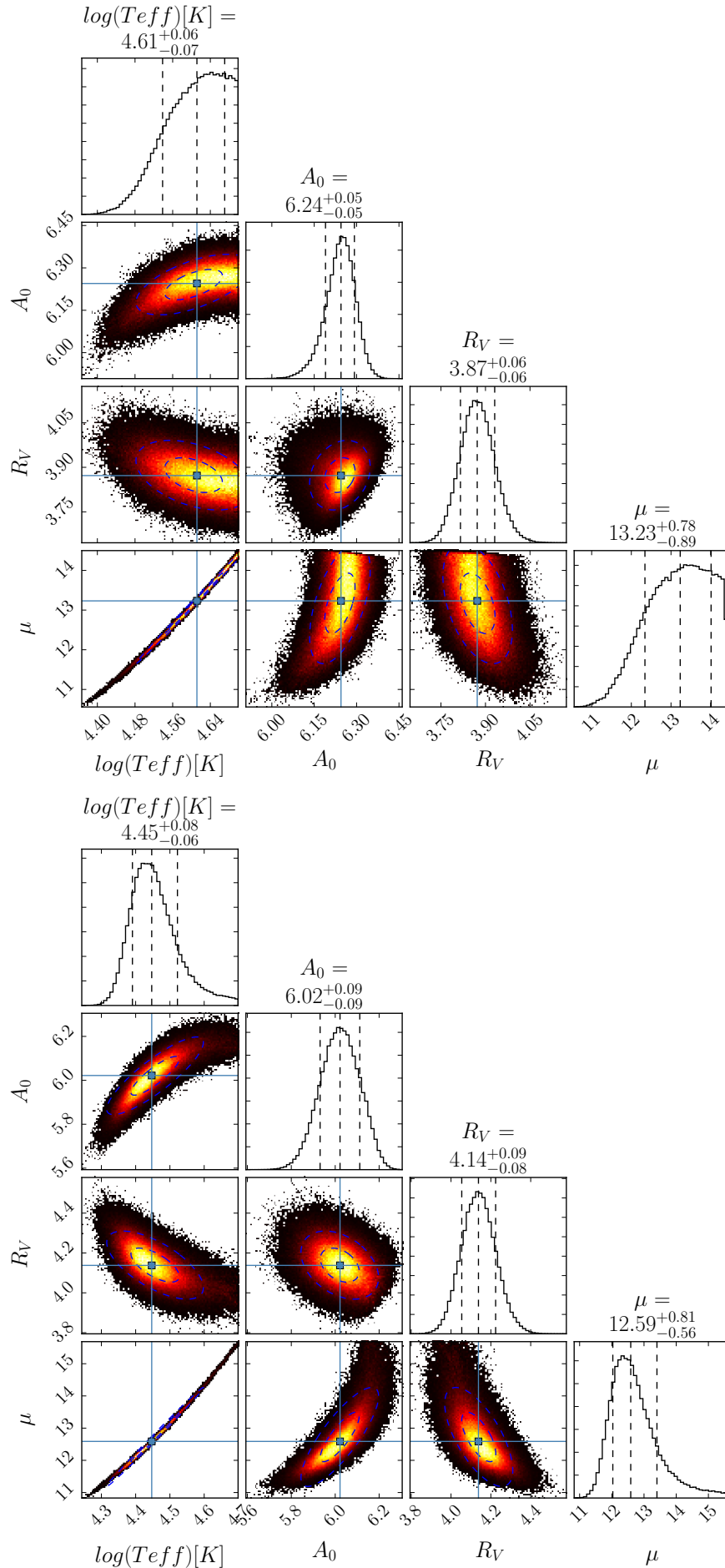
For each of the objects for which we have computed SED fits, the posterior distribution was sampled with 100 *walkers* over 10000 *iterations* with a 1000 iteration burn in. The typical autocorrelation time for each walk (or number of steps per independent sample) was found to be well below 100, which indicates that the posteriors are thoroughly sampled. We can determine the probability distributions for each parameter by marginalising over all other parameters. We visualize this by constructing 1-D histograms of the values of each parameter visited in the random walk. We can also check for covariance or degeneracy between parameters by constructing marginalised 2-D histograms for each pair of parameters. The value adopted for each parameter is the median of the marginalised posterior distribution with upper and lower uncertainties defined by the 16<sup>th</sup> and 84<sup>th</sup> percentiles. Figure 2.7 shows an example of these diagrams for a known O4V and a known B1V star in the sample (#913 and #549 using the numbering system from [Vargas Álvarez et al. \(2013\)](#) from Chapter 3).

The obvious difference between the two cases is apparent in the 1-D marginalisation of parameters. We see that the hotter the object the more skewed the probability distributions in  $\log(T_{\text{eff}})$  and  $\mu$  become. This can be attributed to the fact that the hotter SEDs are approaching the RJ tail. This makes it more difficult to differentiate the temperature of the hottest stars and consequently the luminosity and distance. This makes the drop off in probability at the hot end more shallow. This intrinsic feature also means that the uncertainties on  $\log(T_{\text{eff}})$  and  $\mu$  increase with temperature but has the positive effect of decreasing the uncertainties on  $A_0$  and  $R_V$ . For the later type stars  $\log(T_{\text{eff}})$  is better defined but still uncertain. It is plainly apparent in Figure

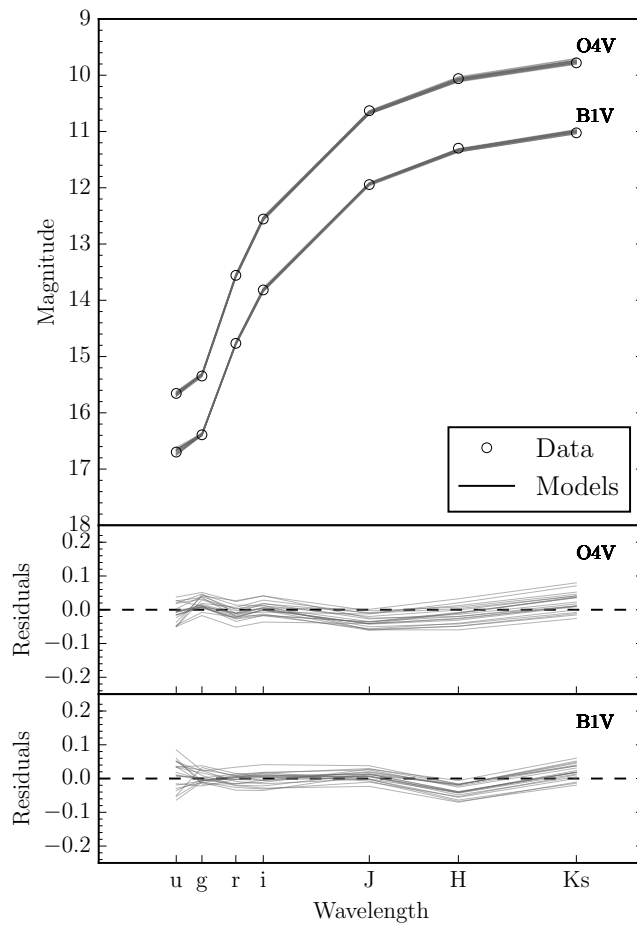
2.7 that  $\log(T_{\text{eff}})$  and  $\mu$  are strongly and positively covariant. The role of the distance modulus is essentially that of a normalisation parameter.

Figure 2.8 shows the results for the O4V star from Figure 2.7 translated into the original SED data space. The top panel shows the observed SED over-plotted by 30 randomly sampled model SEDs that are drawn from the posterior distributions shown in Figure 2.7. The lower panel shows the residuals between them. We can see that for each band, across all the posterior distributions, the differences between the models and the data never exceed  $\sim 0.1$  mag. The discrepancies between the model and data can be attributed to one or more of the following: inaccuracies in the intrinsic SEDs of OB stars in the Padova isochrones; inaccuracies in the shape of the reddening law; a calibration offset between the optical and NIR catalogues.

The posterior distributions obtained tell us the most probable parameters given the data, however they do not tell us anything about ‘goodness-of-fit’. As some objects in our selection may be contaminants or may just have bad photometry, it is important to determine how well the data fit the model in order to obtain a ‘clean’ selection of OB stars. We have opted to use the value of  $\chi^2$ , given by the SED fits, at the median values in the marginalised posterior distribution. We are aware that the posterior medians may not exactly trace the maximum likelihood, but they provide a representative sample. Since we are fitting 7 data points with 4 parameters we expect a  $k = 3$   $\chi^2$  distribution peaking at 1 – the top panel of Figure 3.6 indicates this is what happens and, by implication, that the uncertainties on our data points are not significantly over- or under- estimated. In keeping with this, we have chosen to use the commonly adopted 5% significance level, at  $\chi^2 = 7.82$  as the limit beyond which we judge the fits to the applied model to be unsatisfactory.



**Figure 2.7:** PDFs of the fitting parameters as a result of the MCMC simulation for stars #913 an O4V (top) and #549 and B1V (bottom) using the numbering system from Vargas Álvarez et al. (2013) (see. Section 3.3.1).



**Figure 2.8:** Visualisation of the posterior distributions of objects #913 and #549 (from Vargas Álvarez et al., 2013) in SED data space. The top panel shows 30 model SEDs for both objects (gray solid lines), generated from a random sampling of the posterior parameter distributions shown in Figure 2.7. Our photometric data is plotted on top (circles). The bottom panels show the residuals.

---

# CHAPTER 3: TEST CASE:

## WESTERLUND 2

---

### 3.1 Introduction

In this chapter, I present the results of a pilot study in which I establish and validate my methods. A 2 square-degree field capturing the Carina Arm around the young massive star cluster, Westerlund 2, was selected for this. The confirmed OB stars in this cluster are used to validate our identification method, based on selection from the  $(u - g, g - r)$  diagram for the region. The stellar parameters prove to be sufficient to confirm OB status while the reddening parameters are determined to a precision of  $\sigma(A_0) \sim 0.09$  and  $\sigma(R_V) \sim 0.08$ . Across the 2 square degrees there are 489 objects that fit well as new OB candidates, earlier than  $\sim B2$ . This total includes 74 probable massive O stars, 5 likely blue supergiants and 32 reddened subdwarfs.

The region considered, roughly centres on  $\ell = 284^\circ$ ,  $b = -0.7^\circ$ , in the part of the Plane containing the young massive cluster, Westerlund 2 (Wd 2), the larger associated HII region RCW 49, and the diffuse nebula NGC3199 (see Figure 3.1). The data are taken from two VPHAS+ fields numbered 1678 and 1679. Previous optical and near-infrared studies on the stellar content of Westerlund 2 have focused on the immediate environment of the cluster itself - a patch of sky 4 arcmin across - (Moffat et al., 1991; Ascenso et al., 2007a; Vargas Álvarez et al., 2013), while the x-ray study by Tsujimoto et al. (2007) focused on an area  $\sim 17$  arcmin across. Most recently, Hur et al. (2015) have revisited optical photometry of this cluster over a 17.9' x 9.3' footprint.

By tracing  $8\mu\text{m}$  warm-dust emission Rahman & Murray (2010) have identified this same region as part of a large star-forming complex (G283). The CO data presented by Dame (2007) show persuasively that Wd 2 and its environs fall just inside the sky position of the tangent point of the Carina Arm, but further away. This cluster is estimated to be 1 - 3Myr old (Vargas Álvarez et al., 2013; Ascenso et al., 2007a). It contains a large number of spectroscopically-confirmed OB stars, albeit behind a dust

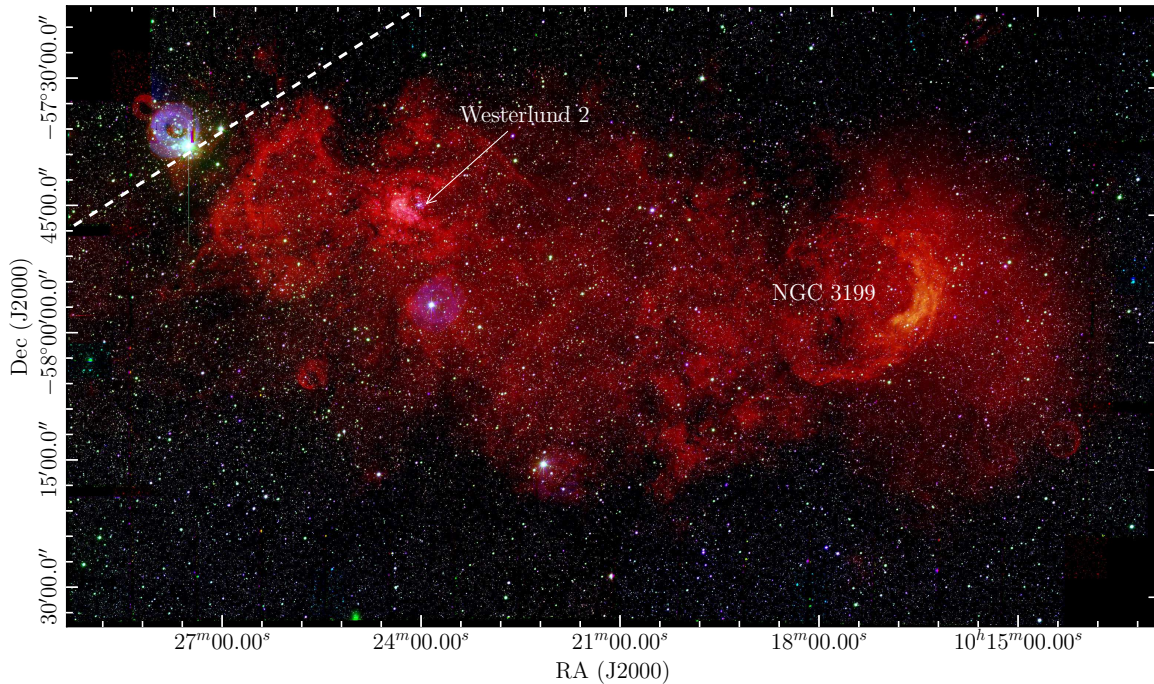


**Figure 3.1:** RGB image of the  $\sim 2$  square degree region ( $H\alpha$ ,  $g$ ,  $i$ ). This region falls within the star forming complex G283 identified by [Rahman & Murray \(2010\)](#) – an elliptical region slightly larger than the sky area shown. Westerlund 2 is embedded in the HII region RCW49, while the diffuse nebulae NGC3199 is located to the right (West) as marked. The dashed line traces the Galactic equator.

column giving rise to over 6 magnitudes of visual extinction ([Moffat et al., 1991](#); [Rauw et al., 2007](#); [Carraro et al., 2012](#); [Vargas Álvarez et al., 2013](#)). Estimates of the distance to Wd 2 in the literature have varied enormously, ranging from 2.8 kpc ([Ascenso et al., 2007a](#)) up to  $\sim 8$  kpc (e.g. [Rauw et al., 2011](#)). However, it is not our aim to enter into this debate. More important is the likelihood that much of the scientific gain from VPHAS+ discoveries of OB stars will be in the domain of visual extinctions of up to 8–10 magnitudes, and distance scales of 2–10 kpc (varying with Galactic longitude). In this regard, the field around Wd 2 is highly typical of the task ahead.

A recent study on Wd 2 by [Vargas Álvarez et al. \(2013\)](#) uses data from the Hubble Space Telescope (HST) that offers much better spatial resolution than is achievable from the ground. As such it is the only dataset that offers better angular resolution than the new VPHAS+ data analysed here. These authors’ values of  $R_V$  and  $A_V$  were derived by fitting, to 32 individual OB stars in or near Wd 2, reddened model optical/near-infrared SEDs appropriate for the selected stars’ spectroscopically-confirmed spectral types. The best fits were computed by seeking the global  $\chi^2$  min-

imum among all plausible values of  $R_V$  and  $A_V$  – resulting in a mean outcome of  $R_V = 3.77 \pm 0.09$  and  $A_V = 6.51 \pm 0.38$  mag combining results from different reddening law prescriptions. We use a comparison of our OnIR SED fit results for this same set of OB stars to bench-mark our method.

This chapter is organised as follows. In Section 3.2.1 more details on the selection of OB stars in this region are shown. Section 3.3 validates the method by comparing my results for Wd 2 stars with those of Vargas Álvarez et al. (2013). The results of the fits to the final list of 527 new OB candidates drawn from across the full 2 square degrees are presented in Section 3.4. This is followed by a discussion of the results in Section 3.5, in which we consider the extinction trends revealed in this region, and draw attention to the newly discovered O stars outside the confines of Wd 2. The outlook and our conclusions are summarised in Section 3.6.

## 3.2 Selection and fitting method

### 3.2.1 Photometric selection and cross matching

Figure 3.2 shows the selection of OB candidates (blue crosses) across the two fields as well as the known OB stars from Vargas Álvarez et al. (2013) that were successfully cross matched with VPHAS+ (shown as red triangles). Over-plotted are the reddening tracks of a B3V, a B1V and that of a pure RJ spectrum all taken from Drew et al. (2014). The tracks we use take into account the measured red leak associated with the  $u$ -band filter.

Previous results from Carraro et al. (2012) and Vargas Álvarez et al. (2013) suggest an  $R_V = 3.8$  reddening law is required towards Wd 2. The B1V and RJ reddening vectors have been drawn using this law. To avoid a bias towards this non-standard reddening law we have used the B3V  $R_V = 3.1$  reddening vector as our lower selection limit and have dropped its position by 0.1 mags in  $u - g$  in order to capture any early B stars that may have been missed. The lower the value of  $R_V$ , the steeper the reddening vector will be.

Each object was then cross matched to within  $1''$  of the best available near infrared detection in order to access  $J, H, K$  photometry. The mean angular cross-match distance was in fact much less than this, being only  $0.09''$ . As the stellar density in the central  $\sim 4'$  of Wd 2 is very high, the [Ascenso et al. \(2007a\)](#) NIR catalogue was the preferred partner on account of its superior angular resolution. Everywhere else 2MASS was used. This follows the approach taken by [Vargas Álvarez et al. \(2013\)](#).

### 3.3 Validation of Method

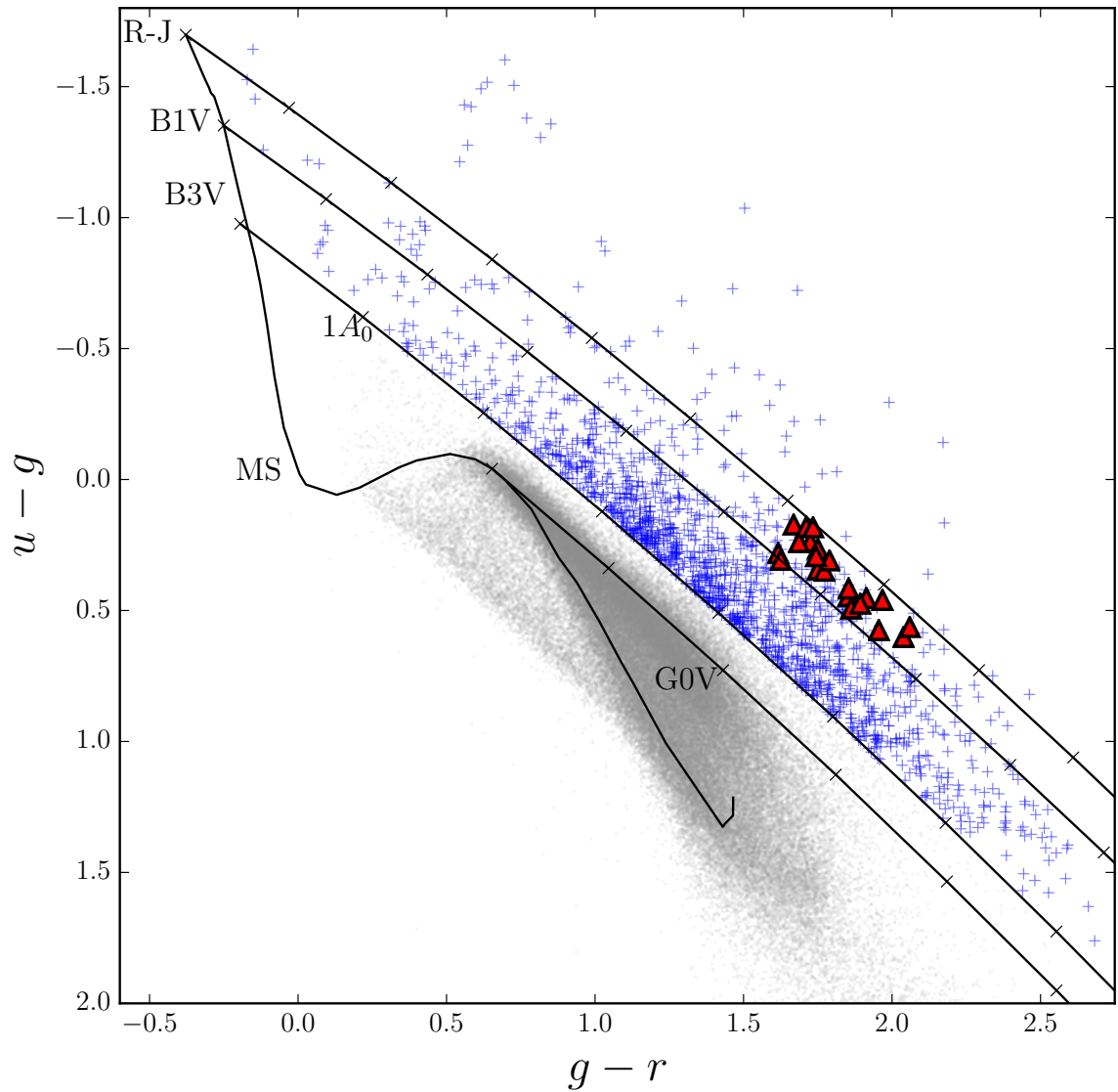
First it is appropriate to verify that our selection method recovers known objects. Second we verify that the fitting algorithm delivers the expected results.

#### 3.3.1 Photometric selection

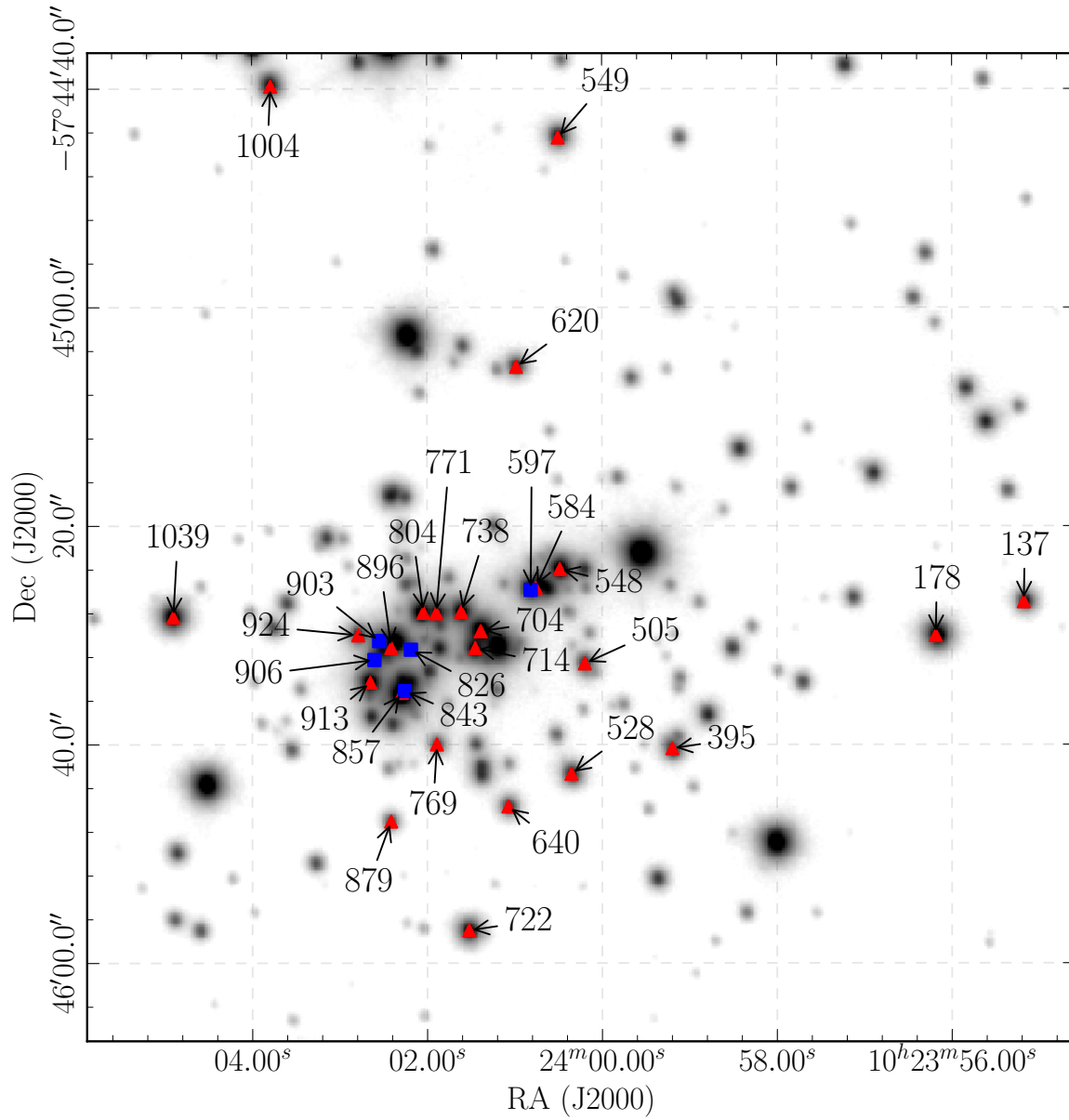
[Vargas Álvarez et al. \(2013\)](#) derived the extinction properties of 29 known OB stars in the central region of Wd 2, of which, 24 were successfully cross matched with VPHAS+ to within  $1''$ . Using the nomenclature from [Vargas Álvarez et al. \(2013\)](#), the five missing objects are #597, #826, #843, #903 and #906. They appear in some of the most crowded regions of the cluster: the angular resolution of VPHAS+ compared to that of HST is insufficient to separate them from brighter neighbours. Figure 3.3 shows the positions of the 24 cross-matched objects and the positions of those that are missing over plotted on the g-band image.

Figure 3.4 is the highly magnified section of Figure 3.2 that contains the objects with known spectral type. The red and blue shaded regions are where we expect to find late-type (O9 - O6) and early-type (O6 - RJ) O stars respectively. We find that the majority of the objects are correctly separated into their respective early or late spectral-type zones defined by the  $R_V = 3.8$  reddening tracks. This gives an early indication that an  $R_V \sim 3.8$  reddening law is required for this sight-line and that the calibration of the data is in good agreement with the synthetic photometry.

Object #771 falls well above the ‘RJ limit’. As a confirmed O8V star, its position in the  $(u - g, g - r)$  diagram is clearly anomalous. Close inspection of the image suggests



**Figure 3.2:** Selection of OB stars in and around Wd2. The lower reddening curve is that of a B3V, dropped by 0.1 in  $u-g$  in order to capture all early type B stars, and is characterised by an  $R_V = 3.1$  law. The other reddening curves are that of a B1V and an ideal Rayleigh-Jeans spectrum and are characterised by an  $R_V = 3.8$  law. Selected OB candidates are blue crosses while the known objects from Vargas Álvarez et al. (2013) are red triangles.



**Figure 3.3:** Inverse VPHAS+  $g$  band image of the central region of Wd 2 showing the objects with known spectral type from [Vargas Álvarez et al. \(2013\)](#). The red triangles are the positions of the objects detected on the ground (by VST) and the blue squares are the positions of those that are distinguished in crowded regions using HST.

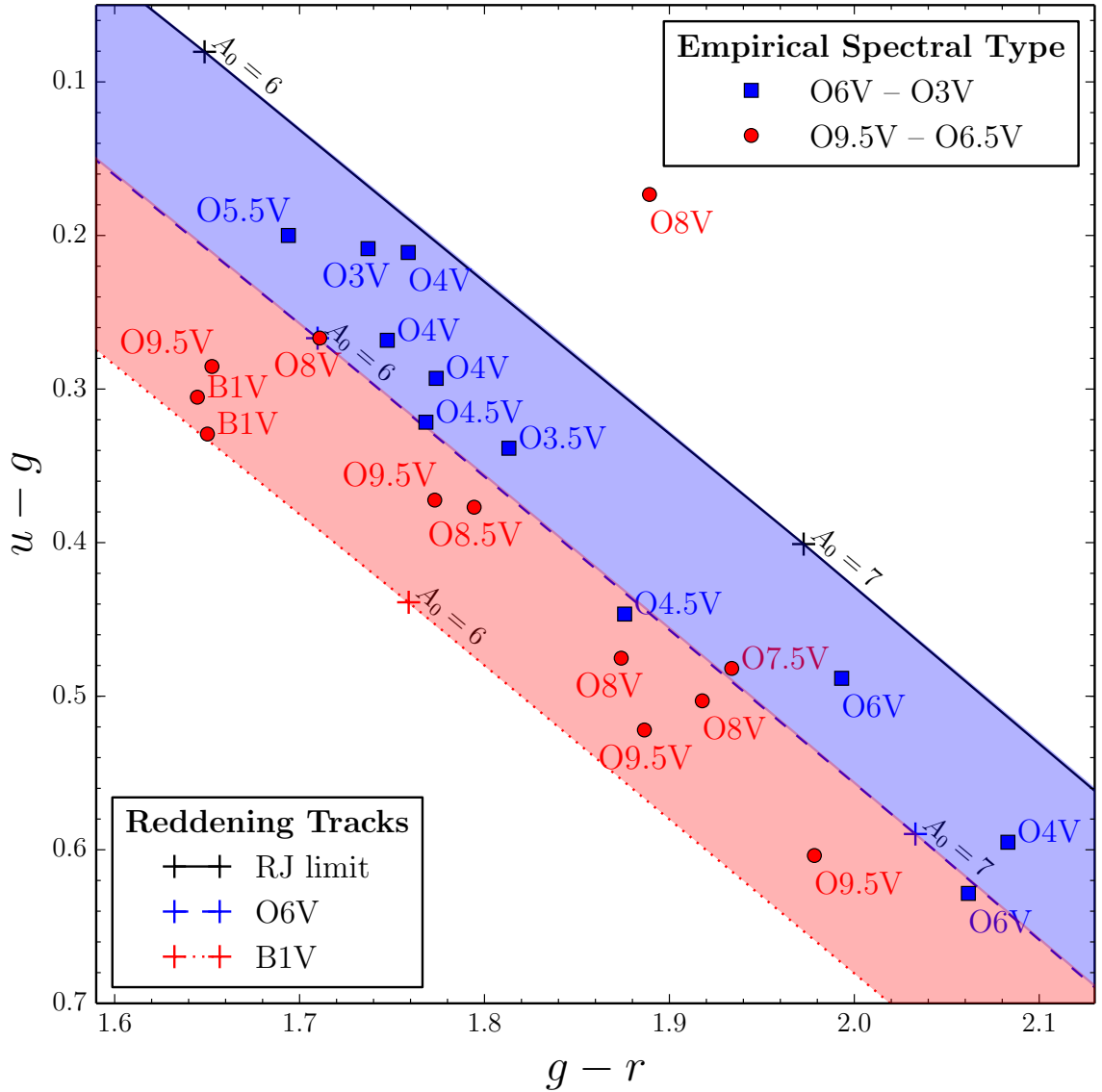


**Figure 3.4:** Testing the selection process of OB stars associated with Wd2. Objects with known spectral type tend to fall into the correct synthetic spectral type range with an  $R_V = 3.8$  reddening law. Objects shown are in the magnitude range ( $14 < g < 18$ ).

that the VPHAS+ photometry of this star is affected by a bright neighbour.

### 3.3.2 SED fitting

Ultimately 21 of the 24 known objects were suitable for SED fitting. These objects are listed in Table 3.1. Two of the objects left out are #896 and #771 for which there is no clear detection in one or more of the the optical bands due to blending. The third is object #1004 for which the near-infrared photometry is incomplete.

We find that we are able to determine the values of  $A_0$  and  $R_V$  with relatively

high precision (better than  $\pm 0.09$  mag and  $\pm 0.08$  respectively in all cases). These uncertainties are similar to those found by [Vargas Álvarez et al. \(2013\)](#). We note that  $R_V$  and  $A_0$  are well defined and show negligible covariance relative to each other and only modest covariance with respect to  $\log(T_{\text{eff}})$  and  $\mu$ .

However, as expected, our determination of temperature and distance are not so informative. For object #913 (see Fig. 2.7),  $\log(T_{\text{eff}}) = 4.61^{+0.06}_{-0.07}$  and  $\mu = 13.23^{+0.78}_{-0.89}$ . This corresponds to values of  $T_{\text{eff}} = 40.7^{+6.0}_{-6.1}$  kK, or a spectral type range from O8V to O2V. The results for  $\mu$  translate to  $d = 4.4^{+1.9}_{-1.5}$  kpc. This already significant distance uncertainty is nevertheless an underestimate given that neither the luminosity class or metallicity uncertainties have been formally incorporated. In addition we are treating all stars as if single which biases the inferred distance moduli to lower values by up to 0.75 mag. Because of the relative lack of constraint on  $\log(T_{\text{eff}})$  from the intrinsic colours of OB stars, the error in  $\log(T_{\text{eff}})$  is driven mainly by the error in  $\mu$ . In comparison the direct effect of binarity on  $\log(T_{\text{eff}})$ , through colour-changes, will be small.

**Table 3.1:** Table comparing the derived stellar parameters of objects with known spectral type from Vargas Álvarez et al. (2013) with the results in this study. The ID given corresponds to the numeration given by Vargas Álvarez et al. (2013). Most of the effective temperatures in the HST column were derived spectroscopically by Vargas Álvarez et al. (2013) and uncertainties were given. The rest have no provided uncertainty as they were estimated from their spectral types using the temperature scales from Martins et al. (2005) and Zorec & Briot (1991).

ID	ST	$A_V$		$R_V$		$\log(T_{\text{eff}})$		$\mu$		$V$	
		VPHAS+	HST	VPHAS+	HST	VPHAS+	HST	VPHAS+	HST	VPHAS+	HST
137	O4 V	$7.47^{+0.04}_{-0.04}$	$7.41 \pm 0.22$	$4.05^{+0.05}_{-0.05}$	$3.84 \pm 0.07$	$4.63^{+0.05}_{-0.06}$	$4.633 \pm 0.004$	$13.43^{+0.62}_{-0.79}$	$13.19 \pm 0.45$	$15.496 \pm +0.056$	$15.591 \pm 0.006$
178	O4 V-III((f))	$6.34^{+0.04}_{-0.04}$	$6.38 \pm 0.07$	$4.03^{+0.06}_{-0.06}$	$3.93 \pm 0.03$	$4.63^{+0.05}_{-0.07}$	$4.629 \pm 0.002$	$13.38^{+0.64}_{-0.82}$	$11.79 \pm 0.16$	$14.385 \pm +0.055$	$14.490 \pm 0.004$
395	O7.5V	$6.78^{+0.07}_{-0.08}$	$6.92 \pm 0.07$	$4.08^{+0.07}_{-0.07}$	$3.77 \pm 0.03$	$4.52^{+0.09}_{-0.07}$	$4.544 \pm 0.000$	$12.91^{+1.09}_{-0.76}$	$12.78 \pm 0.18$	$15.688 \pm +0.056$	$16.019 \pm 0.062$
505	O8.5V	$6.19^{+0.05}_{-0.06}$	$6.36 \pm 0.14$	$3.84^{+0.06}_{-0.06}$	$3.71 \pm 0.06$	$4.59^{+0.07}_{-0.08}$	$4.531 \pm 0.006$	$14.57^{+0.93}_{-0.95}$	$13.29 \pm 0.30$	$15.889 \pm +0.056$	$16.094 \pm 0.005$
528	O8 V	$6.72^{+0.06}_{-0.07}$	$6.97 \pm 0.14$	$4.02^{+0.07}_{-0.06}$	$3.99 \pm 0.05$	$4.56^{+0.09}_{-0.08}$	$4.544 \pm 0.005$	$13.34^{+1.10}_{-0.89}$	$12.55 \pm 0.30$	$15.571 \pm +0.056$	$15.841 \pm 0.005$
548	O4 V	$6.34^{+0.05}_{-0.05}$	$6.48 \pm 0.10$	$4.02^{+0.06}_{-0.06}$	$3.76 \pm 0.04$	$4.61^{+0.06}_{-0.07}$	$4.633 \pm 0.002$	$13.11^{+0.81}_{-0.90}$	$13.19 \pm 0.23$	$14.361 \pm +0.055$	$14.522 \pm 0.002$
549	B1 V	$6.02^{+0.09}_{-0.09}$	$6.09 \pm 0.08$	$4.14^{+0.09}_{-0.08}$	$4.01 \pm 0.04$	$4.45^{+0.08}_{-0.06}$	$4.398 \pm 0.000$	$12.59^{+0.81}_{-0.56}$	$11.68 \pm 0.19$	$15.485 \pm +0.056$	$15.562 \pm 0.005$
584	O8 V	$4.60^{+0.04}_{-0.04}$	$6.19 \pm 0.05$	$2.91^{+0.04}_{-0.04}$	$3.73 \pm 0.02$	$4.66^{+0.03}_{-0.05}$	$4.544 \pm 0.002$	$15.24^{+0.42}_{-0.64}$	$12.94 \pm 0.12$	$14.195 \pm +0.055$	$15.442 \pm 0.004$
620	B1 V	$5.77^{+0.09}_{-0.09}$	$5.77 \pm 0.08$	$4.00^{+0.08}_{-0.08}$	$3.82 \pm 0.04$	$4.46^{+0.08}_{-0.06}$	$4.398 \pm 0.000$	$13.46^{+0.86}_{-0.56}$	$12.56 \pm 0.19$	$16.007 \pm +0.057$	$16.086 \pm 0.006$
640	O9.5V	$6.32^{+0.05}_{-0.07}$	$6.37 \pm 0.05$	$3.97^{+0.07}_{-0.06}$	$3.73 \pm 0.02$	$4.57^{+0.08}_{-0.08}$	$4.505 \pm 0.002$	$14.30^{+1.07}_{-0.91}$	$13.11 \pm 0.13$	$16.065 \pm +0.057$	$16.234 \pm 0.006$
704	O4 V	$6.03^{+0.05}_{-0.05}$	$6.27 \pm 0.29$	$3.94^{+0.06}_{-0.06}$	$3.76 \pm 0.12$	$4.61^{+0.06}_{-0.07}$	$4.681 \pm 0.008$	$12.91^{+0.77}_{-0.85}$	$14.26 \pm 0.63$	$13.844 \pm +0.055$	$14.059 \pm 0.002$
714	O3 V	$5.61^{+0.04}_{-0.05}$	$6.08 \pm 0.11$	$3.67^{+0.06}_{-0.06}$	$3.73 \pm 0.05$	$4.62^{+0.05}_{-0.07}$	$4.643 \pm 0.000$	$14.29^{+0.69}_{-0.82}$	$14.53 \pm 0.26$	$14.642 \pm +0.055$	$15.017 \pm 0.003$
722	O6 V	$7.21^{+0.05}_{-0.06}$	$7.23 \pm 0.04$	$3.94^{+0.06}_{-0.05}$	$3.65 \pm 0.01$	$4.61^{+0.06}_{-0.08}$	$4.584 \pm 0.001$	$12.79^{+0.84}_{-0.94}$	$12.04 \pm 0.11$	$14.944 \pm +0.055$	$15.060 \pm 0.030$
738	O5.5V	$5.84^{+0.05}_{-0.05}$	$6.02 \pm 0.08$	$3.88^{+0.06}_{-0.06}$	$3.73 \pm 0.04$	$4.61^{+0.06}_{-0.07}$	$4.602 \pm 0.000$	$13.91^{+0.81}_{-0.90}$	$13.39 \pm 0.19$	$14.696 \pm +0.055$	$14.896 \pm 0.003$
769	O9.5V	$6.50^{+0.06}_{-0.09}$	$6.63 \pm 0.06$	$3.86^{+0.07}_{-0.06}$	$3.65 \pm 0.02$	$4.54^{+0.10}_{-0.08}$	$4.491 \pm 0.002$	$14.12^{+1.20}_{-0.89}$	$13.04 \pm 0.13$	$16.351 \pm +0.057$	$16.576 \pm 0.008$
804	O6 III	$7.11^{+0.11}_{-0.11}$	$6.91 \pm 0.04$	$4.11^{+0.09}_{-0.09}$	$3.71 \pm 0.01$	$4.60^{+0.07}_{-0.08}$	$4.582 \pm 0.001$	$12.14^{+0.89}_{-0.96}$	$11.78 \pm 0.10$	$14.290 \pm +0.055$	$14.433 \pm 0.003$
857	O4.5V	$6.50^{+0.08}_{-0.08}$	$6.13 \pm 0.08$	$4.17^{+0.09}_{-0.08}$	$3.63 \pm 0.03$	$4.56^{+0.09}_{-0.08}$	$4.623 \pm 0.002$	$11.30^{+1.08}_{-0.91}$	$12.65 \pm 0.18$	$13.335 \pm +0.055$	$13.869 \pm 0.003$
879	O9.5V	$6.77^{+0.06}_{-0.07}$	$6.98 \pm 0.07$	$3.82^{+0.06}_{-0.06}$	$3.70 \pm 0.03$	$4.57^{+0.08}_{-0.08}$	$4.519 \pm 0.003$	$14.37^{+1.05}_{-0.98}$	$13.11 \pm 0.16$	$16.510 \pm +0.058$	$16.645 \pm 0.056$
913	O3-4V	$6.23^{+0.05}_{-0.06}$	$6.42 \pm 0.11$	$3.87^{+0.06}_{-0.06}$	$3.66 \pm 0.04$	$4.61^{+0.06}_{-0.07}$	$4.642 \pm 0.002$	$13.23^{+0.78}_{-0.89}$	$13.45 \pm 0.24$	$14.344 \pm +0.055$	$14.531 \pm 0.002$
924	O8 V	$6.25^{+0.06}_{-0.07}$	$6.40 \pm 0.07$	$3.68^{+0.06}_{-0.06}$	$3.60 \pm 0.03$	$4.57^{+0.08}_{-0.08}$	$4.544 \pm 0.000$	$14.08^{+1.02}_{-0.91}$	$13.16 \pm 0.16$	$15.680 \pm +0.056$	$15.960 \pm 0.005$
1039	O4-5V	$6.43^{+0.05}_{-0.05}$	$6.42 \pm 0.10$	$3.80^{+0.06}_{-0.05}$	$3.47 \pm 0.04$	$4.62^{+0.05}_{-0.07}$	$4.622 \pm 0.002$	$13.26^{+0.70}_{-0.86}$	$12.98 \pm 0.22$	$14.429 \pm +0.055$	$14.523 \pm 0.030$

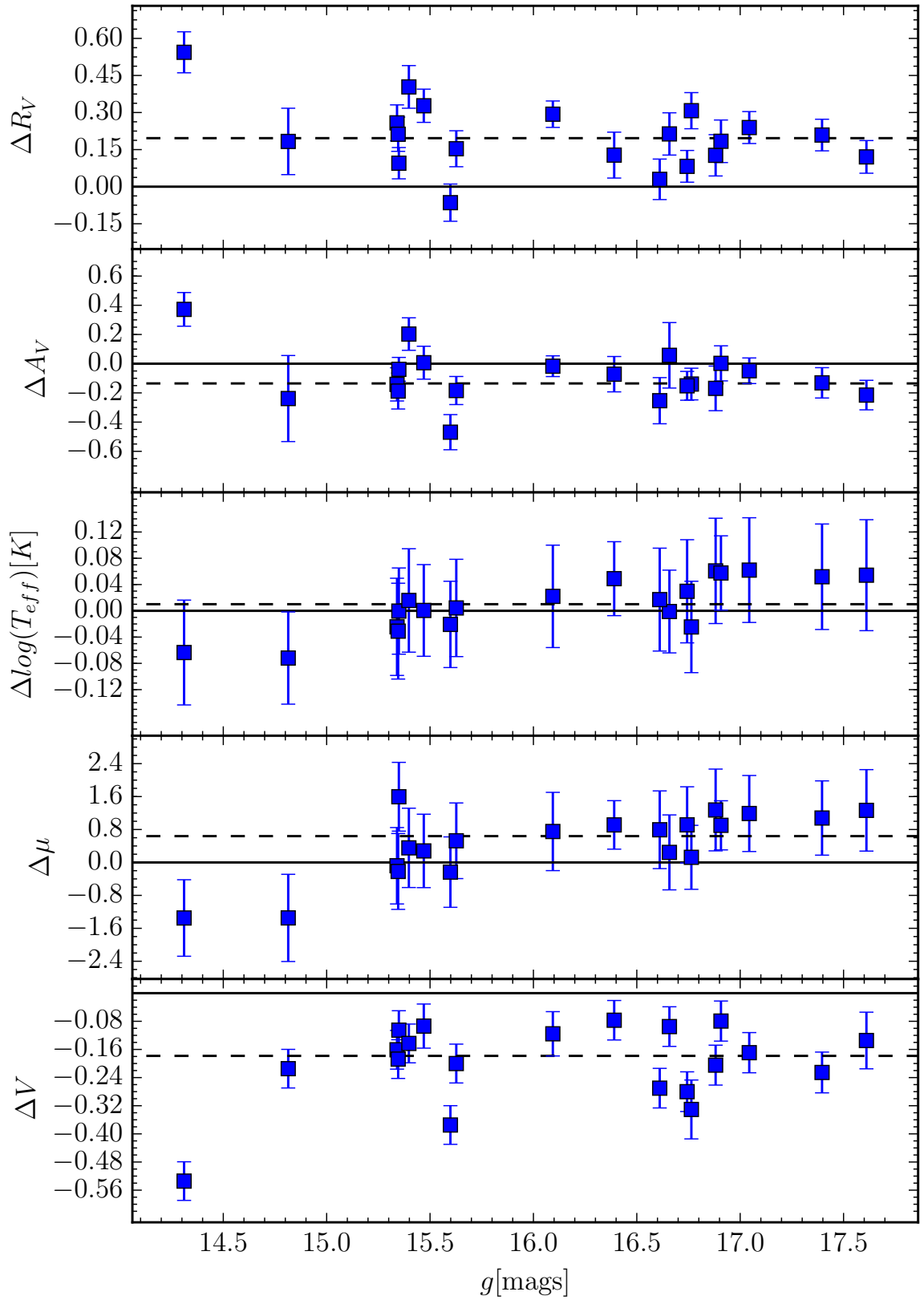
Table 3.1 compares the stellar parameters of the 21 known OB stars derived in this study with those from Vargas Álvarez et al. (2013). Here  $A_0$  has been converted to  $A_V$  and the VPHAS+  $g$  band magnitudes have been converted to  $V$  band using the Sloan to Johnson conversion from Lupton (2005)<sup>1</sup> for ease of comparison. We also note that our SED-derived  $\log(T_{\text{eff}})$  values are compared to spectroscopic values where available (Vargas Álvarez et al., 2013; Rauw et al., 2007). Otherwise effective temperatures are derived from spectral types according to the temperature scales of Martins et al. (2005) and Zorec & Briot (1991). We restrict our comparison to the results in Vargas Álvarez et al. (2013) based on the Fitzpatrick & Massa (2007) extinction curves.

Figure 3.5 plots the difference between the values derived in the two studies. It must be noted that star #584 has not been included in this analysis as extreme blending has substantially affected its photometry (see Figure 3.3 and Table 3.1).

A significant difference is found between the transformed  $V$  band magnitudes in VPHAS+ and HST of  $\sim 0.18$  mag, such that VPHAS+ is brighter. Vargas Álvarez et al. (2013) compare their empirical  $B$  and  $V$  band measurements with those of Moffat et al. (1991) and Rauw et al. (2007) and find that those ground based measurements are also systematically brighter, by 0.18 and 0.15 mag, and by 0.22 and 0.12 respectively. Vargas Álvarez et al. (2013) suggest that the difference may be due to source blending following on from the effects of atmospheric seeing. If this were the case we would expect to find objects in the most crowded/blended region of the cluster to be consistently more discrepant. As we do not see this effect we suspect a real calibration difference. Hur et al. (2015) have also uncovered a similar problem but find good agreement between their optical photometry and that of Rauw et al. (2007). If the scale of Rauw et al. (2007) is the right one, our photometry may be too bright by  $\sim 0.05$  mag. This difference may be traced back to APASS, the current external reference for calibration.

The apparent systematic calibration difference between the two data sets is reflected in the derived values of  $A_V$ . In particular the median of the star-by-star differences in  $A_V$  shows that our extinctions are on average 0.14 mag less than those derived by Vargas Álvarez et al. (2013). The median  $A_V$  with the 16<sup>th</sup> and 84<sup>th</sup> percentiles in

<sup>1</sup><https://www.sdss3.org/dr8/algorithms/sdssUBVRITransform.php>



**Figure 3.5:** The difference between stellar parameters found in this study and those found by Vargas Álvarez et al. (2013). The solid line shows zero difference while the dashed line shows the median difference. The individual numerical values are given in Table 3.1.

this study and in [Vargas Álvarez et al. \(2013\)](#) are;  $A_V(\text{VPHAS+}) = 6.34_{+0.44}^{-0.32}$  and  $A_V(\text{HST}) = 6.41_{+0.56}^{-0.32}$ . With brighter optical magnitudes there is also an offset in  $R_V$  such that our values are higher: the median star-by-star difference in  $R_V$  is 0.20, while sample medians are respectively  $R_V(\text{VPHAS+}) = 3.96_{+0.12}^{-0.14}$  and  $R_V(\text{HST}) = 3.73_{+0.11}^{-0.08}$ .

Despite the expectation of poor constraints on distance, the difference in the median values of  $\mu$  happens to be modest:  $\mu(\text{VPHAS+}) = 13.36_{+0.92}^{-0.57}$  and  $\mu(\text{HST}) = 13.07_{+0.31}^{-1.02}$ . This is likely to be due to the O stars in Wd 2 being on the main sequence, matching our assumption. Similarly there is only a modest offset on average in the measures of effective temperature.

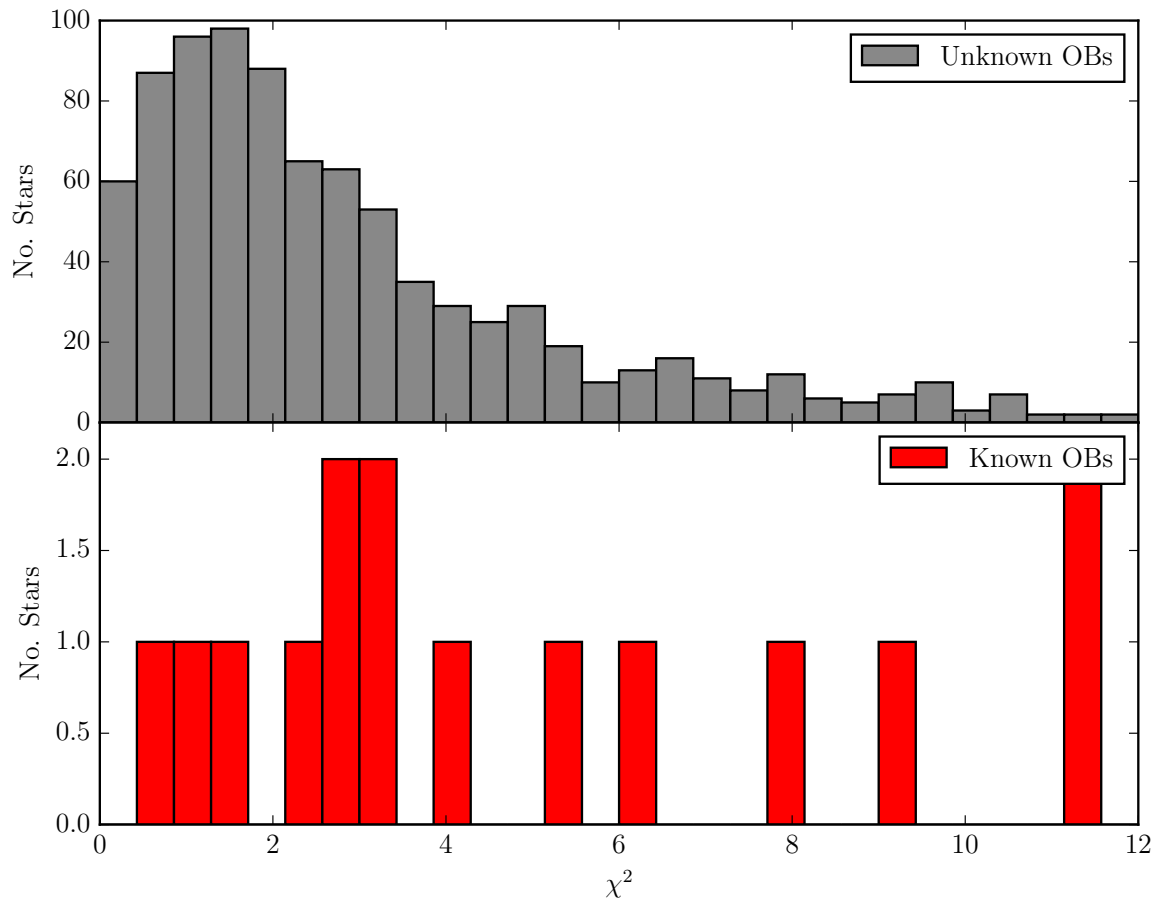
The results of this comparison are encouraging. We have found good quantitative agreement, within the uncertainties, between our derived parameters and those of [Vargas Álvarez et al. \(2013\)](#) drawing on HST optical photometry. Where there are differences, we understand their origin. This gives us confidence that both our method and the underlying VPHAS+ data are producing reliable results.

### 3.4 Results

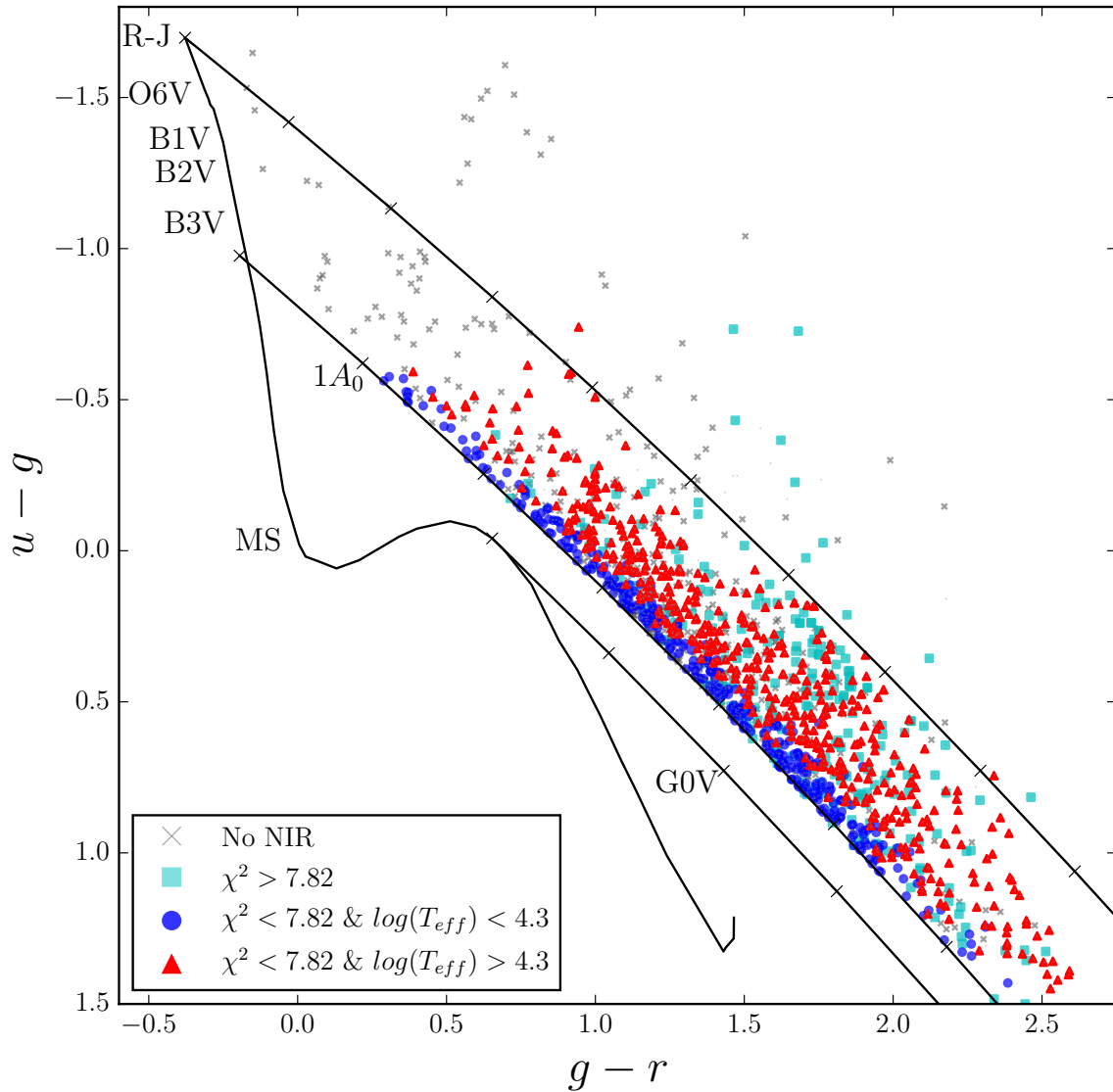
Here we apply the SED fitting methods discussed above to the full selection of OB candidates from our pilot  $\sim 2$  sq.deg field.

Figure 3.6 shows the  $\chi^2$  distribution of the fits to all 1050 objects in the wider selection above the distribution obtained for the known objects from [Vargas Álvarez et al. \(2013\)](#). A cut at  $\chi^2 = 7.82$  cut makes reasonable sense when applied to the  $\chi^2$  distribution for the known objects (in common with [Vargas Álvarez et al., 2013](#)), in that the 10 confirmed OB stars beyond the chosen cut are mainly there because of the impact on the photometry of the blending in the crowded central parts of Wd 2 present in the VST data. For this reason we have still tabulated those objects not meeting our selection criteria but have not used them in any further analysis. We note that if both 2MASS [Skrutskie et al. \(2006\)](#) and [Ascenso et al. \(2007a\)](#) photometry are available we keep which ever yields the better  $\chi^2$ .

Figure 3.7 shows the stages in the selection process: first, those stars without a



**Figure 3.6:**  $\chi^2$  distributions for the known objects (bottom) and the wider selection (top). The  $\chi^2$  distribution for the wider selection peaks at  $\sim 1$  as expected from a distribution with  $k = 3$  degrees of freedom. Using a 5% significance level we judge objects with  $\chi^2 > 7.82$  to be unsatisfactorily fit. The known objects with poor fits are subject to photometric blending in the cluster's core.



**Figure 3.7:**  $(u-g, g-r)$  diagram showing the stages of selection. Red triangles are the final selection used for further discussion. All of the objects clearly above the RJ reddening vector are returned as bad fits.

match to good quality NIR photometry have to be set aside (shown as grey crosses in the Figure); next, those with ‘poor’  $\chi^2$  values (the cyan-coloured squares); finally the good fits are divided in two groups based on their effective temperature. Those with a median posterior effective temperature exceeding 20000K, or equivalently  $\log(T_{eff}) \geq 4.3$ , are shown as red triangles while those that are assigned cooler fits are shown as blue squares. The hotter stars are our target group of spectral type B2 and earlier.

Counter-intuitively perhaps, it can be seen in Figure 3.7 that in the domain where  $g-r < 0.5$ , only 12 stars could be matched with good NIR photometry. This is

**Table 3.2:** Breakdown of the number of new OB candidates, previously identified OB candidates and objects with known spectral type according to effective temperature and fit quality.

All Objects: 1073		
$\log(T_{\text{eff}}) \geq 4.3$	$\chi^2 \leq 7.82$	$\chi^2 > 7.82$
Total	527	145
New Candidate OBs	489	98
Old Candidate OBs	19	28
Known O - B2 stars	19	10
Other	0	1 C star & 6 WR stars
$\log(T_{\text{eff}}) < 4.3$	$\chi^2 \leq 7.82$	$\chi^2 > 7.82$
Total	321	80
New Candidate OBs	320	78
Old Candidate OBs	0	2
Known O - B2 stars	1	0
All $\log(T_{\text{eff}})$	848	225

because lowly reddened UV-excess objects detected in VPHAS+ are commonly too faint for detection in 2MASS due to their blue SEDs – many of these are likely to be underluminous hot compact objects, given the  $g > 13$  criterion. Unsurprisingly the cyan coloured squares representing objects with poor fits are frequently to be found above the Rayleigh-Jeans limit – only 2 objects with accepted fits fall into this part of the diagram. It is reassuring that there is some offset between the  $R_V = 3.1$  B3V reddening vector, serving as lower bound to the selection region, and the spread of hotter objects: it suggests that few, if any, stars hotter than  $\log(T_{\text{eff}}) = 4.3$  have been missed (given our other constraints, such as the magnitude limits). It is worth noting that the selection of objects that occupied the 0.1 mag wide band directly below the B3V reddening vector in  $u - g$  provided just 1 star out of 374 with  $\log(T_{\text{eff}}) \geq 4.3$  and  $\chi^2 < 7.82$ .

The main groupings emerging from the fitting process of all 1073 objects are shown in table 3.2. All of the objects along with their photometry and derived parameters are tabulated in Tables 3.4 and 3.5. (excerpts, the full versions of the tables are in the electronic version of [Mohr-Smith et al. \(2015\)](#)).

### Further cross-matches with previously catalogued objects

All of the objects in the initial selection were cross-matched to  $< 1''$  with the SIMBAD (Wenger et al., 2000) database to check for examples of objects of known type beyond those in Vargas Álvarez et al. (2013).

Tsujimoto et al. (2007) conducted a  $17 \times 17$  arcmin high resolution X-ray imaging survey centred on Wd2 and the surrounding star forming region RCW 49. They identified 17 new X-ray emitting OB candidates in this larger region, enclosing that studied by Vargas Álvarez et al. (2013). On using a  $1''$  cross match radius we find 8 of these objects make it into our selection. Five of the missing objects are picked up by VPHAS+ but have  $g < 13$  and hence were too bright to be selected. Conversely, the remaining 4 objects are detected by VPHAS+ but are too faint ( $g > 20$ ) to be in our selection. It is likely that these objects are highly reddened ( $A_V \gtrsim 9$ ).

Across all other literature sources, accessed via SIMBAD, fourteen further stars of confirmed type were found (see Table 3.3). The breakdown of their classifications is as follows: six stars with a Wolf-Rayet (WR) component, three OV, two OIII, one OVb, one B5Vne, one carbon star and one star listed as M1III. All six WR stars, the carbon star and one of the OV stars could not be fitted convincingly as reddened OB stars (i.e.  $\chi^2 > 7.82$ ), while the others were in the accepted  $\chi^2 < 7.82$  range. The OVb star was confirmed as an O3V + O5.5V binary system by Vargas Álvarez et al. (2013) but was not used in their SED fitting analysis – hence it did not feature in Section 3.3.2. On close inspection of the literature, it became clear that the SIMBAD M1III attribution matching one of our selected objects is wrong, resulting from confusion over the sky position of the previously catalogued HAeBe candidate, THA 35-II-41. THA 35-II-41 is indeed one of our selected objects but it is not at the position attributed to it by Carmona et al. (2010) where these authors observed an M giant spectrum.

We also detect seven bright objects in the originally NIR-selected open cluster DBS2003 45 (Dutra et al., 2003) centred at  $10\text{h}19\text{m}10.5\text{s} -58^\circ 02' 22.6''$ . The study by Zhu et al. (2009) identifies seven OB stars in this cluster estimated as ranging from spectral type B0 to O7 from low resolution NIR spectroscopy. However, six out of seven

---

of the positions given in Table 2 of [Zhu et al. \(2009\)](#) do not match with the VPHAS+ positions nor with any detections in the 2MASS point source catalogue. We therefore suspect that there is an error in the positions that they give, whilst the objects are in common. We find these are among the most highly extinguished objects in our selection with an average  $A_V = 8.37$ .

**Table 3.3:** Objects crossed matched with SIMBAD in the selection which have known spectral type. Derived parameters of highly evolved objects will be inaccurate due to the main-sequence assumption as shown by their large  $\chi^2$  values. On further inspection of the literature the classification object #895 is much different from that in SIMBAD (see Section 3.4)

ID	RA	DEC	Identifier	Spectral Type	$g$	$\log(T_{eff})$	$R_V$	$A_0$	$\mu$	$\chi^2$
282	10 18 04.98	-58 16 26.27	WR 19	WC5+O9	14.02	$4.37^{+0.05}_{-0.04}$	$5.79^{+0.09}_{-0.09}$	$4.14^{+0.09}_{-0.08}$	$9.60^{+0.48}_{-0.38}$	39.60
335	10 18 53.39	-58 07 52.94	WR 19a	WN	15.45	$4.54^{+0.10}_{-0.08}$	$8.59^{+0.06}_{-0.09}$	$4.32^{+0.07}_{-0.06}$	$9.87^{+1.19}_{-0.89}$	10.21
437	10 20 17.50	-57 44 59.39	C* 1665	C*	16.54	$4.66^{+0.02}_{-0.03}$	$12.30^{+0.04}_{-0.04}$	$4.54^{+0.03}_{-0.03}$	$8.05^{+0.32}_{-0.39}$	436.47
560	10 22 05.75	-57 53 46.03	2MASS J10220574-5753460	B5Vne	15.71	$4.42^{+0.07}_{-0.05}$	$5.64^{+0.09}_{-0.09}$	$3.80^{+0.07}_{-0.07}$	$11.98^{+0.68}_{-0.49}$	1.53
644	10 23 23.50	-58 00 20.80	SS 215	O2If*/WN5	13.48	$4.41^{+0.06}_{-0.05}$	$5.67^{+0.09}_{-0.09}$	$4.27^{+0.10}_{-0.09}$	$9.60^{+0.57}_{-0.44}$	16.06
687	10 23 58.01	-57 45 48.93	V* V712 Car	O3If*/WN6+O3If*/WN6	14.48	$4.48^{+0.08}_{-0.06}$	$7.50^{+0.08}_{-0.09}$	$4.27^{+0.07}_{-0.07}$	$9.39^{+0.91}_{-0.63}$	10.47
717	10 24 01.20	-57 45 31.03	Cl* Westerlund 2 MSP 188	O3V+O5.5V	14.34	$4.53^{+0.10}_{-0.08}$	$6.79^{+0.09}_{-0.09}$	$4.41^{+0.10}_{-0.09}$	$10.70^{+1.19}_{-0.88}$	5.69
743	10 24 02.44	-57 44 36.05	Cl Westerlund 2 5	O5/5.5V/III(f)	13.80	$4.54^{+0.09}_{-0.07}$	$5.95^{+0.06}_{-0.08}$	$4.24^{+0.09}_{-0.08}$	$11.18^{+1.08}_{-0.81}$	10.56
770	10 24 06.64	-57 47 15.88	Cl* Westerlund 2 NRM 3	O9.5V	17.61	$4.58^{+0.08}_{-0.08}$	$7.75^{+0.05}_{-0.07}$	$4.14^{+0.06}_{-0.05}$	$13.44^{+1.03}_{-0.98}$	2.07
789	10 24 16.25	-57 43 43.75	Cl* Westerlund 2 NRM 2	O8.5III	15.94	$4.62^{+0.05}_{-0.07}$	$7.38^{+0.04}_{-0.05}$	$4.02^{+0.05}_{-0.05}$	$12.73^{+0.68}_{-0.87}$	2.47
793	10 24 18.40	-57 48 29.77	WR 20b	WN6ha	14.61	$4.38^{+0.06}_{-0.05}$	$7.97^{+0.09}_{-0.10}$	$4.60^{+0.08}_{-0.07}$	$7.94^{+0.55}_{-0.43}$	22.34
797	10 24 21.29	-57 47 27.53	Cl* Westerlund 2 NRM 1	O6V	15.70	$4.64^{+0.04}_{-0.06}$	$7.04^{+0.04}_{-0.04}$	$4.14^{+0.06}_{-0.05}$	$13.12^{+0.55}_{-0.76}$	3.59
822	10 24 39.20	-57 45 21.20	2MASS J10243919-5745211	O5V	16.03	$4.61^{+0.06}_{-0.08}$	$7.03^{+0.04}_{-0.05}$	$4.00^{+0.06}_{-0.05}$	$13.10^{+0.77}_{-0.93}$	1.68
895	10 25 47.07	-58 21 27.66	THA 35-II-41	HAeBe	13.55	$4.56^{+0.09}_{-0.08}$	$4.14^{+0.05}_{-0.07}$	$4.78^{+0.15}_{-0.13}$	$13.31^{+1.08}_{-0.87}$	4.89
907	10 25 56.51	-57 48 43.54	WR 21a	WN+	13.62	$4.37^{+0.05}_{-0.04}$	$6.34^{+0.09}_{-0.09}$	$4.45^{+0.09}_{-0.09}$	$8.59^{+0.49}_{-0.39}$	42.02

**Table 3.4:** Sample table containing the positions and photometry of all 1073 objects. The first five columns are the objects IDs given in this study, VPHAS ID, Moffat et al. (1991), MSP ID, Vargas Álvarez et al. (2013), VA ID, Tsujimoto et al. (2007), TFT ID, and in SIMBAD, SIMBAD ID, where applicable. The full table can be found in the electronic version of Mohr-Smith et al. (2015).

ID	MSP ID	VA ID	TFT ID	SIMBAD ID	ST	RA (J2000)	DEC (J2000)	u	err u	g	err g	r	err r	i	err i	Ha	err Ha	J	err J	H	err H	K	err K
1	-	-	-	-	-	10 13 09.25	-58 01 58.10	15.061	0.002	15.008	0.001	13.643	0.001	12.861	13.044	0.001	0.001	11.696	0.021	11.255	0.022	10.837	0.021
52	-	-	-	-	-	10 14 40.36	-57 24 26.24	16.937	0.006	15.487	0.001	12.959	0.001	11.468	12.345	0.001	0.001	8.693	0.024	7.870	0.036	7.414	0.027
89	-	-	-	-	-	10 15 24.77	-57 44 09.28	20.081	0.101	19.776	0.025	18.265	0.016	17.376	17.914	0.022	0.019	15.900	0.089	15.331	0.094	14.970	0.121
162	-	-	-	-	-	10 16 31.33	-57 48 18.68	19.199	0.034	18.923	0.010	17.323	0.006	16.565	17.392	0.017	0.007	15.246	0.054	14.763	0.079	14.509	0.096
164	-	-	-	-	-	10 16 31.97	-57 56 02.37	19.675	0.050	19.702	0.026	17.937	0.014	17.316	16.223	0.008	0.019	15.476	0.064	14.878	0.062	14.549	0.090
175	-	-	-	-	-	10 16 42.53	-57 32 47.65	17.559	0.009	16.168	0.002	13.576	0.001	12.078	13.053	0.001	0.001	9.327	0.026	8.474	0.049	7.953	0.027
413	-	-	-	-	-	10 19 47.82	-57 50 38.64	17.677	0.014	17.057	0.004	15.127	0.002	13.894	14.697	0.003	0.001	11.830	0.026	11.179	0.027	10.872	0.027
496	-	-	-	-	-	10 21 20.56	-57 43 09.40	15.521	0.003	15.231	0.001	13.666	0.001	12.692	13.284	0.001	0.001	11.014	0.023	10.524	0.023	10.292	0.021
578	-	-	-	-	-	10 22 19.90	-57 46 11.21	17.855	0.011	16.506	0.002	14.037	0.001	12.592	13.513	0.001	0.001	9.870	0.024	9.100	0.024	8.600	0.021
601	-	-	-	-	-	10 22 35.02	-58 33 37.82	16.554	0.005	16.692	0.002	15.716	0.002	15.153	15.471	0.004	0.002	14.220	0.056	13.883	0.066	13.810	0.064
677	182	178	112	Cl* Westerlund 2 MSP 182	O4V-III((f))	10 23 56.18	-57 45 30.00	15.587	0.004	15.349	0.002	13.624	0.001	12.613	13.211	0.001	0.001	10.520	0.015	10.050	0.008	9.750	0.020
712	157	584	-	2MASS J10240073-5745253	O8V	10 24 00.76	-57 45 25.65	15.376	0.004	15.137	0.002	13.450	0.001	12.437	13.044	0.001	0.001	11.660	0.038	11.150	0.027	10.790	0.031
724	263	722	202	Cl* Westerlund 2 MSP 263	O6V	10 24 01.52	-57 45 57.00	16.696	0.008	16.094	0.003	14.055	0.001	12.859	13.633	0.002	0.001	10.520	0.025	9.910	0.035	9.530	0.036
732	167	804	217	Cl* Westerlund 2 MSP 167	O8V	10 24 02.04	-57 45 27.94	15.858	0.005	15.398	0.002	13.430	0.001	12.306	13.007	0.001	0.001	9.960	0.122	9.357	0.158	8.982	0.095
737	203/444	857	224	Cl* Westerlund 2 NRM 4	O4.5V	10 24 02.29	-57 45 35.26	14.604	0.003	14.310	0.001	12.566	0.001	11.560	12.170	0.001	0.001	9.450	0.063	8.950	0.090	8.520	0.050
763	171	1039	298	Cl* Westerlund 2 MSP 171	O4-5V	10 24 04.90	-57 45 28.35	15.886	0.005	15.470	0.002	13.616	0.001	12.552	13.206	0.001	0.001	10.480	0.018	10.000	0.039	9.740	0.033
770	383	-	314	Cl* Westerlund 2 NRM 3	O9.5V	10 24 06.64	-57 47 15.88	18.263	0.023	17.608	0.006	15.502	0.003	14.248	14.952	0.003	0.002	11.736	0.028	11.008	0.025	10.536	0.023
789	-	-	388	Cl* Westerlund 2 NRM 2	O8.5III	10 24 16.25	-57 43 43.75	16.495	0.007	15.936	0.003	13.883	0.001	12.664	13.432	0.001	0.001	10.316	0.023	9.624	0.023	9.236	0.021
797	-	-	405	Cl* Westerlund 2 NRM 1	O6V	10 24 21.29	-57 47 27.53	16.048	0.006	15.703	0.002	13.796	0.001	12.636	13.367	0.001	0.001	10.435	0.024	9.745	0.022	9.386	0.019
822	-	-	447	2MASS J10243919-5745211	O5V	10 24 39.20	-57 45 21.20	16.519	0.007	16.033	0.003	14.084	0.001	12.919	13.644	0.002	0.001	10.709	0.026	10.060	0.027	9.679	0.023

**Table 3.5:** Sample table containing the derived parameters of all 1073 objects. The 16<sup>th</sup>, 50<sup>th</sup> and 84<sup>th</sup> percentiles are given for each parameter as well as the  $\chi^2$  value at the 50<sup>th</sup> percentile. The notes column indicates if the object shows emission (EM), is a sub-luminous candidate (SUB), is a blue supergiant candidate (BSG) or is a new O star candidate near Wd 2 (WD2) with similar reddening. The full table can be found in the electronic version of Mohr-Smith et al. (2015).

ID	$\log(T_{\text{eff}})$ P16 <sup>th</sup>	$\log(T_{\text{eff}})$ P50 <sup>th</sup>	$\log(T_{\text{eff}})$ P84 <sup>th</sup>	A0 P16 <sup>th</sup>	A0 P50 <sup>th</sup>	A0 P84 <sup>th</sup>	RV P16 <sup>th</sup>	RV P50 <sup>th</sup>	RV P84 <sup>th</sup>	DM P16 <sup>th</sup>	DM P50 <sup>th</sup>	DM P84 <sup>th</sup>	$\chi^2$	Notes
1	4.39	4.44	4.39	4.54	4.62	4.54	3.65	3.73	3.65	12.14	12.65	12.14	37.82	EM
52	4.31	4.36	4.31	8.29	8.38	8.29	3.72	3.77	3.72	7.54	7.93	7.54	2.28	BSG
89	4.33	4.43	4.33	5.09	5.26	5.09	3.67	3.79	3.67	15.69	16.57	15.69	1.97	SUB
162	4.40	4.47	4.40	4.69	4.80	4.69	3.27	3.35	3.27	15.89	16.58	15.89	5.05	SUB
164	4.46	4.54	4.46	5.64	5.73	5.64	4.03	4.13	4.03	16.39	17.23	16.39	39.93	EM
175	4.37	4.43	4.37	8.48	8.59	8.48	3.72	3.77	3.72	8.59	9.15	8.59	1.04	BSG
413	4.52	4.61	4.52	6.77	6.83	6.77	3.72	3.77	3.72	13.19	14.23	13.19	6.66	WD2
496	4.46	4.54	4.46	5.53	5.62	5.53	3.69	3.75	3.69	12.08	12.99	12.08	4.61	-
578	4.32	4.37	4.32	8.12	8.22	8.12	3.75	3.80	3.75	8.83	9.23	8.83	2.32	BSG
601	4.32	4.36	4.32	3.35	3.45	3.35	3.57	3.69	3.57	14.46	14.83	14.46	0.97	SUB
677	4.56	4.63	4.56	6.31	6.35	6.31	3.97	4.03	3.97	12.56	13.38	12.56	24.78	-
712	4.61	4.66	4.61	4.56	4.60	4.56	2.86	2.91	2.86	14.60	15.24	14.60	72.87	-
724	4.53	4.61	4.53	7.19	7.25	7.19	3.89	3.94	3.89	11.84	12.79	11.84	7.64	-
732	4.52	4.60	4.52	7.03	7.14	7.03	4.03	4.11	4.03	11.18	12.14	11.18	1.89	-
737	4.48	4.56	4.48	6.43	6.51	6.43	4.10	4.17	4.10	10.39	11.30	10.39	2.52	-
763	4.55	4.62	4.55	6.39	6.44	6.39	3.74	3.80	3.74	12.40	13.26	12.40	18.43	-
770	4.50	4.58	4.50	7.68	7.75	7.68	4.09	4.14	4.09	12.46	13.44	12.46	2.07	-
789	4.55	4.62	4.55	7.33	7.38	7.33	3.98	4.02	3.98	11.85	12.73	11.85	2.47	-
797	4.58	4.64	4.58	7.00	7.04	7.00	4.09	4.14	4.09	12.36	13.12	12.36	3.59	-
822	4.54	4.61	4.54	6.98	7.03	6.98	3.95	4.00	3.95	12.16	13.10	12.16	1.68	-

## Contaminants

Unacceptable fits with  $\chi^2 > 7.82$  have a range of causes. The most frequent are likely to be contact binaries or the products of poor photometry.

Contact binaries may find their way into the selection because they are both quite common and rapidly variable. Figure 3.8 shows how around half of the  $\chi^2 \geq 7.82$  objects clearly separate in the  $(r - i, g - r)$  colour-colour diagram away from the OB stars towards redder  $g - r$  from the perspective of fixed  $r - i$ . This is plausibly the signature of contact binary (W UMa) interlopers. W UMa systems are doubly eclipsing binaries in which the brightness in any one band scarcely remains constant over time. These objects have typical orbital periods of 8 hours with two pronounced minima per cycle (Rucinski, 1992). The u/g/r VST exposures are taken sequentially with about 15 minutes elapsing between u and g, and g and r. If the g band exposure of a W UMa system is taken at or near minimum light, its measured  $u - g$  colour is bluer than true, while  $g - r$  is redder, potentially pushing the star up into our OB selection. However these objects fail to pass as OB stars when the whole OnIR SED fit is performed, hence their poor  $\chi^2$  values. It has been estimated that there is around 1 W UMa system for every  $\sim 130$  main sequence stars (Rucinski, 1992). So finding perhaps as many as  $\sim 100$  in our OB selection, given  $\sim 100000$  stars across the 2 square degrees with u/g/r photometry, is reasonable.

The second common origin for the poor fits is likely due to photometry affected by blending or incorrect cross-matching between bands. In the crowded core of Wd 2 this is an obvious difficulty (see Figs. 3.3 and 3.6).

The literature search already reported in section 3.4 revealed that high  $\chi^2$  may be linked to extreme objects like WR stars (6 examples) and carbon stars (1 only). Another rare contaminant may be white dwarf/M dwarf binaries that can present blue  $u - g$ , alongside red  $r - i$ . In such systems, the blue white-dwarf light begins to be overwhelmed by the red dwarf's light with increasing wavelength, shifting the combined colours below and to the right of the OB reddening track in the  $(g - r, r - i)$  diagram (fig 3.8). These are known to co-locate with reddened OB stars in the  $(u - g, g - r)$

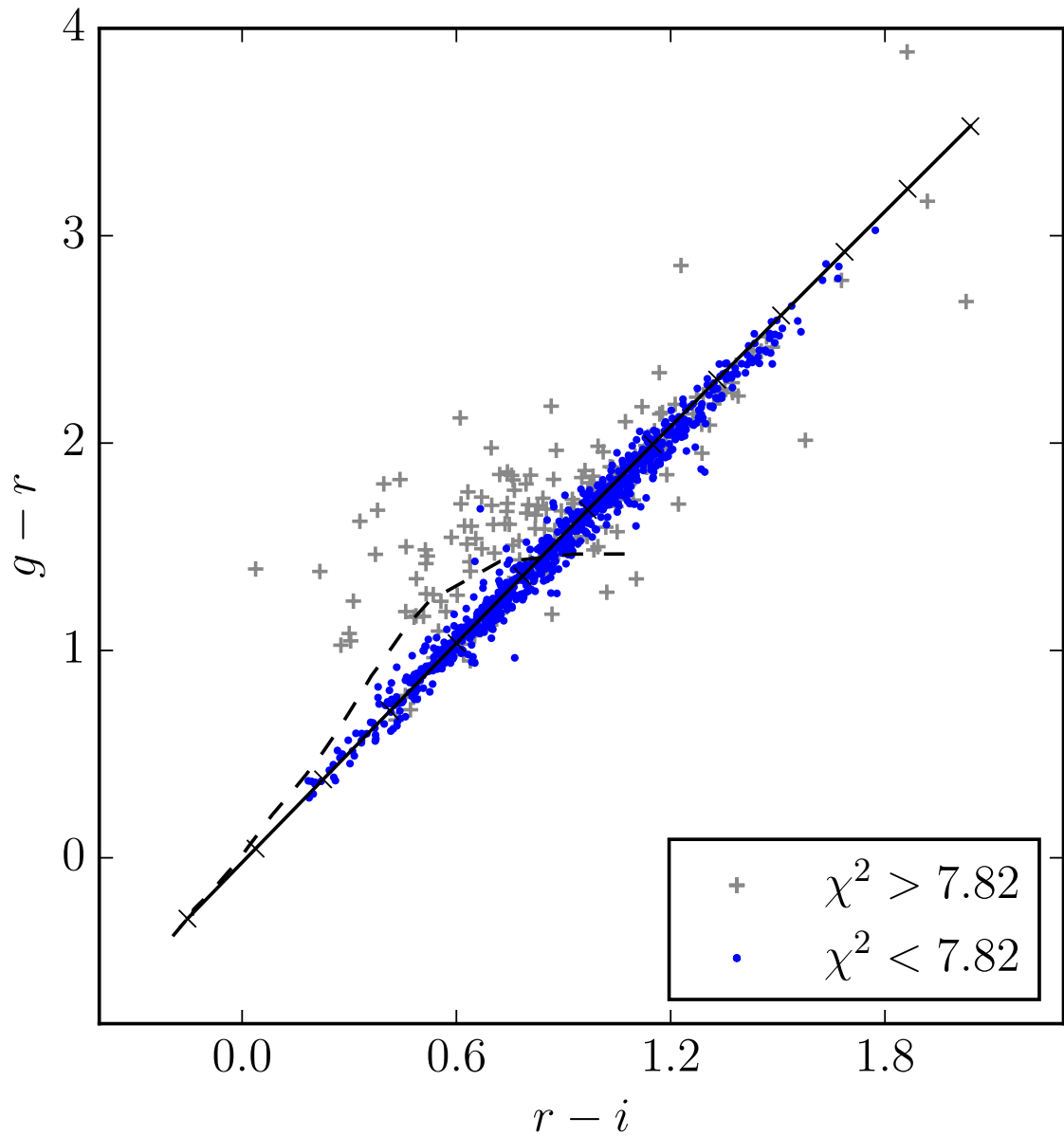


**Figure 3.8:** Positions of objects with  $\chi^2 \leq 7.82$  (blue dots) and  $\chi^2 > 7.82$  (grey crosses) in the  $(r-i, g-r)$  plane. The solid black line is the reddening vector of an O9V with  $R_V = 3.8$ . The dashed line is the unreddened main sequence. We find that a large number of objects with ‘poor’ fits depart from the OB star reddening vector. These objects show colours that can be consistent with eclipsing W UMa contact binaries, given the way in which the survey data are collected.

diagram or they may fall beyond the RJ reddening vector (Smolčić et al., 2004).

### 3.4.1 Parameters of the candidate OB stars

Figure 3.9 shows the distribution of stellar parameters across the entire selection for the objects fitting successfully to a reddened OB-star SED ( $\chi^2 \leq 7.82$  and  $\log(T_{\text{eff}}) \geq 4.3$ ). Coloured in red are the results for all objects within an 8 arcmin box centred on Wd 2 (drawn in Figure 3.14). It can be seen that those objects in or near the cluster are reported to have similar extinction in the range  $5.5 \leq A_0 \leq 7$  (top right panel in Figure 3.9). Otherwise, the reddenings range more broadly across the full 2 square degrees from  $A_0 \simeq 3$  up to  $A_0 \simeq 8$ . Other features of this particular sight-line are that larger than standard  $R_V$  is favoured – a roughly normal distribution in  $R_V$  about a mean value of  $R_V = 3.84 \pm 0.25$  is obtained – and that most of the selected stars are attributed distances of between  $\sim 2$  kpc ( $\mu \simeq 11$ ) and  $\sim 6$  kpc ( $\mu \simeq 14$ ). The objects in/near Wd2 tend toward the higher end of the distance modulus range and show a fairly wide spread in extinction law with  $3.5 \leq R_V \leq 4.5$ .

Echoing the initial mass function (IMF), the distribution in median  $\log(T_{\text{eff}})$  values is heavily skewed towards the lower end. The turn over in the  $\log(T_{\text{eff}})$  distribution at just below  $\log(T_{\text{eff}}) = 4.3$  further supports the conclusion that our initial selection of VPHAS+ sources in the  $(u - g, g - r)$  diagram is essentially complete in the desired O to B2 effective temperature range (given our magnitude limits). The coolest object in the candidate list is  $\sim 16000$  K.

Stars with median estimated effective temperatures in excess of 30000K ( $\log(T_{\text{eff}}) \geq 4.477$ ) are regarded as candidate O stars. Of the new discoveries, 74 meet this criterion. We can further subdivide this group to distinguish the highly probable O stars: 28 objects have a 16<sup>th</sup> percentile  $\log(T_{\text{eff}})$  exceeding 4.477. Seven of these may be sdO stars (see section 3.4.2).

Predictably, many of the hottest candidates are in and around Wd 2: this young massive cluster does indeed stand out in this part of the Galactic Plane. Moreover the top left panel in 3.9 suggests a relative lack of cooler OB stars within the 8 arcmin box

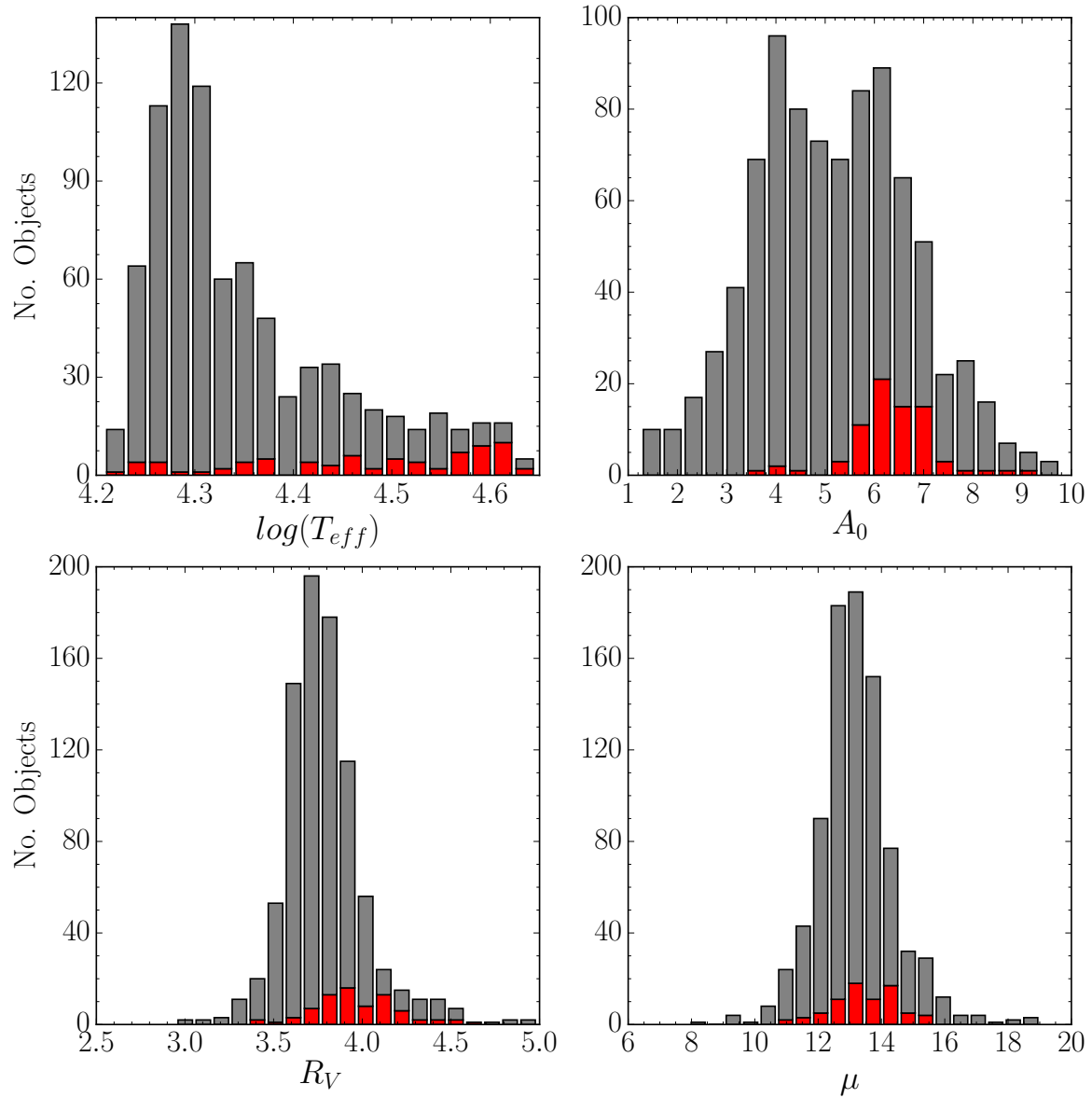
centred on the cluster. This could be taken to imply that the stellar mass function of Wd 2 and environs is top heavy. At the same time, there are biases that can favour the detection of more massive stars at the likely distance of the cluster ( $\mu \sim 13 - 14$ ) – namely, the effects of crowding (less massive fainter stars are more likely to be lost in blends) and of magnitude limited selection. However this is unlikely to be all of the explanation given that there are plenty of examples of  $A_0 \sim 5.5 - 7$  cool candidates with a similar estimated distance modulus. This could be further explored with deeper photometry of the region.

Figure 3.10 shows the upper and lower uncertainties on each parameter as a function of  $g$ -band magnitude for all  $\chi^2 < 7.82$  objects. The uncertainty on  $\log(T_{\text{eff}})$  and  $A_0$  increases for fainter objects, tracking the increase with rising magnitude of the photometric errors. Conversely the uncertainty on  $R_V$  shows a slight increase with decreasing magnitude at the bright end.  $R_V$  is more difficult to determine for bright objects typically as they are more often less obscured. Nevertheless it is evident that both  $R_V$  and  $A_0$  are consistently well determined across the entire magnitude range. Our OnIR SED fits deliver  $A_0$  to within  $\lesssim 0.09$  mag up to 18<sup>th</sup> magnitude, rising up to  $\lesssim 0.25$  mag at 20<sup>th</sup> magnitude. We find the median uncertainty on  $R_V$  to be 0.081.

### 3.4.2 Inferences from the best-fit parameters and other aspects of the photometry

A richer understanding of the candidate objects can be obtained from a combination of more scrutiny of the fit parameters obtained and from a fuller utilisation of the VPHAS+ photometry at our disposal. So far the focus has been on the information to be extracted from the individual OnIR SEDs – treating all candidates as if they are well described as reddened, single, main-sequence OB stars. We can learn more through consideration of the ensemble of objects, and if use is made of the narrowband H $\alpha$  band to separate out emission line stars.

First we acknowledge and relax the main sequence assumption applied so far. The first two panels of Figure 3.11 show scatter plots of the best-fit median distance mod-



**Figure 3.9:** Distribution of the best fit parameters for the selection of objects with  $\chi^2 < 7.82$ . The red bars are objects within an 8 arcmin box of Wd 2 while the grey bars are the wider selection. We find that the objects spatially associated with Wd 2 show a tight distribution in  $A_0$  and provide an over density of objects in the  $5.5 \leq A_0 \leq 7$  range and also show a wider spread in  $R_V$ .

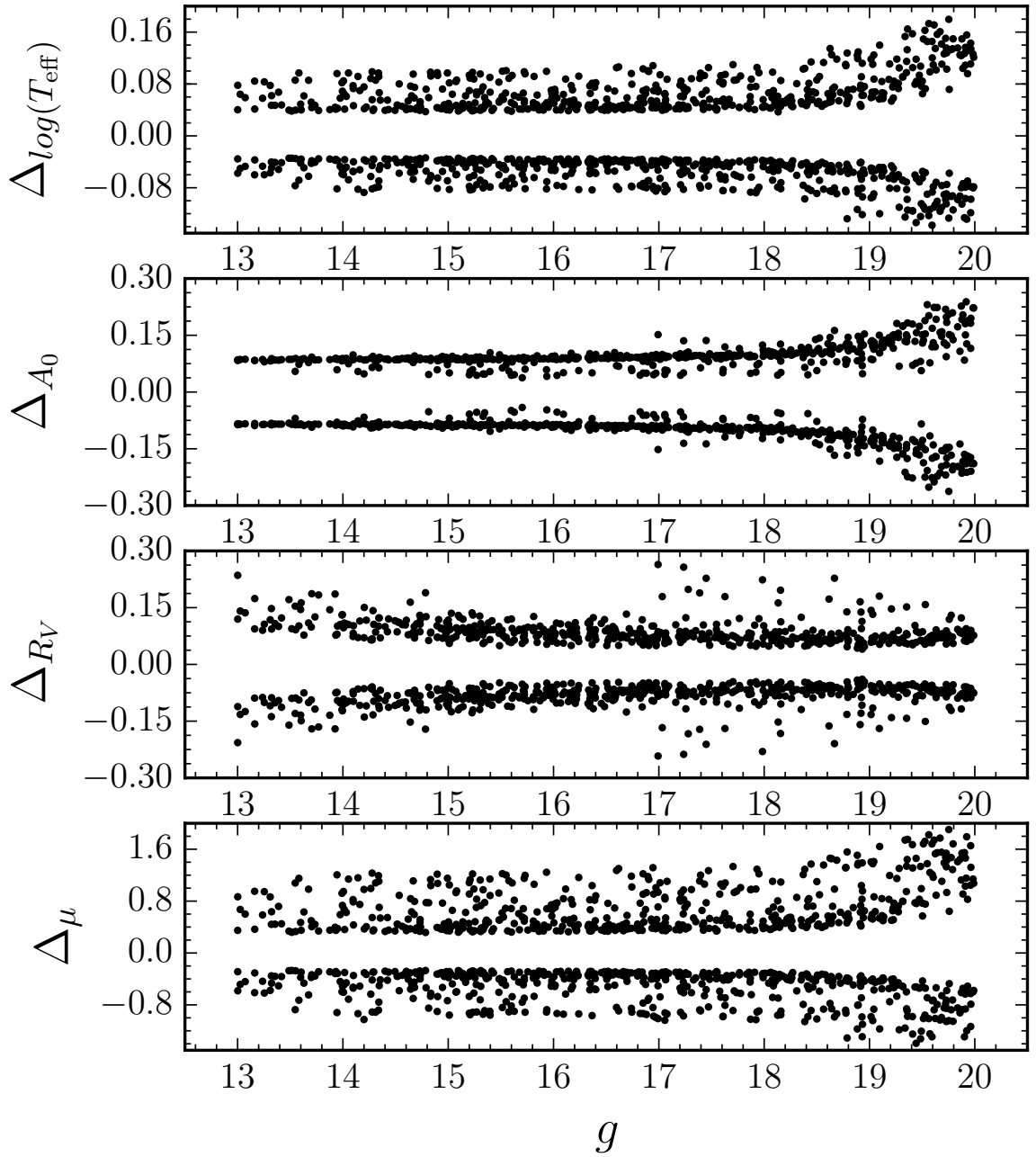


**Figure 3.10:** Uncertainty on each parameter as a function of  $g$  band magnitude. Uncertainties are derived from the 16<sup>th</sup> and 84<sup>th</sup> percentiles of the posterior distributions.

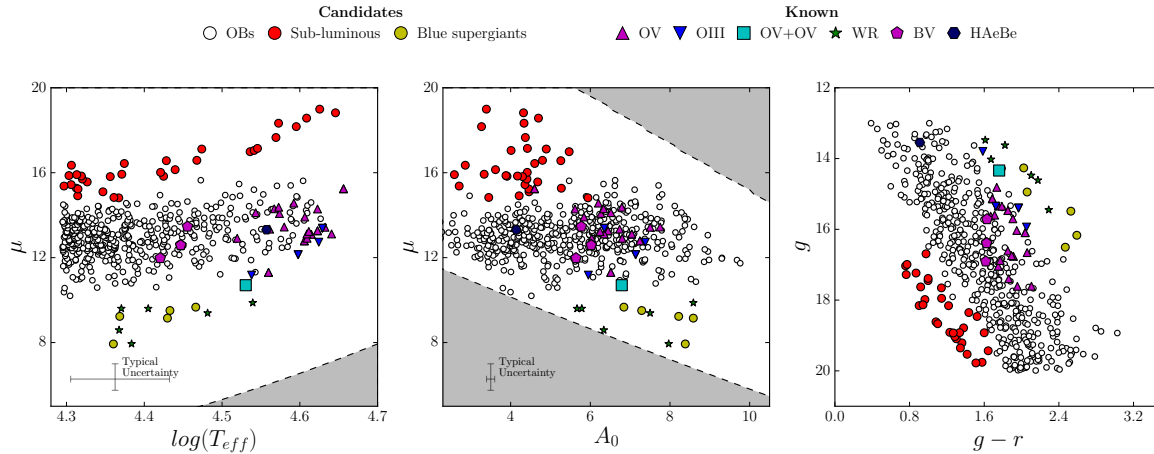


**Figure 3.11:** 2-D distribution of the best fit parameters for the final selection of OB candidates ( $\chi^2 \leq 7.82$  and  $\log(T_{\text{eff}}) \geq 4.3$ ) and objects in the selection with known spectral type (the carbon star lies outside the range of 2 of these diagrams and was therefore not included). Objects shown in red and yellow are thought to be candidate sub-luminous OB stars and candidate blue supergiants respectively. The areas shaded in grey are where we cannot detect OB stars given the survey limits.

ulus,  $\mu$ , vs.  $\log(T_{\text{eff}})$  and vs.  $A_0$  for the candidate OB stars. Different symbols are over-plotted to pick out the already known objects listed in SIMBAD as well as the O stars of Vargas Álvarez et al. (2013). The areas shaded in grey are where we cannot detect OB stars given the survey limits. These regions are where the given combination of parameters yields model SEDs which have  $g > 20$  or  $g < 13$ . The objects plotted as red circles have relatively low extinction but, if we take the returned distance moduli at face value, they would have to be construed as very distant ( $> 10$  kpc) when compared to the known OB stars. It is more plausible that these are intrinsically sub-luminous objects rather than distant OB stars located in remarkably clear reddening holes. Their scattered spatial distribution across the whole field shown in Figure 3.14 supports this argument.

The converse argument can be applied to those objects plotted as yellow circles: they are found to have more than 6 magnitudes of extinction but are seemingly very close (less than  $\sim 700$  pc away,  $\mu < 9$ ). We suspect that these objects are intrinsically much higher-luminosity, evolved B stars. The proximity of these stars in the figures to the (poorly-fit) known WR stars, including the highly-luminous WR20a, lends credibility to this interpretation.

Referring back to the photometry in the form of a  $(g, g - r)$  colour magnitude

diagram (CMD), these interpretations are seen to make sense – the sub-luminous and over-luminous objects form tracks separated from the main-sequence – see the third panel of Figure 3.11. Table 3.6 lists these extreme objects. There will be further discussion of them in Section 3.5. The main concentration of objects appears in the  $11.5 < \mu < 14$  mag range which equates to distances ranging from 2 – 6 kpc. This encloses the derived distance range of  $\sim 4 - 6$  kpc in the Carina arm near its tangent traced in CO by Grabelsky et al. (1988).

We can also use the VPHAS+  $H\alpha$  measurements to uncover any emission line stars in our selection. The presence of emission lines implies the presence of ionized circumstellar gas which, among massive OB stars, most commonly indicates classical Be stars with circumstellar disks. Although the OnIR SEDs of classical Be stars are not greatly different from normal B stars of similar effective temperature, the derived interstellar extinctions from SED fits that do not take into account the circumstellar continuum emission will nevertheless be overestimated. We have used the  $(r-i, r-H\alpha)$  diagram to select all objects that lie more than 0.1 mag in  $r - H\alpha$  above the O9V reddening vector (this equates to  $\sim 10\text{\AA}$  in emission line equivalent width). Figure 3.12 shows this selection. Using the relation between  $EW(H\alpha)$  and added colour excess  $E(B - V)$  due to the presence of a circumstellar disk in classical Be stars from Dachs et al. (1988), we can estimate that the derived reddenings ( $A_0$ ) for our  $H\alpha$ -excess stars will have been inflated by between  $\sim 0.1$  and  $\sim 0.3$  magnitudes. There are 17 of these objects in the  $\chi^2 \leq 7.82$  and  $\log(T_{\text{eff}}) \geq 4.3$  group and a further 63 with  $\chi^2 > 7.82$  and/or  $\log(T_{\text{eff}}) < 4.3$ . Objects with  $H\alpha$  excess are marked in Table 3.5.

### 3.4.3 Reddening

After removing the obvious sub/over-luminous objects and the emission line stars from the selection we are left with a cleaner selection of 458  $\sim$  non-emission OB candidates and 19 known OB stars available for further examination of their reddening properties.

Given our tight grasp on  $A_0$  and  $R_V$ , it is of interest to consider their interdependence.  $R_V$  is plotted as a function of  $A_0$  in Figure 3.13. The left panel of this Figure

**Table 3.6:** Table containing the derived stellar parameters of the sub-luminous and blue supergiant candidates in the  $\chi^2 \leq 7.82$  and  $\log(T_{\text{eff}}) \geq 4.3$  group.

ID	RA	DEC	$g$	$\log(T_{\text{eff}})$	$A_0$	$R_V$	$\mu$	$\chi^2$
Sub-Luminous								
19	10 13 40.87	-57 43 15.38	18.13	$4.65^{+0.04}_{-0.05}$	$4.32^{+0.09}_{-0.09}$	$4.95^{+0.16}_{-0.15}$	$18.82^{+0.50}_{-0.69}$	7.09
28	10 13 54.74	-58 14 33.73	18.91	$4.31^{+0.05}_{-0.04}$	$4.36^{+0.13}_{-0.13}$	$3.82^{+0.17}_{-0.16}$	$15.44^{+0.45}_{-0.37}$	3.53
82	10 15 21.46	-57 53 30.64	19.43	$4.37^{+0.08}_{-0.06}$	$5.94^{+0.13}_{-0.13}$	$4.03^{+0.10}_{-0.10}$	$14.82^{+0.77}_{-0.52}$	1.11
86	10 15 22.76	-57 48 21.73	18.67	$4.57^{+0.08}_{-0.08}$	$4.34^{+0.16}_{-0.17}$	$4.17^{+0.23}_{-0.21}$	$18.33^{+0.98}_{-0.99}$	2.10
89	10 15 24.77	-57 44 09.28	19.78	$4.43^{+0.13}_{-0.09}$	$5.26^{+0.15}_{-0.17}$	$3.79^{+0.13}_{-0.12}$	$16.57^{+1.47}_{-0.88}$	1.97
96	10 15 36.78	-57 46 58.03	17.65	$4.37^{+0.05}_{-0.05}$	$3.34^{+0.10}_{-0.10}$	$3.13^{+0.11}_{-0.10}$	$15.93^{+0.53}_{-0.42}$	0.82
153	10 16 25.54	-58 33 18.54	18.93	$4.61^{+0.06}_{-0.08}$	$4.70^{+0.09}_{-0.09}$	$3.84^{+0.11}_{-0.11}$	$18.57^{+0.83}_{-0.99}$	6.51
162	10 16 31.33	-57 48 18.68	18.92	$4.47^{+0.09}_{-0.07}$	$4.80^{+0.10}_{-0.11}$	$3.35^{+0.09}_{-0.09}$	$16.58^{+1.04}_{-0.69}$	5.05
177	10 16 44.32	-58 01 29.97	19.02	$4.32^{+0.06}_{-0.05}$	$4.17^{+0.13}_{-0.13}$	$3.60^{+0.14}_{-0.13}$	$15.84^{+0.54}_{-0.42}$	2.71
202	10 17 01.28	-58 05 29.31	19.35	$4.47^{+0.11}_{-0.08}$	$4.89^{+0.13}_{-0.14}$	$3.87^{+0.15}_{-0.14}$	$17.11^{+1.34}_{-0.86}$	3.96
219	10 17 15.78	-57 23 13.80	19.53	$4.37^{+0.07}_{-0.06}$	$4.60^{+0.15}_{-0.15}$	$3.57^{+0.16}_{-0.15}$	$16.43^{+0.75}_{-0.54}$	1.31
274	10 17 59.10	-58 01 05.92	18.16	$4.31^{+0.05}_{-0.04}$	$2.86^{+0.13}_{-0.13}$	$3.27^{+0.20}_{-0.18}$	$16.35^{+0.43}_{-0.36}$	3.30
275	10 17 59.67	-57 48 12.93	17.03	$4.30^{+0.04}_{-0.04}$	$2.71^{+0.10}_{-0.10}$	$3.61^{+0.18}_{-0.17}$	$15.37^{+0.35}_{-0.30}$	1.17
292	10 18 11.80	-58 20 12.24	19.21	$4.33^{+0.05}_{-0.05}$	$4.68^{+0.13}_{-0.13}$	$3.82^{+0.15}_{-0.14}$	$15.57^{+0.50}_{-0.41}$	1.62
402	10 19 39.37	-58 29 18.43	19.76	$4.31^{+0.07}_{-0.06}$	$5.27^{+0.15}_{-0.15}$	$3.72^{+0.12}_{-0.11}$	$15.27^{+0.64}_{-0.47}$	3.79
468	10 20 48.03	-57 45 45.52	18.35	$4.35^{+0.05}_{-0.05}$	$4.46^{+0.12}_{-0.12}$	$3.47^{+0.12}_{-0.12}$	$15.10^{+0.51}_{-0.41}$	0.35
472	10 20 53.73	-57 58 41.78	17.95	$4.55^{+0.10}_{-0.08}$	$4.42^{+0.08}_{-0.09}$	$3.94^{+0.12}_{-0.11}$	$17.14^{+1.22}_{-0.89}$	3.28
474	10 20 54.07	-58 02 32.59	18.92	$4.30^{+0.05}_{-0.04}$	$3.88^{+0.12}_{-0.12}$	$3.40^{+0.14}_{-0.13}$	$15.87^{+0.42}_{-0.35}$	6.59
484	10 21 07.91	-57 33 52.74	18.16	$4.57^{+0.09}_{-0.08}$	$4.37^{+0.08}_{-0.09}$	$3.70^{+0.11}_{-0.10}$	$17.66^{+1.09}_{-0.95}$	3.39
486	10 21 10.28	-58 10 46.02	18.62	$4.36^{+0.05}_{-0.05}$	$4.30^{+0.11}_{-0.11}$	$4.33^{+0.17}_{-0.16}$	$15.82^{+0.50}_{-0.43}$	1.42
601	10 22 35.02	-58 33 37.82	16.69	$4.36^{+0.05}_{-0.04}$	$3.45^{+0.10}_{-0.10}$	$3.69^{+0.13}_{-0.13}$	$14.83^{+0.46}_{-0.38}$	0.97
647	10 23 27.84	-57 54 56.79	19.03	$4.54^{+0.11}_{-0.09}$	$5.47^{+0.09}_{-0.10}$	$4.39^{+0.13}_{-0.12}$	$16.99^{+1.38}_{-1.04}$	5.40
810	10 24 31.14	-57 33 45.22	16.99	$4.60^{+0.07}_{-0.08}$	$3.27^{+0.15}_{-0.15}$	$4.03^{+0.26}_{-0.24}$	$18.17^{+0.94}_{-1.01}$	1.71
819	10 24 36.96	-58 22 47.18	17.28	$4.31^{+0.04}_{-0.04}$	$2.59^{+0.11}_{-0.11}$	$3.51^{+0.20}_{-0.18}$	$15.91^{+0.39}_{-0.33}$	5.83
842	10 24 58.98	-57 59 56.24	17.45	$4.42^{+0.07}_{-0.05}$	$3.91^{+0.14}_{-0.14}$	$4.11^{+0.23}_{-0.21}$	$15.83^{+0.77}_{-0.57}$	0.66
870	10 25 25.08	-57 59 04.50	17.98	$4.31^{+0.04}_{-0.04}$	$4.21^{+0.12}_{-0.12}$	$4.99^{+0.22}_{-0.23}$	$14.91^{+0.42}_{-0.33}$	0.71
894	10 25 47.01	-57 46 51.19	19.09	$4.32^{+0.06}_{-0.05}$	$4.41^{+0.15}_{-0.15}$	$3.84^{+0.18}_{-0.17}$	$15.70^{+0.54}_{-0.43}$	1.49
956	10 26 57.82	-57 36 16.66	17.39	$4.54^{+0.09}_{-0.08}$	$4.01^{+0.10}_{-0.10}$	$4.44^{+0.19}_{-0.17}$	$17.05^{+1.11}_{-0.88}$	7.77
989	10 27 34.13	-57 36 25.34	18.79	$4.31^{+0.05}_{-0.04}$	$4.46^{+0.13}_{-0.13}$	$3.59^{+0.14}_{-0.13}$	$15.23^{+0.46}_{-0.39}$	3.04
1024	10 28 14.60	-57 41 36.33	17.24	$4.44^{+0.07}_{-0.06}$	$3.62^{+0.14}_{-0.14}$	$4.22^{+0.26}_{-0.24}$	$16.14^{+0.82}_{-0.61}$	1.70
1052	10 28 50.85	-57 45 56.73	17.63	$4.63^{+0.05}_{-0.06}$	$3.39^{+0.12}_{-0.12}$	$3.80^{+0.18}_{-0.17}$	$18.99^{+0.61}_{-0.81}$	2.77
1059	10 28 56.00	-58 09 02.55	18.46	$4.42^{+0.07}_{-0.05}$	$4.42^{+0.10}_{-0.10}$	$3.27^{+0.09}_{-0.09}$	$16.02^{+0.72}_{-0.53}$	5.96
Blue supergiants								
52	10 14 40.36	-57 24 26.24	15.49	$4.36^{+0.05}_{-0.05}$	$8.38^{+0.10}_{-0.10}$	$3.77^{+0.05}_{-0.05}$	$7.93^{+0.51}_{-0.40}$	2.28
175	10 16 42.53	-57 32 47.65	16.17	$4.43^{+0.08}_{-0.06}$	$8.59^{+0.10}_{-0.10}$	$3.77^{+0.05}_{-0.05}$	$9.15^{+0.82}_{-0.56}$	1.04
188	10 16 53.91	-57 55 02.11	14.26	$4.47^{+0.09}_{-0.06}$	$6.84^{+0.09}_{-0.09}$	$3.81^{+0.06}_{-0.06}$	$9.67^{+0.99}_{-0.63}$	0.25
452	10 20 31.60	-58 03 08.72	14.95	$4.43^{+0.07}_{-0.05}$	$7.29^{+0.09}_{-0.10}$	$4.03^{+0.07}_{-0.07}$	$9.51^{+0.77}_{-0.53}$	0.91
578	10 22 19.90	-57 46 11.21	16.51	$4.37^{+0.06}_{-0.05}$	$8.22^{+0.10}_{-0.10}$	$3.80^{+0.05}_{-0.05}$	$9.23^{+0.54}_{-0.41}$	2.32

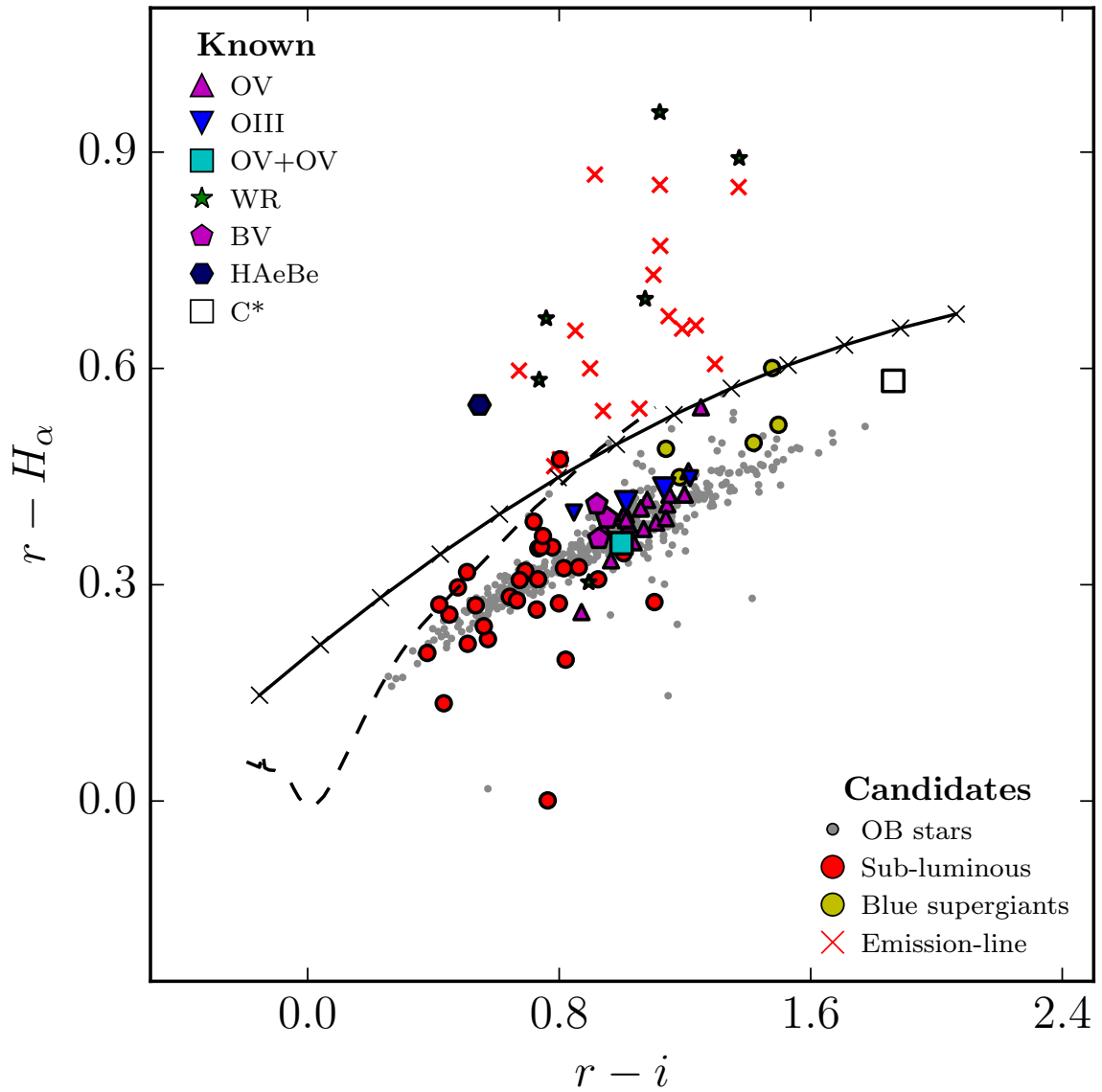


**Figure 3.12:** 13 of the  $\chi^2 \leq 7.82$  and  $\log(T_{\text{eff}}) \geq 4.3$  objects show  $H\alpha$  excess. As emission is usually associated with circumstellar dust; the derived extinction may be incorrect. The solid line is the reddening vector of an O9V raised by 0.1 in  $r - H\alpha$  and the dashed line shows the zero reddened main-sequence.

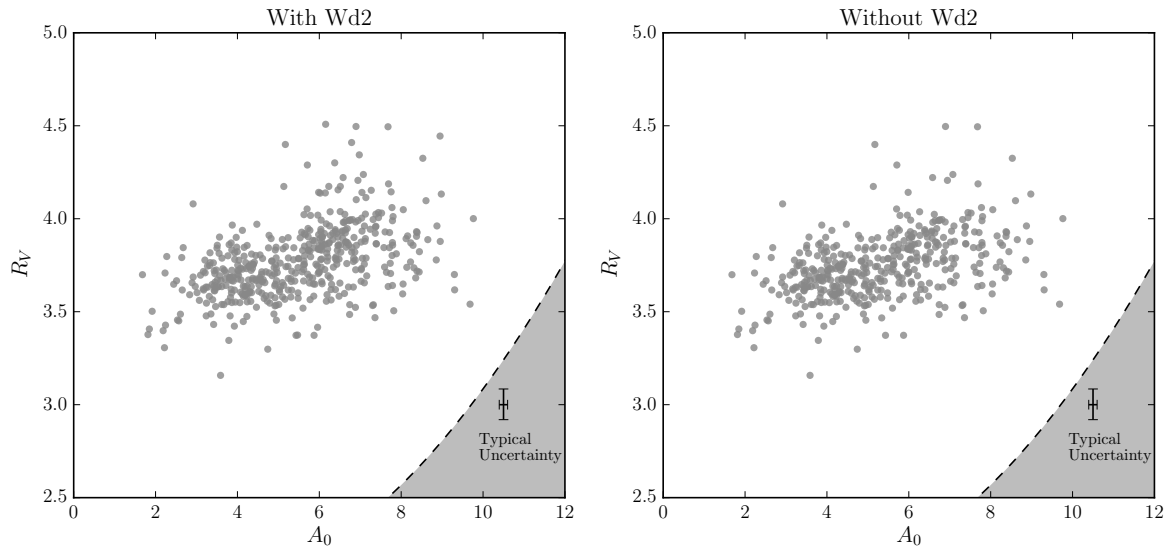


**Figure 3.13:**  $A_0$  vs.  $R_V$  plot for the final selection with and without the objects within the 8 arcmin box surrounding Wd 2. There is a modest increase in  $R_V$  as a function of  $A_0$  in either case with correlation coefficient  $r = 0.47$  and  $r = 0.45$  respectively. The areas shaded in grey are where we cannot detect OB stars given the survey limits.

includes those objects within an 8 arcmin box around Wd 2 and the right hand panel excludes them. In both cases we can see a moderate positive correlation in  $R_V$  as a function of  $A_0$  (correlation coefficient  $r = 0.47$  and  $r = 0.45$  respectively). On comparing the two panels, it is evident that the members of Wd 2 drive up the  $R_V$  trend more sharply when they are included. The shaded background shows that the trends seen are independent of the boundaries set by the survey selection limits. Given that it was demonstrated in Section 3.3.2 that the fitting method generates negligible covariance between  $A_0$  and  $R_V$ , we can say with confidence that the correlation apparent now is related to the physical nature of the volume of space under study.

It is commonly understood that increasing  $R_V$  is linked to increasing typical dust grain size, and that values of 3.5 and more are associated with denser molecular cloud environments (see e.g. [Draine, 2003](#)). The  $\sim 2$  square degrees under examination here sample sight-lines lying just inside the Carina Arm tangent direction. Our pencil beam is evidently one that would initially pass through the atomic diffuse interstellar medium and then enter the dense clouds of the Carina Arm, wherein Wd 2 is located. In this situation it makes sense that as the dust column grows it becomes ever more dominated by the dense/molecular ISM component – i.e.  $R_V$  tends to rise. However the rise is not

dramatic, and the data points show significant dispersion, which may imply that the variation in the dust properties within the sampled volume is not especially coherent. The effect of the bright limit of the survey is to remove sensitivity to  $A_0$  much below 2–3, or to distances less than  $\sim 3$  kpc (see below). Current maps of Galactic spiral arm structure place this distance already within the Carina Arm (Russeil, 2003; Vallée, 2014).

The clear message of Figure 3.13 is that the typical, if necessarily idealised, reddening law for this sight-line can be characterised by  $R_V \sim 3.8$ , which rises much less sharply with decreasing wavelength than the Galactic average of  $R_V = 3.1$ .

## 3.5 Discussion

### 3.5.1 The number and spatial distribution of the OB candidates

Figure 3.14 shows the location of each new candidate in the 2 square degrees for which the SED fit returned  $\chi^2 \leq 7.82$  and  $\log(T_{\text{eff}}) \geq 4.3$ , over-plotted on the VPHAS+ H $\alpha$  mosaic. Each star is colour-coded according to its derived extinction,  $A_0$ . The 527 objects are scattered across the field, with lower reddenings ( $A_0 < 5$ ) dominating in the southern half. Apart from in Westerlund 2 itself, the distribution is sparser and more highly-reddened in the north. Towards the NW and the tangent direction, roughly at RA 10h11m, Dec -56 14 (J2000) (Dame, 2007), the most reddened objects ( $A_0 > 8$ ) are found.

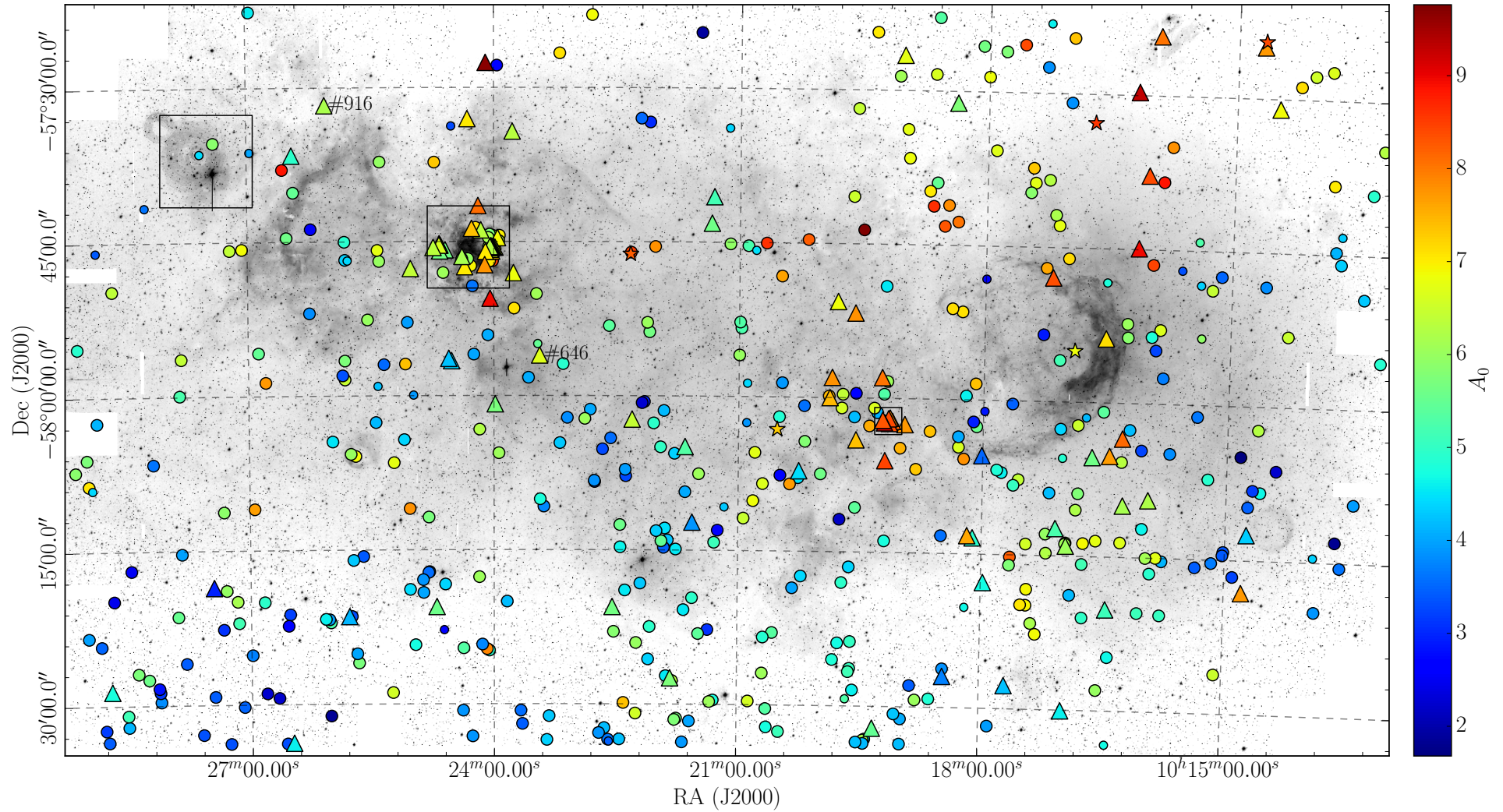


**Figure 3.14:** Known and candidate OB stars, in our selection, coloured according to their inferred reddening ( $A_0$ ) and over-plotted on the high-confidence inverse VPHAS+  $H\alpha$  image. The boxes pick out the known clusters IC 2581, Wd 2, and DBS2003 45 (working from east to west). The symbols used have the following interpretations: O stars with  $\log(T_{\text{eff}}) > 4.477$  are triangles; early B stars,  $4.300 \leq \log(T_{\text{eff}}) \leq 4.477$  are large circles; stars and small circles represent the blue supergiants and under-luminous objects respectively. The white space under the object near the eastern boundary is currently a region of reduced confidence in  $H\alpha$  (without inclusion of the adjacent field). Low resolution spectroscopy of object #916 and #646 suggests their spectral types may be early as O3-O4 (see Chapter 4).

489 of the objects shown have not been identified previously as confirmed or candidate OB stars. Previous works by [Reed \(2003\)](#), and by [Kaltcheva & Golev \(2012\)](#) have noted a further 26 stars earlier than B3 within this region – all of which are brighter than  $V = 11$ , and therefore not in our sample. Also for reasons of brightness, our sample does not include any stars obviously associated with IC 2581. [Turner \(1978\)](#) studied the cluster – home to a number of early B stars – establishing a distance of 2.87 kpc, and a typical reddening corresponding to  $A_0 \sim 1.5$ . For the present selection, this cluster is in combination too close and too lowly-reddened: a B3 main sequence star with  $A_0 = 1.5$  needs to be at a distance of 3.8 kpc to achieve  $g = 13$ . The one star that has been uncovered close to IC 2581 is a candidate sub-luminous object, likely to be at a much shorter distance and unconnected to IC 2581. It can be seen in [Figure 3.13](#) that  $A_0 = 1.9$  for the least reddened candidate OB star in the sample.

It has been argued before by e.g. [Grabelsky et al. \(1988\)](#) and [Dame \(2007\)](#) that the Carina Arm tangent region traced in CO spans the distance range from 3 to 5 kpc. At larger distances the conical volume captured here reaches beyond the Solar Circle where declining amounts of molecular gas are detected. Taking note of these considerations, it seems likely that the high values of  $R_V$ , trending from 3.6 to 3.9, revealed by our SED fits ([Figure 3.13](#)) are largely a product of the dominant and increasing contribution to the total extinction from the dust column of the Carina Arm. Similarly [Povich et al. \(2011\)](#) found it necessary to adopt  $R_V = 4$  for embedded Carina Arm objects at  $l \sim 287^\circ$ . In contrast, [Turner \(1978\)](#) determined  $R_V$  to be  $3.11 \pm 0.18$  across this region, based on bright OB stars with extinctions below  $A_V$  of 2 – clearly the foreground to our sample. Indeed it seems likely that much of the extinction of the OB population spanning  $A_0 \sim 2$  to  $A_0 \sim 9$  accumulates within the Carina Arm. The appearance of [Figure 3.11](#) indicates few detected main sequence OB stars beyond a distance modulus of 14 ( 6 kpc).

### 3.5.2 Westerlund 2

Figures 3.9 and 3.13 tell us that a single value of  $R_V$  cannot be used to describe the extinction law of sight lines towards all objects in Wd 2. Instead we find that  $R_V$  ranges from approximately 3.5 to 4.5 within the cluster. Similar spreads in  $R_V$  within star clusters has previously been found by Fitzpatrick & Massa (2007) and highlights the importance of deriving  $R_V$  on a star-by-star basis. Hur et al. (2015) describe a hybrid extinction model with  $R_V = 3.33 \pm 0.03$  to  $A_0 \sim 3$  (based on three stars), while  $R_V = 4.14 \pm 0.08$  is required for stars in Wd 2. Figure 3.13 cautions against this clear-cut interpretation, even while our results are numerically consistent with theirs. Reality is more fractal and it is best not to place too much weight on very few stars.

In Figure 3.9 we noticed a tight distribution in  $A_0$  for the objects close to Wd 2 as projected on the sky. While there are no new OB star candidates in the central region of Wd 2 (within the 8 arcmin box shown in fig 3.14), there are a handful of probable O stars scattered across the field that share its extinction. All objects that have extinctions consistent to within  $1 \sigma$  of the mean of known objects in Wd 2 ( $5.8 > A_0 > 7.2$ ) and have  $\log(T_{\text{eff}}) > 4.477$  are identified in Table 3.7. It is possible that these have been ejected from Wd 2 by dynamical interactions or after supernova explosions in binary systems (Allen & Poveda, 1971; Gies & Bolton, 1986). Given a derived distance of  $\sim 5$  kpc to Wd 2, an object that is separated from the cluster by  $\sim 20$  arcmin on the sky would have to have travelled a minimum distance of  $\sim 30$  pc in 1–2 Myr. This would equate to a minimum (plane-of-sky) velocity of  $\sim 25$  km/s. Given that massive stars can attain runaway velocities of up to  $\sim 200$  km/s through dynamical encounters between binary systems (Gvaramadze et al., 2010), it is not unreasonable to consider that these objects may have been ejected recently from Wd 2. The study by Roman-Lopes et al. (2011) also highlighted two isolated stars as possible dynamically-ejected runaways from Wd 2 (WR20aa and WR20c). WR20aa (SS215) is in our selection as a poor fit object while WR20c is located just beyond the area studied to the North of the cluster. Alternatively these stars may have formed in situ within the wider star forming region on a similar time scale to the cluster. Low

**Table 3.7:** The reddening parameters and angular separation from the centre of Wd 2 ( RA 10 24 18.5 DEC -57 45 32.3 (J2000)) of new O star candidates with similar reddening to the cluster, outside the 8 arcmin box shown in figure 3.14. All objects have  $\log(T_{\text{eff}}) > 4.477$  and  $5.8 > A_0 > 7.2$ . See Tables 3.4 and 3.5 for the full set of data.

ID	$g$	$A_0$	Separation (ar- cmin)
44	16.62	$6.88^{+0.07}_{-0.09}$	80.21
121	14.28	$6.21^{+0.06}_{-0.08}$	70.59
191	17.43	$6.05^{+0.09}_{-0.09}$	64.98
144	16.94	$6.13^{+0.07}_{-0.09}$	68.46
161	19.28	$7.11^{+0.07}_{-0.12}$	62.73
346	16.60	$6.76^{+0.07}_{-0.09}$	46.51
413	17.06	$6.83^{+0.05}_{-0.06}$	36.42
576	15.40	$6.42^{+0.05}_{-0.07}$	23.13
916	15.01	$6.19^{+0.05}_{-0.07}$	19.67
646	15.58	$6.69^{+0.06}_{-0.08}$	12.60
796	16.37	$7.03^{+0.05}_{-0.07}$	12.50
662	15.33	$6.30^{+0.05}_{-0.06}$	12.06
846	16.82	$6.39^{+0.04}_{-0.05}$	6.03
661	17.21	$6.81^{+0.04}_{-0.05}$	5.05

resolution spectroscopy of object #916 and #646 suggests their spectral types may be as early as O3-O4 (see Chapter 4). Their positions are marked on Figure 3.14.

As a final point of interest, we note that the more reddened cluster DBS2003 45, picked out in figure 3.14 as well, also appears to be surrounded by a scatter of OB stars that are reddened similarly to the cluster.

### 3.5.3 Candidate blue supergiants and sub-luminous stars

The results from Section 3.4.2 suggest the presence of 5 high luminosity B stars scattered across the field. If they are early-B supergiants, their absolute visual magnitudes would be in the region of  $\sim -6.5$  (Crowther et al., 2006). On correcting the previous main-sequence assumption, we find their derived distance moduli,  $\mu$ , rise from  $\sim 9$  to  $\sim 13.5$ , placing them amongst the general OB population that we pick out. Meylan & Maeder (1983) estimate a surface density of around 10 - 20 blue supergiants (BSGs)

per  $\text{kpc}^2$  in the Galactic Plane. Assuming that our selection spans distances from 2 - 6 kpc we are sampling a projected disk surface area of a little over  $1 \text{ kpc}^2$ ; so finding 5 candidates undershoots the surface density prediction but not to the extent that it can be claimed to be inconsistent with it. Given that these candidates are affected by saturation in the  $i$  band ( $i \lesssim 12$ ), there may one or two BSGs that have fallen into the ‘poor-fit’ group due to saturation in the redder bands.

We also find evidence for the presence of a population of subdwarf stars (see table 3.6 and figure 3.11). Of these 9 may be sdO stars, leaving 23 in the sdB category. The absolute magnitudes of the latter range from  $M_V = 3 - 6$  (Stark & Wade, 2003). Since these objects are  $\sim 6$  mag fainter than their main-sequence counterparts, their distance moduli are likely to be  $\sim 10$  as opposed to the estimated values of  $\sim 16$ . This behaviour and the spatial scattering of the subdwarf candidates suggests that we are looking at a group of moderately reddened  $A_0 \lesssim 4$  stars in the foreground of the main OB population. We are biased to select more highly reddened subdwarf stars due to the 2MASS faint limit as discussed in Section 3.4. With access to deeper NIR photometry we would expect to find more lowly reddened sdB stars in the selection.

Although the SED fitting we have performed has no sensitivity to surface gravities and limited sensitivity to stellar effective temperature, the fact that the Carina Arm region studied falls near the tangent has allowed us to pick out the extreme objects purely from their outlier distance moduli – relative to the near MS stars concentrated in the range  $11 < \mu < 14$ . While this approach works here, it is evident that in other sight lines, where the population of OB stars may be spread more uniformly across a larger distance range, the luminosity extremes would not stand out in the same way.

## 3.6 Conclusions

In summary, we have demonstrated a method for selecting and parametrizing the reddening and basic stellar properties of OB stars uniformly across large areas of the Southern sky using VPHAS+, and NIR survey data. The selection presented here has resulted in reddening parameters for 848 O and B stars (see table 3.2). Of these, 489

are well-fit new OB stars hotter than 20000 K, including 74 probable O stars. This has been achieved by reaching down to  $g = 20$  mag and approaches a factor of 10 increase relative to the small number of known and candidate O to B2 stars in the region.

By bringing together VPHAS+  $u, g, r, i$  photometry with NIR 2MASS photometry, we are able to determine both the value of the extinction,  $A_0$ , and test and select the most appropriate reddening law, as parametrised by  $R_V$ , to a high degree of accuracy: both are typically measured to better than 0.1 (magnitudes in the case of  $A_0$ ). Pleasingly there are signs that the still preliminary nature of the photometric calibration of the VPHAS+ survey data blends well with the now well-established 2MASS calibration.

We set out expecting to only gain a crude impression of stellar effective temperatures (and hence distance moduli), and so it has turned out. But we have found good consistency with earlier results in our benchmark region around the much-studied cluster Westerlund 2, confirming that our methods are sound and able to e.g distinguish early O stars from late-O and early-B stars. This represents an efficient start to selection that needs to be followed up by spectroscopic confirmation and measurement of stellar parameters. With precise spectroscopic parameters in hand, the photometry can be re-used for direct and even more precise measurement of reddening laws.

We have also seen how the high resolution and wide field of view of OmegaCam can bring a wider context to the study of open clusters and OB associations, through an ability to identify potentially-related stars that have either been ejected from clusters or simply have formed – perhaps as part of a wider star-formation event – in relative isolation in the surrounding field. This study has also uncovered 5 BSG candidates as well as 32 reddened candidate subdwarfs of which 9 may be sdO stars.

---

# CHAPTER 4: SPECTROSCOPIC CONFIRMATION

---

In Chapter 3 we saw that the apparent yield from blue photometric selection of candidate OB stars was a 10-fold increase in the identified population. Here, we use limited spectroscopic follow up to assess how effective this selection is. This was obtained through the Anglo Australian Observatory (AAO) service observing programme (applied for in autumn 2013).

## 4.1 Spectroscopic observations

Low resolution spectra of 276 OB candidates ( $13 < g < 19$ ) were taken using 2dF on AAOmega in service mode during June and July 2014. Fig. 4.1 shows the positions of the 276 OB candidates coloured by their photometrically determined extinctions, overlaid on the VPHAS+ H $\alpha$  image. The triangular points are candidate O stars and the circular points are candidate B stars. The large black circle shows the AAOmega 2df field of view centred on RA 10 28 45.25 DEC -58 25 56.12 (J2000). The field of view overlaps with the two square degrees studied in Chapter 3. Westerlund 2 is situated in the top right of the image. All candidates are the product of the same selection and SED fitting procedure that was described in the previous chapter.

The 580V and 1700D gratings were used, covering the wavelength range  $\sim 3000 - 6000\text{\AA}$  at a resolution of  $R=1300$  and  $\sim 8450 - 9000\text{\AA}$  at a resolution of  $R=10000$  respectively. We used a 0.5 arcsecond slit and dedicated sky fibres. The data were extracted and reduced to one-dimensional form using the 2dFdr software package with default settings; the wavelength calibration was obtained using a third order polynomial fit. The spectra have a mean signal to noise ratio (S/N) of 37 as measured in the wavelength range  $4560 - 4650\text{\AA}$ . Due to the large magnitude range of the candidates the observations were split in two configurations; a faint set-up and a bright set-up. This was done to avoid saturation of the brighter objects by permitting reduced

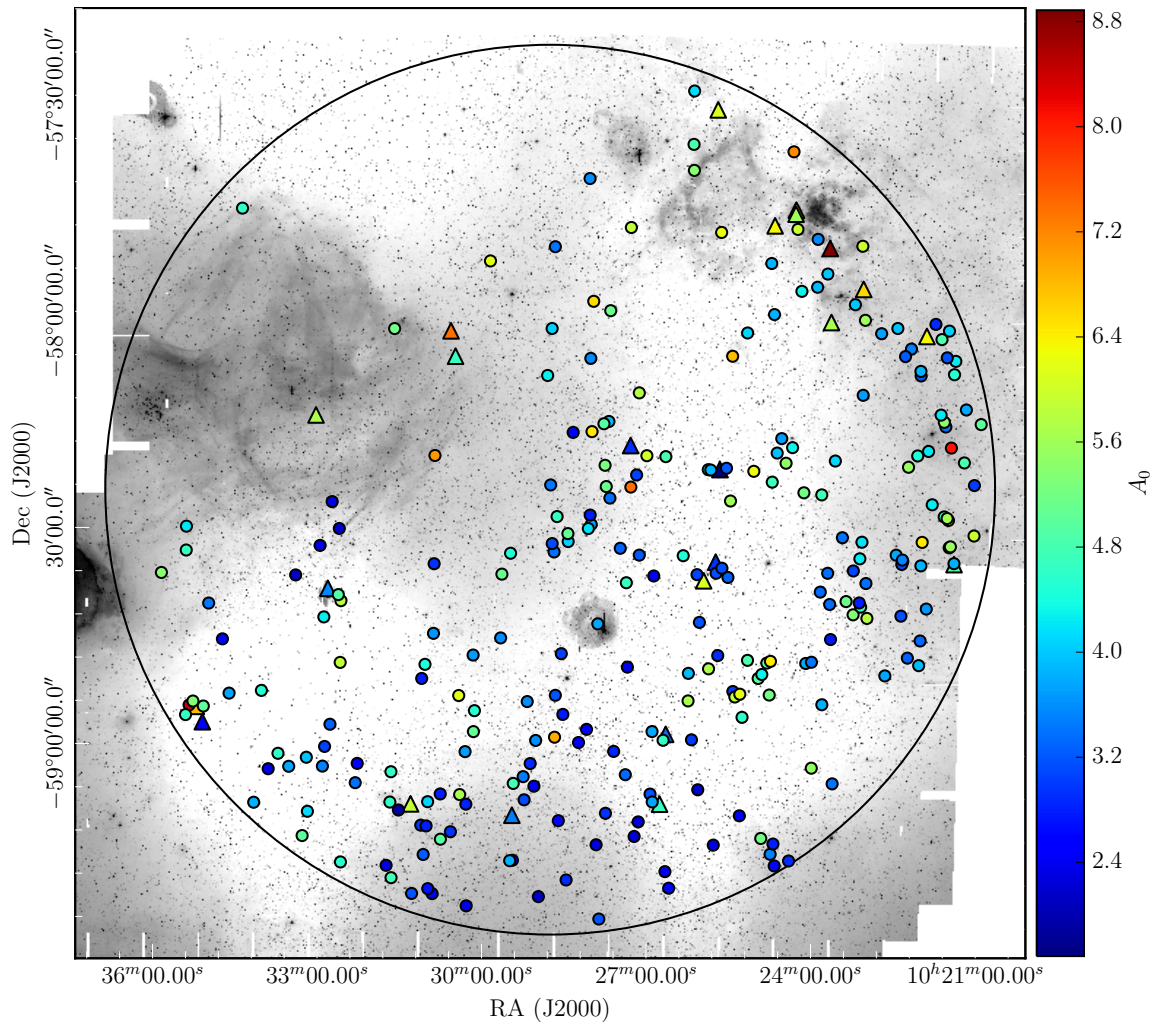


**Figure 4.1:** Positions of the 276 OB candidates coloured by their photometrically determined extinction. Triangles are candidate O stars and circles are candidate B stars. The large black circle represents the AAOmega 2dF field of view.

exposure times compared to those needed for the fainter targets. The faint set-up included objects in the magnitude range  $16 \leq g < 19$  and had a total exposure time of 140 minutes. The bright set-up included objects in the magnitude range  $13 \leq g < 16$  and had a total exposure time of 40 minutes.

Each spectrum was continuum fitted and normalized using a spline fit in the PYRAF package ONEDSPEC. Before further analysis the prominent diffuse interstellar bands (DIBs) at  $\lambda \simeq 4430, 4892, 4748$  and  $5362\text{\AA}$  were cut out.

## 4.2 Broad classification of the spectra

The ‘blue’ and ‘red’ part of each spectrum was visually inspected in order to categorise the objects into spectral types. Of the 276 candidates observed, using the spectral features listed below, we found that the spectral classes break down as follows:

- 196 B stars (HeI absorption)
- 29 O stars (HeI & HeII absorption)
- 27 CBe stars (double peaked Paschen &  $H\beta$  emission & HeI absorption)
- 22 A/F/G stars (calcium triplet absorption, G-band)
- 2 WR stars (previously known)

Including the more exotic CBe and WR stars as our massive star targets, we find contamination from just a handful of lower mass A, F and G type stars. Closer inspection revealed that all of the A/F/G stars had photometry that was likely affected by blending, a very bright neighbouring star or being on the edge of a detector, leading to bad photometry in one or more bands. This unreliable photometry pushed these later type objects into the OB star region on the  $(u - g, g - r)$  colour-colour diagram and hence contaminated our selection.

Fig. 4.2 shows the distribution of spectral classes for the selection. The distribution in red is for those objects that have unacceptable  $\chi^2 > 7.82$  photometric SED fits.

Here we can see that the majority of A/F/G star contaminants have poor photometric fits to main-sequence OB star SEDs because of their contaminated photometry. For small numbers of objects it is quite easy to remove these from the selection process by visually inspecting thumbnails of each star. However, when the numbers grow this becomes increasingly less practical and the benefit becomes less obvious given the small percentage of contaminants. The SED fitting procedure reduces the contamination rate from 8.0% to just 6.3% when making a cut at  $\chi^2 < 7.82$ .

We also note that around 70% of the CBe stars are found to have poor  $\chi^2$  values. Although the OnIR SEDs of classical Be stars are not greatly different from normal B stars of similar effective temperature, the presence of a warm circumstellar disk can affect the NIR colours. It is in fact easy to separate CBe stars from the rest of the population through detection of line emission via the VPHAS+ narrow band H $\alpha$  filter (see section 5.1.2). Both of the previously known WR stars have similar colours to MS OB stars in the optical and are hence in our selection, but they do not fit well to MS OB star OnIR SEDs because of a NIR excess due to their dense stellar winds (Faherty et al., 2014). Visual inspection of the OB stars with poor fits suggests that most of them are likely affected by blending in the NIR photometry. At these longer wavelengths blending will be more common due to the higher stellar density and lower spatial resolution of 2MASS.

### 4.3 Model atmosphere fitting

Each OB star spectrum covering the wavelength range  $\sim 3000 - 6000\text{\AA}$  (225 stars in total) was fitted to a grid of model spectra in order to derive effective temperatures for comparison to our photometric estimates. The method used for the O stars was different from that applied to the B stars in order to adapt to different model grids, supplied in different forms. For the B stars the TLUSTY NLTE grid (Lanz & Hubeny, 2007) was used and the more appropriate NLTE FASTWIND grid was used for the O stars where LTE is known to misrepresent these hot more non-locally coupled atmospheres. As the full spectrum was supplied in the TLUSTY grid the entire spectrum

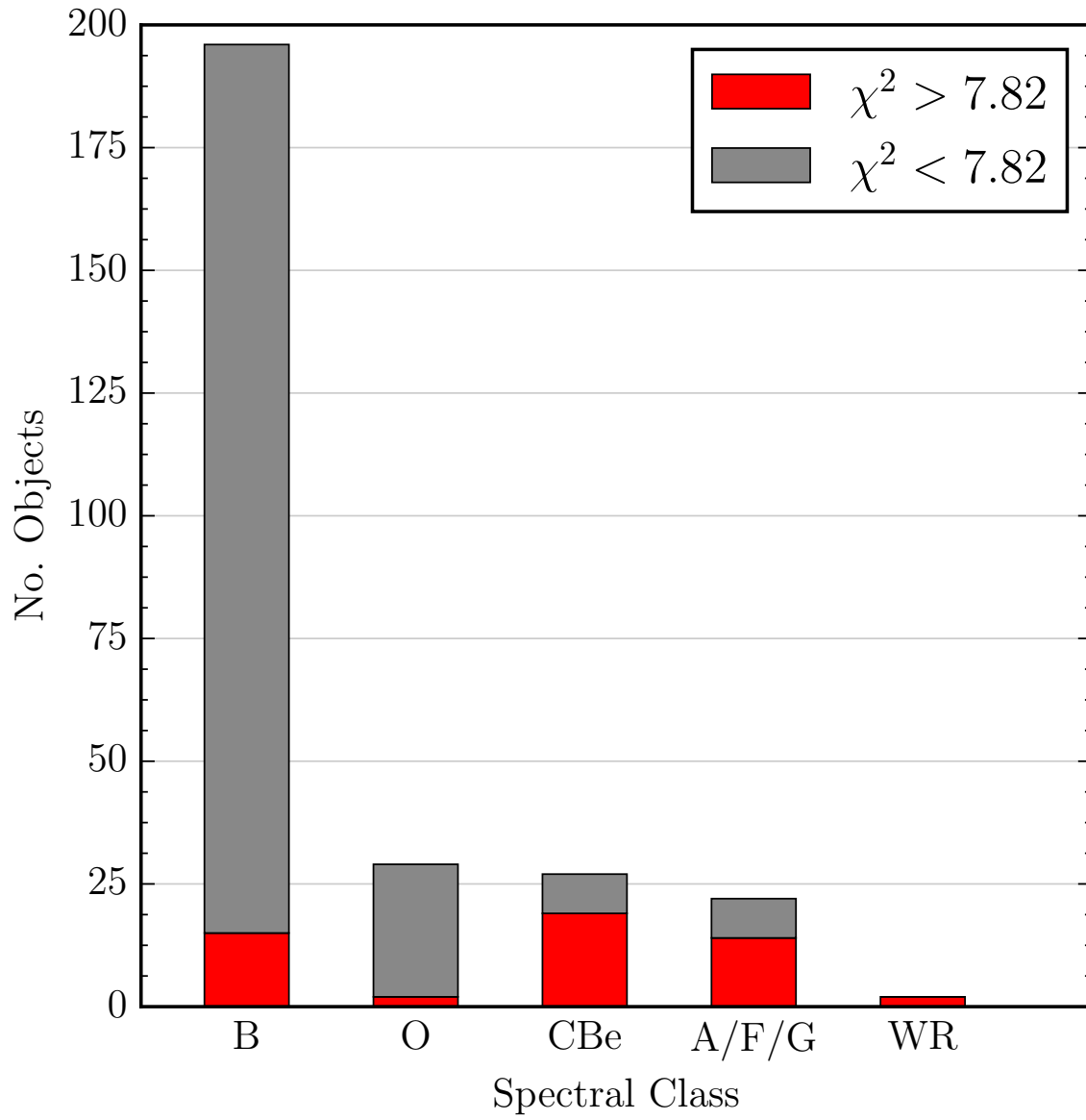


Figure 4.2: Distribution of spectral classes found for sample of stars with AAOmega spectra.

was used in the fitting procedure. The FASTWIND grid contains just the Hydrogen and Helium lines needed to determine effective temperatures and therefore only these lines were used in the fitting procedure. Solar metallicity was adopted in both cases. Since this sight line samples only a restricted range of Galactic radii ( $\sim 7 - 10$  kpc) this is a reasonable approximation.

### 4.3.1 B star model fitting

We begin with a set of TLUSTY model spectra which are parametrised in terms of just effective temperature and surface gravity. Each spectrum in the grid was rotationally broadened ( $v \sin i$ ) to a range of velocities and convolved to match the resolution of the instrument using the PYTHON package PYASTRONOMY. The grid was then linearly interpolated to form a continuous set of models for MCMC sampling, growing the parameter set to three:

$$\theta = \{T_{\text{eff}}, \log(g), v \sin i\} \quad (4.1)$$

The best fit parameters were derived using MCMC sampling with a  $\chi^2$  likelihood function akin to that used in the photometric fits:

$$P(SPEC_{obs} | \theta) \propto \exp\left(-\frac{1}{2} \sum_i^n \frac{(f(obs)_i - f(mod)_i)^2}{\sigma_i^2}\right) \quad (4.2)$$

where  $P(SPEC_{obs} | \theta)$  is the probability of obtaining the observed spectrum ( $SPEC_{obs}$ ) given a set of parameters  $\theta$  and  $f(obs)_i$  and  $f(mod)_i$  as the observed and model normalized flux at each wavelength  $i$ .

We compare the observed spectra to a grid of parametrised TLUSTY models using uniform priors:

$$P(\theta) = \begin{cases} 1 & \text{if } \begin{cases} 15kK \leq T_{\text{eff}} \leq 30kK \\ 1.75 \leq \log(g) \leq 4.75 \\ 0kms^{-1} \leq vsini \leq 600kms^{-1} \end{cases} \\ 0 & \text{else} \end{cases} \quad (4.3)$$

The boundaries of the priors are defined by the limits of the model grid.

### 4.3.2 O star model fitting

We begin with a set of FASTWIND models that consist of the following line profiles: H $\delta$ , HeII 4200, H $\gamma$ , HeI 4387, HeI 4471, HeII 4541, HeII 4686, HeI 4713, H $\beta$  and HeII 5411.

The models are parametrised by the following:

- $T_{\text{eff}}$  (effective temperature)
- $\log(g)$  (surface gravity)
- $Y_{\text{He}}$  (helium abundance)
- $\xi_t$  (micro turbulence)
- $Q$  (mass loss rate)
- $\beta$  (exponent of wind velocity)
- $vsini$  (rotational velocity)
- $RV$  (heliocentric radial velocity)

In this case each line profile was fit independently using the same style of likelihood function as Eqn. 4.2. The overall function is the product of probabilities for all line profiles:

$$P(SPEC_{obs} | \theta) \propto \prod_j^n P(LP_{obs(j)} | \theta) \quad (4.4)$$

Where  $P(SPEC_{obs} | \theta)$  is the probability of obtaining the observed spectrum ( $SPEC_{obs}$ ) given a set of parameters  $\theta$  and where  $P(LP_{obs(j)} | \theta)$  is the probability of obtaining the observed line profile,  $LP_{obs(j)}$ , given a set of parameters  $\theta$ .

The parameters  $\xi_t$  and  $\beta$  were fixed at  $5 \text{ km s}^{-1}$  and 0.8 respectively as our spectra are too low resolution to detect any tangible change in these parameters. As for the B stars, each spectrum in the grid was rotationally broadened ( $v \sin i$ ) with a range of velocities and convolved to match the resolution of the instrument. This leaves us with 6 free parameters:

$$\theta = \{T_{\text{eff}}, \log(g), v \sin i, RV, \log(Q), YHe\} \quad (4.5)$$

The uniform grid was linearly interpolated to form a continuous grid for MCMC sampling. The following uniform priors for each parameter were adopted and are defined by the limits of the model grid:

$$P(\theta) = \begin{cases} 1 & \text{if } \begin{cases} 25kK \leq T_{\text{eff}} \leq 55kK \\ 3.0 \leq \log(g) \leq 4.4 \\ 50kms^{-1} \leq v \sin i \leq 400kms^{-1} \\ -400kms^{-1} \leq RV \leq 400kms^{-1} \\ -14 \leq \log(Q) \leq -12.5 \\ 0.06 \leq YHe \leq 0.17 \end{cases} \\ 0 & \text{else} \end{cases} \quad (4.6)$$

The key constraint expected from these fits is to obtain effective temperatures. There is also useful information to be found in the derived surface gravities and rotational velocities. Given the low resolution nature of the spectra we will be treating the

other parameters as ‘nuisance parameters’ as the derived values are unreliable, have large uncertainties and are not relevant to this discussion. However, their influence on the other parameters is, by default, taken into account when using the marginalised posterior probability distributions. It is noted that we also fitted the O stars to O star NLTE TLUSTY models (Lanz & Hubeny, 2003) using the same method as for the B stars and found little difference in the average derived temperatures and surface gravities when comparing the two models. There was however a tendency for the NLTE models to over-estimate the derived temperature of the hottest O stars by up to  $\sim 5000\text{K}$ .

## 4.4 Results

The median of the posterior probability distributions for each parameter is taken as the best fit value. The 16<sup>th</sup> and 84<sup>th</sup> percentiles are taken as the upper and lower uncertainty on each parameter. Fig. 4.3 shows sample spectra after normalisation and excision of DIBs over-plotted on the best fit model. The top panel is an O star with  $g = 15.5$  and  $S/N = 25$  and the bottom panel is a B star with  $g = 17.2$  and  $S/N = 31$ .

Fig. 4.4 shows the distribution in  $T_{\text{eff}}$ ,  $\log(g)$  and  $v \sin i$  for the spectroscopic fits of OB stars. The distribution in  $T_{\text{eff}}$  peaks at around 20kK and falls off at higher temperatures. This is very similar to the distribution in the photometrically derived temperatures shown in Chapter 3. As expected the majority of stars show MS surface gravities with a median value of  $\sim 3.92$ . The three lowest surface gravity objects  $\log(g) \lesssim 3.2$  are likely evolved B stars. Their relatively cool temperatures ( $19\text{kK} < T_{\text{eff}} < 24\text{kK}$ ) and surface gravities suggest that these are likely to be luminosity class II bright giants (Schmidt-Kaler, 1982). Their over-luminous position in the  $(u - g, g)$  CMD also supports the notion that these are evolved objects (see section 5.1.1). One particular very hot O star (44kK) has also been selected as a subdwarf (ID 1558) using the technique outlined in section 5.1.1. As the FASTWIND grid did not allow values of  $\log(g)$  beyond 4.3 this object was hindered from standing out as a subdwarf:  $\log(g) = 4.2$  was assigned to it. However when this object was fit to the TLUSTY

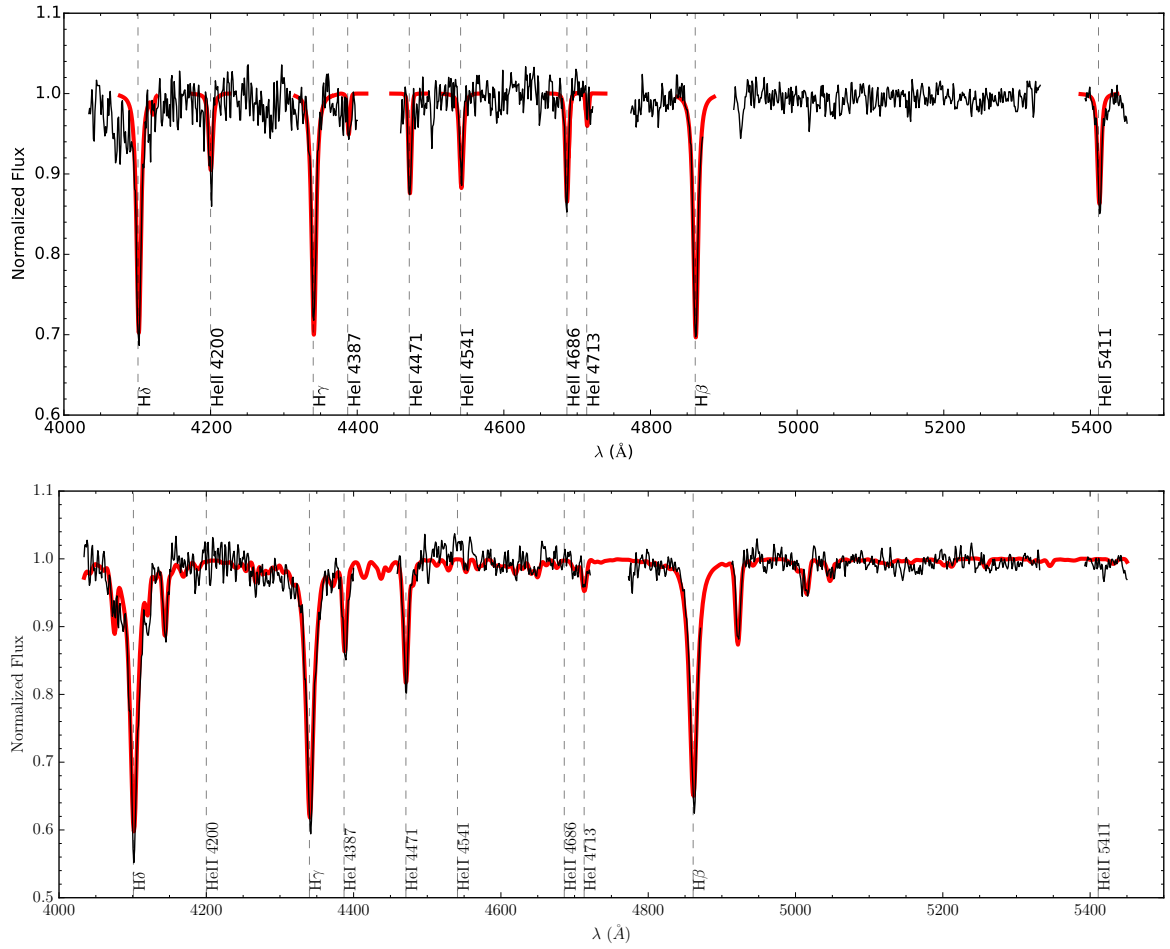


**Figure 4.3:** Example of spectra and best fit models. Top: ID #1374,  $g = 15.5$  mag,  $A_0 = 5.6$ ,  $T_{\text{eff}} = 38600$  K and  $\log(g) = 4.19$ . Bottom: ID #2593  $g = 17.2$  mag,  $A_0 = 4.5$ ,  $T_{\text{eff}} = 23100$  K and  $\log(g) = 4.32$

grid which allowed higher values of surface gravity, it preferred a much higher value of  $\log(g) = 4.7$  making this object an obvious sdO star. The distribution in projected rotational velocities ( $v \sin i$ ) peaks at  $\sim 100 \text{ kms}^{-1}$ , tailing off to a few stars with high  $v \sin i$  values of a few hundred  $\text{kms}^{-1}$  which is consistent with other literature values (see e.g. [Simón-Díaz & Herrero, 2007](#); [Daflon et al., 2007](#)). Due to a combination of spectral resolution and signal noise, the MCMC implied uncertainties on  $v \sin i$  are clearly optimistic. For  $v \sin i$  less than  $\sim 230 \text{ kms}^{-1}$  (i.e. below the velocity resolution in the spectra) there is an unknown systematic uncertainty, related to the instrumental profile that is not taken into account. Continuum choice will also have an impact that isn't measured. Increasingly, for  $v \sin i$  beyond  $\sim 230 \text{ kms}^{-1}$  the uncertainties will be more realistic but still underestimated. No reference objects were observed so it is not feasible to estimate these systematic effects. A table containing the spectroscopic parameters for all OB stars in the selection is shown in [Appendix B.1](#).

## 4.5 Comparison of the spectroscopic best-fit effective temperatures with photometric estimates

Figure [4.5](#) shows the effective temperatures determined from the photometric SED fits compared to those determined by spectroscopy. The red circles show objects with  $\chi^2 > 7.82$  in the SED fitting routine. We find that, despite our reservations about determining effective temperatures through photometry alone, there is a good correlation between the two methods. We do however see a systematic tendency to underestimate the temperature of O stars and over estimate those of the B stars in the photometric method when compared to the spectroscopy. As the photometric calibration appears to be well constrained, this is very likely to be due to inconsistencies between the photometric effective temperature scales in the Padova isochrones and the effective temperature scales adopted for the spectroscopy in TLUSTY and FASTWIND. Another factor that affects the extreme cases is photometric blending or contamination. For example the poor  $\chi^2$  object with the largest disagreement is close to a very red

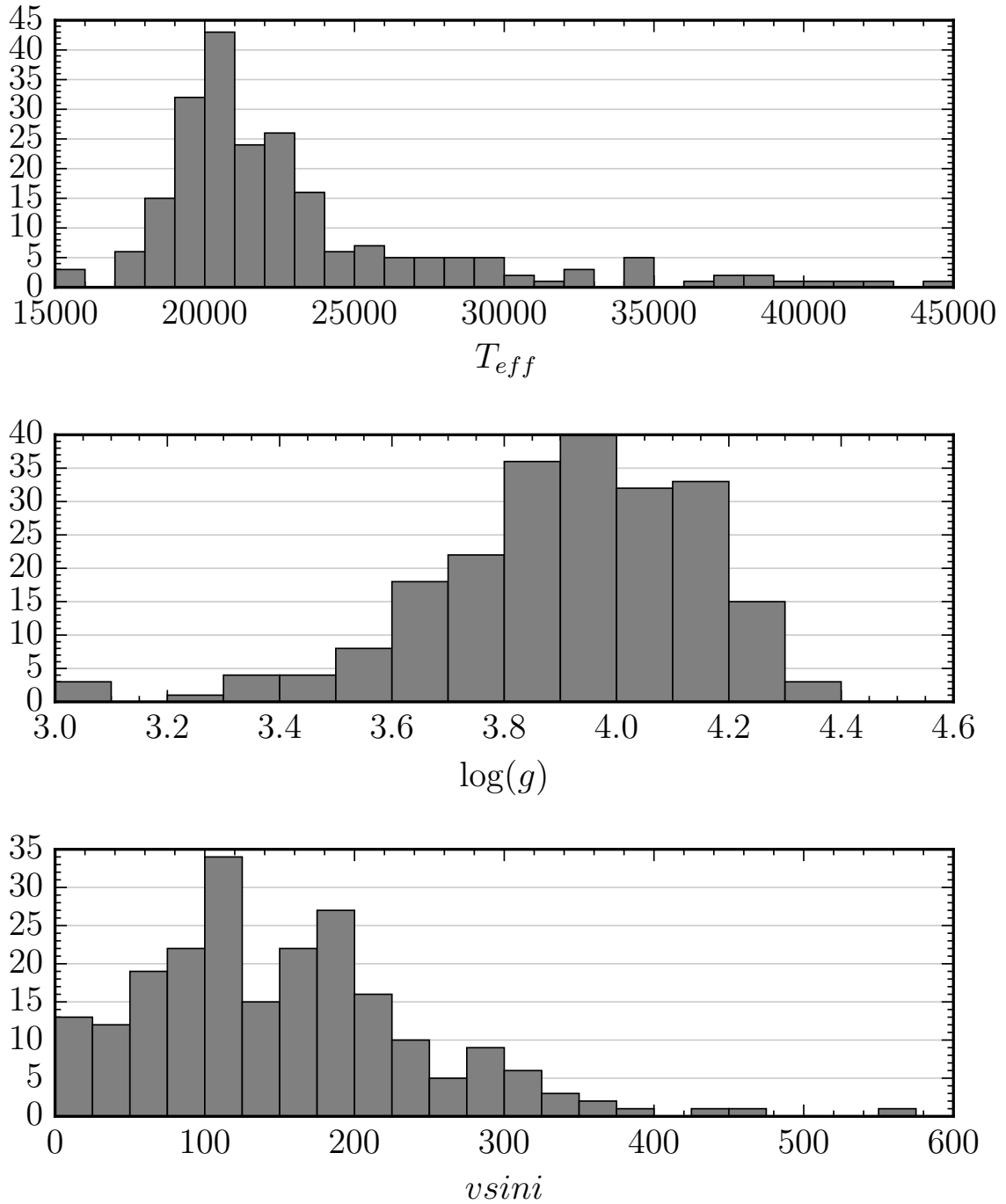


**Figure 4.4:** Distribution of effective temperature, surface gravity and projected rotation speeds for spectroscopic fits.

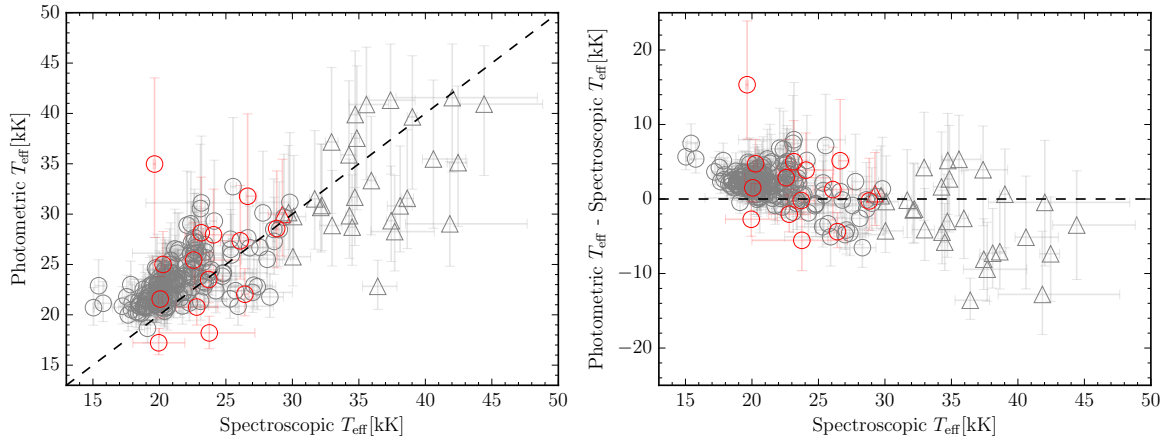


**Figure 4.5:** Comparison of the derived effective temperature from the photometric SED fitting with those derived from spectroscopy. The triangles are O stars and the circles are B stars. Symbols coloured in red had photometric SED fits with  $\chi^2 > 7.82$ .

object which is likely affecting the measured magnitudes, particularly in 2MASS.

With the extra information on temperature provided by the spectroscopic fits, we can check what effect the systematic offset in the photometrically derived  $\log(T_{\text{eff}})$  has on the derived reddening parameters. To do this we re-calculated the SED fits using a much narrower uniform prior on temperature, based on the 16th and 84th percentiles of the marginalized posterior distribution of spectroscopic temperature for each star (as indicated by the horizontal error bars in Fig. 4.5 & Fig. 4.6). Fig. 4.6 shows the impact on the derived values of  $A_0$  and  $R_V$  when the more precise ‘restricted’ temperature prior is used in place of almost no constraint in the SED fitting. Here we can see that for both reddening parameters that restricting  $\log(T_{\text{eff}})$  has a greater effect on stars below  $\sim 25\text{kK}$ . This is due to the higher sensitivity in the shape of the SED as a function of temperature for the cooler stars. At temperatures greater than this, the SEDs begin to approximate the RJ tail and sensitivity to temperature is greatly reduced, such that the shape of the SED is almost entirely dominated by extinction.

It is noted that these systematic effects are very small; for stars with  $T_{\text{eff}} \geq 25\text{kK}$  the median difference in  $A_0$  and  $R_V$  (‘free’ - ‘restricted’) is -0.025 and 0.026 and for those with  $T_{\text{eff}} < 25\text{kK}$  the median difference is 0.09 and -0.07 respectively. In the worst cases these systematic uncertainties are comparable to the random uncertainties on the parameters due to the photometric errors. However, if there is a true disagreement between the photometric and spectroscopic effective temperature scales, we could

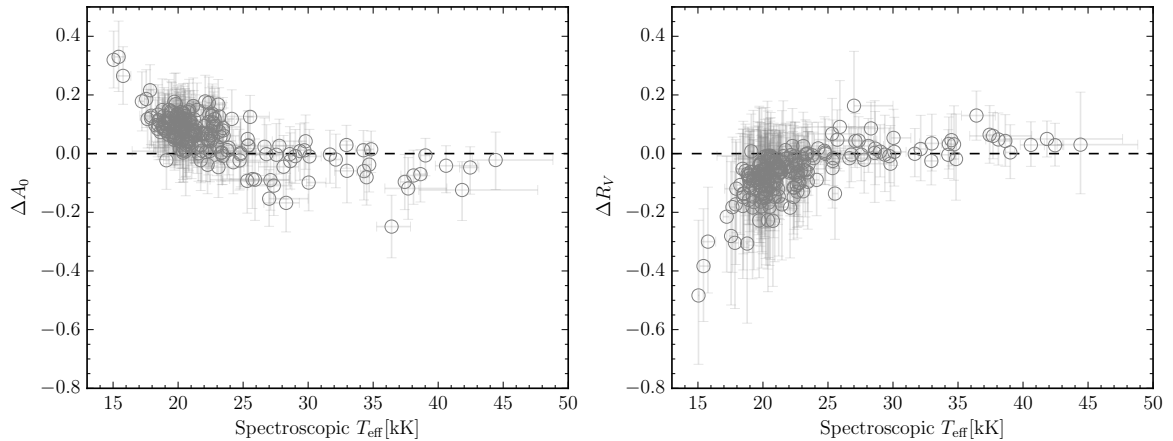


**Figure 4.6:** Change in derived reddening parameters when using a temperature prior defined by the spectroscopic fits (free - fixed).

be forcing photometric fits to systematically ‘incorrect’ SED models by restricting the temperature prior. This idea is supported by systematically poorer fits in the ‘restricted’ case where the median  $\chi^2 = 2.99$  compared to  $\chi^2 = 1.58$  in the ‘free’ case. Putting this another way, regarding the spectroscopic temperature scale as definitive, the photometric SED fits appear to provide precise and reliable extinction parameters, albeit at the cost of a small systematic bias in effective temperature estimation at the present time.

---

# CHAPTER 5: CARINA REGION

---

In this chapter the techniques for selecting and parametrising the OB stars in the Wd 2 test case are utilised over a much wider area on the sky made up of 42 VPHAS+ fields covering over 42 square degrees of the Carina Arm. The footprint of the area on the sky is shown in Fig. 5.1. It is roughly centred on the Carina Nebula ( $\ell = 287.62, b = -0.65$ ) and spans twelve degrees in Galactic longitude and covers up to  $+2^\circ$  and down to  $-3^\circ$  in latitude. The footprint encloses the fields studied in Chapter 3 and those with spectroscopy in Chapter 4 as shown by the large rectangle and circle respectively on the right hand side of the plot.

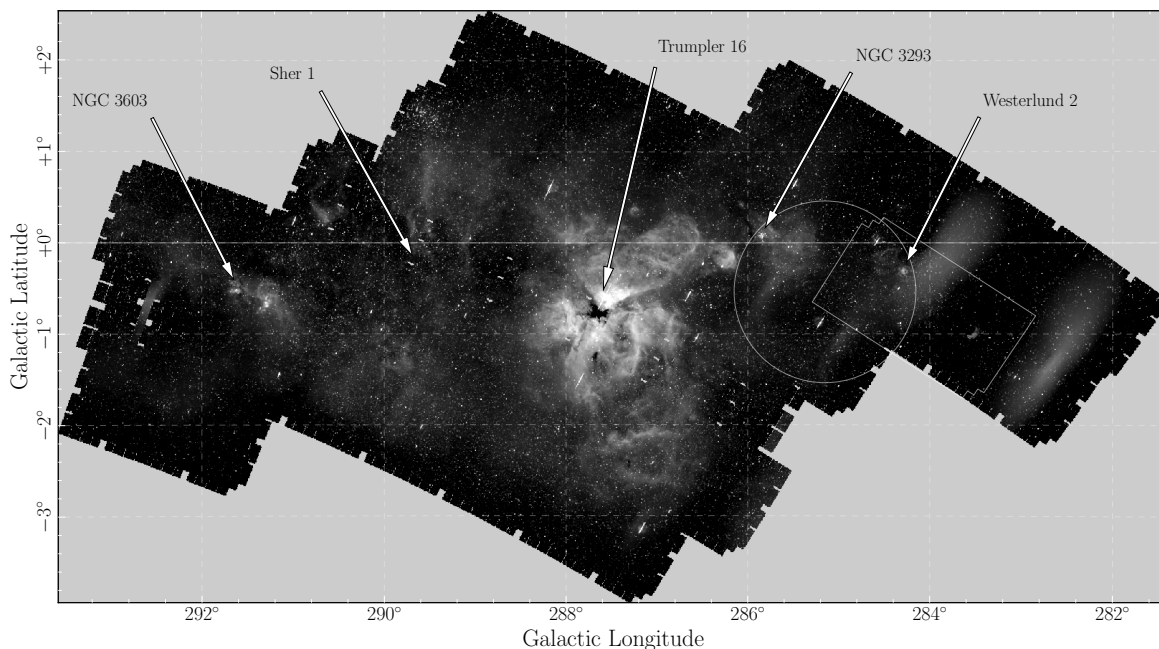


**Figure 5.1:** VPHAS+  $H\alpha$  image showing the footprint of the 42 square degrees in Carina that are studied here. The positions of major OB star clusters are labelled. The white rectangle shows the area studied in Chapter 3 (Mohr-Smith et al., 2015) and the circle shows the area studied in Chapter 4. The two large bright smudges in the far right of the image are due to uncorrected scattered light.

## 5.1 Results of the photometric selection

The selection criteria are unchanged from Chapter 3. Table 5.1 shows the breakdown of the number of OB candidates according to effective temperature and fit quality. In total 14900 OB stars were selected for SED fitting. Around a quarter of the candidates were found to have poor,  $\chi^2 > 7.82$ , SED fits. Of those objects which have acceptable

SED fits, just under half are probable later type B stars with  $\log(T_{\text{eff}}) < 4.3$ . There are 5915 objects in our target effective temperature range,  $\log(T_{\text{eff}}) \geq 4.30$  with acceptable fits. Of these, 905 are probable O stars with  $\log(T_{\text{eff}}) \geq 4.477$ . There are thus around five times as many B2–B0 star candidates as O star candidates.

All candidates were cross matched with SIMBAD to within an acceptance radius of 1 arcsec in order to check if any objects with already known spectral type are selected. Table 5.2 shows a breakdown of the number of selected OB candidates with spectroscopically confirmed types according to SIMBAD and those with spectroscopically confirmed types from AAOmega in Chapter 4, grouped according to effective temperature and fit quality. The majority of objects with known spectral type from SIMBAD were found to be OB and WR stars as expected. There is however contamination from a handful of M giant stars and one carbon star (C\*) in the poor fit,  $\chi^2 > 7.82$ , group that were originally selected. These objects were incorrectly selected as very highly reddened OB stars in the  $(u-g, g-r)$  diagram but nevertheless they are easily removed from the selection using the  $r-i$  colour as discussed in Section 5.1.2. A very positive feature of Table 5.1 is the high success rate in placing stars correctly into the O and B spectral types.

Fig. 5.2 shows the distributions of parameters for all objects with acceptable ( $\chi^2 < 7.82$ ) SED fits. Objects with  $\log(T_{\text{eff}}) \geq 4.30$  (2 s.f) are coloured grey. Similar to the test case in Chapter 3, the entire region shows enhanced values of  $R_V$  with a median value of 3.74. The majority of the candidates have best-fit extinctions in the range ( $4 < A_0 < 6$ ) at likely distances of 3 - 10 kpc. The spatial distribution of the accepted OB stars is shown in Fig. 5.3. The candidate B stars are the red open circles while the candidate O stars are the blue open triangles. Fig. 5.4 shows the distribution in Galactic latitude and longitude of candidate O (blue line) and B (red line) stars. Here it can be seen that the distribution peaks below the  $b = 0$  Galactic equator. This appearance may be linked to the onset of the warping of the Galactic Plane as described by Russeil (2003), Levine et al. (2006) and others. It is also to be expected, to an extent, simply because the Sun is believed to be above the true Galactic equatorial plane (see Goodman et al., 2014). This point will be taken up

**Table 5.1:** Breakdown of the number of OB candidates according to effective temperature and fit quality.

	$\chi^2 \leq 7.82$	$\chi^2 > 7.82$
O Stars: $\log(T_{\text{eff}}) \geq 4.477$	905	1090
B2 - B0: $4.3 \leq \log(T_{\text{eff}}) < 4.477$	5010	1039
Late B: $\log(T_{\text{eff}}) < 4.3$	5170	1686
All $\log(T_{\text{eff}})$	11085	3815

**Table 5.2:** Breakdown of the number of selected OB candidates with spectroscopically confirmed types according to SIMBAD and those with spectroscopically confirmed types from AAOmega in Chapter 4

	$\chi^2 \leq 7.82$	$\chi^2 > 7.82$
<b><math>\log(T_{\text{eff}}) \geq 4.477</math></b>		
AAOmega Confirmed O	18	0
Confirmed B	5	2
Other	3 A/F/G	9 A/F/G
SIMBAD Confirmed O	23	7
Confirmed B	3	4
Other	2 WR	3 WR & 7M
<b><math>4.3 \leq \log(T_{\text{eff}}) &lt; 4.477</math></b>		
AAOmega Confirmed O	10	1
Confirmed B	174	10
Other	6 A/F/G	2 A/F/G
SIMBAD Confirmed O	4	2
Confirmed B	18	15
Other	1WR	13 WR & 1 M & 1 C*
<b><math>\log(T_{\text{eff}}) &lt; 4.3</math></b>		
AAOmega Confirmed O	0	0
Confirmed B	3	2
Other	0	2 A/F/G
SIMBAD Confirmed O	0	0
Confirmed B	6	1
Other	0	10 WR & 1 M

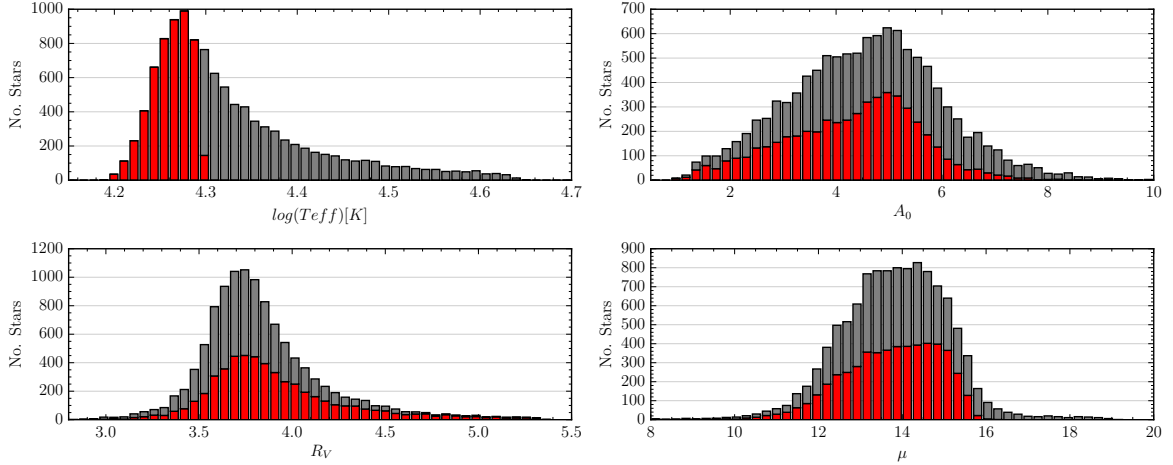


**Figure 5.2:** Distribution of the best fit parameters for the selection of objects with  $\chi^2 < 7.82$ . Objects with  $\log(T_{\text{eff}}) > 4.3$  (2 s.f) are coloured in grey. The remaining cooler objects are coloured red.

again in section 5.2.3. This plot also shows that the number of detected OB candidates decreases with lower Galactic longitude. This effect is likely due to the presence of the Carina Arm tangent at these lower longitudes, where the extinction builds up more quickly with distance (see Fig. 1.5, e.g. Grabelsky et al., 1987; Dame et al., 2001; Dame, 2007). This prevents us from probing so deeply into the Galactic plane and therefore we are sampling a smaller volume, that yields fewer objects. This is also discussed in more detail in Section 5.2.2.

Fig. 5.5 shows the distribution of  $g$  band magnitudes and  $g - K$  colours of all candidates with acceptable SED fits in the target temperature range. Here, we can see that there is a sharp upturn in the number of stars at  $g \sim 20$ . This effect can be attributed to the growing number of sub-luminous objects at these faint magnitudes as discussed in detail in Section 5.1.1. In effect, at the faint end of the distribution, we are seeing the merging of two separate distributions; one for the massive OB stars and one for the sdO and sdB stars. The fact that the magnitude range of the  $g$  and  $K$  band only overlaps between  $13 \lesssim m \lesssim 15$  prevents us from detecting a greater number of intrinsically fainter and less reddened hot stars with lower  $g - K$ . As we are targeting intrinsically bright massive OB stars, rather than sdO and sdB stars, this is not detrimental to the selection. If the faint limit of the selection criterion in the  $g$  band was increased to say, 21 mags, we would be more sensitive to highly-reddened

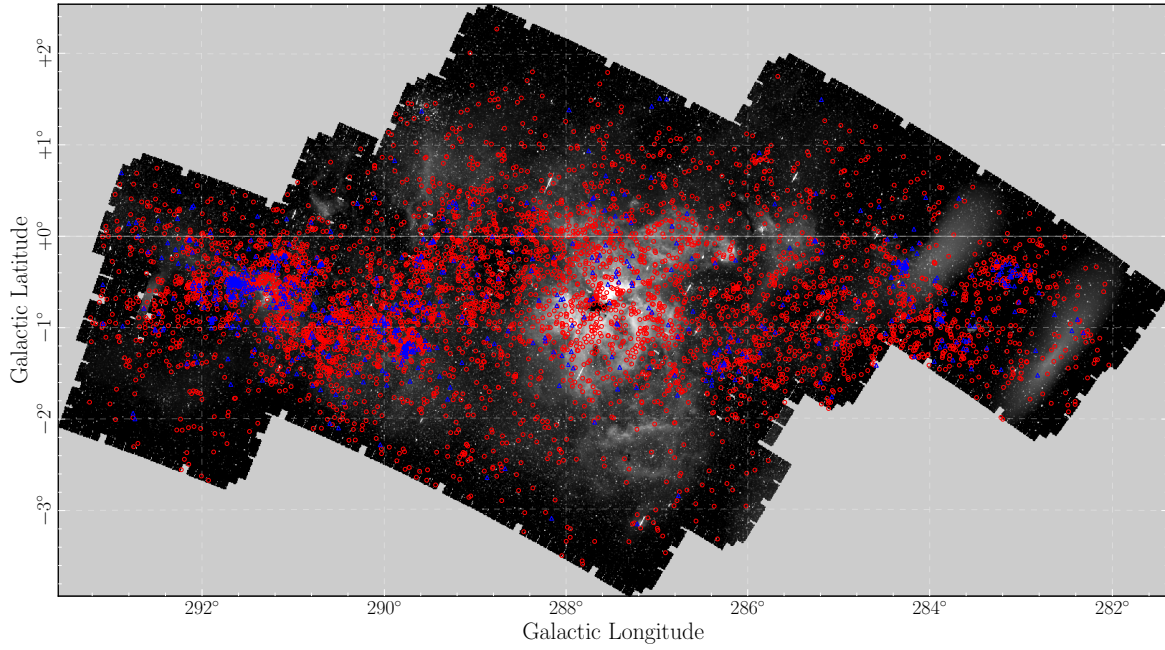


**Figure 5.3:** Distribution of O and early B star candidates across the 42 square degree region overplotted on the VPHAS+  $H\alpha$  mosaic. Red circles are candidate B stars and blue triangles are candidate O stars

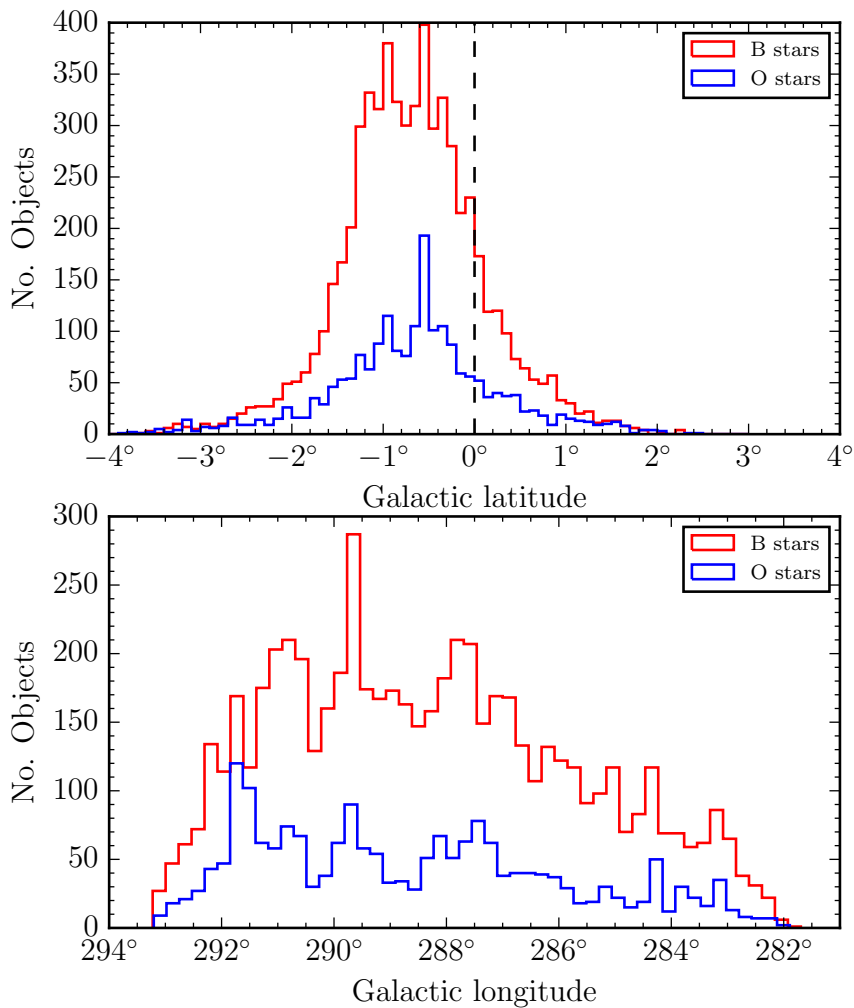


**Figure 5.4:** Distribution in Galactic latitude and longitude of O and early B star candidates. The dashed marks  $b = 0$ .

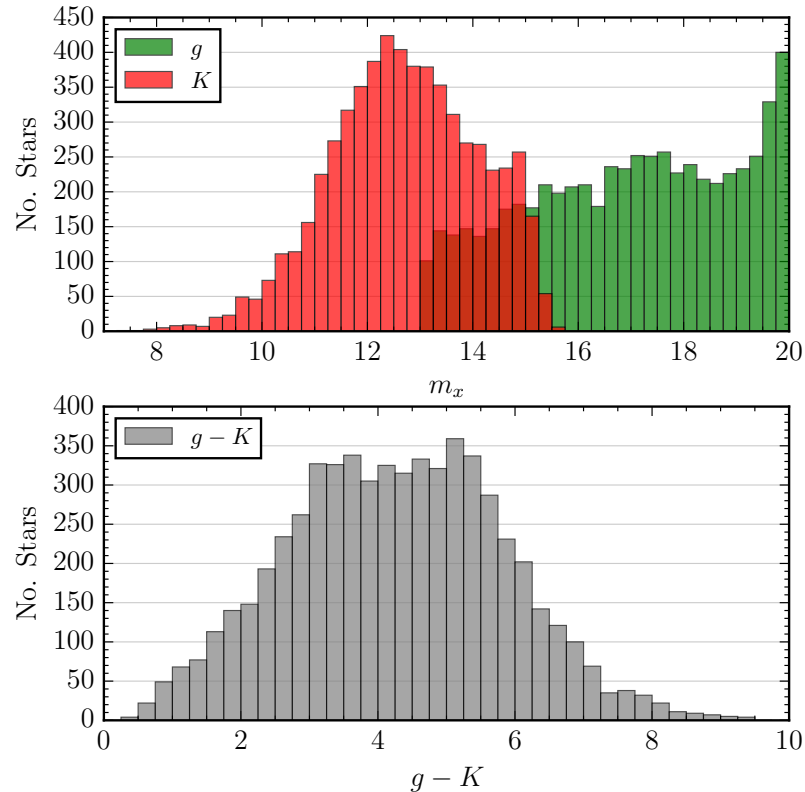


**Figure 5.5:** Top panel:  $g$  and  $K$  band magnitude distribution of  $\chi^2 < 7.82$   $\log(T_{\text{eff}}) > 4.295$  objects. Bottom panel:  $g - K$  distribution.

OB stars with extreme  $g - K$  colours. However, any  $u$  band information will likely be lost, at such high extinctions, beyond the  $u \sim 21$  faint limit of VPHAS+. A sample table, containing all O star candidates with  $\log(T_{\text{eff}}) > 4.477$  and  $\chi^2 < 7.82$ , is shown in the Appendix C.1.

### 5.1.1 Subdwarfs and Over-luminous Stars

Due to the large numbers of objects in this selection it becomes more difficult to separate the sub-luminous and over-luminous stars in the same manner as Chapter 3. This is because the different luminosity groups drawn from a much wider sky area start to become blended in the  $\mu$  vs  $A_0$  and  $\mu$  vs  $\log(T_{\text{eff}})$  diagrams used in the selection. Here, a different technique is necessary.

We can separate sub-luminous and over-luminous stars from our MS OB star targets by primarily using the colour-magnitude diagram (CMD). In the  $(u - g, g)$  CMD the sub-luminous and over-luminous stars will, for a given temperature and distance, form

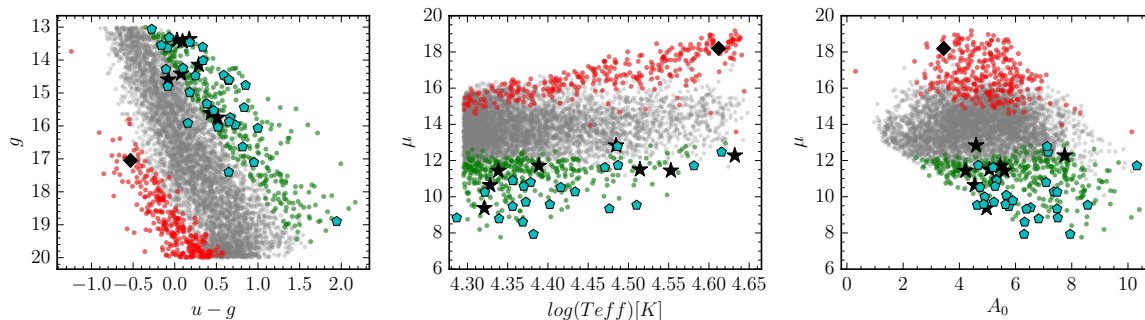


**Figure 5.6:** Objects coloured in red are likely sub-luminous compared to the rest of the population. Objects coloured in green are likely over-luminous when compared to the rest of the population. The black diamond is a known SdO star while the black stars are the low surface gravity objects from Chapter 4. The cyan pentagons are known WR stars and the black star symbols are luminosity class I and II OB stars.

separate sequences below and above the main sequence. As we are looking at a range of distances these sequences become somewhat blended. The aim here is to make a crude cut to pick out probable sub-dwarfs and bright supergiants that stand out from the rest of the population.

In order to perform the selection we first take all objects with acceptable  $\chi^2 < 7.82$  fits and bin the data into deciles in effective temperature. For each bin we then take the lowest effective temperature and the reddening vector corresponding to it, and place the vector at the 95<sup>th</sup> percentile in distance modulus (based on all temperatures) on the  $(u - g, g)$  CMD. All stars fainter than this line are selected as sub-luminous (see Fig. 5.6): they are statistically fainter than the coolest and most distant MS stars in their temperature bin. We also take the highest temperature in each bin and place it at the 5<sup>th</sup> percentile in distance modulus on the  $(u - g, g)$  CMD. All stars brighter than this line are selected as over-luminous: they are statistically brighter than the hottest and closest MS stars in their temperature bin.

Figure 5.6 shows the CMD,  $(\log(T_{\text{eff}}) \text{ vs } \mu)$  and  $(A_0 \text{ vs } \mu)$  with likely MS stars in grey and the selected sub-luminous and over-luminous stars in red and green respectively. The black diamond is the spectroscopically confirmed SdO star which is appropriately selected as under-luminous. The black star symbols are the lowest surface gravity stars with spectra discussed in Chapter 4 along with the luminosity class I and II objects from SIMBAD. The cyan pentagons are known WR stars from SIMBAD. These evolved objects reassuringly tend to co-locate in the diagram with the over-luminous candidates.

It is to be noted that objects with poor  $\chi^2 > 7.82$  SED fits are not part of the over-and-under-luminous selection. This includes most of the WR stars as well as four of the luminosity class I and II objects. Here we can see that separating the under-luminous and over-luminous stars on the CMD also creates a relatively clean selection in the two derived parameter diagrams.

As we have performed SED fits with a MS assumption the under-luminous objects appear as very distant objects with relatively low reddening. The absolute magnitudes of SdO stars range from  $M_V = 3 - 6$  (Stark & Wade, 2003). Since these objects are  $\sim 6$  mag fainter than MS OB stars for a given temperature, their distance moduli are likely to be  $\sim 10 - 12$  as opposed to the SED-fit values of  $\sim 16 - 18$ . This suggests that we are looking at a group of moderately reddened  $A_0 \sim 4 - 5$  stars in the foreground of the main massive OB population. We are biased to select more highly reddened subdwarf stars due to the 2MASS faint limit as noted before in Section 5.1. If this limit was not in place we would expect to find further more lowly reddened sdB stars in the selection.

Conversely the over-luminous objects appear as close-by with relatively high reddening. If these objects are, for example, blue supergiants their absolute visual magnitudes would be around  $\sim -6.5$  (Crowther et al., 2006). If the main-sequence assumption is replaced, we find their derived distance moduli,  $\mu$ , would rise from  $\sim 10$  to  $\sim 14$ , placing them amongst the general OB population.

While this luminosity discrimination isn't perfect it gives an idea of the frequency of these outliers. There will be some over- and under-luminous objects which we cannot distinguish from the MS population and indeed objects falsely labelled as probably under- or over-luminous objects. For example we can see that the distribution in distance blends into the main distribution for the lower temperature sub-luminous objects.

In total 299 objects are tagged as likely to be under-luminous while 344 are tagged over-luminous. This equates to around 5% of the whole sample going into each category, a proportion that is a direct consequence of the distance modulus percentile chosen (95<sup>th</sup> for over-luminous and 5<sup>th</sup> for the sub-luminous) to select these objects on the

CMD. This cut was chosen by visual inspection of the CMD, noting roughly where the sequences separate. [Meylan & Maeder \(1983\)](#) estimate a surface density of 10 - 20 blue supergiants (BSGs) per  $\text{kpc}^2$  in the Galactic Plane. Taking our distance range as 3 - 10 kpc we are sampling a projected disk surface area of a little over  $9 \text{ kpc}^2$ . This suggests that our selection of 344 over-luminous stars is too generous by a factor of two or more. [Han et al. \(2003\)](#) suggests a space density of sdB stars of  $2 - 4 \times 10^{-6} \text{ pc}^{-3}$ . Assuming that we are detecting sdB stars at distances between 1 to 2.5 kpc then we are sampling a volume of around  $\sim 0.06 \text{ kpc}^3$  which predicts around  $\sim 180$  sdB stars. Again this suggests a somewhat over-enthusiastic selection of 344 possible sub-luminous stars. The fact that these selections are generous, suggests that the remaining population is likely to be a relatively clean selection of near main-sequence OB stars. The candidate stars selected as over- and under-luminous are marked as such in [Table C.1](#) in the appendix.

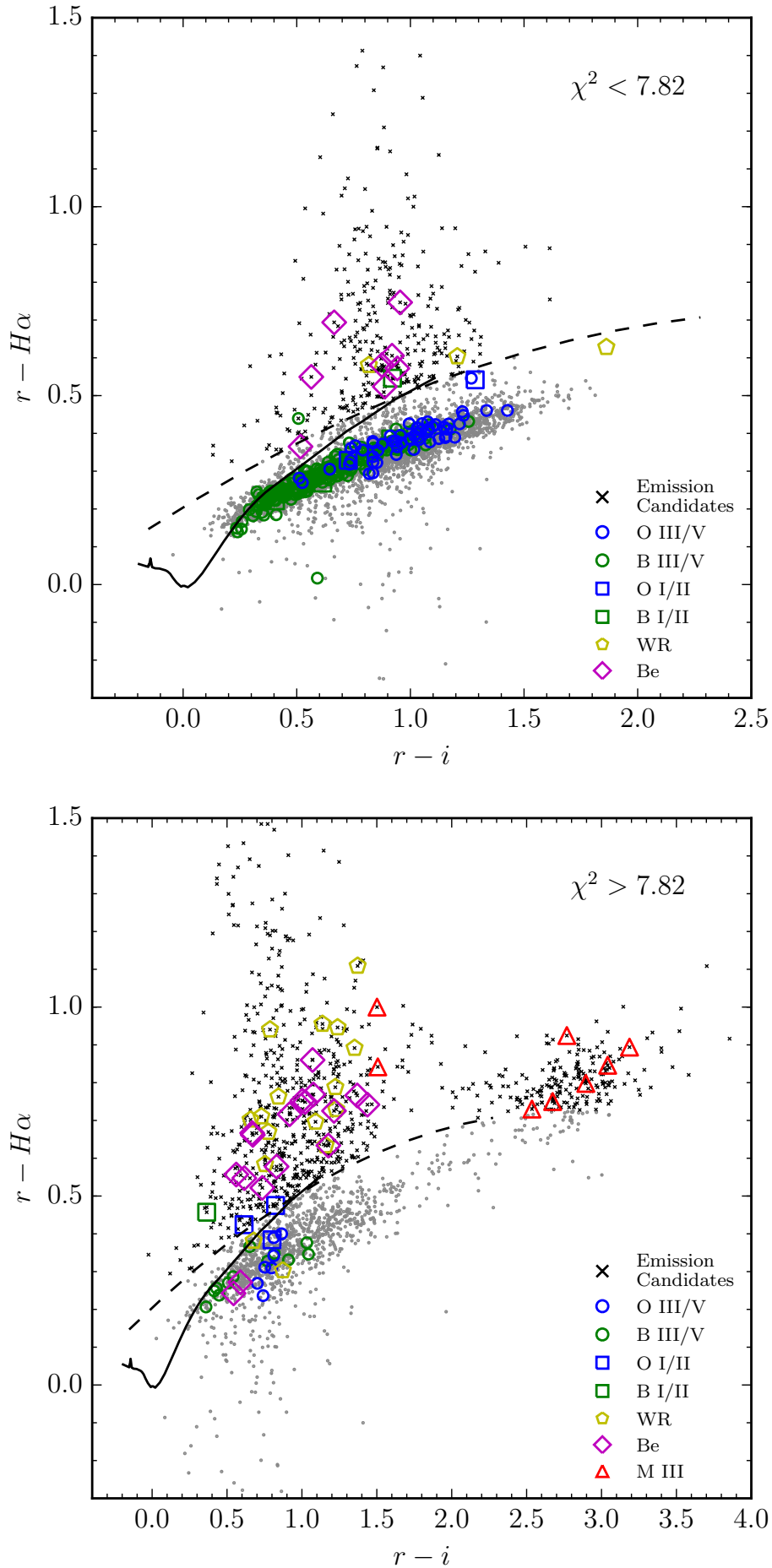
### 5.1.2 Emission line stars

As discussed previously in [section 3.4.2](#), we can also use the VPHAS+  $\text{H}\alpha$  measurements to pick out any emission line stars in our selection. Again, we have used the  $(r - i, r - \text{H}\alpha)$  diagram to select all objects that lie more than 0.1 mag in  $r - \text{H}\alpha$  above the O9V reddening vector (equating to  $\sim 10\text{\AA}$  in emission line equivalent width). [Figure 5.7](#) shows this selection for objects with  $\log(T_{\text{eff}}) \geq 4.3$  in the accepted fit  $\chi \leq 7.82$  group (top panel) and the poor fit  $\chi^2 > 7.82$  group (bottom panel). The black crosses show objects selected as emission line stars, while the various coloured symbols (see legend) show stars with known spectral type from the SIMBAD cross match and those with AAOmega spectra from [Chapter 4](#). Here we can see that the emission line objects co-locate in the diagram with CBe stars and WR stars while the non-emission line objects co-locate in the diagram with the known dwarf and giant OB stars. As discussed in [section 4.2](#) the majority of WR and CBe stars produce poor  $\chi^2$  values when fit to MS OB star SEDs. The bottom panel of [Fig. 5.7](#) shows in addition a group of poor  $\chi^2$  objects with  $r - i > 2$  that co-locate with a group of known M giant stars.

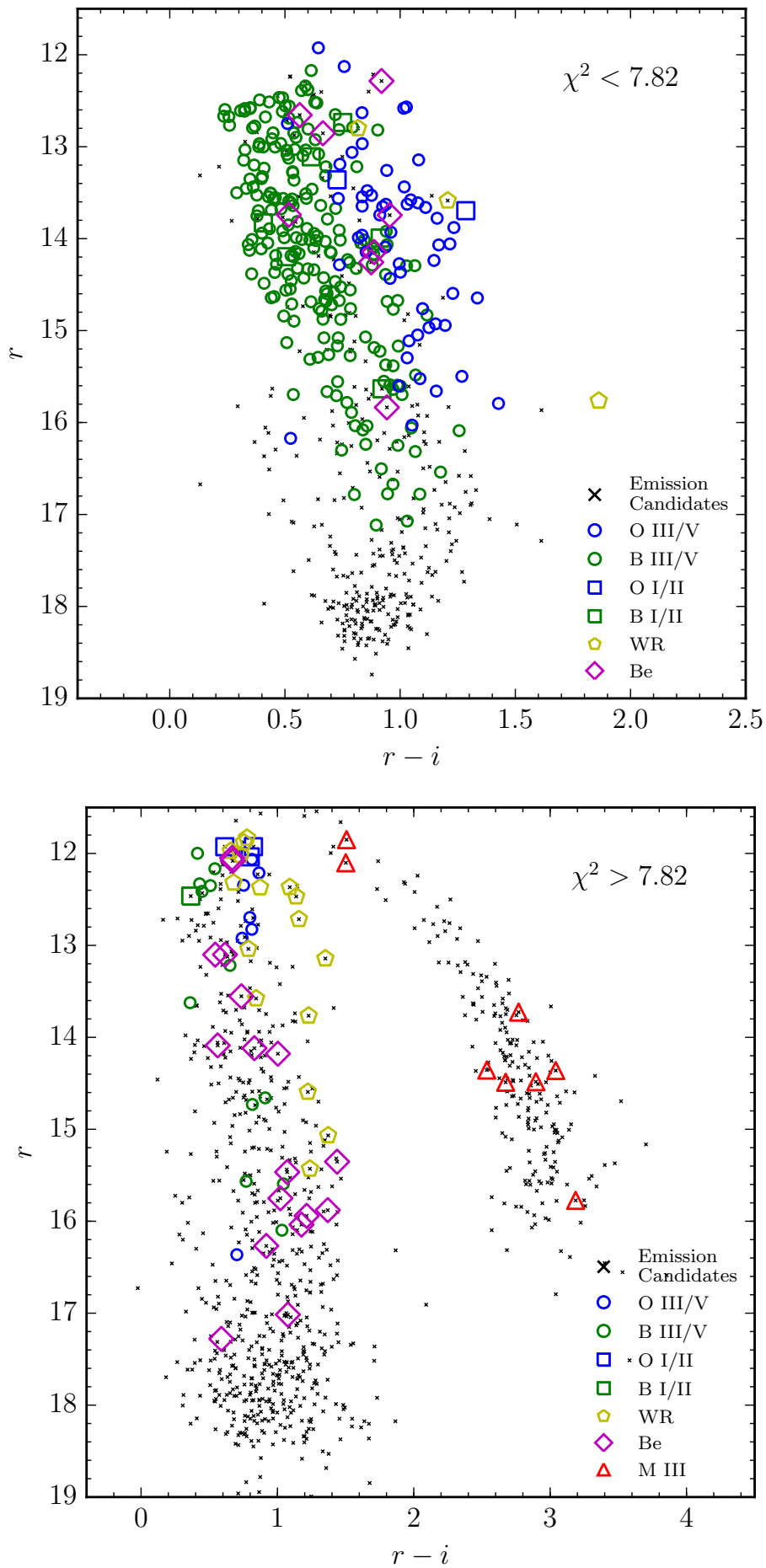
These very red contaminant objects showing extreme  $r - i$  values, are found in the bottom right corner of the  $(u - g, g - r)$  CC diagram, permitting them to enter into the original selection as candidate highly reddened OB stars. It is likely that the  $u$  band photometry for these intrinsically red objects is affected by the red leak in the VPHAS+  $u$  band (see [Drew et al., 2014](#)), pushing them apparently blue-ward into the OB star regime. It is noted that none of these objects are found with acceptable  $\chi^2$  values. This is further illustration of how the SED-fitting is critical in enhancing the selection efficiency.

Fig. 5.8 shows  $(r, r - i)$  CMDs for the emission line stars and those with known spectral type in both the  $\chi^2 \leq 7.82$  (top panel) and  $\chi^2 > 7.82$  (bottom panel) groups. The bottom panel shows that the group of M giants form a separate track when compared to the rest of the population; reaffirming their status as M giant candidates. The CMDs also show that the majority of emission line candidates are relatively faint ( $r \gtrsim 18$ ). The emission line status of these faint objects must be treated with caution as some may be affected by contamination from the bright surrounding HII regions in this area which the CASU pipeline struggles to disentangle. Direct inspection of the images may help to clarify matters, and of course follow-up long-slit spectroscopy would settle this matter.

There are 326 emission line objects in the  $\chi^2 \leq 7.82$  and  $\log(T_{\text{eff}}) \geq 4.3$  group and a further 856 with  $\chi^2 > 7.82$  and/or  $\log(T_{\text{eff}}) < 4.3$ . Objects with H $\alpha$  excess are marked in Table C.1 in the appendix. Objects with H $\alpha$  emission are removed from any further discussion regarding extinction as the derived extinctions may be affected by the presence of a circumstellar disk.



**Figure 5.7:** Emission line stars selected using the VPHAS+ ( $r - i, r - H\alpha$ ) diagram with various stars of known spectral class. The top panel shows OB candidates with  $\chi^2 < 7.82$  and the bottom panel shows OB candidates with  $\chi^2 > 7.82$ .



**Figure 5.8:** CMD for Emission line stars selected using the VPHAS+  $(r-i, r-H\alpha)$  diagram shown in Fig. 5.7.

## 5.2 Extinction properties and spatial distribution

### 5.2.1 Extinction law

The top panel of Fig. 5.9 shows a density contour plot for the candidate OB stars of the amount of extinction,  $A_0$ , as a function of the shape of the extinction law,  $R_V$ . The contours are based on the number of stars per  $[0.1A_0 \times 0.05R_V]$  bin as indicated by the colour bar. Fitzpatrick & Massa (2007) and Hur et al. (2012) found raised values of  $R_V > 3.5$  in the open clusters Trumpler 16 (Tr 16) and NGC 3293 with normal values of  $R_V \sim 3.1$  for foreground stars. The open green circles on Fig. 5.9 are the values derived by Fitzpatrick & Massa (2007) for stars in Tr 16 and NGC 3293. Here, it can be seen that the pattern in values derived for our candidate OB stars blends well with these previous results in showing a preference for lower values of  $R_V$  where  $A_0 < 2.0$ .

Over-plotted on Fig. 5.9 is a regression line for  $A_0 \geq 2.0$  and for  $A_0 < 2.0$ . In the  $A_0 \geq 2.0$  case we can see that the regression line suggests a very slight increase in  $R_V$  with extinction ( $+0.16 R_V$  between 2.0 and 8.0  $A_0$ ). However, the Pearson's correlation coefficient of the regression line is very low ( $r = 0.17$ ) due to the relatively large amount of scatter. We therefore do not claim any significant change in the average extinction law once  $A_0 \geq 2.0$ . In the  $A_0 < 2.0$  case we see a much sharper increase in  $R_V$  over a much shorter range in  $A_0$  ( $+0.52 R_V$  between  $A_0 = 1.0$  and 2.0). Here, the correlation is still weak ( $r = 0.35$ ), due to low numbers of stars and a large scatter, but stronger than for  $A_0 \geq 2.0$ . This pattern perhaps represents a transition down to  $R_V \sim 3.1$  in the foreground of the Carina Arm at  $A_0 \lesssim 1$ . Increasing  $R_V$  tracks increasing typical dust grain size as the Carina star forming complex is entered at  $A_0 \geq 2.0$ .

Since our measures of extinction and extinction law on a star-by-star basis are quite precise, the scatter that we see in  $R_V$  vs  $A_0$  is likely to be real. This demonstrates that prescribing a single value of  $R_V$  for an entire star-forming complex is doomed to mislead, and that care needs to be taken in achieving adequate sampling for the purpose in hand.

It is important to further check the extent to which the distribution in  $A_0$  vs  $R_V$  is astrophysical rather than down to the selection limits imposed by the survey. In

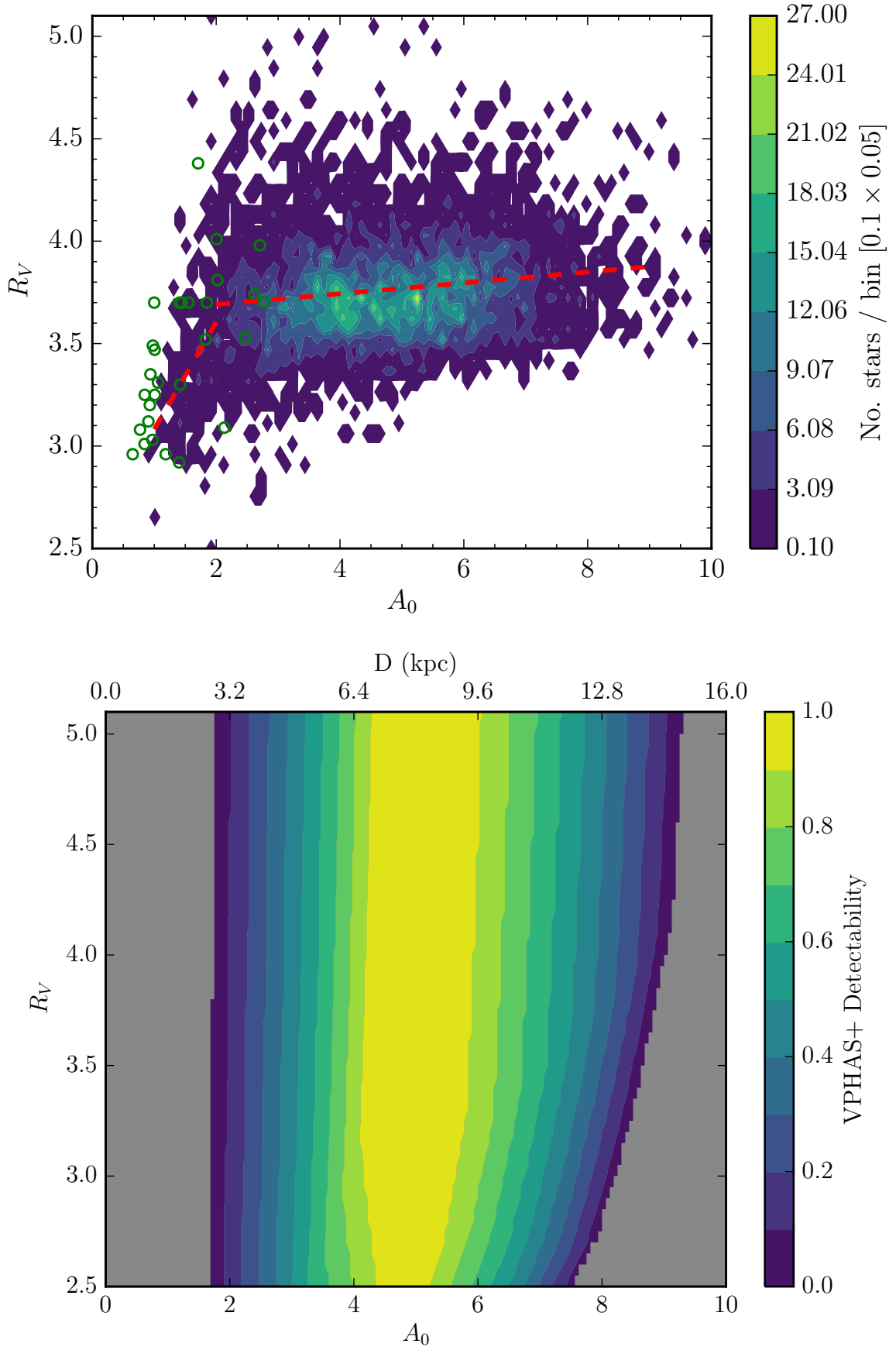


**Figure 5.9: Top:** Density plot showing the distribution in  $A_0$  vs  $R_V$ . The red dashed lines show least squared fits for  $A_0 \leq 2$  and  $A_0 > 2$ . The green circles show derived values for O stars from [Fitzpatrick & Massa \(2007\)](#). **Bottom:** Sensitivity of detecting OB stars in VPHAS+ for different combinations of  $A_0$  and  $R_V$ . An increase in extinction of 0.625 mag/kpc is adopted.

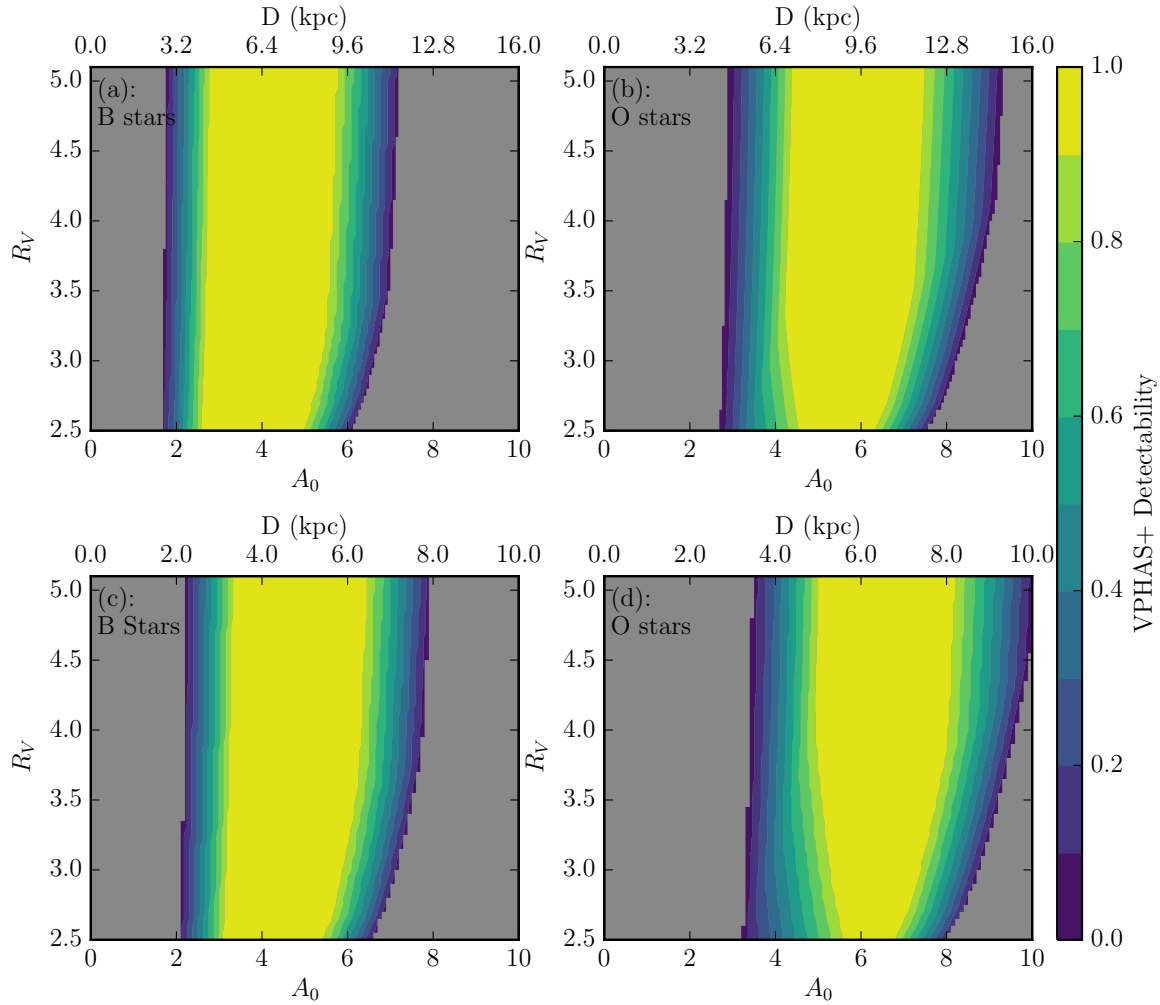


**Figure 5.10:** Detectability of OB stars in VPHAS+ for different combinations of  $A_0$  and  $R_V$ . Panels (a) and (b) separate B and O stars respectively and adopt an increase in extinction of  $0.625 \text{ mag/kpc}$ . Panels (c) and (d) separate B and O stars respectively for the case of a steeper increase in extinction of  $1 \text{ mag/kpc}$ .

order to do this, we can model the impact of the adopted magnitude selection limits on the allowed combinations of  $A_0$  and  $R_V$ . First, we take all of the photometric OB main sequence star models in the grid ( $\log(T_{\text{eff}}) \geq 4.3$ ) and redden them, assuming a rise in  $A_0$  of 0.625 mag/kpc (see section 5.2.2) for all values of  $R_V$ . We can then see which combinations of  $A_0$  and  $R_V$  produce an SED within the survey imposed magnitude limits ( $12 < u < 21$ ,  $12 < i < 21$ ,  $12 < r < 21$  and  $13 < g < 20$ ). The detectability is then taken to be proportional to the number of unique SEDs which meet these requirements given a specified combination of  $A_0$  and  $R_V$  and (by implication) distance. It is noted that this model of detectability is not a model of how many stars we expect to find in selection given  $A_0$  and  $R_V$ , as this would require taking into account the IMF and the effects of sampling a larger volume with increasing distance. Rather, it is a measure of the relative range in OB star temperatures it is possible to detect for given  $A_0$  and  $R_V$ , and implied distance.

The bottom panel of Fig. 5.9 shows a density plot of the overall measure of detectability. The grey areas in the plot are combinations of  $A_0$  and  $R_V$  in which none of the modelled main sequence OB stars could be detected. Here we can see that the main driver in detectability is the amount of extinction,  $A_0$ , rather than the shape of the extinction law,  $R_V$ . It is only at high values of extinction ( $A_0 \gtrsim 8$ ) where the extinction law produces a bias in favour of high  $R_V$ , as the  $u$  band is then more readily pushed beyond the faint limit. We can therefore conclude that the distribution shown in Fig. 5.9 is only mildly affected by the detection limits at the two extremes in  $A_0$ . The fact that we do not see any objects in the  $5 < A_0 < 7$  range with  $R_V \sim 3.1$  is driven more by the characteristics of these sight lines than by selection bias. Fig. 5.9 shows that VPHAS+ is most sensitive in the  $4.0 < A_0 < 6.5$  range which is in agreement with the distribution of selected OB stars in Fig. 5.2. Below this range the sensitivity drops off as the hotter O stars begin to saturate. Conversely, above this range, the sensitivity drops off as the cooler objects become too faint to be detected.

In order to demonstrate this point further, Fig 5.10 shows the sensitivity to combinations of  $A_0$  and  $R_V$  separately for early B stars, ( $4.295 < \log(T_{\text{eff}}) < 4.477$ ; panel a) and for O stars ( $4.477 < \log(T_{\text{eff}}) < 4.7$ ; panel b). Here, we can see that for

the intrinsically-fainter B stars the sensitivity peaks at lower extinction with values of  $2.5 < A_0 < 5$ , whereas the intrinsically brighter O stars have a peak sensitivity in the range  $4.5 < A_0 < 7$ . As expected, this plot also shows that due to the magnitude limits appropriate to VPHAS+ we will be missing any early B stars with extinction beyond  $A_0 \simeq 7$ . In order to pick up these stars the limiting magnitude in the bluer  $u$  and  $g$  bands would need to increase by 2–3 magnitudes. We can also see that we will be missing a significant number of O stars at  $A_0 \gtrsim 8$ . Beyond this only the hottest O stars can be detected.

The treatment here assumes that extinction uniformly increases with distance - given the fractal nature of the ISM in star forming regions, this will not always be the case. Increasing distance and extinction obviously act together to increase apparent magnitude. For example, cooler objects, with high  $A_0$ , would be detected at shorter distances in regions where the extinction builds up more steeply with distance. This is demonstrated in panels (c) and (d) of Fig 5.10 where I have calculated the sensitivity based on a steeper extinction gradient of 1 mag/kpc, compared to the previously adopted value of 0.625 mag/kpc. Here we can see that, for the O stars, the peak sensitivity has now shifted to higher values of  $5 < A_0 < 8$ . Similarly, for the B stars, the peak sensitivity has also shifted to higher values of  $3 < A_0 < 6$ . It is noted that these calculations are based on MS stars; a different set of limits would be applicable to the more luminous (less common) evolved classes of object. Unavoidably, the selection is complex.

### 5.2.2 The changing OB star distribution with increasing extinction

Fig. 5.11 shows the selected OB stars in three different extinction windows ( $A_0 \leq 4$ ,  $4 < A_0 < 6$  and  $A_0 \geq 6$ ). In each plot the objects are colour coded by their derived values of  $A_0$ . What stands out the most is that the distribution in Galactic latitude becomes tighter as  $A_0$  increases, revealing the ever more distant thin Galactic disk. This effect can be attributed to the projection effect on the scale height of

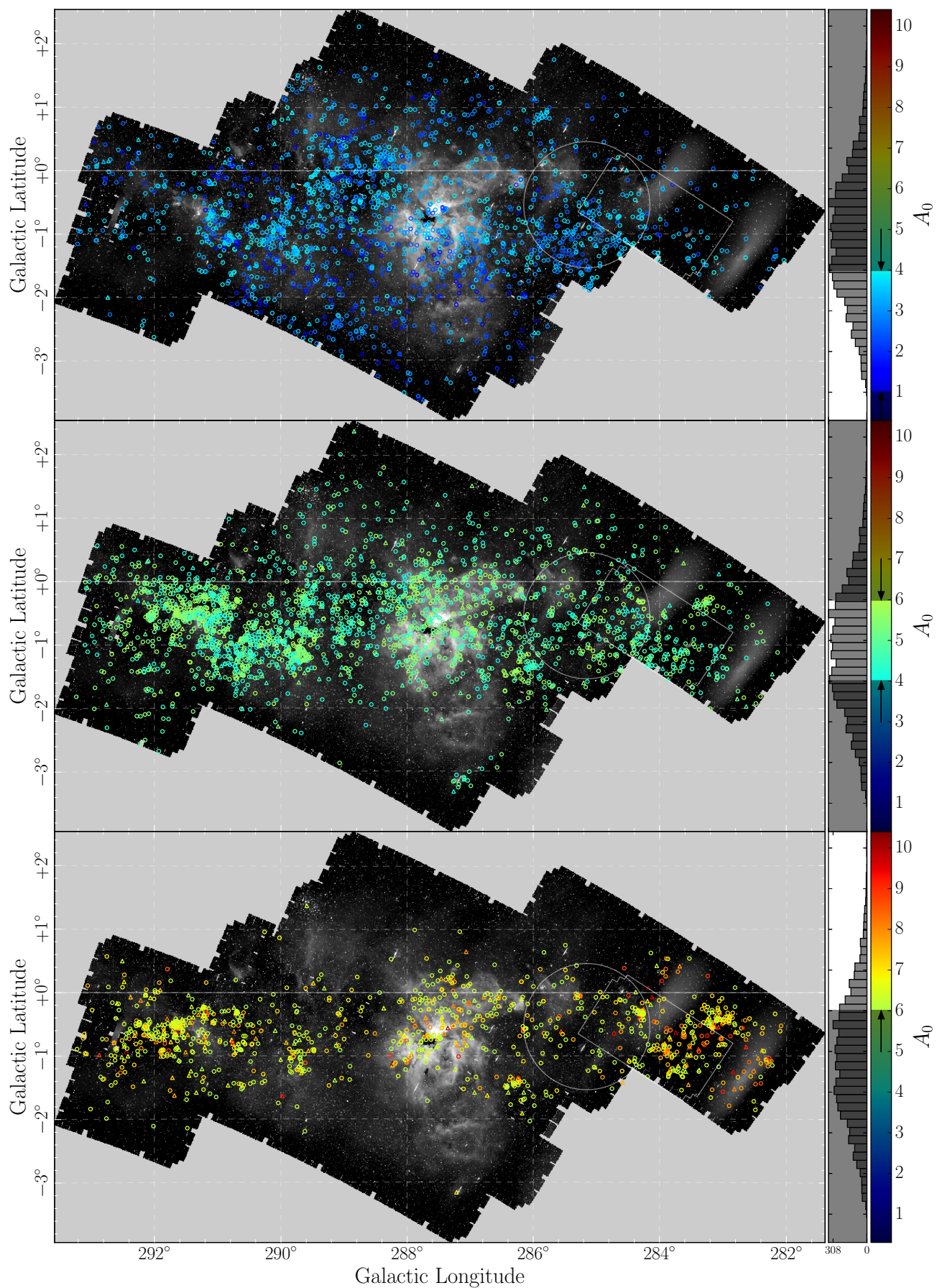


**Figure 5.11:** Series of plots showing the positions of OB stars through windows increasing in  $A_0$ . O stars and early B stars are represented as triangles and circles respectively. The large circle and rectangle represent the area covered by AAOmega follow up and the area covered in [Mohr-Smith et al. \(2015\)](#) respectively. The histogram to the right of the plot shows the distribution in  $A_0$ .

the OB stars as reddening, and the distance to which it loosely correlates, increases. We can use this effect to estimate what distances we are sampling as a function of rising extinction. This method turns out to be more informative than taking our derived distance moduli from SED fitting because of the strong correlation between distance temperature and luminosity class and the relative weakness of the SED fitting constraint on these parameters. Panel (a) of Fig. 5.12 shows that the trend in  $A_0$  vs  $D$  is not particularly meaningful as distance would seem to decrease with extinction beyond  $A_0 = 5$ . Instead, we explore the use of the angular spread of the candidates as a proxy for distance, under the assumption that the OB star scale height in the Galactic disk is independent of Galactocentric radius (Paladini et al., 2004).

First we bin the objects in extinction from  $2.5 > 8.5$  in steps of  $1A_0$ . In each bin the standard deviation in Galactic latitude,  $\sigma_\theta$ , is used as a measure of the angular scale height,  $H_\theta$ . The scale height of OB stars is conventionally defined with respect to an exponential. Gaussian  $\sigma$  can be scaled by a factor of 1.235 to make it an approximately equivalent measure. Assuming an exponential scale height of OB stars ( $h_{OB}$ ) of  $45 \pm 15$ pc (Reed, 2000) we can calculate a corresponding distance using the small angle approximation:

$$D \simeq h_{OB}/1.235 \times \sigma_\theta \quad (5.1)$$

Panels (b), (c) and (d) of Fig. 5.12 show the derived distances as a function of  $A_0$  for three different Galactic longitude ranges. Panel (b) shows the entire longitude range of the studied area while panels (c) and (d) split the longitude range in half. Panel (c), where  $287.6 < l < 293.2$ , includes the part of the footprint that contains the cluster NGC 3603 (3495 stars), while panel (d), where  $282.0 < l < 287.6$  takes in the rest of the foot print containing Wd 2 (1979 stars). Over-plotted on the figures are the distance and extinction to NGC 3603 (green triangle) taken from Sung & Bessell (2004) and the distance and extinction to Wd 2 (red diamond) taken from Dame (2007) and Mohr-Smith et al. (2015) respectively. The error bars shown reflect the uncertainty in  $h_{OB}$ .

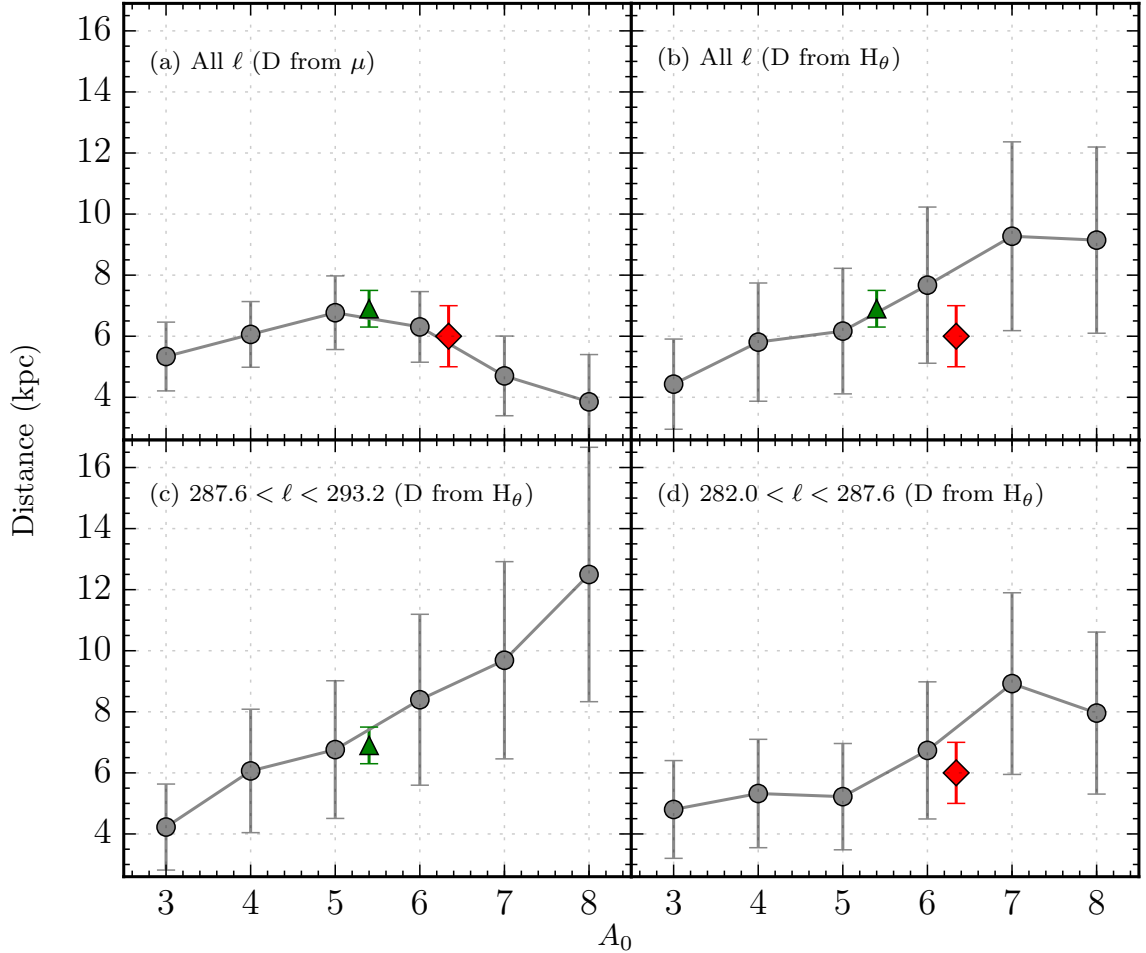


**Figure 5.12:** Panel (a): The mean distance and standard deviation obtained from the best-fitting distance modulus  $\mu$  as a function of best-fit  $A_0$ . Panel (b): here the distance is inferred as a function of  $A_0$  based on the measured angular scale-height ( $H_\theta$ ) of the newly uncovered OB star population, as described in the text. This gives a much more orderly trend, supporting the expectation that the best-fit distance moduli are unreliable. The green symbol places NGC 3603 on the diagram according to the literature consensus on its reddening and distance, while the red point does the same for Westerlund 2. Panels (c) and (d) are the same as (b) except that they split the longitude range in half, with 3495 stars in the higher longitude (NGC 3603) half of the studied range in (c), and 1979 stars in the lower longitude range including Westerlund 2.

Panel (c) shows that for  $287.6 < l < 293.2$  we have a well-behaved steady increase in estimated distance as a function of extinction of 1.6 kpc/mag on average (or 0.625mag/kpc). The literature values of extinction and distance of NGC 3603 fit comfortably into this trend. However, for  $282.0 < l < 287.6$  the build up in extinction is less straight forward. Here we see very little increase in the derived distance between  $A_0 = 3$  and  $A_0 = 6$ . We can also see that Wd 2 is rather heavily extinguished for its distance when compared to the general trend in the panel (b). This behaviour can be attributed to the fact that for the sight lines with  $282.0 < l < 287.6$ , the Carina arm tangent ( $l \simeq 281$ ) is not far away, and the accumulated column density of dust is much more significant when compared to the  $287.6 < l < 293.2$  sight lines (Dame, 2007). These effects are supported by Figs. 1.4 & 1.5 taken directly from Grabelsky et al. (1987) where the intensity of CO emission, effectively a tracer of dust, is around four times greater at  $l \sim 281$  than at  $l \sim 291$ . In Fig. 1.4 there is in fact an obvious gap in CO emission at around  $l \sim 291$  in the direction of NGC 3603 which fits with the only moderate increase in extinction that we see for this sight line. Panel (d) shows that, in the tangent direction, extinction accumulates rapidly to  $D \sim 5$  or 6 kpc and that much of this rise might be achieved by  $\sim 2$  kpc. Beyond  $\sim 5 - 6$  kpc the rise in extinction is less rapid and behaves much in the same way as shown in panel (c). This behaviour is supported in the lower panel of Fig. 1.4 which shows that the CO emission in the tangent direction is concentrated between  $\sim 2 - 6$  kpc, beyond these distances the amount of CO emission falls off rapidly, perhaps coinciding with a return to a more ‘normal’ increase of extinction with distance, similar to the NGC3603 sight line. Fig. 5.4 shows that we are detecting fewer objects near the tangent when compared to the opposite end of the footprint. This can be attributed to the more rapid increase in extinction with distance in this direction. Here, we are unable to detect objects to as high distances and hence find fewer objects.

Marshall et al. (2006) produced a three dimensional extinction map of the Milky Way by comparing empirical colours of giant stars in 2MASS with the expected intrinsic colours from the Besançon stellar population synthesis model. This technique was applied to 64000 sight lines each separated by  $0.25^\circ$  in Galactic longitude. Fig. 5.13

shows the derived extinction as a function of distance from [Marshall et al. \(2006\)](#) for a number of sight lines within the Carina region in this study. The sight lines shown in blue correspond to the higher Galactic longitude side of the region containing NGC 3603 ( $290.5^\circ < \ell < 291.5^\circ$  and  $-1^\circ < b < 0^\circ$ ) while those shown in red correspond to the Carina tangent side of the region ( $282.5^\circ < \ell < 283.5^\circ$  and  $-1^\circ < b < 0^\circ$ ). The lines shown in green correspond to a region slightly offset from the tangent at ( $285.5^\circ < \ell < 286.5^\circ$  and  $-1^\circ < b < 0^\circ$ ). The extinction values in [Marshall et al. \(2006\)](#) are given in terms of the extinction in the K band,  $A_K$ . These values are multiplied by  $\sim 8$  to translate them into  $A_0$  for  $R_V \sim 3.8$ . Over-plotted on Fig. 5.13 are the corresponding values for either side of the region calculated using the scale height technique in this study (panels (c) and (d) from Fig. 5.12). The diamond markers show the Carina tangent side of the foot print while the triangle markers show the opposite end of the foot print. Here we can see that the general trend for the opposing sight lines in [Marshall et al. \(2006\)](#) are in keeping with those suggested in the VPHAS+ data; the extinction builds up more quickly in the Carina tangent side of the footprint. However, there is a systematic over-estimation from the OB-star data of the corresponding distances associated with the tangent far side. The opposite end of the foot print is in much better agreement. This discrepancy is linked to the fact that the [Marshall et al. \(2006\)](#) data shown in red is sampling only the extreme end of the footprint, very close to the tangent region, whereas the OB-star data sample a much wider longitude distribution, including objects further away from the tangent. For this reason, the tangent side OB-star data are in better agreement with the [Marshall et al. \(2006\)](#) data shown in green, which overlap the red and blue data, as these correspond to sight lines offset from the tangent. Despite the large uncertainties associated with the methods used in this study to derive the distances, a consistent plausible picture emerges.

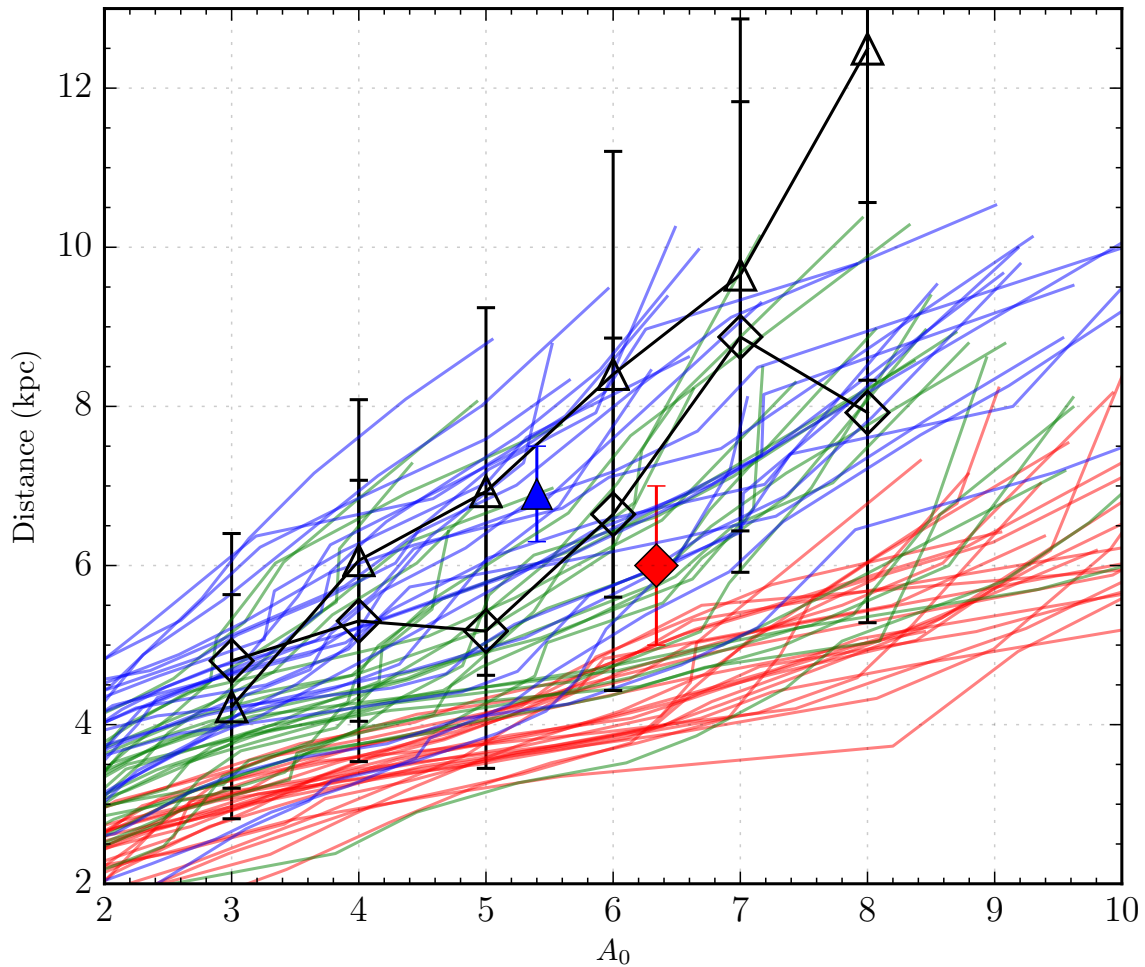


**Figure 5.13:** Comparison of the derived values of extinction as a function of distance between [Marshall et al. \(2006\)](#) and this study for sight lines towards and away from the Carina tangent. The diamond markers show the Carina tangent side of the foot print while the triangle markers show the opposite end of the foot print (VPHAS+ data). The red and the blue lines are those taken from [Marshall et al. \(2006\)](#) and show the Carina tangent side of the footprint and the opposite end of the footprint respectively. The lines shown in green correspond to a region slightly offset from the tangent. The blue triangle and red diamond show the corresponding values for NGC 3603 and Wd 2 respectively.

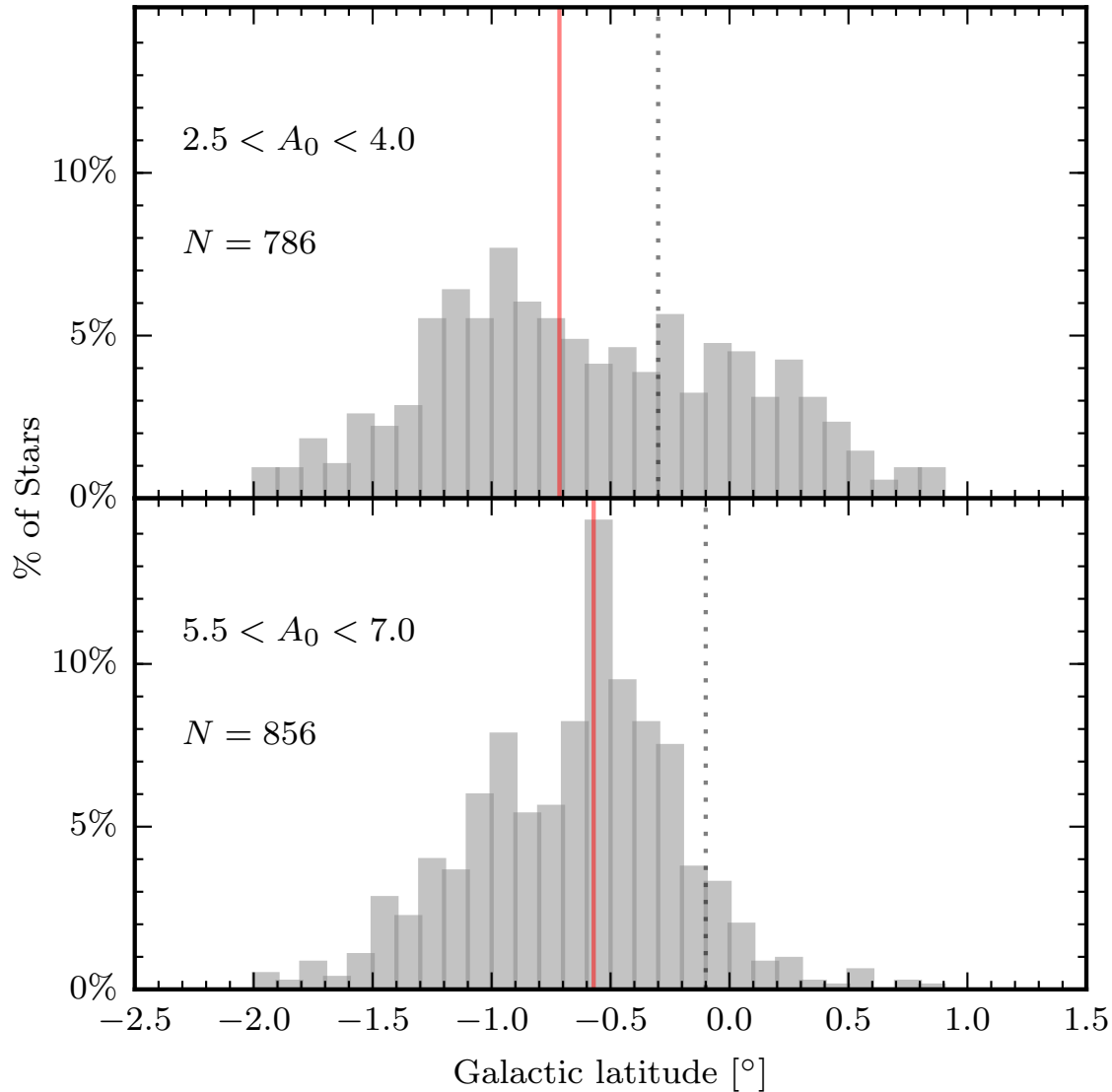
### 5.2.3 Onset of the Galactic warp

Taking the longitude range with the higher densities of OB candidates, offering the clearer view, Fig. 5.14 shows the Galactic latitude distribution for two reddening bins;  $2.5 < A_0 < 4.0$  and  $5.5 < A_0 < 7.0$  corresponding to nearer and significantly more distant reaches of the Galactic Plane centred around heliocentric distances of  $\sim 5$  kpc and  $\sim 9$  kpc respectively (see Fig. 5.12c). Over plotted on these histograms are the corresponding latitudes of the true Galactic mid-plane, as determined after the necessary correction for the height of the Sun above it ( $\sim 25$  pc) taken from Goodman et al. (2014). It can be seen in that the median OB star density (red line) is below the true mid-plane in both cases. Using the difference between these latitudes and the corresponding representative heliocentric distances we can calculate the vertical distance below the mid-plane at which the OB star density peaks. This corresponds to  $\sim 36$  pc below the true mid-plane at  $\sim 5$  kpc and  $\sim 74$  pc below the mid-plane at  $\sim 9$  kpc.

This result hints at the beginnings of the negative Galactic warp sampled at heliocentric distance of  $\sim 5$  and  $\sim 9$  kpc. Assuming a distances of 8 kpc from the sun to the Galactic centre, at a Galactic longitude of  $l = 291^\circ$ , heliocentric distances of 5 and 9 kpc correspond to Galactocentric distances of 7.8 and 9.7 kpc respectively. Based on the distribution of neutral hydrogen, from the 21-cm line, which is overwhelmingly concentrated in the thin disk, Kalberla & Kerp (2009) suggest that there is little warping of the Plane out to Galactocentric radii of  $\sim 9$  kpc. What we see here is probably consistent with this. Beyond this distance they and Levine et al. (2006) see a rapid increase in the warp down to  $\sim 500$  pc at a Galactocentric distance of  $\sim 15$  kpc, far beyond the distances probed here.

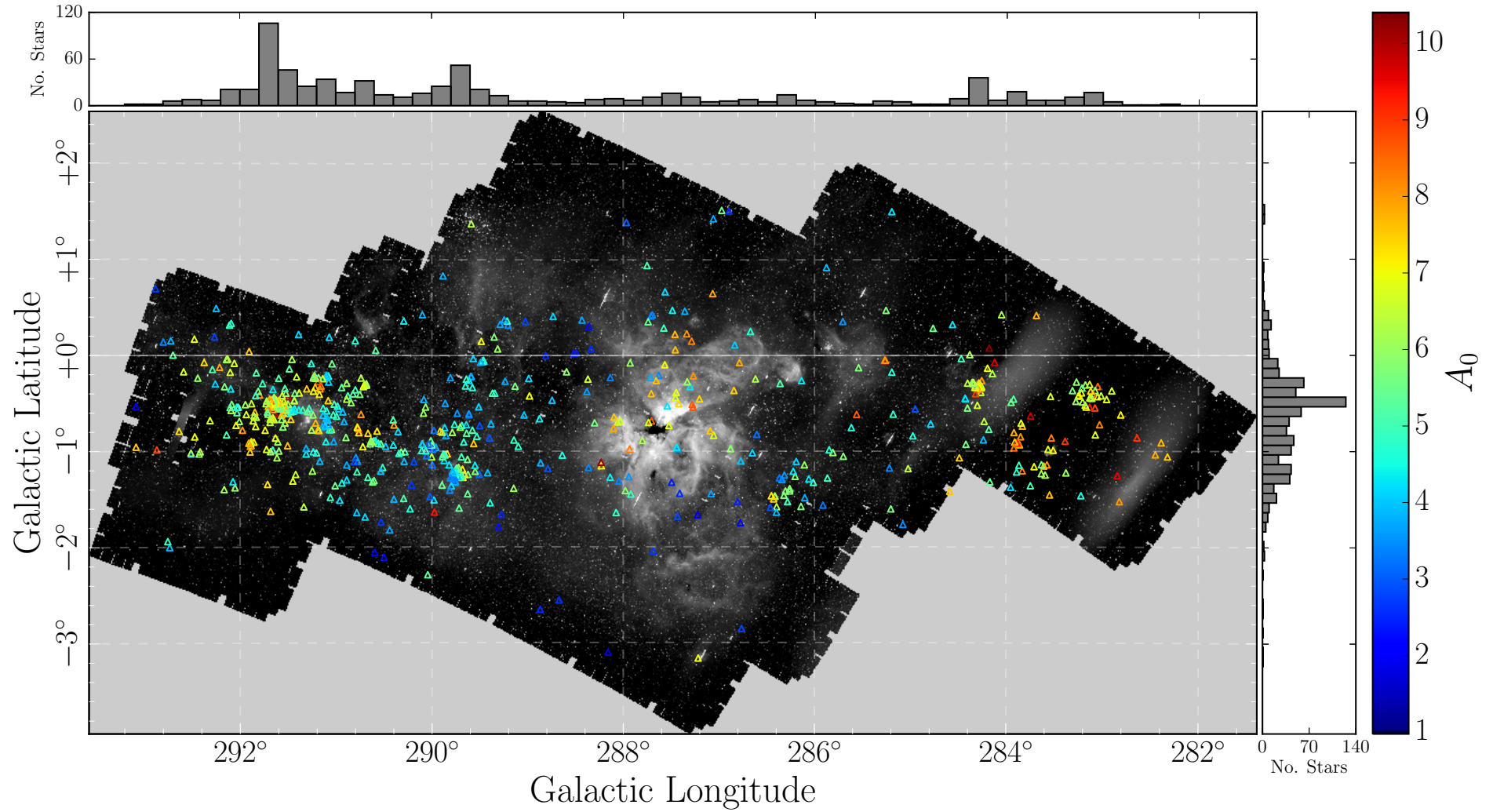
## 5.3 Clustering of O stars

Fig. 5.15 shows the distribution of O stars ( $\log(T_{\text{eff}}) > 4.477$ ) across the whole region coloured according to their extinction. The panels above and to the left of the main plot show the corresponding distributions in Galactic longitude and latitude respectively.



**Figure 5.14:** The top and bottom panels respectively give the Galactic latitude distributions of OB stars with best fitting extinctions in the ranges  $2.5 < A_0 < 4.0$  and  $5.5 < A_0 < 7.0$ , drawn from the Galactic longitude range  $287.6 < \ell < 293.2$ . As discussed in the text, it is very likely that the lower reddening range samples distances along the line of sight, that scatter around 5 kpc. The higher reddening range, in the bottom panel, is likely to pick out distances from around 7 kpc (roughly the distance to NGC 3603, that helps populate the taller histogram peak) out to, potentially 10 kpc or more. In either panel, the grey dotted line identifies the approximate position of the true mid-plane of the Galactic disc for the typical distance (see text and [Goodman et al. \(2014\)](#)). The red dotted line picks out the median Galactic latitude of the OB star distribution. The separation between these two latitudes is clearly greater in the higher-reddening distribution associated with the appreciably greater line-of-sight distance. It is also evident that the distribution width is smaller in this case, as expected.

Here we can see that the majority of the O stars in the selection are concentrated around the cluster NGC 3603 ( $l \sim 291^\circ$ ). Many known O stars in the Carina Nebula/Carina OB1 association at  $l \sim 288^\circ$  are missing from the selection as they are brighter than our bright selection limit. However we do pick up a handful of reddened O star candidates and many reddened B star candidates (see Fig. 5.11) which are far more extinguished than the typical values of  $A_V \sim 2.5$  of known clusters such as Trumpler 14 and 16 (Hur et al., 2012). These objects are likely to be situated behind or deeper into the nebula than the well studied population beyond the nominal distance of  $\sim 2.9$  kpc (Hur et al., 2012). Fig. 5.15 also shows that there are fewer O stars in the low longitude side of the region, in which the reddening accumulates more rapidly. The reasons behind this are discussed in Section 5.2.2. In the next subsection, I will lay out some of the insights provided by the wider field around NGC3603, before going on to a discussion of newly apparent asterisms or possibly genuine clusters.



**Figure 5.15:** Spatial distribution of candidate O stars across the Carina region, coloured by the extinction. The histograms above and to the right of the plot show the Galactic longitude and latitude distribution respectively

### 5.3.1 NGC 3603

As well as uncovering O stars near the central region of the NGC 3603, we also uncover many more objects in an extended halo around the dense core. Many of these objects have similar extinction to the cluster and extend into the surrounding G291 star forming region identified by [Rahman & Murray \(2010\)](#). The top panel of Fig. 5.16, taken directly from [Rahman & Murray \(2010\)](#), shows the  $8\mu\text{m}$  Midcourse Space Experiment (MSX) image of the G291 star forming region. The G291 region is made up of two star forming complexes SFC27 and SFC28. [Rahman & Murray \(2010\)](#) separate these regions based on a substantial difference in their H I velocities. They state that for SFC27 and SFC28,  $v_{LSR} = -22 \text{ km s}^{-1}$  and  $v_{LSR} = 16 \text{ km s}^{-1}$  corresponding to distances of 3 kpc and 7.4 kpc respectively.

The bottom panel of Fig. 5.16 shows the VPHAS+  $\text{H}\alpha$  image with the selected candidate OB stars over-plotted and coloured by their derived extinction. In total there are 958 B star candidates and 300 O star candidates within the G291 ellipse shown on the figure. Here we can see that the majority of the massive star population, dominated by NGC 3603, favours the SFC28 region. There are 395 B star candidates and 199 O star candidates in the SFC28 ellipse compared to 432 B star candidates and 79 O star candidates in SFC27. Given the much closer distance of SFC27 compared to SFC28 it makes sense that we detect relatively more B stars in SFC27 and more O stars in SFC28, given the selection limits discussed in section 5.2.1. In the overlap region between SFC27 and SFC28 is the NGC 3576 HII region. The top panel of Fig. 5.17 shows a zoomed in view of the region containing both NGC 3603 (left of image) and NGC 3576 (right of image). NGC 3576 is situated in the foreground of G291 at  $\sim 2.4$  kpc ([Persi et al., 1994](#)) and is home to an embedded young massive star cluster located at  $l = 291.267 - b = 0.709$ , measuring about 10 arc minutes across and containing possibly  $\sim 7$  NIR-detected early B and O type stars. ([Persi et al., 1994](#); [Purcell et al., 2009](#)). Despite being very close, the cluster has a very high extinction of  $A_V > 10$ . It is therefore not surprising that we do not detect any OB stars associated with this cluster.

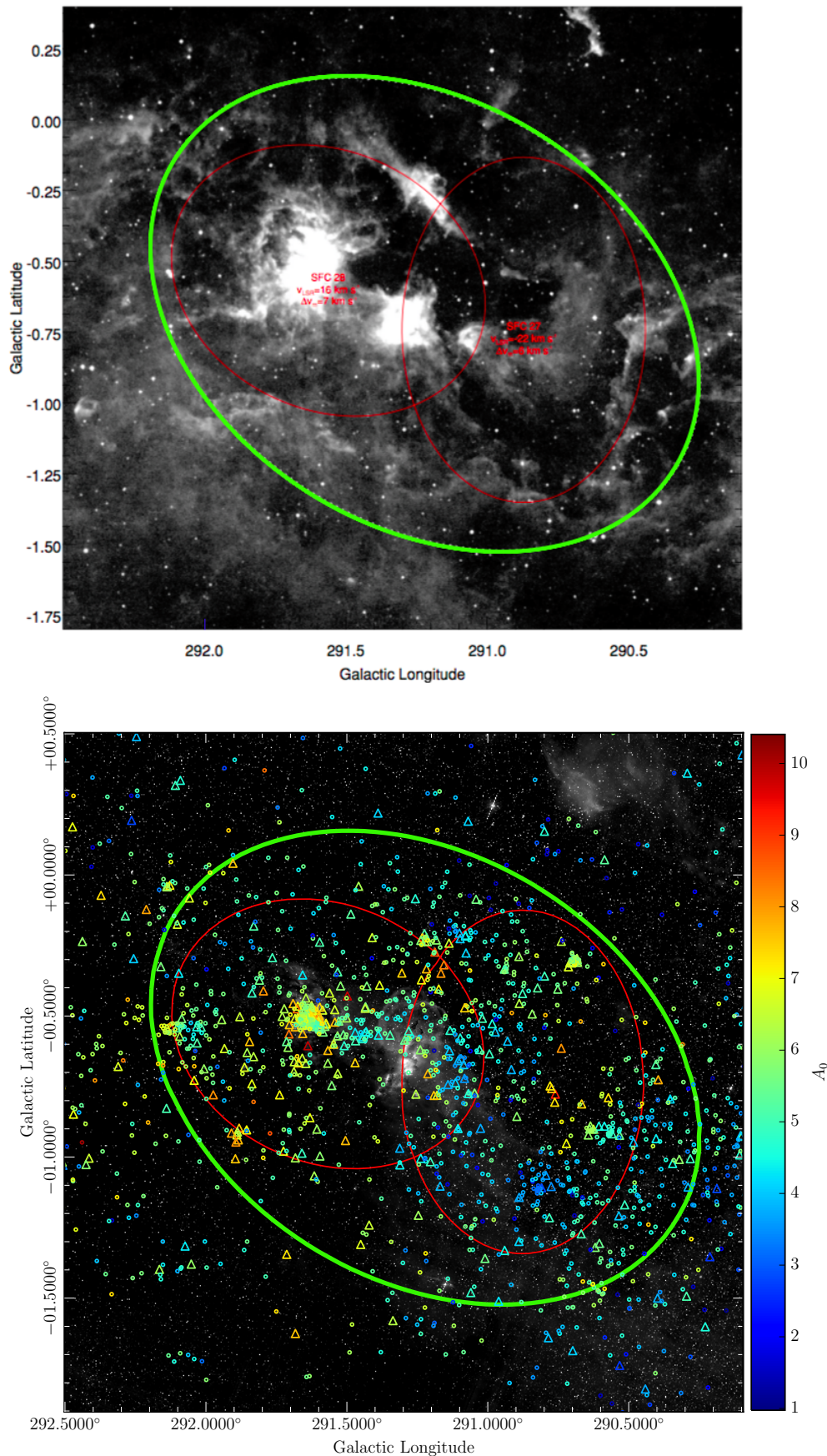


**Figure 5.16:** The G291 star forming complex (Rahman & Murray, 2010). Top panel: taken directly from Rahman & Murray (2010). Bottom panel: VPHAS+  $H\alpha$  image with OB stars over-plotted. Triangles are candidate O stars and circles are candidate B stars. Objects are coloured by their extinction.

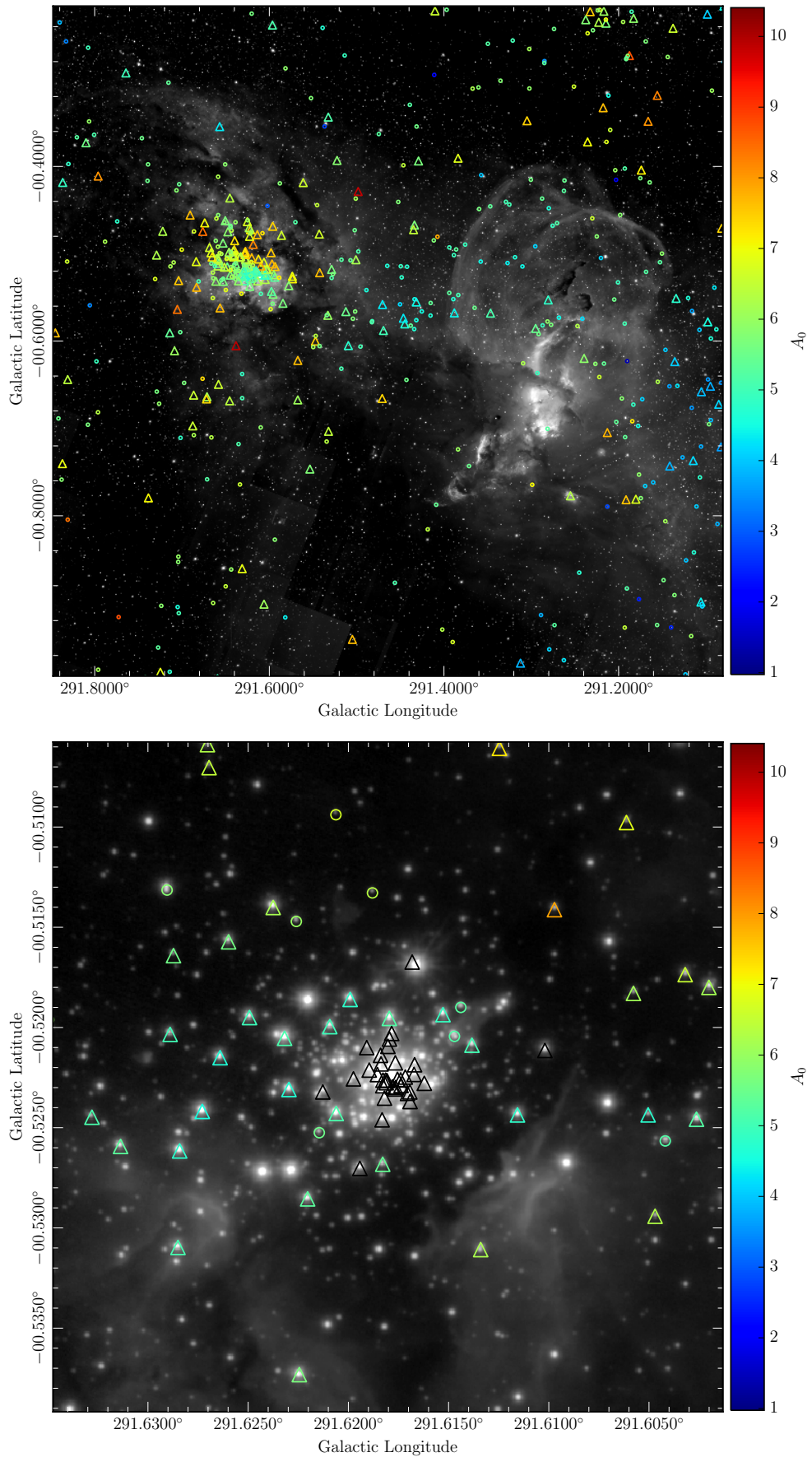


**Figure 5.17:** Top: A zoomed in view of the region containing both NGC 3603 (left of image) and NGC 3576 (right of image). NGC 3576 is situated in the foreground of G291 at  $\sim 2.4$  kpc. Bottom: A zoomed in view of VPHAS+  $r$  band image of the core of NGC 3603. The coloured circles and triangles are candidate OB stars from this study. The black triangles are the O stars from [Melena et al. \(2008\)](#).

The lower panel of Fig. 5.17 shows an even closer view of the VPHAS+  $r$  band image of NGC 3603 ( $\sim 2$  arcmin<sup>2</sup>). A study by Melena et al. (2008) collects photometry for 51 early type stars in the core of NGC3603. Of those 51 objects 17 are in our selection. In Fig. 5.17 it can be seen that we are missing objects (shown as black triangles) from the central  $\sim 10$  arcsecond diameter of the cluster core. This is the most dense region of the cluster and objects are lost due to blending in one or both of 2MASS (typical seeing  $\sim 2$ arcsec) or VPHAS+ (typical seeing  $\sim 1$ arcsec). Of the missing 34 objects just four have 2MASS photometry, which may be compromised by blending. These are not complete in all VPHAS+ bands and so didn't make it into the selection. Conversely, fifteen of the missing 34 objects are actually complete in the original VPHAS+ data so could benefit from cross matching with a higher resolution NIR data.

Fig. 5.18 shows the  $\sim 6 \times 6$  arcmin<sup>2</sup> region surrounding NGC3603. The lower panel is an extinction map of the region in the form of a Voronoi tessellation diagram. Each Voronoi cell contains one star and has been coloured by the value of  $A_0$  derived for that star. The top panel shows the positions of the corresponding stars over-plotted on the VPHAS+  $H\alpha$  image, coloured according to extinction. The white star symbol marks the centre of the cluster. Clayton (1986) identified the presence of an expanding gas shell surrounding NGC 3603 driven by the radiation pressure of the OB stars within the cluster. This shell structure is around 45 arcseconds in diameter and is indicated by the black and white circle in the upper and lower panels of the plot respectively.

More recently, Pang et al. (2011) have examined the extinction properties of the gas surrounding the cluster and found a preference for lower extinction within the expanding shell compared to the surrounding area. More specifically, they found that the extinction builds up more quickly to the North and South of the cluster when compared to the East and West direction. The derived extinction of the stars shown in Fig. 5.18 not only supports the extinction in the central region of the cluster being lower but also endorses a stronger increase in extinction in the North-South direction compared to the East-West direction. Pang et al. (2011) suggest that the ionizing radiation and/or stellar winds of the OB stars sweep away the ISM leaving a cavity in the dust within the expanding shell, thus lowering the extinction there. Melena et al.

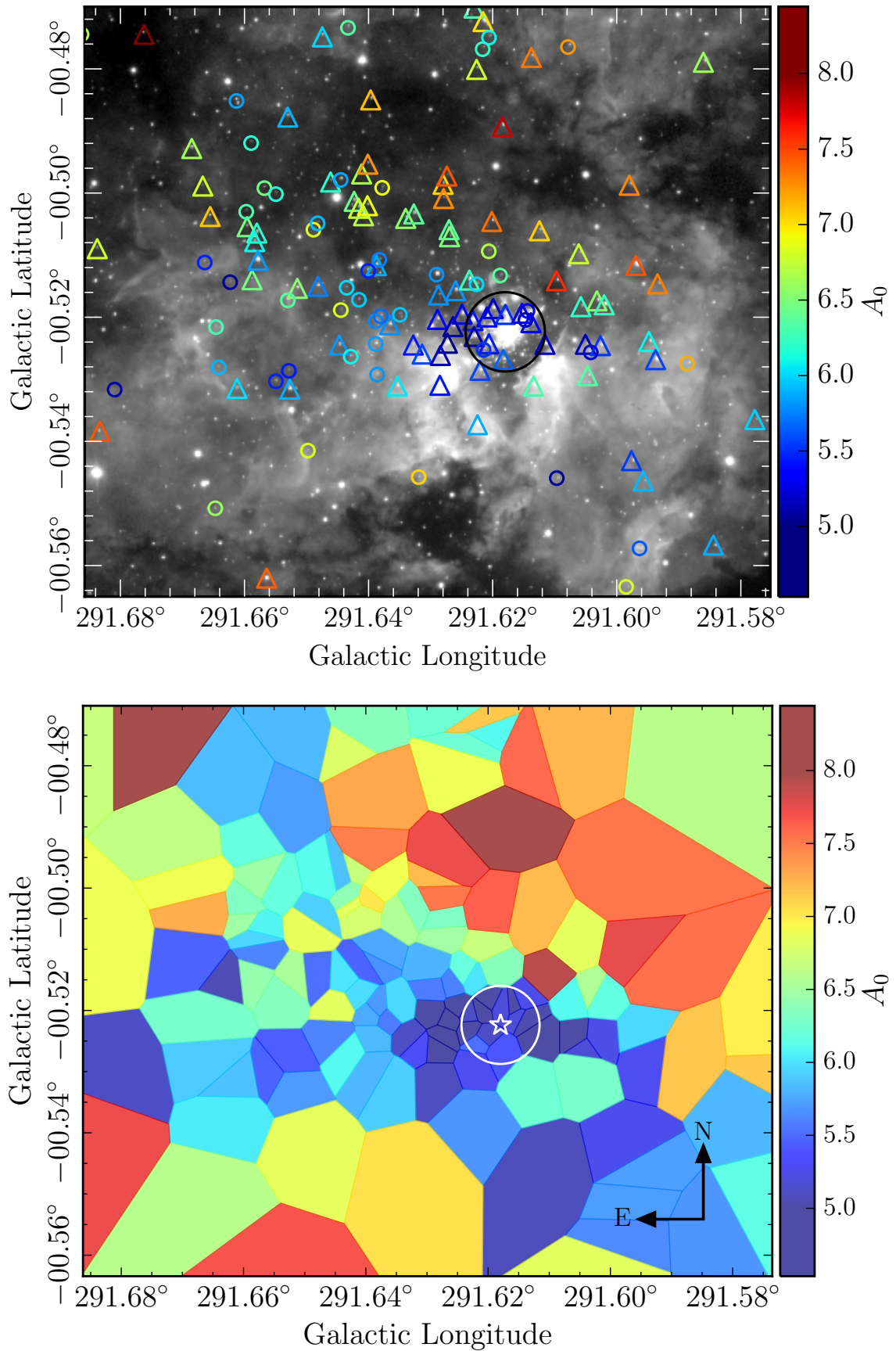


**Figure 5.18:** Top: Corresponding positions of OB stars over plotted on the VPHAS+  $H\alpha$  image, coloured by their extinction. Bottom: Extinction map in the form of a Voronoi tessellation diagram for the region surrounding NGC 3603. In both diagrams the circle drawn represents the location of the expanding shell (Pang et al., 2011). The region shown spans  $6 \times 6$  arcmin<sup>2</sup>, or a sky area of  $12 \times 12$  pc<sup>2</sup> at  $D = 6.9$  kpc

(2008) provide colour excesses ( $E(B - V)$ ) for the objects in the central 10 arc seconds of the cluster core. Although we are missing a number of these objects, those that we do pick up have a similar extinction to those that are missing, assuming  $R_V \sim 3.8$ , and are within the outline of the expanding shell. This implies that the story would be very similar if these stars were included in the plot.

### 5.3.2 New Clusters

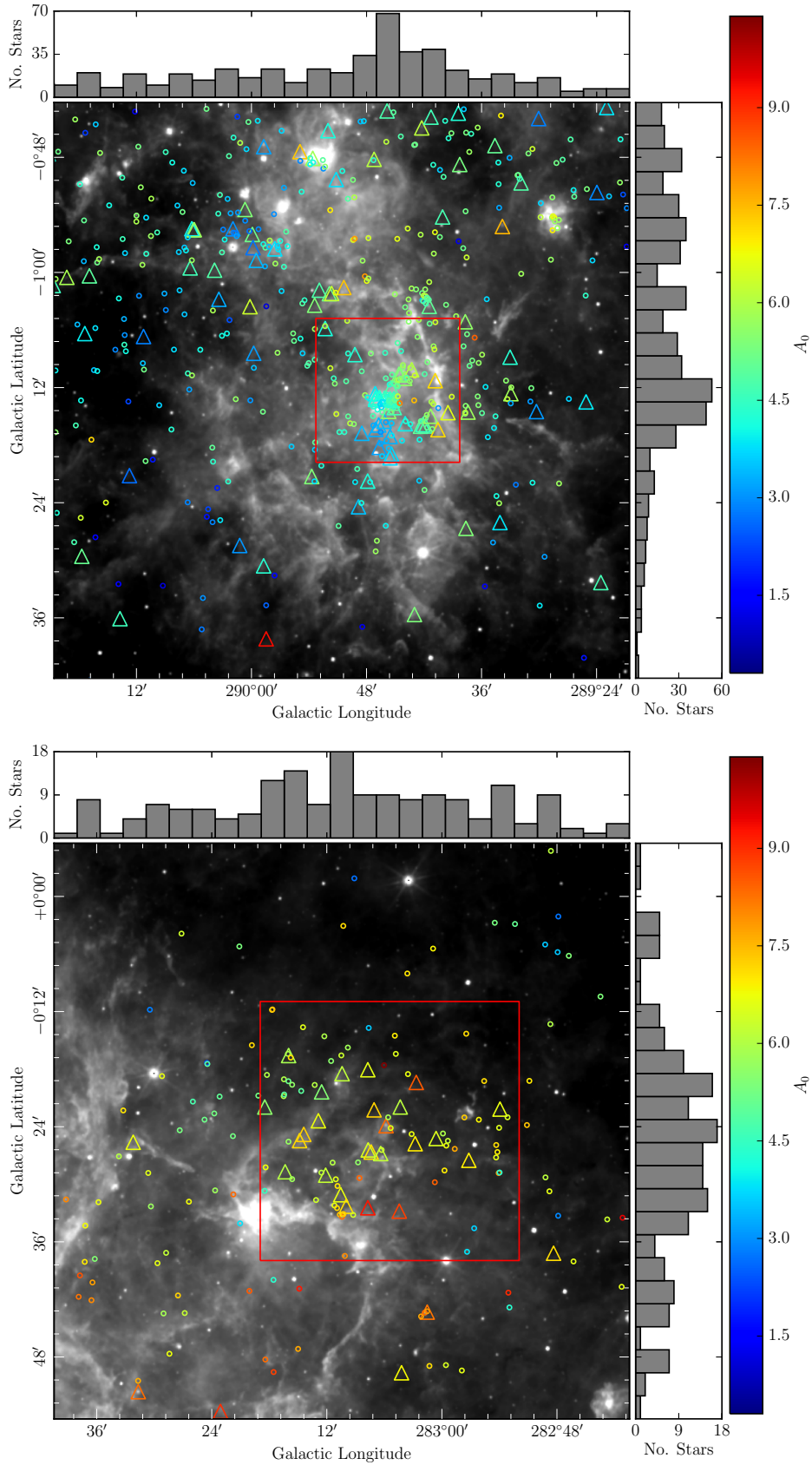
As well as picking up new stars that are associated with known clusters we also highlight two new distinct clusterings of O stars as seen in the large spatial plot, Fig. 5.15. The first, located at  $\sim l = 289.76, \sim b = -1.30$ , we shall call, Cl 1, and the second at  $\sim l = 283.16, \sim b = -0.50$  shall be called Cl 2. Without accurate measurements of distance and proper motions it is difficult to determine if these are genuine clusters or associations. However, if they are genuine, we might expect to find that they are aligned with warm dust and/or HII emission thanks to their massive star content.

Fig. 5.19 shows a closer view of these potential clusters/associations over-plotted on the WISE 12 micron image, with each OB star coloured by its derived extinction. The region shown covers 1 square degree. The upper panel shows Cl 1 and the lower panel shows Cl 2. The histograms above and to the right of the images show the distribution in Galactic longitude and latitude respectively of the region shown. Fig. 5.20 is the same as above but over plotted on the VPHAS+  $H\alpha$  image. Although somewhat arbitrary, the red boxes drawn on the images give a rough indication of the boundaries of the clusters/associations and are based on where the stellar density falls off. The red box for Cl 1 measures  $15 \text{ arcmin}^2$  and for Cl 2 it measures  $24 \text{ arcmin}^2$ . Fig. 5.21 shows the distribution in  $A_0$  for Cl 1 (left panel) and Cl 2 (right panel) within the red box (red bars) and outside the red box (grey bars).

In the top panel of Figs. 5.19 and 5.20 we can see that there is a clear peak in stellar density within the red box. The main concentration of stars in Cl 1 coincides with bright emission from warm dust in the 12 micron image as well as with some relatively faint emission from the ionised gas in the  $H\alpha$  image. Although, there is a

fairly large spread in extinction ( $3 < A_0 < 6$ ) peaking at  $A_0 \sim 4.5$  for stars within the red box the distribution is a little tighter than for those beyond the red box. The fact that the 12 micron emission extends well beyond the peak in stellar density suggests that this cluster/association is probably part of a wider star forming region. Based on its similar extinction and close Galactic longitude, Cl 1 is likely to be at a similar distance to NGC 3603, perhaps around  $\sim 6-7$  kpc.

The more highly reddened Cl 2 appears to be much more spatially dispersed but has a much tighter distribution in extinction ( $5.5 < A_0 < 7.5$ ) peaking at  $A_0 \sim 6$ . The peak in warm dust emission shown in the WISE 12 micron image does not seem to coincide with the peak in stellar density and there is no  $H\alpha$  emission seen in the VPHAS+ image. This suggests that, if this is a genuine cluster, it has time to clear the local ISM and dynamically evolve. It looks like more of an OB association than a cluster. Cl 2 shares a similar extinction to Wd 2 and is not far away in Galactic longitude and therefore may share a similar distance of  $\sim 5 - 6$  kpc. Assuming this distance, this association would be  $\sim 35 - 40$  pc across which is much larger than typical open clusters which are usually no more than a few pc across ([Portegies Zwart et al., 2010](#)).



**Figure 5.19:** Possible new clusters/OB associations over plotted on the associated warm dust emission from the WISE 12 micron image. The top panel shows Cl 1 and the bottom panel shows Cl 2. The histograms above and to the right of the plot show the Galactic longitude and latitude distribution respectively. The red boxes which measure  $15^2$  arcmin and  $24^2$  arcmin respectively roughly indicate where the stellar density falls off.

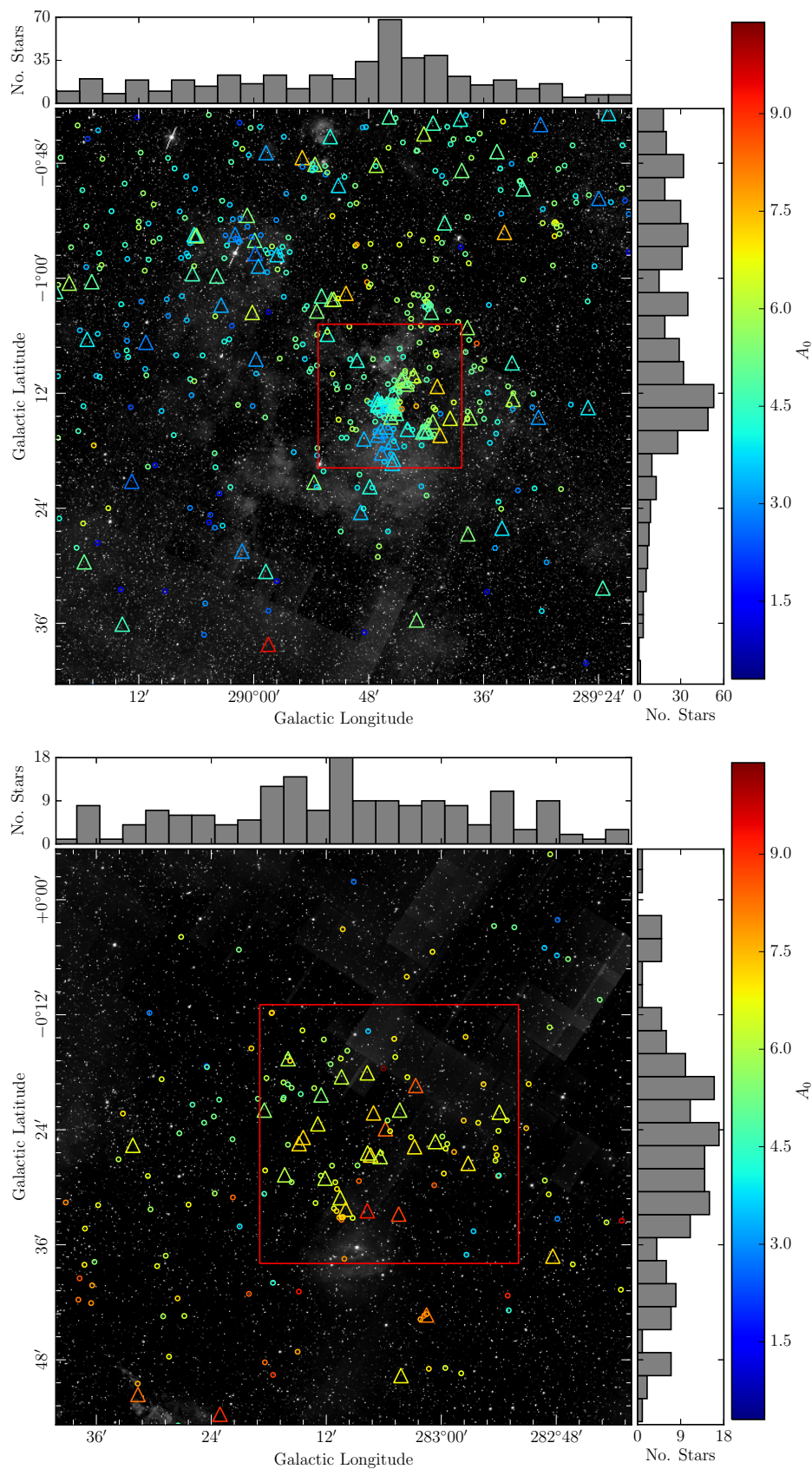


**Figure 5.20:** Possible new clusters/OB associations over plotted on the H $\alpha$  emission from the VPHAS+ image. The top panel shows Cl 1 and the bottom panel shows Cl 2. The histograms above and to the right of the plot show the Galactic longitude and latitude distribution respectively. The red boxes which measure  $15^2$  arcmin and  $24^2$  arcmin respectively roughly indicate where the stellar density falls off.

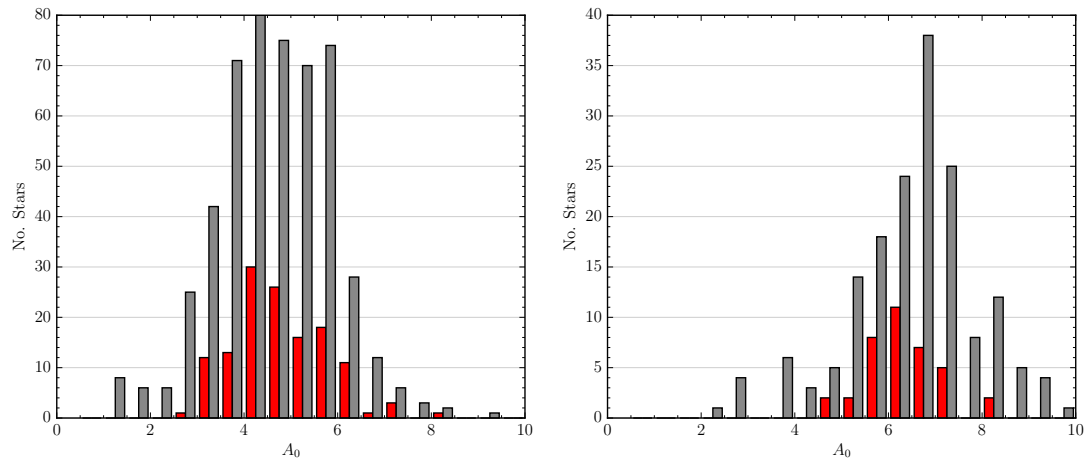


**Figure 5.21:**  $A_0$  distributions of Cl 1 (left panel) and Cl 2 (right panel)

---

# CHAPTER 6: COMPARISONS WITH SELECTED CATALOGUES

---

In this chapter I make comparisons between the catalogue of OB stars from VPHAS+ with two of the largest OB star catalogues from the literature; ‘The Catalog of Galactic OB stars’ by [Reed \(2003\)](#) and ‘The Galactic O star catalogue’ (GOSC) by [Maíz Apellániz et al. \(2013\)](#). I also make comparisons between the VPHAS+ OB star catalogue and a list of HII regions from the Red MSX Source (RMS) survey.

## 6.1 OB star catalogues

The [Reed \(2003\)](#) ‘Catalog of Galactic OB stars’ is currently the largest data set which attempts to include spectroscopically confirmed and photometric candidate OB stars drawn from across the literature up until the year 2003. The catalogue includes spectroscopically confirmed main sequence stars earlier than B2 or luminosity class I-IV stars earlier than B9. It also includes candidate OB stars which have a UB<sub>V</sub> Q value of less than -0.667, roughly corresponding to earlier than main sequence B2. Coloured in green on the upper panel of [Fig. 6.1](#) is a histogram of the B band magnitudes of all stars (earlier than B2 if a spectral type is given) that fall into the 42 square degree Carina footprint and are listed in the [Reed \(2003\)](#) catalogue. In total there are 845 confirmed or suspected OB stars from the [Reed \(2003\)](#) catalogue in this region. Here it can be seen that 94% of the stars in the catalogue are brighter than  $B = 13$ . The mean B band magnitude is 10.58. Also plotted on the upper panel of [Fig. 6.1](#) is the VPHAS+  $g$  band (similar to the B band) histogram for the candidate OB stars selected in this study. The mean  $g$  band magnitude is 16.99. Although in more recent years there have been more discoveries of fainter OB stars in this region, particular around the massive star clusters NGC 3603 and Wd 2 (see e.g. [Vargas Álvarez et al., 2013](#); [Hur et al., 2015](#)), we can see that the VPHAS+ selection is probing a much deeper magnitude range than has been achieved before. There is a noticeable deficit of stars with  $g/B \sim 12 - 13$

between the two catalogues which are missing from this study due to the bright limit. In total, this study has uncovered around seven times more OB stars in this region than in the [Reed \(2003\)](#) catalogue. There are a total of 22 objects in the [Reed \(2003\)](#) catalogue with a quoted B and V band magnitude  $> 13$ , which we would expect to be able to detect in VPHAS+. Of these objects 6 successfully cross match to the VPHAS+ catalogue to within a 1 arcsec radius. Eight of the missing 16 objects are spectroscopically confirmed O stars missing in the core of NGC 3603 due to blending. The remainder are photometric candidates in [Reed \(2003\)](#). They may be missing in the VPHAS+ catalogue due to them being incorrectly identified as OB candidates in [Reed \(2003\)](#) or their photometry may be incomplete or affected by blending in VPHAS+.

The Galactic O star Catalogue (GOSC) ([Maíz Apellániz et al., 2013](#)) is the largest collection of high-resolution spectroscopically confirmed Galactic O stars. Currently the total number of stars in this catalogue stands at 590 and, as shown in [Fig. 1.9](#) which is taken directly from [Maíz Apellániz et al. \(2016\)](#), it is complete up to  $B = 8$ . Coloured green in the lower panel of [Fig. 6.1](#) is the B band magnitude distribution for O stars in the GOSC catalogue that fall into the 42 square degree Carina region. In total there are 106 stars from GOSC in this region. Also plotted on the lower panel of [Fig. 6.1](#) are the  $g$  band apparent magnitudes of the O star candidates, whose SED fits give  $\log(T_{\text{eff}}) > 4.477$  and  $\chi^2 < 7.82$ , uncovered by VPHAS+ in this study.

Here, we can see the large number of much-fainter O star candidates that we are uncovering compared to what O stars have already been spectroscopically observed by GOSC. This study offers a reliable catalogue of nearly a 1000 candidate O star targets homogeneously selected for future follow-up with spectroscopy.

The VPHAS+ catalogue was also cross matched with a catalogue of Galactic WR stars<sup>1</sup> drawn from across the literature that was initially put together by [Rosslowe & Crowther \(2015\)](#). In the 42 square degree Carina region there are a total of 52 WR stars of which 32 are faint enough to be in our catalogue. As we saw in [Table 5.2](#), 29 of these were successfully cross matched to the catalogue. As discussed previously, the vast majority of WR stars return  $\chi^2 > 7.82$  SED fits due to the presence of NIR

<sup>1</sup><http://pacrowther.staff.shef.ac.uk/WRcat/index.php>

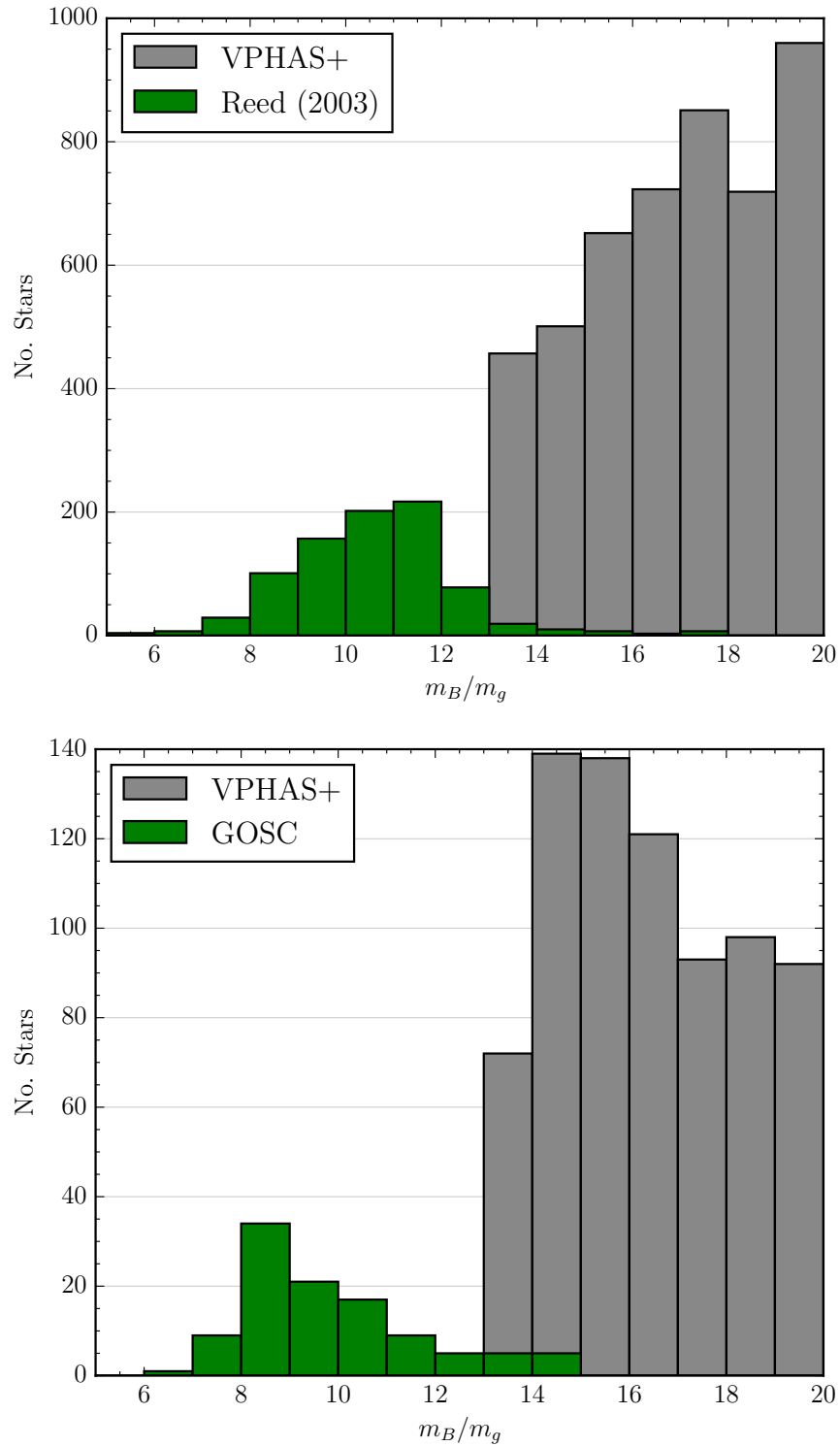


**Figure 6.1:** Top: Comparison of the B band apparent magnitudes of OB stars in the [Reed \(2003\)](#) catalogue (green) with the  $g$  band apparent magnitudes of candidate OB stars in this study (grey). Bottom: Comparison of the B band apparent magnitudes of O stars only, from GOSC (green) with the  $g$  band apparent magnitudes of candidate O stars in this study (grey).

excess.

## 6.2 RMS HII regions

The selected candidate O and B stars are all capable of ionising the ISM. As such it might be expected that many will be located within detectable H II regions. Furthermore, reddening may make the detection of H $\alpha$  nebulosity uncertain. Therefore it is useful to access longer wavelengths. The Red MSX Source (RMS) survey ([Lumsden et al., 2013](#)) is a mid infra-red survey designed to search the Galaxy for massive young stellar objects (MYSOs). The survey also identified a number of extended sources which are potentially compact and diffuse HII regions with similar near- and mid-IR colours to MYSOs. The aim here is to cross-match the VPHAS+ OB star catalogue with the RMS catalogue to see if any of the candidate OB stars are likely to be the ionizers of such compact/diffuse HII regions, and to appraise how often the nebulosity is apparent also.

The catalogue of OB stars was cross matched with the RMS catalogue of HII regions to within 15 arcmin. In total 85 O stars and 96 B stars were successfully cross matched within this limiting radius. All 85 RMS HII regions that were cross matched with O stars also successfully cross matched with the B stars. The blue line in [Fig. 6.2](#) shows the cumulative distribution in cross match radius for O stars (left panel) and B stars (right panel). In this plot it can be seen that the median cross match radius for the B stars is less than for the O stars. In the case of a random distribution, this result could simply be attributed to the B stars being more numerous and therefore more likely to align with an HII region. In order to determine if these cross matches are likely to be genuine or if they are just chance alignments, the cross match was performed a second time but with a fixed offset of 0.5 degrees applied to the Galactic longitudes of the candidate OB stars in order to crudely pseudo-randomise their positions. A K-S test between the two cumulative distributions in cross match radius was then performed. The cumulative distribution for the alternative catalogue cross match radius is the green line shown in [Fig. 6.2](#). Here, the p-value obtained for both the O star and B

star case is very small (near zero) allowing us to reject the null hypothesis that the two samples were drawn from the same distribution. This suggests that cross match between OB star candidates at their true positions and the RMS HII regions is genuine rather than due to chance alignment. The median separation between the RMS HII regions and the O and B stars is  $\sim 230$ arcsec and  $\sim 87$ arcsec respectively.

Figs. 6.3 and 6.4 show a selection of thumbnails where our OB candidates have been successfully cross matched with the RMS HII regions to within 20 arcsec (two MSX beamwidths). For each of these HII regions there is a VPHAS+ H $\alpha$  image, which shows emission from the HII region, and a WISE 12  $\mu$ m image to show any accompanying warm dust emission. The black circles with white crosses the positions of HII regions given by the RMS catalogue. Empty circles and triangles are B stars and O star candidates respectively. Diamonds are OB candidates with poor  $\chi^2$  fits. Thumbnails are not shown of HII regions that are obviously connected to the extensive and well known nebulosity near NGC 3603, Wd 2 and the Carina Nebula.

Here, we can see that we have uncovered the potential ionizers of 16 different HII regions. For around 11 of the HII regions, a single star seems to be responsible for the bright emission, while the rest have multiple stars that may contribute. Acknowledging the large uncertainties on effective temperature, eight of the HII regions are associated with probable B stars ( $\log(T_{\text{eff}}) < 4.477$ ), with no nearby O star ( $\log(T_{\text{eff}}) > 4.477$ ). Although these cross matches are convincing, accurate distances to both the HII regions and the companion OB star would be needed to determine if the two are truly related. In a number of cases, (RMS IDs 389, 446, 456, 470, 471, 653, 696 and 4783) the HII regions are very faint or seemingly non existent in the VPHAS+ image but show obvious signs of warm dust emission in the complementary WISE 12 micron images. It is not obvious that the optical HII regions are missing due to extinction, as the OB stars associated with these regions are no more highly reddened than those that do show H $\alpha$  emission in the optical. The mean extinction for objects with and without a visible HII region in VPHAS+ is  $A_0 = 6.4$  and  $A_0 = 6.7$  respectively. One interesting example is RMS ID 469 where the brightest H $\alpha$  emission coincides with the weakest 12  $\mu$ m emission and vice versa. Here, some of the bright 12  $\mu$ m emission may be due

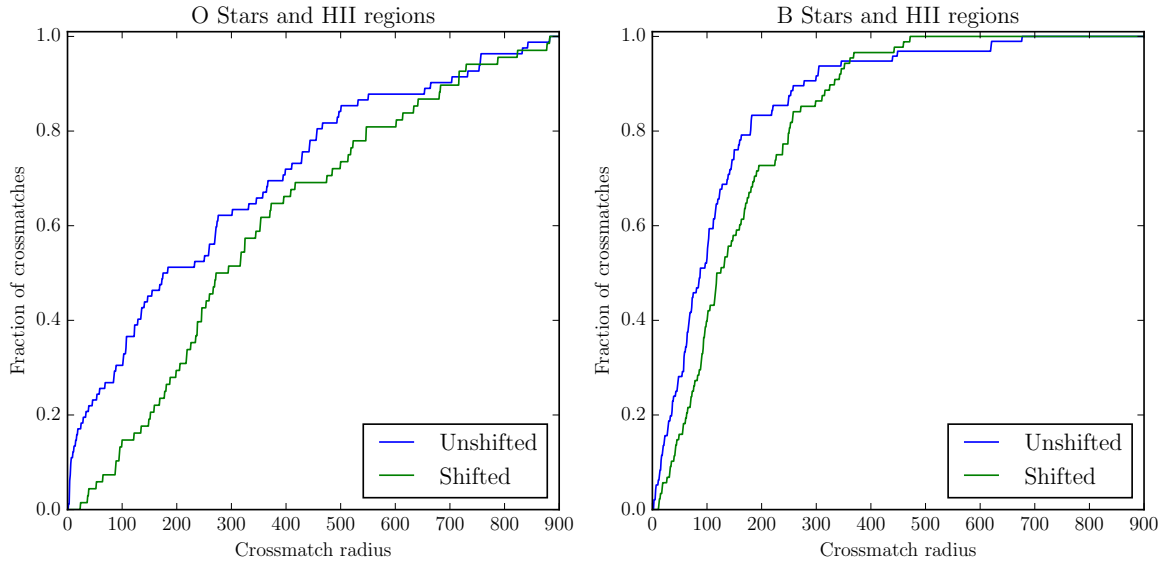


**Figure 6.2:** Cumulative distributions in cross match radius between RMS HII regions and the VPHAS+ O star candidates (left) and B star candidates (right). The green line shows the distribution for when the position of the OB stars have been shifted and the blue line when they are unchanged. A k-s test between the blue and green distributions produces near zero p-values in both cases suggesting that the cross matches are not down to random alignment.

to an increased column density of dust rather than due to warming. If this is the case then you would expect the optical emission to be more extinguished in these regions. In order to determine if the bright  $12\mu\text{m}$  emission is truly due to warm dust longer wavelength data would be needed to obtain colour information.

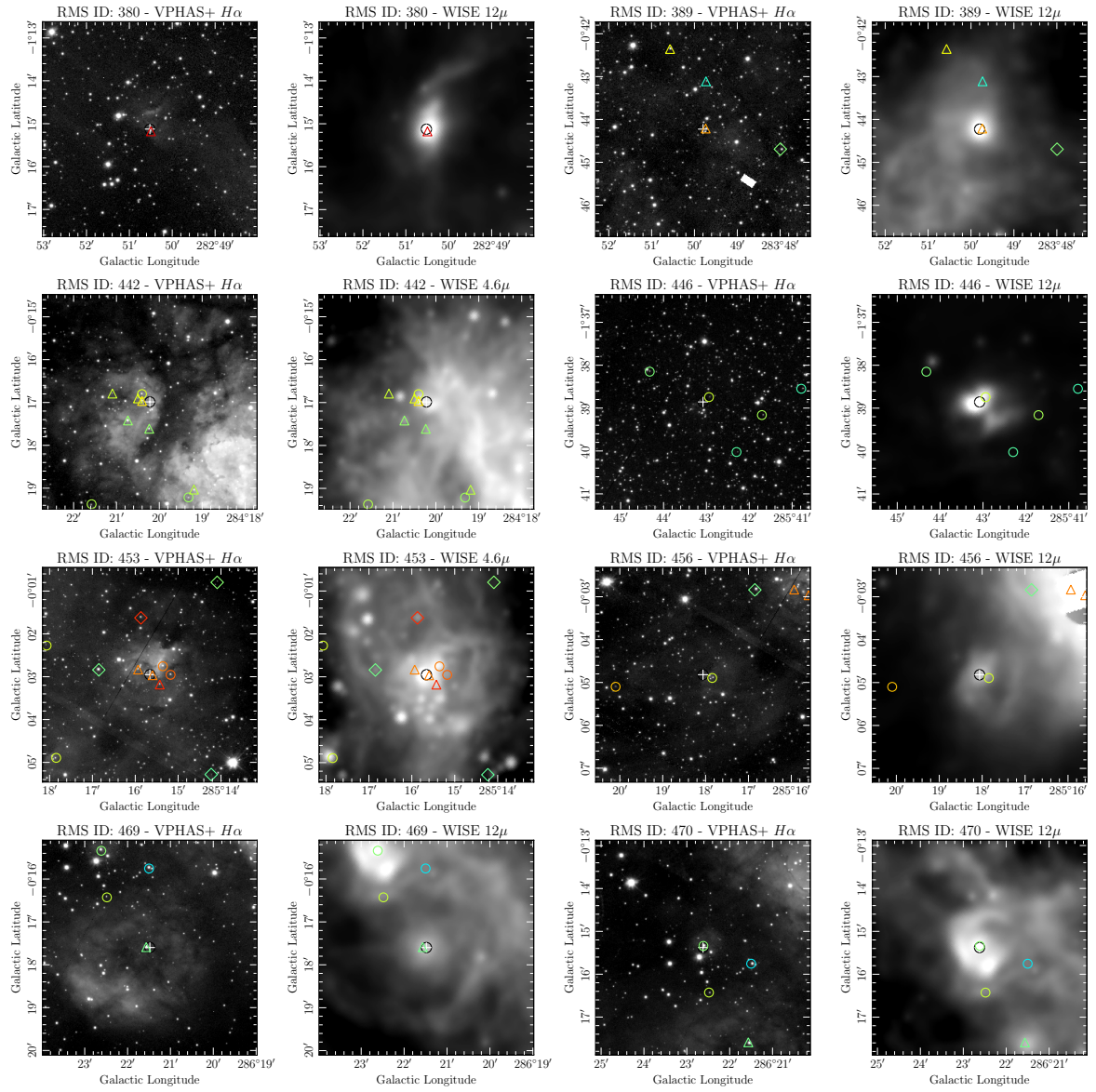


**Figure 6.3:** Selection of HII regions cross matched with OB star candidates from VPHAS+. Triangles are O stars, circles are B stars and diamonds are objects with poor  $\chi^2$  values from their SED fits.

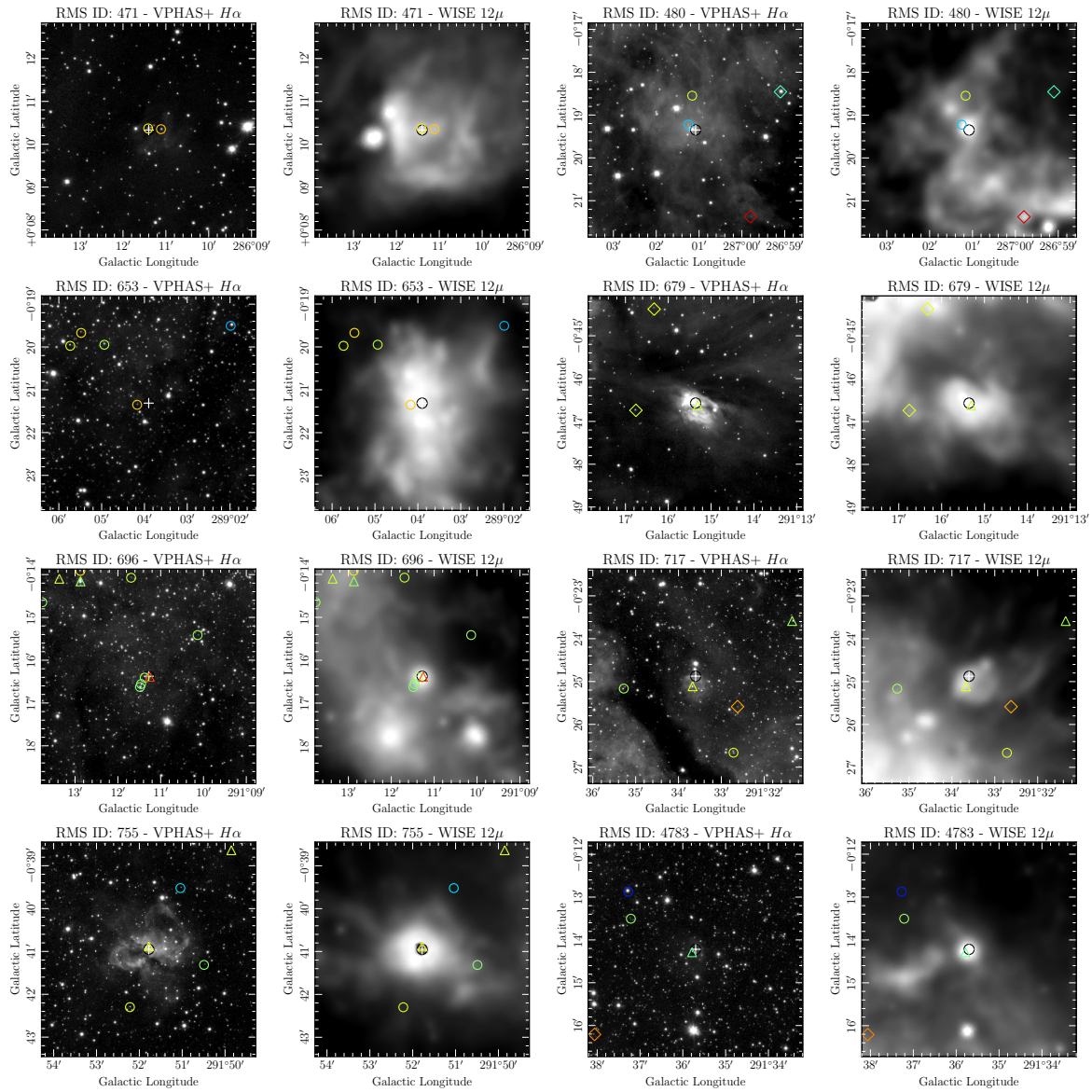


**Figure 6.4:** Selection of HII regions: cross matched with OB star candidates from VPHAS+. Triangles are O stars, circles are B stars and diamonds are objects with poor  $\chi^2$  values from their SED fits.

---

# CHAPTER 7: CONCLUSIONS AND FUTURE WORK

---

## 7.1 Conclusion

In summary, I have demonstrated a method for selecting and parametrizing the reddening and basic stellar properties of OB stars uniformly across large areas of the Southern sky using VPHAS+, and NIR survey data. The selection has resulted in a reliable catalogue of 5915 high confidence OB stars earlier than  $\sim B2$  from across 42 square degrees straddling the Galactic mid-plane. Of these, 905 are probable O stars. This has been achieved by reaching down to  $g = 20$  mag and approaches a factor of 10 increase relative to the small numbers of known and candidate O to B2 stars at brighter magnitudes. The region explored spanned  $\sim 12$  degrees running from the Carina Arm tangent to the much studied massive cluster NGC 3603.

By bringing together VPHAS+  $u, g, r, i$  photometry with NIR 2MASS photometry, we are able to determine both the value of the extinction,  $A_0$ , and the shape of the reddening law, as parametrised by  $R_V$ , to good precision: both are typically measured to better than 0.1 (magnitudes in the case of  $A_0$ ). Using a statistically much larger sample across a large area on the sky, I have confirmed previous results that sight lines into the Carina Arm require flatter reddening laws with  $3.5 \lesssim R_V \lesssim 4.0$  for  $A_0 \geq 2.0$ . More normal values of  $3.1 \lesssim R_V \lesssim 3.5$  appear to apply to foreground objects with  $A_0 \lesssim 2$ . This suggests that the average dust grain size within the Carina Arm star forming region is larger than that in the inter-arm region – a result that is consistent with the high molecular cloud content of a grand spiral arm design. Analysis in Chapter 5 has also shown that the extinction builds up more quickly closer to the Carina Arm tangent where the dust column density is expected to be significantly higher.

A crude impression of stellar effective temperatures (and hence distance moduli) was expected, and so it has turned out. However, I have found good consistency with previously published results in the benchmark region around the much-studied clus-

ter Westerlund 2, providing a first indication that the methods are sound and able to distinguish O stars from early-B stars. This distinction was further confirmed in Chapter 4 where a representative sample of 276 OB candidates were followed up with AAOmega spectroscopy. Despite a clear systemic difference between the photometrically derived effective temperatures and those derived from spectroscopy (particularly for the O stars), the OnIR SED fitting proved good enough to distinguish likely O from early B stars. I also showed that the systematic offset in effective temperature only has a modest effect on the derived extinction parameters for the B stars ( $A_0 \sim +0.09$  and  $R_V \sim -0.07$ ) and an even smaller effect on the O stars ( $A_0 \sim +0.025$  and  $R_{V-s} \sim -0.026$ ). This is a reflection of the convergence of the O star SED onto the Rayleigh-Jeans limit as effective temperature rises to  $\sim 40000\text{K}$  and more. The follow-up spectroscopy also confirmed that there are very low levels of contamination ( $\sim 6\%$ ) from late type stars within the selection.

Further exploitation of the parameters derived from the photometry has also enabled a crude distinction between main sequence OB stars and the subdwarfs at lower luminosities, and higher-luminosity evolved massive OB stars. The narrow band  $\text{H}\alpha$  filter in the VPHAS+ survey has also enabled the selection of emission line objects. The majority of these are likely to be classical Be stars while some may be examples of yet to be discovered WR stars. This method of selection does not explicitly find new WR stars because these objects typically present with NIR excesses, and therefore yield poor SED fits.

I have also demonstrated how the high resolution and wide field of view of Omega-Cam can bring a wider context to the study of star forming regions, away from the dense well studied cores of open clusters and OB associations, extending into previously uncharted areas on the sky. This provides the ability to identify potentially-related stars that have either been ejected from clusters or simply have formed in relative isolation in the surrounding field – perhaps as part of a wider star-formation event. In particular, a large number of new candidate reddened O stars have been found at extended angular separation from the young massive stars cluster in NGC 3603 and a handful have been found around Wd 2. Searching for OB stars in wider regions also allows

for the discovery of new clusters and OB associations; like the two potential new clusters/associations uncovered in Chapter 5. However, accurate distances and kinematics will be needed to confirm their status as clusters or associations. I have also paired up the ionization sources of a number of HII regions catalogued by the RMS survey. I have also shown how the large number of new discoveries can be put to work to reveal the overall structure of the disk – here, in revealing the evidence of incipient disk warping.

## 7.2 Improvements

As the catalogue is magnitude limited, a large number of highly reddened early B stars will be missing from the selection as discussed in Section 5.2.1. In order to sweep up these objects, deeper observations in both the  $g$  and  $u$  bands would be needed. This would also allow for the detection of O stars with extreme reddenings of  $A_0 > 10$  and/or at greater distances ( $D \gtrsim 10\text{kpc}$ ). Pleasingly there are signs that the still preliminary nature of the photometric calibration of the VPHAS+ survey data blends well with the now well-established 2MASS calibration. However the global calibration of VPHAS+ can still be improved upon by using a higher resolution and deeper survey as the external reference for calibrating the  $g$ ,  $r$  and  $i$  band. A possible candidate for such a reference over some of the area is the Pan-STARRS survey (Magnier et al., 2013) which will soon be made public. The method could also be improved by combining the optical VPHAS+ data with deeper higher resolution NIR data from a survey such as VVV. This would enable cleaner and more numerous cross matches within crowded regions such as the cores of clusters, and across a wider  $g - K$  range.

The Bayesian SED fitting technique may be improved by using more complex priors on distance and effective temperature. For example, a prior that reflects the IMF may be used on effective temperature. In this scenario, the posterior probability distribution in effective temperature would be skewed towards lower temperatures. Given the tendency in the O star range to systematically under estimate effective temperatures with a uniform prior, this alone would in fact cause an even greater disagreement. The could be an improvement in the B star range. Using a prior that reflects the

increase in volume sampled as a function of distance may counteract the bias in the O star range. The posterior probability distributions in distance modulus would then be skewed towards higher values as it is more likely for an object to be at a greater distance given the increase in volume sampled. In the presence of the degeneracy between effective temperature and distance this may skew the effective temperatures back towards higher values. However, the exact effects of changing the priors would need to be tested and in combination they may not change the results significantly. The systematic offset in effective temperature may also be alleviated by using the same set of model atmospheres to derive synthetic photometry for SED fitting as those used for fitting the spectroscopy. In effect we are currently comparing two distinct sets of models. An alternative could be to use a set of Non-LTE models such as CMFGEN (Hillier & Lanz, 2001). However, there is currently no public repository for a well sampled grid of such models that includes model atmospheres with temperatures spanning 15000K to 50000K or higher.

### 7.3 Future work

Future work emerging from this study will include:

- Applying the automated method across the entire VPHAS+ footprint
- Investigating variable extinction laws within clusters
- Analysing already obtained XSHOOTER spectroscopy
- Further spectroscopic follow-up

Further low resolution spectroscopic follow up of the catalogue will allow us to further understand the advantages and limitations of the SED fitting technique through greater number statistics – so far there is little insight on the subdwarf and evolved OB star candidates. The catalogue also provides reliable targets for future high resolution spectroscopic follow up. This would provide much needed empirical evidence in large

numbers that will aid understanding the evolution of OB stars in the Milky Way (Castro et al., 2014).

High resolution XSHOOTER spectroscopy has already been obtained for two of the candidate ‘runaway’ early O stars near Wd 2 as discussed in section 3.5.2 as well as for two control stars in the centre of the cluster. This data will allow accurate radial velocity measurements to be made in order to determine if these objects have been ejected from Wd 2 or if they are more likely to have formed in situ. Clearly much more can be done in this area for this and other clusters.

One aspect of further analysis that might be attempted is on variable extinction laws within clusters. As was shown in Chapter 5 sight lines within Carina show considerable extinction law variation with values of  $R_V$  mostly ranging from 3.5 to 4.0. Some of this variation may be informative. As an example, Fig. 7.1 shows the VPHAS+  $H\alpha$  image centred on Wd 2, measuring 3 arcmin across. Over-plotted are the the OB candidates coloured by their derived values of  $R_V$ . Here, we can see a tendency for lower values of  $R_V$  in the central core of the cluster compared to the outskirts. This could be due to radiation pressure from the massive stars in the cluster core driving the larger dust grains out into the local ISM, a process described by Draine (2011). If this is the case it might be expected that this pattern is also seen in other clusters. In order to see if the same applies to NGC 3603 we would need higher resolution NIR data as there are presently no  $R_V$  measurements in the core of NGC 3603 due to blending. For Wd 2, superior NIR data presented by Ascenso et al. (2007a) was adopted.

In the coming months, I aim to take the method established in this thesis and apply it to all VPHAS+ fields that have been observed to date. Fig. 7.2 shows a plot of the survey footprint with fields complete in all VPHAS+ filters coloured in green up to April 2016. The extension of my work will take in a strip  $\sim \pm 2$  degrees across the entire Southern Galactic mid-plane (a sky area of over 700 square degrees), within which we expect to find the majority of massive OB stars. This will surely result in the largest catalogue of Galactic OB stars to date, exceeding previous lists by up to a factor of at least a few. Garmany et al. (1982) were able to claim a volume-limited census to  $\sim 2.5$  kpc 3 decades ago – now it should be possible to expand the effective volume by a

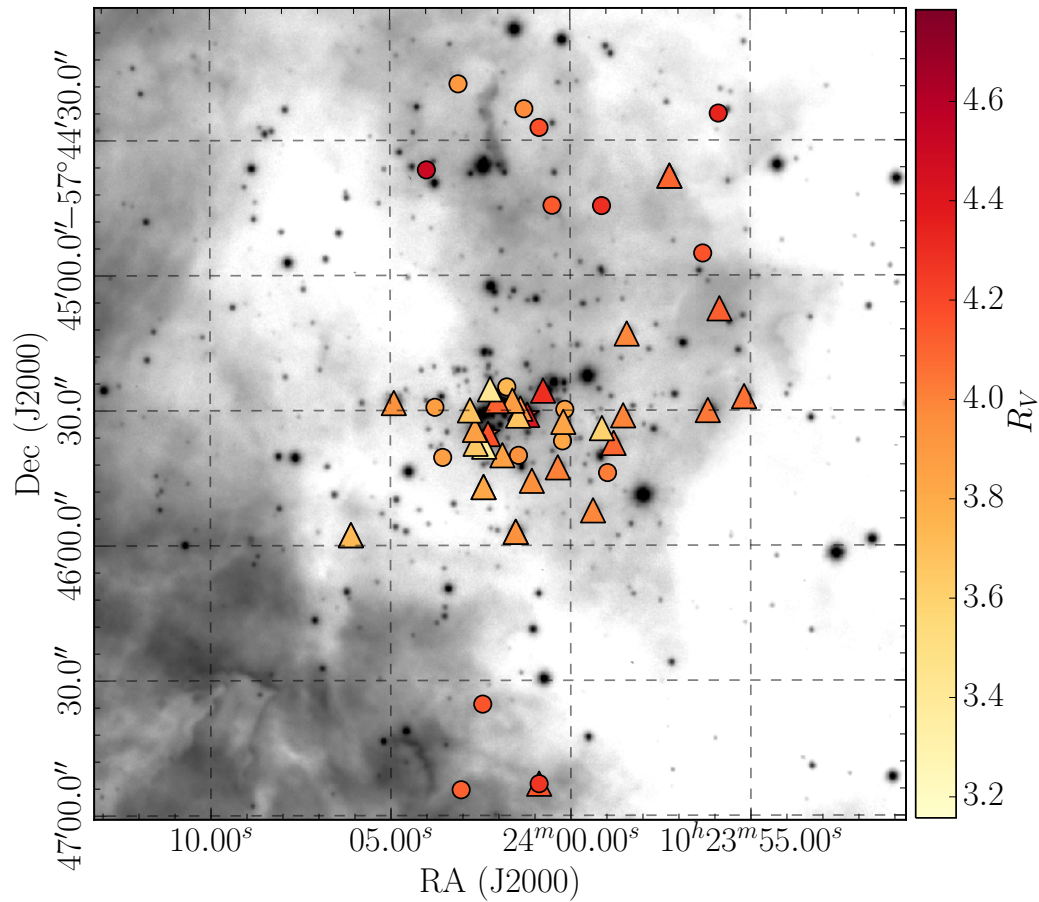


**Figure 7.1:** Candidate OB stars over plotted on the VPHAS+  $H\alpha$  image of Wd 2, coloured by their derived values of  $R_V$ . Objects in the core of the cluster tend to show lower values of  $R_V$  compared to the outskirts of the cluster.

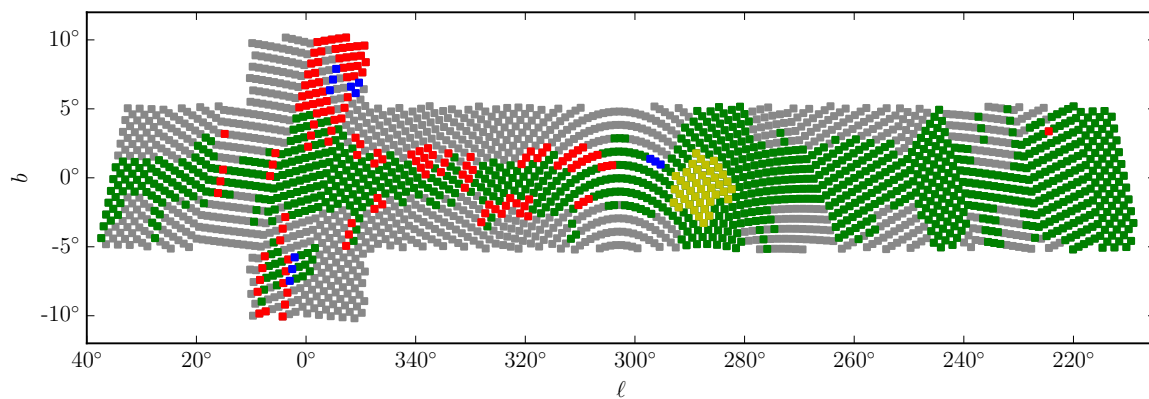


**Figure 7.2:** VPHAS+ survey footprint in Galactic coordinates. The coloured points show which fields have been completed only in the ‘red’ set (red points), only in the ‘blue’ set (blue points) and those that are complete in both sets (green points) and those yet to be observed (grey points) up to April 2016. The points coloured in yellow are the fields used in this study

factor of 2 or more. Building this catalogue in very near future would make it available before the initial release of Gaia data in 2017 that will provide the first parallaxes to these objects. Obtaining distances to a statistically large sample of Galactic OB stars will allow us to begin to build an accurate 3D picture of the spatial distribution of recent and ongoing star formation in the Milky Way and test the new generation of reddening maps and methods (e.g. [Sale & Magorrian, 2014](#); [Green et al., 2014](#)). Proper motions and distances from Gaia will also enable the discovery and confirmation of new young clusters and OB associations. Our high quality extinction estimates are critical to Gaia exploitation, since without reliable reddening corrections the luminosities of massive O and early B stars will remain unknown, despite knowledge of the distance from parallax measurements.

The work to be done will include: i) Bringing all the relevant VPHAS+ u band data onto an astrophysically sound scale relative to the longer wavelength bands. ii) Applying my selection technique across the Southern Galactic mid-plane. iii) Organizing the selections into an annotated catalogue (e.g. distinguishing high quality candidate OB stars from the other groups that also pass through the selection).

# References

- Allen, C. & Poveda, A. 1971, *Ap&SS*, 13, 350 [\[ADS\]](#)
- Allen, D. A. & Hillier, D. J. 1993, *Proceedings of the Astronomical Society of Australia*, 10, 338 [\[ADS\]](#)
- Ascenso, J., Alves, J., Beletsky, Y., & Lago, M. T. V. T. 2007a, *A&A*, 466, 137 [\[ADS\]](#)
- Ascenso, J., Alves, J., Vicente, S., & Lago, M. T. V. T. 2007b, *A&A*, 476, 199 [\[ADS\]](#)
- Astropy Collaboration, Robitaille, T. P., Tollerud, E. J., Greenfield, P., Droettboom, M., Bray, E., Aldcroft, T., Davis, M., Ginsburg, A., Price-Whelan, A. M., Kerzendorf, W. E., Conley, A., Crighton, N., Barbary, K., Muna, D., Ferguson, H., Grollier, F., Parikh, M. M., Nair, P. H., Unther, H. M., Deil, C., Woillez, J., Conseil, S., Kramer, R., Turner, J. E. H., Singer, L., Fox, R., Weaver, B. A., Zabalza, V., Edwards, Z. I., Azalee Bostroem, K., Burke, D. J., Casey, A. R., Crawford, S. M., Dencheva, N., Ely, J., Jenness, T., Labrie, K., Lim, P. L., Pierfederici, F., Pontzen, A., Ptak, A., Refsdal, B., Servillat, M., & Streicher, O. 2013, *A&A*, 558, A33 [\[ADS\]](#)
- Bailer-Jones, C. A. L. 2011, *MNRAS*, 411, 435 [\[ADS\]](#)
- Bertelli, G., Bressan, A., Chiosi, C., Fagotto, F., & Nasi, E. 1994, *A&AS*, 106, 275 [\[ADS\]](#)
- Bestenlehner, J. M., Vink, J. S., Gräfener, G., Najarro, F., Evans, C. J., Bastian, N., Bonanos, A. Z., Bressert, E., Crowther, P. A., Doran, E., Friedrich, K., Hénault-Brunet, V., Herrero, A., de Koter, A., Langer, N., Lennon, D. J., Maíz Apellániz, J., Sana, H., Soszynski, I., & Taylor, W. D. 2011, *A&A*, 530, L14 [\[ADS\]](#)
- Blaauw, A. 1961, *Bull. Astron. Inst. Netherlands*, 15, 265 [\[ADS\]](#)
- Bonanos, A. Z., Lennon, D. J., Köhlinger, F., van Loon, J. T., Massa, D. L., Sewilo, M., Evans, C. J., Panagia, N., Babler, B. L., Block, M., Bracker, S., Engelbracht, C. W., Gordon, K. D., Hora, J. L., Indebetouw, R., Meade, M. R., Meixner, M., Misselt, K. A., Robitaille, T. P., Shiao, B., & Whitney, B. A. 2010, *AJ*, 140, 416 [\[ADS\]](#)
- Bressan, A., Marigo, P., Girardi, L., Salasnich, B., Dal Cero, C., Rubele, S., & Nanni, A. 2012, *MNRAS*, 427, 127 [\[ADS\]](#)
- Cardelli, J. A., Clayton, G. C., & Mathis, J. S. 1989, *ApJ*, 345, 245 [\[ADS\]](#)
- Carmona, A., van den Ancker, M. E., Audard, M., Henning, T., Setiawan, J., & Rodmann, J. 2010, *A&A*, 517, A67 [\[ADS\]](#)
- Carraro, G., Turner, D., Majaess, D., & Baume, G. 2012, *ArXiv e-prints* [\[ADS\]](#)
- Castro, N., Fossati, L., Langer, N., Simón-Díaz, S., Schneider, F. R. N., & Izzard, R. G. 2014, *A&A*, 570, L13 [\[ADS\]](#)

- Chiappini, C., Matteucci, F., & Romano, D. 2001, *ApJ*, 554, 1044 [ADS]
- Clayton, C. A. 1986, *MNRAS*, 219, 895 [ADS]
- Crowther, P. A. 2007, *ARA&A*, 45, 177 [ADS]
- Crowther, P. A., Lennon, D. J., & Walborn, N. R. 2006, *A&A*, 446, 279 [ADS]
- Dachs, J., Kiehling, R., & Engels, D. 1988, *A&A*, 194, 167 [ADS]
- Daffon, S., Cunha, K., de Araújo, F. X., Wolff, S., & Przybilla, N. 2007, *AJ*, 134, 1570 [ADS]
- Dame, T. M. 2007, *ApJ*, 665, L163 [ADS]
- Dame, T. M., Hartmann, D., & Thaddeus, P. 2001, *ApJ*, 547, 792 [ADS]
- Davidson, K. & Humphreys, R. M. 1997, *ARA&A*, 35, 1 [ADS]
- de Wit, W. J., Testi, L., Palla, F., & Zinnecker, H. 2005, *A&A*, 437, 247 [ADS]
- Draine, B. T. 2003, *ARA&A*, 41, 241 [ADS]
- . 2011, *ApJ*, 732, 100 [ADS]
- Drew, J. E., Gonzalez-Solares, E., Greimel, R., Irwin, M. J., Küpcü Yoldas, A., Lewis, J., Barentsen, G., Eisloffel, J., Farnhill, H. J., Martin, W. E., Walsh, J. R., Walton, N. A., Mohr-Smith, M., Raddi, R., Sale, S. E., Wright, N. J., Groot, P., Barlow, M. J., Corradi, R. L. M., Drake, J. J., Fabregat, J., Frew, D. J., Gänsicke, B. T., Knigge, C., Mampaso, A., Morris, R. A. H., Naylor, T., Parker, Q. A., Phillipps, S., Ruhland, C., Steeghs, D., Unruh, Y. C., Vink, J. S., Wesson, R., & Zijlstra, A. A. 2014, *MNRAS*, 440, 2036 [ADS]
- Dutra, C. M., Bica, E., Soares, J., & Barbuy, B. 2003, *A&A*, 400, 533 [ADS]
- Eisenhauer, F., Genzel, R., Alexander, T., Abuter, R., Paumard, T., Ott, T., Gilbert, A., Gillessen, S., Horrobin, M., Trippe, S., Bonnet, H., Dumas, C., Hubin, N., Kaufer, A., Kissler-Patig, M., Monnet, G., Ströbele, S., Szeifert, T., Eckart, A., Schödel, R., & Zucker, S. 2005, *ApJ*, 628, 246 [ADS]
- Elmegreen, B. G. 2011, in *EAS Publications Series*, Vol. 51, *EAS Publications Series*, 19–30 [ADS]
- Evans, C. J., Taylor, W. D., Hénault-Brunet, V., Sana, H., de Koter, A., Simón-Díaz, S., Carraro, G., Bagnoli, T., Bastian, N., Bestenlehner, J. M., Bonanos, A. Z., Bressert, E., Brott, I., Campbell, M. A., Cantiello, M., Clark, J. S., Costa, E., Crowther, P. A., de Mink, S. E., Doran, E., Dufton, P. L., Dunstall, P. R., Friedrich, K., Garcia, M., Gieles, M., Gräfener, G., Herrero, A., Howarth, I. D., Izzard, R. G., Langer, N., Lennon, D. J., Maíz Apellániz, J., Markova, N., Najarro, F., Puls, J., Ramirez, O. H., Sabín-Sanjulián, C., Smartt, S. J., Stroud, V. E., van Loon, J. T., Vink, J. S., & Walborn, N. R. 2011, *A&A*, 530, A108 [ADS]
- Faherty, J. K., Shara, M. M., Zurek, D., Kanarek, G., & Moffat, A. F. J. 2014, *AJ*, 147, 115 [ADS]

- Fitzpatrick, E. L. 2004, in *Astronomical Society of the Pacific Conference Series*, Vol. 309, *Astrophysics of Dust*, 33 [ADS]
- Fitzpatrick, E. L. & Massa, D. 2007, *ApJ*, 663, 320 [ADS]
- Foreman-Mackey, D., Hogg, D. W., Lang, D., & Goodman, J. 2013, *PASP*, 125, 306 [ADS]
- Garmany, C. D., Conti, P. S., & Chiosi, C. 1982, *ApJ*, 263, 777 [ADS]
- Gies, D. R. & Bolton, C. T. 1986, *ApJS*, 61, 419 [ADS]
- Goodman, A. A., Alves, J., Beaumont, C. N., Benjamin, R. A., Borkin, M. A., Burkert, A., Dame, T. M., Jackson, J., Kauffmann, J., Robitaille, T., & Smith, R. J. 2014, *ApJ*, 797, 53 [ADS]
- Grabelsky, D. A., Cohen, R. S., Bronfman, L., & Thaddeus, P. 1988, *ApJ*, 331, 181 [ADS]
- Grabelsky, D. A., Cohen, R. S., Bronfman, L., Thaddeus, P., & May, J. 1987, *ApJ*, 315, 122 [ADS]
- Green, G. M., Schlafly, E. F., Finkbeiner, D. P., Jurić, M., Rix, H.-W., Burgett, W., Chambers, K. C., Draper, P. W., Flewelling, H., Kudritzki, R. P., Magnier, E., Martin, N., Metcalfe, N., Tonry, J., Wainscoat, R., & Waters, C. 2014, *ApJ*, 783, 114 [ADS]
- Gvaramadze, V. V., Gualandris, A., & Portegies Zwart, S. 2010, in *IAU Symposium*, Vol. 266, *IAU Symposium*, 413–416 [ADS]
- Hamann, W.-R., Gräfener, G., & Liermann, A. 2006, *A&A*, 457, 1015 [ADS]
- Han, Z., Podsiadlowski, P., Maxted, P. F. L., & Marsh, T. R. 2003, *MNRAS*, 341, 669 [ADS]
- Herbst, W. 1976, *ApJ*, 208, 923 [ADS]
- Hillier, D. J. & Lanz, T. 2001, in *Astronomical Society of the Pacific Conference Series*, Vol. 247, *Spectroscopic Challenges of Photoionized Plasmas*, 343 [ADS]
- Hur, H., Park, B.-G., Sung, H., Bessell, M. S., Lim, B., Chun, M.-Y., & Sohn, S. T. 2015, *MNRAS*, 446, 3797 [ADS]
- Hur, H., Sung, H., & Bessell, M. S. 2012, *AJ*, 143, 41 [ADS]
- Johnson, H. L. & Morgan, W. W. 1953a, *ApJ*, 117, 313 [ADS]
- . 1953b, *ApJ*, 117, 313 [ADS]
- Jurić, M., Ivezić, Ž., Brooks, A., Lupton, R. H., Schlegel, D., Finkbeiner, D., Padmanabhan, N., Bond, N., Sesar, B., Rockosi, C. M., Knapp, G. R., Gunn, J. E., Sumi, T., Schneider, D. P., Barentine, J. C., Brewington, H. J., Brinkmann, J., Fukugita, M., Harvanek, M., Kleinman, S. J., Krzesinski, J., Long, D., Neilsen, Jr., E. H., Nitta, A., Snedden, S. A., & York, D. G. 2008, *ApJ*, 673, 864 [ADS]

- Kalberla, P. M. W. & Kerp, J. 2009, *ARA&A*, 47, 27 [ADS]
- Kaltcheva, N. T. & Golev, V. K. 2012, *PASP*, 124, 128 [ADS]
- Kobulnicky, H. A., Kiminki, D. C., Lundquist, M. J., Burke, J., Chapman, J., Keller, E., Lester, K., Rolan, E. K., Topel, E., Bhattacharjee, A., Smullen, R. A., Vargas Álvarez, C. A., Runnoe, J. C., Dale, D. A., & Brotherton, M. M. 2014, *ApJS*, 213, 34 [ADS]
- Kroupa, P. 2001, *MNRAS*, 322, 231 [ADS]
- Lamb, J. B., Oey, M. S., Segura-Cox, D. M., Graus, A. S., Kiminki, D. C., Golden-Marx, J. B., & Parker, J. W. 2016, *ApJ*, 817, 113 [ADS]
- Langer, N. 2012, *ARA&A*, 50, 107 [ADS]
- Lanz, T. & Hubeny, I. 2003, *ApJS*, 146, 417 [ADS]
- . 2007, *ApJS*, 169, 83 [ADS]
- Levine, E. S., Blitz, L., & Heiles, C. 2006, *ApJ*, 643, 881 [ADS]
- Luck, R. E., Moffett, T. J., Barnes, III, T. G., & Gieren, W. P. 1998, *AJ*, 115, 605 [ADS]
- Lumsden, S. L., Hoare, M. G., Urquhart, J. S., Oudmaijer, R. D., Davies, B., Mottram, J. C., Cooper, H. D. B., & Moore, T. J. T. 2013, *ApJS*, 208, 11 [ADS]
- Maeder, A. & Meynet, G. 2010, *New Astronomy Reviews*, 54, 32, ;ice:title;Proceedings: A Life With Stars; /ce:title;
- Magnier, E. A., Schlafly, E., Finkbeiner, D., Juric, M., Tonry, J. L., Burgett, W. S., Chambers, K. C., Flewelling, H. A., Kaiser, N., Kudritzki, R.-P., Morgan, J. S., Price, P. A., Sweeney, W. E., & Stubbs, C. W. 2013, *ApJS*, 205, 20 [ADS]
- Maíz Apellániz, J., Sota, A., Arias, J. I., Barbá, R. H., Walborn, N. R., Simón-Díaz, S., Negueruela, I., Marco, A., Leão, J. R. S., Herrero, A., Gamen, R. C., & Alfaro, E. J. 2016, *ApJS*, 224, 4 [ADS]
- Maíz Apellániz, J., Sota, A., Morrell, N. I., Barbá, R. H., Walborn, N. R., Alfaro, E. J., Gamen, R. C., Arias, J. I., & Gallego Calvente, A. T. 2013, in *Massive Stars: From alpha to Omega*, 198 [ADS]
- Maíz-Apellániz, J., Walborn, N. R., Galué, H. Á., & Wei, L. H. 2004, *ApJS*, 151, 103 [ADS]
- Marshall, D. J., Robin, A. C., Reylé, C., Schultheis, M., & Picaud, S. 2006, *A&A*, 453, 635 [ADS]
- Martins, F. & Plez, B. 2006, *A&A*, 457, 637 [ADS]
- Martins, F., Schaerer, D., & Hillier, D. J. 2005, *A&A*, 436, 1049 [ADS]
- Mason, B. D., Hartkopf, W. I., Gies, D. R., Henry, T. J., & Helsel, J. W. 2009, *AJ*, 137, 3358 [ADS]

- Mauerhan, J. C., Cotera, A., Dong, H., Morris, M. R., Wang, Q. D., Stolovy, S. R., & Lang, C. 2010, *ApJ*, 725, 188 [ADS]
- Melena, N. W., Massey, P., Morrell, N. I., & Zangari, A. M. 2008, *AJ*, 135, 878 [ADS]
- Meylan, G. & Maeder, A. 1983, *A&A*, 124, 84 [ADS]
- Meynet, G. & Maeder, A. 2005, *A&A*, 429, 581 [ADS]
- Moffat, A. F. J., Shara, M. M., & Potter, M. 1991, *AJ*, 102, 642 [ADS]
- Mohr-Smith, M., Drew, J. E., Barentsen, G., Wright, N. J., Napiwotzki, R., Corradi, R. L. M., Eisloffel, J., Groot, P., Kalari, V., Parker, Q. A., Raddi, R., Sale, S. E., Unruh, Y. C., Vink, J. S., & Wesson, R. 2015, *MNRAS*, 450, 3855 [ADS]
- Munari, U., Sordo, R., Castelli, F., & Zwitter, T. 2005, *A&A*, 442, 1127 [ADS]
- Napiwotzki, R. & Silva, M. D. V. 2012, *Mem. Soc. Astron. Italiana*, 83, 272 [ADS]
- Paladini, R., Davies, R. D., & De Zotti, G. 2004, *MNRAS*, 347, 237 [ADS]
- Pang, X., Pasquali, A., & Grebel, E. K. 2011, *AJ*, 142, 132 [ADS]
- Parker, R. J. & Goodwin, S. P. 2007, *MNRAS*, 380, 1271 [ADS]
- Patat, F., Moehler, S., O'Brien, K., Pompei, E., Bensby, T., Carraro, G., de Ugarte Postigo, A., Fox, A., Gavignaud, I., James, G., Korhonen, H., Ledoux, C., Randall, S., Sana, H., Smoker, J., Stefl, S., & Szeifert, T. 2011, *A&A*, 527, A91 [ADS]
- Perets, H. B. & Šubr, L. 2012, *ApJ*, 751, 133 [ADS]
- Persi, P., Roth, M., Tapia, M., Ferrari-Toniolo, M., & Marenzi, A. R. 1994, *A&A*, 282, 474 [ADS]
- Poelarends, A. J. T., Herwig, F., Langer, N., & Heger, A. 2008, *ApJ*, 675, 614 [ADS]
- Portegies Zwart, S. F., McMillan, S. L. W., & Gieles, M. 2010, *ARA&A*, 48, 431 [ADS]
- Poveda, A., Ruiz, J., & Allen, C. 1967, *Boletín de los Observatorios Tonantzintla y Tacubaya*, 4, 86 [ADS]
- Povich, M. S., Townsley, L. K., Broos, P. S., Gagné, M., Babler, B. L., Indebetouw, R., Majewski, S. R., Meade, M. R., Getman, K. V., Robitaille, T. P., & Townsend, R. H. D. 2011, *ApJS*, 194, 6 [ADS]
- Purcell, C. R., Minier, V., Longmore, S. N., André, P., Walsh, A. J., Jones, P., Herpin, F., Hill, T., Cunningham, M. R., & Burton, M. G. 2009, *A&A*, 504, 139 [ADS]
- Rahman, M. & Murray, N. 2010, *ApJ*, 719, 1104 [ADS]
- Rauw, G., Manfroid, J., Gosset, E., Nazé, Y., Sana, H., De Becker, M., Foellmi, C., & Moffat, A. F. J. 2007, *A&A*, 463, 981 [ADS]
- Rauw, G., Sana, H., & Nazé, Y. 2011, *A&A*, 535, A40 [ADS]
- Reed, B. C. 2000, *AJ*, 120, 314 [ADS]

- . 2003, *AJ*, 125, 2531 [\[ADS\]](#)
- Robitaille, T. P. & Whitney, B. A. 2010, *ApJ*, 710, L11 [\[ADS\]](#)
- Rolleston, W. R. J., Smartt, S. J., Dufton, P. L., & Ryans, R. S. I. 2000, *A&A*, 363, 537 [\[ADS\]](#)
- Roman-Lopes, A., Barba, R. H., & Morrell, N. I. 2011, *MNRAS*, 416, 501 [\[ADS\]](#)
- Rosslowe, C. K. & Crowther, P. A. 2015, *MNRAS*, 447, 2322 [\[ADS\]](#)
- Rucinski, S. M. 1992, *AJ*, 104, 1968 [\[ADS\]](#)
- Russeil, D. 2003, *A&A*, 397, 133 [\[ADS\]](#)
- Sale, S. E., Drew, J. E., Barentsen, G., Farnhill, H. J., Raddi, R., Barlow, M. J., Eislöffel, J., Vink, J. S., Rodríguez-Gil, P., & Wright, N. J. 2014, *MNRAS*, 443, 2907 [\[ADS\]](#)
- Sale, S. E., Drew, J. E., Knigge, C., Zijlstra, A. A., Irwin, M. J., Morris, R. A. H., Phillipps, S., Drake, J. J., Greimel, R., Unruh, Y. C., Groot, P. J., Mampaso, A., & Walton, N. A. 2010, *MNRAS*, 402, 713 [\[ADS\]](#)
- Sale, S. E. & Magorrian, J. 2014, *MNRAS*, 445, 256 [\[ADS\]](#)
- Salpeter, E. E. 1955, *ApJ*, 121, 161 [\[ADS\]](#)
- Sana, H., de Koter, A., de Mink, S. E., Dunstall, P. R., Evans, C. J., Hénault-Brunet, V., Maíz Apellániz, J., Ramírez-Agudelo, O. H., Taylor, W. D., Walborn, N. R., Clark, J. S., Crowther, P. A., Herrero, A., Gieles, M., Langer, N., Lennon, D. J., & Vink, J. S. 2013, *A&A*, 550, A107 [\[ADS\]](#)
- Sana, H., Dunstall, P. R., Hénault-Brunet, V., Walborn, N. R., de Koter, A., de Mink, S. E., Dufton, P. L., Evans, C. J., Maíz Apellániz, J., Taylor, W. D., & Vink, J. S. 2012, in *Astronomical Society of the Pacific Conference Series*, Vol. 465, *Proceedings of a Scientific Meeting in Honor of Anthony F. J. Moffat*, 284 [\[ADS\]](#)
- Sana, H. & Evans, C. J. 2011, in *IAU Symposium*, Vol. 272, *Active OB Stars: Structure, Evolution, Mass Loss, and Critical Limits*, 474–485 [\[ADS\]](#)
- Sander, A., Hamann, W.-R., & Todt, H. 2012, *A&A*, 540, A144 [\[ADS\]](#)
- Schmidt-Kaler. 1982, *Landolt-Börnstein: Numerical Data and Functional Relationships in Science and Technology - New Series* " Gruppe/Group 6 Astronomy and Astrophysics " Volume 2 Schaifers/Voigt: *Astronomy and Astrophysics / Astronomie und Astrophysik* " Stars and Star Clusters / Sterne und Sternhaufen (Springer-Verlag, Berlin)
- Shanks, T., Metcalfe, N., Chehade, B., Findlay, J. R., Irwin, M. J., Gonzalez-Solares, E., Lewis, J. R., Yoldas, A. K., Mann, R. G., Read, M. A., Sutorius, E. T. W., & Voutsinas, S. 2015, *MNRAS*, 451, 4238 [\[ADS\]](#)
- Simón-Díaz, S., Castro, N., Garcia, M., Herrero, A., & Markova, N. 2011, *Bulletin de la Societe Royale des Sciences de Liege*, 80, 514 [\[ADS\]](#)

- Simón-Díaz, S. & Herrero, A. 2007, *A&A*, 468, 1063 [ADS]
- Skrutskie, M. F., Cutri, R. M., Stiening, R., Weinberg, M. D., Schneider, S., Carpenter, J. M., Beichman, C., Capps, R., Chester, T., Elias, J., Huchra, J., Liebert, J., Lonsdale, C., Monet, D. G., Price, S., Seitzer, P., Jarrett, T., Kirkpatrick, J. D., Gizis, J. E., Howard, E., Evans, T., Fowler, J., Fullmer, L., Hurt, R., Light, R., Kopan, E. L., Marsh, K. A., McCallon, H. L., Tam, R., Van Dyk, S., & Wheelock, S. 2006, *AJ*, 131, 1163 [ADS]
- Smartt, S. J. 2009, *ARA&A*, 47, 63 [ADS]
- Smartt, S. J. & Rolleston, W. R. J. 1997, *ApJ*, 481, L47 [ADS]
- Smith, N. 2006b, *ApJ*, 644, 1151 [ADS]
- Smolčić, V., Ivezić, Ž., Knapp, G. R., Lupton, R. H., Pavlovski, K., Ilijić, S., Schlegel, D., Smith, J. A., McGehee, P. M., Silvestri, N. M., Hawley, S. L., Rockosi, C., Gunn, J. E., Strauss, M. A., Fan, X., Eisenstein, D., & Harris, H. 2004, *ApJ*, 615, L141 [ADS]
- Sparke, L. S. & Gallagher, III, J. S. 2000, *Galaxies in the universe : an introduction*, 416 [ADS]
- Stark, A. A. & Lee, Y. 2005, *ApJ*, 619, L159 [ADS]
- Stark, M. A. & Wade, R. A. 2003, *AJ*, 126, 1455 [ADS]
- Sung, H. & Bessell, M. S. 2004, *AJ*, 127, 1014 [ADS]
- Taylor, M. B. 2005, in *Astronomical Society of the Pacific Conference Series*, Vol. 347, *Astronomical Data Analysis Software and Systems XIV*, 29 [ADS]
- Tsujimoto, M., Feigelson, E. D., Townsley, L. K., Broos, P. S., Getman, K. V., Wang, J., Garmire, G. P., Baba, D., Nagayama, T., Tamura, M., & Churchwell, E. B. 2007, *ApJ*, 665, 719 [ADS]
- Turner, D. G. 1978, *AJ*, 83, 1081 [ADS]
- Vallée, J. P. 2005, *AJ*, 130, 569 [ADS]
- . 2014, *AJ*, 148, 5 [ADS]
- van der Hucht, K. A. 2001, *VizieR Online Data Catalog*, 3215, 0 [ADS]
- Vargas Álvarez, C. A., Kobulnicky, H. A., Bradley, D. R., Kannappan, S. J., Norris, M. A., Cool, R. J., & Miller, B. P. 2013, *AJ*, 145, 125 [ADS]
- Walborn, N. R. 1995, in *Revista Mexicana de Astronomia y Astrofisica Conference Series*, Vol. 2, *Revista Mexicana de Astronomia y Astrofisica Conference Series*, 51 [ADS]
- Wanajo, S., Tamamura, M., Itoh, N., Nomoto, K., Ishimaru, Y., Beers, T. C., & Nozawa, S. 2003, *ApJ*, 593, 968 [ADS]

- Wenger, M., Ochsenbein, F., Egret, D., Dubois, P., Bonnarel, F., Borde, S., Genova, F., Jasniewicz, G., Laloë, S., Lesteven, S., & Monier, R. 2000, *A&AS*, 143, 9 [\[ADS\]](#)
- Zhu, Q., Davies, B., Figer, D. F., & Trombley, C. 2009, *ApJ*, 702, 929 [\[ADS\]](#)
- Zinnecker, H. & Yorke, H. W. 2007, *ARA&A*, 45, 481 [\[ADS\]](#)
- Zorec, J. & Briot, D. 1991, *A&A*, 245, 150 [\[ADS\]](#)

# APPENDIX A: REDDENING TABLES AND FIGURES

**Table A.1:** VST/OmegaCam synthetic colours for main-sequence dwarfs in the  $(u-g)$ ,  $(g-r)$  plane reddened with an  $R_V = 2.5$  extinction law. Objects in *italics* are affected by the  $u$  and  $g$  filter red leaks. The top panel of Fig. A.1 plots these values.

$R_V = 2.5$										
Spectral Type	$A_0 = 0$		$A_0 = 2$		$A_0 = 4$		$A_0 = 6$		$A_0 = 8$	
	$(u-g)$	$(g-r)$	$(u-g)$	$(g-r)$	$(u-g)$	$(g-r)$	$(u-g)$	$(g-r)$	$(u-g)$	$(g-r)$
O6V	-1.494	-0.299	-0.456	0.669	0.630	1.590	1.707	2.470	<i>2.338</i>	<i>3.319</i>
O8V	-1.463	-0.287	-0.426	0.678	0.659	1.597	1.734	2.475	<i>2.352</i>	<i>3.322</i>
O9V	-1.446	-0.282	-0.409	0.683	0.676	1.600	1.749	2.477	<i>2.359</i>	<i>3.324</i>
B0V	-1.433	-0.271	-0.397	0.693	0.687	1.610	1.757	2.487	<i>2.357</i>	<i>3.333</i>
B1V	-1.324	-0.240	-0.289	0.721	0.792	1.636	1.850	2.512	<i>2.386</i>	<i>3.357</i>
B2V	-1.209	-0.218	-0.177	0.743	0.902	1.657	1.947	2.531	<i>2.417</i>	<i>3.376</i>
B3V	-1.053	-0.186	-0.023	0.773	1.050	1.686	2.074	2.559	<i>2.446</i>	<i>3.403</i>
B5V	-0.828	-0.139	0.198	0.818	1.264	1.728	2.252	2.600	<i>2.474</i>	<i>3.443</i>
B6V	-0.728	-0.121	0.295	0.834	1.357	1.743	2.326	2.615	<i>2.483</i>	<i>3.457</i>
B7V	-0.580	-0.100	0.439	0.854	1.493	1.762	2.433	2.632	<i>2.494</i>	<i>3.473</i>
B8V	-0.388	-0.076	0.624	0.876	1.668	1.782	<i>2.566</i>	<i>2.650</i>	<i>2.505</i>	<i>3.491</i>
B9V	-0.198	-0.046	0.810	0.903	1.845	1.807	<i>2.694</i>	<i>2.674</i>	<i>2.504</i>	<i>3.513</i>
A0V	-0.053	-0.005	0.957	0.940	1.987	1.841	<i>2.792</i>	<i>2.706</i>	<i>2.489</i>	<i>3.543</i>
A1V	-0.019	0.005	0.990	0.950	2.018	1.851	<i>2.809</i>	<i>2.715</i>	<i>2.479</i>	<i>3.552</i>
A2V	0.021	0.025	1.030	0.969	2.058	1.868	<i>2.832</i>	<i>2.732</i>	<i>2.464</i>	<i>3.569</i>
A3V	0.038	0.059	1.054	0.999	2.086	1.897	<i>2.847</i>	<i>2.758</i>	<i>2.443</i>	<i>3.594</i>
A5V	0.067	0.125	1.089	1.062	2.121	1.956	<i>2.850</i>	<i>2.815</i>	<i>2.377</i>	<i>3.649</i>
A6V	0.044	0.199	1.073	1.132	2.109	2.023	<i>2.816</i>	<i>2.880</i>	<i>2.295</i>	<i>3.712</i>
F0V	-0.026	0.329	1.016	1.257	2.058	2.144	<i>2.725</i>	<i>2.998</i>	<i>2.125</i>	<i>3.829</i>
F2V	-0.049	0.387	0.999	1.313	2.043	2.197	<i>2.687</i>	<i>3.050</i>	<i>2.048</i>	<i>3.880</i>
F5V	-0.066	0.495	0.994	1.414	2.041	2.294	<i>2.631</i>	<i>3.144</i>	<i>1.914</i>	<i>3.971</i>
F8V	-0.040	0.576	1.029	1.490	2.075	2.365	<i>2.607</i>	<i>3.212</i>	<i>1.815</i>	<i>4.037</i>
G0V	-0.001	0.630	1.075	1.540	2.117	2.412	<i>2.600</i>	<i>3.257</i>	<i>1.754</i>	<i>4.081</i>
G2V	0.042	0.670	1.121	1.577	2.160	2.447	<i>2.597</i>	<i>3.290</i>	<i>1.707</i>	<i>4.113</i>
G5V	0.162	0.756	1.249	1.657	2.272	2.523	<i>2.591</i>	<i>3.363</i>	<i>1.603</i>	<i>4.185</i>
G8V	0.355	0.845	1.448	1.742	2.440	2.606	<i>2.590</i>	<i>3.445</i>	<i>1.491</i>	<i>4.266</i>
K0V	0.451	0.904	1.544	1.798	2.510	2.659	<i>2.557</i>	<i>3.497</i>	<i>1.405</i>	<i>4.316</i>
K1V	0.523	0.939	1.616	1.832	<i>2.563</i>	<i>2.692</i>	<i>2.539</i>	<i>3.529</i>	<i>1.355</i>	<i>4.348</i>
K2V	0.602	0.978	1.694	1.870	<i>2.615</i>	<i>2.730</i>	<i>2.514</i>	<i>3.566</i>	<i>1.297</i>	<i>4.385</i>
M2V	1.238	1.425	2.203	2.311	<i>2.400</i>	<i>3.161</i>	<i>1.332</i>	<i>3.984</i>	<i>-0.106</i>	<i>4.787</i>
K3V	0.756	1.049	1.843	1.939	<i>2.711</i>	<i>2.798</i>	<i>2.462</i>	<i>3.634</i>	<i>1.192</i>	<i>4.452</i>
K4V	0.841	1.092	1.925	1.980	<i>2.756</i>	<i>2.839</i>	<i>2.422</i>	<i>3.675</i>	<i>1.125</i>	<i>4.493</i>
K5V	1.064	1.198	2.132	2.084	<i>2.847</i>	<i>2.942</i>	<i>2.297</i>	<i>3.776</i>	<i>0.946</i>	<i>4.593</i>
K7V	1.364	1.386	2.378	2.268	<i>2.797</i>	<i>3.119</i>	<i>1.898</i>	<i>3.948</i>	<i>0.484</i>	<i>4.757</i>
M0V	1.348	1.394	2.354	2.276	<i>2.732</i>	<i>3.128</i>	<i>1.798</i>	<i>3.955</i>	<i>0.378</i>	<i>4.763</i>
M1V	1.311	1.422	2.297	2.305	<i>2.585</i>	<i>3.155</i>	<i>1.579</i>	<i>3.979</i>	<i>0.151</i>	<i>4.784</i>
M2V	1.238	1.425	2.203	2.311	<i>2.400</i>	<i>3.161</i>	<i>1.332</i>	<i>3.984</i>	<i>-0.106</i>	<i>4.787</i>

**Table A.2:** VST/OmegaCam synthetic colours for main-sequence dwarfs in the  $(u-g)$ ,  $(g-r)$  plane reddened with an  $R_V = 3.1$  extinction law. Objects in *italics* are affected by the  $u$  and  $g$  filter red leaks. The middle panel of Fig. A.1 plots these values.

$R_V = 3.1$										
Spectral Type	$A_0 = 0$		$A_0 = 2$		$A_0 = 4$		$A_0 = 6$		$A_0 = 8$	
	$(u-g)$	$(g-r)$	$(u-g)$	$(g-r)$	$(u-g)$	$(g-r)$	$(u-g)$	$(g-r)$	$(u-g)$	$(g-r)$
<i>O6V</i>	-1.494	-0.299	-0.753	0.504	0.028	1.280	0.834	2.031	1.584	2.761
<i>O8V</i>	-1.463	-0.287	-0.722	0.514	0.058	1.288	0.864	2.037	1.610	2.765
<i>O9V</i>	-1.446	-0.282	-0.705	0.518	0.075	1.292	0.880	2.040	1.624	2.768
<i>B0V</i>	-1.433	-0.271	-0.692	0.529	0.087	1.301	0.891	2.050	1.632	2.777
<i>B1V</i>	-1.324	-0.240	-0.584	0.558	0.195	1.329	0.995	2.076	1.719	2.802
<i>B2V</i>	-1.209	-0.218	-0.470	0.579	0.307	1.350	1.104	2.096	1.808	2.821
<i>B3V</i>	-1.053	-0.186	-0.315	0.610	0.460	1.379	1.250	2.125	1.923	2.849
<i>B5V</i>	-0.828	-0.139	-0.092	0.655	0.680	1.423	1.460	2.166	<i>2.080</i>	<i>2.890</i>
<i>B6V</i>	-0.728	-0.121	0.007	0.672	0.776	1.439	1.550	2.182	<i>2.144</i>	<i>2.905</i>
<i>B7V</i>	-0.580	-0.100	0.152	0.692	0.918	1.458	1.682	2.200	<i>2.234</i>	<i>2.922</i>
<i>B8V</i>	-0.388	-0.076	0.340	0.714	1.101	1.478	1.850	2.219	<i>2.344</i>	<i>2.940</i>
<i>B9V</i>	-0.198	-0.046	0.528	0.742	1.285	1.504	2.019	2.244	<i>2.445</i>	<i>2.964</i>
<i>A0V</i>	-0.053	-0.005	0.675	0.780	1.431	1.540	2.153	2.277	<i>2.514</i>	<i>2.995</i>
<i>A1V</i>	-0.019	0.005	0.709	0.790	1.464	1.550	2.181	2.287	<i>2.525</i>	<i>3.005</i>
<i>A2V</i>	0.021	0.025	0.749	0.809	1.505	1.568	2.217	2.304	<i>2.538</i>	<i>3.021</i>
<i>A3V</i>	0.038	0.059	0.771	0.840	1.531	1.597	2.241	2.332	<i>2.541</i>	<i>3.048</i>
<i>A5V</i>	0.067	0.125	0.805	0.904	1.567	1.658	2.269	2.390	<i>2.523</i>	<i>3.105</i>
<i>A6V</i>	0.044	0.199	0.788	0.975	1.554	1.726	2.252	2.456	<i>2.474</i>	<i>3.169</i>
<i>F0V</i>	-0.026	0.329	0.728	1.101	1.501	1.849	2.192	2.577	<i>2.356</i>	<i>3.288</i>
<i>F2V</i>	-0.049	0.387	0.709	1.157	1.486	1.904	2.171	2.630	<i>2.304</i>	<i>3.341</i>
<i>F5V</i>	-0.066	0.495	0.701	1.260	1.483	2.003	2.155	2.726	<i>2.220</i>	<i>3.434</i>
<i>F8V</i>	-0.040	0.576	0.734	1.337	1.520	2.076	<i>2.173</i>	<i>2.796</i>	<i>2.168</i>	<i>3.502</i>
<i>G0V</i>	-0.001	0.630	0.779	1.388	1.566	2.124	<i>2.201</i>	<i>2.842</i>	<i>2.140</i>	<i>3.547</i>
<i>G2V</i>	0.042	0.670	0.825	1.425	1.612	2.160	<i>2.230</i>	<i>2.877</i>	<i>2.120</i>	<i>3.580</i>
<i>G5V</i>	0.162	0.756	0.952	1.507	1.736	2.238	<i>2.306</i>	<i>2.952</i>	<i>2.073</i>	<i>3.653</i>
<i>G8V</i>	0.355	0.845	1.149	1.593	1.924	2.321	<i>2.414</i>	<i>3.035</i>	<i>2.024</i>	<i>3.735</i>
<i>K0V</i>	0.451	0.904	1.247	1.649	2.012	2.376	<i>2.446</i>	<i>3.088</i>	<i>1.967</i>	<i>3.787</i>
<i>K1V</i>	0.523	0.939	1.319	1.683	2.077	2.409	<i>2.471</i>	<i>3.120</i>	<i>1.934</i>	<i>3.819</i>
<i>K2V</i>	0.602	0.978	1.398	1.722	2.145	2.447	<i>2.492</i>	<i>3.158</i>	<i>1.893</i>	<i>3.857</i>
<i>M2V</i>	1.238	1.425	1.959	2.165	<i>2.318</i>	<i>2.884</i>	<i>1.754</i>	<i>3.585</i>	<i>0.587</i>	<i>4.273</i>
<i>K3V</i>	0.756	1.049	1.550	1.791	2.275	2.516	<i>2.523</i>	<i>3.226</i>	<i>1.816</i>	<i>3.925</i>
<i>K4V</i>	0.841	1.092	1.634	1.833	2.342	2.558	<i>2.528</i>	<i>3.268</i>	<i>1.762</i>	<i>3.966</i>
<i>K5V</i>	1.064	1.198	1.848	1.938	2.501	2.661	<i>2.512</i>	<i>3.370</i>	<i>1.609</i>	<i>4.067</i>
<i>K7V</i>	1.364	1.386	2.116	2.122	<i>2.610</i>	<i>2.841</i>	<i>2.261</i>	<i>3.545</i>	<i>1.173</i>	<i>4.238</i>
<i>M0V</i>	1.348	1.394	2.095	2.131	<i>2.566</i>	<i>2.850</i>	<i>2.174</i>	<i>3.553</i>	<i>1.068</i>	<i>4.245</i>
<i>M1V</i>	1.311	1.422	2.046	2.160	<i>2.462</i>	<i>2.878</i>	<i>1.981</i>	<i>3.580</i>	<i>0.842</i>	<i>4.268</i>
<i>M2V</i>	1.238	1.425	1.959	2.165	<i>2.318</i>	<i>2.884</i>	<i>1.754</i>	<i>3.585</i>	<i>0.587</i>	<i>4.273</i>

**Table A.3:** VST/OmegaCam synthetic colours for main-sequence dwarfs in the  $(u-g), (g-r)$  plane reddened with an  $R_V = 3.8$  extinction law. Objects in *italics* are affected by the  $u$  and  $g$  filter red leaks. The bottom panel of Fig. A.1 plots these values.

$R_V = 3.8$										
Spectral Type	$A_0 = 0$		$A_0 = 2$		$A_0 = 4$		$A_0 = 6$		$A_0 = 8$	
	$(u-g)$	$(g-r)$	$(u-g)$	$(g-r)$	$(u-g)$	$(g-r)$	$(u-g)$	$(g-r)$	$(u-g)$	$(g-r)$
<i>O6V</i>	-1.494	-0.299	-0.910	0.373	-0.299	1.029	0.334	1.671	0.968	2.299
<i>O8V</i>	-1.463	-0.287	-0.879	0.383	-0.269	1.037	0.364	1.677	0.997	2.304
<i>O9V</i>	-1.446	-0.282	-0.862	0.387	-0.251	1.041	0.381	1.680	1.013	2.306
<i>B0V</i>	-1.433	-0.271	-0.849	0.398	-0.239	1.051	0.393	1.690	1.023	2.316
<i>B1V</i>	-1.324	-0.240	-0.741	0.427	-0.131	1.079	0.500	1.717	1.124	2.342
<i>B2V</i>	-1.209	-0.218	-0.627	0.449	-0.018	1.101	0.611	1.738	1.229	2.362
<i>B3V</i>	-1.053	-0.186	-0.472	0.480	0.136	1.131	0.762	1.767	1.369	2.391
<i>B5V</i>	-0.828	-0.139	-0.247	0.526	0.358	1.175	0.980	1.810	1.568	2.432
<i>B6V</i>	-0.728	-0.121	-0.149	0.543	0.455	1.191	1.074	1.826	1.652	2.447
<i>B7V</i>	-0.580	-0.100	-0.003	0.563	0.599	1.211	1.212	1.844	1.775	2.466
<i>B8V</i>	-0.388	-0.076	0.186	0.585	0.784	1.232	1.391	1.864	1.930	2.485
<i>B9V</i>	-0.198	-0.046	0.375	0.614	0.971	1.259	1.570	1.890	2.082	2.509
<i>A0V</i>	-0.053	-0.005	0.522	0.652	1.118	1.295	1.713	1.925	2.199	2.542
<i>A1V</i>	-0.019	0.005	0.556	0.663	1.151	1.305	1.744	1.934	<i>2.222</i>	<i>2.552</i>
<i>A2V</i>	0.021	0.025	0.596	0.682	1.192	1.324	1.783	1.952	<i>2.252</i>	<i>2.569</i>
<i>A3V</i>	0.038	0.059	0.617	0.713	1.216	1.354	1.809	1.981	<i>2.270</i>	<i>2.596</i>
<i>A5V</i>	0.067	0.125	0.650	0.777	1.252	1.416	1.843	2.041	<i>2.285</i>	<i>2.655</i>
<i>A6V</i>	0.044	0.199	0.631	0.849	1.238	1.485	1.829	2.108	<i>2.258</i>	<i>2.721</i>
<i>F0V</i>	-0.026	0.329	0.570	0.976	1.183	1.610	1.775	2.231	<i>2.180</i>	<i>2.842</i>
<i>F2V</i>	-0.049	0.387	0.550	1.033	1.166	1.665	1.758	2.285	<i>2.149</i>	<i>2.895</i>
<i>F5V</i>	-0.066	0.495	0.540	1.137	1.162	1.766	1.752	2.383	<i>2.110</i>	<i>2.991</i>
<i>F8V</i>	-0.040	0.576	0.573	1.215	1.198	1.841	1.782	2.455	<i>2.104</i>	<i>3.061</i>
<i>G0V</i>	-0.001	0.630	0.616	1.266	1.244	1.890	1.822	2.503	<i>2.112</i>	<i>3.107</i>
<i>G2V</i>	0.042	0.670	0.662	1.304	1.290	1.926	1.862	2.538	<i>2.122</i>	<i>3.141</i>
<i>G5V</i>	0.162	0.756	0.787	1.387	1.417	2.006	1.969	2.615	<i>2.150</i>	<i>3.217</i>
<i>G8V</i>	0.355	0.845	0.984	1.473	1.611	2.090	2.128	2.699	<i>2.192</i>	<i>3.299</i>
<i>K0V</i>	0.451	0.904	1.081	1.530	1.704	2.146	<i>2.194</i>	<i>2.753</i>	<i>2.184</i>	<i>3.352</i>
<i>K1V</i>	0.523	0.939	1.154	1.564	1.773	2.179	<i>2.243</i>	<i>2.786</i>	<i>2.182</i>	<i>3.385</i>
<i>K2V</i>	0.602	0.978	1.233	1.603	1.847	2.218	<i>2.291</i>	<i>2.824</i>	<i>2.173</i>	<i>3.423</i>
<i>M2V</i>	1.238	1.425	1.817	2.048	<i>2.198</i>	<i>2.659</i>	<i>1.979</i>	<i>3.259</i>	<i>1.108</i>	<i>3.850</i>
<i>K3V</i>	0.756	1.049	1.386	1.673	1.988	2.287	<i>2.378</i>	<i>2.892</i>	<i>2.149</i>	<i>3.491</i>
<i>K4V</i>	0.841	1.092	1.470	1.715	2.063	2.329	<i>2.417</i>	<i>2.934</i>	<i>2.124</i>	<i>3.533</i>
<i>K5V</i>	1.064	1.198	1.687	1.820	2.250	2.432	<i>2.492</i>	<i>3.037</i>	<i>2.032</i>	<i>3.635</i>
<i>K7V</i>	1.364	1.386	1.965	2.006	<i>2.433</i>	<i>2.615</i>	<i>2.405</i>	<i>3.216</i>	<i>1.669</i>	<i>3.810</i>
<i>M0V</i>	1.348	1.394	1.946	2.014	<i>2.399</i>	<i>2.624</i>	<i>2.335</i>	<i>3.225</i>	<i>1.570</i>	<i>3.818</i>
<i>M1V</i>	1.311	1.422	1.900	2.043	<i>2.318</i>	<i>2.653</i>	<i>2.176</i>	<i>3.252</i>	<i>1.355</i>	<i>3.844</i>
<i>M2V</i>	1.238	1.425	1.817	2.048	<i>2.198</i>	<i>2.659</i>	<i>1.979</i>	<i>3.259</i>	<i>1.108</i>	<i>3.850</i>

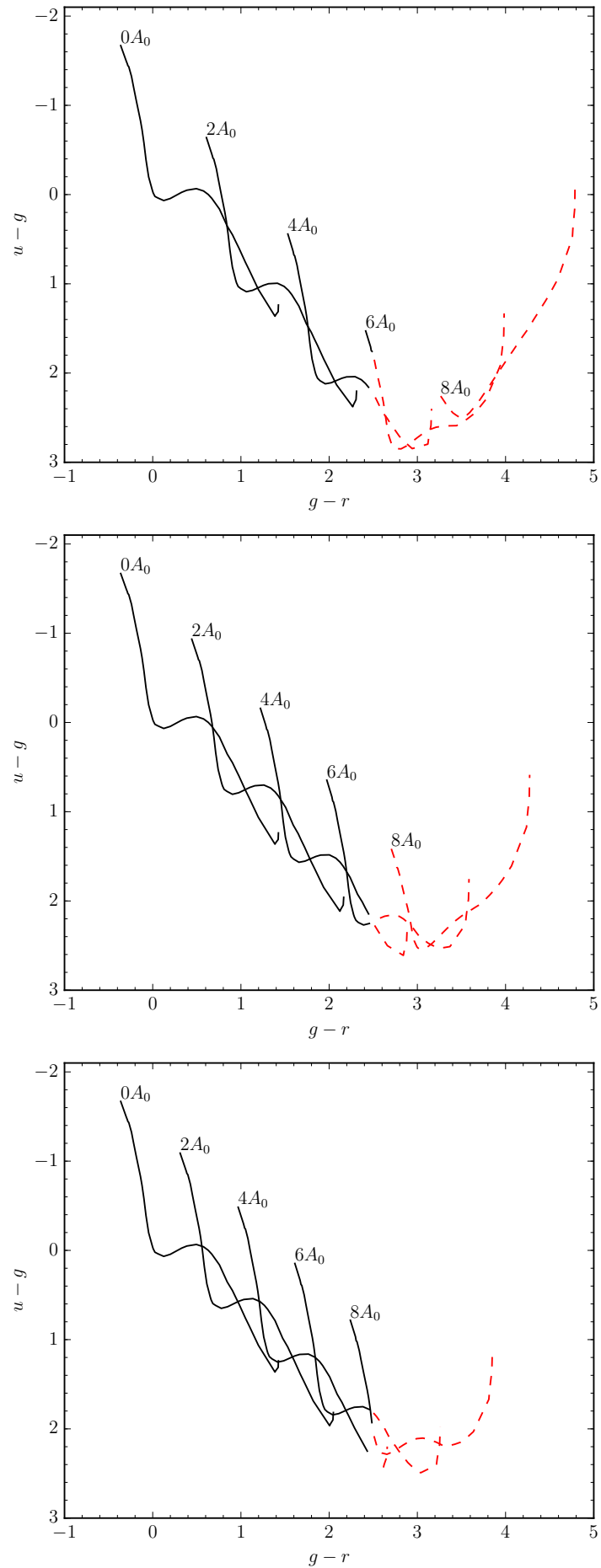


**Figure A.1:** VST/OmegaCam synthetic colours for main-sequence dwarfs in the  $(u-g)$ ,  $(g-r)$  plane reddened with an  $R_V = 2.5$ ,  $3.1$  and  $3.8$  extinction law from top to bottom. The dashed red tracks are affected by the  $u$  and  $g$  filter red leaks.

**Table A.4:** VST/OmegaCam synthetic colours for main-sequence dwarfs in the  $(r - i), (r - H\alpha)$  plane reddened with an  $R_V = 2.5$  extinction law. The top panel of Fig. A.2 plots these values.

$R_V = 2.5$										
Spectral Type	$A_0 = 0$		$A_0 = 2$		$A_0 = 4$		$A_0 = 6$		$A_0 = 8$	
	$(r - i)$	$(r - H\alpha)$								
O6V	-0.145	0.071	0.337	0.235	0.801	0.365	1.248	0.461	1.682	0.527
O8V	-0.152	0.055	0.332	0.221	0.798	0.352	1.248	0.450	1.683	0.517
O9V	-0.153	0.049	0.331	0.216	0.798	0.348	1.248	0.446	1.684	0.513
B0V	-0.150	0.054	0.335	0.220	0.801	0.351	1.252	0.449	1.688	0.516
B1V	-0.136	0.048	0.348	0.214	0.815	0.345	1.266	0.443	1.702	0.509
B2V	-0.123	0.045	0.361	0.211	0.828	0.341	1.278	0.438	1.714	0.504
B3V	-0.104	0.044	0.380	0.209	0.847	0.338	1.297	0.434	1.733	0.499
B5V	-0.077	0.039	0.406	0.202	0.872	0.330	1.322	0.425	1.757	0.488
B6V	-0.068	0.036	0.415	0.198	0.881	0.326	1.330	0.420	1.766	0.484
B7V	-0.057	0.029	0.426	0.192	0.892	0.319	1.341	0.413	1.776	0.476
B8V	-0.045	0.018	0.439	0.180	0.904	0.307	1.353	0.400	1.788	0.463
B9V	-0.028	0.006	0.455	0.167	0.920	0.293	1.369	0.386	1.804	0.448
A0V	-0.009	-0.005	0.474	0.155	0.939	0.280	1.388	0.372	1.823	0.433
A1V	-0.003	-0.003	0.479	0.157	0.944	0.281	1.393	0.373	1.827	0.434
A2V	0.006	-0.004	0.488	0.156	0.953	0.280	1.402	0.371	1.836	0.432
A3V	0.021	-0.008	0.503	0.151	0.967	0.275	1.415	0.365	1.849	0.425
A5V	0.051	0.005	0.532	0.162	0.995	0.283	1.443	0.371	1.876	0.429
A6V	0.083	0.027	0.563	0.181	1.025	0.300	1.471	0.386	1.903	0.442
F0V	0.149	0.084	0.626	0.232	1.085	0.346	1.529	0.427	1.960	0.478
F2V	0.177	0.109	0.653	0.255	1.111	0.366	1.555	0.445	1.984	0.495
F5V	0.225	0.149	0.699	0.290	1.156	0.398	1.598	0.473	2.026	0.520
F8V	0.259	0.173	0.731	0.312	1.187	0.417	1.628	0.490	2.055	0.534
G0V	0.280	0.188	0.751	0.325	1.206	0.428	1.646	0.500	2.074	0.543
G2V	0.295	0.197	0.766	0.333	1.220	0.435	1.660	0.506	2.087	0.548
G5V	0.327	0.217	0.797	0.350	1.250	0.450	1.689	0.518	2.115	0.558
G8V	0.358	0.233	0.827	0.364	1.279	0.461	1.716	0.527	2.141	0.565
K0V	0.385	0.245	0.852	0.374	1.303	0.469	1.740	0.534	2.165	0.570
K1V	0.399	0.251	0.866	0.379	1.316	0.473	1.753	0.537	2.177	0.573
K2V	0.415	0.258	0.882	0.385	1.332	0.478	1.768	0.540	2.192	0.575
M2V	1.111	0.526	1.590	0.630	2.052	0.703	2.499	0.746	2.933	0.764
K3V	0.445	0.270	0.910	0.395	1.359	0.486	1.794	0.547	2.218	0.580
K4V	0.464	0.278	0.929	0.401	1.377	0.491	1.812	0.551	2.235	0.583
K5V	0.521	0.302	0.985	0.422	1.433	0.509	1.867	0.565	2.289	0.595
K7V	0.721	0.390	1.189	0.502	1.641	0.582	2.078	0.632	2.505	0.657
M0V	0.787	0.413	1.257	0.524	1.711	0.603	2.151	0.653	2.580	0.676
M1V	0.931	0.470	1.405	0.578	1.863	0.654	2.307	0.701	2.738	0.722
M2V	1.111	0.526	1.590	0.630	2.052	0.703	2.499	0.746	2.933	0.764

**Table A.5:** VST/OmegaCam synthetic colours for main-sequence dwarfs in the  $(r - i)$ ,  $(r - H\alpha)$  plane reddened with an  $R_V = 3.1$  extinction law. The middle panel of Fig. A.2 plots these values.

$R_V = 3.1$										
Spectral Type	$A_0 = 0$		$A_0 = 2$		$A_0 = 4$		$A_0 = 6$		$A_0 = 8$	
	$(r - i)$	$(r - H\alpha)$								
<i>O6V</i>	-0.145	0.071	0.280	0.213	0.694	0.330	1.097	0.422	1.491	0.490
<i>O8V</i>	-0.152	0.055	0.275	0.199	0.690	0.317	1.096	0.410	1.491	0.479
<i>O9V</i>	-0.153	0.049	0.274	0.193	0.690	0.312	1.096	0.405	1.492	0.475
<i>B0V</i>	-0.150	0.054	0.278	0.198	0.694	0.316	1.100	0.409	1.496	0.478
<i>B1V</i>	-0.136	0.048	0.291	0.192	0.708	0.310	1.114	0.403	1.510	0.472
<i>B2V</i>	-0.123	0.045	0.304	0.188	0.721	0.306	1.126	0.398	1.523	0.466
<i>B3V</i>	-0.104	0.044	0.323	0.186	0.740	0.303	1.145	0.394	1.541	0.462
<i>B5V</i>	-0.077	0.039	0.349	0.180	0.765	0.295	1.170	0.386	1.566	0.452
<i>B6V</i>	-0.068	0.036	0.358	0.177	0.774	0.291	1.179	0.381	1.575	0.448
<i>B7V</i>	-0.057	0.029	0.369	0.170	0.785	0.284	1.190	0.374	1.586	0.440
<i>B8V</i>	-0.045	0.018	0.382	0.158	0.797	0.272	1.202	0.362	1.598	0.427
<i>B9V</i>	-0.028	0.006	0.398	0.145	0.813	0.259	1.218	0.348	1.614	0.413
<i>A0V</i>	-0.009	-0.005	0.418	0.133	0.833	0.246	1.238	0.334	1.633	0.399
<i>A1V</i>	-0.003	-0.003	0.423	0.135	0.838	0.248	1.243	0.335	1.638	0.399
<i>A2V</i>	0.006	-0.004	0.432	0.134	0.847	0.247	1.251	0.334	1.646	0.397
<i>A3V</i>	0.021	-0.008	0.446	0.130	0.861	0.241	1.265	0.328	1.660	0.391
<i>A5V</i>	0.051	0.005	0.476	0.141	0.890	0.250	1.293	0.335	1.687	0.396
<i>A6V</i>	0.083	0.027	0.507	0.160	0.920	0.268	1.322	0.350	1.716	0.410
<i>F0V</i>	0.149	0.084	0.570	0.212	0.981	0.315	1.382	0.393	1.774	0.449
<i>F2V</i>	0.177	0.109	0.598	0.235	1.008	0.336	1.408	0.413	1.799	0.466
<i>F5V</i>	0.225	0.149	0.644	0.271	1.053	0.369	1.452	0.442	1.842	0.493
<i>F8V</i>	0.259	0.173	0.677	0.294	1.084	0.389	1.482	0.460	1.872	0.509
<i>G0V</i>	0.280	0.188	0.697	0.307	1.104	0.400	1.501	0.470	1.890	0.518
<i>G2V</i>	0.295	0.197	0.712	0.315	1.118	0.408	1.515	0.477	1.904	0.524
<i>G5V</i>	0.327	0.217	0.743	0.332	1.149	0.423	1.545	0.490	1.933	0.535
<i>G8V</i>	0.358	0.233	0.773	0.347	1.177	0.435	1.573	0.500	1.960	0.543
<i>K0V</i>	0.385	0.245	0.799	0.357	1.203	0.444	1.597	0.507	1.984	0.549
<i>K1V</i>	0.399	0.251	0.812	0.362	1.216	0.448	1.610	0.511	1.996	0.552
<i>K2V</i>	0.415	0.258	0.828	0.368	1.231	0.453	1.625	0.515	2.011	0.555
<i>M2V</i>	1.111	0.526	1.537	0.616	1.952	0.683	2.357	0.728	2.753	0.753
<i>K3V</i>	0.445	0.270	0.857	0.378	1.259	0.461	1.653	0.522	2.038	0.560
<i>K4V</i>	0.464	0.278	0.876	0.385	1.278	0.467	1.671	0.526	2.056	0.564
<i>K5V</i>	0.521	0.302	0.932	0.406	1.333	0.486	1.726	0.542	2.111	0.578
<i>K7V</i>	0.721	0.390	1.136	0.487	1.542	0.560	1.938	0.612	2.326	0.642
<i>M0V</i>	0.787	0.413	1.205	0.510	1.612	0.582	2.010	0.633	2.401	0.662
<i>M1V</i>	0.931	0.470	1.353	0.564	1.764	0.633	2.165	0.681	2.559	0.709
<i>M2V</i>	1.111	0.526	1.537	0.616	1.952	0.683	2.357	0.728	2.753	0.753

**Table A.6:** VST/OmegaCam synthetic colours for main-sequence dwarfs in the  $(r - i), (r - H\alpha)$  plane reddened with an  $R_V = 3.8$  extinction law. The bottom panel of Fig. A.2 plots these values.

$R_V = 3.8$										
Spectral Type	$A_0 = 0$		$A_0 = 2$		$A_0 = 4$		$A_0 = 6$		$A_0 = 8$	
	$(r - i)$	$(r - H\alpha)$								
<i>O6V</i>	-0.145	0.071	0.236	0.195	0.609	0.300	0.977	0.386	1.339	0.454
<i>O8V</i>	-0.152	0.055	0.230	0.180	0.606	0.286	0.975	0.374	1.338	0.442
<i>O9V</i>	-0.153	0.049	0.229	0.175	0.605	0.282	0.975	0.369	1.339	0.438
<i>B0V</i>	-0.150	0.054	0.233	0.179	0.609	0.286	0.979	0.373	1.343	0.442
<i>B1V</i>	-0.136	0.048	0.247	0.174	0.623	0.280	0.993	0.367	1.357	0.435
<i>B2V</i>	-0.123	0.045	0.260	0.170	0.636	0.276	1.006	0.362	1.370	0.430
<i>B3V</i>	-0.104	0.044	0.279	0.168	0.655	0.273	1.025	0.359	1.389	0.426
<i>B5V</i>	-0.077	0.039	0.305	0.162	0.681	0.266	1.050	0.351	1.414	0.417
<i>B6V</i>	-0.068	0.036	0.314	0.159	0.690	0.262	1.059	0.347	1.423	0.413
<i>B7V</i>	-0.057	0.029	0.325	0.152	0.701	0.255	1.070	0.339	1.434	0.405
<i>B8V</i>	-0.045	0.018	0.338	0.140	0.713	0.243	1.083	0.327	1.446	0.392
<i>B9V</i>	-0.028	0.006	0.354	0.128	0.729	0.230	1.099	0.313	1.462	0.378
<i>A0V</i>	-0.009	-0.005	0.373	0.116	0.749	0.218	1.118	0.300	1.481	0.365
<i>A1V</i>	-0.003	-0.003	0.379	0.117	0.754	0.219	1.123	0.301	1.486	0.365
<i>A2V</i>	0.006	-0.004	0.388	0.117	0.763	0.218	1.132	0.300	1.495	0.364
<i>A3V</i>	0.021	-0.008	0.402	0.112	0.777	0.213	1.146	0.294	1.509	0.357
<i>A5V</i>	0.051	0.005	0.432	0.124	0.806	0.222	1.174	0.302	1.537	0.364
<i>A6V</i>	0.083	0.027	0.463	0.144	0.837	0.240	1.204	0.318	1.566	0.378
<i>F0V</i>	0.149	0.084	0.527	0.196	0.899	0.289	1.265	0.363	1.625	0.419
<i>F2V</i>	0.177	0.109	0.555	0.219	0.926	0.310	1.291	0.383	1.651	0.438
<i>F5V</i>	0.225	0.149	0.602	0.256	0.972	0.344	1.336	0.414	1.695	0.466
<i>F8V</i>	0.259	0.173	0.634	0.278	1.004	0.365	1.367	0.432	1.725	0.483
<i>G0V</i>	0.280	0.188	0.655	0.292	1.024	0.376	1.387	0.443	1.745	0.492
<i>G2V</i>	0.295	0.197	0.670	0.300	1.038	0.384	1.401	0.450	1.758	0.499
<i>G5V</i>	0.327	0.217	0.701	0.318	1.069	0.400	1.431	0.464	1.788	0.510
<i>G8V</i>	0.358	0.233	0.731	0.332	1.098	0.413	1.459	0.475	1.815	0.520
<i>K0V</i>	0.385	0.245	0.757	0.343	1.123	0.421	1.484	0.482	1.840	0.526
<i>K1V</i>	0.399	0.251	0.771	0.348	1.137	0.426	1.497	0.486	1.853	0.529
<i>K2V</i>	0.415	0.258	0.787	0.354	1.153	0.431	1.513	0.490	1.868	0.533
<i>M2V</i>	1.111	0.526	1.496	0.605	1.874	0.666	2.245	0.710	2.611	0.739
<i>K3V</i>	0.445	0.270	0.816	0.365	1.181	0.440	1.540	0.498	1.895	0.539
<i>K4V</i>	0.464	0.278	0.835	0.372	1.199	0.446	1.559	0.503	1.913	0.543
<i>K5V</i>	0.521	0.302	0.891	0.393	1.255	0.465	1.615	0.520	1.969	0.558
<i>K7V</i>	0.721	0.390	1.095	0.475	1.464	0.542	1.827	0.592	2.185	0.625
<i>M0V</i>	0.787	0.413	1.164	0.498	1.534	0.564	1.899	0.613	2.259	0.646
<i>M1V</i>	0.931	0.470	1.312	0.552	1.686	0.616	2.054	0.663	2.417	0.693
<i>M2V</i>	1.111	0.526	1.496	0.605	1.874	0.666	2.245	0.710	2.611	0.739

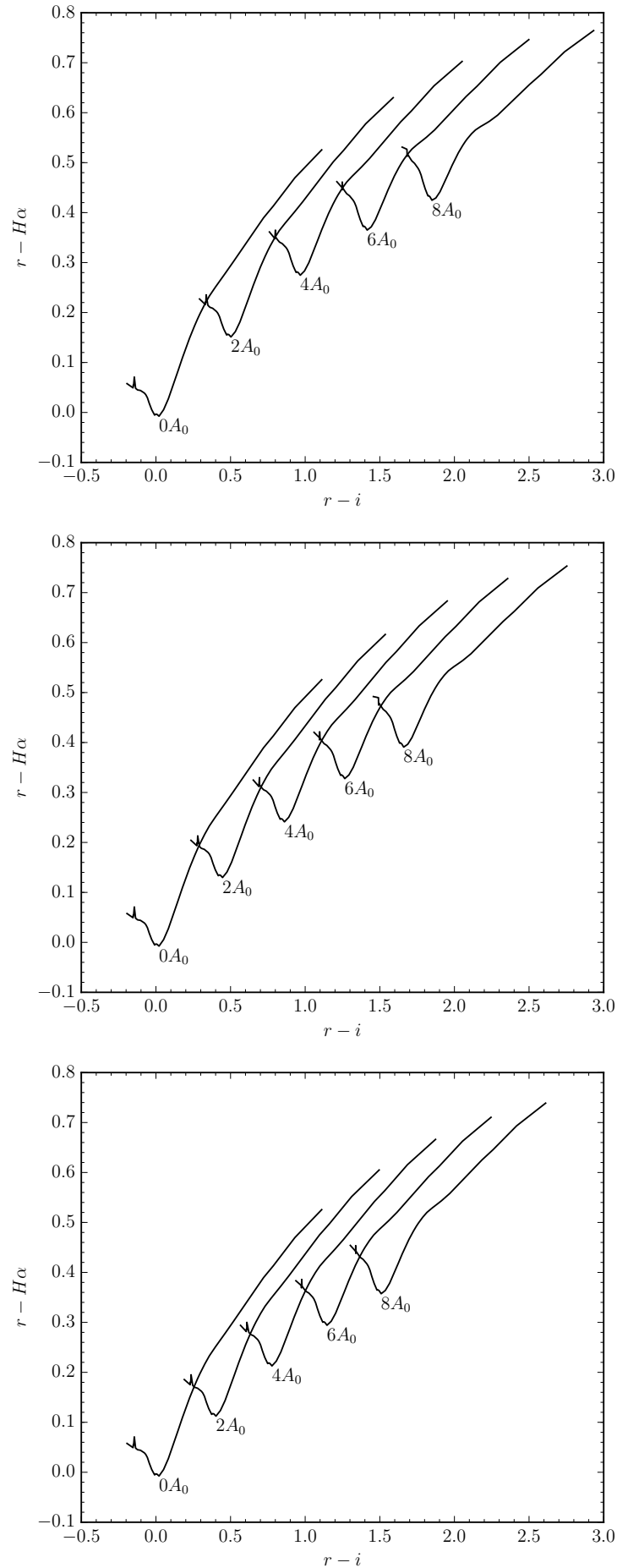


**Figure A.2:** VST/OmegaCam synthetic colours for main-sequence dwarfs in the  $(r-i)$ ,  $(r-H\alpha)$  plane reddened with an  $R_V = 2.5$ ,  $3.1$  and  $3.8$  extinction law from top to bottom.

# APPENDIX B: TABLE OF OB CANDIDATES FOLLOWED UP WITH AAOMEGA SPECTROSCOPY

**Table B.1:** Table of OB candidates followed up with AAOMega spectroscopy. The table contains the positions of the objects, the photometrically derived extinctions and effective temperatures as well as the spectroscopically derived effective temperatures, surface gravities and rotational velocities.

ID	$\ell$ [°]	b [°]	$A_0$ [mag]	Phot. $T_{\text{eff}}$ [kK]	Spec. $T_{\text{eff}}$ [kK]	$\log(g)$ [dex]	$vsini$ [kms $^{-1}$ ]
1558	284.64454	-1.30688	3.45 $^{+0.07}_{-0.07}$	40.93 $^{+5.79}_{-7.08}$	44.42 $^{+4.40}_{-1.80}$	4.18 $^{+0.08}_{-0.10}$	199 $^{+58}_{-49}$
1338	284.37839	0.00914	6.17 $^{+0.05}_{-0.07}$	37.35 $^{+6.89}_{-6.95}$	42.46 $^{+0.67}_{-0.82}$	3.87 $^{+0.04}_{-0.05}$	124 $^{+23}_{-16}$
1294	284.31756	-0.39893	8.94 $^{+0.04}_{-0.05}$	41.57 $^{+5.33}_{-7.40}$	42.02 $^{+6.40}_{-4.23}$	3.94 $^{+0.19}_{-0.33}$	205 $^{+85}_{-70}$
1236	284.27644	-0.16351	7.29 $^{+0.09}_{-0.10}$	29.04 $^{+6.17}_{-4.21}$	41.84 $^{+5.82}_{-3.33}$	3.98 $^{+0.18}_{-0.24}$	216 $^{+69}_{-67}$
1273	284.29885	-0.51977	6.67 $^{+0.06}_{-0.08}$	35.47 $^{+7.84}_{-6.88}$	40.61 $^{+2.44}_{-0.82}$	3.88 $^{+0.04}_{-0.06}$	156 $^{+27}_{-18}$
1356	284.40202	-0.54809	5.68 $^{+0.05}_{-0.06}$	39.66 $^{+6.07}_{-7.18}$	39.02 $^{+0.34}_{-0.38}$	4.23 $^{+0.05}_{-0.08}$	311 $^{+20}_{-43}$
1374	284.41811	-0.92735	5.61 $^{+0.08}_{-0.09}$	31.57 $^{+6.81}_{-4.99}$	38.64 $^{+0.47}_{-0.42}$	4.19 $^{+0.07}_{-0.10}$	120 $^{+19}_{-13}$
2766	285.69824	-1.05342	5.78 $^{+0.08}_{-0.09}$	30.82 $^{+5.94}_{-4.58}$	38.10 $^{+0.92}_{-0.97}$	4.11 $^{+0.13}_{-0.21}$	209 $^{+30}_{-40}$
3414	286.11988	-0.56819	6.71 $^{+0.10}_{-0.10}$	28.26 $^{+5.57}_{-3.91}$	37.69 $^{+2.98}_{-1.79}$	3.91 $^{+0.23}_{-0.22}$	305 $^{+29}_{-39}$
1856	284.96360	-1.21836	5.25 $^{+0.08}_{-0.09}$	29.34 $^{+5.43}_{-4.04}$	37.43 $^{+0.35}_{-0.35}$	4.19 $^{+0.05}_{-0.08}$	102 $^{+5}_{-2}$
1314	284.34006	-0.28272	7.02 $^{+0.04}_{-0.05}$	41.31 $^{+5.58}_{-7.34}$	37.38 $^{+1.85}_{-1.61}$	3.96 $^{+0.24}_{-0.24}$	291 $^{+41}_{-49}$
1550	284.63880	-0.49941	6.87 $^{+0.10}_{-0.09}$	22.83 $^{+2.60}_{-2.29}$	36.42 $^{+1.45}_{-1.15}$	4.15 $^{+0.11}_{-0.16}$	199 $^{+62}_{-61}$
2550	285.53899	-0.12740	5.73 $^{+0.06}_{-0.08}$	33.33 $^{+6.38}_{-5.39}$	35.94 $^{+0.34}_{-0.30}$	3.89 $^{+0.02}_{-0.05}$	238 $^{+25}_{-19}$
1354	284.40103	-0.28898	6.37 $^{+0.05}_{-0.05}$	40.89 $^{+5.69}_{-7.48}$	35.57 $^{+1.66}_{-1.31}$	4.09 $^{+0.14}_{-0.24}$	321 $^{+23}_{-45}$
2164	285.21643	-1.17513	3.42 $^{+0.05}_{-0.07}$	37.54 $^{+7.18}_{-7.11}$	34.85 $^{+0.21}_{-0.40}$	4.18 $^{+0.04}_{-0.11}$	103 $^{+21}_{-2}$
1318	284.34556	-0.29031	5.62 $^{+0.05}_{-0.06}$	39.89 $^{+6.32}_{-7.24}$	34.72 $^{+0.39}_{-0.41}$	4.21 $^{+0.07}_{-0.14}$	312 $^{+21}_{-26}$
2994	285.84627	-0.98638	4.71 $^{+0.07}_{-0.09}$	31.68 $^{+6.33}_{-4.80}$	34.69 $^{+0.18}_{-0.27}$	4.28 $^{+0.02}_{-0.05}$	104 $^{+10}_{-3}$
1708	284.82866	-0.26531	5.22 $^{+0.09}_{-0.09}$	28.71 $^{+5.18}_{-3.79}$	34.49 $^{+0.24}_{-0.30}$	4.28 $^{+0.02}_{-0.04}$	115 $^{+14}_{-10}$
1567	284.65778	-0.77555	5.55 $^{+0.08}_{-0.09}$	29.84 $^{+5.62}_{-4.24}$	34.29 $^{+0.19}_{-0.29}$	4.27 $^{+0.02}_{-0.07}$	103 $^{+7}_{-2}$
1164	284.22781	-0.68789	6.40 $^{+0.06}_{-0.08}$	35.89 $^{+7.35}_{-6.90}$	34.25 $^{+0.54}_{-0.62}$	3.72 $^{+0.09}_{-0.13}$	227 $^{+19}_{-21}$
1173	284.24987	-0.43274	6.06 $^{+0.09}_{-0.10}$	28.87 $^{+5.47}_{-4.03}$	32.99 $^{+0.75}_{-0.95}$	4.22 $^{+0.06}_{-0.14}$	225 $^{+62}_{-65}$
2921	285.80714	-1.01425	5.98 $^{+0.05}_{-0.07}$	37.17 $^{+7.41}_{-7.10}$	32.95 $^{+0.49}_{-0.47}$	4.12 $^{+0.10}_{-0.09}$	215 $^{+19}_{-18}$
2127	285.19168	-0.17393	4.72 $^{+0.07}_{-0.08}$	30.86 $^{+6.09}_{-4.48}$	32.22 $^{+0.23}_{-0.50}$	4.29 $^{+0.01}_{-0.03}$	343 $^{+5}_{-20}$
2109	285.17743	-0.61318	4.73 $^{+0.08}_{-0.09}$	30.09 $^{+5.81}_{-4.35}$	32.13 $^{+0.39}_{-0.48}$	4.22 $^{+0.05}_{-0.07}$	110 $^{+16}_{-8}$
1408	284.46722	-0.03133	4.93 $^{+0.07}_{-0.09}$	31.51 $^{+6.78}_{-5.00}$	31.68 $^{+0.31}_{-0.39}$	4.23 $^{+0.05}_{-0.09}$	113 $^{+22}_{-10}$
1513	284.59906	-1.02230	4.26 $^{+0.08}_{-0.09}$	29.76 $^{+6.07}_{-4.23}$	30.10 $^{+0.91}_{-0.15}$	3.92 $^{+0.15}_{-0.02}$	122 $^{+11}_{-10}$
1141	284.20148	-0.71191	4.93 $^{+0.09}_{-0.09}$	25.77 $^{+3.63}_{-2.90}$	30.04 $^{+1.33}_{-0.17}$	3.54 $^{+0.22}_{-0.04}$	129 $^{+21}_{-14}$
1165	284.23541	-0.88100	3.86 $^{+0.07}_{-0.08}$	33.32 $^{+7.24}_{-5.33}$	29.81 $^{+0.07}_{-2.56}$	4.01 $^{+0.03}_{-0.44}$	153 $^{+11}_{-23}$
1355	284.40119	-1.07503	5.66 $^{+0.09}_{-0.09}$	27.28 $^{+4.62}_{-3.26}$	29.71 $^{+0.46}_{-0.91}$	4.22 $^{+0.06}_{-0.11}$	117 $^{+18}_{-11}$
1243	284.28086	-0.75062	3.91 $^{+0.08}_{-0.09}$	29.70 $^{+6.25}_{-4.26}$	29.37 $^{+0.04}_{-0.04}$	4.02 $^{+0.01}_{-0.01}$	14 $^{+15}_{-10}$
2606	285.57825	-1.09409	4.89 $^{+0.09}_{-0.09}$	29.97 $^{+5.48}_{-4.13}$	29.25 $^{+0.67}_{-1.08}$	4.24 $^{+0.05}_{-0.09}$	273 $^{+57}_{-72}$
1266	284.29394	-0.87970	5.47 $^{+0.09}_{-0.09}$	26.68 $^{+4.12}_{-3.21}$	29.02 $^{+0.23}_{-0.49}$	3.91 $^{+0.08}_{-0.07}$	188 $^{+21}_{-22}$
1791	284.90913	-0.90977	3.20 $^{+0.09}_{-0.09}$	28.56 $^{+5.73}_{-3.91}$	28.82 $^{+0.11}_{-0.08}$	4.08 $^{+0.01}_{-0.01}$	8 $^{+12}_{-6}$
1808	284.92434	-0.33711	3.60 $^{+0.09}_{-0.09}$	27.29 $^{+4.39}_{-3.29}$	28.63 $^{+0.11}_{-0.14}$	4.05 $^{+0.02}_{-0.02}$	141 $^{+5}_{-6}$

Continued on next page...

ID	$\ell$	b	$A_0$	Phot. $T_{\text{eff}}$	Spec. $T_{\text{eff}}$	$\log(g)$	$vsini$
1639	284.73663	-1.10861	3.39 <sup>+0.08</sup> <sub>-0.09</sub>	28.48 <sup>+5.02</sup> <sub>-3.73</sub>	28.59 <sup>+0.19</sup> <sub>-0.14</sub>	4.13 <sup>+0.02</sup> <sub>-0.02</sub>	73 <sup>+8</sup> <sub>-11</sub>
1334	284.36814	-1.14149	6.04 <sup>+0.09</sup> <sub>-0.09</sub>	21.78 <sup>+2.35</sup> <sub>-2.02</sub>	28.31 <sup>+1.02</sup> <sub>-1.71</sub>	3.99 <sup>+0.19</sup> <sub>-0.19</sub>	58 <sup>+51</sup> <sub>-40</sub>
1945	285.03451	-1.18191	5.98 <sup>+0.09</sup> <sub>-0.10</sub>	25.51 <sup>+3.58</sup> <sub>-2.96</sub>	28.11 <sup>+1.16</sup> <sub>-1.92</sub>	4.19 <sup>+0.23</sup> <sub>-0.24</sub>	115 <sup>+71</sup> <sub>-72</sub>
2662	285.61449	-0.75291	4.54 <sup>+0.08</sup> <sub>-0.09</sub>	30.12 <sup>+6.13</sup> <sub>-4.46</sub>	27.79 <sup>+1.72</sup> <sub>-0.28</sub>	3.81 <sup>+0.25</sup> <sub>-0.04</sub>	6 <sup>+11</sup> <sub>-5</sub>
1747	284.86811	-0.46289	5.86 <sup>+0.10</sup> <sub>-0.09</sub>	26.69 <sup>+4.32</sup> <sub>-3.20</sub>	27.56 <sup>+1.53</sup> <sub>-2.68</sub>	4.11 <sup>+0.27</sup> <sub>-0.27</sub>	92 <sup>+76</sup> <sub>-62</sub>
1431	284.49702	-0.08363	5.46 <sup>+0.09</sup> <sub>-0.09</sub>	22.79 <sup>+2.65</sup> <sub>-2.28</sub>	27.36 <sup>+1.39</sup> <sub>-2.01</sub>	4.32 <sup>+0.20</sup> <sub>-0.23</sub>	133 <sup>+69</sup> <sub>-77</sub>
2342	285.35511	-0.66325	5.19 <sup>+0.10</sup> <sub>-0.09</sub>	22.94 <sup>+2.87</sup> <sub>-2.27</sub>	27.11 <sup>+1.40</sup> <sub>-2.30</sub>	3.88 <sup>+0.12</sup> <sub>-0.18</sub>	60 <sup>+37</sup> <sub>-38</sub>
2914	285.80207	-1.07655	2.83 <sup>+0.09</sup> <sub>-0.08</sub>	22.22 <sup>+2.34</sup> <sub>-1.98</sub>	27.00 <sup>+3.00</sup> <sub>-0.00</sub>	3.75 <sup>+0.50</sup> <sub>-0.00</sub>	0 <sup>+7</sup> <sub>-0</sub>
1353	284.40085	-1.08042	6.23 <sup>+0.09</sup> <sub>-0.09</sub>	25.74 <sup>+3.78</sup> <sub>-2.94</sub>	26.79 <sup>+1.22</sup> <sub>-1.35</sub>	3.85 <sup>+0.16</sup> <sub>-0.16</sub>	72 <sup>+51</sup> <sub>-47</sub>
1263	284.29188	-0.86154	4.30 <sup>+0.09</sup> <sub>-0.09</sub>	27.64 <sup>+4.89</sup> <sub>-3.43</sub>	26.64 <sup>+0.26</sup> <sub>-0.31</sub>	3.70 <sup>+0.03</sup> <sub>-0.03</sub>	4 <sup>+6</sup> <sub>-3</sub>
1795	284.91442	-0.89035	2.99 <sup>+0.08</sup> <sub>-0.09</sub>	31.77 <sup>+8.18</sup> <sub>-5.02</sub>	26.63 <sup>+0.69</sup> <sub>-0.12</sub>	4.08 <sup>+0.04</sup> <sub>-0.01</sub>	74 <sup>+9</sup> <sub>-9</sub>
1152	284.21773	-0.79669	4.54 <sup>+0.09</sup> <sub>-0.09</sub>	21.05 <sup>+2.35</sup> <sub>-1.93</sub>	26.43 <sup>+0.31</sup> <sub>-0.26</sub>	3.66 <sup>+0.03</sup> <sub>-0.04</sub>	232 <sup>+12</sup> <sub>-9</sub>
1565	284.65688	-0.85548	5.32 <sup>+0.10</sup> <sub>-0.10</sub>	27.35 <sup>+5.50</sup> <sub>-3.80</sub>	26.08 <sup>+1.47</sup> <sub>-1.49</sub>	4.18 <sup>+0.17</sup> <sub>-0.17</sub>	372 <sup>+39</sup> <sub>-39</sub>
3134	285.93272	-1.13862	4.87 <sup>+0.11</sup> <sub>-0.11</sub>	20.85 <sup>+2.04</sup> <sub>-1.89</sub>	25.91 <sup>+2.66</sup> <sub>-3.46</sub>	4.07 <sup>+0.43</sup> <sub>-0.49</sub>	472 <sup>+83</sup> <sub>-115</sub>
1602	284.70199	-1.15676	5.43 <sup>+0.09</sup> <sub>-0.09</sub>	22.39 <sup>+2.46</sup> <sub>-2.11</sub>	25.72 <sup>+1.72</sup> <sub>-1.75</sub>	4.09 <sup>+0.20</sup> <sub>-0.21</sub>	98 <sup>+59</sup> <sub>-63</sub>
1832	284.94718	-0.55783	2.95 <sup>+0.06</sup> <sub>-0.08</sub>	32.73 <sup>+6.86</sup> <sub>-5.17</sub>	25.54 <sup>+0.25</sup> <sub>-0.19</sub>	4.17 <sup>+0.03</sup> <sub>-0.03</sub>	80 <sup>+14</sup> <sub>-16</sub>
1581	284.67868	-1.18017	5.96 <sup>+0.10</sup> <sub>-0.10</sub>	25.94 <sup>+4.04</sup> <sub>-3.25</sub>	25.41 <sup>+3.50</sup> <sub>-4.61</sub>	3.88 <sup>+0.45</sup> <sub>-0.46</sub>	277 <sup>+119</sup> <sub>-117</sub>
1227	284.27348	-0.69497	3.55 <sup>+0.09</sup> <sub>-0.09</sub>	26.50 <sup>+3.96</sup> <sub>-3.09</sub>	25.36 <sup>+0.19</sup> <sub>-0.26</sub>	3.91 <sup>+0.02</sup> <sub>-0.03</sub>	88 <sup>+14</sup> <sub>-14</sub>
3290	286.03910	-0.58023	3.81 <sup>+0.09</sup> <sub>-0.08</sub>	27.50 <sup>+4.46</sup> <sub>-3.34</sub>	25.35 <sup>+0.17</sup> <sub>-0.18</sub>	3.58 <sup>+0.02</sup> <sub>-0.02</sub>	2 <sup>+3</sup> <sub>-1</sub>
1580	284.67791	-1.15032	4.77 <sup>+0.09</sup> <sub>-0.09</sub>	21.59 <sup>+2.26</sup> <sub>-1.94</sub>	25.32 <sup>+1.97</sup> <sub>-1.92</sub>	4.20 <sup>+0.21</sup> <sub>-0.21</sub>	167 <sup>+50</sup> <sub>-62</sub>
1414	284.47914	-1.09329	6.58 <sup>+0.10</sup> <sub>-0.09</sub>	24.83 <sup>+3.36</sup> <sub>-2.82</sub>	24.81 <sup>+3.28</sup> <sub>-3.53</sub>	3.90 <sup>+0.36</sup> <sub>-0.35</sub>	197 <sup>+83</sup> <sub>-90</sub>
1816	284.93088	-1.15181	5.10 <sup>+0.10</sup> <sub>-0.09</sub>	24.09 <sup>+3.07</sup> <sub>-2.53</sub>	24.79 <sup>+2.50</sup> <sub>-2.85</sub>	4.27 <sup>+0.28</sup> <sub>-0.33</sub>	211 <sup>+91</sup> <sub>-100</sub>
1329	284.35953	-0.91936	4.27 <sup>+0.09</sup> <sub>-0.09</sub>	23.83 <sup>+3.02</sup> <sub>-2.47</sub>	24.73 <sup>+1.59</sup> <sub>-1.46</sub>	4.22 <sup>+0.18</sup> <sub>-0.17</sub>	152 <sup>+46</sup> <sub>-56</sub>
1812	284.92673	-0.59715	6.11 <sup>+0.09</sup> <sub>-0.09</sub>	22.39 <sup>+2.53</sup> <sub>-2.19</sub>	24.25 <sup>+2.66</sup> <sub>-2.78</sub>	4.14 <sup>+0.32</sup> <sub>-0.35</sub>	136 <sup>+106</sup> <sub>-90</sub>
1378	284.42418	-0.73052	3.75 <sup>+0.09</sup> <sub>-0.09</sub>	29.31 <sup>+6.05</sup> <sub>-4.34</sub>	24.13 <sup>+0.19</sup> <sub>-0.34</sub>	3.95 <sup>+0.03</sup> <sub>-0.03</sub>	206 <sup>+7</sup> <sub>-7</sub>
1635	284.73163	-0.75386	6.25 <sup>+0.09</sup> <sub>-0.09</sub>	25.64 <sup>+3.91</sup> <sub>-3.05</sub>	24.07 <sup>+2.08</sup> <sub>-2.16</sub>	4.28 <sup>+0.25</sup> <sub>-0.27</sub>	154 <sup>+82</sup> <sub>-92</sub>
3281	286.03235	-0.26009	5.46 <sup>+0.09</sup> <sub>-0.08</sub>	24.48 <sup>+2.94</sup> <sub>-2.52</sub>	23.90 <sup>+0.61</sup> <sub>-0.95</sub>	3.07 <sup>+0.07</sup> <sub>-0.11</sub>	172 <sup>+24</sup> <sub>-28</sub>
1139	284.19941	-0.77157	4.30 <sup>+0.09</sup> <sub>-0.09</sub>	23.52 <sup>+2.80</sup> <sub>-2.34</sub>	23.78 <sup>+0.51</sup> <sub>-0.44</sub>	4.12 <sup>+0.06</sup> <sub>-0.06</sub>	103 <sup>+21</sup> <sub>-25</sub>
1912	285.01020	-0.02493	6.21 <sup>+0.10</sup> <sub>-0.10</sub>	18.20 <sup>+1.66</sup> <sub>-1.57</sub>	23.75 <sup>+3.43</sup> <sub>-3.76</sub>	4.22 <sup>+0.36</sup> <sub>-0.51</sub>	284 <sup>+179</sup> <sub>-173</sub>
1609	284.70759	-0.79709	4.79 <sup>+0.09</sup> <sub>-0.09</sub>	23.22 <sup>+2.74</sup> <sub>-2.40</sub>	23.71 <sup>+1.03</sup> <sub>-1.06</sub>	4.05 <sup>+0.14</sup> <sub>-0.14</sub>	65 <sup>+46</sup> <sub>-43</sub>
1361	284.40522	-1.06835	4.47 <sup>+0.09</sup> <sub>-0.09</sub>	24.06 <sup>+2.92</sup> <sub>-2.44</sub>	23.50 <sup>+1.19</sup> <sub>-1.17</sub>	4.11 <sup>+0.15</sup> <sub>-0.15</sub>	54 <sup>+47</sup> <sub>-37</sub>
2301	285.32266	-1.29429	3.82 <sup>+0.09</sup> <sub>-0.09</sub>	26.25 <sup>+3.81</sup> <sub>-3.01</sub>	23.45 <sup>+0.36</sup> <sub>-0.39</sub>	3.71 <sup>+0.05</sup> <sub>-0.05</sub>	120 <sup>+15</sup> <sub>-18</sub>
1256	284.28575	-0.75998	3.25 <sup>+0.09</sup> <sub>-0.09</sub>	26.96 <sup>+4.38</sup> <sub>-3.30</sub>	23.45 <sup>+0.16</sup> <sub>-0.15</sub>	3.89 <sup>+0.02</sup> <sub>-0.02</sub>	85 <sup>+12</sup> <sub>-12</sub>
3384	286.10560	-0.57577	5.13 <sup>+0.09</sup> <sub>-0.09</sub>	23.19 <sup>+2.65</sup> <sub>-2.24</sub>	23.44 <sup>+0.59</sup> <sub>-0.59</sub>	3.95 <sup>+0.07</sup> <sub>-0.07</sub>	46 <sup>+32</sup> <sub>-31</sub>
1861	284.96622	-1.17229	5.11 <sup>+0.09</sup> <sub>-0.09</sub>	22.79 <sup>+2.61</sup> <sub>-2.13</sub>	23.35 <sup>+2.60</sup> <sub>-2.81</sub>	4.16 <sup>+0.30</sup> <sub>-0.32</sub>	308 <sup>+85</sup> <sub>-83</sub>
1160	284.22301	-0.92752	5.07 <sup>+0.09</sup> <sub>-0.09</sub>	23.31 <sup>+2.71</sup> <sub>-2.29</sub>	23.30 <sup>+0.46</sup> <sub>-0.61</sub>	3.72 <sup>+0.06</sup> <sub>-0.06</sub>	217 <sup>+11</sup> <sub>-11</sub>
2690	285.63760	-0.77719	2.83 <sup>+0.09</sup> <sub>-0.08</sub>	25.21 <sup>+3.37</sup> <sub>-2.65</sub>	23.26 <sup>+0.14</sup> <sub>-0.15</sub>	4.05 <sup>+0.02</sup> <sub>-0.02</sub>	6 <sup>+8</sup> <sub>-4</sub>
1342	284.38647	-0.91560	4.53 <sup>+0.09</sup> <sub>-0.09</sub>	25.75 <sup>+3.51</sup> <sub>-2.89</sub>	23.17 <sup>+0.37</sup> <sub>-0.49</sub>	3.90 <sup>+0.05</sup> <sub>-0.05</sub>	143 <sup>+17</sup> <sub>-16</sub>
1925	285.02131	-1.18215	6.46 <sup>+0.08</sup> <sub>-0.11</sub>	31.12 <sup>+6.63</sup> <sub>-5.57</sub>	23.16 <sup>+3.86</sup> <sub>-4.18</sub>	4.12 <sup>+0.38</sup> <sub>-0.45</sub>	199 <sup>+166</sup> <sub>-133</sub>
2497	285.48302	-1.03472	3.52 <sup>+0.09</sup> <sub>-0.09</sub>	25.30 <sup>+3.48</sup> <sub>-2.79</sub>	23.15 <sup>+0.16</sup> <sub>-0.21</sub>	3.63 <sup>+0.02</sup> <sub>-0.02</sub>	165 <sup>+5</sup> <sub>-5</sub>
2593	285.57024	-0.90338	4.60 <sup>+0.09</sup> <sub>-0.09</sub>	21.34 <sup>+2.22</sup> <sub>-1.87</sub>	23.10 <sup>+1.96</sup> <sub>-1.98</sub>	4.32 <sup>+0.22</sup> <sub>-0.23</sub>	261 <sup>+57</sup> <sub>-58</sub>
1379	284.42443	-0.45116	4.37 <sup>+0.08</sup> <sub>-0.08</sub>	30.55 <sup>+6.39</sup> <sub>-4.43</sub>	23.09 <sup>+0.61</sup> <sub>-0.62</sub>	3.97 <sup>+0.08</sup> <sub>-0.07</sub>	307 <sup>+16</sup> <sub>-16</sub>
1864	284.96644	-0.23210	4.01 <sup>+0.09</sup> <sub>-0.09</sub>	22.13 <sup>+2.48</sup> <sub>-2.01</sub>	22.99 <sup>+0.31</sup> <sub>-0.31</sub>	3.72 <sup>+0.04</sup> <sub>-0.04</sub>	7 <sup>+11</sup> <sub>-5</sub>
1772	284.88997	-0.62127	4.93 <sup>+0.09</sup> <sub>-0.09</sub>	26.16 <sup>+4.04</sup> <sub>-2.97</sub>	22.91 <sup>+0.33</sup> <sub>-0.28</sub>	3.42 <sup>+0.03</sup> <sub>-0.03</sub>	99 <sup>+14</sup> <sub>-13</sub>
2890	285.78911	-1.11981	5.04 <sup>+0.09</sup> <sub>-0.09</sub>	20.77 <sup>+2.04</sup> <sub>-1.79</sub>	22.81 <sup>+1.59</sup> <sub>-1.54</sub>	4.17 <sup>+0.20</sup> <sub>-0.19</sub>	200 <sup>+59</sup> <sub>-63</sub>
2204	285.24038	-1.15365	3.86 <sup>+0.10</sup> <sub>-0.09</sub>	27.17 <sup>+4.91</sup> <sub>-3.49</sub>	22.81 <sup>+0.47</sup> <sub>-0.30</sub>	3.83 <sup>+0.05</sup> <sub>-0.04</sub>	150 <sup>+13</sup> <sub>-12</sub>

Continued on next page...

ID	$\ell$	b	$A_0$	Phot. $T_{\text{eff}}$	Spec. $T_{\text{eff}}$	$\log(g)$	$vsini$
1963	285.05029	-0.63829	$3.44^{+0.09}_{-0.09}$	$27.52^{+4.35}_{-3.38}$	$22.73^{+0.41}_{-0.31}$	$3.83^{+0.04}_{-0.04}$	$288^{+12}_{-11}$
2000	285.08859	-0.75067	$3.31^{+0.09}_{-0.09}$	$25.57^{+3.59}_{-2.79}$	$22.70^{+0.12}_{-0.14}$	$4.06^{+0.02}_{-0.02}$	$130^{+8}_{-8}$
1469	284.55690	-0.82900	$4.17^{+0.09}_{-0.09}$	$24.55^{+3.09}_{-2.51}$	$22.68^{+0.52}_{-0.40}$	$4.11^{+0.06}_{-0.05}$	$129^{+20}_{-20}$
1527	284.62269	-1.05298	$4.32^{+0.09}_{-0.09}$	$26.41^{+3.82}_{-3.04}$	$22.67^{+0.47}_{-0.34}$	$3.81^{+0.05}_{-0.04}$	$109^{+16}_{-20}$
2081	285.15308	-0.54251	$3.49^{+0.08}_{-0.09}$	$28.36^{+4.91}_{-3.64}$	$22.64^{+0.33}_{-0.28}$	$3.92^{+0.04}_{-0.04}$	$22^{+29}_{-16}$
1457	284.53933	-1.10535	$3.62^{+0.09}_{-0.08}$	$28.39^{+5.28}_{-3.55}$	$22.60^{+0.29}_{-0.21}$	$3.67^{+0.03}_{-0.03}$	$303^{+7}_{-10}$
2610	285.58382	-0.85472	$6.26^{+0.09}_{-0.09}$	$24.38^{+3.21}_{-2.58}$	$22.57^{+3.49}_{-3.12}$	$3.87^{+0.39}_{-0.38}$	$151^{+113}_{-98}$
2576	285.56115	-0.70101	$3.73^{+0.09}_{-0.08}$	$25.24^{+3.18}_{-2.64}$	$22.55^{+0.44}_{-0.41}$	$4.00^{+0.06}_{-0.06}$	$74^{+25}_{-35}$
1528	284.62372	-0.88068	$4.88^{+0.09}_{-0.09}$	$24.52^{+2.93}_{-2.52}$	$22.51^{+0.50}_{-0.48}$	$3.47^{+0.06}_{-0.06}$	$557^{+16}_{-15}$
1512	284.59894	-1.28761	$3.38^{+0.09}_{-0.09}$	$23.85^{+2.74}_{-2.43}$	$22.50^{+0.14}_{-0.16}$	$3.85^{+0.02}_{-0.02}$	$103^{+11}_{-14}$
3167	285.95651	-0.24451	$4.76^{+0.09}_{-0.09}$	$22.71^{+2.62}_{-2.18}$	$22.45^{+2.19}_{-1.82}$	$3.85^{+0.27}_{-0.23}$	$192^{+66}_{-75}$
1267	284.29415	-0.70297	$3.25^{+0.08}_{-0.08}$	$27.17^{+4.06}_{-3.17}$	$22.41^{+0.27}_{-0.28}$	$3.74^{+0.04}_{-0.04}$	$59^{+18}_{-26}$
3032	285.87442	-0.76083	$3.32^{+0.08}_{-0.08}$	$24.59^{+3.01}_{-2.48}$	$22.41^{+0.17}_{-0.20}$	$3.84^{+0.02}_{-0.02}$	$246^{+5}_{-5}$
3144	285.93860	-0.83543	$3.55^{+0.08}_{-0.09}$	$23.96^{+2.79}_{-2.36}$	$22.36^{+0.35}_{-0.33}$	$3.97^{+0.04}_{-0.04}$	$174^{+12}_{-12}$
1283	284.30809	-1.04126	$3.05^{+0.09}_{-0.09}$	$29.18^{+5.48}_{-4.01}$	$22.36^{+0.15}_{-0.22}$	$3.86^{+0.02}_{-0.02}$	$192^{+5}_{-6}$
1561	284.65002	-1.06947	$3.12^{+0.08}_{-0.08}$	$26.08^{+3.47}_{-2.77}$	$22.35^{+0.11}_{-0.08}$	$3.94^{+0.01}_{-0.01}$	$101^{+7}_{-9}$
1695	284.81303	-0.78574	$5.69^{+0.10}_{-0.10}$	$23.72^{+3.06}_{-2.51}$	$22.32^{+2.11}_{-2.14}$	$3.98^{+0.26}_{-0.25}$	$102^{+68}_{-66}$
1496	284.58161	-0.47053	$4.14^{+0.09}_{-0.09}$	$21.19^{+2.10}_{-1.79}$	$22.27^{+0.30}_{-0.38}$	$4.06^{+0.04}_{-0.04}$	$164^{+12}_{-13}$
1842	284.95429	-1.16864	$4.38^{+0.09}_{-0.09}$	$22.24^{+2.49}_{-2.10}$	$22.15^{+1.53}_{-1.47}$	$4.20^{+0.18}_{-0.18}$	$73^{+57}_{-49}$
1640	284.74083	-1.07290	$3.37^{+0.09}_{-0.09}$	$24.26^{+2.76}_{-2.53}$	$22.10^{+0.30}_{-0.30}$	$4.08^{+0.04}_{-0.04}$	$37^{+26}_{-24}$
2021	285.10960	-0.64905	$2.79^{+0.08}_{-0.08}$	$28.72^{+4.97}_{-3.63}$	$22.09^{+0.16}_{-0.17}$	$3.78^{+0.02}_{-0.02}$	$85^{+11}_{-12}$
2464	285.45424	-0.94725	$3.64^{+0.09}_{-0.09}$	$25.00^{+3.65}_{-2.83}$	$22.03^{+0.35}_{-0.32}$	$3.84^{+0.04}_{-0.04}$	$25^{+25}_{-18}$
1310	284.33341	-0.54060	$4.05^{+0.09}_{-0.09}$	$23.86^{+2.84}_{-2.41}$	$21.89^{+0.30}_{-0.38}$	$4.01^{+0.04}_{-0.05}$	$201^{+13}_{-14}$
2037	285.11693	-0.82649	$4.76^{+0.10}_{-0.09}$	$22.26^{+2.51}_{-2.12}$	$21.83^{+0.34}_{-0.35}$	$3.38^{+0.05}_{-0.04}$	$117^{+18}_{-17}$
1382	284.42795	-1.13541	$5.60^{+0.09}_{-0.09}$	$23.90^{+2.85}_{-2.38}$	$21.80^{+0.31}_{-0.34}$	$3.35^{+0.04}_{-0.04}$	$201^{+13}_{-14}$
1968	285.05394	-1.09482	$5.80^{+0.10}_{-0.09}$	$23.54^{+2.91}_{-2.50}$	$21.76^{+4.08}_{-3.97}$	$4.15^{+0.38}_{-0.43}$	$297^{+171}_{-169}$
1860	284.96556	-1.41368	$5.58^{+0.09}_{-0.09}$	$20.88^{+2.13}_{-1.81}$	$21.74^{+1.98}_{-1.77}$	$3.78^{+0.26}_{-0.24}$	$80^{+70}_{-54}$
1665	284.77608	-1.17962	$2.80^{+0.08}_{-0.09}$	$21.66^{+2.19}_{-1.94}$	$21.56^{+0.18}_{-0.18}$	$4.19^{+0.02}_{-0.02}$	$179^{+6}_{-7}$
3086	285.91123	-0.79877	$3.08^{+0.08}_{-0.08}$	$22.09^{+2.22}_{-1.94}$	$21.47^{+0.19}_{-0.24}$	$3.78^{+0.02}_{-0.03}$	$162^{+8}_{-8}$
1970	285.05426	-0.84524	$2.49^{+0.08}_{-0.08}$	$26.44^{+3.70}_{-2.87}$	$21.46^{+0.14}_{-0.14}$	$4.05^{+0.02}_{-0.02}$	$19^{+18}_{-13}$
1464	284.54597	-1.08836	$3.81^{+0.09}_{-0.09}$	$22.85^{+2.57}_{-2.14}$	$21.42^{+0.41}_{-0.38}$	$4.02^{+0.05}_{-0.06}$	$184^{+15}_{-15}$
1440	284.50925	-1.13863	$3.91^{+0.09}_{-0.09}$	$23.51^{+2.84}_{-2.29}$	$21.37^{+0.32}_{-0.25}$	$3.96^{+0.04}_{-0.03}$	$250^{+11}_{-11}$
1386	284.43155	-1.13573	$5.71^{+0.10}_{-0.09}$	$24.88^{+3.47}_{-2.80}$	$21.34^{+3.45}_{-3.37}$	$3.95^{+0.37}_{-0.34}$	$182^{+91}_{-101}$
1569	284.66358	-0.74483	$3.99^{+0.08}_{-0.09}$	$22.92^{+2.47}_{-2.16}$	$21.31^{+0.26}_{-0.32}$	$3.89^{+0.04}_{-0.04}$	$41^{+27}_{-26}$
3190	285.97398	-0.37663	$3.49^{+0.09}_{-0.09}$	$23.01^{+2.49}_{-2.16}$	$21.31^{+0.22}_{-0.23}$	$3.37^{+0.03}_{-0.03}$	$278^{+8}_{-8}$
1466	284.54919	-1.23118	$3.74^{+0.09}_{-0.08}$	$23.28^{+2.76}_{-2.23}$	$21.29^{+0.28}_{-0.28}$	$3.72^{+0.04}_{-0.03}$	$50^{+23}_{-30}$
1539	284.63080	-1.33515	$3.98^{+0.09}_{-0.09}$	$22.94^{+2.73}_{-2.16}$	$21.26^{+0.40}_{-0.37}$	$3.90^{+0.05}_{-0.05}$	$112^{+20}_{-26}$
3456	286.15112	-0.57196	$4.72^{+0.09}_{-0.09}$	$23.38^{+2.73}_{-2.36}$	$21.21^{+0.48}_{-0.56}$	$3.82^{+0.06}_{-0.07}$	$177^{+18}_{-19}$
2331	285.34437	-1.20834	$3.38^{+0.09}_{-0.09}$	$23.13^{+2.66}_{-2.25}$	$21.21^{+0.36}_{-0.23}$	$4.02^{+0.05}_{-0.05}$	$80^{+23}_{-37}$
2091	285.16508	-1.42419	$2.61^{+0.09}_{-0.09}$	$24.77^{+3.15}_{-2.56}$	$21.21^{+0.17}_{-0.18}$	$3.84^{+0.02}_{-0.02}$	$58^{+15}_{-24}$
1402	284.45185	-0.36021	$3.91^{+0.09}_{-0.09}$	$26.54^{+3.95}_{-3.16}$	$21.16^{+0.50}_{-0.48}$	$4.04^{+0.06}_{-0.06}$	$178^{+19}_{-20}$
1549	284.63752	-0.72140	$3.75^{+0.09}_{-0.09}$	$23.44^{+2.90}_{-2.36}$	$21.16^{+0.31}_{-0.28}$	$4.07^{+0.04}_{-0.04}$	$334^{+12}_{-11}$
1395	284.44061	-1.17309	$3.91^{+0.09}_{-0.09}$	$24.44^{+3.20}_{-2.52}$	$21.16^{+0.25}_{-0.24}$	$3.69^{+0.03}_{-0.03}$	$8^{+13}_{-6}$
3186	285.97144	-0.61283	$4.59^{+0.09}_{-0.09}$	$23.44^{+2.86}_{-2.34}$	$21.07^{+0.61}_{-0.63}$	$3.76^{+0.07}_{-0.08}$	$74^{+32}_{-43}$
1278	284.30153	-0.98429	$4.93^{+0.09}_{-0.09}$	$21.67^{+2.34}_{-1.98}$	$21.04^{+1.74}_{-1.59}$	$4.18^{+0.20}_{-0.18}$	$185^{+52}_{-58}$
1854	284.96226	-0.48429	$3.96^{+0.09}_{-0.08}$	$24.15^{+3.11}_{-2.42}$	$21.02^{+0.24}_{-0.23}$	$3.66^{+0.03}_{-0.03}$	$15^{+18}_{-11}$

Continued on next page...

ID	$\ell$	b	$A_0$	Phot. $T_{\text{eff}}$	Spec. $T_{\text{eff}}$	$\log(g)$	$vsini$
2818	285.73625	-1.02935	$2.85^{+0.08}_{-0.09}$	$23.56^{+2.64}_{-2.25}$	$20.90^{+0.19}_{-0.25}$	$4.02^{+0.03}_{-0.03}$	$157^{+8}_{-9}$
2677	285.62588	-0.38123	$2.22^{+0.10}_{-0.09}$	$24.14^{+3.20}_{-2.54}$	$20.90^{+0.10}_{-0.16}$	$4.10^{+0.02}_{-0.02}$	$114^{+7}_{-8}$
1121	284.17655	-0.70375	$4.17^{+0.09}_{-0.09}$	$26.74^{+4.03}_{-3.10}$	$20.85^{+0.70}_{-0.65}$	$3.64^{+0.08}_{-0.08}$	$127^{+29}_{-34}$
1345	284.38825	-0.46144	$3.98^{+0.09}_{-0.09}$	$22.04^{+2.34}_{-2.06}$	$20.82^{+1.28}_{-1.11}$	$4.16^{+0.14}_{-0.13}$	$183^{+42}_{-46}$
3263	286.02161	-0.90793	$4.21^{+0.09}_{-0.09}$	$21.70^{+2.29}_{-1.93}$	$20.82^{+0.55}_{-0.32}$	$3.88^{+0.05}_{-0.04}$	$141^{+17}_{-18}$
1921	285.02001	-1.07917	$2.94^{+0.09}_{-0.08}$	$24.17^{+2.93}_{-2.40}$	$20.81^{+0.24}_{-0.21}$	$3.94^{+0.03}_{-0.03}$	$108^{+9}_{-10}$
2553	285.54024	-1.12391	$2.44^{+0.09}_{-0.09}$	$24.99^{+3.54}_{-2.57}$	$20.76^{+0.18}_{-0.16}$	$3.64^{+0.02}_{-0.02}$	$108^{+8}_{-9}$
1534	284.62649	-0.75214	$4.36^{+0.09}_{-0.09}$	$21.87^{+2.26}_{-1.99}$	$20.75^{+0.62}_{-0.55}$	$3.78^{+0.06}_{-0.08}$	$206^{+17}_{-17}$
1324	284.35226	-0.44718	$4.05^{+0.09}_{-0.08}$	$22.76^{+2.52}_{-2.14}$	$20.74^{+0.32}_{-0.37}$	$3.80^{+0.04}_{-0.05}$	$181^{+12}_{-12}$
1330	284.35966	-0.32290	$6.03^{+0.10}_{-0.10}$	$22.38^{+2.67}_{-2.32}$	$20.67^{+3.05}_{-2.70}$	$4.31^{+0.30}_{-0.39}$	$302^{+157}_{-155}$
2039	285.11855	-0.66906	$3.78^{+0.09}_{-0.09}$	$21.53^{+2.12}_{-1.91}$	$20.60^{+1.13}_{-1.02}$	$4.18^{+0.14}_{-0.13}$	$150^{+47}_{-57}$
1956	285.04407	-0.61107	$5.22^{+0.11}_{-0.11}$	$20.73^{+2.44}_{-2.25}$	$20.59^{+5.43}_{-4.12}$	$4.05^{+0.42}_{-0.48}$	$281^{+173}_{-172}$
1463	284.54569	-1.11345	$3.20^{+0.09}_{-0.09}$	$23.74^{+2.92}_{-2.37}$	$20.58^{+0.20}_{-0.20}$	$4.05^{+0.02}_{-0.03}$	$54^{+17}_{-24}$
3234	286.00608	-0.79626	$3.84^{+0.09}_{-0.09}$	$20.84^{+2.03}_{-1.73}$	$20.57^{+0.33}_{-0.31}$	$4.11^{+0.04}_{-0.04}$	$193^{+12}_{-14}$
3016	285.86600	-0.87092	$2.54^{+0.09}_{-0.09}$	$23.12^{+2.50}_{-2.17}$	$20.57^{+0.19}_{-0.19}$	$3.84^{+0.02}_{-0.02}$	$151^{+8}_{-10}$
1721	284.84081	-1.20247	$3.50^{+0.09}_{-0.09}$	$24.00^{+3.06}_{-2.44}$	$20.53^{+0.34}_{-0.18}$	$3.90^{+0.04}_{-0.03}$	$155^{+11}_{-21}$
2082	285.15442	-1.56514	$2.68^{+0.09}_{-0.08}$	$24.17^{+3.00}_{-2.42}$	$20.51^{+0.19}_{-0.19}$	$3.79^{+0.02}_{-0.02}$	$204^{+7}_{-7}$
1237	284.27652	-0.63794	$4.01^{+0.09}_{-0.09}$	$23.73^{+2.89}_{-2.43}$	$20.49^{+0.44}_{-0.43}$	$3.62^{+0.06}_{-0.05}$	$184^{+19}_{-17}$
2354	285.36847	-1.07229	$2.51^{+0.08}_{-0.08}$	$24.55^{+2.89}_{-2.51}$	$20.43^{+0.24}_{-0.25}$	$3.86^{+0.03}_{-0.03}$	$111^{+13}_{-16}$
2103	285.17585	-0.65988	$5.11^{+0.10}_{-0.09}$	$20.26^{+2.04}_{-1.80}$	$20.40^{+2.65}_{-2.30}$	$4.01^{+0.31}_{-0.30}$	$96^{+86}_{-66}$
2858	285.76057	-0.53949	$4.33^{+0.09}_{-0.09}$	$20.36^{+2.00}_{-1.68}$	$20.39^{+1.29}_{-1.16}$	$3.61^{+0.16}_{-0.16}$	$439^{+58}_{-56}$
2222	285.25158	-1.45206	$2.39^{+0.09}_{-0.09}$	$24.41^{+3.26}_{-2.49}$	$20.38^{+0.27}_{-0.27}$	$3.67^{+0.03}_{-0.03}$	$89^{+16}_{-20}$
1540	284.63279	-0.99038	$3.53^{+0.09}_{-0.09}$	$22.23^{+2.41}_{-2.04}$	$20.37^{+0.24}_{-0.25}$	$3.82^{+0.03}_{-0.03}$	$175^{+10}_{-10}$
1867	284.96984	-0.62353	$3.08^{+0.09}_{-0.09}$	$23.15^{+2.58}_{-2.26}$	$20.37^{+0.13}_{-0.15}$	$4.03^{+0.02}_{-0.02}$	$125^{+7}_{-6}$
3061	285.89265	-0.90705	$3.42^{+0.09}_{-0.09}$	$22.59^{+2.45}_{-2.14}$	$20.35^{+0.34}_{-0.30}$	$3.74^{+0.04}_{-0.04}$	$297^{+11}_{-11}$
2426	285.42933	-1.26197	$2.97^{+0.10}_{-0.09}$	$21.57^{+2.48}_{-1.96}$	$20.35^{+0.16}_{-0.16}$	$3.95^{+0.02}_{-0.02}$	$196^{+7}_{-6}$
2285	285.31328	-0.63176	$4.55^{+0.09}_{-0.09}$	$21.29^{+2.17}_{-1.90}$	$20.33^{+0.20}_{-0.19}$	$3.04^{+0.02}_{-0.02}$	$185^{+8}_{-8}$
1269	284.29631	-0.89081	$3.44^{+0.09}_{-0.08}$	$22.65^{+2.47}_{-2.05}$	$20.31^{+0.27}_{-0.24}$	$3.81^{+0.03}_{-0.03}$	$201^{+10}_{-11}$
2325	285.34026	-1.14814	$2.90^{+0.09}_{-0.09}$	$25.00^{+3.28}_{-2.64}$	$20.27^{+0.13}_{-0.14}$	$3.51^{+0.02}_{-0.02}$	$8^{+12}_{-6}$
2167	285.21749	-1.32346	$2.23^{+0.09}_{-0.08}$	$22.87^{+2.45}_{-2.13}$	$20.23^{+0.27}_{-0.28}$	$3.87^{+0.03}_{-0.03}$	$46^{+25}_{-26}$
1789	284.90795	-0.93527	$3.34^{+0.09}_{-0.08}$	$24.13^{+2.97}_{-2.42}$	$20.23^{+0.18}_{-0.16}$	$3.58^{+0.02}_{-0.02}$	$26^{+20}_{-17}$
2599	285.57582	-1.13958	$3.14^{+0.09}_{-0.09}$	$22.16^{+2.28}_{-2.00}$	$20.20^{+0.39}_{-0.37}$	$3.90^{+0.05}_{-0.05}$	$123^{+19}_{-20}$
1136	284.19570	-0.67442	$2.90^{+0.09}_{-0.08}$	$21.28^{+2.03}_{-1.78}$	$20.20^{+0.33}_{-0.17}$	$4.08^{+0.04}_{-0.03}$	$166^{+13}_{-13}$
3207	285.98861	-0.46422	$2.63^{+0.09}_{-0.09}$	$23.11^{+2.66}_{-2.24}$	$20.20^{+0.12}_{-0.12}$	$3.78^{+0.01}_{-0.02}$	$103^{+7}_{-8}$
1552	284.63960	-1.10936	$3.44^{+0.08}_{-0.08}$	$22.48^{+2.34}_{-2.07}$	$20.18^{+0.27}_{-0.25}$	$3.98^{+0.04}_{-0.03}$	$217^{+9}_{-10}$
2765	285.69712	-1.07982	$2.91^{+0.09}_{-0.08}$	$23.64^{+2.76}_{-2.25}$	$20.15^{+0.16}_{-0.13}$	$3.83^{+0.02}_{-0.02}$	$86^{+10}_{-13}$
1955	285.04405	-1.23092	$4.66^{+0.09}_{-0.09}$	$20.74^{+1.94}_{-1.76}$	$20.14^{+2.57}_{-2.00}$	$4.08^{+0.25}_{-0.23}$	$143^{+71}_{-80}$
2586	285.56670	-1.46511	$3.25^{+0.09}_{-0.08}$	$23.50^{+2.62}_{-2.23}$	$20.12^{+0.18}_{-0.16}$	$3.60^{+0.02}_{-0.02}$	$269^{+7}_{-7}$
1291	284.31507	-0.62927	$3.78^{+0.09}_{-0.09}$	$22.82^{+2.46}_{-2.28}$	$20.11^{+0.30}_{-0.23}$	$3.82^{+0.04}_{-0.03}$	$332^{+11}_{-11}$
1669	284.78259	-0.71570	$3.28^{+0.09}_{-0.08}$	$21.51^{+2.07}_{-1.81}$	$20.10^{+0.25}_{-0.14}$	$3.88^{+0.03}_{-0.02}$	$337^{+9}_{-9}$
2649	285.60859	-0.31922	$2.36^{+0.09}_{-0.09}$	$21.56^{+2.23}_{-1.90}$	$20.06^{+0.16}_{-0.13}$	$4.23^{+0.02}_{-0.02}$	$176^{+8}_{-8}$
1372	284.41481	-1.03008	$4.32^{+0.10}_{-0.09}$	$21.97^{+2.57}_{-2.01}$	$20.03^{+0.31}_{-0.28}$	$3.62^{+0.04}_{-0.04}$	$142^{+18}_{-18}$
1811	284.92668	-0.91298	$3.22^{+0.08}_{-0.08}$	$23.03^{+2.52}_{-2.15}$	$20.01^{+0.15}_{-0.15}$	$3.90^{+0.02}_{-0.02}$	$216^{+6}_{-6}$
3125	285.92807	-1.10812	$2.37^{+0.09}_{-0.08}$	$23.65^{+2.70}_{-2.27}$	$19.98^{+0.09}_{-0.10}$	$4.12^{+0.02}_{-0.02}$	$33^{+22}_{-21}$
1728	284.85155	-0.22670	$6.64^{+0.09}_{-0.09}$	$17.22^{+1.42}_{-1.19}$	$19.94^{+1.97}_{-1.94}$	$3.20^{+0.24}_{-0.23}$	$224^{+73}_{-77}$
1960	285.04651	-0.46407	$2.50^{+0.09}_{-0.09}$	$23.01^{+2.80}_{-2.29}$	$19.90^{+0.22}_{-0.14}$	$3.93^{+0.02}_{-0.02}$	$117^{+6}_{-6}$

Continued on next page...

ID	$\ell$	b	$A_0$	Phot. $T_{\text{eff}}$	Spec. $T_{\text{eff}}$	$\log(g)$	$vsini$
2362	285.37408	-1.31762	$2.32^{+0.08}_{-0.08}$	$21.28^{+2.01}_{-1.79}$	$19.90^{+0.12}_{-0.16}$	$4.09^{+0.02}_{-0.02}$	$113^{+11}_{-11}$
2367	285.37910	-1.44823	$2.42^{+0.09}_{-0.08}$	$23.23^{+2.59}_{-2.11}$	$19.89^{+0.25}_{-0.34}$	$3.95^{+0.02}_{-0.03}$	$250^{+8}_{-8}$
2378	285.39118	-1.48568	$2.63^{+0.09}_{-0.09}$	$23.05^{+2.48}_{-2.17}$	$19.86^{+0.20}_{-0.23}$	$3.97^{+0.03}_{-0.03}$	$48^{+23}_{-28}$
3415	286.12044	-0.55359	$5.43^{+0.09}_{-0.09}$	$21.22^{+2.08}_{-1.90}$	$19.83^{+0.63}_{-0.63}$	$3.89^{+0.08}_{-0.08}$	$101^{+36}_{-48}$
2923	285.80853	-0.92719	$4.68^{+0.10}_{-0.09}$	$24.52^{+3.49}_{-2.63}$	$19.82^{+0.45}_{-0.49}$	$3.56^{+0.06}_{-0.06}$	$177^{+19}_{-19}$
1752	284.86999	-1.29948	$3.89^{+0.09}_{-0.08}$	$21.02^{+2.01}_{-1.79}$	$19.81^{+0.16}_{-0.19}$	$3.47^{+0.02}_{-0.02}$	$34^{+21}_{-22}$
2055	285.13114	-1.51997	$2.85^{+0.08}_{-0.09}$	$22.26^{+2.19}_{-2.00}$	$19.81^{+0.16}_{-0.15}$	$3.68^{+0.02}_{-0.02}$	$60^{+11}_{-9}$
1517	284.60814	-1.21555	$3.20^{+0.08}_{-0.09}$	$21.40^{+2.14}_{-1.85}$	$19.80^{+0.23}_{-0.25}$	$3.94^{+0.03}_{-0.03}$	$81^{+18}_{-23}$
1307	284.33105	-0.36651	$3.61^{+0.09}_{-0.09}$	$22.97^{+2.56}_{-2.19}$	$19.80^{+0.22}_{-0.29}$	$3.70^{+0.04}_{-0.04}$	$32^{+20}_{-20}$
1697	284.81612	-0.70078	$3.92^{+0.09}_{-0.09}$	$21.07^{+2.06}_{-1.83}$	$19.73^{+1.18}_{-0.95}$	$4.15^{+0.14}_{-0.12}$	$85^{+55}_{-56}$
2542	285.53206	-1.22142	$2.66^{+0.10}_{-0.09}$	$20.96^{+2.09}_{-1.79}$	$19.73^{+0.21}_{-0.24}$	$3.94^{+0.03}_{-0.03}$	$355^{+9}_{-9}$
2753	285.68411	-0.39247	$2.42^{+0.09}_{-0.09}$	$21.04^{+2.06}_{-1.77}$	$19.72^{+0.19}_{-0.18}$	$4.26^{+0.03}_{-0.02}$	$292^{+8}_{-8}$
3030	285.87236	-1.20358	$2.77^{+0.09}_{-0.08}$	$24.65^{+3.03}_{-2.47}$	$19.71^{+0.16}_{-0.16}$	$3.85^{+0.02}_{-0.02}$	$181^{+7}_{-7}$
2169	285.21889	-0.66129	$3.10^{+0.09}_{-0.08}$	$21.55^{+2.17}_{-1.85}$	$19.68^{+0.21}_{-0.22}$	$4.00^{+0.03}_{-0.03}$	$54^{+21}_{-29}$
1578	284.67582	-1.14025	$2.85^{+0.09}_{-0.09}$	$21.34^{+2.22}_{-1.87}$	$19.64^{+0.15}_{-0.21}$	$4.02^{+0.02}_{-0.03}$	$86^{+12}_{-13}$
1825	284.94239	-1.46943	$3.46^{+0.09}_{-0.09}$	$21.66^{+2.29}_{-1.93}$	$19.63^{+0.25}_{-0.28}$	$3.63^{+0.03}_{-0.03}$	$91^{+14}_{-17}$
2668	285.61832	-1.15594	$3.57^{+0.05}_{-0.07}$	$38.65^{+7.37}_{-8.61}$	$19.63^{+0.08}_{-0.10}$	$3.58^{+0.01}_{-0.01}$	$171^{+5}_{-5}$
1604	284.70398	-1.04403	$3.44^{+0.09}_{-0.09}$	$21.02^{+2.02}_{-1.74}$	$19.60^{+0.15}_{-0.13}$	$4.11^{+0.02}_{-0.02}$	$145^{+13}_{-13}$
2009	285.09949	-1.08016	$3.99^{+0.09}_{-0.09}$	$22.92^{+2.86}_{-2.24}$	$19.52^{+0.24}_{-0.32}$	$3.57^{+0.03}_{-0.04}$	$171^{+13}_{-12}$
2179	285.22493	-0.68026	$3.43^{+0.09}_{-0.08}$	$23.05^{+2.86}_{-2.12}$	$19.47^{+0.15}_{-0.14}$	$3.34^{+0.02}_{-0.02}$	$111^{+7}_{-8}$
3124	285.92806	-0.19719	$4.22^{+0.09}_{-0.09}$	$21.80^{+2.27}_{-1.92}$	$19.30^{+0.27}_{-0.23}$	$3.08^{+0.03}_{-0.03}$	$157^{+12}_{-13}$
2387	285.39933	-1.34193	$2.26^{+0.08}_{-0.08}$	$22.26^{+2.15}_{-1.96}$	$19.30^{+0.23}_{-0.22}$	$3.92^{+0.03}_{-0.03}$	$275^{+9}_{-9}$
1701	284.82067	-0.69710	$4.55^{+0.09}_{-0.09}$	$22.95^{+2.63}_{-2.24}$	$19.28^{+0.30}_{-0.37}$	$3.65^{+0.04}_{-0.04}$	$184^{+12}_{-13}$
2733	285.67002	-1.24639	$2.60^{+0.09}_{-0.09}$	$20.72^{+1.96}_{-1.72}$	$19.26^{+0.27}_{-0.26}$	$4.19^{+0.04}_{-0.04}$	$99^{+21}_{-25}$
2042	285.11985	-1.57214	$2.95^{+0.09}_{-0.09}$	$22.14^{+2.40}_{-2.01}$	$19.22^{+0.27}_{-0.30}$	$3.77^{+0.04}_{-0.04}$	$158^{+13}_{-15}$
2500	285.48490	-1.31382	$2.31^{+0.08}_{-0.09}$	$21.78^{+2.20}_{-1.93}$	$19.20^{+0.14}_{-0.14}$	$3.94^{+0.02}_{-0.02}$	$235^{+5}_{-5}$
2429	285.43254	-0.78905	$3.54^{+0.10}_{-0.09}$	$18.66^{+1.72}_{-1.45}$	$19.10^{+0.23}_{-0.23}$	$3.79^{+0.03}_{-0.03}$	$108^{+12}_{-13}$
2867	285.77049	-1.03003	$4.15^{+0.09}_{-0.09}$	$20.76^{+2.06}_{-1.79}$	$19.08^{+0.29}_{-0.34}$	$4.17^{+0.04}_{-0.04}$	$174^{+18}_{-18}$
2534	285.52116	-1.07434	$2.92^{+0.09}_{-0.09}$	$21.36^{+2.10}_{-1.87}$	$19.01^{+0.27}_{-0.28}$	$3.93^{+0.04}_{-0.04}$	$263^{+12}_{-12}$
2384	285.39821	-1.01466	$2.81^{+0.09}_{-0.08}$	$21.62^{+2.15}_{-1.86}$	$18.99^{+0.27}_{-0.25}$	$3.87^{+0.03}_{-0.04}$	$387^{+11}_{-11}$
1972	285.05864	-0.78661	$3.31^{+0.08}_{-0.08}$	$21.65^{+2.08}_{-1.84}$	$18.96^{+0.25}_{-0.24}$	$3.96^{+0.03}_{-0.03}$	$139^{+13}_{-13}$
1920	285.01762	-0.99145	$3.24^{+0.08}_{-0.09}$	$21.40^{+2.01}_{-1.90}$	$18.96^{+0.18}_{-0.15}$	$3.81^{+0.02}_{-0.02}$	$53^{+18}_{-25}$
2989	285.84146	-1.13007	$3.30^{+0.09}_{-0.09}$	$21.97^{+2.25}_{-1.95}$	$18.92^{+0.25}_{-0.23}$	$3.92^{+0.03}_{-0.03}$	$99^{+14}_{-19}$
1940	285.03206	-1.16858	$3.07^{+0.08}_{-0.08}$	$20.69^{+1.87}_{-1.71}$	$18.92^{+0.09}_{-0.13}$	$3.60^{+0.02}_{-0.02}$	$66^{+12}_{-14}$
1863	284.96633	-0.89334	$3.13^{+0.09}_{-0.09}$	$20.74^{+2.02}_{-1.76}$	$18.84^{+0.21}_{-0.19}$	$3.92^{+0.03}_{-0.02}$	$120^{+11}_{-12}$
3409	286.11811	-0.82680	$3.89^{+0.09}_{-0.09}$	$20.85^{+2.09}_{-1.83}$	$18.81^{+0.38}_{-0.37}$	$3.67^{+0.05}_{-0.05}$	$193^{+16}_{-17}$
2390	285.39991	-1.08919	$2.58^{+0.09}_{-0.09}$	$22.52^{+2.46}_{-2.15}$	$18.79^{+0.06}_{-0.07}$	$4.03^{+0.01}_{-0.01}$	$207^{+3}_{-4}$
2376	285.39079	-0.96773	$3.23^{+0.08}_{-0.09}$	$20.17^{+1.74}_{-1.66}$	$18.65^{+0.26}_{-0.25}$	$3.98^{+0.04}_{-0.04}$	$232^{+12}_{-12}$
2933	285.81180	-1.06874	$3.03^{+0.09}_{-0.08}$	$21.12^{+2.00}_{-1.77}$	$18.54^{+0.33}_{-0.33}$	$3.90^{+0.05}_{-0.04}$	$65^{+33}_{-39}$
2939	285.81593	-1.28309	$2.36^{+0.10}_{-0.09}$	$19.23^{+1.62}_{-1.45}$	$18.49^{+0.24}_{-0.23}$	$4.06^{+0.03}_{-0.03}$	$36^{+28}_{-26}$
2160	285.21387	-0.99614	$2.45^{+0.09}_{-0.08}$	$20.91^{+1.99}_{-1.67}$	$18.49^{+0.10}_{-0.10}$	$3.99^{+0.01}_{-0.02}$	$115^{+7}_{-8}$
2982	285.83858	-1.01228	$1.95^{+0.09}_{-0.09}$	$21.32^{+2.21}_{-1.83}$	$18.45^{+0.13}_{-0.13}$	$3.98^{+0.02}_{-0.02}$	$94^{+11}_{-14}$
2519	285.50754	-0.79086	$3.83^{+0.09}_{-0.08}$	$21.39^{+2.20}_{-1.84}$	$18.43^{+0.40}_{-0.43}$	$3.77^{+0.06}_{-0.06}$	$233^{+18}_{-16}$
2307	285.33002	-0.89175	$3.11^{+0.09}_{-0.08}$	$20.33^{+1.86}_{-1.61}$	$18.26^{+0.25}_{-0.26}$	$3.89^{+0.04}_{-0.04}$	$93^{+22}_{-30}$
2117	285.18460	-0.67607	$4.12^{+0.09}_{-0.09}$	$21.18^{+2.07}_{-1.85}$	$17.95^{+1.00}_{-0.90}$	$4.09^{+0.15}_{-0.15}$	$90^{+70}_{-61}$
3025	285.86958	-1.21874	$2.45^{+0.09}_{-0.09}$	$19.34^{+1.72}_{-1.50}$	$17.91^{+0.16}_{-0.14}$	$4.08^{+0.02}_{-0.02}$	$161^{+11}_{-14}$

Continued on next page...

ID	$\ell$	b	$A_0$	Phot. $T_{\text{eff}}$	Spec. $T_{\text{eff}}$	$\log(g)$	$vsini$
2724	285.66102	-1.34944	$2.19^{+0.08}_{-0.08}$	$23.00^{+2.34}_{-2.11}$	$17.85^{+0.28}_{-0.15}$	$3.78^{+0.03}_{-0.03}$	$70^{+15}_{-17}$
2615	285.58614	-1.34879	$2.91^{+0.09}_{-0.09}$	$19.99^{+1.82}_{-1.59}$	$17.65^{+0.17}_{-0.18}$	$3.84^{+0.03}_{-0.03}$	$233^{+14}_{-11}$
2863	285.76754	-0.42266	$2.17^{+0.09}_{-0.08}$	$21.79^{+2.15}_{-1.89}$	$17.55^{+0.14}_{-0.15}$	$3.93^{+0.02}_{-0.02}$	$229^{+12}_{-9}$
2857	285.76036	-1.11674	$2.97^{+0.09}_{-0.09}$	$20.85^{+1.94}_{-1.75}$	$17.21^{+0.18}_{-0.28}$	$3.43^{+0.03}_{-0.03}$	$145^{+12}_{-13}$
3082	285.91025	-1.19416	$3.18^{+0.09}_{-0.09}$	$20.50^{+1.89}_{-1.74}$	$15.77^{+0.60}_{-0.46}$	$3.65^{+0.10}_{-0.09}$	$189^{+54}_{-61}$
1458	284.54001	-1.10852	$3.34^{+0.09}_{-0.09}$	$20.42^{+1.92}_{-1.70}$	$15.43^{+0.48}_{-0.30}$	$3.90^{+0.10}_{-0.09}$	$92^{+70}_{-62}$
3305	286.04985	-0.77698	$2.40^{+0.09}_{-0.09}$	$20.71^{+2.01}_{-1.74}$	$15.04^{+0.06}_{-0.03}$	$3.55^{+0.02}_{-0.02}$	$213^{+15}_{-22}$

# APPENDIX C: TABLE OF CANDIDATE O STARS

**Table C.1:** Photometry and derived parameters from the SED fits for candidate O stars with  $\chi^2 < 7.82$  and  $\log(T_{\text{eff}}) > 4.477$ . The notes column indicates if an object has been selected as subluminoous (SUB), over luminous (LUM) or as an emission-line objects (EM).

ID	$\ell$	$b$	u	g	r	i	H $\alpha$	J	H	K	$\log(T_{\text{eff}})$	$A_0$	$R_V$	$\mu$	$\chi^2$	Notes
27	282.22378	-1.45943	18.35	18.58	17.25	16.53	16.92	15.13	14.68	14.43	4.62 <sup>+0.05</sup> <sub>-0.07</sub>	4.90 <sup>+0.06</sup> <sub>-0.07</sub>	4.06 <sup>+0.09</sup> <sub>-0.09</sub>	18.21 <sup>+0.68</sup> <sub>-0.83</sub>	2.68	–
48	282.32016	-1.05674	18.07	16.93	14.57	13.22	14.13	10.86	10.17	9.86	4.52 <sup>+0.10</sup> <sub>-0.08</sub>	7.54 <sup>+0.07</sup> <sub>-0.09</sub>	3.50 <sup>+0.05</sup> <sub>-0.04</sub>	12.13 <sup>+1.24</sup> <sub>-0.85</sub>	4.33	–
63	282.38547	-0.91021	19.10	17.80	15.31	13.89	14.89	11.52	10.85	10.46	4.53 <sup>+0.10</sup> <sub>-0.08</sub>	7.71 <sup>+0.07</sup> <sub>-0.09</sub>	3.39 <sup>+0.04</sup> <sub>-0.04</sub>	12.82 <sup>+1.19</sup> <sub>-0.86</sub>	1.33	–
85	282.44597	-1.03506	17.23	15.98	13.52	12.10	13.03	9.67	8.93	8.54	4.51 <sup>+0.10</sup> <sub>-0.08</sub>	7.85 <sup>+0.07</sup> <sub>-0.10</sub>	3.52 <sup>+0.04</sup> <sub>-0.04</sub>	10.64 <sup>+1.14</sup> <sub>-0.80</sub>	1.60	–
147	282.63270	-1.97146	19.65	19.50	18.12	17.28	17.81	15.95	15.43	15.38	4.48 <sup>+0.10</sup> <sub>-0.08</sub>	4.84 <sup>+0.13</sup> <sub>-0.13</sub>	3.66 <sup>+0.13</sup> <sub>-0.13</sub>	17.41 <sup>+1.16</sup> <sub>-0.82</sub>	2.84	–
151	282.63620	-0.85915	20.52	19.11	16.47	14.90	16.02	11.95	11.05	10.60	4.51 <sup>+0.11</sup> <sub>-0.10</sub>	9.04 <sup>+0.08</sup> <sub>-0.13</sub>	3.83 <sup>+0.05</sup> <sub>-0.05</sub>	12.52 <sup>+1.37</sup> <sub>-1.05</sub>	4.80	–
195	282.77527	-1.85239	19.95	19.72	18.14	17.24	17.77	15.93	15.36	15.26	4.58 <sup>+0.08</sup> <sub>-0.09</sub>	5.07 <sup>+0.11</sup> <sub>-0.11</sub>	3.41 <sup>+0.10</sup> <sub>-0.10</sub>	18.42 <sup>+1.16</sup> <sub>-1.05</sub>	3.19	–
212	282.80590	-0.61975	18.04	17.11	14.96	13.69	14.54	11.44	10.78	10.46	4.49 <sup>+0.10</sup> <sub>-0.07</sub>	7.16 <sup>+0.08</sup> <sub>-0.10</sub>	3.64 <sup>+0.05</sup> <sub>-0.05</sub>	12.43 <sup>+1.16</sup> <sub>-0.72</sub>	4.31	–
218	282.81973	-1.52385	20.90	19.64	17.23	15.81	16.77	13.24	12.47	12.06	4.49 <sup>+0.14</sup> <sub>-0.12</sub>	8.06 <sup>+0.10</sup> <sub>-0.17</sub>	3.71 <sup>+0.05</sup> <sub>-0.05</sub>	13.91 <sup>+1.63</sup> <sub>-1.16</sub>	2.13	–
226	282.84160	-1.25296	20.84	19.45	16.74	15.13	16.25	11.99	11.00	10.48	4.52 <sup>+0.11</sup> <sub>-0.11</sub>	9.55 <sup>+0.07</sup> <sub>-0.14</sub>	4.01 <sup>+0.05</sup> <sub>-0.05</sub>	12.49 <sup>+1.35</sup> <sub>-1.16</sub>	1.28	–
248	282.89901	-0.36939	20.43	19.52	17.44	16.23	17.04	14.16	13.63	13.30	4.48 <sup>+0.11</sup> <sub>-0.10</sub>	6.66 <sup>+0.10</sup> <sub>-0.15</sub>	3.48 <sup>+0.06</sup> <sub>-0.06</sub>	15.23 <sup>+1.33</sup> <sub>-0.98</sub>	3.27	–
277	282.95318	-0.45835	20.56	19.88	17.86	16.68	17.46	14.58	13.87	13.50	4.52 <sup>+0.11</sup> <sub>-0.10</sub>	6.94 <sup>+0.08</sup> <sub>-0.13</sub>	3.81 <sup>+0.07</sup> <sub>-0.06</sub>	15.83 <sup>+1.30</sup> <sub>-1.08</sub>	1.61	–
292	282.97708	-1.19048	19.15	19.09	17.61	16.80	17.29	15.30	14.82	14.67	4.56 <sup>+0.09</sup> <sub>-0.08</sub>	5.15 <sup>+0.08</sup> <sub>-0.09</sub>	3.79 <sup>+0.10</sup> <sub>-0.09</sub>	17.60 <sup>+1.09</sup> <sub>-0.94</sub>	1.41	–
314	283.01007	-0.42048	16.48	15.81	13.82	12.67	13.41	10.73	10.14	9.81	4.57 <sup>+0.09</sup> <sub>-0.08</sub>	6.53 <sup>+0.05</sup> <sub>-0.07</sub>	3.57 <sup>+0.05</sup> <sub>-0.05</sub>	12.79 <sup>+1.08</sup> <sub>-0.97</sub>	1.16	–
327	283.02548	-0.72208	20.47	19.38	16.95	15.49	16.51	12.90	12.08	11.66	4.58 <sup>+0.08</sup> <sub>-0.11</sub>	8.27 <sup>+0.05</sup> <sub>-0.09</sub>	3.76 <sup>+0.05</sup> <sub>-0.05</sub>	14.50 <sup>+1.08</sup> <sub>-1.20</sub>	2.09	–
337	283.04451	-0.32310	20.85	19.51	16.88	15.35	16.32	12.68	11.89	11.40	4.54 <sup>+0.11</sup> <sub>-0.12</sub>	8.52 <sup>+0.07</sup> <sub>-0.14</sub>	3.60 <sup>+0.05</sup> <sub>-0.04</sub>	13.82 <sup>+1.34</sup> <sub>-1.30</sub>	1.82	–
340	283.04643	-0.42953	19.84	18.85	16.66	15.40	16.24	13.26	12.59	12.34	4.52 <sup>+0.10</sup> <sub>-0.09</sub>	7.00 <sup>+0.07</sup> <sub>-0.11</sub>	3.48 <sup>+0.05</sup> <sub>-0.05</sub>	14.59 <sup>+1.26</sup> <sub>-0.94</sub>	6.81	–
351	283.06527	0.12084	17.81	18.12	16.92	16.29	16.59	15.35	14.85	14.76	4.63 <sup>+0.05</sup> <sub>-0.07</sub>	4.06 <sup>+0.08</sup> <sub>-0.08</sub>	3.62 <sup>+0.11</sup> <sub>-0.10</sub>	18.71 <sup>+0.63</sup> <sub>-0.83</sub>	6.80	–
354	283.07012	-0.82747	17.51	16.61	14.50	13.28	14.08	11.17	10.55	10.23	4.48 <sup>+0.09</sup> <sub>-0.07</sub>	6.84 <sup>+0.08</sup> <sub>-0.09</sub>	3.55 <sup>+0.05</sup> <sub>-0.05</sub>	12.14 <sup>+1.03</sup> <sub>-0.68</sub>	1.89	–
355	283.07236	-0.36579	16.62	16.09	14.23	13.14	13.81	11.35	10.79	10.57	4.60 <sup>+0.07</sup> <sub>-0.09</sub>	6.11 <sup>+0.05</sup> <sub>-0.06</sub>	3.52 <sup>+0.05</sup> <sub>-0.05</sub>	13.89 <sup>+0.91</sup> <sub>-1.03</sub>	4.63	–
357	283.07404	-0.54669	19.77	18.29	15.61	14.02	15.12	11.21	10.39	9.99	4.57 <sup>+0.09</sup> <sub>-0.10</sub>	8.80 <sup>+0.05</sup> <sub>-0.09</sub>	3.60 <sup>+0.04</sup> <sub>-0.04</sub>	12.64 <sup>+1.15</sup> <sub>-1.09</sub>	7.51	–
373	283.09686	-1.05699	17.39	18.13	17.18	16.61	16.94	15.38	15.00	14.86	4.64 <sup>+0.04</sup> <sub>-0.06</sub>	4.31 <sup>+0.09</sup> <sub>-0.09</sub>	4.97 <sup>+0.16</sup> <sub>-0.15</sub>	18.74 <sup>+0.56</sup> <sub>-0.74</sub>	5.66	–
374	283.09707	-0.39828	20.34	19.30	16.85	15.40	16.39	12.73	11.88	11.51	4.59 <sup>+0.07</sup> <sub>-0.10</sub>	8.39 <sup>+0.05</sup> <sub>-0.07</sub>	3.81 <sup>+0.05</sup> <sub>-0.05</sub>	14.47 <sup>+0.94</sup> <sub>-1.12</sub>	5.56	–
384	283.10638	-0.44663	16.05	15.52	13.64	12.56	13.25	10.71	10.16	9.91	4.59 <sup>+0.07</sup> <sub>-0.08</sub>	6.19 <sup>+0.05</sup> <sub>-0.06</sub>	3.56 <sup>+0.05</sup> <sub>-0.05</sub>	13.18 <sup>+0.87</sup> <sub>-0.96</sub>	2.68	–
396	283.11785	-0.37073	20.70	19.70	17.45	16.15	16.97	13.86	13.28	12.93	4.55 <sup>+0.10</sup> <sub>-0.13</sub>	7.25 <sup>+0.07</sup> <sub>-0.13</sub>	3.52 <sup>+0.06</sup> <sub>-0.06</sub>	15.53 <sup>+1.27</sup> <sub>-1.34</sub>	4.09	–
401	283.12290	-0.44398	18.78	18.04	15.92	14.75	15.53	12.49	11.85	11.57	4.57 <sup>+0.08</sup> <sub>-0.08</sub>	7.08 <sup>+0.06</sup> <sub>-0.07</sub>	3.72 <sup>+0.05</sup> <sub>-0.05</sub>	14.40 <sup>+1.03</sup> <sub>-0.92</sub>	4.98	–

Continued on next page...

ID	$\ell$	$b$	u	g	r	i	H $\alpha$	J	H	K	$\log(T_{\text{eff}})$	$A_0$	$R_V$	$\mu$	$\chi^2$	Notes
404	283.12811	-0.44032	17.44	16.85	14.89	13.74	14.46	11.76	11.22	10.94	4.62 <sup>+0.06</sup> <sub>-0.08</sub>	6.50 <sup>+0.04</sup> <sub>-0.05</sub>	3.59 <sup>+0.05</sup> <sub>-0.05</sub>	14.46 <sup>+0.77</sup> <sub>-0.94</sub>	4.09	–
405	283.12869	-0.54084	19.62	18.01	15.23	13.60	14.72	10.62	9.70	9.21	4.48 <sup>+0.11</sup> <sub>-0.08</sub>	9.24 <sup>+0.09</sup> <sub>-0.12</sub>	3.72 <sup>+0.05</sup> <sub>-0.04</sub>	10.85 <sup>+1.27</sup> <sub>-0.84</sub>	1.85	–
406	283.12876	-0.30103	17.16	16.30	14.24	13.05	13.83	11.02	10.43	10.12	4.49 <sup>+0.11</sup> <sub>-0.07</sub>	6.65 <sup>+0.09</sup> <sub>-0.10</sub>	3.51 <sup>+0.05</sup> <sub>-0.05</sub>	12.15 <sup>+1.25</sup> <sub>-0.74</sub>	1.84	–
430	283.16624	-0.53818	18.61	17.67	15.53	14.25	15.10	12.05	11.37	11.06	4.49 <sup>+0.10</sup> <sub>-0.07</sub>	7.12 <sup>+0.08</sup> <sub>-0.09</sub>	3.63 <sup>+0.05</sup> <sub>-0.05</sub>	13.00 <sup>+1.13</sup> <sub>-0.73</sub>	3.72	–
439	283.17345	-0.30791	15.58	15.02	13.17	12.12	12.76	10.24	9.72	9.40	4.51 <sup>+0.09</sup> <sub>-0.07</sub>	6.16 <sup>+0.07</sup> <sub>-0.09</sub>	3.64 <sup>+0.06</sup> <sub>-0.06</sub>	11.66 <sup>+1.03</sup> <sub>-0.73</sub>	0.82	–
442	283.17584	-0.51816	18.33	17.51	15.47	14.27	15.05	12.24	11.61	11.28	4.48 <sup>+0.09</sup> <sub>-0.07</sub>	6.69 <sup>+0.09</sup> <sub>-0.10</sub>	3.58 <sup>+0.06</sup> <sub>-0.05</sub>	13.18 <sup>+1.03</sup> <sub>-0.70</sub>	1.72	–
460	283.20201	-0.48417	17.77	17.18	15.34	14.25	14.94	12.34	11.78	11.50	4.50 <sup>+0.10</sup> <sub>-0.07</sub>	6.25 <sup>+0.08</sup> <sub>-0.09</sub>	3.68 <sup>+0.06</sup> <sub>-0.06</sub>	13.59 <sup>+1.17</sup> <sub>-0.73</sub>	2.44	–
464	283.20900	-0.33948	16.58	16.23	14.61	13.66	14.25	12.03	11.59	11.36	4.52 <sup>+0.10</sup> <sub>-0.07</sub>	5.47 <sup>+0.07</sup> <sub>-0.08</sub>	3.58 <sup>+0.06</sup> <sub>-0.06</sub>	13.79 <sup>+1.19</sup> <sub>-0.74</sub>	3.05	–
468	283.21468	-0.38967	16.71	15.92	13.84	12.65	13.42	10.63	10.03	9.72	4.55 <sup>+0.09</sup> <sub>-0.08</sub>	6.70 <sup>+0.06</sup> <sub>-0.08</sub>	3.51 <sup>+0.05</sup> <sub>-0.05</sub>	12.41 <sup>+1.17</sup> <sub>-0.87</sub>	1.08	–
474	283.21946	-1.46297	15.15	15.09	13.75	13.02	13.43	11.71	11.35	11.17	4.48 <sup>+0.09</sup> <sub>-0.06</sub>	4.54 <sup>+0.08</sup> <sub>-0.09</sub>	3.60 <sup>+0.08</sup> <sub>-0.08</sub>	13.28 <sup>+0.98</sup> <sub>-0.63</sub>	1.33	–
487	283.24010	-0.41335	20.44	19.37	17.14	15.82	16.71	13.58	12.90	12.60	4.53 <sup>+0.11</sup> <sub>-0.11</sub>	7.26 <sup>+0.07</sup> <sub>-0.13</sub>	3.52 <sup>+0.05</sup> <sub>-0.05</sub>	15.00 <sup>+1.37</sup> <sub>-1.19</sub>	5.20	–
494	283.24735	-0.42416	20.44	19.56	17.36	16.05	16.95	13.87	13.23	12.92	4.59 <sup>+0.08</sup> <sub>-0.10</sub>	7.16 <sup>+0.06</sup> <sub>-0.08</sub>	3.53 <sup>+0.06</sup> <sub>-0.05</sub>	16.05 <sup>+0.98</sup> <sub>-1.17</sub>	3.93	–
510	283.26641	-0.27639	16.30	15.79	14.02	13.01	13.68	11.22	10.70	10.45	4.49 <sup>+0.10</sup> <sub>-0.07</sub>	5.90 <sup>+0.08</sup> <sub>-0.09</sub>	3.61 <sup>+0.06</sup> <sub>-0.06</sub>	12.52 <sup>+1.10</sup> <sub>-0.69</sub>	1.67	–
518	283.27241	-0.47827	16.29	15.85	14.09	13.04	13.71	11.24	10.71	10.43	4.58 <sup>+0.08</sup> <sub>-0.08</sub>	6.04 <sup>+0.05</sup> <sub>-0.07</sub>	3.67 <sup>+0.06</sup> <sub>-0.05</sub>	13.49 <sup>+1.02</sup> <sub>-0.96</sub>	1.59	–
544	283.30781	-0.36578	14.81	14.55	12.91	12.03	12.54	10.35	9.84	9.62	4.55 <sup>+0.09</sup> <sub>-0.08</sub>	5.59 <sup>+0.06</sup> <sub>-0.08</sub>	3.73 <sup>+0.07</sup> <sub>-0.06</sub>	12.37 <sup>+1.07</sup> <sub>-0.86</sub>	2.71	–
555	283.33196	-0.99985	18.32	18.66	17.56	16.97	17.29	15.80	15.17	15.31	4.55 <sup>+0.08</sup> <sub>-0.08</sub>	4.29 <sup>+0.16</sup> <sub>-0.16</sub>	4.17 <sup>+0.23</sup> <sub>-0.21</sub>	18.09 <sup>+1.05</sup> <sub>-0.94</sub>	2.70	–
586	283.37539	-1.22501	20.21	19.57	17.62	16.49	nan	14.86	14.23	13.99	4.58 <sup>+0.08</sup> <sub>-0.10</sub>	6.02 <sup>+0.07</sup> <sub>-0.09</sub>	3.32 <sup>+0.06</sup> <sub>-0.06</sub>	17.12 <sup>+1.03</sup> <sub>-1.10</sub>	6.10	–
593	283.38483	-0.89466	20.32	19.09	16.50	14.97	16.02	12.01	11.16	10.65	4.56 <sup>+0.09</sup> <sub>-0.10</sub>	9.02 <sup>+0.06</sup> <sub>-0.09</sub>	3.92 <sup>+0.05</sup> <sub>-0.05</sub>	13.20 <sup>+1.11</sup> <sub>-1.09</sub>	3.46	–
676	283.50830	-0.98960	20.13	19.27	17.06	15.83	16.38	13.65	13.01	12.63	4.56 <sup>+0.09</sup> <sub>-0.09</sub>	7.13 <sup>+0.05</sup> <sub>-0.08</sub>	3.58 <sup>+0.05</sup> <sub>-0.05</sub>	15.47 <sup>+1.12</sup> <sub>-1.01</sub>	0.43	EM
685	283.52763	-0.86026	20.67	19.40	16.88	15.43	16.43	12.76	11.99	11.54	4.51 <sup>+0.12</sup> <sub>-0.11</sub>	8.33 <sup>+0.08</sup> <sub>-0.14</sub>	3.70 <sup>+0.05</sup> <sub>-0.05</sub>	13.60 <sup>+1.42</sup> <sub>-1.11</sub>	0.94	–
693	283.53650	-0.42700	16.97	16.59	14.90	13.79	14.28	11.64	11.00	10.57	4.48 <sup>+0.11</sup> <sub>-0.07</sub>	6.73 <sup>+0.09</sup> <sub>-0.10</sub>	4.34 <sup>+0.09</sup> <sub>-0.08</sub>	12.48 <sup>+1.28</sup> <sub>-0.76</sub>	4.33	EM
700	283.54576	-1.45506	20.97	19.89	17.63	16.29	17.19	13.89	13.08	12.71	4.48 <sup>+0.13</sup> <sub>-0.12</sub>	7.70 <sup>+0.11</sup> <sub>-0.17</sub>	3.79 <sup>+0.06</sup> <sub>-0.06</sub>	14.49 <sup>+1.53</sup> <sub>-1.15</sub>	3.05	–
708	283.56172	-0.97938	14.98	14.26	12.24	11.08	11.76	8.97	8.30	7.94	4.49 <sup>+0.10</sup> <sub>-0.07</sub>	6.84 <sup>+0.08</sup> <sub>-0.09</sub>	3.77 <sup>+0.06</sup> <sub>-0.06</sub>	9.91 <sup>+1.13</sup> <sub>-0.69</sub>	0.28	–
714	283.57306	-1.14095	19.53	18.38	15.95	14.58	15.51	11.97	11.18	10.78	4.50 <sup>+0.10</sup> <sub>-0.07</sub>	8.11 <sup>+0.07</sup> <sub>-0.10</sub>	3.75 <sup>+0.05</sup> <sub>-0.05</sub>	12.73 <sup>+1.16</sup> <sub>-0.78</sub>	2.45	–
724	283.59204	-1.24742	14.79	14.27	12.47	11.40	12.03	9.52	8.97	8.67	4.51 <sup>+0.09</sup> <sub>-0.07</sub>	6.19 <sup>+0.07</sup> <sub>-0.09</sub>	3.72 <sup>+0.07</sup> <sub>-0.06</sub>	10.92 <sup>+1.13</sup> <sub>-0.78</sub>	1.75	–
731	283.60401	-1.08072	18.91	19.01	17.72	17.03	17.40	15.87	15.36	15.10	4.54 <sup>+0.09</sup> <sub>-0.08</sub>	4.47 <sup>+0.10</sup> <sub>-0.11</sub>	3.72 <sup>+0.13</sup> <sub>-0.12</sub>	18.02 <sup>+1.08</sup> <sub>-0.89</sub>	2.88	–
733	283.60589	-1.15355	18.92	17.91	15.58	14.26	15.15	11.81	11.13	10.77	4.56 <sup>+0.09</sup> <sub>-0.09</sub>	7.67 <sup>+0.06</sup> <sub>-0.08</sub>	3.65 <sup>+0.05</sup> <sub>-0.05</sub>	13.52 <sup>+1.09</sup> <sub>-1.00</sub>	2.43	–
746	283.62122	0.29277	20.12	19.98	18.33	17.42	17.99	15.86	15.30	14.94	4.61 <sup>+0.06</sup> <sub>-0.08</sub>	5.58 <sup>+0.09</sup> <sub>-0.10</sub>	3.72 <sup>+0.10</sup> <sub>-0.10</sub>	18.51 <sup>+0.84</sup> <sub>-1.03</sub>	3.14	–
756	283.63086	-1.13990	16.63	16.23	14.54	13.59	14.17	11.91	11.46	11.23	4.51 <sup>+0.09</sup> <sub>-0.07</sub>	5.57 <sup>+0.07</sup> <sub>-0.09</sub>	3.55 <sup>+0.06</sup> <sub>-0.06</sub>	13.60 <sup>+1.06</sup> <sub>-0.72</sub>	2.28	–
758	283.63158	-1.23256	17.44	16.94	15.18	14.14	14.79	12.23	11.71	11.43	4.48 <sup>+0.10</sup> <sub>-0.07</sub>	6.10 <sup>+0.08</sup> <sub>-0.10</sub>	3.76 <sup>+0.07</sup> <sub>-0.07</sub>	13.37 <sup>+1.18</sup> <sub>-0.72</sub>	3.95	–
774	283.67085	-1.07771	19.04	19.14	17.88	17.26	17.47	16.21	15.81	15.41	4.50 <sup>+0.08</sup> <sub>-0.07</sub>	4.12 <sup>+0.14</sup> <sub>-0.14</sub>	3.55 <sup>+0.16</sup> <sub>-0.15</sub>	18.01 <sup>+1.01</sup> <sub>-0.78</sub>	3.61	SUB/EM
777	283.67206	-1.11521	19.13	19.29	18.00	17.22	17.69	15.86	15.48	14.93	4.60 <sup>+0.07</sup> <sub>-0.08</sub>	4.99 <sup>+0.11</sup> <sub>-0.11</sub>	4.10 <sup>+0.14</sup> <sub>-0.13</sub>	18.50 <sup>+0.89</sup> <sub>-1.00</sub>	4.30	–
785	283.68417	0.41788	20.84	19.67	17.27	15.92	16.84	13.44	12.69	12.36	4.50 <sup>+0.12</sup> <sub>-0.11</sub>	7.81 <sup>+0.09</sup> <sub>-0.15</sub>	3.64 <sup>+0.06</sup> <sub>-0.05</sub>	14.29 <sup>+1.43</sup> <sub>-1.10</sub>	3.71	–

Continued on next page...

ID	$\ell$	$b$	u	g	r	i	H $\alpha$	J	H	K	$\log(T_{\text{eff}})$	$A_0$	$R_V$	$\mu$	$\chi^2$	Notes
801	283.70709	-1.16032	16.12	15.53	13.57	12.40	12.92	10.29	9.60	9.13	4.53 <sup>+0.10</sup> <sub>-0.08</sub>	6.98 <sup>+0.06</sup> <sub>-0.09</sub>	3.96 <sup>+0.06</sup> <sub>-0.06</sub>	11.61 <sup>+1.19</sup> <sub>-0.85</sub>	6.54	LUM/EM
813	283.72805	0.49976	19.85	19.68	17.97	17.03	17.61	15.44	14.88	14.53	4.61 <sup>+0.06</sup> <sub>-0.07</sub>	5.69 <sup>+0.09</sup> <sub>-0.09</sub>	3.69 <sup>+0.09</sup> <sub>-0.09</sub>	18.15 <sup>+0.74</sup> <sub>-0.91</sub>	3.64	-
826	283.74478	-0.63041	20.96	19.59	16.80	15.18	16.30	11.86	10.93	10.34	4.55 <sup>+0.10</sup> <sub>-0.12</sub>	9.84 <sup>+0.06</sup> <sub>-0.05</sub>	4.05 <sup>+0.05</sup> <sub>-0.05</sub>	12.62 <sup>+1.25</sup> <sub>-1.27</sub>	4.88	-
827	283.74598	-1.35949	14.28	14.14	12.67	11.82	12.32	10.39	9.94	9.68	4.53 <sup>+0.10</sup> <sub>-0.07</sub>	5.08 <sup>+0.06</sup> <sub>-0.08</sub>	3.68 <sup>+0.08</sup> <sub>-0.07</sub>	12.30 <sup>+1.17</sup> <sub>-0.77</sub>	1.21	-
877	283.82885	-0.71850	17.82	18.01	16.82	16.18	16.57	15.01	14.56	14.45	4.53 <sup>+0.10</sup> <sub>-0.09</sub>	4.30 <sup>+0.08</sup> <sub>-0.09</sub>	3.84 <sup>+0.12</sup> <sub>-0.12</sub>	17.11 <sup>+1.18</sup> <sub>-0.83</sub>	1.84	-
879	283.82897	-0.73685	18.73	17.86	15.65	14.34	15.20	11.82	11.11	10.71	4.56 <sup>+0.09</sup> <sub>-0.08</sub>	7.77 <sup>+0.06</sup> <sub>-0.08</sub>	3.89 <sup>+0.05</sup> <sub>-0.05</sub>	13.37 <sup>+1.08</sup> <sub>-0.91</sub>	3.37	-
884	283.83054	-1.20438	20.52	19.33	16.90	15.47	16.47	12.79	12.00	11.56	4.49 <sup>+0.12</sup> <sub>-0.10</sub>	8.27 <sup>+0.09</sup> <sub>-0.13</sub>	3.81 <sup>+0.05</sup> <sub>-0.05</sub>	13.37 <sup>+1.38</sup> <sub>-0.97</sub>	1.93	-
891	283.84011	-0.37448	18.02	18.15	16.93	16.25	16.60	15.08	14.60	14.59	4.54 <sup>+0.10</sup> <sub>-0.10</sub>	4.35 <sup>+0.09</sup> <sub>-0.09</sub>	3.74 <sup>+0.12</sup> <sub>-0.11</sub>	17.28 <sup>+1.23</sup> <sub>-0.88</sub>	2.87	-
893	283.84282	-0.70593	17.60	17.05	15.07	13.91	14.69	11.83	11.18	10.87	4.62 <sup>+0.06</sup> <sub>-0.08</sub>	6.81 <sup>+0.05</sup> <sub>-0.06</sub>	3.79 <sup>+0.05</sup> <sub>-0.05</sub>	14.34 <sup>+0.75</sup> <sub>-1.00</sub>	1.89	-
896	283.84849	-0.84851	17.79	16.96	14.75	13.43	14.30	10.81	10.03	9.60	4.55 <sup>+0.09</sup> <sub>-0.08</sub>	8.03 <sup>+0.06</sup> <sub>-0.05</sub>	4.07 <sup>+0.06</sup> <sub>-0.05</sub>	12.08 <sup>+1.13</sup> <sub>-0.89</sub>	2.42	-
904	283.85874	-0.93225	20.29	19.48	17.27	15.96	16.83	13.48	12.80	12.39	4.60 <sup>+0.07</sup> <sub>-0.08</sub>	7.72 <sup>+0.05</sup> <sub>-0.07</sub>	3.88 <sup>+0.05</sup> <sub>-0.05</sub>	15.48 <sup>+0.86</sup> <sub>-0.97</sub>	3.11	-
912	283.86504	-1.14576	15.60	15.51	14.14	13.33	13.80	11.90	11.49	11.29	4.49 <sup>+0.09</sup> <sub>-0.07</sub>	4.88 <sup>+0.07</sup> <sub>-0.09</sub>	3.74 <sup>+0.08</sup> <sub>-0.08</sub>	13.52 <sup>+1.05</sup> <sub>-0.69</sub>	1.86	-
913	283.86510	-1.54400	18.79	18.92	17.65	16.89	17.29	15.70	15.09	15.06	4.58 <sup>+0.08</sup> <sub>-0.09</sub>	4.68 <sup>+0.09</sup> <sub>-0.09</sub>	3.87 <sup>+0.12</sup> <sub>-0.11</sub>	18.22 <sup>+0.98</sup> <sub>-1.02</sub>	5.81	-
918	283.87303	-0.91706	19.30	18.41	16.05	14.70	15.58	12.11	11.29	10.85	4.60 <sup>+0.06</sup> <sub>-0.07</sub>	8.15 <sup>+0.05</sup> <sub>-0.05</sub>	3.93 <sup>+0.05</sup> <sub>-0.05</sub>	13.95 <sup>+0.81</sup> <sub>-0.86</sub>	0.80	-
921	283.87587	-0.91029	19.01	17.92	15.53	14.13	15.05	11.42	10.56	10.14	4.49 <sup>+0.10</sup> <sub>-0.07</sub>	8.35 <sup>+0.08</sup> <sub>-0.10</sub>	3.95 <sup>+0.06</sup> <sub>-0.06</sub>	11.88 <sup>+1.11</sup> <sub>-0.73</sub>	1.58	-
925	283.87904	-0.91720	19.09	18.15	15.76	14.35	15.31	11.63	10.82	10.44	4.61 <sup>+0.06</sup> <sub>-0.08</sub>	8.37 <sup>+0.05</sup> <sub>-0.06</sub>	3.95 <sup>+0.05</sup> <sub>-0.05</sub>	13.60 <sup>+0.81</sup> <sub>-0.94</sub>	4.09	-
930	283.88519	-0.90709	20.42	19.48	17.08	15.67	16.63	13.00	12.18	11.77	4.60 <sup>+0.07</sup> <sub>-0.09</sub>	8.33 <sup>+0.06</sup> <sub>-0.08</sub>	3.91 <sup>+0.06</sup> <sub>-0.06</sub>	14.79 <sup>+0.91</sup> <sub>-1.09</sub>	1.79	-
931	283.88521	-0.91207	20.27	18.78	15.99	14.35	15.48	11.35	10.42	9.96	4.57 <sup>+0.08</sup> <sub>-0.10</sub>	9.34 <sup>+0.06</sup> <sub>-0.09</sub>	3.75 <sup>+0.04</sup> <sub>-0.04</sub>	12.53 <sup>+1.07</sup> <sub>-1.09</sub>	2.72	-
939	283.88979	-1.21592	15.18	15.20	13.91	13.14	13.60	11.80	11.41	11.24	4.52 <sup>+0.10</sup> <sub>-0.07</sub>	4.67 <sup>+0.07</sup> <sub>-0.09</sub>	3.75 <sup>+0.08</sup> <sub>-0.08</sub>	13.77 <sup>+1.22</sup> <sub>-0.77</sub>	1.64	-
958	283.90845	-0.90338	19.54	18.63	16.46	15.17	16.03	12.74	11.98	11.63	4.49 <sup>+0.11</sup> <sub>-0.08</sub>	7.60 <sup>+0.08</sup> <sub>-0.10</sub>	3.88 <sup>+0.06</sup> <sub>-0.06</sub>	13.53 <sup>+1.33</sup> <sub>-0.79</sub>	4.11	-
965	283.91700	-0.80465	20.37	19.57	17.39	16.11	16.95	13.61	12.78	12.43	4.53 <sup>+0.10</sup> <sub>-0.08</sub>	7.79 <sup>+0.08</sup> <sub>-0.09</sub>	4.04 <sup>+0.07</sup> <sub>-0.07</sub>	14.67 <sup>+1.17</sup> <sub>-0.91</sub>	1.19	-
968	283.91775	-0.96423	20.62	19.44	16.99	15.55	16.51	12.78	11.96	11.59	4.51 <sup>+0.12</sup> <sub>-0.11</sub>	8.44 <sup>+0.08</sup> <sub>-0.14</sub>	3.86 <sup>+0.05</sup> <sub>-0.05</sub>	13.61 <sup>+1.40</sup> <sub>-1.12</sub>	7.22	-
972	283.92122	-0.45493	14.34	14.23	12.77	11.89	12.39	10.39	9.94	9.73	4.57 <sup>+0.08</sup> <sub>-0.08</sub>	5.19 <sup>+0.05</sup> <sub>-0.07</sub>	3.74 <sup>+0.07</sup> <sub>-0.07</sub>	12.85 <sup>+1.00</sup> <sub>-0.93</sub>	1.93	-
994	283.94769	-0.48908	15.52	15.22	13.66	12.71	13.28	11.01	10.52	10.29	4.49 <sup>+0.10</sup> <sub>-0.07</sub>	5.58 <sup>+0.08</sup> <sub>-0.09</sub>	3.79 <sup>+0.08</sup> <sub>-0.07</sub>	12.43 <sup>+1.11</sup> <sub>-0.72</sub>	3.79	-
998	283.95096	-1.37519	13.89	13.94	12.71	12.00	12.39	10.88	10.52	10.39	4.51 <sup>+0.10</sup> <sub>-0.07</sub>	4.20 <sup>+0.07</sup> <sub>-0.09</sub>	3.51 <sup>+0.08</sup> <sub>-0.08</sub>	12.89 <sup>+1.15</sup> <sub>-0.77</sub>	1.66	-
1046	284.04689	0.42547	15.37	14.80	12.89	11.85	12.45	9.94	9.44	9.14	4.54 <sup>+0.09</sup> <sub>-0.07</sub>	6.20 <sup>+0.06</sup> <sub>-0.08</sub>	3.57 <sup>+0.06</sup> <sub>-0.05</sub>	11.76 <sup>+1.10</sup> <sub>-0.83</sub>	1.66	-
1086	284.11950	-0.07137	20.84	18.91	15.90	14.13	15.40	11.00	10.13	9.65	4.54 <sup>+0.11</sup> <sub>-0.12</sub>	9.67 <sup>+0.07</sup> <sub>-0.14</sub>	3.54 <sup>+0.04</sup> <sub>-0.04</sub>	11.89 <sup>+1.34</sup> <sub>-1.29</sub>	7.51	-
1102	284.14213	-0.18889	15.83	15.31	13.45	12.36	13.03	10.44	9.93	9.62	4.58 <sup>+0.08</sup> <sub>-0.08</sub>	6.28 <sup>+0.05</sup> <sub>-0.07</sub>	3.64 <sup>+0.05</sup> <sub>-0.05</sub>	12.74 <sup>+1.01</sup> <sub>-0.97</sub>	2.36	-
1116	284.16849	-1.31921	15.15	14.89	13.36	12.44	13.01	10.80	10.31	10.11	4.51 <sup>+0.10</sup> <sub>-0.07</sub>	5.45 <sup>+0.07</sup> <sub>-0.09</sub>	3.77 <sup>+0.08</sup> <sub>-0.07</sub>	12.37 <sup>+1.13</sup> <sub>-0.74</sub>	5.18	-
1119	284.17576	0.07782	20.84	18.90	15.74	13.90	15.13	10.51	9.57	9.03	4.58 <sup>+0.08</sup> <sub>-0.09</sub>	10.32 <sup>+0.05</sup> <sub>-0.08</sub>	3.65 <sup>+0.04</sup> <sub>-0.04</sub>	11.71 <sup>+1.03</sup> <sub>-1.08</sub>	6.84	-
1126	284.17909	-0.77150	16.16	15.92	14.41	13.53	14.05	11.94	11.50	11.28	4.49 <sup>+0.10</sup> <sub>-0.07</sub>	5.27 <sup>+0.08</sup> <sub>-0.09</sub>	3.70 <sup>+0.08</sup> <sub>-0.07</sub>	13.42 <sup>+1.11</sup> <sub>-0.68</sub>	1.96	-
1133	284.19334	-0.13258	17.08	16.35	14.30	13.08	13.85	10.92	10.27	9.93	4.58 <sup>+0.08</sup> <sub>-0.08</sub>	7.01 <sup>+0.05</sup> <sub>-0.07</sub>	3.72 <sup>+0.05</sup> <sub>-0.05</sub>	12.91 <sup>+1.08</sup> <sub>-0.97</sub>	1.83	-
1157	284.22199	-0.12858	16.37	16.97	16.22	15.73	15.92	14.90	14.57	14.74	4.60 <sup>+0.07</sup> <sub>-0.08</sub>	3.26 <sup>+0.15</sup> <sub>-0.15</sub>	4.02 <sup>+0.26</sup> <sub>-0.24</sub>	18.16 <sup>+0.95</sup> <sub>-0.99</sub>	3.23	-

Continued on next page...

ID	$\ell$	$b$	u	g	r	i	H $\alpha$	J	H	K	log( $T_{\text{eff}}$ )	$A_0$	$R_V$	$\mu$	$\chi^2$	Notes
1164	284.22782	-0.68788	15.80	15.38	13.60	12.53	13.17	10.57	9.97	9.65	4.55 <sup>+0.09</sup> <sub>-0.08</sub>	6.40 <sup>+0.06</sup> <sub>-0.08</sub>	3.91 <sup>+0.07</sup> <sub>-0.06</sub>	12.40 <sup>+1.12</sup> <sub>-0.94</sub>	1.11	–
1165	284.23543	-0.88100	13.35	13.58	12.51	11.89	12.20	10.87	10.59	10.42	4.52 <sup>+0.09</sup> <sub>-0.07</sub>	3.86 <sup>+0.07</sup> <sub>-0.08</sub>	3.63 <sup>+0.09</sup> <sub>-0.09</sub>	13.10 <sup>+1.14</sup> <sub>-0.76</sub>	0.42	–
1175	284.25379	-0.26128	19.79	18.92	16.60	15.22	16.16	12.60	11.83	11.44	4.61 <sup>+0.06</sup> <sub>-0.08</sub>	8.11 <sup>+0.04</sup> <sub>-0.05</sub>	3.91 <sup>+0.05</sup> <sub>-0.05</sub>	14.69 <sup>+0.79</sup> <sub>-0.95</sub>	4.57	–
1176	284.25472	-0.32226	17.65	17.22	15.37	14.25	14.97	12.07	11.38	11.09	4.58 <sup>+0.08</sup> <sub>-0.08</sub>	6.88 <sup>+0.05</sup> <sub>-0.07</sub>	4.09 <sup>+0.07</sup> <sub>-0.06</sub>	14.09 <sup>+1.02</sup> <sub>-0.98</sub>	4.42	–
1179	284.25649	-0.33083	17.65	17.31	15.59	14.57	15.09	12.52	11.90	11.53	4.49 <sup>+0.09</sup> <sub>-0.07</sub>	6.46 <sup>+0.08</sup> <sub>-0.09</sub>	4.20 <sup>+0.09</sup> <sub>-0.08</sub>	13.47 <sup>+1.07</sup> <sub>-0.68</sub>	0.28	EM
1183	284.25811	-0.33623	17.21	16.64	14.59	13.37	14.14	10.96	10.26	9.86	4.62 <sup>+0.06</sup> <sub>-0.08</sub>	7.49 <sup>+0.04</sup> <sub>-0.05</sub>	4.09 <sup>+0.05</sup> <sub>-0.05</sub>	13.22 <sup>+0.75</sup> <sub>-0.92</sub>	2.88	–
1189	284.26045	-0.33575	15.58	15.33	13.62	12.59	13.21	10.63	10.05	9.73	4.60 <sup>+0.06</sup> <sub>-0.07</sub>	6.33 <sup>+0.04</sup> <sub>-0.05</sub>	4.06 <sup>+0.06</sup> <sub>-0.06</sub>	13.07 <sup>+0.80</sup> <sub>-0.88</sub>	1.80	–
1195	284.26216	-0.32909	17.72	17.19	15.23	14.09	14.86	11.86	11.23	10.87	4.58 <sup>+0.07</sup> <sub>-0.08</sub>	6.99 <sup>+0.05</sup> <sub>-0.07</sub>	3.97 <sup>+0.06</sup> <sub>-0.06</sub>	13.87 <sup>+0.96</sup> <sub>-0.90</sub>	1.97	–
1197	284.26333	-0.38413	17.61	17.19	15.29	14.19	14.87	12.05	11.44	11.08	4.60 <sup>+0.06</sup> <sub>-0.08</sub>	6.79 <sup>+0.05</sup> <sub>-0.06</sub>	3.99 <sup>+0.06</sup> <sub>-0.05</sub>	14.37 <sup>+0.83</sup> <sub>-0.91</sub>	1.75	–
1201	284.26504	-0.33323	17.99	17.52	15.60	14.52	15.24	12.39	11.74	11.36	4.56 <sup>+0.08</sup> <sub>-0.07</sub>	6.80 <sup>+0.09</sup> <sub>-0.09</sub>	3.99 <sup>+0.08</sup> <sub>-0.08</sub>	14.19 <sup>+1.01</sup> <sub>-0.86</sub>	1.03	–
1204	284.26645	-0.33436	17.39	16.99	15.15	14.06	14.76	11.90	11.22	10.86	4.56 <sup>+0.09</sup> <sub>-0.08</sub>	6.85 <sup>+0.08</sup> <sub>-0.09</sub>	4.16 <sup>+0.09</sup> <sub>-0.08</sub>	13.56 <sup>+1.11</sup> <sub>-0.91</sub>	0.72	–
1212	284.26840	-0.32930	15.37	15.12	13.45	12.42	13.04	10.15	9.64	9.23	4.50 <sup>+0.10</sup> <sub>-0.07</sub>	6.71 <sup>+0.10</sup> <sub>-0.10</sub>	4.51 <sup>+0.12</sup> <sub>-0.11</sub>	11.18 <sup>+1.22</sup> <sub>-0.79</sub>	3.51	–
1215	284.26975	-0.33719	17.66	17.26	15.42	14.33	15.01	12.22	11.61	11.32	4.61 <sup>+0.06</sup> <sub>-0.08</sub>	6.66 <sup>+0.04</sup> <sub>-0.05</sub>	3.97 <sup>+0.06</sup> <sub>-0.06</sub>	14.68 <sup>+0.81</sup> <sub>-0.93</sub>	5.71	–
1216	284.27003	-0.33005	14.60	14.32	12.58	11.57	12.22	9.27	8.67	8.37	4.53 <sup>+0.10</sup> <sub>-0.08</sub>	6.77 <sup>+0.08</sup> <sub>-0.09</sub>	4.40 <sup>+0.10</sup> <sub>-0.09</sub>	10.69 <sup>+1.20</sup> <sub>-0.87</sub>	4.69	–
1217	284.27017	-0.33379	17.05	16.59	14.75	13.66	14.34	11.58	10.94	10.58	4.55 <sup>+0.10</sup> <sub>-0.08</sub>	6.69 <sup>+0.06</sup> <sub>-0.08</sub>	4.01 <sup>+0.07</sup> <sub>-0.07</sub>	13.26 <sup>+1.21</sup> <sub>-0.93</sub>	0.63	–
1220	284.27092	-0.29714	17.47	17.06	15.30	14.24	14.88	12.30	11.73	11.42	4.56 <sup>+0.09</sup> <sub>-0.08</sub>	6.31 <sup>+0.06</sup> <sub>-0.06</sub>	3.88 <sup>+0.07</sup> <sub>-0.06</sub>	14.18 <sup>+1.11</sup> <sub>-0.90</sub>	1.56	–
1221	284.27116	-0.32831	15.85	15.38	13.35	12.29	13.01	9.96	9.36	8.98	4.59 <sup>+0.07</sup> <sub>-0.07</sub>	7.06 <sup>+0.10</sup> <sub>-0.11</sub>	4.03 <sup>+0.09</sup> <sub>-0.08</sub>	12.07 <sup>+0.90</sup> <sub>-0.87</sub>	5.91	–
1223	284.27196	-0.33363	17.38	17.03	15.29	14.27	14.91	12.30	11.82	11.35	4.56 <sup>+0.09</sup> <sub>-0.08</sub>	6.22 <sup>+0.06</sup> <sub>-0.07</sub>	3.91 <sup>+0.07</sup> <sub>-0.07</sub>	14.34 <sup>+1.12</sup> <sub>-0.93</sub>	5.13	–
1226	284.27271	-0.32974	14.59	14.29	12.56	11.54	12.17	9.45	8.95	8.52	4.56 <sup>+0.08</sup> <sub>-0.08</sub>	6.50 <sup>+0.07</sup> <sub>-0.08</sub>	4.16 <sup>+0.09</sup> <sub>-0.08</sub>	11.33 <sup>+1.06</sup> <sub>-0.90</sub>	2.25	–
1231	284.27449	-0.33576	16.69	16.08	14.05	12.84	13.63	10.56	9.89	9.55	4.60 <sup>+0.07</sup> <sub>-0.08</sub>	7.20 <sup>+0.05</sup> <sub>-0.06</sub>	3.92 <sup>+0.05</sup> <sub>-0.05</sub>	12.77 <sup>+0.87</sup> <sub>-0.92</sub>	3.36	–
1232	284.27469	-0.33236	18.18	17.59	15.65	14.50	15.27	12.33	11.82	11.38	4.57 <sup>+0.09</sup> <sub>-0.09</sub>	6.77 <sup>+0.06</sup> <sub>-0.07</sub>	3.81 <sup>+0.06</sup> <sub>-0.06</sub>	14.36 <sup>+1.12</sup> <sub>-0.99</sub>	6.96	–
1238	284.27659	-0.32502	15.88	15.45	13.61	12.53	13.21	10.53	9.96	9.59	4.59 <sup>+0.07</sup> <sub>-0.08</sub>	6.51 <sup>+0.05</sup> <sub>-0.06</sub>	3.89 <sup>+0.06</sup> <sub>-0.06</sub>	12.82 <sup>+0.93</sup> <sub>-0.96</sub>	1.53	–
1246	284.28159	-0.34966	20.24	19.34	17.04	15.66	16.20	12.83	11.96	11.43	4.51 <sup>+0.11</sup> <sub>-0.10</sub>	8.57 <sup>+0.09</sup> <sub>-0.12</sub>	4.27 <sup>+0.08</sup> <sub>-0.07</sub>	13.42 <sup>+1.32</sup> <sub>-1.04</sub>	0.75	EM
1248	284.28245	-0.28698	16.48	15.92	13.88	12.65	13.43	10.32	9.62	9.24	4.62 <sup>+0.05</sup> <sub>-0.07</sub>	7.36 <sup>+0.04</sup> <sub>-0.05</sub>	4.02 <sup>+0.05</sup> <sub>-0.05</sub>	12.69 <sup>+0.72</sup> <sub>-0.86</sub>	2.52	–
1250	284.28319	-0.33049	19.78	19.00	16.93	15.72	16.50	13.53	12.85	12.56	4.53 <sup>+0.10</sup> <sub>-0.08</sub>	7.03 <sup>+0.07</sup> <sub>-0.10</sub>	3.73 <sup>+0.06</sup> <sub>-0.05</sub>	14.89 <sup>+1.23</sup> <sub>-0.89</sub>	4.66	–
1268	284.29580	-0.34822	18.25	17.59	15.50	14.23	14.95	11.74	11.01	10.54	4.58 <sup>+0.08</sup> <sub>-0.08</sub>	7.73 <sup>+0.05</sup> <sub>-0.06</sub>	4.14 <sup>+0.06</sup> <sub>-0.05</sub>	13.43 <sup>+1.03</sup> <sub>-0.91</sub>	2.34	–
1273	284.29885	-0.51977	16.09	15.56	13.66	12.55	13.24	10.49	9.86	9.52	4.55 <sup>+0.10</sup> <sub>-0.08</sub>	6.67 <sup>+0.06</sup> <sub>-0.08</sub>	3.87 <sup>+0.06</sup> <sub>-0.06</sub>	12.19 <sup>+1.20</sup> <sub>-0.93</sub>	0.78	–
1294	284.31755	-0.39894	18.86	18.11	15.79	14.37	15.33	11.45	10.45	9.96	4.62 <sup>+0.06</sup> <sub>-0.08</sub>	8.94 <sup>+0.04</sup> <sub>-0.05</sub>	4.44 <sup>+0.05</sup> <sub>-0.05</sub>	13.17 <sup>+0.74</sup> <sub>-0.94</sub>	1.94	–
1296	284.31987	-0.31719	17.12	16.93	15.33	14.34	15.00	12.45	11.87	11.57	4.59 <sup>+0.07</sup> <sub>-0.08</sub>	6.13 <sup>+0.05</sup> <sub>-0.06</sub>	4.13 <sup>+0.07</sup> <sub>-0.07</sub>	14.73 <sup>+0.91</sup> <sub>-0.98</sub>	1.63	–
1303	284.32504	-0.33362	16.04	15.69	13.79	12.62	13.37	10.44	9.74	9.39	4.64 <sup>+0.04</sup> <sub>-0.06</sub>	7.02 <sup>+0.04</sup> <sub>-0.04</sub>	4.13 <sup>+0.06</sup> <sub>-0.05</sub>	13.14 <sup>+0.53</sup> <sub>-0.78</sub>	3.93	–
1313	284.33724	-0.29353	16.87	16.72	15.23	14.31	14.86	12.63	12.13	11.82	4.54 <sup>+0.10</sup> <sub>-0.08</sub>	5.61 <sup>+0.06</sup> <sub>-0.09</sub>	4.01 <sup>+0.08</sup> <sub>-0.07</sub>	14.45 <sup>+1.27</sup> <sub>-0.88</sub>	1.31	–
1314	284.34005	-0.28273	16.51	16.02	14.08	12.90	13.64	10.71	10.06	9.68	4.62 <sup>+0.06</sup> <sub>-0.08</sub>	7.02 <sup>+0.04</sup> <sub>-0.05</sub>	3.99 <sup>+0.06</sup> <sub>-0.05</sub>	13.12 <sup>+0.77</sup> <sub>-0.95</sub>	1.85	–
1316	284.34163	-0.28174	19.27	18.76	16.94	15.84	16.56	13.79	13.11	12.82	4.49 <sup>+0.09</sup> <sub>-0.07</sub>	6.58 <sup>+0.08</sup> <sub>-0.09</sub>	3.97 <sup>+0.08</sup> <sub>-0.07</sub>	14.81 <sup>+1.11</sup> <sub>-0.71</sub>	1.77	–

Continued on next page...

ID	$\ell$	$b$	u	g	r	i	H $\alpha$	J	H	K	$\log(T_{\text{eff}})$	$A_0$	$R_V$	$\mu$	$\chi^2$	Notes
1318	284.34555	-0.29031	15.31	15.18	13.64	12.73	13.27	11.03	10.56	10.28	4.60 <sup>+0.07</sup> <sub>-0.08</sub>	5.62 <sup>+0.05</sup> <sub>-0.06</sub>	3.91 <sup>+0.07</sup> <sub>-0.06</sub>	13.68 <sup>+0.90</sup> <sub>-0.94</sub>	2.16	-
1323	284.35157	-0.27985	19.19	18.76	17.00	15.95	16.59	14.00	13.41	13.10	4.52 <sup>+0.10</sup> <sub>-0.07</sub>	6.31 <sup>+0.07</sup> <sub>-0.09</sub>	3.91 <sup>+0.07</sup> <sub>-0.07</sub>	15.40 <sup>+1.22</sup> <sub>-0.77</sub>	0.92	-
1338	284.37839	0.00914	15.53	14.99	13.14	12.06	12.73	10.21	9.68	9.41	4.57 <sup>+0.08</sup> <sub>-0.08</sub>	6.17 <sup>+0.05</sup> <sub>-0.07</sub>	3.58 <sup>+0.05</sup> <sub>-0.05</sub>	12.41 <sup>+1.02</sup> <sub>-0.93</sub>	2.19	-
1354	284.40103	-0.28897	17.14	16.80	15.03	13.97	14.62	12.01	11.42	11.13	4.61 <sup>+0.06</sup> <sub>-0.08</sub>	6.37 <sup>+0.05</sup> <sub>-0.05</sub>	3.93 <sup>+0.06</sup> <sub>-0.06</sub>	14.56 <sup>+0.80</sup> <sub>-0.96</sub>	2.47	-
1356	284.40202	-0.54809	15.32	15.25	13.73	12.83	13.35	11.11	10.58	10.34	4.60 <sup>+0.07</sup> <sub>-0.08</sub>	5.68 <sup>+0.05</sup> <sub>-0.06</sub>	4.05 <sup>+0.07</sup> <sub>-0.07</sub>	13.66 <sup>+0.87</sup> <sub>-0.94</sub>	2.07	-
1368	284.40944	0.40951	18.63	18.65	17.30	16.58	16.94	15.18	14.70	14.55	4.49 <sup>+0.09</sup> <sub>-0.07</sub>	4.80 <sup>+0.09</sup> <sub>-0.10</sub>	3.89 <sup>+0.11</sup> <sub>-0.11</sub>	16.75 <sup>+1.12</sup> <sub>-0.72</sub>	1.65	-
1374	284.41812	-0.92735	15.85	15.53	13.93	12.97	13.55	11.33	10.78	10.54	4.50 <sup>+0.09</sup> <sub>-0.07</sub>	5.61 <sup>+0.08</sup> <sub>-0.09</sub>	3.75 <sup>+0.07</sup> <sub>-0.07</sub>	12.75 <sup>+1.10</sup> <sub>-0.72</sub>	2.14	-
1379	284.42443	-0.45116	15.74	15.80	14.60	13.87	14.26	12.65	12.29	12.10	4.49 <sup>+0.09</sup> <sub>-0.06</sub>	4.37 <sup>+0.08</sup> <sub>-0.08</sub>	3.74 <sup>+0.10</sup> <sub>-0.09</sub>	14.29 <sup>+1.05</sup> <sub>-0.66</sub>	1.04	-
1380	284.42632	-0.44554	15.08	15.18	14.03	13.35	13.72	12.16	11.81	11.70	4.48 <sup>+0.09</sup> <sub>-0.06</sub>	4.19 <sup>+0.08</sup> <sub>-0.09</sub>	3.72 <sup>+0.10</sup> <sub>-0.09</sub>	13.80 <sup>+1.03</sup> <sub>-0.65</sub>	4.18	-
1408	284.46722	-0.03133	15.23	14.97	13.46	12.62	13.12	11.17	10.82	10.61	4.50 <sup>+0.09</sup> <sub>-0.07</sub>	4.93 <sup>+0.07</sup> <sub>-0.09</sub>	3.44 <sup>+0.07</sup> <sub>-0.06</sub>	12.90 <sup>+1.10</sup> <sub>-0.73</sub>	2.43	-
1423	284.48641	-1.06831	19.05	18.21	16.10	14.83	15.66	12.41	11.70	11.28	4.48 <sup>+0.10</sup> <sub>-0.07</sub>	7.51 <sup>+0.09</sup> <sub>-0.10</sub>	3.95 <sup>+0.06</sup> <sub>-0.06</sub>	13.09 <sup>+1.15</sup> <sub>-0.76</sub>	2.01	-
1437	284.50634	-0.46535	17.02	17.43	16.45	15.85	16.16	14.79	14.35	14.30	4.58 <sup>+0.08</sup> <sub>-0.08</sub>	4.04 <sup>+0.13</sup> <sub>-0.13</sub>	4.16 <sup>+0.20</sup> <sub>-0.19</sub>	17.51 <sup>+1.03</sup> <sub>-0.99</sub>	1.27	-
1445	284.52236	0.00883	16.87	17.37	16.39	15.91	16.11	14.88	14.39	14.14	4.54 <sup>+0.09</sup> <sub>-0.08</sub>	3.99 <sup>+0.09</sup> <sub>-0.10</sub>	4.43 <sup>+0.20</sup> <sub>-0.18</sub>	17.01 <sup>+1.12</sup> <sub>-0.88</sub>	6.00	-
1471	284.55812	0.32404	13.29	13.49	12.30	11.64	11.99	10.43	10.13	9.94	4.57 <sup>+0.08</sup> <sub>-0.08</sub>	4.28 <sup>+0.05</sup> <sub>-0.06</sub>	3.75 <sup>+0.09</sup> <sub>-0.08</sub>	13.17 <sup>+1.04</sup> <sub>-0.92</sub>	1.67	-
1475	284.55982	-0.87683	18.87	18.81	17.43	16.64	17.12	15.48	15.07	14.79	4.57 <sup>+0.08</sup> <sub>-0.08</sub>	4.56 <sup>+0.09</sup> <sub>-0.10</sub>	3.43 <sup>+0.11</sup> <sub>-0.10</sub>	18.09 <sup>+1.05</sup> <sub>-0.97</sub>	2.71	-
1501	284.58726	-1.41781	19.80	18.78	16.55	15.23	16.67	12.78	12.07	11.72	4.48 <sup>+0.11</sup> <sub>-0.09</sub>	7.60 <sup>+0.10</sup> <sub>-0.12</sub>	3.77 <sup>+0.06</sup> <sub>-0.06</sub>	13.48 <sup>+1.22</sup> <sub>-0.87</sub>	2.48	-
1558	284.64454	-1.30688	16.52	17.05	16.17	15.65	15.90	14.81	14.54	14.44	4.61 <sup>+0.06</sup> <sub>-0.08</sub>	3.45 <sup>+0.07</sup> <sub>-0.07</sub>	3.84 <sup>+0.14</sup> <sub>-0.12</sub>	18.19 <sup>+0.82</sup> <sub>-0.93</sub>	1.02	-
1657	284.76158	0.28442	17.76	17.63	16.09	15.19	15.76	13.46	13.06	12.77	4.58 <sup>+0.08</sup> <sub>-0.08</sub>	5.57 <sup>+0.05</sup> <sub>-0.07</sub>	3.89 <sup>+0.07</sup> <sub>-0.07</sub>	15.95 <sup>+0.98</sup> <sub>-0.91</sub>	4.72	-
1671	284.78596	-0.71369	12.95	13.53	12.63	12.09	12.11	10.91	10.59	10.29	4.55 <sup>+0.09</sup> <sub>-0.07</sub>	4.12 <sup>+0.06</sup> <sub>-0.07</sub>	4.77 <sup>+0.15</sup> <sub>-0.14</sub>	13.26 <sup>+1.09</sup> <sub>-0.85</sub>	4.39	EM
1832	284.94718	-0.55783	13.81	14.32	13.56	13.12	13.32	12.43	12.26	12.15	4.51 <sup>+0.09</sup> <sub>-0.07</sub>	2.95 <sup>+0.06</sup> <sub>-0.08</sub>	3.62 <sup>+0.13</sup> <sub>-0.11</sub>	14.82 <sup>+1.09</sup> <sub>-0.74</sub>	0.52	-
1851	284.96032	-0.91334	16.80	17.20	15.87	14.97	15.49	13.03	12.38	12.03	4.64 <sup>+0.04</sup> <sub>-0.05</sub>	6.17 <sup>+0.06</sup> <sub>-0.06</sub>	5.23 <sup>+0.09</sup> <sub>-0.10</sub>	15.83 <sup>+0.51</sup> <sub>-0.69</sub>	4.22	-
1869	284.97164	-0.83938	15.91	15.70	14.23	13.38	13.68	12.24	11.85	11.61	4.51 <sup>+0.10</sup> <sub>-0.07</sub>	4.57 <sup>+0.07</sup> <sub>-0.08</sub>	3.25 <sup>+0.06</sup> <sub>-0.06</sub>	14.17 <sup>+1.16</sup> <sub>-0.74</sub>	6.37	EM
1900	285.00263	-1.18342	15.68	16.43	15.72	15.17	15.27	14.19	14.00	13.90	4.63 <sup>+0.05</sup> <sub>-0.07</sub>	3.65 <sup>+0.14</sup> <sub>-0.15</sub>	4.76 <sup>+0.25</sup> <sub>-0.23</sub>	17.67 <sup>+0.68</sup> <sub>-0.94</sub>	4.82	-
1906	285.00609	-1.18520	16.38	17.08	16.25	15.74	16.06	14.71	14.40	14.29	4.62 <sup>+0.07</sup> <sub>-0.07</sub>	3.78 <sup>+0.07</sup> <sub>-0.13</sub>	4.62 <sup>+0.15</sup> <sub>-0.13</sub>	18.05 <sup>+1.07</sup> <sub>-0.90</sub>	2.29	-
1925	285.02131	-1.18215	19.37	18.72	16.79	15.69	16.36	13.65	13.07	12.82	4.49 <sup>+0.09</sup> <sub>-0.08</sub>	6.46 <sup>+0.08</sup> <sub>-0.11</sub>	3.67 <sup>+0.06</sup> <sub>-0.06</sub>	14.85 <sup>+1.07</sup> <sub>-0.80</sub>	4.34	-
1987	285.07558	-1.76510	13.20	13.63	12.75	12.18	12.45	11.28	11.02	10.96	4.59 <sup>+0.08</sup> <sub>-0.08</sub>	3.52 <sup>+0.05</sup> <sub>-0.07</sub>	3.75 <sup>+0.11</sup> <sub>-0.10</sub>	14.36 <sup>+1.03</sup> <sub>-0.98</sub>	5.59	-
2077	285.15176	-0.53853	18.72	18.91	17.55	16.82	17.21	15.41	14.81	14.44	4.59 <sup>+0.07</sup> <sub>-0.08</sub>	5.12 <sup>+0.09</sup> <sub>-0.09</sub>	4.22 <sup>+0.12</sup> <sub>-0.11</sub>	17.82 <sup>+0.93</sup> <sub>-0.93</sub>	6.65	-
2109	285.17742	-0.61319	15.54	15.57	14.29	13.55	13.96	12.17	11.75	11.52	4.48 <sup>+0.08</sup> <sub>-0.06</sub>	4.73 <sup>+0.08</sup> <sub>-0.09</sub>	3.95 <sup>+0.09</sup> <sub>-0.09</sub>	13.59 <sup>+0.95</sup> <sub>-0.65</sub>	0.14	-
2127	285.19169	-0.17393	14.54	14.53	13.19	12.45	12.83	11.10	10.69	10.46	4.49 <sup>+0.09</sup> <sub>-0.06</sub>	4.72 <sup>+0.07</sup> <sub>-0.08</sub>	3.79 <sup>+0.09</sup> <sub>-0.08</sub>	12.66 <sup>+0.99</sup> <sub>-0.66</sub>	0.16	-
2129	285.19263	1.50246	14.76	14.83	13.62	12.92	13.30	11.74	11.43	11.25	4.52 <sup>+0.10</sup> <sub>-0.07</sub>	4.25 <sup>+0.07</sup> <sub>-0.08</sub>	3.60 <sup>+0.09</sup> <sub>-0.08</sub>	13.80 <sup>+1.15</sup> <sub>-0.75</sub>	0.74	-
2141	285.20185	-1.60295	16.90	16.64	15.02	14.09	14.64	12.44	11.89	11.60	4.52 <sup>+0.10</sup> <sub>-0.07</sub>	5.66 <sup>+0.07</sup> <sub>-0.09</sub>	3.81 <sup>+0.07</sup> <sub>-0.06</sub>	14.03 <sup>+1.16</sup> <sub>-0.77</sub>	0.95	-
2150	285.20582	1.20905	19.28	19.32	17.91	17.04	17.54	15.40	14.74	14.49	4.58 <sup>+0.08</sup> <sub>-0.09</sub>	5.64 <sup>+0.09</sup> <sub>-0.09</sub>	4.34 <sup>+0.12</sup> <sub>-0.11</sub>	17.60 <sup>+1.06</sup> <sub>-1.06</sub>	1.64	-
2164	285.21643	-1.17514	13.12	13.61	12.77	12.24	12.47	11.41	11.13	11.03	4.57 <sup>+0.08</sup> <sub>-0.08</sub>	3.42 <sup>+0.05</sup> <sub>-0.07</sub>	3.85 <sup>+0.12</sup> <sub>-0.11</sub>	14.33 <sup>+1.06</sup> <sub>-0.95</sub>	1.51	-

Continued on next page...

ID	$\ell$	$b$	u	g	r	i	H $\alpha$	J	H	K	$\log(T_{\text{eff}})$	$A_0$	$R_V$	$\mu$	$\chi^2$	Notes
2225	285.25235	0.47173	17.11	16.86	15.26	14.35	14.88	12.60	12.08	11.83	4.51 <sup>+0.09</sup> <sub>-0.07</sub>	5.70 <sup>+0.07</sup> <sub>-0.09</sub>	3.88 <sup>+0.08</sup> <sub>-0.07</sub>	14.13 <sup>+1.06</sup> <sub>-0.75</sub>	1.88	–
2236	285.25713	-0.05303	19.97	18.79	16.11	14.62	15.66	11.60	10.75	10.27	4.59 <sup>+0.07</sup> <sub>-0.09</sub>	9.09 <sup>+0.05</sup> <sub>-0.07</sub>	3.89 <sup>+0.05</sup> <sub>-0.05</sub>	13.09 <sup>+0.92</sup> <sub>-1.07</sub>	6.32	–
2241	285.25997	-0.04941	19.49	18.62	16.32	15.05	15.79	12.39	11.61	11.02	4.49 <sup>+0.09</sup> <sub>-0.07</sub>	8.13 <sup>+0.09</sup> <sub>-0.10</sub>	4.12 <sup>+0.07</sup> <sub>-0.07</sub>	12.90 <sup>+1.00</sup> <sub>-0.70</sub>	3.62	–
2246	285.26556	-0.04719	18.94	18.16	15.86	14.58	15.45	11.95	11.17	10.72	4.60 <sup>+0.07</sup> <sub>-0.08</sub>	8.09 <sup>+0.06</sup> <sub>-0.07</sub>	4.05 <sup>+0.06</sup> <sub>-0.05</sub>	13.80 <sup>+0.89</sup> <sub>-0.96</sub>	2.30	–
2252	285.27325	-1.04995	19.25	19.26	17.91	17.07	17.50	15.61	15.14	14.88	4.57 <sup>+0.09</sup> <sub>-0.09</sub>	5.12 <sup>+0.11</sup> <sub>-0.11</sub>	3.98 <sup>+0.13</sup> <sub>-0.12</sub>	17.89 <sup>+1.14</sup> <sub>-1.10</sub>	2.07	–
2518	285.50561	-0.72612	18.86	19.00	17.67	16.91	17.42	15.39	14.96	14.61	4.58 <sup>+0.07</sup> <sub>-0.08</sub>	5.12 <sup>+0.09</sup> <sub>-0.09</sub>	4.17 <sup>+0.12</sup> <sub>-0.12</sub>	17.90 <sup>+0.96</sup> <sub>-0.98</sub>	1.31	–
2550	285.53900	-0.12740	15.70	15.34	13.63	12.69	13.28	10.96	10.52	10.17	4.52 <sup>+0.08</sup> <sub>-0.07</sub>	5.73 <sup>+0.06</sup> <sub>-0.08</sub>	3.67 <sup>+0.07</sup> <sub>-0.06</sub>	12.67 <sup>+1.00</sup> <sub>-0.77</sub>	2.52	–
2574	285.55938	-0.61533	20.85	19.31	16.63	15.08	16.12	12.29	11.50	11.10	4.54 <sup>+0.11</sup> <sub>-0.14</sub>	8.67 <sup>+0.07</sup> <sub>-0.16</sub>	3.58 <sup>+0.05</sup> <sub>-0.05</sub>	13.45 <sup>+1.36</sup> <sub>-1.44</sub>	6.07	–
2662	285.61448	-0.75292	13.95	13.95	12.68	11.93	12.32	10.62	10.27	10.06	4.48 <sup>+0.09</sup> <sub>-0.06</sub>	4.54 <sup>+0.08</sup> <sub>-0.09</sub>	3.74 <sup>+0.09</sup> <sub>-0.09</sub>	12.16 <sup>+1.01</sup> <sub>-0.66</sub>	1.52	–
2687	285.63699	-0.97408	17.64	18.05	17.05	16.45	16.72	15.42	14.96	15.15	4.60 <sup>+0.07</sup> <sub>-0.08</sub>	3.97 <sup>+0.10</sup> <sub>-0.10</sub>	4.01 <sup>+0.15</sup> <sub>-0.15</sub>	18.52 <sup>+0.86</sup> <sub>-1.02</sub>	4.14	–
2766	285.69824	-1.05342	16.39	16.06	14.43	13.48	14.04	11.69	11.16	10.94	4.49 <sup>+0.08</sup> <sub>-0.06</sub>	5.78 <sup>+0.08</sup> <sub>-0.09</sub>	3.84 <sup>+0.07</sup> <sub>-0.07</sub>	12.98 <sup>+0.97</sup> <sub>-0.67</sub>	3.83	–
2771	285.70405	0.35604	14.57	14.94	13.91	13.47	13.64	12.49	12.25	12.07	4.50 <sup>+0.08</sup> <sub>-0.06</sub>	3.56 <sup>+0.07</sup> <sub>-0.08</sub>	3.76 <sup>+0.11</sup> <sub>-0.10</sub>	14.49 <sup>+0.92</sup> <sub>-0.65</sub>	6.75	–
2892	285.79081	-2.02509	18.97	19.10	17.83	17.04	17.56	15.52	14.98	14.65	4.54 <sup>+0.10</sup> <sub>-0.09</sub>	5.21 <sup>+0.10</sup> <sub>-0.11</sub>	4.38 <sup>+0.15</sup> <sub>-0.14</sub>	17.41 <sup>+1.20</sup> <sub>-1.02</sub>	1.24	–
2921	285.80713	-1.01425	16.27	15.94	14.27	13.28	13.89	11.42	10.89	10.67	4.57 <sup>+0.09</sup> <sub>-0.08</sub>	5.98 <sup>+0.05</sup> <sub>-0.07</sub>	3.83 <sup>+0.07</sup> <sub>-0.06</sub>	13.62 <sup>+1.10</sup> <sub>-0.96</sub>	6.71	–
2994	285.84627	-0.98639	14.63	14.76	13.58	12.83	13.24	11.45	11.05	10.81	4.50 <sup>+0.09</sup> <sub>-0.07</sub>	4.71 <sup>+0.07</sup> <sub>-0.09</sub>	4.12 <sup>+0.11</sup> <sub>-0.10</sub>	13.11 <sup>+1.02</sup> <sub>-0.69</sub>	1.22	–
3015	285.86419	-1.28089	14.35	14.42	13.11	12.36	12.61	10.92	10.49	10.21	4.53 <sup>+0.10</sup> <sub>-0.07</sub>	4.93 <sup>+0.06</sup> <sub>-0.08</sub>	4.03 <sup>+0.09</sup> <sub>-0.08</sub>	12.82 <sup>+1.19</sup> <sub>-0.74</sub>	0.79	EM
3034	285.87491	0.91925	13.28	13.57	12.58	12.00	12.29	10.91	10.66	10.44	4.48 <sup>+0.09</sup> <sub>-0.06</sub>	3.86 <sup>+0.08</sup> <sub>-0.09</sub>	3.95 <sup>+0.12</sup> <sub>-0.12</sub>	12.63 <sup>+1.08</sup> <sub>-0.64</sub>	1.45	–
3085	285.91076	-1.56440	13.91	14.21	13.27	12.73	13.00	11.86	11.70	11.58	4.49 <sup>+0.10</sup> <sub>-0.07</sub>	3.32 <sup>+0.08</sup> <sub>-0.09</sub>	3.44 <sup>+0.10</sup> <sub>-0.09</sub>	13.98 <sup>+1.16</sup> <sub>-0.69</sub>	2.54	–
3106	285.92149	0.06546	19.65	19.73	18.16	17.34	17.91	15.63	15.03	14.79	4.60 <sup>+0.07</sup> <sub>-0.09</sub>	5.68 <sup>+0.09</sup> <sub>-0.10</sub>	4.13 <sup>+0.12</sup> <sub>-0.12</sub>	18.09 <sup>+0.92</sup> <sub>-1.04</sub>	4.73	–
3197	285.97972	1.14523	18.32	18.61	17.39	16.81	17.02	15.84	15.43	15.15	4.59 <sup>+0.06</sup> <sub>-0.07</sub>	4.00 <sup>+0.10</sup> <sub>-0.10</sub>	3.58 <sup>+0.13</sup> <sub>-0.13</sub>	18.76 <sup>+0.74</sup> <sub>-0.80</sub>	6.63	–
3198	285.98020	-2.56271	18.14	18.54	17.41	16.84	17.12	15.93	15.44	15.23	4.60 <sup>+0.05</sup> <sub>-0.06</sub>	3.95 <sup>+0.11</sup> <sub>-0.11</sub>	3.78 <sup>+0.15</sup> <sub>-0.15</sub>	18.92 <sup>+0.64</sup> <sub>-0.79</sub>	5.27	–
3245	286.01144	-1.32687	16.13	16.11	14.79	14.02	14.44	12.59	12.18	12.01	4.52 <sup>+0.09</sup> <sub>-0.07</sub>	4.83 <sup>+0.06</sup> <sub>-0.08</sub>	3.82 <sup>+0.09</sup> <sub>-0.08</sub>	14.54 <sup>+1.15</sup> <sub>-0.79</sub>	2.70	–
3297	286.04468	-1.32775	17.04	17.32	16.28	15.67	15.98	14.51	14.25	13.98	4.49 <sup>+0.08</sup> <sub>-0.06</sub>	4.07 <sup>+0.09</sup> <sub>-0.09</sub>	4.03 <sup>+0.14</sup> <sub>-0.13</sub>	16.30 <sup>+0.96</sup> <sub>-0.69</sub>	1.12	–
3312	286.05886	-1.29040	14.36	14.52	13.36	12.70	13.03	11.46	11.17	10.95	4.51 <sup>+0.10</sup> <sub>-0.07</sub>	4.29 <sup>+0.07</sup> <sub>-0.08</sub>	3.84 <sup>+0.10</sup> <sub>-0.09</sub>	13.40 <sup>+1.15</sup> <sub>-0.72</sub>	2.05	–
3377	286.10111	-1.48521	13.61	13.94	12.95	12.40	12.68	11.37	11.12	11.00	4.52 <sup>+0.09</sup> <sub>-0.07</sub>	3.71 <sup>+0.06</sup> <sub>-0.08</sub>	3.77 <sup>+0.11</sup> <sub>-0.10</sub>	13.65 <sup>+1.15</sup> <sub>-0.75</sub>	2.35	–
3382	286.10491	-1.14333	17.25	16.90	15.24	14.26	14.85	12.40	11.83	11.59	4.49 <sup>+0.09</sup> <sub>-0.06</sub>	5.98 <sup>+0.08</sup> <sub>-0.09</sub>	3.91 <sup>+0.07</sup> <sub>-0.07</sub>	13.63 <sup>+1.07</sup> <sub>-0.66</sub>	4.43	–
3432	286.13500	-0.26249	13.79	14.09	13.01	12.35	12.71	11.10	10.78	10.62	4.59 <sup>+0.07</sup> <sub>-0.08</sub>	4.30 <sup>+0.05</sup> <sub>-0.06</sub>	4.02 <sup>+0.10</sup> <sub>-0.09</sub>	13.97 <sup>+0.91</sup> <sub>-0.92</sub>	4.66	–
3441	286.14068	-1.57794	16.36	16.10	14.48	13.54	14.09	11.87	11.35	11.02	4.53 <sup>+0.09</sup> <sub>-0.07</sub>	5.71 <sup>+0.06</sup> <sub>-0.08</sub>	3.83 <sup>+0.07</sup> <sub>-0.07</sub>	13.65 <sup>+1.14</sup> <sub>-0.83</sub>	1.06	–
3453	286.15030	-1.58007	20.03	19.84	18.08	17.08	17.68	15.33	14.71	14.33	4.61 <sup>+0.06</sup> <sub>-0.08</sub>	6.10 <sup>+0.08</sup> <sub>-0.08</sub>	3.86 <sup>+0.09</sup> <sub>-0.09</sub>	17.91 <sup>+0.79</sup> <sub>-0.98</sub>	3.09	–
3505	286.17590	-1.91123	19.04	18.80	17.00	15.99	16.60	13.91	13.06	12.72	4.56 <sup>+0.08</sup> <sub>-0.08</sub>	6.84 <sup>+0.06</sup> <sub>-0.07</sub>	4.39 <sup>+0.08</sup> <sub>-0.07</sub>	15.46 <sup>+1.05</sup> <sub>-0.91</sub>	6.90	–
3523	286.18469	-0.10107	20.32	20.00	18.11	17.05	16.69	15.03	14.22	13.95	4.56 <sup>+0.09</sup> <sub>-0.11</sub>	6.74 <sup>+0.07</sup> <sub>-0.10</sub>	4.07 <sup>+0.09</sup> <sub>-0.09</sub>	16.69 <sup>+1.13</sup> <sub>-1.19</sub>	4.91	SUB/EM
3531	286.19067	-1.10800	16.28	16.39	15.17	14.53	14.52	13.48	13.14	12.95	4.51 <sup>+0.09</sup> <sub>-0.07</sub>	4.03 <sup>+0.07</sup> <sub>-0.08</sub>	3.49 <sup>+0.09</sup> <sub>-0.09</sub>	15.47 <sup>+1.10</sup> <sub>-0.74</sub>	1.26	EM
3553	286.20202	-1.26364	18.37	18.15	16.59	15.68	16.18	13.82	13.33	13.08	4.50 <sup>+0.10</sup> <sub>-0.07</sub>	5.80 <sup>+0.08</sup> <sub>-0.10</sub>	4.04 <sup>+0.09</sup> <sub>-0.08</sub>	15.24 <sup>+1.16</sup> <sub>-0.76</sub>	2.54	–

Continued on next page...

ID	$\ell$	$b$	u	g	r	i	H $\alpha$	J	H	K	$\log(T_{\text{eff}})$	$A_0$	$R_V$	$\mu$	$\chi^2$	Notes
3574	286.21424	-0.50726	20.18	19.98	18.37	17.46	18.03	15.87	15.16	15.09	4.54 <sup>+0.10</sup> <sub>-0.11</sub>	5.63 <sup>+0.12</sup> <sub>-0.14</sub>	3.85 <sup>+0.12</sup> <sub>-0.12</sub>	17.69 <sup>+1.20</sup> <sub>-1.24</sub>	3.30	—
3588	286.22195	-1.21016	13.91	14.17	13.04	12.39	12.75	11.15	10.83	10.63	4.56 <sup>+0.08</sup> <sub>-0.07</sub>	4.32 <sup>+0.05</sup> <sub>-0.07</sub>	3.96 <sup>+0.10</sup> <sub>-0.09</sub>	13.68 <sup>+0.97</sup> <sub>-0.86</sub>	1.44	—
3644	286.25818	-1.39355	17.22	16.84	15.17	14.18	14.76	12.32	11.81	11.48	4.48 <sup>+0.09</sup> <sub>-0.07</sub>	5.98 <sup>+0.08</sup> <sub>-0.09</sub>	3.89 <sup>+0.07</sup> <sub>-0.07</sub>	13.49 <sup>+1.09</sup> <sub>-0.69</sub>	1.42	—
3646	286.25945	-1.41573	18.66	18.38	16.76	15.87	16.41	14.09	13.53	13.34	4.49 <sup>+0.08</sup> <sub>-0.06</sub>	5.73 <sup>+0.07</sup> <sub>-0.09</sub>	3.90 <sup>+0.08</sup> <sub>-0.07</sub>	15.37 <sup>+0.97</sup> <sub>-0.66</sub>	5.40	—
3647	286.25999	-1.39469	17.79	17.48	15.85	14.92	15.47	13.12	12.66	12.32	4.50 <sup>+0.10</sup> <sub>-0.07</sub>	5.77 <sup>+0.08</sup> <sub>-0.09</sub>	3.86 <sup>+0.08</sup> <sub>-0.07</sub>	14.50 <sup>+1.15</sup> <sub>-0.72</sub>	3.00	—
3649	286.26184	-0.21325	19.65	19.62	18.04	17.24	nan	15.40	14.80	14.56	4.51 <sup>+0.10</sup> <sub>-0.09</sub>	5.81 <sup>+0.10</sup> <sub>-0.11</sub>	4.30 <sup>+0.12</sup> <sub>-0.12</sub>	16.83 <sup>+1.20</sup> <sub>-0.98</sub>	5.72	—
3677	286.28125	-1.52851	15.13	15.12	13.76	12.97	13.41	11.51	11.10	10.88	4.54 <sup>+0.09</sup> <sub>-0.07</sub>	4.95 <sup>+0.06</sup> <sub>-0.08</sub>	3.84 <sup>+0.08</sup> <sub>-0.08</sub>	13.57 <sup>+1.14</sup> <sub>-0.79</sub>	0.73	—
3711	286.30320	-1.41676	16.43	16.17	14.54	13.58	14.15	11.88	11.30	10.97	4.53 <sup>+0.10</sup> <sub>-0.08</sub>	5.83 <sup>+0.07</sup> <sub>-0.08</sub>	3.90 <sup>+0.07</sup> <sub>-0.06</sub>	13.49 <sup>+1.17</sup> <sub>-0.80</sub>	2.10	—
3729	286.31445	-1.24976	14.07	14.46	13.55	13.03	13.27	12.07	11.81	11.70	4.51 <sup>+0.09</sup> <sub>-0.07</sub>	3.55 <sup>+0.07</sup> <sub>-0.09</sub>	3.84 <sup>+0.12</sup> <sub>-0.11</sub>	14.24 <sup>+1.10</sup> <sub>-0.73</sub>	1.24	—
3740	286.31895	-1.46131	16.13	15.84	14.18	13.24	13.81	11.46	10.97	10.69	4.54 <sup>+0.09</sup> <sub>-0.07</sub>	5.80 <sup>+0.06</sup> <sub>-0.08</sub>	3.81 <sup>+0.07</sup> <sub>-0.06</sub>	13.33 <sup>+1.13</sup> <sub>-0.82</sub>	1.22	—
3764	286.34039	-1.29766	13.77	14.12	13.19	12.66	12.90	11.66	11.42	11.28	4.49 <sup>+0.08</sup> <sub>-0.06</sub>	3.60 <sup>+0.07</sup> <sub>-0.09</sub>	3.86 <sup>+0.12</sup> <sub>-0.11</sub>	13.53 <sup>+0.91</sup> <sub>-0.65</sub>	1.64	—
3780	286.35942	-0.29314	14.39	14.25	12.80	11.94	12.43	10.40	9.95	9.73	4.53 <sup>+0.09</sup> <sub>-0.07</sub>	5.20 <sup>+0.06</sup> <sub>-0.08</sub>	3.79 <sup>+0.08</sup> <sub>-0.07</sub>	12.28 <sup>+1.14</sup> <sub>-0.81</sub>	1.92	—
3790	286.36621	-1.27916	13.29	13.74	12.88	12.41	12.61	11.59	11.43	11.24	4.51 <sup>+0.09</sup> <sub>-0.07</sub>	3.24 <sup>+0.07</sup> <sub>-0.08</sub>	3.70 <sup>+0.12</sup> <sub>-0.11</sub>	13.87 <sup>+1.10</sup> <sub>-0.74</sub>	1.94	—
3832	286.39573	-1.58073	18.47	18.01	16.20	15.19	15.82	13.24	12.66	12.32	4.49 <sup>+0.09</sup> <sub>-0.07</sub>	6.27 <sup>+0.09</sup> <sub>-0.10</sub>	3.87 <sup>+0.07</sup> <sub>-0.07</sub>	14.32 <sup>+1.02</sup> <sub>-0.68</sub>	0.25	—
3836	286.39755	-1.63901	13.82	14.07	13.02	12.44	12.71	11.34	11.06	10.92	4.48 <sup>+0.07</sup> <sub>-0.06</sub>	3.87 <sup>+0.08</sup> <sub>-0.08</sub>	3.80 <sup>+0.11</sup> <sub>-0.09</sub>	13.09 <sup>+0.84</sup> <sub>-0.62</sub>	1.67	—
3861	286.41319	-1.46904	17.87	17.51	15.78	14.80	15.38	12.88	12.27	11.97	4.49 <sup>+0.08</sup> <sub>-0.07</sub>	6.19 <sup>+0.08</sup> <sub>-0.09</sub>	4.00 <sup>+0.07</sup> <sub>-0.07</sub>	14.03 <sup>+0.98</sup> <sub>-0.70</sub>	0.64	—
3862	286.41392	-1.47357	18.53	18.28	16.63	15.68	16.24	13.67	13.14	12.81	4.52 <sup>+0.10</sup> <sub>-0.07</sub>	6.21 <sup>+0.07</sup> <sub>-0.08</sub>	4.18 <sup>+0.09</sup> <sub>-0.08</sub>	15.10 <sup>+1.16</sup> <sub>-0.75</sub>	3.17	—
3877	286.42639	-1.49964	20.10	19.42	17.33	16.14	16.96	13.76	12.95	12.57	4.50 <sup>+0.10</sup> <sub>-0.07</sub>	7.47 <sup>+0.08</sup> <sub>-0.10</sub>	4.10 <sup>+0.07</sup> <sub>-0.07</sub>	14.52 <sup>+1.14</sup> <sub>-0.75</sub>	0.68	—
3904	286.45034	-1.46653	20.20	19.58	17.59	16.43	17.19	14.08	13.43	12.98	4.51 <sup>+0.12</sup> <sub>-0.09</sub>	7.24 <sup>+0.08</sup> <sub>-0.12</sub>	4.09 <sup>+0.07</sup> <sub>-0.07</sub>	15.14 <sup>+1.41</sup> <sub>-0.96</sub>	2.45	—
3920	286.46085	-1.58800	12.93	13.56	12.91	12.51	12.62	11.78	11.60	11.52	4.52 <sup>+0.09</sup> <sub>-0.07</sub>	2.92 <sup>+0.07</sup> <sub>-0.08</sub>	4.04 <sup>+0.16</sup> <sub>-0.14</sub>	14.18 <sup>+1.12</sup> <sub>-0.73</sub>	2.07	—
4057	286.55450	-0.08387	20.11	19.91	18.09	17.13	17.20	14.82	14.21	13.75	4.52 <sup>+0.10</sup> <sub>-0.10</sub>	6.88 <sup>+0.09</sup> <sub>-0.12</sub>	4.47 <sup>+0.10</sup> <sub>-0.10</sub>	15.99 <sup>+1.23</sup> <sub>-1.02</sub>	7.68	SUB/EM
4129	286.60316	-0.82492	12.79	13.27	12.54	12.00	12.21	11.23	10.99	10.90	4.53 <sup>+0.10</sup> <sub>-0.08</sub>	3.22 <sup>+0.06</sup> <sub>-0.09</sub>	3.86 <sup>+0.14</sup> <sub>-0.12</sub>	13.67 <sup>+1.23</sup> <sub>-0.85</sub>	4.80	—
4158	286.61708	-0.24435	20.04	19.57	17.80	16.79	17.35	14.78	14.21	14.03	4.49 <sup>+0.13</sup> <sub>-0.10</sub>	6.26 <sup>+0.10</sup> <sub>-0.15</sub>	3.91 <sup>+0.08</sup> <sub>-0.08</sub>	15.92 <sup>+1.50</sup> <sub>-1.02</sub>	6.80	—
4203	286.64888	-1.01800	13.63	13.87	12.75	12.14	12.44	10.99	10.65	10.47	4.50 <sup>+0.08</sup> <sub>-0.06</sub>	4.12 <sup>+0.07</sup> <sub>-0.08</sub>	3.89 <sup>+0.10</sup> <sub>-0.10</sub>	12.87 <sup>+0.97</sup> <sub>-0.69</sub>	0.38	—
4228	286.66935	0.25148	15.45	15.36	13.99	13.23	13.63	11.86	11.48	11.30	4.48 <sup>+0.07</sup> <sub>-0.06</sub>	4.69 <sup>+0.07</sup> <sub>-0.09</sub>	3.65 <sup>+0.08</sup> <sub>-0.08</sub>	13.35 <sup>+0.83</sup> <sub>-0.63</sub>	1.63	—
4246	286.68315	-0.11287	20.35	19.96	18.06	17.03	17.68	14.94	14.40	14.06	4.54 <sup>+0.10</sup> <sub>-0.11</sub>	6.51 <sup>+0.10</sup> <sub>-0.13</sub>	3.89 <sup>+0.10</sup> <sub>-0.09</sub>	16.57 <sup>+1.29</sup> <sub>-1.20</sub>	2.62	—
4247	286.68338	-0.82772	18.86	18.98	17.68	16.93	17.34	15.74	15.13	14.89	4.58 <sup>+0.08</sup> <sub>-0.09</sub>	4.70 <sup>+0.11</sup> <sub>-0.11</sub>	3.86 <sup>+0.14</sup> <sub>-0.13</sub>	18.18 <sup>+1.05</sup> <sub>-1.01</sub>	3.64	—
4345	286.72876	-1.62830	19.95	19.62	17.70	16.63	17.31	14.51	13.69	13.40	4.58 <sup>+0.07</sup> <sub>-0.09</sub>	6.93 <sup>+0.06</sup> <sub>-0.08</sub>	4.15 <sup>+0.08</sup> <sub>-0.08</sub>	16.38 <sup>+0.97</sup> <sub>-1.00</sub>	6.70	—
4410	286.76266	-2.85311	13.06	13.77	13.04	12.69	12.78	12.09	11.93	11.81	4.59 <sup>+0.07</sup> <sub>-0.07</sub>	2.77 <sup>+0.05</sup> <sub>-0.05</sub>	3.73 <sup>+0.13</sup> <sub>-0.12</sub>	15.42 <sup>+0.85</sup> <sub>-0.84</sub>	2.99	—
4431	286.77048	-1.10299	12.94	13.32	12.35	11.79	12.01	10.65	10.35	10.16	4.51 <sup>+0.09</sup> <sub>-0.07</sub>	3.97 <sup>+0.07</sup> <sub>-0.08</sub>	4.21 <sup>+0.13</sup> <sub>-0.12</sub>	12.58 <sup>+1.05</sup> <sub>-0.71</sub>	1.44	—
4438	286.77482	-1.74885	12.55	13.33	12.86	12.60	12.66	12.15	12.01	11.99	4.48 <sup>+0.09</sup> <sub>-0.06</sub>	2.21 <sup>+0.08</sup> <sub>-0.09</sub>	3.99 <sup>+0.21</sup> <sub>-0.20</sub>	14.31 <sup>+1.05</sup> <sub>-0.62</sub>	1.22	—
4465	286.78495	-0.07461	20.53	19.72	17.38	16.01	16.92	13.49	12.80	12.45	4.60 <sup>+0.07</sup> <sub>-0.10</sub>	7.85 <sup>+0.05</sup> <sub>-0.07</sub>	3.71 <sup>+0.06</sup> <sub>-0.06</sub>	15.60 <sup>+0.90</sup> <sub>-1.15</sub>	7.63	—
4520	286.80433	-1.52904	12.22	13.05	12.54	12.23	12.28	11.65	11.57	11.52	4.58 <sup>+0.07</sup> <sub>-0.07</sub>	2.48 <sup>+0.05</sup> <sub>-0.06</sub>	4.05 <sup>+0.17</sup> <sub>-0.16</sub>	14.98 <sup>+0.93</sup> <sub>-0.86</sub>	3.78	—

Continued on next page...

ID	$\ell$	$b$	u	g	r	i	H $\alpha$	J	H	K	log( $T_{\text{eff}}$ )	$A_0$	$R_V$	$\mu$	$\chi^2$	Notes
4551	286.81566	0.77420	18.51	18.50	17.27	16.53	16.94	15.39	15.10	14.89	4.48 <sup>+0.10</sup> <sub>-0.07</sub>	4.21 <sup>+0.12</sup> <sub>-0.11</sub>	3.49 <sup>+0.13</sup> <sub>-0.13</sub>	17.09 <sup>+1.22</sup> <sub>-0.77</sub>	1.93	–
4584	286.83433	0.11063	14.55	14.78	13.66	13.05	13.38	11.92	11.63	11.51	4.54 <sup>+0.09</sup> <sub>-0.07</sub>	4.01 <sup>+0.07</sup> <sub>-0.08</sub>	3.70 <sup>+0.10</sup> <sub>-0.09</sub>	14.35 <sup>+1.07</sup> <sub>-0.82</sub>	1.60	–
4608	286.84167	-0.36556	20.01	18.97	16.73	15.44	16.30	13.05	12.34	11.99	4.48 <sup>+0.12</sup> <sub>-0.11</sub>	7.49 <sup>+0.10</sup> <sub>-0.15</sub>	3.71 <sup>+0.06</sup> <sub>-0.06</sub>	13.83 <sup>+1.42</sup> <sub>-1.06</sub>	2.94	–
4685	286.87741	-0.97465	18.43	18.12	16.45	15.53	16.01	13.71	13.23	12.82	4.48 <sup>+0.10</sup> <sub>-0.07</sub>	5.88 <sup>+0.09</sup> <sub>-0.10</sub>	3.93 <sup>+0.08</sup> <sub>-0.08</sub>	14.82 <sup>+1.14</sup> <sub>-0.69</sub>	2.76	–
4705	286.89426	1.50945	12.90	13.52	12.88	12.50	12.62	11.98	11.87	11.76	4.51 <sup>+0.09</sup> <sub>-0.06</sub>	2.53 <sup>+0.07</sup> <sub>-0.08</sub>	3.52 <sup>+0.14</sup> <sub>-0.13</sub>	14.44 <sup>+1.02</sup> <sub>-0.70</sub>	1.09	–
4761	286.93065	-1.58151	18.07	18.13	16.74	15.79	16.34	13.83	13.06	12.71	4.49 <sup>+0.10</sup> <sub>-0.07</sub>	6.30 <sup>+0.09</sup> <sub>-0.09</sub>	4.99 <sup>+0.14</sup> <sub>-0.13</sub>	14.67 <sup>+1.20</sup> <sub>-0.74</sub>	2.32	–
4765	286.93209	-0.12212	20.12	19.81	18.01	17.08	17.13	15.21	14.58	14.36	4.51 <sup>+0.11</sup> <sub>-0.09</sub>	6.07 <sup>+0.12</sup> <sub>-0.13</sub>	3.86 <sup>+0.11</sup> <sub>-0.11</sub>	16.65 <sup>+1.33</sup> <sub>-1.01</sub>	3.38	SUB/EM
4833	286.97023	1.51731	17.14	17.16	15.76	14.94	15.39	13.36	12.69	12.52	4.54 <sup>+0.09</sup> <sub>-0.08</sub>	5.45 <sup>+0.06</sup> <sub>-0.08</sub>	4.24 <sup>+0.10</sup> <sub>-0.09</sub>	15.20 <sup>+1.11</sup> <sub>-0.87</sub>	7.41	–
4839	286.97151	-0.71588	19.56	19.31	17.56	16.68	16.19	14.86	14.18	13.88	4.50 <sup>+0.09</sup> <sub>-0.08</sub>	6.04 <sup>+0.08</sup> <sub>-0.11</sub>	4.01 <sup>+0.09</sup> <sub>-0.09</sub>	16.10 <sup>+1.11</sup> <sub>-0.85</sub>	7.14	SUB/EM
5022	287.05378	-0.83533	15.74	15.41	13.69	12.61	13.27	10.44	9.79	9.44	4.57 <sup>+0.09</sup> <sub>-0.08</sub>	6.76 <sup>+0.05</sup> <sub>-0.07</sub>	4.28 <sup>+0.07</sup> <sub>-0.07</sub>	12.25 <sup>+1.10</sup> <sub>-0.95</sub>	2.67	–
5026	287.05763	1.42962	15.35	15.59	14.54	13.94	14.22	12.98	12.70	12.57	4.51 <sup>+0.10</sup> <sub>-0.07</sub>	3.72 <sup>+0.07</sup> <sub>-0.09</sub>	3.56 <sup>+0.10</sup> <sub>-0.09</sub>	15.16 <sup>+1.19</sup> <sub>-0.78</sub>	0.59	–
5036	287.06420	0.64763	20.46	19.90	17.95	16.71	17.55	14.22	13.20	12.74	4.48 <sup>+0.15</sup> <sub>-0.12</sub>	7.91 <sup>+0.12</sup> <sub>-0.18</sub>	4.65 <sup>+0.10</sup> <sub>-0.09</sub>	14.42 <sup>+1.75</sup> <sub>-1.18</sub>	3.09	–
5074	287.08172	-1.44573	12.64	13.11	12.28	11.73	11.89	10.72	10.45	10.29	4.51 <sup>+0.09</sup> <sub>-0.07</sub>	3.67 <sup>+0.07</sup> <sub>-0.08</sub>	4.25 <sup>+0.15</sup> <sub>-0.13</sub>	12.79 <sup>+1.06</sup> <sub>-0.74</sub>	1.73	–
5090	287.09109	-0.78824	19.94	19.31	17.32	16.10	16.48	13.63	12.89	12.49	4.51 <sup>+0.11</sup> <sub>-0.08</sub>	7.54 <sup>+0.07</sup> <sub>-0.10</sub>	4.23 <sup>+0.08</sup> <sub>-0.07</sub>	14.57 <sup>+1.36</sup> <sub>-0.85</sub>	2.63	EM
5104	287.09676	-3.13121	18.16	18.35	17.18	16.48	16.76	15.31	14.89	14.71	4.56 <sup>+0.09</sup> <sub>-0.08</sub>	4.38 <sup>+0.10</sup> <sub>-0.10</sub>	3.85 <sup>+0.14</sup> <sub>-0.13</sub>	17.80 <sup>+1.12</sup> <sub>-0.96</sub>	1.47	–
5123	287.10375	-0.48850	18.07	18.27	17.14	16.39	16.82	15.40	14.88	14.81	4.60 <sup>+0.07</sup> <sub>-0.08</sub>	4.27 <sup>+0.13</sup> <sub>-0.13</sub>	3.73 <sup>+0.15</sup> <sub>-0.15</sub>	18.32 <sup>+0.88</sup> <sub>-1.03</sub>	5.97	–
5153	287.12023	-0.40640	20.03	19.97	18.22	17.25	17.86	15.56	15.02	14.72	4.61 <sup>+0.06</sup> <sub>-0.09</sub>	5.84 <sup>+0.09</sup> <sub>-0.09</sub>	3.72 <sup>+0.10</sup> <sub>-0.10</sub>	18.27 <sup>+0.78</sup> <sub>-1.03</sub>	4.39	–
5157	287.12641	-2.67416	17.39	17.73	16.70	16.13	16.43	15.19	14.71	14.49	4.53 <sup>+0.09</sup> <sub>-0.07</sub>	3.93 <sup>+0.09</sup> <sub>-0.10</sub>	3.95 <sup>+0.15</sup> <sub>-0.14</sub>	17.29 <sup>+1.16</sup> <sub>-0.80</sub>	3.18	–
5219	287.15394	-1.76240	19.57	19.55	18.11	17.31	17.76	15.81	15.35	15.29	4.55 <sup>+0.09</sup> <sub>-0.09</sub>	5.08 <sup>+0.12</sup> <sub>-0.12</sub>	3.84 <sup>+0.13</sup> <sub>-0.13</sub>	17.96 <sup>+1.10</sup> <sub>-1.05</sub>	1.49	–
5312	287.20311	-0.45373	19.77	18.84	16.69	15.41	16.20	13.02	12.35	11.98	4.48 <sup>+0.12</sup> <sub>-0.10</sub>	7.42 <sup>+0.10</sup> <sub>-0.14</sub>	3.83 <sup>+0.06</sup> <sub>-0.06</sub>	13.80 <sup>+1.45</sup> <sub>-0.97</sub>	2.78	–
5321	287.20667	-0.83342	20.39	19.99	18.09	16.83	17.61	14.19	13.24	12.75	4.52 <sup>+0.12</sup> <sub>-0.12</sub>	8.11 <sup>+0.08</sup> <sub>-0.14</sub>	4.88 <sup>+0.10</sup> <sub>-0.09</sub>	14.85 <sup>+1.49</sup> <sub>-1.20</sub>	1.98	–
5342	287.21664	-3.16340	20.08	19.39	17.39	16.21	16.96	14.09	13.35	12.98	4.48 <sup>+0.12</sup> <sub>-0.11</sub>	6.95 <sup>+0.10</sup> <sub>-0.15</sub>	3.89 <sup>+0.07</sup> <sub>-0.07</sub>	14.86 <sup>+1.39</sup> <sub>-1.05</sub>	1.74	–
5359	287.22345	-1.66564	12.50	13.23	12.71	12.47	12.53	12.06	11.98	11.99	4.49 <sup>+0.08</sup> <sub>-0.06</sub>	2.07 <sup>+0.07</sup> <sub>-0.08</sub>	3.45 <sup>+0.16</sup> <sub>-0.14</sub>	14.42 <sup>+0.96</sup> <sub>-0.60</sub>	2.97	–
5365	287.22857	-0.78806	19.93	19.92	18.27	17.18	17.37	14.99	14.10	13.71	4.59 <sup>+0.08</sup> <sub>-0.10</sub>	7.09 <sup>+0.07</sup> <sub>-0.09</sub>	4.86 <sup>+0.12</sup> <sub>-0.11</sub>	16.73 <sup>+0.98</sup> <sub>-1.18</sub>	2.78	SUB/EM
5386	287.23804	-1.21419	20.11	19.80	18.00	17.08	17.24	15.08	14.34	13.99	4.48 <sup>+0.11</sup> <sub>-0.10</sub>	6.43 <sup>+0.10</sup> <sub>-0.14</sub>	4.19 <sup>+0.10</sup> <sub>-0.09</sub>	15.95 <sup>+1.23</sup> <sub>-0.98</sub>	6.55	SUB/EM
5433	287.26126	-3.32242	18.35	18.58	17.35	16.70	17.01	15.60	15.31	15.29	4.60 <sup>+0.06</sup> <sub>-0.07</sub>	4.12 <sup>+0.11</sup> <sub>-0.11</sub>	3.56 <sup>+0.13</sup> <sub>-0.13</sub>	18.73 <sup>+0.79</sup> <sub>-0.89</sub>	1.56	–
5440	287.26686	-0.21384	19.61	18.96	16.89	15.59	16.26	12.95	12.10	11.68	4.56 <sup>+0.09</sup> <sub>-0.09</sub>	8.07 <sup>+0.06</sup> <sub>-0.09</sub>	4.37 <sup>+0.07</sup> <sub>-0.07</sub>	14.24 <sup>+1.13</sup> <sub>-1.04</sub>	2.65	EM
5451	287.26987	-0.54177	19.39	18.37	16.05	14.57	15.60	11.74	10.85	10.32	4.51 <sup>+0.11</sup> <sub>-0.09</sub>	8.70 <sup>+0.08</sup> <sub>-0.11</sub>	4.19 <sup>+0.07</sup> <sub>-0.06</sub>	12.29 <sup>+1.34</sup> <sub>-0.92</sub>	3.22	–
5475	287.27820	-0.51156	20.67	19.42	16.96	15.44	16.50	12.63	11.76	11.31	4.54 <sup>+0.11</sup> <sub>-0.14</sub>	8.71 <sup>+0.08</sup> <sub>-0.16</sub>	3.92 <sup>+0.06</sup> <sub>-0.06</sub>	13.59 <sup>+1.41</sup> <sub>-1.50</sub>	4.00	–
5491	287.28450	0.14990	20.71	19.52	17.06	15.59	16.48	13.08	12.19	11.76	4.54 <sup>+0.11</sup> <sub>-0.12</sub>	8.25 <sup>+0.07</sup> <sub>-0.14</sub>	3.73 <sup>+0.05</sup> <sub>-0.05</sub>	14.14 <sup>+1.32</sup> <sub>-1.27</sub>	4.63	–
5525	287.30162	-0.32561	13.48	13.57	12.45	11.67	12.10	10.52	10.19	10.02	4.53 <sup>+0.10</sup> <sub>-0.08</sub>	4.28 <sup>+0.06</sup> <sub>-0.08</sub>	3.67 <sup>+0.09</sup> <sub>-0.08</sub>	12.77 <sup>+1.18</sup> <sub>-0.84</sub>	7.11	–
5570	287.33089	-0.27428	15.14	14.75	13.06	12.05	12.66	10.21	9.68	9.40	4.53 <sup>+0.10</sup> <sub>-0.08</sub>	6.00 <sup>+0.06</sup> <sub>-0.09</sub>	3.81 <sup>+0.07</sup> <sub>-0.06</sub>	11.86 <sup>+1.15</sup> <sub>-0.86</sub>	2.45	–
5577	287.33570	0.22728	20.87	19.69	17.25	15.76	16.81	13.29	12.51	12.08	4.55 <sup>+0.10</sup> <sub>-0.12</sub>	8.08 <sup>+0.07</sup> <sub>-0.13</sub>	3.62 <sup>+0.05</sup> <sub>-0.05</sub>	14.67 <sup>+1.23</sup> <sub>-1.32</sub>	4.50	–

Continued on next page...

ID	$\ell$	$b$	u	g	r	i	H $\alpha$	J	H	K	$\log(T_{\text{eff}})$	$A_0$	$R_V$	$\mu$	$\chi^2$	Notes
5614	287.35339	-0.56176	19.82	19.48	17.24	15.67	16.40	12.25	11.03	10.38	4.63 <sup>+0.05</sup> <sub>-0.07</sub>	10.14 <sup>+0.04</sup> <sub>-0.05</sub>	5.32 <sup>+0.05</sup> <sub>-0.07</sub>	13.59 <sup>+0.61</sup> <sub>-0.85</sub>	5.07	SUB/EM
5619	287.35586	0.46316	14.10	14.32	13.26	12.61	12.96	11.67	11.40	11.24	4.55 <sup>+0.09</sup> <sub>-0.08</sub>	3.78 <sup>+0.06</sup> <sub>-0.07</sub>	3.50 <sup>+0.09</sup> <sub>-0.08</sub>	14.27 <sup>+1.13</sup> <sub>-0.88</sub>	1.97	-
5648	287.37407	-3.28974	17.14	17.70	16.92	16.46	16.63	15.62	15.34	15.12	4.51 <sup>+0.09</sup> <sub>-0.07</sub>	3.34 <sup>+0.10</sup> <sub>-0.10</sub>	4.20 <sup>+0.22</sup> <sub>-0.19</sub>	17.80 <sup>+1.04</sup> <sub>-0.78</sub>	0.36	-
5728	287.40516	-0.16098	15.29	16.20	15.64	15.28	15.42	14.66	14.40	14.35	4.62 <sup>+0.05</sup> <sub>-0.07</sub>	2.86 <sup>+0.07</sup> <sub>-0.07</sub>	4.61 <sup>+0.20</sup> <sub>-0.19</sub>	18.26 <sup>+0.70</sup> <sub>-0.84</sub>	1.72	-
5744	287.40922	-1.44177	12.18	13.02	12.56	12.25	12.34	11.69	11.50	11.40	4.51 <sup>+0.10</sup> <sub>-0.07</sub>	2.56 <sup>+0.07</sup> <sub>-0.08</sub>	4.58 <sup>+0.27</sup> <sub>-0.22</sub>	14.08 <sup>+1.23</sup> <sub>-0.77</sub>	0.23	-
5751	287.41285	-0.64554	19.69	19.37	17.50	16.30	16.91	13.72	12.89	12.44	4.56 <sup>+0.09</sup> <sub>-0.10</sub>	7.81 <sup>+0.06</sup> <sub>-0.09</sub>	4.74 <sup>+0.09</sup> <sub>-0.08</sub>	15.07 <sup>+1.16</sup> <sub>-1.11</sub>	1.88	SUB/EM
5766	287.41911	-0.50301	20.44	19.95	18.08	16.90	17.73	14.50	13.71	13.31	4.50 <sup>+0.13</sup> <sub>-0.13</sub>	7.39 <sup>+0.10</sup> <sub>-0.17</sub>	4.45 <sup>+0.10</sup> <sub>-0.09</sub>	15.25 <sup>+1.56</sup> <sub>-1.26</sub>	1.02	-
5790	287.42909	-0.97388	13.91	14.33	13.49	12.93	13.15	11.97	11.65	11.52	4.48 <sup>+0.08</sup> <sub>-0.06</sub>	3.63 <sup>+0.08</sup> <sub>-0.08</sub>	4.18 <sup>+0.15</sup> <sub>-0.14</sub>	13.71 <sup>+0.95</sup> <sub>-0.62</sub>	1.63	-
5798	287.43288	-1.68184	14.00	14.53	13.76	13.37	13.48	12.71	12.55	12.46	4.50 <sup>+0.09</sup> <sub>-0.07</sub>	2.82 <sup>+0.08</sup> <sub>-0.09</sub>	3.55 <sup>+0.13</sup> <sub>-0.11</sub>	14.97 <sup>+1.11</sup> <sub>-0.70</sub>	0.66	-
5831	287.44158	-0.95909	15.75	16.14	15.13	14.56	14.90	13.25	12.90	12.69	4.49 <sup>+0.09</sup> <sub>-0.07</sub>	4.30 <sup>+0.09</sup> <sub>-0.09</sub>	4.55 <sup>+0.17</sup> <sub>-0.15</sub>	14.85 <sup>+1.06</sup> <sub>-0.69</sub>	1.25	-
5839	287.44443	-0.55023	19.62	19.77	18.28	17.37	18.74	15.53	14.55	14.18	4.56 <sup>+0.09</sup> <sub>-0.10</sub>	6.43 <sup>+0.10</sup> <sub>-0.11</sub>	4.99 <sup>+0.15</sup> <sub>-0.14</sub>	16.96 <sup>+1.18</sup> <sub>-1.16</sub>	6.42	-
5843	287.44613	-0.38631	16.95	16.66	14.97	13.86	14.58	11.68	10.97	10.60	4.57 <sup>+0.09</sup> <sub>-0.10</sub>	6.88 <sup>+0.06</sup> <sub>-0.08</sub>	4.42 <sup>+0.08</sup> <sub>-0.07</sub>	13.44 <sup>+1.12</sup> <sub>-1.10</sub>	3.10	-
5850	287.45117	-2.17365	19.89	19.96	18.45	17.59	18.05	16.28	15.56	15.44	4.60 <sup>+0.05</sup> <sub>-0.08</sub>	5.22 <sup>+0.13</sup> <sub>-0.13</sub>	3.78 <sup>+0.14</sup> <sub>-0.13</sub>	18.90 <sup>+0.68</sup> <sub>-0.96</sub>	4.85	-
5859	287.45320	-0.43955	17.54	16.97	15.09	13.94	14.72	11.80	11.17	10.87	4.54 <sup>+0.09</sup> <sub>-0.08</sub>	6.78 <sup>+0.06</sup> <sub>-0.08</sub>	3.90 <sup>+0.06</sup> <sub>-0.06</sub>	13.39 <sup>+1.16</sup> <sub>-0.84</sub>	4.62	-
5865	287.45560	0.06016	19.79	18.72	16.40	15.03	15.98	12.64	11.94	11.60	4.57 <sup>+0.09</sup> <sub>-0.09</sub>	7.64 <sup>+0.06</sup> <sub>-0.09</sub>	3.59 <sup>+0.05</sup> <sub>-0.05</sub>	14.37 <sup>+1.12</sup> <sub>-1.05</sub>	4.36	-
5873	287.45916	0.22214	20.83	19.93	17.72	16.44	17.33	14.04	13.21	12.76	4.50 <sup>+0.13</sup> <sub>-0.12</sub>	7.72 <sup>+0.09</sup> <sub>-0.16</sub>	3.96 <sup>+0.07</sup> <sub>-0.07</sub>	14.77 <sup>+1.60</sup> <sub>-1.20</sub>	2.20	-
5901	287.46892	-0.29321	20.39	19.94	18.23	17.19	17.65	15.36	14.60	14.39	4.48 <sup>+0.13</sup> <sub>-0.11</sub>	6.22 <sup>+0.12</sup> <sub>-0.16</sub>	4.00 <sup>+0.10</sup> <sub>-0.10</sub>	16.30 <sup>+1.52</sup> <sub>-1.07</sub>	4.73	SUB/EM
5944	287.48562	0.47270	14.85	14.87	13.65	12.89	13.33	11.65	11.29	11.11	4.49 <sup>+0.11</sup> <sub>-0.07</sub>	4.43 <sup>+0.08</sup> <sub>-0.09</sub>	3.69 <sup>+0.09</sup> <sub>-0.09</sub>	13.32 <sup>+1.28</sup> <sub>-0.71</sub>	2.36	-
5956	287.49210	-0.66900	19.65	19.42	17.71	16.64	17.20	14.65	13.81	13.54	4.58 <sup>+0.08</sup> <sub>-0.11</sub>	6.67 <sup>+0.07</sup> <sub>-0.10</sub>	4.32 <sup>+0.11</sup> <sub>-0.11</sub>	16.50 <sup>+1.03</sup> <sub>-1.28</sub>	5.14	-
5961	287.49471	-1.32610	12.37	13.17	12.63	12.35	12.45	11.84	11.72	11.66	4.55 <sup>+0.08</sup> <sub>-0.07</sub>	2.40 <sup>+0.06</sup> <sub>-0.07</sub>	3.89 <sup>+0.18</sup> <sub>-0.16</sub>	14.81 <sup>+1.02</sup> <sub>-0.82</sub>	0.94	-
6002	287.51036	-0.83807	19.88	19.63	17.96	17.01	17.24	15.14	14.39	14.19	4.51 <sup>+0.12</sup> <sub>-0.11</sub>	6.21 <sup>+0.09</sup> <sub>-0.14</sub>	4.18 <sup>+0.10</sup> <sub>-0.09</sub>	16.40 <sup>+1.40</sup> <sub>-1.13</sub>	4.90	SUB/EM
6019	287.51625	1.22528	19.54	19.59	18.11	17.30	17.80	15.90	15.27	15.22	4.61 <sup>+0.06</sup> <sub>-0.08</sub>	5.15 <sup>+0.11</sup> <sub>-0.11</sub>	3.82 <sup>+0.12</sup> <sub>-0.11</sub>	18.64 <sup>+0.82</sup> <sub>-0.97</sub>	4.18	-
6036	287.52219	-0.73213	19.85	19.34	17.40	16.26	17.12	14.07	13.44	13.02	4.52 <sup>+0.11</sup> <sub>-0.11</sub>	6.92 <sup>+0.07</sup> <sub>-0.13</sub>	3.99 <sup>+0.08</sup> <sub>-0.08</sub>	15.37 <sup>+1.34</sup> <sub>-1.14</sub>	1.43	-
6054	287.53232	-0.86044	19.28	19.25	17.68	16.70	16.81	14.53	13.90	13.58	4.57 <sup>+0.09</sup> <sub>-0.10</sub>	6.58 <sup>+0.07</sup> <sub>-0.09</sub>	4.69 <sup>+0.10</sup> <sub>-0.10</sub>	16.42 <sup>+1.10</sup> <sub>-1.09</sub>	3.08	SUB/EM
6071	287.53972	-0.52833	15.30	15.61	14.61	13.98	14.34	12.77	12.39	12.22	4.50 <sup>+0.10</sup> <sub>-0.07</sub>	4.23 <sup>+0.07</sup> <sub>-0.09</sub>	4.28 <sup>+0.14</sup> <sub>-0.13</sub>	14.54 <sup>+1.12</sup> <sub>-0.73</sub>	0.99	-
6118	287.56277	0.66649	15.23	15.32	14.13	13.43	13.78	12.34	12.00	11.81	4.51 <sup>+0.09</sup> <sub>-0.07</sub>	4.16 <sup>+0.07</sup> <sub>-0.09</sub>	3.58 <sup>+0.09</sup> <sub>-0.08</sub>	14.34 <sup>+1.11</sup> <sub>-0.77</sub>	1.14	-
6124	287.56532	-0.09674	17.29	16.42	14.32	13.04	13.88	10.87	10.22	9.85	4.50 <sup>+0.10</sup> <sub>-0.07</sub>	7.08 <sup>+0.08</sup> <sub>-0.09</sub>	3.67 <sup>+0.06</sup> <sub>-0.05</sub>	11.96 <sup>+1.19</sup> <sub>-0.78</sub>	3.33	-
6143	287.57556	0.28728	14.81	14.74	13.32	12.46	12.98	11.06	10.65	10.41	4.58 <sup>+0.08</sup> <sub>-0.08</sub>	5.00 <sup>+0.05</sup> <sub>-0.06</sub>	3.67 <sup>+0.07</sup> <sub>-0.07</sub>	13.66 <sup>+1.00</sup> <sub>-0.93</sub>	1.47	-
6157	287.58605	-0.94097	16.22	16.88	16.17	15.63	15.78	14.16	13.93	13.81	4.58 <sup>+0.08</sup> <sub>-0.07</sub>	4.13 <sup>+0.09</sup> <sub>-0.10</sub>	5.30 <sup>+0.07</sup> <sub>-0.13</sub>	17.03 <sup>+1.00</sup> <sub>-0.82</sub>	7.19	-
6171	287.59023	1.15270	17.51	17.66	16.56	15.91	16.21	14.86	14.55	14.46	4.50 <sup>+0.09</sup> <sub>-0.07</sub>	3.91 <sup>+0.10</sup> <sub>-0.11</sub>	3.57 <sup>+0.13</sup> <sub>-0.13</sub>	16.86 <sup>+1.07</sup> <sub>-0.78</sub>	1.04	-
6186	287.59442	-0.83807	19.75	19.55	17.93	17.10	16.80	15.28	14.74	14.65	4.48 <sup>+0.11</sup> <sub>-0.09</sub>	5.68 <sup>+0.12</sup> <sub>-0.14</sub>	4.01 <sup>+0.12</sup> <sub>-0.12</sub>	16.46 <sup>+1.31</sup> <sub>-0.90</sub>	4.94	SUB/EM
6235	287.61773	-0.69090	19.96	19.86	18.29	17.26	17.38	15.07	14.48	14.22	4.55 <sup>+0.10</sup> <sub>-0.13</sub>	6.57 <sup>+0.10</sup> <sub>-0.13</sub>	4.59 <sup>+0.15</sup> <sub>-0.13</sub>	16.77 <sup>+1.26</sup> <sub>-1.38</sub>	4.38	SUB/EM
6266	287.62797	-0.20789	13.75	14.10	13.20	12.67	12.94	11.78	11.55	11.43	4.49 <sup>+0.09</sup> <sub>-0.06</sub>	3.42 <sup>+0.08</sup> <sub>-0.08</sub>	3.70 <sup>+0.12</sup> <sub>-0.11</sub>	13.76 <sup>+0.99</sup> <sub>-0.66</sub>	0.85	-

Continued on next page...

ID	$\ell$	$b$	u	g	r	i	H $\alpha$	J	H	K	log( $T_{\text{eff}}$ )	$A_0$	$R_V$	$\mu$	$\chi^2$	Notes
6336	287.65593	-0.26291	20.60	19.93	17.81	16.53	17.30	14.10	13.35	12.92	4.55 <sup>+0.11</sup> <sub>-0.12</sub>	7.64 <sup>+0.08</sup> <sub>-0.13</sub>	4.05 <sup>+0.08</sup> <sub>-0.08</sub>	15.43 <sup>+1.33</sup> <sub>-1.29</sub>	1.30	-
6391	287.67357	-0.67477	19.18	18.92	17.07	15.74	16.68	13.07	12.11	11.57	4.60 <sup>+0.07</sup> <sub>-0.08</sub>	8.30 <sup>+0.05</sup> <sub>-0.06</sub>	5.03 <sup>+0.08</sup> <sub>-0.07</sub>	14.63 <sup>+0.87</sup> <sub>-1.01</sub>	6.91	-
6428	287.68516	-2.04547	14.27	14.87	14.20	13.79	13.96	13.21	13.05	13.02	4.53 <sup>+0.09</sup> <sub>-0.08</sub>	2.68 <sup>+0.07</sup> <sub>-0.08</sub>	3.57 <sup>+0.14</sup> <sub>-0.12</sub>	15.88 <sup>+1.15</sup> <sub>-0.84</sub>	1.67	-
6458	287.69556	0.42487	14.01	14.39	13.51	12.95	13.24	12.10	11.88	11.73	4.53 <sup>+0.10</sup> <sub>-0.08</sub>	3.42 <sup>+0.07</sup> <sub>-0.08</sub>	3.67 <sup>+0.11</sup> <sub>-0.10</sub>	14.55 <sup>+1.24</sup> <sub>-0.87</sub>	1.68	-
6480	287.70478	-0.68509	16.74	16.16	13.96	12.59	13.49	9.76	8.88	8.33	4.62 <sup>+0.05</sup> <sub>-0.07</sub>	8.62 <sup>+0.04</sup> <sub>-0.05</sub>	4.53 <sup>+0.05</sup> <sub>-0.05</sub>	11.66 <sup>+0.68</sup> <sub>-0.84</sub>	3.46	-
6489	287.70677	-0.39850	20.37	19.36	17.15	15.84	16.72	13.41	12.63	12.29	4.48 <sup>+0.12</sup> <sub>-0.11</sub>	7.63 <sup>+0.10</sup> <sub>-0.17</sub>	3.85 <sup>+0.06</sup> <sub>-0.06</sub>	14.04 <sup>+1.43</sup> <sub>-1.09</sub>	3.38	-
6500	287.70958	0.41365	13.42	13.74	12.85	12.27	12.57	11.46	11.21	11.09	4.50 <sup>+0.09</sup> <sub>-0.07</sub>	3.39 <sup>+0.07</sup> <sub>-0.09</sub>	3.58 <sup>+0.11</sup> <sub>-0.10</sub>	13.58 <sup>+1.09</sup> <sub>-0.72</sub>	2.58	-
6513	287.71471	-0.23120	13.36	13.59	12.58	11.93	12.27	10.99	10.71	10.56	4.50 <sup>+0.08</sup> <sub>-0.07</sub>	3.73 <sup>+0.07</sup> <sub>-0.08</sub>	3.59 <sup>+0.10</sup> <sub>-0.09</sub>	13.02 <sup>+0.99</sup> <sub>-0.70</sub>	2.60	-
6566	287.73580	-0.69971	16.91	16.49	14.74	13.66	14.32	11.59	10.94	10.56	4.48 <sup>+0.09</sup> <sub>-0.06</sub>	6.59 <sup>+0.08</sup> <sub>-0.09</sub>	4.17 <sup>+0.08</sup> <sub>-0.08</sub>	12.41 <sup>+1.01</sup> <sub>-0.65</sub>	0.79	-
6577	287.73980	0.35342	15.60	15.12	13.45	12.45	13.07	10.88	10.45	10.19	4.48 <sup>+0.10</sup> <sub>-0.07</sub>	5.42 <sup>+0.08</sup> <sub>-0.10</sub>	3.43 <sup>+0.06</sup> <sub>-0.06</sub>	12.23 <sup>+1.12</sup> <sub>-0.70</sub>	3.20	-
6584	287.74256	-3.62010	16.60	17.45	16.94	16.60	16.67	15.93	15.78	15.47	4.53 <sup>+0.07</sup> <sub>-0.07</sub>	2.83 <sup>+0.12</sup> <sub>-0.13</sub>	4.87 <sup>+0.30</sup> <sub>-0.31</sub>	18.46 <sup>+0.91</sup> <sub>-0.77</sub>	1.13	-
6603	287.75109	0.94079	15.74	15.66	14.25	13.43	13.87	11.90	11.49	11.25	4.52 <sup>+0.09</sup> <sub>-0.07</sub>	5.09 <sup>+0.07</sup> <sub>-0.08</sub>	3.84 <sup>+0.08</sup> <sub>-0.08</sub>	13.71 <sup>+1.11</sup> <sub>-0.77</sub>	1.52	-
6666	287.77523	0.09986	18.14	18.47	17.23	16.57	16.88	15.40	14.84	14.75	4.62 <sup>+0.05</sup> <sub>-0.07</sub>	4.51 <sup>+0.09</sup> <sub>-0.09</sub>	3.98 <sup>+0.12</sup> <sub>-0.12</sub>	18.54 <sup>+0.66</sup> <sub>-0.84</sub>	5.79	-
6720	287.79994	-0.88845	14.91	14.96	13.48	12.50	13.11	10.55	9.90	9.57	4.62 <sup>+0.06</sup> <sub>-0.08</sub>	6.28 <sup>+0.04</sup> <sub>-0.05</sub>	4.62 <sup>+0.08</sup> <sub>-0.07</sub>	13.05 <sup>+0.78</sup> <sub>-0.95</sub>	2.20	-
6738	287.80847	-1.00688	20.03	19.97	18.39	17.48	17.78	15.48	14.88	14.39	4.51 <sup>+0.12</sup> <sub>-0.11</sub>	6.26 <sup>+0.14</sup> <sub>-0.16</sub>	4.55 <sup>+0.17</sup> <sub>-0.16</sub>	16.64 <sup>+1.50</sup> <sub>-1.17</sub>	1.48	SUB/EM
6808	287.84112	-1.03083	19.85	19.88	18.54	17.77	nan	16.33	15.97	15.20	4.48 <sup>+0.12</sup> <sub>-0.10</sub>	5.09 <sup>+0.16</sup> <sub>-0.18</sub>	4.18 <sup>+0.19</sup> <sub>-0.18</sub>	17.56 <sup>+1.36</sup> <sub>-1.05</sub>	4.85	-
6815	287.84306	-1.41284	18.75	19.24	18.07	17.41	17.68	15.74	15.29	14.73	4.59 <sup>+0.07</sup> <sub>-0.07</sub>	5.32 <sup>+0.10</sup> <sub>-0.10</sub>	5.17 <sup>+0.14</sup> <sub>-0.15</sub>	18.11 <sup>+0.92</sup> <sub>-0.89</sub>	5.41	-
6942	287.88987	-0.52276	18.91	19.12	17.86	17.02	17.30	15.42	14.79	14.74	4.60 <sup>+0.07</sup> <sub>-0.09</sub>	5.38 <sup>+0.13</sup> <sub>-0.13</sub>	4.52 <sup>+0.17</sup> <sub>-0.16</sub>	17.98 <sup>+0.93</sup> <sub>-1.13</sub>	3.03	-
7023	287.92084	-1.44939	16.87	16.86	15.52	14.70	15.20	13.33	12.90	12.65	4.54 <sup>+0.10</sup> <sub>-0.08</sub>	4.89 <sup>+0.06</sup> <sub>-0.08</sub>	3.81 <sup>+0.09</sup> <sub>-0.08</sub>	15.44 <sup>+1.18</sup> <sub>-0.87</sub>	1.14	-
7032	287.92453	-0.93498	19.81	19.83	18.26	17.41	17.25	15.49	14.95	14.45	4.53 <sup>+0.10</sup> <sub>-0.09</sub>	6.04 <sup>+0.10</sup> <sub>-0.11</sub>	4.45 <sup>+0.13</sup> <sub>-0.12</sub>	17.04 <sup>+1.19</sup> <sub>-1.01</sub>	4.45	SUB/EM
7040	287.92784	-0.07751	19.36	18.94	17.29	16.20	16.94	14.46	13.88	13.63	4.55 <sup>+0.10</sup> <sub>-0.09</sub>	5.97 <sup>+0.07</sup> <sub>-0.10</sub>	3.76 <sup>+0.08</sup> <sub>-0.07</sub>	16.32 <sup>+1.23</sup> <sub>-1.05</sub>	7.67	-
7052	287.93327	-0.97834	20.54	19.90	17.82	16.45	17.14	13.69	12.89	12.36	4.57 <sup>+0.09</sup> <sub>-0.11</sub>	8.34 <sup>+0.06</sup> <sub>-0.10</sub>	4.46 <sup>+0.08</sup> <sub>-0.08</sub>	15.01 <sup>+1.15</sup> <sub>-1.23</sub>	5.64	EM
7073	287.94191	-1.26715	13.76	14.25	13.39	12.88	13.12	11.97	11.66	11.49	4.52 <sup>+0.09</sup> <sub>-0.07</sub>	3.58 <sup>+0.06</sup> <sub>-0.08</sub>	4.14 <sup>+0.13</sup> <sub>-0.12</sub>	14.15 <sup>+1.06</sup> <sub>-0.73</sub>	0.91	-
7075	287.94292	-0.06395	19.99	19.74	18.10	17.22	17.70	15.80	15.12	14.99	4.54 <sup>+0.10</sup> <sub>-0.10</sub>	5.32 <sup>+0.13</sup> <sub>-0.14</sub>	3.56 <sup>+0.12</sup> <sub>-0.11</sub>	17.76 <sup>+1.27</sup> <sub>-1.15</sub>	2.79	-
7127	287.96709	1.39013	13.52	14.01	13.20	12.65	12.91	12.00	11.87	11.72	4.61 <sup>+0.06</sup> <sub>-0.08</sub>	3.03 <sup>+0.05</sup> <sub>-0.06</sub>	3.39 <sup>+0.10</sup> <sub>-0.09</sub>	15.50 <sup>+0.83</sup> <sub>-0.96</sub>	5.04	-
7152	287.97780	-1.41257	17.21	17.02	15.41	14.44	15.04	12.70	12.18	11.89	4.61 <sup>+0.06</sup> <sub>-0.08</sub>	5.83 <sup>+0.05</sup> <sub>-0.06</sub>	3.90 <sup>+0.07</sup> <sub>-0.06</sub>	15.33 <sup>+0.84</sup> <sub>-0.92</sub>	1.06	-
7279	288.03050	-0.68621	19.43	18.96	16.98	15.95	16.48	13.86	13.23	12.84	4.56 <sup>+0.09</sup> <sub>-0.08</sub>	6.71 <sup>+0.06</sup> <sub>-0.08</sub>	3.89 <sup>+0.07</sup> <sub>-0.07</sub>	15.60 <sup>+1.07</sup> <sub>-0.94</sub>	4.16	EM
7321	288.04411	1.16301	17.74	18.04	16.99	16.34	16.72	15.21	14.75	14.91	4.55 <sup>+0.09</sup> <sub>-0.08</sub>	4.19 <sup>+0.09</sup> <sub>-0.09</sub>	4.05 <sup>+0.15</sup> <sub>-0.14</sub>	17.55 <sup>+1.14</sup> <sub>-0.92</sub>	6.03	-
7325	288.04560	-1.31315	12.81	13.37	12.64	12.16	12.36	11.27	10.97	10.84	4.48 <sup>+0.09</sup> <sub>-0.06</sub>	3.40 <sup>+0.08</sup> <sub>-0.09</sub>	4.43 <sup>+0.17</sup> <sub>-0.15</sub>	13.07 <sup>+0.97</sup> <sub>-0.67</sub>	1.04	-
7354	288.05795	-0.69545	19.13	18.50	16.56	15.41	16.16	13.36	12.64	12.39	4.54 <sup>+0.10</sup> <sub>-0.09</sub>	6.75 <sup>+0.06</sup> <sub>-0.09</sub>	3.80 <sup>+0.06</sup> <sub>-0.06</sub>	14.92 <sup>+1.19</sup> <sub>-0.97</sub>	7.13	-
7383	288.07156	0.60340	20.24	19.92	18.20	17.29	17.93	15.76	15.01	14.96	4.53 <sup>+0.11</sup> <sub>-0.11</sub>	5.57 <sup>+0.12</sup> <sub>-0.14</sub>	3.62 <sup>+0.11</sup> <sub>-0.10</sub>	17.45 <sup>+1.37</sup> <sub>-1.19</sub>	6.33	-
7387	288.07482	-1.64232	16.25	16.28	14.95	14.19	14.52	12.80	12.35	12.14	4.52 <sup>+0.09</sup> <sub>-0.07</sub>	4.84 <sup>+0.07</sup> <sub>-0.08</sub>	3.88 <sup>+0.09</sup> <sub>-0.08</sub>	14.66 <sup>+1.09</sup> <sub>-0.77</sub>	0.63	-
7409	288.09097	-0.41842	16.41	16.98	16.03	15.45	15.75	14.40	13.97	13.82	4.63 <sup>+0.05</sup> <sub>-0.07</sub>	4.06 <sup>+0.07</sup> <sub>-0.08</sub>	4.43 <sup>+0.14</sup> <sub>-0.13</sub>	17.67 <sup>+0.67</sup> <sub>-0.85</sub>	2.27	-

Continued on next page...

ID	$\ell$	$b$	u	g	r	i	H $\alpha$	J	H	K	$\log(T_{\text{eff}})$	$A_0$	$R_V$	$\mu$	$\chi^2$	Notes
7418	288.09754	-0.64311	20.11	19.43	17.38	16.11	16.84	13.69	12.97	12.53	4.54 <sup>+0.11</sup> <sub>-0.12</sub>	7.56 <sup>+0.08</sup> <sub>-0.14</sub>	4.10 <sup>+0.07</sup> <sub>-0.07</sub>	14.92 <sup>+1.35</sup> <sub>-1.27</sub>	2.56	–
7429	288.10173	-0.76245	20.45	19.63	17.45	16.15	17.02	13.58	12.80	12.43	4.53 <sup>+0.11</sup> <sub>-0.12</sub>	7.88 <sup>+0.07</sup> <sub>-0.13</sub>	4.04 <sup>+0.07</sup> <sub>-0.06</sub>	14.74 <sup>+1.31</sup> <sub>-1.23</sub>	4.25	–
7441	288.10864	-1.01871	20.23	19.84	18.14	17.14	17.51	15.73	15.10	14.82	4.56 <sup>+0.09</sup> <sub>-0.11</sub>	5.48 <sup>+0.12</sup> <sub>-0.14</sub>	3.42 <sup>+0.11</sup> <sub>-0.10</sub>	17.84 <sup>+1.16</sup> <sub>-1.27</sub>	5.29	SUB/EM
7449	288.11287	-2.90224	15.72	16.38	15.80	15.44	15.54	14.97	14.76	15.04	4.51 <sup>+0.09</sup> <sub>-0.07</sub>	2.41 <sup>+0.10</sup> <sub>-0.10</sub>	3.54 <sup>+0.24</sup> <sub>-0.21</sub>	17.48 <sup>+1.14</sup> <sub>-0.76</sub>	3.40	–
7497	288.13587	-0.23050	13.73	14.08	13.18	12.67	12.92	11.78	11.58	11.45	4.48 <sup>+0.08</sup> <sub>-0.06</sub>	3.35 <sup>+0.08</sup> <sub>-0.08</sub>	3.65 <sup>+0.11</sup> <sub>-0.10</sub>	13.70 <sup>+0.93</sup> <sub>-0.61</sub>	1.33	–
7502	288.13764	-1.27220	14.21	14.42	13.34	12.64	13.05	11.42	11.02	10.84	4.51 <sup>+0.10</sup> <sub>-0.07</sub>	4.36 <sup>+0.07</sup> <sub>-0.09</sub>	4.07 <sup>+0.11</sup> <sub>-0.10</sub>	13.28 <sup>+1.18</sup> <sub>-0.78</sub>	2.16	–
7531	288.15206	-0.50610	16.43	16.87	15.82	15.18	15.53	13.79	13.39	13.31	4.61 <sup>+0.06</sup> <sub>-0.08</sub>	4.49 <sup>+0.08</sup> <sub>-0.08</sub>	4.47 <sup>+0.13</sup> <sub>-0.12</sub>	16.91 <sup>+0.77</sup> <sub>-0.99</sub>	2.66	–
7547	288.16019	-3.10146	13.49	14.26	13.84	13.62	13.63	13.35	13.34	13.43	4.49 <sup>+0.10</sup> <sub>-0.07</sub>	1.72 <sup>+0.08</sup> <sub>-0.09</sub>	3.13 <sup>+0.17</sup> <sub>-0.15</sub>	15.93 <sup>+1.20</sup> <sub>-0.70</sub>	5.76	–
7688	288.22981	-1.15233	16.37	16.33	14.75	13.68	14.38	11.34	10.51	10.06	4.51 <sup>+0.10</sup> <sub>-0.07</sub>	7.20 <sup>+0.07</sup> <sub>-0.09</sub>	5.14 <sup>+0.11</sup> <sub>-0.10</sub>	12.18 <sup>+1.22</sup> <sub>-0.80</sub>	1.22	–
7689	288.23212	-1.11675	20.42	19.07	16.40	14.67	15.90	11.36	10.23	9.60	4.51 <sup>+0.12</sup> <sub>-0.13</sub>	10.13 <sup>+0.09</sup> <sub>-0.17</sub>	4.32 <sup>+0.06</sup> <sub>-0.06</sub>	11.40 <sup>+1.45</sup> <sub>-1.33</sub>	5.29	–
7764	288.26927	-2.17969	18.03	18.21	17.11	16.51	16.79	15.59	15.29	15.18	4.52 <sup>+0.09</sup> <sub>-0.08</sub>	3.67 <sup>+0.11</sup> <sub>-0.12</sub>	3.39 <sup>+0.15</sup> <sub>-0.14</sub>	17.82 <sup>+1.11</sup> <sub>-0.85</sub>	0.38	–
7822	288.29954	-0.70407	16.76	16.57	15.05	14.16	14.65	12.46	11.87	11.62	4.48 <sup>+0.08</sup> <sub>-0.06</sub>	5.64 <sup>+0.09</sup> <sub>-0.09</sub>	4.06 <sup>+0.08</sup> <sub>-0.08</sub>	13.58 <sup>+0.95</sup> <sub>-0.63</sub>	2.33	–
7868	288.32421	-0.44436	18.40	18.58	17.27	16.53	16.96	15.24	14.65	14.36	4.60 <sup>+0.07</sup> <sub>-0.08</sub>	4.90 <sup>+0.08</sup> <sub>-0.08</sub>	4.05 <sup>+0.11</sup> <sub>-0.11</sub>	17.90 <sup>+0.85</sup> <sub>-0.95</sub>	5.35	–
7896	288.33671	0.06897	13.42	13.94	13.27	12.86	13.05	12.34	12.19	12.13	4.48 <sup>+0.09</sup> <sub>-0.06</sub>	2.55 <sup>+0.08</sup> <sub>-0.09</sub>	3.39 <sup>+0.13</sup> <sub>-0.12</sub>	14.45 <sup>+1.00</sup> <sub>-0.64</sub>	1.00	–
7906	288.33908	0.61633	18.68	18.74	17.25	16.33	16.88	14.67	14.07	13.91	4.63 <sup>+0.05</sup> <sub>-0.06</sub>	5.67 <sup>+0.08</sup> <sub>-0.08</sub>	4.15 <sup>+0.10</sup> <sub>-0.09</sub>	17.60 <sup>+0.63</sup> <sub>-0.82</sub>	3.42	–
7952	288.35967	0.30449	12.39	13.08	12.59	12.18	12.32	11.83	11.70	11.64	4.53 <sup>+0.09</sup> <sub>-0.07</sub>	2.28 <sup>+0.06</sup> <sub>-0.08</sub>	3.49 <sup>+0.16</sup> <sub>-0.13</sub>	14.57 <sup>+1.10</sup> <sub>-0.81</sub>	6.40	–
7958	288.36301	-1.17115	13.99	14.46	13.64	13.10	13.38	12.26	11.99	11.88	4.55 <sup>+0.09</sup> <sub>-0.08</sub>	3.42 <sup>+0.05</sup> <sub>-0.08</sub>	3.89 <sup>+0.12</sup> <sub>-0.11</sub>	14.94 <sup>+1.15</sup> <sub>-0.89</sub>	1.63	–
7967	288.36593	-0.92344	19.00	19.04	17.70	16.86	17.32	15.21	14.60	14.18	4.48 <sup>+0.10</sup> <sub>-0.08</sub>	5.62 <sup>+0.11</sup> <sub>-0.11</sub>	4.58 <sup>+0.16</sup> <sub>-0.14</sub>	16.21 <sup>+1.22</sup> <sub>-0.82</sub>	1.28	–
7973	288.36948	-0.24718	20.39	19.59	17.57	16.41	17.19	14.35	13.76	13.48	4.49 <sup>+0.12</sup> <sub>-0.09</sub>	6.62 <sup>+0.09</sup> <sub>-0.13</sub>	3.59 <sup>+0.06</sup> <sub>-0.06</sub>	15.49 <sup>+1.41</sup> <sub>-0.96</sub>	2.85	–
7994	288.38059	-0.37732	13.56	13.94	12.97	12.41	12.69	11.51	11.23	11.09	4.55 <sup>+0.09</sup> <sub>-0.07</sub>	3.61 <sup>+0.06</sup> <sub>-0.07</sub>	3.70 <sup>+0.10</sup> <sub>-0.09</sub>	14.14 <sup>+1.06</sup> <sub>-0.81</sub>	0.41	–
8082	288.43128	0.37089	13.47	13.76	12.77	12.14	12.44	11.26	10.97	10.84	4.56 <sup>+0.06</sup> <sub>-0.08</sub>	3.65 <sup>+0.06</sup> <sub>-0.08</sub>	3.56 <sup>+0.11</sup> <sub>-0.09</sub>	13.94 <sup>+1.14</sup> <sub>-0.96</sub>	3.21	–
8101	288.44562	0.13668	16.69	17.42	16.72	16.25	16.63	15.41	15.13	15.05	4.60 <sup>+0.16</sup> <sub>-0.09</sub>	3.40 <sup>+0.16</sup> <sub>-0.16</sub>	4.57 <sup>+0.30</sup> <sub>-0.29</sub>	18.63 <sup>+0.85</sup> <sub>-1.10</sub>	0.99	–
8183	288.49038	0.02867	13.60	14.16	13.53	13.13	13.32	12.64	12.53	12.50	4.48 <sup>+0.09</sup> <sub>-0.06</sub>	2.42 <sup>+0.08</sup> <sub>-0.09</sub>	3.32 <sup>+0.13</sup> <sub>-0.12</sub>	14.87 <sup>+1.02</sup> <sub>-0.64</sub>	2.02	–
8231	288.51906	0.02261	12.47	13.12	12.56	12.23	12.36	11.74	11.61	11.60	4.49 <sup>+0.09</sup> <sub>-0.06</sub>	2.35 <sup>+0.08</sup> <sub>-0.08</sub>	3.58 <sup>+0.17</sup> <sub>-0.14</sub>	14.02 <sup>+1.06</sup> <sub>-0.64</sub>	1.43	–
8287	288.54951	0.32516	19.67	19.30	17.61	16.60	17.23	14.94	14.32	14.13	4.56 <sup>+0.09</sup> <sub>-0.10</sub>	5.82 <sup>+0.07</sup> <sub>-0.09</sub>	3.69 <sup>+0.08</sup> <sub>-0.08</sub>	17.04 <sup>+1.16</sup> <sub>-1.08</sub>	3.91	–
8357	288.59280	-0.17019	18.14	17.81	16.16	15.19	15.78	13.40	12.84	12.60	4.51 <sup>+0.09</sup> <sub>-0.07</sub>	5.89 <sup>+0.07</sup> <sub>-0.09</sub>	3.87 <sup>+0.08</sup> <sub>-0.07</sub>	14.80 <sup>+1.12</sup> <sub>-0.75</sub>	2.34	–
8379	288.60918	0.03411	19.46	19.82	18.43	17.62	18.11	15.82	15.35	15.18	4.63 <sup>+0.05</sup> <sub>-0.07</sub>	5.71 <sup>+0.11</sup> <sub>-0.11</sub>	4.71 <sup>+0.15</sup> <sub>-0.13</sub>	18.69 <sup>+0.64</sup> <sub>-0.82</sub>	7.49	–
8416	288.63797	-1.04164	13.87	13.87	12.54	11.82	12.21	10.52	10.16	9.91	4.48 <sup>+0.08</sup> <sub>-0.06</sub>	4.56 <sup>+0.08</sup> <sub>-0.09</sub>	3.70 <sup>+0.09</sup> <sub>-0.08</sub>	12.09 <sup>+0.97</sup> <sub>-0.67</sub>	1.21	–
8475	288.67110	-2.55571	14.54	15.15	14.51	14.14	14.26	13.59	13.43	13.38	4.49 <sup>+0.09</sup> <sub>-0.06</sub>	2.57 <sup>+0.08</sup> <sub>-0.09</sub>	3.63 <sup>+0.16</sup> <sub>-0.15</sub>	15.80 <sup>+1.02</sup> <sub>-0.64</sub>	0.32	–
8551	288.71077	-2.06787	16.15	16.90	16.33	15.96	16.08	15.23	14.96	14.75	4.50 <sup>+0.10</sup> <sub>-0.07</sub>	2.99 <sup>+0.10</sup> <sub>-0.10</sub>	4.75 <sup>+0.30</sup> <sub>-0.25</sub>	17.31 <sup>+1.17</sup> <sub>-0.76</sub>	0.60	–
8592	288.73330	0.40845	14.95	15.08	13.94	13.23	13.63	12.17	11.84	11.67	4.53 <sup>+0.10</sup> <sub>-0.08</sub>	4.10 <sup>+0.06</sup> <sub>-0.08</sub>	3.59 <sup>+0.09</sup> <sub>-0.08</sub>	14.40 <sup>+1.23</sup> <sub>-0.84</sub>	2.10	–
8612	288.74416	-0.46719	13.42	13.78	12.73	12.12	12.43	11.10	10.80	10.61	4.59 <sup>+0.07</sup> <sub>-0.08</sub>	3.93 <sup>+0.05</sup> <sub>-0.07</sub>	3.82 <sup>+0.10</sup> <sub>-0.09</sub>	14.10 <sup>+0.96</sup> <sub>-0.99</sub>	0.93	–
8693	288.78868	-1.18230	13.10	13.73	12.97	12.53	12.72	11.94	11.71	11.64	4.61 <sup>+0.06</sup> <sub>-0.08</sub>	2.91 <sup>+0.04</sup> <sub>-0.05</sub>	3.61 <sup>+0.11</sup> <sub>-0.10</sub>	15.46 <sup>+0.83</sup> <sub>-0.96</sub>	2.09	–

Continued on next page...

ID	$\ell$	$b$	u	g	r	i	H $\alpha$	J	H	K	$\log(T_{\text{eff}})$	$A_0$	$R_V$	$\mu$	$\chi^2$	Notes
8733	288.81086	-0.00250	13.07	13.67	13.05	12.68	12.84	12.14	12.04	11.98	4.50 <sup>+0.08</sup> <sub>-0.07</sub>	2.49 <sup>+0.07</sup> <sub>-0.08</sub>	3.51 <sup>+0.15</sup> <sub>-0.13</sub>	14.51 <sup>+0.95</sup> <sub>-0.70</sub>	1.09	—
8789	288.83931	2.37978	16.88	17.31	16.18	15.49	15.81	14.03	13.30	13.12	4.57 <sup>+0.08</sup> <sub>-0.08</sub>	5.13 <sup>+0.07</sup> <sub>-0.08</sub>	4.96 <sup>+0.15</sup> <sub>-0.12</sub>	16.15 <sup>+1.03</sup> <sub>-0.90</sub>	5.29	—
8825	288.86487	-1.12192	13.85	14.26	13.26	12.69	12.99	11.72	11.42	11.29	4.60 <sup>+0.07</sup> <sub>-0.07</sub>	3.76 <sup>+0.05</sup> <sub>-0.06</sub>	3.79 <sup>+0.10</sup> <sub>-0.09</sub>	14.87 <sup>+0.88</sup> <sub>-0.88</sub>	0.58	—
8829	288.86930	-2.65363	13.85	14.49	13.87	13.51	13.61	12.99	12.84	12.74	4.50 <sup>+0.09</sup> <sub>-0.06</sub>	2.53 <sup>+0.07</sup> <sub>-0.08</sub>	3.67 <sup>+0.16</sup> <sub>-0.14</sub>	15.27 <sup>+1.03</sup> <sub>-0.66</sub>	0.42	—
8837	288.87577	-0.66055	14.98	15.06	13.82	13.12	13.51	11.84	11.54	11.33	4.51 <sup>+0.10</sup> <sub>-0.07</sub>	4.41 <sup>+0.07</sup> <sub>-0.09</sub>	3.72 <sup>+0.09</sup> <sub>-0.08</sub>	13.76 <sup>+1.23</sup> <sub>-0.75</sub>	1.88	—
8895	288.90325	-1.50268	19.16	19.24	18.00	17.26	17.78	15.74	15.53	15.13	4.48 <sup>+0.11</sup> <sub>-0.07</sub>	4.85 <sup>+0.12</sup> <sub>-0.13</sub>	4.16 <sup>+0.18</sup> <sub>-0.16</sub>	17.17 <sup>+1.24</sup> <sub>-0.79</sub>	2.80	—
8986	288.95044	0.98827	19.71	19.54	18.05	17.17	17.76	15.75	15.18	14.88	4.54 <sup>+0.10</sup> <sub>-0.10</sub>	5.22 <sup>+0.11</sup> <sub>-0.12</sub>	3.74 <sup>+0.11</sup> <sub>-0.11</sub>	17.72 <sup>+1.25</sup> <sub>-1.13</sub>	2.67	—
9043	288.98084	-0.42276	18.96	17.99	15.72	14.39	15.24	12.45	11.75	11.43	4.62 <sup>+0.05</sup> <sub>-0.08</sub>	6.97 <sup>+0.05</sup> <sub>-0.06</sub>	3.33 <sup>+0.04</sup> <sub>-0.04</sub>	15.03 <sup>+0.73</sup> <sub>-0.98</sub>	7.63	—
9054	288.98842	-0.23914	14.46	14.54	13.34	12.66	13.03	11.53	11.19	11.02	4.48 <sup>+0.08</sup> <sub>-0.06</sub>	4.14 <sup>+0.08</sup> <sub>-0.09</sub>	3.60 <sup>+0.09</sup> <sub>-0.08</sub>	13.16 <sup>+0.88</sup> <sub>-0.64</sub>	0.22	—
9106	289.02309	0.35628	13.83	14.41	13.70	13.28	13.47	12.67	12.47	12.42	4.55 <sup>+0.09</sup> <sub>-0.07</sub>	2.81 <sup>+0.06</sup> <sub>-0.07</sub>	3.60 <sup>+0.12</sup> <sub>-0.11</sub>	15.44 <sup>+1.12</sup> <sub>-0.84</sub>	1.51	—
9139	289.03666	-1.35611	18.59	18.80	17.45	16.75	17.16	15.62	15.20	15.01	4.63 <sup>+0.05</sup> <sub>-0.06</sub>	4.42 <sup>+0.09</sup> <sub>-0.09</sub>	3.59 <sup>+0.11</sup> <sub>-0.10</sub>	18.93 <sup>+0.63</sup> <sub>-0.79</sub>	4.12	—
9146	289.03792	-0.62153	14.17	14.44	13.41	12.81	13.15	11.73	11.38	11.24	4.49 <sup>+0.08</sup> <sub>-0.06</sub>	3.94 <sup>+0.08</sup> <sub>-0.09</sub>	3.92 <sup>+0.11</sup> <sub>-0.11</sub>	13.47 <sup>+0.95</sup> <sub>-0.67</sub>	0.95	—
9177	289.05282	-1.46905	18.88	19.18	17.82	17.09	17.63	15.50	15.18	14.88	4.63 <sup>+0.05</sup> <sub>-0.07</sub>	5.14 <sup>+0.09</sup> <sub>-0.10</sub>	4.27 <sup>+0.13</sup> <sub>-0.12</sub>	18.64 <sup>+0.64</sup> <sub>-0.83</sub>	7.48	—
9262	289.09731	-0.94925	15.39	15.28	13.88	13.10	13.56	11.72	11.34	11.09	4.49 <sup>+0.09</sup> <sub>-0.06</sub>	4.79 <sup>+0.08</sup> <sub>-0.09</sub>	3.65 <sup>+0.08</sup> <sub>-0.08</sub>	13.28 <sup>+1.09</sup> <sub>-0.67</sub>	0.43	—
9268	289.10155	-0.86628	18.29	18.62	17.48	16.81	17.23	15.60	15.19	14.82	4.60 <sup>+0.07</sup> <sub>-0.08</sub>	4.49 <sup>+0.10</sup> <sub>-0.10</sub>	4.15 <sup>+0.15</sup> <sub>-0.13</sub>	18.41 <sup>+0.90</sup> <sub>-0.96</sub>	1.36	—
9325	289.13070	-0.32083	15.76	15.49	13.90	12.98	13.55	11.24	10.72	10.48	4.50 <sup>+0.10</sup> <sub>-0.07</sub>	5.68 <sup>+0.07</sup> <sub>-0.09</sub>	3.86 <sup>+0.07</sup> <sub>-0.07</sub>	12.72 <sup>+1.13</sup> <sub>-0.72</sub>	2.07	—
9347	289.14334	-0.88364	16.00	15.95	14.60	13.81	14.26	12.41	11.98	11.73	4.48 <sup>+0.09</sup> <sub>-0.06</sub>	4.86 <sup>+0.08</sup> <sub>-0.09</sub>	3.84 <sup>+0.09</sup> <sub>-0.08</sub>	13.84 <sup>+1.03</sup> <sub>-0.66</sub>	0.36	—
9355	289.14633	-1.38825	17.55	17.08	15.26	14.24	14.91	12.44	11.95	11.63	4.55 <sup>+0.08</sup> <sub>-0.08</sub>	6.00 <sup>+0.06</sup> <sub>-0.08</sub>	3.61 <sup>+0.06</sup> <sub>-0.06</sub>	14.41 <sup>+1.03</sup> <sub>-0.90</sub>	0.87	—
9421	289.18132	-0.73823	18.09	18.23	17.02	16.36	16.75	15.26	14.98	14.83	4.56 <sup>+0.09</sup> <sub>-0.08</sub>	4.10 <sup>+0.09</sup> <sub>-0.09</sub>	3.51 <sup>+0.11</sup> <sub>-0.11</sub>	17.95 <sup>+1.11</sup> <sub>-0.94</sub>	0.48	—
9448	289.19249	1.00633	16.09	16.56	15.73	15.21	15.39	14.47	14.08	14.07	4.54 <sup>+0.09</sup> <sub>-0.06</sub>	3.34 <sup>+0.07</sup> <sub>-0.08</sub>	3.82 <sup>+0.14</sup> <sub>-0.13</sub>	16.96 <sup>+1.13</sup> <sub>-0.86</sub>	5.94	—
9464	289.20398	0.31705	14.01	14.51	13.69	13.22	13.45	12.28	12.02	11.83	4.48 <sup>+0.08</sup> <sub>-0.06</sub>	3.49 <sup>+0.07</sup> <sub>-0.08</sub>	4.27 <sup>+0.15</sup> <sub>-0.14</sub>	14.08 <sup>+0.85</sup> <sub>-0.61</sub>	0.96	—
9482	289.21260	0.36064	15.10	15.08	13.74	12.98	13.44	11.54	11.16	10.89	4.48 <sup>+0.08</sup> <sub>-0.06</sub>	4.85 <sup>+0.08</sup> <sub>-0.08</sub>	3.88 <sup>+0.08</sup> <sub>-0.08</sub>	13.02 <sup>+0.98</sup> <sub>-0.62</sub>	1.14	—
9522	289.23526	-0.26877	14.03	14.27	13.27	12.67	12.99	11.69	11.39	11.28	4.48 <sup>+0.09</sup> <sub>-0.06</sub>	3.71 <sup>+0.08</sup> <sub>-0.09</sub>	3.70 <sup>+0.10</sup> <sub>-0.10</sub>	13.47 <sup>+1.03</sup> <sub>-0.64</sub>	1.59	—
9542	289.24445	0.37258	13.91	14.31	13.31	12.77	13.05	11.79	11.47	11.31	4.56 <sup>+0.08</sup> <sub>-0.08</sub>	3.78 <sup>+0.06</sup> <sub>-0.07</sub>	3.89 <sup>+0.11</sup> <sub>-0.10</sub>	14.40 <sup>+1.02</sup> <sub>-0.86</sub>	0.80	—
9597	289.27527	-1.66047	14.65	15.28	14.63	14.25	14.43	13.85	13.63	13.52	4.53 <sup>+0.09</sup> <sub>-0.07</sub>	2.49 <sup>+0.08</sup> <sub>-0.09</sub>	3.43 <sup>+0.16</sup> <sub>-0.14</sub>	16.43 <sup>+1.11</sup> <sub>-0.78</sub>	3.23	—
9617	289.28693	0.32692	13.36	13.69	12.73	12.20	12.45	11.23	10.93	10.81	4.49 <sup>+0.08</sup> <sub>-0.06</sub>	3.63 <sup>+0.08</sup> <sub>-0.09</sub>	3.83 <sup>+0.11</sup> <sub>-0.10</sub>	13.07 <sup>+0.96</sup> <sub>-0.66</sub>	0.74	—
9642	289.30409	-1.79116	12.58	13.38	12.80	12.50	12.57	12.06	11.93	11.93	4.60 <sup>+0.07</sup> <sub>-0.08</sub>	2.33 <sup>+0.05</sup> <sub>-0.06</sub>	3.56 <sup>+0.15</sup> <sub>-0.13</sub>	15.62 <sup>+0.91</sup> <sub>-0.95</sub>	2.29	—
9657	289.31277	0.06842	16.68	16.25	14.48	13.48	14.08	11.62	11.10	10.85	4.55 <sup>+0.09</sup> <sub>-0.08</sub>	6.03 <sup>+0.06</sup> <sub>-0.08</sub>	3.70 <sup>+0.06</sup> <sub>-0.06</sub>	13.57 <sup>+1.13</sup> <sub>-0.87</sub>	3.93	—
9694	289.33635	0.22049	18.85	18.81	17.32	16.47	16.99	14.82	14.18	13.93	4.55 <sup>+0.09</sup> <sub>-0.08</sub>	5.64 <sup>+0.08</sup> <sub>-0.08</sub>	4.19 <sup>+0.10</sup> <sub>-0.10</sub>	16.70 <sup>+1.07</sup> <sub>-0.89</sub>	2.10	—
9705	289.34324	-0.39437	15.00	15.03	13.77	13.04	13.45	11.73	11.32	11.17	4.50 <sup>+0.09</sup> <sub>-0.07</sub>	4.57 <sup>+0.07</sup> <sub>-0.09</sub>	3.79 <sup>+0.09</sup> <sub>-0.09</sub>	13.44 <sup>+1.03</sup> <sub>-0.69</sub>	2.47	—
9719	289.34930	0.19281	17.93	17.60	15.96	15.02	15.61	13.22	12.73	12.50	4.52 <sup>+0.10</sup> <sub>-0.08</sub>	5.77 <sup>+0.07</sup> <sub>-0.09</sub>	3.80 <sup>+0.07</sup> <sub>-0.07</sub>	14.83 <sup>+1.17</sup> <sub>-0.81</sub>	4.70	—
9754	289.36698	-0.39340	16.89	16.71	15.25	14.39	14.89	12.89	12.38	12.23	4.49 <sup>+0.09</sup> <sub>-0.07</sub>	5.14 <sup>+0.08</sup> <sub>-0.10</sub>	3.75 <sup>+0.08</sup> <sub>-0.07</sub>	14.37 <sup>+1.00</sup> <sub>-0.72</sub>	5.37	—
9780	289.38267	-0.71353	14.45	14.71	13.67	13.05	13.38	12.10	11.73	11.60	4.51 <sup>+0.10</sup> <sub>-0.07</sub>	3.82 <sup>+0.08</sup> <sub>-0.09</sub>	3.71 <sup>+0.11</sup> <sub>-0.11</sub>	14.15 <sup>+1.19</sup> <sub>-0.79</sub>	1.30	—

Continued on next page...

ID	$\ell$	$b$	u	g	r	i	H $\alpha$	J	H	K	$\log(T_{\text{eff}})$	$A_0$	$R_V$	$\mu$	$\chi^2$	Notes
9797	289.39258	-1.53871	13.87	13.99	12.72	12.02	12.41	10.76	10.29	10.02	4.51 <sup>+0.09</sup> <sub>-0.07</sub>	4.65 <sup>+0.07</sup> <sub>-0.08</sub>	3.97 <sup>+0.10</sup> <sub>-0.09</sub>	12.51 <sup>+1.11</sup> <sub>-0.73</sub>	3.12	—
9811	289.39956	-0.86104	13.30	13.84	13.11	12.67	12.85	12.02	11.77	11.72	4.52 <sup>+0.09</sup> <sub>-0.07</sub>	2.94 <sup>+0.07</sup> <sub>-0.08</sub>	3.73 <sup>+0.13</sup> <sub>-0.12</sub>	14.41 <sup>+1.13</sup> <sub>-0.75</sub>	2.33	—
9839	289.41834	-1.22487	13.25	13.56	12.51	11.96	12.22	10.87	10.61	10.42	4.53 <sup>+0.09</sup> <sub>-0.07</sub>	3.89 <sup>+0.06</sup> <sub>-0.08</sub>	3.84 <sup>+0.11</sup> <sub>-0.10</sub>	13.16 <sup>+1.10</sup> <sub>-0.82</sub>	1.81	—
9899	289.45639	-0.05910	14.48	14.71	13.63	13.03	13.37	11.97	11.64	11.47	4.48 <sup>+0.08</sup> <sub>-0.06</sub>	3.93 <sup>+0.07</sup> <sub>-0.08</sub>	3.80 <sup>+0.10</sup> <sub>-0.09</sub>	13.65 <sup>+0.93</sup> <sub>-0.60</sub>	0.07	—
9901	289.45783	-0.05859	14.16	14.42	13.39	12.82	13.13	11.85	11.51	11.38	4.48 <sup>+0.08</sup> <sub>-0.06</sub>	3.73 <sup>+0.08</sup> <sub>-0.09</sub>	3.73 <sup>+0.11</sup> <sub>-0.11</sub>	13.56 <sup>+0.96</sup> <sub>-0.62</sub>	0.81	—
9910	289.46167	-0.04904	14.56	14.55	13.20	12.43	12.88	11.09	10.65	10.48	4.54 <sup>+0.09</sup> <sub>-0.07</sub>	4.76 <sup>+0.06</sup> <sub>-0.07</sub>	3.72 <sup>+0.08</sup> <sub>-0.07</sub>	13.21 <sup>+1.14</sup> <sub>-0.78</sub>	1.23	—
9921	289.46592	-0.06360	14.52	14.59	13.34	12.63	13.03	11.31	10.91	10.68	4.48 <sup>+0.08</sup> <sub>-0.06</sub>	4.60 <sup>+0.08</sup> <sub>-0.09</sub>	3.92 <sup>+0.10</sup> <sub>-0.09</sub>	12.83 <sup>+0.92</sup> <sub>-0.65</sub>	0.25	—
9967	289.48389	0.14862	20.07	19.64	17.70	16.68	17.39	14.34	13.65	13.24	4.49 <sup>+0.09</sup> <sub>-0.10</sub>	7.07 <sup>+0.09</sup> <sub>-0.10</sub>	4.29 <sup>+0.09</sup> <sub>-0.08</sub>	15.14 <sup>+1.10</sup> <sub>-0.76</sub>	5.74	—
9983	289.49052	-0.06971	13.20	13.55	12.56	12.03	12.30	11.03	10.71	10.56	4.50 <sup>+0.08</sup> <sub>-0.06</sub>	3.75 <sup>+0.07</sup> <sub>-0.08</sub>	3.91 <sup>+0.11</sup> <sub>-0.11</sub>	12.99 <sup>+0.96</sup> <sub>-0.68</sub>	0.70	—
10003	289.50092	-0.73273	13.46	14.04	13.30	12.88	13.05	12.23	12.06	11.99	4.57 <sup>+0.08</sup> <sub>-0.08</sub>	2.86 <sup>+0.05</sup> <sub>-0.06</sub>	3.57 <sup>+0.12</sup> <sub>-0.11</sub>	15.31 <sup>+1.04</sup> <sub>-0.88</sub>	0.52	—
10010	289.50464	-1.24172	13.94	14.38	13.57	13.08	13.31	12.38	12.14	12.02	4.49 <sup>+0.09</sup> <sub>-0.06</sub>	3.09 <sup>+0.07</sup> <sub>-0.09</sub>	3.63 <sup>+0.12</sup> <sub>-0.11</sub>	14.43 <sup>+1.01</sup> <sub>-0.65</sub>	0.94	—
10021	289.51104	-0.53604	13.67	13.86	12.73	12.11	12.42	10.95	10.63	10.46	4.49 <sup>+0.09</sup> <sub>-0.07</sub>	4.10 <sup>+0.08</sup> <sub>-0.09</sub>	3.82 <sup>+0.11</sup> <sub>-0.10</sub>	12.67 <sup>+0.99</sup> <sub>-0.69</sub>	0.51	—
10055	289.53129	-0.84450	16.79	16.70	15.33	14.55	14.99	13.12	12.76	12.53	4.48 <sup>+0.08</sup> <sub>-0.06</sub>	4.80 <sup>+0.08</sup> <sub>-0.09</sub>	3.73 <sup>+0.08</sup> <sub>-0.07</sub>	14.63 <sup>+0.93</sup> <sub>-0.65</sub>	1.62	—
10090	289.54877	-2.42556	17.93	18.39	17.35	16.79	17.10	15.95	15.48	15.16	4.60 <sup>+0.05</sup> <sub>-0.07</sub>	3.83 <sup>+0.12</sup> <sub>-0.12</sub>	3.88 <sup>+0.17</sup> <sub>-0.17</sub>	18.95 <sup>+0.65</sup> <sub>-0.83</sub>	4.87	—
10092	289.54902	-1.21059	15.86	15.61	14.00	13.06	13.64	11.30	10.77	10.47	4.51 <sup>+0.10</sup> <sub>-0.07</sub>	5.80 <sup>+0.07</sup> <sub>-0.09</sub>	3.94 <sup>+0.08</sup> <sub>-0.07</sub>	12.81 <sup>+1.15</sup> <sub>-0.80</sub>	0.20	—
10098	289.55039	-1.14720	13.63	13.88	12.74	12.10	12.42	10.92	10.55	10.35	4.56 <sup>+0.09</sup> <sub>-0.08</sub>	4.29 <sup>+0.05</sup> <sub>-0.07</sub>	3.94 <sup>+0.10</sup> <sub>-0.09</sub>	13.34 <sup>+1.11</sup> <sub>-0.89</sub>	0.58	—
10126	289.56384	-0.92023	19.09	18.18	15.95	14.69	15.51	12.32	11.60	11.16	4.50 <sup>+0.09</sup> <sub>-0.07</sub>	7.53 <sup>+0.08</sup> <sub>-0.09</sub>	3.80 <sup>+0.05</sup> <sub>-0.05</sub>	13.16 <sup>+1.10</sup> <sub>-0.71</sub>	0.60	—
10135	289.56784	-0.03128	14.69	14.80	13.52	12.82	13.14	11.85	11.51	11.28	4.59 <sup>+0.07</sup> <sub>-0.08</sub>	4.11 <sup>+0.05</sup> <sub>-0.06</sub>	3.36 <sup>+0.07</sup> <sub>-0.07</sub>	14.84 <sup>+0.89</sup> <sub>-0.95</sub>	6.84	—
10136	289.56804	-1.43453	17.26	17.72	16.66	16.10	16.39	15.11	14.82	14.66	4.62 <sup>+0.05</sup> <sub>-0.07</sub>	3.84 <sup>+0.07</sup> <sub>-0.08</sub>	3.82 <sup>+0.12</sup> <sub>-0.11</sub>	18.54 <sup>+0.67</sup> <sub>-0.83</sub>	2.33	—
10161	289.57684	-0.77968	15.26	15.01	13.49	12.60	13.13	11.13	10.75	10.56	4.55 <sup>+0.09</sup> <sub>-0.08</sub>	5.07 <sup>+0.06</sup> <sub>-0.08</sub>	3.47 <sup>+0.07</sup> <sub>-0.06</sub>	13.44 <sup>+1.11</sup> <sub>-0.88</sub>	2.86	—
10162	289.57694	-0.33405	16.22	16.19	14.88	14.13	14.56	12.82	12.44	12.24	4.48 <sup>+0.09</sup> <sub>-0.07</sub>	4.59 <sup>+0.08</sup> <sub>-0.10</sub>	3.69 <sup>+0.09</sup> <sub>-0.08</sub>	14.39 <sup>+1.05</sup> <sub>-0.68</sub>	0.54	—
10193	289.58756	-0.21989	13.54	13.85	12.82	12.23	12.53	11.22	11.01	10.84	4.55 <sup>+0.10</sup> <sub>-0.08</sub>	3.75 <sup>+0.06</sup> <sub>-0.08</sub>	3.65 <sup>+0.10</sup> <sub>-0.09</sub>	13.86 <sup>+1.19</sup> <sub>-0.88</sub>	1.69	—
10195	289.58799	1.37518	19.00	18.70	17.01	15.99	16.55	14.16	13.36	13.07	4.52 <sup>+0.10</sup> <sub>-0.08</sub>	6.33 <sup>+0.07</sup> <sub>-0.09</sub>	4.14 <sup>+0.08</sup> <sub>-0.08</sub>	15.44 <sup>+1.21</sup> <sub>-0.84</sub>	7.68	—
10214	289.59441	-0.21808	16.46	16.49	15.14	14.42	14.53	13.62	13.36	13.20	4.63 <sup>+0.05</sup> <sub>-0.07</sub>	3.76 <sup>+0.05</sup> <sub>-0.05</sub>	2.89 <sup>+0.06</sup> <sub>-0.06</sub>	17.27 <sup>+0.62</sup> <sub>-0.84</sub>	5.46	EM
10246	289.60845	0.61961	16.66	17.10	16.26	15.72	15.91	14.78	14.51	14.30	4.50 <sup>+0.10</sup> <sub>-0.07</sub>	3.59 <sup>+0.09</sup> <sub>-0.10</sub>	4.13 <sup>+0.18</sup> <sub>-0.17</sub>	16.71 <sup>+1.12</sup> <sub>-0.71</sub>	1.01	—
10257	289.61237	-0.26034	14.66	14.82	13.65	12.99	13.36	11.78	11.56	11.31	4.53 <sup>+0.10</sup> <sub>-0.07</sub>	4.21 <sup>+0.07</sup> <sub>-0.08</sub>	3.71 <sup>+0.10</sup> <sub>-0.09</sub>	14.05 <sup>+1.24</sup> <sub>-0.83</sub>	3.52	—
10259	289.61302	-0.61981	12.65	13.14	12.29	11.89	12.02	10.96	10.77	10.64	4.48 <sup>+0.08</sup> <sub>-0.06</sub>	3.28 <sup>+0.08</sup> <sub>-0.08</sub>	3.98 <sup>+0.14</sup> <sub>-0.13</sub>	12.87 <sup>+0.92</sup> <sub>-0.60</sub>	5.13	—
10262	289.61386	-0.60832	14.66	14.97	14.00	13.44	13.72	12.57	12.25	12.14	4.50 <sup>+0.09</sup> <sub>-0.06</sub>	3.55 <sup>+0.07</sup> <sub>-0.08</sub>	3.66 <sup>+0.11</sup> <sub>-0.10</sub>	14.57 <sup>+1.02</sup> <sub>-0.68</sub>	1.35	—
10283	289.62350	-1.24261	16.41	16.15	14.54	13.62	14.18	11.87	11.34	11.01	4.50 <sup>+0.09</sup> <sub>-0.07</sub>	5.77 <sup>+0.08</sup> <sub>-0.09</sub>	3.95 <sup>+0.08</sup> <sub>-0.07</sub>	13.17 <sup>+1.10</sup> <sub>-0.69</sub>	0.25	—
10292	289.62718	-1.44454	16.13	16.08	14.69	13.82	14.35	12.20	11.70	11.41	4.52 <sup>+0.09</sup> <sub>-0.07</sub>	5.41 <sup>+0.07</sup> <sub>-0.09</sub>	4.14 <sup>+0.09</sup> <sub>-0.09</sub>	13.82 <sup>+1.07</sup> <sub>-0.79</sub>	0.92	—
10298	289.62828	-1.08567	15.14	14.90	13.31	12.41	12.94	10.73	10.24	9.94	4.53 <sup>+0.10</sup> <sub>-0.07</sub>	5.61 <sup>+0.06</sup> <sub>-0.08</sub>	3.83 <sup>+0.08</sup> <sub>-0.07</sub>	12.49 <sup>+1.19</sup> <sub>-0.79</sub>	0.53	—
10330	289.63797	-0.81251	16.47	16.23	14.68	13.81	14.31	12.27	11.79	11.53	4.49 <sup>+0.09</sup> <sub>-0.07</sub>	5.29 <sup>+0.08</sup> <sub>-0.09</sub>	3.70 <sup>+0.07</sup> <sub>-0.07</sub>	13.71 <sup>+1.04</sup> <sub>-0.69</sub>	0.25	—
10334	289.63965	-0.24656	14.08	14.07	12.71	11.99	12.39	10.56	10.16	9.90	4.48 <sup>+0.08</sup> <sub>-0.06</sub>	4.81 <sup>+0.08</sup> <sub>-0.09</sub>	3.87 <sup>+0.09</sup> <sub>-0.08</sub>	12.03 <sup>+0.93</sup> <sub>-0.64</sub>	1.16	—

Continued on next page...

ID	$\ell$	$b$	u	g	r	i	H $\alpha$	J	H	K	log( $T_{\text{eff}}$ )	$A_0$	$R_V$	$\mu$	$\chi^2$	Notes
10339	289.64049	-0.72340	16.01	16.10	14.89	14.21	14.58	13.07	12.70	12.49	4.49 <sup>+0.10</sup> <sub>-0.06</sub>	4.24 <sup>+0.08</sup> <sub>-0.09</sub>	3.68 <sup>+0.09</sup> <sub>-0.08</sub>	14.73 <sup>+1.10</sup> <sub>-0.65</sub>	0.86	—
10359	289.64949	-0.31801	15.62	15.61	14.29	13.54	13.98	12.19	11.88	11.64	4.50 <sup>+0.08</sup> <sub>-0.06</sub>	4.61 <sup>+0.07</sup> <sub>-0.08</sub>	3.68 <sup>+0.08</sup> <sub>-0.07</sub>	14.00 <sup>+0.90</sup> <sub>-0.66</sub>	2.60	—
10378	289.65836	-1.24356	18.91	18.41	16.56	15.48	16.18	13.41	12.79	12.42	4.49 <sup>+0.09</sup> <sub>-0.07</sub>	6.60 <sup>+0.08</sup> <sub>-0.09</sub>	3.98 <sup>+0.07</sup> <sub>-0.07</sub>	14.43 <sup>+1.07</sup> <sub>-0.74</sub>	0.14	—
10394	289.66782	-0.90367	14.67	14.72	13.42	12.68	13.09	11.33	10.94	10.72	4.52 <sup>+0.10</sup> <sub>-0.07</sub>	4.70 <sup>+0.06</sup> <sub>-0.08</sub>	3.83 <sup>+0.09</sup> <sub>-0.08</sub>	13.31 <sup>+1.20</sup> <sub>-0.76</sub>	0.18	—
10413	289.67572	-1.27318	16.88	16.44	14.58	13.43	14.15	11.20	10.47	9.99	4.53 <sup>+0.10</sup> <sub>-0.08</sub>	7.15 <sup>+0.06</sup> <sub>-0.09</sub>	4.30 <sup>+0.07</sup> <sub>-0.07</sub>	12.39 <sup>+1.17</sup> <sub>-0.89</sub>	3.75	—
10422	289.68061	-1.18807	18.38	17.75	15.75	14.58	15.36	12.40	11.60	11.18	4.49 <sup>+0.11</sup> <sub>-0.07</sub>	7.15 <sup>+0.08</sup> <sub>-0.10</sub>	4.05 <sup>+0.07</sup> <sub>-0.07</sub>	13.12 <sup>+1.34</sup> <sub>-0.75</sub>	3.85	—
10438	289.68791	-0.73024	14.24	14.34	13.01	12.26	12.63	11.01	10.60	10.41	4.60 <sup>+0.07</sup> <sub>-0.08</sub>	4.62 <sup>+0.05</sup> <sub>-0.06</sub>	3.68 <sup>+0.08</sup> <sub>-0.07</sub>	13.91 <sup>+0.88</sup> <sub>-0.98</sub>	0.89	—
10439	289.68846	-1.24970	16.55	16.37	14.84	13.91	14.48	12.21	11.68	11.35	4.52 <sup>+0.09</sup> <sub>-0.07</sub>	5.70 <sup>+0.07</sup> <sub>-0.09</sub>	4.01 <sup>+0.08</sup> <sub>-0.07</sub>	13.83 <sup>+1.13</sup> <sub>-0.77</sub>	0.83	—
10448	289.69096	-1.05896	15.00	14.92	13.51	12.70	13.16	11.24	10.81	10.54	4.50 <sup>+0.09</sup> <sub>-0.07</sub>	5.03 <sup>+0.07</sup> <sub>-0.08</sub>	3.82 <sup>+0.08</sup> <sub>-0.08</sub>	12.88 <sup>+1.07</sup> <sub>-0.71</sub>	0.60	—
10472	289.69742	-1.26674	15.80	15.85	14.57	13.83	14.26	12.42	12.00	11.73	4.48 <sup>+0.09</sup> <sub>-0.06</sub>	4.81 <sup>+0.08</sup> <sub>-0.09</sub>	4.03 <sup>+0.10</sup> <sub>-0.09</sub>	13.83 <sup>+1.02</sup> <sub>-0.64</sub>	0.34	—
10484	289.70192	-1.26441	15.92	16.05	14.84	14.15	14.54	12.87	12.47	12.25	4.50 <sup>+0.09</sup> <sub>-0.07</sub>	4.51 <sup>+0.08</sup> <sub>-0.08</sub>	3.95 <sup>+0.10</sup> <sub>-0.10</sub>	14.60 <sup>+1.06</sup> <sub>-0.72</sub>	0.15	—
10490	289.70402	-0.74895	17.30	16.86	15.08	14.04	14.66	12.19	11.67	11.33	4.54 <sup>+0.09</sup> <sub>-0.08</sub>	6.12 <sup>+0.08</sup> <sub>-0.08</sub>	3.74 <sup>+0.07</sup> <sub>-0.07</sub>	13.97 <sup>+1.16</sup> <sub>-0.89</sub>	1.01	—
10496	289.70602	-1.26720	15.28	15.30	13.94	13.15	13.62	11.69	11.26	11.01	4.57 <sup>+0.08</sup> <sub>-0.08</sub>	5.02 <sup>+0.05</sup> <sub>-0.07</sub>	3.92 <sup>+0.08</sup> <sub>-0.08</sub>	14.05 <sup>+1.04</sup> <sub>-0.91</sub>	0.45	—
10517	289.71659	-1.59425	14.82	14.69	13.25	12.35	12.83	10.79	10.31	10.03	4.53 <sup>+0.09</sup> <sub>-0.08</sub>	5.36 <sup>+0.06</sup> <sub>-0.08</sub>	3.91 <sup>+0.08</sup> <sub>-0.07</sub>	12.67 <sup>+1.12</sup> <sub>-0.84</sub>	1.81	—
10527	289.72139	-1.16902	17.08	16.81	15.17	14.21	14.82	12.36	11.80	11.45	4.51 <sup>+0.09</sup> <sub>-0.07</sub>	6.03 <sup>+0.07</sup> <sub>-0.09</sub>	4.05 <sup>+0.08</sup> <sub>-0.07</sub>	13.74 <sup>+1.07</sup> <sub>-0.74</sub>	0.34	—
10539	289.72830	-0.12468	20.20	19.97	18.32	17.44	17.97	15.50	15.03	14.64	4.49 <sup>+0.11</sup> <sub>-0.10</sub>	5.95 <sup>+0.13</sup> <sub>-0.14</sub>	4.11 <sup>+0.13</sup> <sub>-0.12</sub>	16.67 <sup>+1.35</sup> <sub>-1.00</sub>	2.88	—
10546	289.73273	-1.26275	13.01	13.37	12.31	11.80	12.04	10.69	10.39	10.18	4.51 <sup>+0.08</sup> <sub>-0.06</sub>	3.94 <sup>+0.07</sup> <sub>-0.08</sub>	4.04 <sup>+0.11</sup> <sub>-0.11</sub>	12.66 <sup>+0.99</sup> <sub>-0.68</sub>	4.11	—
10548	289.73352	-1.18401	15.32	15.18	13.67	12.77	13.29	11.08	10.59	10.27	4.54 <sup>+0.09</sup> <sub>-0.07</sub>	5.60 <sup>+0.06</sup> <sub>-0.08</sub>	4.00 <sup>+0.08</sup> <sub>-0.08</sub>	12.96 <sup>+1.13</sup> <sub>-0.83</sub>	0.73	—
10550	289.73562	-0.60374	13.46	13.82	12.87	12.33	12.60	11.41	11.17	11.05	4.54 <sup>+0.09</sup> <sub>-0.07</sub>	3.54 <sup>+0.06</sup> <sub>-0.08</sub>	3.67 <sup>+0.11</sup> <sub>-0.09</sub>	13.91 <sup>+1.15</sup> <sub>-0.80</sub>	0.79	—
10565	289.74134	-1.17805	15.59	15.50	14.01	13.12	13.64	11.54	11.05	10.77	4.59 <sup>+0.07</sup> <sub>-0.08</sub>	5.43 <sup>+0.05</sup> <sub>-0.06</sub>	3.90 <sup>+0.07</sup> <sub>-0.07</sub>	14.02 <sup>+0.97</sup> <sub>-0.97</sub>	1.41	—
10570	289.74350	-1.17673	15.58	15.46	14.00	13.13	13.64	11.53	11.05	10.77	4.53 <sup>+0.10</sup> <sub>-0.08</sub>	5.38 <sup>+0.07</sup> <sub>-0.08</sub>	3.93 <sup>+0.08</sup> <sub>-0.08</sub>	13.30 <sup>+1.24</sup> <sub>-0.83</sub>	0.45	—
10603	289.75178	-1.23479	15.00	15.03	13.74	12.99	13.42	11.65	11.29	11.09	4.53 <sup>+0.09</sup> <sub>-0.07</sub>	4.64 <sup>+0.07</sup> <sub>-0.08</sub>	3.76 <sup>+0.09</sup> <sub>-0.08</sub>	13.70 <sup>+1.04</sup> <sub>-0.78</sub>	1.00	—
10604	289.75217	-1.21961	15.31	15.41	14.18	13.46	13.87	12.24	11.84	11.67	4.55 <sup>+0.09</sup> <sub>-0.08</sub>	4.46 <sup>+0.06</sup> <sub>-0.08</sub>	3.74 <sup>+0.09</sup> <sub>-0.08</sub>	14.59 <sup>+1.16</sup> <sub>-0.90</sub>	1.21	—
10614	289.75501	-1.22704	15.82	15.68	14.24	13.41	13.91	11.91	11.47	11.25	4.49 <sup>+0.10</sup> <sub>-0.07</sub>	5.07 <sup>+0.09</sup> <sub>-0.10</sub>	3.77 <sup>+0.09</sup> <sub>-0.09</sub>	13.40 <sup>+1.14</sup> <sub>-0.73</sub>	0.53	—
10617	289.75520	-1.22251	13.96	14.03	12.71	11.97	12.37	10.64	10.22	10.01	4.54 <sup>+0.09</sup> <sub>-0.07</sub>	4.72 <sup>+0.06</sup> <sub>-0.07</sub>	3.82 <sup>+0.09</sup> <sub>-0.08</sub>	12.83 <sup>+1.08</sup> <sub>-0.83</sub>	0.40	—
10624	289.75653	-1.31575	13.91	14.30	13.40	12.86	13.13	11.79	11.53	11.37	4.48 <sup>+0.08</sup> <sub>-0.06</sub>	3.73 <sup>+0.09</sup> <sub>-0.09</sub>	4.16 <sup>+0.15</sup> <sub>-0.14</sub>	13.54 <sup>+0.97</sup> <sub>-0.65</sub>	0.90	—
10626	289.75725	-1.20051	15.04	15.09	13.79	13.02	13.46	11.65	11.20	10.98	4.53 <sup>+0.09</sup> <sub>-0.07</sub>	4.83 <sup>+0.06</sup> <sub>-0.08</sub>	3.91 <sup>+0.09</sup> <sub>-0.08</sub>	13.65 <sup>+1.10</sup> <sub>-0.80</sub>	0.55	—
10628	289.75804	-1.22084	15.95	16.02	14.75	14.01	14.43	12.71	12.32	12.04	4.52 <sup>+0.10</sup> <sub>-0.07</sub>	4.65 <sup>+0.08</sup> <sub>-0.09</sub>	3.86 <sup>+0.10</sup> <sub>-0.09</sub>	14.60 <sup>+1.21</sup> <sub>-0.78</sub>	0.98	—
10631	289.75895	-1.28511	13.38	13.81	12.96	12.43	12.68	11.62	11.41	11.24	4.53 <sup>+0.10</sup> <sub>-0.07</sub>	3.33 <sup>+0.06</sup> <sub>-0.08</sub>	3.71 <sup>+0.11</sup> <sub>-0.10</sub>	14.06 <sup>+1.23</sup> <sub>-0.79</sub>	1.62	—
10632	289.75909	-1.21982	14.55	14.71	13.55	12.87	13.24	11.71	11.36	11.12	4.50 <sup>+0.10</sup> <sub>-0.07</sub>	4.26 <sup>+0.08</sup> <sub>-0.09</sub>	3.82 <sup>+0.10</sup> <sub>-0.09</sub>	13.52 <sup>+1.15</sup> <sub>-0.73</sub>	0.87	—
10633	289.75912	-1.32202	13.83	14.11	13.13	12.53	12.84	11.58	11.25	11.12	4.48 <sup>+0.09</sup> <sub>-0.06</sub>	3.72 <sup>+0.08</sup> <sub>-0.09</sub>	3.77 <sup>+0.11</sup> <sub>-0.10</sub>	13.35 <sup>+0.98</sup> <sub>-0.66</sub>	1.74	—
10643	289.76145	-1.24134	17.64	17.35	15.74	14.81	15.43	13.09	12.59	12.30	4.48 <sup>+0.09</sup> <sub>-0.06</sub>	5.66 <sup>+0.08</sup> <sub>-0.09</sub>	3.84 <sup>+0.08</sup> <sub>-0.07</sub>	14.32 <sup>+0.99</sup> <sub>-0.65</sub>	0.41	—
10653	289.76425	-0.71943	14.92	14.88	13.54	12.74	13.19	11.41	11.02	10.82	4.55 <sup>+0.09</sup> <sub>-0.08</sub>	4.73 <sup>+0.06</sup> <sub>-0.08</sub>	3.64 <sup>+0.08</sup> <sub>-0.07</sub>	13.68 <sup>+1.15</sup> <sub>-0.87</sub>	0.96	—

Continued on next page...

ID	$\ell$	$b$	u	g	r	i	H $\alpha$	J	H	K	$\log(T_{\text{eff}})$	$A_0$	$R_V$	$\mu$	$\chi^2$	Notes
10664	289.76667	-1.22062	15.31	15.39	14.12	13.35	13.80	12.04	11.60	11.40	4.55 <sup>+0.09</sup> <sub>-0.08</sub>	4.72 <sup>+0.06</sup> <sub>-0.07</sub>	3.87 <sup>+0.09</sup> <sub>-0.08</sub>	14.31 <sup>+1.08</sup> <sub>-0.89</sub>	0.67	-
10668	289.76877	-1.21852	13.69	13.90	12.73	12.06	12.39	10.84	10.42	10.23	4.53 <sup>+0.09</sup> <sub>-0.07</sub>	4.42 <sup>+0.06</sup> <sub>-0.08</sub>	3.98 <sup>+0.10</sup> <sub>-0.09</sub>	12.95 <sup>+1.12</sup> <sub>-0.78</sub>	0.56	-
10669	289.76932	-1.25850	14.42	14.88	14.03	13.53	13.78	12.67	12.36	12.27	4.51 <sup>+0.09</sup> <sub>-0.07</sub>	3.43 <sup>+0.07</sup> <sub>-0.08</sub>	3.95 <sup>+0.13</sup> <sub>-0.12</sub>	14.84 <sup>+1.07</sup> <sub>-0.73</sub>	1.31	-
10695	289.77745	-1.21718	14.19	14.38	13.22	12.52	12.90	11.32	10.95	10.69	4.54 <sup>+0.09</sup> <sub>-0.08</sub>	4.42 <sup>+0.07</sup> <sub>-0.08</sub>	3.92 <sup>+0.10</sup> <sub>-0.10</sub>	13.54 <sup>+1.16</sup> <sub>-0.86</sub>	1.50	-
10698	289.77790	-1.30394	14.69	15.10	14.28	13.78	14.02	12.97	12.76	12.67	4.48 <sup>+0.08</sup> <sub>-0.06</sub>	3.18 <sup>+0.07</sup> <sub>-0.08</sub>	3.69 <sup>+0.12</sup> <sub>-0.11</sub>	14.90 <sup>+0.87</sup> <sub>-0.60</sub>	1.34	-
10701	289.77882	-1.26503	13.28	13.74	12.88	12.35	12.60	11.53	11.31	11.15	4.56 <sup>+0.09</sup> <sub>-0.08</sub>	3.37 <sup>+0.05</sup> <sub>-0.07</sub>	3.75 <sup>+0.11</sup> <sub>-0.10</sub>	14.31 <sup>+1.10</sup> <sub>-0.90</sub>	1.17	-
10715	289.78396	-1.27254	13.92	14.31	13.47	12.95	13.17	12.14	11.89	11.77	4.48 <sup>+0.09</sup> <sub>-0.06</sub>	3.28 <sup>+0.08</sup> <sub>-0.08</sub>	3.73 <sup>+0.12</sup> <sub>-0.11</sub>	14.02 <sup>+1.06</sup> <sub>-0.63</sub>	0.76	-
10719	289.78413	-1.21780	15.22	15.44	14.32	13.66	14.01	12.55	12.24	12.06	4.56 <sup>+0.09</sup> <sub>-0.08</sub>	4.11 <sup>+0.07</sup> <sub>-0.08</sub>	3.74 <sup>+0.10</sup> <sub>-0.10</sub>	15.08 <sup>+1.13</sup> <sub>-0.89</sub>	0.61	-
10721	289.78420	-1.22052	14.39	14.65	13.52	12.86	13.21	11.74	11.42	11.27	4.59 <sup>+0.07</sup> <sub>-0.08</sub>	4.14 <sup>+0.05</sup> <sub>-0.06</sub>	3.74 <sup>+0.08</sup> <sub>-0.08</sub>	14.68 <sup>+0.90</sup> <sub>-0.94</sub>	1.09	-
10723	289.78482	-1.21064	14.11	14.45	13.46	12.86	13.15	11.84	11.57	11.42	4.57 <sup>+0.08</sup> <sub>-0.08</sub>	3.82 <sup>+0.05</sup> <sub>-0.07</sub>	3.80 <sup>+0.10</sup> <sub>-0.10</sub>	14.58 <sup>+1.08</sup> <sub>-0.87</sub>	1.14	-
10725	289.78678	-0.80352	17.74	17.42	15.76	14.76	15.35	12.93	12.33	12.00	4.52 <sup>+0.10</sup> <sub>-0.07</sub>	6.08 <sup>+0.08</sup> <sub>-0.09</sub>	3.99 <sup>+0.09</sup> <sub>-0.08</sub>	14.35 <sup>+1.19</sup> <sub>-0.78</sub>	0.81	-
10749	289.79798	-1.36249	15.46	15.63	14.48	13.79	14.18	12.65	12.34	12.12	4.54 <sup>+0.09</sup> <sub>-0.07</sub>	4.21 <sup>+0.06</sup> <sub>-0.08</sub>	3.72 <sup>+0.09</sup> <sub>-0.08</sub>	14.96 <sup>+1.16</sup> <sub>-0.81</sub>	1.37	-
10763	289.80671	-0.23100	13.23	13.56	12.56	12.03	12.31	11.06	10.80	10.66	4.51 <sup>+0.09</sup> <sub>-0.07</sub>	3.63 <sup>+0.07</sup> <sub>-0.08</sub>	3.72 <sup>+0.11</sup> <sub>-0.10</sub>	13.23 <sup>+1.11</sup> <sub>-0.73</sub>	0.73	-
10766	289.80813	-1.27943	12.55	13.02	12.14	11.71	11.85	10.77	10.54	10.36	4.48 <sup>+0.08</sup> <sub>-0.06</sub>	3.41 <sup>+0.08</sup> <sub>-0.08</sub>	4.04 <sup>+0.13</sup> <sub>-0.13</sub>	12.61 <sup>+0.90</sup> <sub>-0.59</sub>	3.32	EM
10778	289.81396	-1.40707	14.45	14.88	13.96	13.43	13.71	12.58	12.34	12.18	4.57 <sup>+0.08</sup> <sub>-0.07</sub>	3.47 <sup>+0.06</sup> <sub>-0.07</sub>	3.71 <sup>+0.11</sup> <sub>-0.10</sub>	15.47 <sup>+1.10</sup> <sub>-0.86</sub>	0.49	-
10780	289.81592	0.91779	17.11	17.57	16.83	16.28	16.50	15.50	15.29	15.19	4.48 <sup>+0.10</sup> <sub>-0.07</sub>	3.23 <sup>+0.12</sup> <sub>-0.11</sub>	3.94 <sup>+0.23</sup> <sub>-0.21</sub>	17.42 <sup>+1.16</sup> <sub>-0.74</sub>	5.12	-
10788	289.82017	-1.14273	15.50	15.64	14.51	13.82	14.18	12.62	12.28	12.11	4.50 <sup>+0.10</sup> <sub>-0.07</sub>	4.26 <sup>+0.08</sup> <sub>-0.09</sub>	3.82 <sup>+0.11</sup> <sub>-0.10</sub>	14.45 <sup>+1.15</sup> <sub>-0.74</sub>	0.94	-
10795	289.82214	0.92030	17.28	17.70	16.66	16.02	16.37	15.06	14.63	14.53	4.63 <sup>+0.05</sup> <sub>-0.07</sub>	3.98 <sup>+0.07</sup> <sub>-0.07</sub>	3.89 <sup>+0.12</sup> <sub>-0.11</sub>	18.43 <sup>+0.66</sup> <sub>-0.89</sub>	4.39	-
10823	289.83942	-1.02621	17.20	16.62	14.61	13.41	14.16	11.09	10.34	9.91	4.57 <sup>+0.08</sup> <sub>-0.09</sub>	7.39 <sup>+0.05</sup> <sub>-0.08</sub>	4.11 <sup>+0.06</sup> <sub>-0.06</sub>	12.74 <sup>+1.07</sup> <sub>-1.00</sub>	1.09	-
10839	289.85268	-0.83860	13.50	13.79	12.74	12.14	12.45	11.16	10.88	10.72	4.55 <sup>+0.08</sup> <sub>-0.08</sub>	3.80 <sup>+0.05</sup> <sub>-0.08</sub>	3.65 <sup>+0.10</sup> <sub>-0.09</sub>	13.68 <sup>+1.05</sup> <sub>-0.86</sub>	0.28	-
10852	289.86061	-1.03656	17.33	16.95	15.23	14.19	14.84	12.30	11.68	11.41	4.55 <sup>+0.09</sup> <sub>-0.09</sub>	6.23 <sup>+0.06</sup> <sub>-0.08</sub>	3.91 <sup>+0.07</sup> <sub>-0.06</sub>	14.08 <sup>+1.15</sup> <sub>-0.95</sub>	2.72	-
10853	289.86106	-0.49966	14.02	14.28	13.24	12.67	12.96	11.72	11.48	11.33	4.52 <sup>+0.07</sup> <sub>-0.07</sub>	3.65 <sup>+0.07</sup> <sub>-0.08</sub>	3.53 <sup>+0.10</sup> <sub>-0.08</sub>	14.04 <sup>+1.12</sup> <sub>-0.78</sub>	0.22	-
10866	289.86456	-1.03690	16.42	16.47	15.08	14.26	14.74	12.77	12.28	12.04	4.59 <sup>+0.05</sup> <sub>-0.08</sub>	5.18 <sup>+0.05</sup> <sub>-0.06</sub>	3.98 <sup>+0.08</sup> <sub>-0.07</sub>	15.36 <sup>+0.90</sup> <sub>-0.94</sub>	0.80	-
10869	289.86696	-0.75370	13.61	13.98	12.91	12.29	12.60	11.20	10.81	10.60	4.58 <sup>+0.08</sup> <sub>-0.07</sub>	4.17 <sup>+0.06</sup> <sub>-0.06</sub>	4.07 <sup>+0.10</sup> <sub>-0.10</sub>	13.91 <sup>+0.97</sup> <sub>-0.87</sub>	2.00	-
10874	289.87188	-1.09747	13.61	13.85	12.74	12.09	12.41	10.95	10.65	10.44	4.55 <sup>+0.09</sup> <sub>-0.07</sub>	4.14 <sup>+0.06</sup> <sub>-0.07</sub>	3.82 <sup>+0.09</sup> <sub>-0.08</sub>	13.38 <sup>+1.07</sup> <sub>-0.84</sub>	1.02	-
10883	289.87592	0.26242	16.25	16.74	15.88	15.42	15.71	14.56	14.28	14.32	4.54 <sup>+0.09</sup> <sub>-0.07</sub>	3.26 <sup>+0.10</sup> <sub>-0.10</sub>	3.76 <sup>+0.18</sup> <sub>-0.17</sub>	17.17 <sup>+1.15</sup> <sub>-0.83</sub>	2.39	-
10895	289.88199	-1.03084	16.01	16.02	14.73	13.94	14.39	12.59	12.15	11.89	4.48 <sup>+0.07</sup> <sub>-0.06</sub>	4.79 <sup>+0.07</sup> <sub>-0.09</sub>	3.93 <sup>+0.09</sup> <sub>-0.08</sub>	14.00 <sup>+0.82</sup> <sub>-0.64</sub>	1.37	-
10898	289.88386	0.83176	14.17	14.42	13.37	12.74	13.07	11.74	11.48	11.28	4.53 <sup>+0.09</sup> <sub>-0.07</sub>	3.84 <sup>+0.06</sup> <sub>-0.08</sub>	3.66 <sup>+0.10</sup> <sub>-0.09</sub>	14.07 <sup>+1.14</sup> <sub>-0.79</sub>	1.18	-
10912	289.89017	-1.05692	15.64	15.62	14.20	13.33	13.85	11.79	11.25	10.97	4.58 <sup>+0.08</sup> <sub>-0.08</sub>	5.40 <sup>+0.05</sup> <sub>-0.07</sub>	4.04 <sup>+0.08</sup> <sub>-0.08</sub>	14.18 <sup>+1.01</sup> <sub>-0.95</sub>	1.78	-
10918	289.89344	-0.80184	16.80	16.72	15.22	14.31	14.85	12.59	12.01	11.65	4.54 <sup>+0.08</sup> <sub>-0.07</sub>	5.80 <sup>+0.06</sup> <sub>-0.08</sub>	4.24 <sup>+0.09</sup> <sub>-0.08</sub>	14.25 <sup>+0.99</sup> <sub>-0.80</sub>	2.69	-
10923	289.89515	-1.35458	15.71	15.57	14.10	13.25	13.76	11.62	11.11	10.81	4.48 <sup>+0.08</sup> <sub>-0.06</sub>	5.42 <sup>+0.08</sup> <sub>-0.09</sub>	4.03 <sup>+0.08</sup> <sub>-0.08</sub>	12.80 <sup>+0.89</sup> <sub>-0.61</sub>	0.30	-
10964	289.91560	-0.79016	18.25	17.68	15.68	14.49	15.25	12.18	11.45	11.00	4.56 <sup>+0.09</sup> <sub>-0.08</sub>	7.35 <sup>+0.05</sup> <sub>-0.08</sub>	4.12 <sup>+0.06</sup> <sub>-0.06</sub>	13.73 <sup>+1.11</sup> <sub>-0.89</sub>	1.28	-
11010	289.94767	0.31477	18.82	18.95	17.68	16.96	17.38	15.81	15.18	15.05	4.57 <sup>+0.09</sup> <sub>-0.09</sub>	4.59 <sup>+0.10</sup> <sub>-0.11</sub>	3.83 <sup>+0.14</sup> <sub>-0.13</sub>	18.19 <sup>+1.10</sup> <sub>-0.99</sub>	3.72	-

Continued on next page...

ID	$\ell$	$b$	u	g	r	i	H $\alpha$	J	H	K	$\log(T_{\text{eff}})$	$A_0$	$R_V$	$\mu$	$\chi^2$	Notes
11026	289.95943	-0.95903	12.91	13.27	12.24	11.74	11.91	10.68	10.38	10.27	4.52 <sup>+0.08</sup> <sub>-0.06</sub>	3.78 <sup>+0.06</sup> <sub>-0.08</sub>	3.87 <sup>+0.11</sup> <sub>-0.09</sub>	12.89 <sup>+1.02</sup> <sub>-0.70</sub>	4.29	—
11045	289.97441	-1.63652	19.57	18.64	16.22	14.69	15.77	11.62	10.57	10.07	4.59 <sup>+0.07</sup> <sub>-0.11</sub>	9.35 <sup>+0.05</sup> <sub>-0.08</sub>	4.41 <sup>+0.06</sup> <sub>-0.06</sub>	12.91 <sup>+0.94</sup> <sub>-1.27</sub>	3.81	—
11053	289.97863	-0.78158	13.61	13.99	13.04	12.49	12.78	11.85	11.60	11.50	4.58 <sup>+0.08</sup> <sub>-0.08</sub>	3.18 <sup>+0.05</sup> <sub>-0.06</sub>	3.25 <sup>+0.09</sup> <sub>-0.08</sub>	14.93 <sup>+0.97</sup> <sub>-0.90</sub>	3.43	—
11054	289.97888	-1.50970	13.97	14.25	13.15	12.44	12.82	11.34	10.96	10.72	4.59 <sup>+0.07</sup> <sub>-0.08</sub>	4.29 <sup>+0.05</sup> <sub>-0.06</sub>	3.95 <sup>+0.09</sup> <sub>-0.09</sub>	14.17 <sup>+0.91</sup> <sub>-0.93</sub>	4.33	—
11065	289.98418	0.21214	17.32	17.83	16.86	16.46	16.79	15.51	15.26	15.25	4.55 <sup>+0.08</sup> <sub>-0.07</sub>	3.45 <sup>+0.11</sup> <sub>-0.10</sub>	3.86 <sup>+0.19</sup> <sub>-0.17</sub>	18.22 <sup>+0.97</sup> <sub>-0.84</sub>	7.76	—
11074	289.99163	-0.97897	14.92	15.30	14.39	13.85	14.11	13.03	12.76	12.64	4.53 <sup>+0.09</sup> <sub>-0.07</sub>	3.41 <sup>+0.07</sup> <sub>-0.08</sub>	3.64 <sup>+0.11</sup> <sub>-0.10</sub>	15.49 <sup>+1.14</sup> <sub>-0.82</sub>	0.77	—
11082	289.99612	-1.14050	13.85	14.22	13.36	12.84	13.09	12.11	11.89	11.80	4.50 <sup>+0.10</sup> <sub>-0.07</sub>	3.14 <sup>+0.07</sup> <sub>-0.09</sub>	3.44 <sup>+0.11</sup> <sub>-0.10</sub>	14.34 <sup>+1.13</sup> <sub>-0.71</sub>	1.00	—
11085	289.99729	-0.95698	12.97	13.49	12.74	12.32	12.51	11.80	11.59	11.50	4.51 <sup>+0.08</sup> <sub>-0.06</sub>	2.72 <sup>+0.06</sup> <sub>-0.08</sub>	3.40 <sup>+0.12</sup> <sub>-0.11</sub>	14.17 <sup>+1.00</sup> <sub>-0.69</sub>	2.27	—
11087	289.99839	-0.93403	15.58	15.52	14.12	13.28	13.76	11.83	11.25	11.05	4.52 <sup>+0.10</sup> <sub>-0.08</sub>	5.17 <sup>+0.08</sup> <sub>-0.09</sub>	3.94 <sup>+0.09</sup> <sub>-0.09</sub>	13.53 <sup>+1.21</sup> <sub>-0.83</sub>	2.52	—
11090	290.00254	-1.05951	18.30	17.87	16.09	15.07	15.73	13.13	12.48	12.16	4.48 <sup>+0.09</sup> <sub>-0.06</sub>	6.32 <sup>+0.08</sup> <sub>-0.09</sub>	3.97 <sup>+0.07</sup> <sub>-0.07</sub>	14.08 <sup>+1.03</sup> <sub>-0.66</sub>	0.65	—
11101	290.01117	-0.89059	17.52	17.32	15.83	14.95	15.52	13.35	12.82	12.57	4.48 <sup>+0.10</sup> <sub>-0.07</sub>	5.40 <sup>+0.09</sup> <sub>-0.10</sub>	3.90 <sup>+0.09</sup> <sub>-0.08</sub>	14.61 <sup>+1.18</sup> <sub>-0.68</sub>	0.49	—
11110	290.02045	-1.47437	13.33	13.91	13.22	12.71	12.93	12.02	11.83	11.73	4.59 <sup>+0.08</sup> <sub>-0.09</sub>	3.04 <sup>+0.05</sup> <sub>-0.07</sub>	3.78 <sup>+0.13</sup> <sub>-0.12</sub>	15.25 <sup>+1.01</sup> <sub>-1.06</sub>	4.59	—
11136	290.03215	-0.92421	13.71	14.13	13.31	12.83	13.05	12.13	11.91	11.89	4.50 <sup>+0.10</sup> <sub>-0.07</sub>	3.01 <sup>+0.08</sup> <sub>-0.09</sub>	3.48 <sup>+0.12</sup> <sub>-0.11</sub>	14.37 <sup>+1.15</sup> <sub>-0.74</sub>	2.04	—
11163	290.04404	-2.29045	18.09	17.96	16.43	15.58	15.94	14.07	13.48	13.25	4.55 <sup>+0.09</sup> <sub>-0.08</sub>	5.38 <sup>+0.06</sup> <sub>-0.08</sub>	3.84 <sup>+0.08</sup> <sub>-0.08</sub>	16.02 <sup>+1.18</sup> <sub>-0.89</sub>	3.48	EM
11182	290.05664	-1.04668	14.44	14.88	14.03	13.52	13.76	12.80	12.51	12.42	4.52 <sup>+0.09</sup> <sub>-0.07</sub>	3.23 <sup>+0.06</sup> <sub>-0.08</sub>	3.65 <sup>+0.12</sup> <sub>-0.11</sub>	15.15 <sup>+1.08</sup> <sub>-0.76</sub>	2.32	—
11191	290.06419	-0.99610	17.73	17.72	16.42	15.64	16.10	14.25	13.83	13.55	4.49 <sup>+0.09</sup> <sub>-0.07</sub>	4.83 <sup>+0.07</sup> <sub>-0.09</sub>	3.92 <sup>+0.10</sup> <sub>-0.09</sub>	15.72 <sup>+0.99</sup> <sub>-0.68</sub>	1.43	—
11193	290.06626	-0.53868	20.63	19.99	18.10	17.07	17.73	15.40	14.68	14.55	4.49 <sup>+0.13</sup> <sub>-0.12</sub>	5.96 <sup>+0.12</sup> <sub>-0.18</sub>	3.47 <sup>+0.09</sup> <sub>-0.09</sub>	16.60 <sup>+1.52</sup> <sub>-1.22</sub>	3.97	—
11222	290.08407	-0.45954	14.95	15.14	14.06	13.44	13.77	12.41	12.16	12.00	4.49 <sup>+0.09</sup> <sub>-0.07</sub>	3.80 <sup>+0.08</sup> <sub>-0.09</sub>	3.57 <sup>+0.10</sup> <sub>-0.09</sub>	14.31 <sup>+1.05</sup> <sub>-0.69</sub>	0.93	—
11233	290.08790	-0.60251	16.32	15.85	14.09	13.08	13.68	11.25	10.73	10.41	4.49 <sup>+0.09</sup> <sub>-0.07</sub>	6.00 <sup>+0.08</sup> <sub>-0.09</sub>	3.73 <sup>+0.07</sup> <sub>-0.06</sub>	12.50 <sup>+1.03</sup> <sub>-0.69</sub>	0.52	—
11248	290.09870	0.42583	15.36	15.57	14.46	13.87	14.21	12.93	12.55	12.38	4.48 <sup>+0.08</sup> <sub>-0.06</sub>	3.83 <sup>+0.08</sup> <sub>-0.09</sub>	3.64 <sup>+0.10</sup> <sub>-0.09</sub>	14.59 <sup>+0.95</sup> <sub>-0.63</sub>	4.65	—
11249	290.09935	-0.92583	14.73	14.70	13.19	12.26	12.74	10.58	10.03	9.67	4.61 <sup>+0.06</sup> <sub>-0.07</sub>	5.76 <sup>+0.05</sup> <sub>-0.05</sub>	4.15 <sup>+0.08</sup> <sub>-0.07</sub>	13.19 <sup>+0.78</sup> <sub>-0.91</sub>	2.73	—
11252	290.10119	-0.92572	16.08	16.25	15.03	14.31	14.71	13.03	12.64	12.42	4.56 <sup>+0.09</sup> <sub>-0.08</sub>	4.58 <sup>+0.06</sup> <sub>-0.07</sub>	3.92 <sup>+0.10</sup> <sub>-0.09</sub>	15.47 <sup>+1.16</sup> <sub>-0.92</sub>	0.56	—
11261	290.10367	-0.92413	14.03	14.39	13.32	12.68	13.01	11.63	11.34	11.19	4.63 <sup>+0.05</sup> <sub>-0.07</sub>	3.98 <sup>+0.04</sup> <sub>-0.05</sub>	3.77 <sup>+0.08</sup> <sub>-0.08</sub>	15.09 <sup>+0.66</sup> <sub>-0.86</sub>	1.63	—
11266	290.10658	-0.99214	14.75	14.92	13.66	12.94	13.34	11.62	11.24	11.04	4.60 <sup>+0.07</sup> <sub>-0.08</sub>	4.63 <sup>+0.05</sup> <sub>-0.06</sub>	3.87 <sup>+0.08</sup> <sub>-0.08</sub>	14.48 <sup>+0.89</sup> <sub>-0.94</sub>	0.90	—
11398	290.18761	-1.11133	14.27	14.80	14.05	13.61	13.81	13.03	12.77	12.74	4.54 <sup>+0.09</sup> <sub>-0.07</sub>	2.84 <sup>+0.07</sup> <sub>-0.08</sub>	3.50 <sup>+0.13</sup> <sub>-0.12</sub>	15.67 <sup>+1.15</sup> <sub>-0.82</sub>	1.27	—
11436	290.21213	-1.35299	13.60	14.15	13.48	13.05	13.17	12.54	12.35	12.26	4.49 <sup>+0.09</sup> <sub>-0.07</sub>	2.64 <sup>+0.08</sup> <sub>-0.09</sub>	3.52 <sup>+0.14</sup> <sub>-0.13</sub>	14.75 <sup>+1.04</sup> <sub>-0.70</sub>	2.44	—
11464	290.22858	-1.60146	15.91	15.83	14.52	13.71	14.16	12.42	12.06	11.88	4.50 <sup>+0.10</sup> <sub>-0.07</sub>	4.59 <sup>+0.07</sup> <sub>-0.09</sub>	3.57 <sup>+0.08</sup> <sub>-0.08</sub>	14.17 <sup>+1.12</sup> <sub>-0.72</sub>	2.74	—
11535	290.28170	-1.00591	15.74	15.53	14.07	13.22	13.73	11.80	11.39	11.18	4.49 <sup>+0.10</sup> <sub>-0.07</sub>	4.94 <sup>+0.08</sup> <sub>-0.09</sub>	3.55 <sup>+0.07</sup> <sub>-0.07</sub>	13.42 <sup>+1.21</sup> <sub>-0.74</sub>	0.99	—
11544	290.28974	-1.10619	14.20	14.43	13.35	12.71	13.04	11.68	11.41	11.24	4.56 <sup>+0.09</sup> <sub>-0.08</sub>	3.90 <sup>+0.06</sup> <sub>-0.08</sub>	3.61 <sup>+0.09</sup> <sub>-0.09</sub>	14.29 <sup>+1.11</sup> <sub>-0.96</sub>	0.92	—
11547	290.29272	0.36083	14.86	14.94	13.70	13.00	13.38	11.83	11.45	11.29	4.52 <sup>+0.09</sup> <sub>-0.07</sub>	4.33 <sup>+0.07</sup> <sub>-0.08</sub>	3.63 <sup>+0.08</sup> <sub>-0.08</sub>	13.91 <sup>+1.06</sup> <sub>-0.78</sub>	0.69	—
11552	290.29501	-1.49313	16.79	16.54	15.03	14.15	14.70	12.69	12.22	12.03	4.49 <sup>+0.09</sup> <sub>-0.07</sub>	5.10 <sup>+0.08</sup> <sub>-0.09</sub>	3.59 <sup>+0.07</sup> <sub>-0.07</sub>	14.16 <sup>+1.10</sup> <sub>-0.68</sub>	2.09	—
11578	290.32093	-1.00849	16.43	16.12	14.48	13.47	14.09	11.72	11.20	10.88	4.56 <sup>+0.09</sup> <sub>-0.09</sub>	5.89 <sup>+0.06</sup> <sub>-0.08</sub>	3.82 <sup>+0.07</sup> <sub>-0.06</sub>	13.76 <sup>+1.09</sup> <sub>-0.97</sub>	2.02	—
11594	290.33703	0.35494	18.55	19.12	18.18	17.45	17.92	15.92	15.50	14.98	4.63 <sup>+0.05</sup> <sub>-0.06</sub>	5.03 <sup>+0.08</sup> <sub>-0.09</sub>	5.30 <sup>+0.07</sup> <sub>-0.11</sub>	18.96 <sup>+0.60</sup> <sub>-0.80</sub>	4.13	—

Continued on next page...

ID	$\ell$	$b$	u	g	r	i	H $\alpha$	J	H	K	$\log(T_{\text{eff}})$	$A_0$	$R_V$	$\mu$	$\chi^2$	Notes
11608	290.34452	-1.02272	15.49	15.62	14.37	13.63	14.08	12.39	12.00	11.82	4.59 <sup>+0.07</sup> <sub>-0.08</sub>	4.53 <sup>+0.05</sup> <sub>-0.06</sub>	3.75 <sup>+0.08</sup> <sub>-0.07</sub>	15.26 <sup>+0.90</sup> <sub>-0.92</sub>	0.84	—
11618	290.35312	-0.79405	13.55	13.76	12.69	11.98	12.34	10.86	10.53	10.38	4.56 <sup>+0.09</sup> <sub>-0.08</sub>	4.16 <sup>+0.07</sup> <sub>-0.08</sub>	3.79 <sup>+0.11</sup> <sub>-0.10</sub>	13.47 <sup>+1.13</sup> <sub>-0.96</sub>	3.40	—
11665	290.39551	-0.72590	18.30	17.64	15.52	14.23	15.09	11.73	10.97	10.55	4.61 <sup>+0.06</sup> <sub>-0.08</sub>	7.79 <sup>+0.05</sup> <sub>-0.06</sub>	4.11 <sup>+0.06</sup> <sub>-0.05</sub>	13.78 <sup>+0.82</sup> <sub>-0.94</sub>	1.83	—
11667	290.39779	-1.49996	14.06	14.47	13.49	12.87	13.20	11.96	11.65	11.45	4.59 <sup>+0.07</sup> <sub>-0.08</sub>	3.78 <sup>+0.05</sup> <sub>-0.06</sub>	3.83 <sup>+0.09</sup> <sub>-0.09</sub>	14.95 <sup>+0.94</sup> <sub>-0.90</sub>	3.47	—
11674	290.40310	-0.93468	15.47	15.51	14.26	13.55	13.95	12.33	11.99	11.83	4.51 <sup>+0.09</sup> <sub>-0.07</sub>	4.35 <sup>+0.07</sup> <sub>-0.09</sub>	3.62 <sup>+0.09</sup> <sub>-0.08</sub>	14.25 <sup>+1.06</sup> <sub>-0.74</sub>	1.00	—
11676	290.40416	-0.67211	16.91	16.64	15.10	14.22	14.75	12.66	12.28	12.09	4.51 <sup>+0.09</sup> <sub>-0.07</sub>	5.16 <sup>+0.07</sup> <sub>-0.09</sub>	3.54 <sup>+0.07</sup> <sub>-0.06</sub>	14.43 <sup>+1.11</sup> <sub>-0.74</sub>	5.08	—
11733	290.44101	-1.82203	16.09	16.33	15.32	14.71	15.05	13.72	13.56	13.30	4.48 <sup>+0.10</sup> <sub>-0.10</sub>	3.71 <sup>+0.10</sup> <sub>-0.11</sub>	3.67 <sup>+0.16</sup> <sub>-0.15</sub>	15.54 <sup>+1.24</sup> <sub>-0.69</sub>	1.45	—
11762	290.46580	-0.46644	19.89	19.89	18.24	17.27	17.83	15.58	15.16	14.72	4.63 <sup>+0.05</sup> <sub>-0.07</sub>	5.76 <sup>+0.09</sup> <sub>-0.09</sub>	3.84 <sup>+0.10</sup> <sub>-0.10</sub>	18.55 <sup>+0.66</sup> <sub>-0.90</sub>	6.09	—
11792	290.48311	-0.94776	13.86	14.03	12.96	12.26	12.61	11.23	10.90	10.73	4.51 <sup>+0.10</sup> <sub>-0.07</sub>	4.01 <sup>+0.08</sup> <sub>-0.09</sub>	3.66 <sup>+0.10</sup> <sub>-0.09</sub>	13.28 <sup>+1.24</sup> <sub>-0.78</sub>	3.61	—
11810	290.49707	-1.54270	17.06	17.69	16.83	16.23	16.57	15.37	14.83	14.77	4.63 <sup>+0.05</sup> <sub>-0.07</sub>	3.90 <sup>+0.11</sup> <sub>-0.12</sub>	4.48 <sup>+0.18</sup> <sub>-0.19</sub>	18.69 <sup>+0.63</sup> <sub>-0.91</sub>	4.54	—
11820	290.50165	-2.10599	13.05	13.83	13.32	12.96	13.09	12.60	12.48	12.45	4.61 <sup>+0.06</sup> <sub>-0.08</sub>	2.26 <sup>+0.04</sup> <sub>-0.05</sub>	3.49 <sup>+0.14</sup> <sub>-0.12</sub>	16.35 <sup>+0.82</sup> <sub>-0.98</sub>	3.12	—
11841	290.51442	-1.16932	15.67	15.62	14.32	13.47	13.96	12.05	11.68	11.40	4.49 <sup>+0.08</sup> <sub>-0.06</sub>	4.89 <sup>+0.07</sup> <sub>-0.08</sub>	3.85 <sup>+0.09</sup> <sub>-0.08</sub>	13.64 <sup>+0.96</sup> <sub>-0.68</sub>	4.25	—
11868	290.53217	-1.73886	14.06	14.66	14.06	13.62	13.80	13.07	12.95	12.82	4.51 <sup>+0.10</sup> <sub>-0.07</sub>	2.64 <sup>+0.08</sup> <sub>-0.09</sub>	3.67 <sup>+0.16</sup> <sub>-0.14</sub>	15.43 <sup>+1.16</sup> <sub>-0.77</sub>	3.67	—
11869	290.53240	-0.92293	16.51	16.36	14.86	13.96	14.53	12.26	11.84	11.53	4.54 <sup>+0.09</sup> <sub>-0.08</sub>	5.53 <sup>+0.06</sup> <sub>-0.08</sub>	3.93 <sup>+0.08</sup> <sub>-0.08</sub>	14.21 <sup>+1.11</sup> <sub>-0.85</sub>	3.82	—
11874	290.53501	-1.20832	14.13	14.38	13.31	12.67	13.03	11.64	11.33	11.12	4.54 <sup>+0.09</sup> <sub>-0.07</sub>	3.98 <sup>+0.06</sup> <sub>-0.08</sub>	3.75 <sup>+0.10</sup> <sub>-0.09</sub>	13.98 <sup>+1.16</sup> <sub>-0.83</sub>	1.31	—
11907	290.55946	-0.91757	15.89	15.80	14.42	13.60	14.09	12.15	11.79	11.60	4.53 <sup>+0.10</sup> <sub>-0.07</sub>	4.89 <sup>+0.06</sup> <sub>-0.08</sub>	3.66 <sup>+0.08</sup> <sub>-0.07</sub>	14.24 <sup>+1.17</sup> <sub>-0.81</sub>	3.60	—
11933	290.57023	-0.86194	15.40	15.94	15.26	14.81	14.98	14.15	13.99	13.98	4.51 <sup>+0.10</sup> <sub>-0.07</sub>	2.78 <sup>+0.14</sup> <sub>-0.13</sub>	3.61 <sup>+0.25</sup> <sub>-0.23</sub>	16.58 <sup>+1.25</sup> <sub>-0.81</sub>	1.86	—
11937	290.57246	-0.78957	19.62	18.56	16.28	14.97	15.85	12.72	12.03	11.72	4.52 <sup>+0.11</sup> <sub>-0.08</sub>	7.30 <sup>+0.08</sup> <sub>-0.10</sub>	3.50 <sup>+0.05</sup> <sub>-0.05</sub>	14.00 <sup>+1.32</sup> <sub>-0.87</sub>	1.91	—
11960	290.58607	0.05420	18.24	17.93	16.39	15.41	15.85	13.93	13.49	13.25	4.55 <sup>+0.10</sup> <sub>-0.09</sub>	5.29 <sup>+0.06</sup> <sub>-0.09</sub>	3.52 <sup>+0.07</sup> <sub>-0.07</sub>	16.09 <sup>+1.22</sup> <sub>-0.98</sub>	4.97	—
11961	290.58659	-0.89052	16.99	17.01	15.76	15.03	15.46	13.74	13.47	13.20	4.48 <sup>+0.08</sup> <sub>-0.07</sub>	4.42 <sup>+0.08</sup> <sub>-0.09</sub>	3.68 <sup>+0.09</sup> <sub>-0.09</sub>	15.41 <sup>+1.02</sup> <sub>-0.69</sub>	3.76	—
11979	290.59721	-2.05635	14.18	14.89	14.38	14.01	14.14	13.76	13.68	13.65	4.57 <sup>+0.08</sup> <sub>-0.08</sub>	2.05 <sup>+0.06</sup> <sub>-0.07</sub>	3.09 <sup>+0.15</sup> <sub>-0.13</sub>	17.13 <sup>+1.05</sup> <sub>-0.96</sub>	4.98	—
11990	290.60426	-1.30602	18.06	17.84	16.32	15.42	15.99	13.78	13.34	13.00	4.48 <sup>+0.09</sup> <sub>-0.06</sub>	5.45 <sup>+0.09</sup> <sub>-0.10</sub>	3.88 <sup>+0.09</sup> <sub>-0.09</sub>	15.01 <sup>+1.10</sup> <sub>-0.65</sub>	1.07	—
11993	290.60594	-0.89048	15.05	15.18	13.91	13.15	13.59	11.87	11.54	11.35	4.62 <sup>+0.05</sup> <sub>-0.08</sub>	4.55 <sup>+0.05</sup> <sub>-0.05</sub>	3.70 <sup>+0.08</sup> <sub>-0.07</sub>	15.12 <sup>+0.73</sup> <sub>-0.93</sub>	2.21	—
12001	290.60938	-2.01071	18.70	18.95	17.69	16.93	17.34	15.85	15.36	15.37	4.63 <sup>+0.04</sup> <sub>-0.06</sub>	4.43 <sup>+0.11</sup> <sub>-0.10</sub>	3.69 <sup>+0.12</sup> <sub>-0.12</sub>	19.17 <sup>+0.52</sup> <sub>-0.77</sub>	5.72	—
12018	290.61906	-1.32014	16.00	15.62	13.93	12.96	13.57	11.24	10.74	10.45	4.52 <sup>+0.10</sup> <sub>-0.07</sub>	5.76 <sup>+0.07</sup> <sub>-0.09</sub>	3.68 <sup>+0.07</sup> <sub>-0.07</sub>	12.84 <sup>+1.22</sup> <sub>-0.79</sub>	0.40	—
12019	290.62019	-1.76551	18.95	19.13	17.91	17.13	17.57	15.84	15.27	15.17	4.59 <sup>+0.07</sup> <sub>-0.09</sub>	4.81 <sup>+0.12</sup> <sub>-0.12</sub>	4.08 <sup>+0.16</sup> <sub>-0.14</sub>	18.43 <sup>+0.97</sup> <sub>-1.06</sub>	2.09	—
12027	290.62523	-0.90093	19.73	18.90	16.86	15.65	16.46	13.57	13.03	12.65	4.49 <sup>+0.13</sup> <sub>-0.10</sub>	6.72 <sup>+0.11</sup> <sub>-0.14</sub>	3.60 <sup>+0.07</sup> <sub>-0.07</sub>	14.64 <sup>+1.53</sup> <sub>-1.00</sub>	2.29	—
12051	290.63606	-0.88975	20.18	19.72	17.95	16.91	17.59	14.98	14.56	14.14	4.50 <sup>+0.12</sup> <sub>-0.11</sub>	6.11 <sup>+0.11</sup> <sub>-0.16</sub>	3.77 <sup>+0.09</sup> <sub>-0.09</sub>	16.33 <sup>+1.48</sup> <sub>-1.17</sub>	2.76	—
12057	290.63856	-0.90043	16.91	16.66	14.99	14.00	14.64	12.18	11.73	11.47	4.62 <sup>+0.06</sup> <sub>-0.07</sub>	5.88 <sup>+0.05</sup> <sub>-0.05</sub>	3.79 <sup>+0.06</sup> <sub>-0.06</sub>	15.01 <sup>+0.75</sup> <sub>-0.92</sub>	6.18	—
12063	290.64354	-0.92174	17.10	16.65	14.92	13.89	14.54	12.12	11.59	11.34	4.54 <sup>+0.09</sup> <sub>-0.08</sub>	5.92 <sup>+0.07</sup> <sub>-0.08</sub>	3.64 <sup>+0.06</sup> <sub>-0.06</sub>	14.01 <sup>+1.07</sup> <sub>-0.86</sub>	1.98	—
12086	290.66137	-0.96057	20.26	19.78	17.98	16.95	17.63	15.17	14.68	14.44	4.55 <sup>+0.11</sup> <sub>-0.12</sub>	5.92 <sup>+0.10</sup> <sub>-0.13</sub>	3.57 <sup>+0.09</sup> <sub>-0.09</sub>	17.16 <sup>+1.32</sup> <sub>-1.33</sub>	1.19	—
12093	290.66732	-0.81169	17.24	16.28	14.06	12.77	13.61	10.44	9.79	9.34	4.48 <sup>+0.09</sup> <sub>-0.07</sub>	7.40 <sup>+0.09</sup> <sub>-0.09</sub>	3.71 <sup>+0.05</sup> <sub>-0.05</sub>	11.19 <sup>+1.07</sup> <sub>-0.67</sub>	2.08	—
12094	290.66854	-1.27234	15.76	15.62	14.19	13.32	13.84	11.92	11.45	11.24	4.53 <sup>+0.09</sup> <sub>-0.07</sub>	5.03 <sup>+0.06</sup> <sub>-0.08</sub>	3.68 <sup>+0.07</sup> <sub>-0.07</sub>	13.88 <sup>+1.12</sup> <sub>-0.81</sub>	2.01	—

Continued on next page...

ID	$\ell$	$b$	u	g	r	i	H $\alpha$	J	H	K	$\log(T_{\text{eff}})$	$A_0$	$R_V$	$\mu$	$\chi^2$	Notes
12114	290.68135	-0.30980	16.09	15.55	13.69	12.65	13.28	10.84	10.32	9.94	4.51 <sup>+0.09</sup> <sub>-0.07</sub>	6.10 <sup>+0.07</sup> <sub>-0.08</sub>	3.61 <sup>+0.06</sup> <sub>-0.05</sub>	12.22 <sup>+1.06</sup> <sub>-0.71</sub>	2.39	—
12116	290.68294	-0.30062	16.31	15.95	14.27	13.34	13.90	11.71	11.29	10.96	4.52 <sup>+0.09</sup> <sub>-0.07</sub>	5.54 <sup>+0.07</sup> <sub>-0.08</sub>	3.58 <sup>+0.06</sup> <sub>-0.06</sub>	13.50 <sup>+1.11</sup> <sub>-0.78</sub>	1.96	—
12120	290.68369	-0.29569	19.84	19.19	17.26	16.18	16.89	14.29	13.76	13.47	4.51 <sup>+0.11</sup> <sub>-0.09</sub>	6.23 <sup>+0.08</sup> <sub>-0.12</sub>	3.54 <sup>+0.07</sup> <sub>-0.06</sub>	15.78 <sup>+1.30</sup> <sub>-0.97</sub>	0.47	—
12131	290.68682	-0.30392	18.18	17.44	15.44	14.34	15.05	12.44	11.86	11.54	4.48 <sup>+0.09</sup> <sub>-0.07</sub>	6.34 <sup>+0.09</sup> <sub>-0.10</sub>	3.50 <sup>+0.06</sup> <sub>-0.06</sub>	13.55 <sup>+1.07</sup> <sub>-0.70</sub>	0.21	—
12164	290.69652	-0.30652	18.51	17.89	16.00	14.97	15.63	13.13	12.60	12.32	4.48 <sup>+0.10</sup> <sub>-0.07</sub>	6.05 <sup>+0.10</sup> <sub>-0.10</sub>	3.53 <sup>+0.08</sup> <sub>-0.07</sub>	14.34 <sup>+1.15</sup> <sub>-0.74</sub>	0.25	—
12172	290.69855	-1.68624	14.06	14.19	13.03	12.38	12.75	11.23	10.99	10.71	4.48 <sup>+0.09</sup> <sub>-0.06</sub>	4.11 <sup>+0.08</sup> <sub>-0.09</sub>	3.69 <sup>+0.10</sup> <sub>-0.09</sub>	12.89 <sup>+0.99</sup> <sub>-0.63</sub>	4.56	—
12183	290.70268	-0.31208	18.96	18.23	16.21	15.07	15.81	13.10	12.56	12.29	4.55 <sup>+0.09</sup> <sub>-0.08</sub>	6.46 <sup>+0.06</sup> <sub>-0.08</sub>	3.48 <sup>+0.05</sup> <sub>-0.05</sub>	15.03 <sup>+1.17</sup> <sub>-0.93</sub>	1.87	—
12193	290.70893	-0.31025	18.20	17.42	15.34	14.20	14.96	12.17	11.62	11.26	4.51 <sup>+0.10</sup> <sub>-0.07</sub>	6.61 <sup>+0.08</sup> <sub>-0.09</sub>	3.52 <sup>+0.05</sup> <sub>-0.05</sub>	13.52 <sup>+1.23</sup> <sub>-0.77</sub>	0.91	—
12205	290.71263	-1.72900	18.41	18.61	17.55	16.83	17.29	15.59	15.39	15.03	4.50 <sup>+0.11</sup> <sub>-0.08</sub>	4.31 <sup>+0.12</sup> <sub>-0.12</sub>	4.06 <sup>+0.18</sup> <sub>-0.17</sub>	17.36 <sup>+1.33</sup> <sub>-0.82</sub>	4.80	—
12209	290.71424	-0.32554	17.77	16.91	14.78	13.57	14.36	11.52	10.94	10.58	4.53 <sup>+0.09</sup> <sub>-0.08</sub>	6.78 <sup>+0.06</sup> <sub>-0.09</sub>	3.49 <sup>+0.05</sup> <sub>-0.05</sub>	13.07 <sup>+1.13</sup> <sub>-0.83</sub>	1.06	—
12222	290.72113	-0.95182	19.03	18.23	16.14	14.92	15.73	12.74	12.11	11.76	4.53 <sup>+0.09</sup> <sub>-0.08</sub>	7.02 <sup>+0.06</sup> <sub>-0.09</sub>	3.68 <sup>+0.05</sup> <sub>-0.05</sub>	14.16 <sup>+1.13</sup> <sub>-0.83</sub>	1.34	—
12246	290.73940	-0.23511	17.21	16.51	14.54	13.42	14.14	11.48	10.93	10.60	4.51 <sup>+0.09</sup> <sub>-0.07</sub>	6.40 <sup>+0.07</sup> <sub>-0.09</sub>	3.55 <sup>+0.06</sup> <sub>-0.05</sub>	12.87 <sup>+1.08</sup> <sub>-0.78</sub>	0.61	—
12247	290.73942	-0.61437	20.52	19.42	17.01	15.59	16.58	13.07	12.30	11.86	4.56 <sup>+0.09</sup> <sub>-0.10</sub>	8.08 <sup>+0.07</sup> <sub>-0.09</sub>	3.72 <sup>+0.05</sup> <sub>-0.05</sub>	14.57 <sup>+1.16</sup> <sub>-1.08</sub>	1.28	—
12264	290.75180	-0.40483	16.75	16.29	14.54	13.55	14.16	11.89	11.42	11.14	4.53 <sup>+0.10</sup> <sub>-0.08</sub>	5.68 <sup>+0.07</sup> <sub>-0.09</sub>	3.50 <sup>+0.06</sup> <sub>-0.06</sub>	13.68 <sup>+1.25</sup> <sub>-0.84</sub>	0.44	—
12272	290.76035	-0.77706	19.91	18.40	15.64	14.02	15.11	10.98	10.07	9.55	4.50 <sup>+0.11</sup> <sub>-0.09</sub>	9.34 <sup>+0.08</sup> <sub>-0.11</sub>	3.82 <sup>+0.05</sup> <sub>-0.04</sub>	11.43 <sup>+1.26</sup> <sub>-0.90</sub>	1.62	—
12276	290.76249	-0.80560	20.26	19.51	17.41	16.17	16.98	13.86	13.23	12.79	4.53 <sup>+0.10</sup> <sub>-0.11</sub>	7.28 <sup>+0.08</sup> <sub>-0.12</sub>	3.86 <sup>+0.07</sup> <sub>-0.06</sub>	15.17 <sup>+1.27</sup> <sub>-1.13</sub>	2.24	—
12292	290.77372	-0.75715	20.81	19.87	17.61	16.30	17.20	13.91	13.19	12.77	4.51 <sup>+0.12</sup> <sub>-0.14</sub>	7.60 <sup>+0.09</sup> <sub>-0.18</sub>	3.75 <sup>+0.06</sup> <sub>-0.06</sub>	14.86 <sup>+1.46</sup> <sub>-1.37</sub>	0.23	—
12295	290.77500	-1.10443	13.00	13.33	12.45	11.83	12.13	10.99	10.69	10.61	4.51 <sup>+0.10</sup> <sub>-0.07</sub>	3.49 <sup>+0.07</sup> <sub>-0.09</sub>	3.67 <sup>+0.12</sup> <sub>-0.11</sub>	13.19 <sup>+1.22</sup> <sub>-0.79</sub>	6.37	—
12298	290.77787	-0.56370	17.49	17.56	16.28	15.57	15.96	14.40	13.88	13.74	4.52 <sup>+0.09</sup> <sub>-0.07</sub>	4.53 <sup>+0.07</sup> <sub>-0.08</sub>	3.76 <sup>+0.10</sup> <sub>-0.09</sub>	16.22 <sup>+1.12</sup> <sub>-0.75</sub>	3.76	—
12299	290.77908	-0.74782	18.88	18.16	16.09	14.85	15.67	12.63	11.97	11.58	4.58 <sup>+0.08</sup> <sub>-0.09</sub>	7.17 <sup>+0.07</sup> <sub>-0.08</sub>	3.81 <sup>+0.06</sup> <sub>-0.06</sub>	14.53 <sup>+1.04</sup> <sub>-1.04</sub>	1.28	—
12301	290.78085	-0.58539	18.31	18.43	17.21	16.51	16.89	15.37	14.99	14.72	4.54 <sup>+0.09</sup> <sub>-0.08</sub>	4.34 <sup>+0.12</sup> <sub>-0.13</sub>	3.70 <sup>+0.16</sup> <sub>-0.14</sub>	17.60 <sup>+1.14</sup> <sub>-0.90</sub>	1.24	—
12306	290.78174	-1.21518	15.19	15.05	13.63	12.80	13.29	11.38	10.95	10.78	4.51 <sup>+0.09</sup> <sub>-0.07</sub>	4.92 <sup>+0.07</sup> <sub>-0.09</sub>	3.64 <sup>+0.07</sup> <sub>-0.07</sub>	13.19 <sup>+1.05</sup> <sub>-0.74</sub>	3.50	—
12312	290.78494	-1.64075	13.23	13.42	12.30	11.65	11.99	10.62	10.33	10.15	4.55 <sup>+0.09</sup> <sub>-0.08</sub>	3.96 <sup>+0.06</sup> <sub>-0.08</sub>	3.56 <sup>+0.08</sup> <sub>-0.08</sub>	13.14 <sup>+1.10</sup> <sub>-0.88</sub>	0.52	—
12323	290.79087	-0.48485	18.04	18.00	16.62	15.88	16.29	14.78	14.30	14.07	4.52 <sup>+0.09</sup> <sub>-0.07</sub>	4.45 <sup>+0.07</sup> <sub>-0.09</sub>	3.46 <sup>+0.08</sup> <sub>-0.08</sub>	16.68 <sup>+1.05</sup> <sub>-0.78</sub>	6.92	—
12327	290.79396	-1.06477	14.29	14.58	13.60	13.02	13.34	12.12	11.84	11.73	4.51 <sup>+0.08</sup> <sub>-0.07</sub>	3.57 <sup>+0.07</sup> <sub>-0.08</sub>	3.59 <sup>+0.10</sup> <sub>-0.09</sub>	14.22 <sup>+0.99</sup> <sub>-0.69</sub>	1.27	—
12338	290.79881	-0.35821	15.82	15.58	14.09	13.23	13.75	11.81	11.41	11.19	4.49 <sup>+0.10</sup> <sub>-0.07</sub>	4.96 <sup>+0.08</sup> <sub>-0.09</sub>	3.52 <sup>+0.07</sup> <sub>-0.07</sub>	13.42 <sup>+1.11</sup> <sub>-0.68</sub>	0.85	—
12340	290.79920	0.15501	18.84	18.55	16.88	16.08	16.43	14.91	14.40	14.31	4.57 <sup>+0.08</sup> <sub>-0.08</sub>	4.69 <sup>+0.08</sup> <sub>-0.09</sub>	3.07 <sup>+0.07</sup> <sub>-0.07</sub>	17.52 <sup>+1.01</sup> <sub>-0.97</sub>	6.26	—
12359	290.80915	-1.10911	13.91	14.40	13.68	13.19	13.43	12.58	12.41	12.34	4.52 <sup>+0.11</sup> <sub>-0.07</sub>	2.84 <sup>+0.07</sup> <sub>-0.08</sub>	3.47 <sup>+0.12</sup> <sub>-0.11</sub>	15.05 <sup>+1.28</sup> <sub>-0.80</sub>	3.77	—
12388	290.82352	-0.40030	15.20	14.96	13.43	12.54	13.04	10.97	10.57	10.28	4.50 <sup>+0.11</sup> <sub>-0.07</sub>	5.27 <sup>+0.08</sup> <sub>-0.09</sub>	3.68 <sup>+0.08</sup> <sub>-0.07</sub>	12.52 <sup>+1.32</sup> <sub>-0.74</sub>	1.82	—
12415	290.83617	-1.46654	20.43	19.92	18.10	16.95	17.67	15.10	14.40	13.98	4.53 <sup>+0.12</sup> <sub>-0.13</sub>	6.46 <sup>+0.09</sup> <sub>-0.15</sub>	3.84 <sup>+0.09</sup> <sub>-0.08</sub>	16.51 <sup>+1.43</sup> <sub>-1.32</sub>	7.45	—
12416	290.83674	-0.75338	18.81	18.92	17.44	16.54	16.88	14.81	14.06	13.87	4.62 <sup>+0.05</sup> <sub>-0.08</sub>	5.96 <sup>+0.06</sup> <sub>-0.06</sub>	4.49 <sup>+0.09</sup> <sub>-0.09</sub>	17.36 <sup>+0.73</sup> <sub>-0.93</sub>	4.97	SUB/EM
12429	290.84256	-0.49276	17.12	16.57	14.77	13.73	14.40	11.95	11.45	11.16	4.48 <sup>+0.09</sup> <sub>-0.06</sub>	5.91 <sup>+0.08</sup> <sub>-0.09</sub>	3.56 <sup>+0.06</sup> <sub>-0.06</sub>	13.15 <sup>+1.05</sup> <sub>-0.66</sub>	1.17	—
12431	290.84390	-0.17978	19.44	19.54	18.10	17.21	17.75	15.75	15.26	14.83	4.63 <sup>+0.05</sup> <sub>-0.07</sub>	5.37 <sup>+0.11</sup> <sub>-0.11</sub>	4.01 <sup>+0.12</sup> <sub>-0.12</sub>	18.66 <sup>+0.68</sup> <sub>-0.92</sub>	4.68	—

Continued on next page...

ID	$\ell$	$b$	u	g	r	i	H $\alpha$	J	H	K	$\log(T_{\text{eff}})$	$A_0$	$R_V$	$\mu$	$\chi^2$	Notes
12476	290.87690	-0.42029	15.95	15.77	14.30	13.46	13.96	12.04	11.66	11.45	4.53 <sup>+0.09</sup> <sub>-0.07</sub>	4.93 <sup>+0.06</sup> <sub>-0.08</sub>	3.53 <sup>+0.07</sup> <sub>-0.07</sub>	14.09 <sup>+1.13</sup> <sub>-0.80</sub>	1.10	—
12485	290.88160	0.13445	17.67	17.87	16.80	16.14	16.48	15.20	14.85	14.93	4.54 <sup>+0.10</sup> <sub>-0.08</sub>	3.80 <sup>+0.10</sup> <sub>-0.10</sub>	3.49 <sup>+0.13</sup> <sub>-0.12</sub>	17.69 <sup>+1.23</sup> <sub>-0.91</sub>	3.86	—
12498	290.88853	-0.45545	16.01	15.41	13.49	12.38	13.03	10.47	9.92	9.62	4.56 <sup>+0.08</sup> <sub>-0.08</sub>	6.34 <sup>+0.05</sup> <sub>-0.07</sub>	3.58 <sup>+0.06</sup> <sub>-0.05</sub>	12.51 <sup>+1.06</sup> <sub>-0.92</sub>	1.12	—
12499	290.88895	-1.14288	14.75	15.03	14.05	13.41	13.76	12.48	12.28	12.03	4.54 <sup>+0.10</sup> <sub>-0.08</sub>	3.71 <sup>+0.07</sup> <sub>-0.08</sub>	3.63 <sup>+0.11</sup> <sub>-0.10</sub>	14.97 <sup>+1.22</sup> <sub>-0.90</sub>	4.61	—
12501	290.88945	-1.29920	14.35	14.47	13.33	12.62	13.01	11.51	11.12	11.00	4.51 <sup>+0.09</sup> <sub>-0.07</sub>	4.18 <sup>+0.07</sup> <sub>-0.09</sub>	3.69 <sup>+0.09</sup> <sub>-0.08</sub>	13.42 <sup>+1.09</sup> <sub>-0.76</sub>	3.50	—
12502	290.88964	-0.28885	20.33	19.70	17.80	16.74	17.48	15.01	14.39	14.14	4.51 <sup>+0.11</sup> <sub>-0.09</sub>	6.04 <sup>+0.09</sup> <sub>-0.12</sub>	3.48 <sup>+0.07</sup> <sub>-0.07</sub>	16.42 <sup>+1.27</sup> <sub>-0.95</sub>	1.67	—
12517	290.89696	-0.85606	17.83	17.41	15.74	14.70	15.39	12.96	12.44	12.20	4.53 <sup>+0.09</sup> <sub>-0.08</sub>	5.85 <sup>+0.06</sup> <sub>-0.08</sub>	3.68 <sup>+0.07</sup> <sub>-0.06</sub>	14.73 <sup>+1.12</sup> <sub>-0.84</sub>	4.33	—
12550	290.91653	-0.69002	15.44	15.65	14.62	13.99	14.34	13.00	12.66	12.54	4.50 <sup>+0.10</sup> <sub>-0.07</sub>	3.83 <sup>+0.09</sup> <sub>-0.09</sub>	3.68 <sup>+0.12</sup> <sub>-0.11</sub>	14.91 <sup>+1.20</sup> <sub>-0.74</sub>	1.03	—
12564	290.92980	-0.58924	14.53	14.73	13.64	12.99	13.34	11.91	11.64	11.45	4.53 <sup>+0.09</sup> <sub>-0.07</sub>	3.99 <sup>+0.06</sup> <sub>-0.08</sub>	3.66 <sup>+0.09</sup> <sub>-0.08</sub>	14.24 <sup>+1.07</sup> <sub>-0.79</sub>	1.54	—
12587	290.94026	-1.33108	15.51	15.62	14.40	13.67	14.09	12.45	12.08	11.85	4.54 <sup>+0.09</sup> <sub>-0.08</sub>	4.48 <sup>+0.06</sup> <sub>-0.08</sub>	3.80 <sup>+0.09</sup> <sub>-0.08</sub>	14.68 <sup>+1.13</sup> <sub>-0.84</sub>	1.35	—
12589	290.94140	-0.33377	15.81	15.44	13.83	12.87	13.45	11.32	10.93	10.65	4.52 <sup>+0.11</sup> <sub>-0.07</sub>	5.33 <sup>+0.07</sup> <sub>-0.09</sub>	3.47 <sup>+0.06</sup> <sub>-0.06</sub>	13.18 <sup>+1.33</sup> <sub>-0.81</sub>	3.87	—
12599	290.94671	-0.49165	16.59	17.29	16.46	15.96	15.90	15.26	14.86	14.86	4.64 <sup>+0.04</sup> <sub>-0.06</sub>	3.45 <sup>+0.18</sup> <sub>-0.17</sub>	4.16 <sup>+0.28</sup> <sub>-0.26</sub>	18.81 <sup>+0.58</sup> <sub>-0.82</sub>	4.12	SUB/EM
12621	290.96145	-1.51116	15.25	15.39	14.22	13.48	13.90	12.37	12.04	11.88	4.57 <sup>+0.08</sup> <sub>-0.08</sub>	4.23 <sup>+0.05</sup> <sub>-0.07</sub>	3.60 <sup>+0.09</sup> <sub>-0.07</sub>	15.08 <sup>+1.06</sup> <sub>-0.95</sub>	2.53	—
12641	290.97342	-0.55635	14.68	14.93	13.79	13.13	13.47	12.07	11.80	11.63	4.61 <sup>+0.06</sup> <sub>-0.08</sub>	4.02 <sup>+0.05</sup> <sub>-0.06</sub>	3.57 <sup>+0.08</sup> <sub>-0.07</sub>	15.27 <sup>+0.85</sup> <sub>-0.95</sub>	1.28	—
12650	290.98439	-0.52741	16.37	16.29	14.95	14.17	14.61	12.85	12.53	12.36	4.51 <sup>+0.10</sup> <sub>-0.07</sub>	4.58 <sup>+0.07</sup> <sub>-0.09</sub>	3.53 <sup>+0.09</sup> <sub>-0.08</sub>	14.77 <sup>+1.15</sup> <sub>-0.74</sub>	2.07	—
12655	290.98942	-1.44319	20.27	19.83	18.10	17.11	17.66	15.40	14.73	14.53	4.48 <sup>+0.13</sup> <sub>-0.12</sub>	5.90 <sup>+0.12</sup> <sub>-0.16</sub>	3.75 <sup>+0.10</sup> <sub>-0.10</sub>	16.51 <sup>+1.54</sup> <sub>-1.16</sub>	1.92	—
12661	290.99433	-0.63417	16.57	16.43	15.02	14.18	14.68	12.77	12.38	12.14	4.49 <sup>+0.09</sup> <sub>-0.07</sub>	4.91 <sup>+0.08</sup> <sub>-0.09</sub>	3.66 <sup>+0.08</sup> <sub>-0.08</sub>	14.39 <sup>+1.04</sup> <sub>-0.71</sub>	1.23	—
12678	291.00994	-1.35953	16.86	16.48	14.82	13.87	14.47	12.20	11.74	11.51	4.51 <sup>+0.10</sup> <sub>-0.07</sub>	5.56 <sup>+0.07</sup> <sub>-0.09</sub>	3.60 <sup>+0.07</sup> <sub>-0.07</sub>	13.83 <sup>+1.14</sup> <sub>-0.72</sub>	1.31	—
12693	291.01940	-0.50806	15.36	15.15	13.65	12.78	13.27	11.33	10.90	10.71	4.52 <sup>+0.10</sup> <sub>-0.07</sub>	5.05 <sup>+0.07</sup> <sub>-0.09</sub>	3.56 <sup>+0.07</sup> <sub>-0.07</sub>	13.20 <sup>+1.17</sup> <sub>-0.78</sub>	0.90	—
12710	291.02575	-0.89824	14.24	14.56	13.61	13.01	13.35	12.07	11.85	11.54	4.50 <sup>+0.10</sup> <sub>-0.07</sub>	3.73 <sup>+0.08</sup> <sub>-0.09</sub>	3.85 <sup>+0.13</sup> <sub>-0.12</sub>	14.02 <sup>+1.13</sup> <sub>-0.73</sub>	4.19	—
12712	291.02901	-0.61906	15.08	14.99	13.55	12.71	13.20	11.33	10.94	10.74	4.60 <sup>+0.07</sup> <sub>-0.09</sub>	4.91 <sup>+0.05</sup> <sub>-0.06</sub>	3.56 <sup>+0.07</sup> <sub>-0.06</sub>	14.17 <sup>+1.12</sup> <sub>-1.02</sub>	1.27	—
12724	291.04172	-0.08613	17.26	16.78	15.07	14.06	14.70	12.44	11.95	11.75	4.53 <sup>+0.06</sup> <sub>-0.08</sub>	5.59 <sup>+0.04</sup> <sub>-0.08</sub>	3.43 <sup>+0.06</sup> <sub>-0.05</sub>	14.35 <sup>+0.75</sup> <sub>-0.85</sub>	3.97	—
12737	291.04689	-0.77325	15.45	15.43	13.94	12.99	13.59	11.27	10.71	10.40	4.62 <sup>+0.07</sup> <sub>-0.08</sub>	5.81 <sup>+0.05</sup> <sub>-0.05</sub>	4.19 <sup>+0.07</sup> <sub>-0.07</sub>	13.98 <sup>+0.96</sup> <sub>-0.95</sub>	1.79	—
12759	291.06036	-1.48060	14.19	14.19	12.80	11.99	12.45	10.66	10.25	10.02	4.59 <sup>+0.07</sup> <sub>-0.08</sub>	4.84 <sup>+0.06</sup> <sub>-0.06</sub>	3.68 <sup>+0.07</sup> <sub>-0.07</sub>	13.39 <sup>+1.12</sup> <sub>-0.97</sub>	0.94	—
12784	291.06886	-0.77515	15.06	15.33	14.17	13.44	13.86	12.20	11.81	11.60	4.63 <sup>+0.05</sup> <sub>-0.07</sub>	4.53 <sup>+0.05</sup> <sub>-0.05</sub>	4.00 <sup>+0.09</sup> <sub>-0.08</sub>	15.42 <sup>+0.68</sup> <sub>-0.89</sub>	1.60	—
12788	291.06991	0.19066	16.55	16.55	15.32	14.60	15.02	13.50	13.16	13.06	4.49 <sup>+0.10</sup> <sub>-0.07</sub>	4.14 <sup>+0.08</sup> <sub>-0.10</sub>	3.42 <sup>+0.10</sup> <sub>-0.09</sub>	15.36 <sup>+1.18</sup> <sub>-0.75</sub>	1.92	—
12800	291.07738	-0.27651	14.28	14.43	13.25	12.54	12.92	11.46	11.14	11.02	4.59 <sup>+0.07</sup> <sub>-0.08</sub>	4.12 <sup>+0.05</sup> <sub>-0.06</sub>	3.50 <sup>+0.08</sup> <sub>-0.07</sub>	14.41 <sup>+0.94</sup> <sub>-0.97</sub>	2.94	—
12807	291.07908	-0.21361	16.55	16.46	15.14	14.37	14.80	13.13	12.72	12.59	4.48 <sup>+0.09</sup> <sub>-0.06</sub>	4.50 <sup>+0.08</sup> <sub>-0.09</sub>	3.53 <sup>+0.08</sup> <sub>-0.07</sub>	14.70 <sup>+1.03</sup> <sub>-0.65</sub>	4.07	—
12809	291.07950	-0.21635	14.72	14.70	13.41	12.63	13.06	11.43	11.12	10.93	4.56 <sup>+0.09</sup> <sub>-0.09</sub>	4.43 <sup>+0.05</sup> <sub>-0.08</sub>	3.46 <sup>+0.07</sup> <sub>-0.07</sub>	13.97 <sup>+1.15</sup> <sub>-0.96</sub>	2.03	—
12813	291.08199	-0.47085	20.18	19.17	16.84	15.54	16.45	13.25	12.55	12.28	4.57 <sup>+0.09</sup> <sub>-0.12</sub>	7.41 <sup>+0.06</sup> <sub>-0.10</sub>	3.52 <sup>+0.05</sup> <sub>-0.05</sub>	15.11 <sup>+1.14</sup> <sub>-1.29</sub>	5.11	—
12816	291.08263	-0.72109	14.35	14.67	13.73	13.14	13.46	12.27	11.94	11.81	4.52 <sup>+0.10</sup> <sub>-0.07</sub>	3.61 <sup>+0.07</sup> <sub>-0.08</sub>	3.72 <sup>+0.11</sup> <sub>-0.10</sub>	14.43 <sup>+1.14</sup> <sub>-0.75</sub>	2.10	—
12821	291.08530	-0.67236	14.55	14.84	13.71	13.03	13.42	11.95	11.65	11.46	4.61 <sup>+0.06</sup> <sub>-0.08</sub>	4.12 <sup>+0.06</sup> <sub>-0.07</sub>	3.72 <sup>+0.10</sup> <sub>-0.09</sub>	15.20 <sup>+0.77</sup> <sub>-0.93</sub>	1.23	—
12841	291.09488	-0.65170	14.86	15.06	14.00	13.37	13.71	12.42	12.09	11.98	4.51 <sup>+0.09</sup> <sub>-0.07</sub>	3.77 <sup>+0.07</sup> <sub>-0.08</sub>	3.55 <sup>+0.10</sup> <sub>-0.09</sub>	14.47 <sup>+1.08</sup> <sub>-0.74</sub>	2.13	—

Continued on next page...

ID	$\ell$	$b$	u	g	r	i	H $\alpha$	J	H	K	$\log(T_{\text{eff}})$	$A_0$	$R_V$	$\mu$	$\chi^2$	Notes
12847	291.09784	-0.57794	15.13	15.14	13.81	13.02	13.48	11.79	11.44	11.24	4.58 <sup>+0.08</sup> <sub>-0.08</sub>	4.56 <sup>+0.05</sup> <sub>-0.06</sub>	3.53 <sup>+0.07</sup> <sub>-0.07</sub>	14.58 <sup>+1.00</sup> <sub>-0.91</sub>	1.34	—
12849	291.09839	-0.22569	14.95	15.04	13.87	13.19	13.57	12.12	11.79	11.65	4.50 <sup>+0.09</sup> <sub>-0.06</sub>	4.04 <sup>+0.07</sup> <sub>-0.08</sub>	3.51 <sup>+0.08</sup> <sub>-0.08</sub>	14.05 <sup>+1.04</sup> <sub>-0.69</sub>	0.83	—
12852	291.10073	-0.20595	14.38	14.47	13.30	12.63	13.00	11.59	11.27	11.12	4.50 <sup>+0.09</sup> <sub>-0.07</sub>	4.00 <sup>+0.07</sup> <sub>-0.09</sub>	3.49 <sup>+0.08</sup> <sub>-0.08</sub>	13.54 <sup>+1.06</sup> <sub>-0.72</sub>	0.77	—
12862	291.10523	-0.65796	14.07	14.31	13.26	12.62	12.96	11.61	11.29	11.11	4.52 <sup>+0.10</sup> <sub>-0.07</sub>	3.92 <sup>+0.07</sup> <sub>-0.09</sub>	3.74 <sup>+0.10</sup> <sub>-0.09</sub>	13.73 <sup>+1.17</sup> <sub>-0.76</sub>	1.12	—
12864	291.10572	-0.89881	15.07	15.09	13.88	13.13	13.58	11.87	11.52	11.36	4.49 <sup>+0.09</sup> <sub>-0.06</sub>	4.42 <sup>+0.08</sup> <sub>-0.09</sub>	3.71 <sup>+0.09</sup> <sub>-0.09</sub>	13.54 <sup>+1.00</sup> <sub>-0.64</sub>	3.35	—
12875	291.11026	-0.19047	18.08	18.22	17.10	16.37	16.91	15.45	14.94	14.95	4.57 <sup>+0.09</sup> <sub>-0.09</sub>	4.02 <sup>+0.11</sup> <sub>-0.11</sub>	3.50 <sup>+0.14</sup> <sub>-0.13</sub>	18.12 <sup>+1.12</sup> <sub>-1.03</sub>	6.75	—
12884	291.11457	-0.73679	15.17	15.40	14.29	13.58	13.99	12.52	12.17	11.97	4.58 <sup>+0.08</sup> <sub>-0.08</sub>	4.16 <sup>+0.05</sup> <sub>-0.07</sub>	3.74 <sup>+0.09</sup> <sub>-0.08</sub>	15.29 <sup>+1.02</sup> <sub>-0.96</sub>	2.64	—
12911	291.13416	-0.55107	16.34	16.23	14.83	14.02	14.49	12.72	12.28	12.08	4.51 <sup>+0.10</sup> <sub>-0.07</sub>	4.76 <sup>+0.07</sup> <sub>-0.09</sub>	3.58 <sup>+0.08</sup> <sub>-0.07</sub>	14.51 <sup>+1.16</sup> <sub>-0.74</sub>	1.10	—
12913	291.13567	-0.62349	14.38	14.67	13.56	12.92	13.28	11.86	11.58	11.34	4.58 <sup>+0.07</sup> <sub>-0.08</sub>	4.06 <sup>+0.05</sup> <sub>-0.06</sub>	3.76 <sup>+0.09</sup> <sub>-0.08</sub>	14.72 <sup>+0.96</sup> <sub>-0.90</sub>	2.72	—
12917	291.13770	-0.24180	17.24	16.60	14.68	13.54	14.23	11.49	10.93	10.57	4.51 <sup>+0.09</sup> <sub>-0.07</sub>	6.59 <sup>+0.07</sup> <sub>-0.09</sub>	3.73 <sup>+0.06</sup> <sub>-0.06</sub>	12.81 <sup>+1.08</sup> <sub>-0.76</sub>	2.69	—
12921	291.14143	-0.74304	15.59	15.91	14.91	14.28	14.63	13.34	13.06	12.88	4.57 <sup>+0.08</sup> <sub>-0.08</sub>	3.78 <sup>+0.05</sup> <sub>-0.07</sub>	3.69 <sup>+0.10</sup> <sub>-0.09</sub>	16.15 <sup>+1.03</sup> <sub>-0.94</sub>	2.20	—
12945	291.15575	-0.31863	20.70	19.52	17.10	15.65	16.66	13.04	12.20	11.82	4.52 <sup>+0.11</sup> <sub>-0.10</sub>	8.25 <sup>+0.08</sup> <sub>-0.13</sub>	3.77 <sup>+0.05</sup> <sub>-0.05</sub>	13.95 <sup>+1.40</sup> <sub>-1.09</sub>	3.93	—
12962	291.16619	-0.34836	20.16	19.09	16.62	15.18	16.18	12.67	11.92	11.53	4.60 <sup>+0.07</sup> <sub>-0.09</sub>	8.06 <sup>+0.05</sup> <sub>-0.07</sub>	3.61 <sup>+0.05</sup> <sub>-0.05</sub>	14.64 <sup>+0.92</sup> <sub>-1.09</sub>	2.50	—
12967	291.16927	-1.10322	14.67	14.90	13.81	13.14	13.52	12.19	11.84	11.72	4.58 <sup>+0.08</sup> <sub>-0.08</sub>	3.91 <sup>+0.05</sup> <sub>-0.06</sub>	3.54 <sup>+0.09</sup> <sub>-0.08</sub>	15.01 <sup>+1.01</sup> <sub>-0.90</sub>	2.68	—
12977	291.17400	-0.40420	19.35	18.64	16.54	15.32	15.71	13.18	12.47	12.03	4.56 <sup>+0.09</sup> <sub>-0.09</sub>	7.13 <sup>+0.08</sup> <sub>-0.10</sub>	3.79 <sup>+0.07</sup> <sub>-0.06</sub>	14.78 <sup>+1.17</sup> <sub>-1.06</sub>	1.95	EM
12992	291.18023	-0.78108	17.16	16.76	14.91	13.77	14.49	11.68	11.05	10.69	4.62 <sup>+0.05</sup> <sub>-0.08</sub>	6.76 <sup>+0.04</sup> <sub>-0.05</sub>	4.00 <sup>+0.06</sup> <sub>-0.05</sub>	14.21 <sup>+0.71</sup> <sub>-0.97</sub>	2.23	—
12997	291.18289	-0.23044	15.96	15.50	13.76	12.73	13.37	10.99	10.46	10.15	4.50 <sup>+0.10</sup> <sub>-0.07</sub>	5.90 <sup>+0.08</sup> <sub>-0.09</sub>	3.67 <sup>+0.06</sup> <sub>-0.06</sub>	12.35 <sup>+1.16</sup> <sub>-0.72</sub>	1.19	—
13005	291.18760	-0.27308	20.85	19.68	17.19	15.73	16.74	12.88	11.96	11.54	4.50 <sup>+0.11</sup> <sub>-0.10</sub>	8.73 <sup>+0.09</sup> <sub>-0.13</sub>	3.99 <sup>+0.06</sup> <sub>-0.06</sub>	13.36 <sup>+1.32</sup> <sub>-0.99</sub>	1.68	—
13015	291.19146	-0.78165	18.18	17.49	15.42	14.14	15.00	11.72	11.00	10.57	4.57 <sup>+0.09</sup> <sub>-0.09</sub>	7.60 <sup>+0.05</sup> <sub>-0.08</sub>	4.05 <sup>+0.06</sup> <sub>-0.05</sub>	13.38 <sup>+1.10</sup> <sub>-1.00</sub>	2.75	—
13037	291.20360	-1.01653	15.38	15.41	14.08	13.21	13.73	11.82	11.43	11.22	4.62 <sup>+0.06</sup> <sub>-0.08</sub>	4.93 <sup>+0.05</sup> <sub>-0.05</sub>	3.77 <sup>+0.08</sup> <sub>-0.07</sub>	14.88 <sup>+0.77</sup> <sub>-0.95</sub>	5.57	—
13038	291.20373	-0.86273	20.39	19.83	17.89	16.68	17.52	14.52	13.93	13.63	4.58 <sup>+0.08</sup> <sub>-0.10</sub>	6.88 <sup>+0.07</sup> <sub>-0.09</sub>	3.82 <sup>+0.08</sup> <sub>-0.07</sub>	16.65 <sup>+1.02</sup> <sub>-1.21</sub>	5.52	—
13051	291.21290	-0.70476	20.73	19.82	17.64	16.29	17.23	13.83	13.09	12.73	4.56 <sup>+0.10</sup> <sub>-0.13</sub>	7.73 <sup>+0.07</sup> <sub>-0.13</sub>	3.86 <sup>+0.07</sup> <sub>-0.07</sub>	15.31 <sup>+1.26</sup> <sub>-1.40</sub>	6.44	—
13055	291.21453	-0.23598	15.16	14.85	13.24	12.28	12.84	10.55	10.06	9.83	4.51 <sup>+0.10</sup> <sub>-0.07</sub>	5.68 <sup>+0.08</sup> <sub>-0.09</sub>	3.78 <sup>+0.08</sup> <sub>-0.08</sub>	12.17 <sup>+1.25</sup> <sub>-0.78</sub>	2.86	—
13058	291.21693	-0.22230	19.49	19.06	17.33	16.28	16.96	14.45	13.86	13.70	4.55 <sup>+0.10</sup> <sub>-0.10</sub>	6.05 <sup>+0.07</sup> <sub>-0.10</sub>	3.74 <sup>+0.08</sup> <sub>-0.07</sub>	16.41 <sup>+1.22</sup> <sub>-1.15</sub>	5.62	—
13059	291.21702	-0.50563	15.24	15.79	14.91	14.53	14.79	13.72	13.35	13.33	4.54 <sup>+0.09</sup> <sub>-0.07</sub>	3.23 <sup>+0.14</sup> <sub>-0.14</sub>	3.86 <sup>+0.25</sup> <sub>-0.23</sub>	16.27 <sup>+1.11</sup> <sub>-0.85</sub>	4.81	—
13061	291.21770	-0.33278	19.28	18.19	15.83	14.47	15.40	12.06	11.38	11.04	4.57 <sup>+0.09</sup> <sub>-0.09</sub>	7.66 <sup>+0.06</sup> <sub>-0.09</sub>	3.56 <sup>+0.05</sup> <sub>-0.05</sub>	13.83 <sup>+1.11</sup> <sub>-1.06</sub>	4.30	—
13072	291.22280	-0.23496	19.60	19.06	17.25	16.15	16.88	14.23	13.68	13.32	4.50 <sup>+0.11</sup> <sub>-0.09</sub>	6.30 <sup>+0.09</sup> <sub>-0.12</sub>	3.78 <sup>+0.07</sup> <sub>-0.07</sub>	15.47 <sup>+1.27</sup> <sub>-0.93</sub>	2.23	—
13076	291.22464	-0.20812	16.95	16.71	15.20	14.29	14.85	12.80	12.35	12.14	4.52 <sup>+0.10</sup> <sub>-0.07</sub>	5.20 <sup>+0.07</sup> <sub>-0.08</sub>	3.60 <sup>+0.07</sup> <sub>-0.06</sub>	14.67 <sup>+1.17</sup> <sub>-0.80</sub>	2.18	—
13088	291.23260	-0.22274	19.87	19.08	16.98	15.69	16.55	13.33	12.56	12.20	4.54 <sup>+0.10</sup> <sub>-0.09</sub>	7.53 <sup>+0.06</sup> <sub>-0.09</sub>	3.93 <sup>+0.06</sup> <sub>-0.06</sub>	14.69 <sup>+1.20</sup> <sub>-0.96</sub>	2.77	—
13093	291.23552	-0.37193	18.06	17.19	15.09	13.82	14.68	11.66	11.02	10.72	4.54 <sup>+0.10</sup> <sub>-0.08</sub>	7.03 <sup>+0.06</sup> <sub>-0.09</sub>	3.60 <sup>+0.06</sup> <sub>-0.05</sub>	13.27 <sup>+1.30</sup> <sub>-0.94</sub>	5.92	—
13097	291.23769	-0.23203	17.33	16.98	15.30	14.30	14.93	12.58	12.12	11.83	4.58 <sup>+0.08</sup> <sub>-0.08</sub>	5.77 <sup>+0.05</sup> <sub>-0.07</sub>	3.65 <sup>+0.06</sup> <sub>-0.06</sub>	14.96 <sup>+1.03</sup> <sub>-0.94</sub>	2.39	—
13098	291.23786	-1.00481	15.69	15.77	14.60	13.82	14.26	12.62	12.29	12.09	4.55 <sup>+0.10</sup> <sub>-0.08</sub>	4.41 <sup>+0.06</sup> <sub>-0.08</sub>	3.70 <sup>+0.09</sup> <sub>-0.08</sub>	15.00 <sup>+1.24</sup> <sub>-0.91</sub>	4.90	—
13099	291.23954	-0.61981	17.37	16.99	15.34	14.32	14.96	12.57	12.02	11.71	4.51 <sup>+0.10</sup> <sub>-0.07</sub>	5.90 <sup>+0.07</sup> <sub>-0.09</sub>	3.81 <sup>+0.07</sup> <sub>-0.07</sub>	14.04 <sup>+1.24</sup> <sub>-0.77</sub>	2.55	—

Continued on next page...

ID	$\ell$	$b$	u	g	r	i	H $\alpha$	J	H	K	$\log(T_{\text{eff}})$	$A_0$	$R_V$	$\mu$	$\chi^2$	Notes
13106	291.24645	-1.20664	18.45	17.90	16.11	15.06	15.75	13.20	12.65	12.40	4.48 <sup>+0.11</sup> <sub>-0.08</sub>	6.06 <sup>+0.10</sup> <sub>-0.12</sub>	3.67 <sup>+0.07</sup> <sub>-0.06</sub>	14.34 <sup>+1.31</sup> <sub>-0.80</sub>	1.96	—
13117	291.25518	-0.77712	15.10	14.95	13.35	12.35	13.00	10.42	9.76	9.41	4.58 <sup>+0.08</sup> <sub>-0.08</sub>	6.33 <sup>+0.05</sup> <sub>-0.06</sub>	4.33 <sup>+0.08</sup> <sub>-0.07</sub>	12.45 <sup>+0.98</sup> <sub>-0.94</sub>	1.31	—
13118	291.25701	-0.08403	15.03	14.89	13.46	12.64	13.14	11.35	11.00	10.81	4.54 <sup>+0.09</sup> <sub>-0.08</sub>	4.68 <sup>+0.07</sup> <sub>-0.07</sub>	3.41 <sup>+0.07</sup> <sub>-0.07</sub>	13.66 <sup>+1.14</sup> <sub>-0.84</sub>	1.16	—
13161	291.28062	-0.55286	14.61	14.51	13.13	12.30	12.78	10.99	10.54	10.32	4.50 <sup>+0.10</sup> <sub>-0.07</sub>	4.82 <sup>+0.07</sup> <sub>-0.09</sub>	3.65 <sup>+0.08</sup> <sub>-0.07</sub>	12.68 <sup>+1.17</sup> <sub>-0.70</sub>	2.58	—
13187	291.29505	-0.58545	17.60	17.32	15.74	14.80	15.37	13.20	12.72	12.48	4.53 <sup>+0.10</sup> <sub>-0.08</sub>	5.46 <sup>+0.08</sup> <sub>-0.09</sub>	3.67 <sup>+0.08</sup> <sub>-0.08</sub>	15.01 <sup>+1.18</sup> <sub>-0.83</sub>	1.42	—
13204	291.30489	-0.34768	20.47	19.49	17.28	15.93	16.86	13.56	12.93	12.51	4.53 <sup>+0.11</sup> <sub>-0.10</sub>	7.49 <sup>+0.07</sup> <sub>-0.11</sub>	3.69 <sup>+0.06</sup> <sub>-0.05</sub>	14.86 <sup>+1.39</sup> <sub>-1.05</sub>	5.38	—
13209	291.31192	-1.02800	16.20	16.18	14.96	14.19	14.64	12.94	12.60	12.51	4.49 <sup>+0.10</sup> <sub>-0.07</sub>	4.39 <sup>+0.08</sup> <sub>-0.09</sub>	3.59 <sup>+0.09</sup> <sub>-0.09</sub>	14.72 <sup>+1.17</sup> <sub>-0.69</sub>	7.23	—
13212	291.31237	-0.96874	13.75	14.01	12.92	12.25	12.64	11.30	11.01	10.92	4.62 <sup>+0.05</sup> <sub>-0.07</sub>	3.83 <sup>+0.05</sup> <sub>-0.05</sub>	3.45 <sup>+0.08</sup> <sub>-0.08</sub>	14.81 <sup>+0.70</sup> <sub>-0.91</sub>	3.32	—
13234	291.33651	-1.57993	19.46	18.74	16.86	15.71	16.45	13.76	13.19	12.94	4.48 <sup>+0.12</sup> <sub>-0.12</sub>	6.35 <sup>+0.09</sup> <sub>-0.12</sub>	3.61 <sup>+0.06</sup> <sub>-0.06</sub>	14.85 <sup>+1.34</sup> <sub>-0.85</sub>	5.90	—
13244	291.34668	-0.56801	14.62	14.49	13.02	12.13	12.66	10.67	10.27	10.02	4.58 <sup>+0.08</sup> <sub>-0.08</sub>	5.12 <sup>+0.05</sup> <sub>-0.06</sub>	3.64 <sup>+0.07</sup> <sub>-0.06</sub>	13.27 <sup>+0.98</sup> <sub>-0.94</sub>	2.21	—
13280	291.38386	-0.39058	18.32	17.72	15.74	14.56	15.35	12.48	11.87	11.50	4.58 <sup>+0.08</sup> <sub>-0.08</sub>	6.81 <sup>+0.05</sup> <sub>-0.07</sub>	3.77 <sup>+0.06</sup> <sub>-0.05</sub>	14.54 <sup>+1.00</sup> <sub>-0.94</sub>	1.60	—
13285	291.38816	-0.56770	15.91	15.97	14.72	13.98	14.43	12.72	12.46	12.23	4.54 <sup>+0.09</sup> <sub>-0.07</sub>	4.41 <sup>+0.06</sup> <sub>-0.08</sub>	3.62 <sup>+0.09</sup> <sub>-0.08</sub>	15.04 <sup>+1.10</sup> <sub>-0.83</sub>	3.37	—
13288	291.38944	0.21954	14.53	14.65	13.47	12.77	13.16	11.68	11.36	11.21	4.56 <sup>+0.09</sup> <sub>-0.08</sub>	4.13 <sup>+0.05</sup> <sub>-0.08</sub>	3.52 <sup>+0.08</sup> <sub>-0.07</sub>	14.29 <sup>+1.08</sup> <sub>-0.93</sub>	1.37	—
13305	291.41028	-0.22191	17.79	17.02	15.06	13.85	14.62	11.83	11.25	10.92	4.49 <sup>+0.10</sup> <sub>-0.07</sub>	6.61 <sup>+0.08</sup> <sub>-0.10</sub>	3.61 <sup>+0.06</sup> <sub>-0.06</sub>	12.93 <sup>+1.19</sup> <sub>-0.73</sub>	4.88	—
13315	291.42101	-1.24120	19.94	19.17	17.19	16.02	16.84	14.01	13.39	13.14	4.50 <sup>+0.10</sup> <sub>-0.08</sub>	6.57 <sup>+0.08</sup> <sub>-0.11</sub>	3.59 <sup>+0.06</sup> <sub>-0.05</sub>	15.22 <sup>+1.20</sup> <sub>-0.82</sub>	4.57	—
13320	291.42917	-0.39374	17.81	17.23	15.47	14.44	15.10	12.76	12.28	12.08	4.49 <sup>+0.10</sup> <sub>-0.07</sub>	5.66 <sup>+0.08</sup> <sub>-0.09</sub>	3.40 <sup>+0.06</sup> <sub>-0.06</sub>	14.17 <sup>+1.15</sup> <sub>-0.71</sub>	4.57	—
13325	291.43170	-0.55524	15.40	15.38	14.10	13.33	13.79	12.11	11.77	11.57	4.52 <sup>+0.10</sup> <sub>-0.07</sub>	4.46 <sup>+0.07</sup> <sub>-0.08</sub>	3.56 <sup>+0.09</sup> <sub>-0.09</sub>	14.19 <sup>+1.16</sup> <sub>-0.80</sub>	1.40	—
13329	291.43380	-0.46709	15.38	15.25	13.76	12.87	13.42	11.08	10.57	10.30	4.51 <sup>+0.09</sup> <sub>-0.07</sub>	5.70 <sup>+0.07</sup> <sub>-0.09</sub>	4.15 <sup>+0.09</sup> <sub>-0.08</sub>	12.57 <sup>+1.06</sup> <sub>-0.72</sub>	1.91	—
13331	291.43485	-0.47242	16.84	16.25	14.36	13.26	13.98	11.26	10.65	10.33	4.50 <sup>+0.09</sup> <sub>-0.07</sub>	6.49 <sup>+0.08</sup> <sub>-0.08</sub>	3.77 <sup>+0.07</sup> <sub>-0.06</sub>	12.45 <sup>+1.07</sup> <sub>-0.72</sub>	0.69	—
13341	291.44488	-0.58033	16.57	16.54	15.22	14.43	14.91	13.12	12.77	12.57	4.54 <sup>+0.10</sup> <sub>-0.08</sub>	4.64 <sup>+0.06</sup> <sub>-0.08</sub>	3.61 <sup>+0.08</sup> <sub>-0.07</sub>	15.36 <sup>+1.23</sup> <sub>-0.85</sub>	1.93	—
13346	291.44645	-0.57375	16.09	16.10	14.88	14.14	14.58	12.92	12.60	12.47	4.48 <sup>+0.10</sup> <sub>-0.07</sub>	4.30 <sup>+0.08</sup> <sub>-0.09</sub>	3.60 <sup>+0.10</sup> <sub>-0.09</sub>	14.56 <sup>+1.18</sup> <sub>-0.67</sub>	3.41	—
13354	291.45096	-1.31004	20.22	19.56	17.59	16.44	17.22	14.26	13.71	13.44	4.53 <sup>+0.11</sup> <sub>-0.12</sub>	6.81 <sup>+0.09</sup> <sub>-0.14</sub>	3.81 <sup>+0.08</sup> <sub>-0.08</sub>	15.75 <sup>+1.40</sup> <sub>-1.29</sub>	6.31	—
13359	291.45827	-0.03986	20.32	19.77	17.99	16.91	17.67	15.08	14.42	14.20	4.49 <sup>+0.13</sup> <sub>-0.11</sub>	6.19 <sup>+0.10</sup> <sub>-0.16</sub>	3.77 <sup>+0.08</sup> <sub>-0.08</sub>	16.26 <sup>+1.49</sup> <sub>-1.15</sub>	3.45	—
13362	291.46931	-0.58784	14.95	15.00	13.63	12.78	13.30	11.36	10.91	10.75	4.63 <sup>+0.05</sup> <sub>-0.07</sub>	5.01 <sup>+0.05</sup> <sub>-0.06</sub>	3.82 <sup>+0.07</sup> <sub>-0.07</sub>	14.52 <sup>+0.66</sup> <sub>-0.89</sub>	3.66	—
13364	291.47037	-0.55814	15.01	15.19	14.03	13.27	13.72	12.12	11.82	11.60	4.61 <sup>+0.06</sup> <sub>-0.08</sub>	4.32 <sup>+0.05</sup> <sub>-0.06</sub>	3.70 <sup>+0.08</sup> <sub>-0.08</sub>	15.22 <sup>+0.84</sup> <sub>-0.96</sub>	4.88	—
13365	291.47071	-0.66572	20.81	19.93	17.79	16.49	17.39	14.09	13.48	13.10	4.53 <sup>+0.12</sup> <sub>-0.14</sub>	7.46 <sup>+0.10</sup> <sub>-0.17</sub>	3.82 <sup>+0.08</sup> <sub>-0.07</sub>	15.34 <sup>+1.51</sup> <sub>-1.44</sub>	6.85	—
13377	291.48597	-0.13868	13.85	13.71	12.25	11.33	11.71	9.85	9.39	9.12	4.57 <sup>+0.09</sup> <sub>-0.09</sub>	5.26 <sup>+0.05</sup> <sub>-0.07</sub>	3.74 <sup>+0.07</sup> <sub>-0.06</sub>	12.25 <sup>+1.13</sup> <sub>-1.02</sub>	3.03	LUM/EM
13390	291.49824	-0.42868	20.56	19.05	16.23	14.54	15.74	11.37	10.34	9.71	4.51 <sup>+0.11</sup> <sub>-0.09</sub>	9.84 <sup>+0.08</sup> <sub>-0.12</sub>	3.98 <sup>+0.05</sup> <sub>-0.05</sub>	11.60 <sup>+1.26</sup> <sub>-0.93</sub>	5.03	—
13392	291.50082	-0.50687	17.25	16.81	15.04	13.97	14.67	12.21	11.59	11.23	4.56 <sup>+0.09</sup> <sub>-0.09</sub>	6.17 <sup>+0.06</sup> <sub>-0.08</sub>	3.75 <sup>+0.07</sup> <sub>-0.06</sub>	14.15 <sup>+1.12</sup> <sub>-0.99</sub>	4.69	—
13399	291.50487	-0.94160	18.76	17.69	15.38	13.99	14.92	11.61	10.94	10.56	4.58 <sup>+0.08</sup> <sub>-0.09</sub>	7.64 <sup>+0.05</sup> <sub>-0.07</sub>	3.59 <sup>+0.05</sup> <sub>-0.04</sub>	13.48 <sup>+1.05</sup> <sub>-1.01</sub>	4.52	—
13404	291.50949	-0.60512	16.07	16.01	14.70	13.88	14.38	12.52	12.12	11.97	4.52 <sup>+0.09</sup> <sub>-0.07</sub>	4.75 <sup>+0.07</sup> <sub>-0.08</sub>	3.68 <sup>+0.08</sup> <sub>-0.07</sub>	14.50 <sup>+1.13</sup> <sub>-0.78</sub>	5.46	—
13407	291.51233	-0.56623	16.77	16.67	15.18	14.23	14.84	12.65	12.16	11.93	4.61 <sup>+0.06</sup> <sub>-0.08</sub>	5.48 <sup>+0.05</sup> <sub>-0.06</sub>	3.85 <sup>+0.07</sup> <sub>-0.07</sub>	15.49 <sup>+0.79</sup> <sub>-0.93</sub>	3.05	—
13416	291.52245	-0.39312	17.78	17.25	15.47	14.44	15.11	12.70	12.22	11.98	4.53 <sup>+0.10</sup> <sub>-0.08</sub>	5.82 <sup>+0.07</sup> <sub>-0.09</sub>	3.48 <sup>+0.06</sup> <sub>-0.06</sub>	14.48 <sup>+1.19</sup> <sub>-0.86</sub>	2.56	—

Continued on next page...

ID	$\ell$	$b$	u	g	r	i	H $\alpha$	J	H	K	$\log(T_{\text{eff}})$	$A_0$	$R_V$	$\mu$	$\chi^2$	Notes
13422	291.52865	-0.51790	17.56	17.09	15.41	14.39	15.06	12.74	12.21	11.99	4.49 <sup>+0.11</sup> <sub>-0.07</sub>	5.67 <sup>+0.08</sup> <sub>-0.09</sub>	3.56 <sup>+0.06</sup> <sub>-0.06</sub>	14.08 <sup>+1.23</sup> <sub>-0.70</sub>	4.94	—
13425	291.53222	-0.70333	20.02	19.33	17.43	16.31	17.06	14.31	13.73	13.49	4.50 <sup>+0.14</sup> <sub>-0.13</sub>	6.44 <sup>+0.09</sup> <sub>-0.17</sub>	3.68 <sup>+0.07</sup> <sub>-0.07</sub>	15.53 <sup>+1.62</sup> <sub>-1.27</sub>	4.00	—
13426	291.53247	-0.34348	17.24	16.90	15.34	14.43	14.98	12.94	12.51	12.30	4.48 <sup>+0.09</sup> <sub>-0.06</sub>	5.15 <sup>+0.08</sup> <sub>-0.09</sub>	3.48 <sup>+0.07</sup> <sub>-0.07</sub>	14.38 <sup>+1.07</sup> <sub>-0.67</sub>	1.46	—
13427	291.53294	-0.57045	18.53	18.12	16.46	15.42	16.12	13.58	13.05	12.75	4.48 <sup>+0.09</sup> <sub>-0.07</sub>	5.99 <sup>+0.08</sup> <sub>-0.10</sub>	3.87 <sup>+0.08</sup> <sub>-0.08</sub>	14.69 <sup>+1.06</sup> <sub>-0.69</sub>	3.66	—
13437	291.54234	-0.52169	18.53	17.74	15.53	14.20	15.14	11.78	11.06	10.69	4.62 <sup>+0.06</sup> <sub>-0.08</sub>	7.68 <sup>+0.04</sup> <sub>-0.05</sub>	3.85 <sup>+0.05</sup> <sub>-0.05</sub>	14.05 <sup>+0.76</sup> <sub>-0.95</sub>	3.86	—
13440	291.54284	-0.47745	19.21	18.46	16.48	15.28	16.09	13.26	12.68	12.34	4.52 <sup>+0.11</sup> <sub>-0.08</sub>	6.65 <sup>+0.07</sup> <sub>-0.09</sub>	3.61 <sup>+0.06</sup> <sub>-0.05</sub>	14.67 <sup>+1.30</sup> <sub>-0.81</sub>	3.44	—
13448	291.54721	-0.60001	19.78	18.99	16.86	15.55	16.48	13.21	12.50	12.16	4.59 <sup>+0.08</sup> <sub>-0.09</sub>	7.46 <sup>+0.05</sup> <sub>-0.07</sub>	3.81 <sup>+0.06</sup> <sub>-0.06</sub>	15.18 <sup>+0.99</sup> <sub>-1.07</sub>	5.91	—
13455	291.55353	-0.74654	18.69	18.35	16.71	15.72	16.35	14.06	13.50	13.23	4.52 <sup>+0.09</sup> <sub>-0.07</sub>	5.74 <sup>+0.07</sup> <sub>-0.09</sub>	3.75 <sup>+0.07</sup> <sub>-0.06</sub>	15.71 <sup>+1.10</sup> <sub>-0.81</sub>	1.88	—
13457	291.55446	-0.32759	20.28	19.86	18.09	17.07	17.71	15.35	14.95	14.69	4.56 <sup>+0.09</sup> <sub>-0.12</sub>	5.76 <sup>+0.10</sup> <sub>-0.12</sub>	3.50 <sup>+0.09</sup> <sub>-0.09</sub>	17.54 <sup>+1.14</sup> <sub>-1.31</sub>	2.63	—
13461	291.56119	-0.41851	17.95	17.24	15.28	14.11	14.84	12.12	11.52	11.14	4.51 <sup>+0.10</sup> <sub>-0.07</sub>	6.62 <sup>+0.08</sup> <sub>-0.09</sub>	3.67 <sup>+0.06</sup> <sub>-0.06</sub>	13.36 <sup>+1.19</sup> <sub>-0.75</sub>	1.95	—
13466	291.56738	-0.62215	19.35	18.44	16.19	14.82	15.79	12.43	11.73	11.36	4.59 <sup>+0.07</sup> <sub>-0.09</sub>	7.65 <sup>+0.05</sup> <sub>-0.07</sub>	3.72 <sup>+0.05</sup> <sub>-0.05</sub>	14.44 <sup>+0.95</sup> <sub>-1.04</sub>	4.40	—
13467	291.56741	-0.66734	16.07	15.73	14.02	12.99	13.63	11.19	10.61	10.29	4.57 <sup>+0.08</sup> <sub>-0.08</sub>	6.09 <sup>+0.05</sup> <sub>-0.07</sub>	3.85 <sup>+0.06</sup> <sub>-0.06</sub>	13.27 <sup>+1.07</sup> <sub>-0.88</sub>	1.31	—
13471	291.57352	-0.52866	16.00	15.53	13.55	12.38	12.98	10.18	9.47	9.04	4.62 <sup>+0.06</sup> <sub>-0.07</sub>	7.16 <sup>+0.04</sup> <sub>-0.05</sub>	4.08 <sup>+0.05</sup> <sub>-0.05</sub>	12.47 <sup>+0.76</sup> <sub>-0.87</sub>	2.28	EM
13472	291.57361	-0.52577	19.67	19.02	17.08	15.88	16.56	13.72	13.02	12.66	4.52 <sup>+0.11</sup> <sub>-0.09</sub>	6.99 <sup>+0.09</sup> <sub>-0.11</sub>	3.95 <sup>+0.08</sup> <sub>-0.07</sub>	14.90 <sup>+1.36</sup> <sub>-0.95</sub>	2.45	—
13473	291.57410	-0.55117	20.28	19.87	18.08	17.03	17.58	15.15	14.55	14.51	4.57 <sup>+0.09</sup> <sub>-0.11</sub>	6.15 <sup>+0.09</sup> <sub>-0.10</sub>	3.73 <sup>+0.09</sup> <sub>-0.08</sub>	17.35 <sup>+1.10</sup> <sub>-1.20</sub>	6.90	—
13478	291.57774	-0.53649	18.72	18.29	16.60	15.58	16.27	13.88	13.32	13.07	4.52 <sup>+0.10</sup> <sub>-0.08</sub>	5.82 <sup>+0.07</sup> <sub>-0.09</sub>	3.68 <sup>+0.07</sup> <sub>-0.06</sub>	15.44 <sup>+1.24</sup> <sub>-0.85</sub>	3.08	—
13484	291.58443	-0.55670	17.70	17.37	15.75	14.75	15.38	13.08	12.55	12.35	4.55 <sup>+0.09</sup> <sub>-0.09</sub>	5.69 <sup>+0.06</sup> <sub>-0.08</sub>	3.70 <sup>+0.07</sup> <sub>-0.06</sub>	15.13 <sup>+1.16</sup> <sub>-0.98</sub>	4.70	—
13486	291.58603	-0.47893	16.86	16.51	14.67	13.53	14.24	11.53	10.88	10.58	4.64 <sup>+0.04</sup> <sub>-0.06</sub>	6.63 <sup>+0.04</sup> <sub>-0.04</sub>	3.95 <sup>+0.05</sup> <sub>-0.05</sub>	14.36 <sup>+0.55</sup> <sub>-0.82</sub>	4.45	—
13490	291.59344	-0.51462	18.57	17.92	15.85	14.57	15.78	12.17	11.43	11.06	4.62 <sup>+0.06</sup> <sub>-0.07</sub>	7.56 <sup>+0.04</sup> <sub>-0.05</sub>	4.02 <sup>+0.05</sup> <sub>-0.05</sub>	14.44 <sup>+0.75</sup> <sub>-0.91</sub>	4.08	—
13492	291.59375	-0.52683	15.02	14.97	13.46	12.56	13.09	11.05	10.59	10.37	4.63 <sup>+0.05</sup> <sub>-0.06</sub>	5.29 <sup>+0.04</sup> <sub>-0.04</sub>	3.74 <sup>+0.06</sup> <sub>-0.06</sub>	14.22 <sup>+0.62</sup> <sub>-0.82</sub>	2.68	—
13494	291.59482	-0.52392	16.81	16.53	14.86	13.82	14.52	12.07	11.50	11.26	4.62 <sup>+0.05</sup> <sub>-0.07</sub>	5.97 <sup>+0.04</sup> <sub>-0.05</sub>	3.80 <sup>+0.06</sup> <sub>-0.05</sub>	14.83 <sup>+0.72</sup> <sub>-0.92</sub>	3.82	—
13495	291.59552	-0.99644	18.68	18.23	16.50	15.50	16.17	13.81	13.19	12.96	4.51 <sup>+0.10</sup> <sub>-0.08</sub>	5.84 <sup>+0.09</sup> <sub>-0.11</sub>	3.66 <sup>+0.08</sup> <sub>-0.08</sub>	15.26 <sup>+1.24</sup> <sub>-0.86</sub>	1.53	—
13496	291.59574	-0.54637	18.67	18.32	16.72	15.71	16.30	14.01	13.44	13.26	4.50 <sup>+0.11</sup> <sub>-0.08</sub>	5.73 <sup>+0.09</sup> <sub>-0.10</sub>	3.79 <sup>+0.09</sup> <sub>-0.08</sub>	15.38 <sup>+1.31</sup> <sub>-0.82</sub>	4.70	—
13497	291.59609	-0.46854	17.25	16.78	14.87	13.64	14.41	11.29	10.54	10.12	4.61 <sup>+0.06</sup> <sub>-0.08</sub>	7.43 <sup>+0.04</sup> <sub>-0.06</sub>	4.27 <sup>+0.06</sup> <sub>-0.05</sub>	13.45 <sup>+0.79</sup> <sub>-0.95</sub>	2.58	—
13498	291.59618	-0.55126	20.13	19.79	18.11	17.17	nan	15.44	15.03	14.56	4.52 <sup>+0.10</sup> <sub>-0.08</sub>	5.72 <sup>+0.10</sup> <sub>-0.11</sub>	3.73 <sup>+0.10</sup> <sub>-0.10</sub>	17.14 <sup>+1.22</sup> <sub>-0.93</sub>	2.07	—
13500	291.59641	-0.23814	16.71	16.58	15.11	14.23	14.78	12.78	12.35	12.13	4.59 <sup>+0.08</sup> <sub>-0.09</sub>	5.12 <sup>+0.05</sup> <sub>-0.06</sub>	3.63 <sup>+0.07</sup> <sub>-0.06</sub>	15.47 <sup>+0.98</sup> <sub>-1.02</sub>	1.79	—
13501	291.59693	-0.51165	16.26	15.75	13.70	12.41	13.15	9.98	9.17	8.74	4.63 <sup>+0.05</sup> <sub>-0.06</sub>	7.75 <sup>+0.04</sup> <sub>-0.05</sub>	4.25 <sup>+0.06</sup> <sub>-0.05</sub>	12.28 <sup>+0.63</sup> <sub>-0.81</sub>	3.22	—
13502	291.59762	-0.54310	17.48	17.27	15.78	14.88	15.52	13.33	12.87	12.68	4.53 <sup>+0.10</sup> <sub>-0.07</sub>	5.26 <sup>+0.06</sup> <sub>-0.08</sub>	3.70 <sup>+0.07</sup> <sub>-0.07</sub>	15.27 <sup>+1.17</sup> <sub>-0.81</sub>	4.76	—
13503	291.59798	-0.49874	18.48	17.80	15.74	14.44	15.18	12.07	11.32	10.94	4.60 <sup>+0.07</sup> <sub>-0.09</sub>	7.54 <sup>+0.05</sup> <sub>-0.07</sub>	4.01 <sup>+0.06</sup> <sub>-0.05</sub>	14.06 <sup>+0.94</sup> <sub>-1.11</sub>	4.39	—
13509	291.60201	-0.51800	16.43	16.12	14.41	13.34	14.02	11.50	10.92	10.65	4.62 <sup>+0.06</sup> <sub>-0.08</sub>	6.16 <sup>+0.06</sup> <sub>-0.07</sub>	3.86 <sup>+0.06</sup> <sub>-0.06</sub>	14.17 <sup>+0.78</sup> <sub>-0.94</sub>	2.83	—
13511	291.60263	-0.52458	15.93	15.89	14.43	13.48	13.95	12.02	11.59	11.35	4.64 <sup>+0.04</sup> <sub>-0.07</sub>	5.25 <sup>+0.06</sup> <sub>-0.06</sub>	3.74 <sup>+0.08</sup> <sub>-0.07</sub>	15.32 <sup>+0.55</sup> <sub>-0.84</sub>	6.24	—
13512	291.60320	-0.51736	17.54	17.19	15.38	14.24	15.00	12.26	11.60	11.34	4.64 <sup>+0.04</sup> <sub>-0.06</sub>	6.56 <sup>+0.04</sup> <sub>-0.04</sub>	3.93 <sup>+0.06</sup> <sub>-0.05</sub>	15.08 <sup>+0.58</sup> <sub>-0.78</sub>	6.30	—
13517	291.60470	-0.52942	18.41	17.97	16.24	15.17	nan	13.23	12.66	12.32	4.52 <sup>+0.10</sup> <sub>-0.08</sub>	6.29 <sup>+0.07</sup> <sub>-0.09</sub>	3.92 <sup>+0.08</sup> <sub>-0.07</sub>	14.63 <sup>+1.23</sup> <sub>-0.81</sub>	2.31	—

Continued on next page...

ID	$\ell$	$b$	u	g	r	i	H $\alpha$	J	H	K	$\log(T_{\text{eff}})$	$A_0$	$R_V$	$\mu$	$\chi^2$	Notes
13518	291.60505	-0.52436	17.54	17.44	16.10	15.29	16.20	13.91	13.46	13.37	4.49 <sup>+0.09</sup> <sub>-0.07</sub>	4.73 <sup>+0.09</sup> <sub>-0.09</sub>	3.66 <sup>+0.09</sup> <sub>-0.09</sub>	15.54 <sup>+1.07</sup> <sub>-0.70</sub>	3.53	–
13519	291.60578	-0.51830	18.54	18.16	16.48	15.42	16.13	13.61	12.97	12.73	4.54 <sup>+0.10</sup> <sub>-0.08</sub>	6.11 <sup>+0.06</sup> <sub>-0.09</sub>	3.87 <sup>+0.07</sup> <sub>-0.06</sub>	15.29 <sup>+1.24</sup> <sub>-0.88</sub>	5.70	–
13520	291.60609	-0.90122	17.43	17.08	15.31	14.22	14.92	12.44	11.93	11.63	4.63 <sup>+0.05</sup> <sub>-0.07</sub>	6.06 <sup>+0.04</sup> <sub>-0.04</sub>	3.67 <sup>+0.05</sup> <sub>-0.05</sub>	15.42 <sup>+0.63</sup> <sub>-0.84</sub>	4.06	–
13521	291.60613	-0.50977	18.91	18.55	16.73	15.58	16.07	13.53	12.74	12.34	4.60 <sup>+0.07</sup> <sub>-0.09</sub>	6.85 <sup>+0.08</sup> <sub>-0.08</sub>	4.16 <sup>+0.08</sup> <sub>-0.08</sub>	15.66 <sup>+0.92</sup> <sub>-1.03</sub>	5.49	EM
13526	291.60972	-0.51412	18.70	18.13	15.97	14.62	15.63	12.15	11.31	10.91	4.65 <sup>+0.04</sup> <sub>-0.06</sub>	7.92 <sup>+0.04</sup> <sub>-0.04</sub>	4.15 <sup>+0.05</sup> <sub>-0.05</sub>	14.63 <sup>+0.49</sup> <sub>-0.72</sub>	7.62	–
13529	291.61156	-0.52436	15.18	15.29	13.97	13.13	13.67	11.79	11.44	11.22	4.64 <sup>+0.04</sup> <sub>-0.06</sub>	4.78 <sup>+0.04</sup> <sub>-0.04</sub>	3.73 <sup>+0.06</sup> <sub>-0.07</sub>	15.18 <sup>+0.60</sup> <sub>-0.78</sub>	5.11	–
13530	291.61246	-0.50607	18.62	18.16	16.24	15.04	15.72	12.71	12.03	11.72	4.63 <sup>+0.05</sup> <sub>-0.07</sub>	7.22 <sup>+0.05</sup> <sub>-0.05</sub>	4.14 <sup>+0.06</sup> <sub>-0.06</sub>	15.20 <sup>+0.66</sup> <sub>-0.85</sub>	5.56	–
13531	291.61340	-0.53108	17.05	16.64	14.94	13.87	13.86	11.98	11.42	11.02	4.51 <sup>+0.11</sup> <sub>-0.07</sub>	6.24 <sup>+0.10</sup> <sub>-0.10</sub>	3.95 <sup>+0.10</sup> <sub>-0.09</sub>	13.29 <sup>+1.30</sup> <sub>-0.81</sub>	2.51	EM
13532	291.61376	-0.47815	19.13	18.39	16.32	15.03	15.64	12.63	11.92	11.43	4.55 <sup>+0.10</sup> <sub>-0.09</sub>	7.60 <sup>+0.07</sup> <sub>-0.09</sub>	4.04 <sup>+0.07</sup> <sub>-0.06</sub>	14.05 <sup>+1.22</sup> <sub>-1.03</sub>	3.41	EM
13533	291.61384	-0.52088	15.72	15.81	14.50	13.71	13.84	12.33	11.84	11.51	4.58 <sup>+0.08</sup> <sub>-0.08</sub>	5.04 <sup>+0.16</sup> <sub>-0.16</sub>	4.07 <sup>+0.19</sup> <sub>-0.17</sub>	14.72 <sup>+1.08</sup> <sub>-1.05</sub>	0.70	EM
13541	291.61528	-0.51936	15.46	15.43	14.05	13.21	13.58	11.84	11.34	11.27	4.59 <sup>+0.08</sup> <sub>-0.09</sub>	4.91 <sup>+0.14</sup> <sub>-0.13</sub>	3.71 <sup>+0.14</sup> <sub>-0.14</sub>	14.51 <sup>+1.04</sup> <sub>-1.06</sub>	2.29	EM
13542	291.61558	-1.06675	18.90	18.42	16.54	15.46	16.17	13.65	13.08	12.80	4.60 <sup>+0.07</sup> <sub>-0.08</sub>	6.19 <sup>+0.05</sup> <sub>-0.06</sub>	3.60 <sup>+0.06</sup> <sub>-0.06</sub>	16.12 <sup>+0.87</sup> <sub>-1.01</sub>	1.41	–
13546	291.61795	-0.51955	14.28	14.34	12.97	12.13	12.63	10.63	10.19	9.95	4.60 <sup>+0.07</sup> <sub>-0.08</sub>	5.19 <sup>+0.14</sup> <sub>-0.13</sub>	4.03 <sup>+0.15</sup> <sub>-0.14</sub>	13.33 <sup>+0.92</sup> <sub>-0.97</sub>	0.76	–
13549	291.61829	-0.52682	16.53	16.52	15.12	14.22	14.89	12.63	12.12	11.91	4.59 <sup>+0.07</sup> <sub>-0.08</sub>	5.42 <sup>+0.11</sup> <sub>-0.12</sub>	4.06 <sup>+0.13</sup> <sub>-0.12</sub>	15.17 <sup>+0.94</sup> <sub>-0.85</sub>	2.27	–
13550	291.61844	-0.48928	18.79	18.04	15.89	14.50	15.39	11.86	11.02	10.59	4.60 <sup>+0.07</sup> <sub>-0.08</sub>	8.21 <sup>+0.05</sup> <sub>-0.06</sub>	4.22 <sup>+0.06</sup> <sub>-0.06</sub>	13.67 <sup>+0.98</sup> <sub>-1.00</sub>	5.19	–
13555	291.61991	-0.51860	14.94	14.98	13.64	12.81	13.32	11.50	11.11	10.93	4.62 <sup>+0.06</sup> <sub>-0.08</sub>	4.78 <sup>+0.09</sup> <sub>-0.09</sub>	3.69 <sup>+0.10</sup> <sub>-0.09</sub>	14.60 <sup>+0.76</sup> <sub>-0.97</sub>	2.72	–
13556	291.62014	-0.50458	18.86	18.17	16.08	14.75	15.66	12.35	11.57	11.22	4.61 <sup>+0.06</sup> <sub>-0.08</sub>	7.65 <sup>+0.05</sup> <sub>-0.06</sub>	4.01 <sup>+0.06</sup> <sub>-0.05</sub>	14.55 <sup>+0.81</sup> <sub>-1.00</sub>	6.74	–
13560	291.62061	-0.52429	13.84	13.96	12.69	11.84	12.26	10.41	9.94	9.64	4.61 <sup>+0.06</sup> <sub>-0.08</sub>	5.12 <sup>+0.09</sup> <sub>-0.09</sub>	4.14 <sup>+0.11</sup> <sub>-0.10</sub>	13.16 <sup>+0.84</sup> <sub>-0.99</sub>	3.92	–
13562	291.62093	-0.51996	15.26	15.33	14.01	13.17	13.70	11.79	11.45	11.10	4.60 <sup>+0.07</sup> <sub>-0.08</sub>	4.95 <sup>+0.11</sup> <sub>-0.11</sub>	3.89 <sup>+0.12</sup> <sub>-0.11</sub>	14.58 <sup>+0.91</sup> <sub>-1.00</sub>	3.75	–
13567	291.62155	-0.47237	16.27	15.74	13.81	12.61	13.35	10.41	9.65	9.28	4.58 <sup>+0.08</sup> <sub>-0.08</sub>	7.16 <sup>+0.06</sup> <sub>-0.07</sub>	4.08 <sup>+0.06</sup> <sub>-0.06</sub>	12.30 <sup>+0.97</sup> <sub>-0.98</sub>	2.09	–
13571	291.62203	-0.52855	15.51	15.43	13.95	13.02	13.61	11.49	11.02	10.86	4.63 <sup>+0.05</sup> <sub>-0.07</sub>	5.29 <sup>+0.05</sup> <sub>-0.05</sub>	3.73 <sup>+0.07</sup> <sub>-0.06</sub>	14.67 <sup>+0.64</sup> <sub>-0.85</sub>	4.94	–
13572	291.62245	-0.53732	14.93	14.83	13.29	12.33	12.81	10.67	10.16	9.86	4.62 <sup>+0.05</sup> <sub>-0.07</sub>	5.69 <sup>+0.05</sup> <sub>-0.06</sub>	3.96 <sup>+0.08</sup> <sub>-0.07</sub>	13.53 <sup>+0.73</sup> <sub>-0.93</sub>	2.16	–
13573	291.62259	-0.48008	19.10	18.45	16.53	15.32	16.11	13.22	12.49	12.20	4.53 <sup>+0.10</sup> <sub>-0.09</sub>	6.89 <sup>+0.07</sup> <sub>-0.10</sub>	3.87 <sup>+0.07</sup> <sub>-0.06</sub>	14.64 <sup>+1.26</sup> <sub>-0.97</sub>	6.33	–
13577	291.62297	-0.52309	14.71	14.80	13.51	12.70	13.21	11.47	11.03	10.85	4.62 <sup>+0.06</sup> <sub>-0.07</sub>	4.67 <sup>+0.04</sup> <sub>-0.05</sub>	3.71 <sup>+0.07</sup> <sub>-0.07</sub>	14.57 <sup>+0.73</sup> <sub>-0.90</sub>	2.77	–
13578	291.62300	-0.47020	17.49	17.08	15.35	14.27	14.97	12.36	11.81	11.53	4.58 <sup>+0.08</sup> <sub>-0.09</sub>	6.23 <sup>+0.06</sup> <sub>-0.07</sub>	3.83 <sup>+0.07</sup> <sub>-0.06</sub>	14.56 <sup>+1.02</sup> <sub>-1.02</sub>	4.55	–
13579	291.62318	-0.52054	13.93	14.00	12.67	11.80	12.25	10.37	9.90	9.64	4.61 <sup>+0.06</sup> <sub>-0.08</sub>	5.11 <sup>+0.05</sup> <sub>-0.06</sub>	3.98 <sup>+0.08</sup> <sub>-0.07</sub>	13.23 <sup>+0.82</sup> <sub>-0.98</sub>	4.15	–
13580	291.62375	-0.51401	16.11	15.71	13.97	12.90	13.59	11.06	10.46	10.18	4.57 <sup>+0.08</sup> <sub>-0.08</sub>	6.19 <sup>+0.05</sup> <sub>-0.07</sub>	3.82 <sup>+0.06</sup> <sub>-0.06</sub>	13.18 <sup>+1.07</sup> <sub>-0.94</sub>	2.65	–
13584	291.62493	-0.51950	15.48	15.50	14.14	13.29	13.82	11.91	11.50	11.26	4.61 <sup>+0.06</sup> <sub>-0.08</sub>	4.96 <sup>+0.07</sup> <sub>-0.07</sub>	3.78 <sup>+0.09</sup> <sub>-0.08</sub>	14.90 <sup>+0.81</sup> <sub>-0.81</sub>	2.58	–
13585	291.62520	-0.46322	17.06	16.52	14.58	13.39	14.11	11.37	10.72	10.37	4.61 <sup>+0.06</sup> <sub>-0.08</sub>	6.77 <sup>+0.04</sup> <sub>-0.05</sub>	3.80 <sup>+0.06</sup> <sub>-0.05</sub>	13.79 <sup>+0.81</sup> <sub>-0.94</sub>	2.51	–
13587	291.62598	-0.51573	16.62	16.40	14.85	13.88	14.50	12.23	11.75	11.48	4.57 <sup>+0.08</sup> <sub>-0.08</sub>	5.60 <sup>+0.06</sup> <sub>-0.07</sub>	3.80 <sup>+0.08</sup> <sub>-0.07</sub>	14.55 <sup>+1.05</sup> <sub>-0.93</sub>	2.50	–
13590	291.62640	-0.52151	15.46	15.49	14.18	13.37	13.89	12.13	11.69	11.57	4.61 <sup>+0.06</sup> <sub>-0.07</sub>	4.64 <sup>+0.04</sup> <sub>-0.05</sub>	3.60 <sup>+0.07</sup> <sub>-0.06</sub>	15.20 <sup>+0.81</sup> <sub>-0.91</sub>	5.53	–
13591	291.62695	-0.50704	19.50	18.98	17.15	16.03	16.78	14.10	13.44	13.10	4.53 <sup>+0.10</sup> <sub>-0.08</sub>	6.49 <sup>+0.08</sup> <sub>-0.10</sub>	3.86 <sup>+0.07</sup> <sub>-0.07</sub>	15.55 <sup>+1.26</sup> <sub>-0.90</sub>	2.18	–
13592	291.62703	-0.50589	17.23	16.93	15.17	14.07	14.75	12.17	11.60	11.30	4.63 <sup>+0.05</sup> <sub>-0.07</sub>	6.32 <sup>+0.05</sup> <sub>-0.05</sub>	3.89 <sup>+0.06</sup> <sub>-0.06</sub>	15.04 <sup>+0.61</sup> <sub>-0.85</sub>	3.82	–

Continued on next page...

ID	$\ell$	$b$	u	g	r	i	H $\alpha$	J	H	K	$\log(T_{\text{eff}})$	$A_0$	$R_V$	$\mu$	$\chi^2$	Notes
13594	291.62729	-0.52419	14.15	14.31	13.06	12.27	12.71	11.11	10.65	10.51	4.63 <sup>+0.05</sup> <sub>-0.07</sub>	4.53 <sup>+0.05</sup> <sub>-0.06</sub>	3.72 <sup>+0.08</sup> <sub>-0.08</sub>	14.36 <sup>+0.67</sup> <sub>-0.84</sub>	4.46	—
13596	291.62738	-0.49725	21.07	19.98	17.74	16.41	17.23	13.95	13.17	12.77	4.48 <sup>+0.15</sup> <sub>-0.15</sub>	7.74 <sup>+0.13</sup> <sub>-0.23</sub>	3.86 <sup>+0.08</sup> <sub>-0.08</sub>	14.51 <sup>+1.79</sup> <sub>-1.41</sub>	2.14	—
13597	291.62792	-0.50088	20.05	19.46	17.33	16.04	16.89	13.74	12.99	12.52	4.60 <sup>+0.07</sup> <sub>-0.09</sub>	7.53 <sup>+0.05</sup> <sub>-0.07</sub>	3.95 <sup>+0.06</sup> <sub>-0.06</sub>	15.78 <sup>+0.88</sup> <sub>-1.12</sub>	4.64	—
13599	291.62799	-0.49859	19.67	18.81	16.73	15.45	16.35	13.19	12.49	12.19	4.52 <sup>+0.11</sup> <sub>-0.10</sub>	7.22 <sup>+0.08</sup> <sub>-0.12</sub>	3.77 <sup>+0.06</sup> <sub>-0.06</sub>	14.44 <sup>+1.37</sup> <sub>-1.05</sub>	5.16	—
13600	291.62842	-0.52616	14.65	14.71	13.38	12.55	12.93	11.30	10.87	10.65	4.62 <sup>+0.06</sup> <sub>-0.08</sub>	4.75 <sup>+0.05</sup> <sub>-0.06</sub>	3.69 <sup>+0.08</sup> <sub>-0.07</sub>	14.37 <sup>+0.77</sup> <sub>-0.92</sub>	3.90	—
13601	291.62850	-0.53097	15.15	15.17	13.81	12.98	13.20	11.52	11.08	10.78	4.57 <sup>+0.09</sup> <sub>-0.08</sub>	5.10 <sup>+0.08</sup> <sub>-0.08</sub>	3.96 <sup>+0.10</sup> <sub>-0.09</sub>	13.85 <sup>+1.10</sup> <sub>-0.94</sub>	1.80	EM
13602	291.62873	-0.51641	19.00	18.63	17.02	16.02	16.72	14.40	13.84	13.70	4.51 <sup>+0.10</sup> <sub>-0.08</sub>	5.58 <sup>+0.10</sup> <sub>-0.10</sub>	3.64 <sup>+0.10</sup> <sub>-0.09</sub>	16.03 <sup>+1.27</sup> <sub>-0.84</sub>	3.79	—
13603	291.62890	-0.52034	16.65	16.58	15.19	14.33	14.89	12.94	12.47	12.28	4.57 <sup>+0.08</sup> <sub>-0.08</sub>	5.00 <sup>+0.07</sup> <sub>-0.08</sub>	3.73 <sup>+0.09</sup> <sub>-0.08</sub>	15.41 <sup>+1.05</sup> <sub>-0.95</sub>	2.83	—
13609	291.63110	-0.86052	20.30	19.40	17.35	16.10	16.99	13.93	13.34	12.96	4.48 <sup>+0.14</sup> <sub>-0.13</sub>	6.94 <sup>+0.10</sup> <sub>-0.20</sub>	3.67 <sup>+0.07</sup> <sub>-0.07</sub>	14.85 <sup>+1.65</sup> <sub>-1.28</sub>	4.69	—
13611	291.63137	-0.52593	15.79	15.71	14.25	13.33	13.81	11.80	11.32	11.13	4.61 <sup>+0.06</sup> <sub>-0.08</sub>	5.31 <sup>+0.07</sup> <sub>-0.07</sub>	3.81 <sup>+0.08</sup> <sub>-0.08</sub>	14.63 <sup>+0.83</sup> <sub>-0.94</sub>	3.08	—
13615	291.63270	-0.50336	17.68	17.24	15.44	14.35	15.05	12.45	11.85	11.55	4.59 <sup>+0.07</sup> <sub>-0.08</sub>	6.34 <sup>+0.07</sup> <sub>-0.07</sub>	3.80 <sup>+0.07</sup> <sub>-0.06</sub>	14.79 <sup>+0.93</sup> <sub>-1.00</sub>	1.97	—
13617	291.63279	-0.52448	17.53	17.33	15.88	14.99	16.00	13.58	13.03	12.82	4.48 <sup>+0.09</sup> <sub>-0.07</sub>	5.13 <sup>+0.09</sup> <sub>-0.10</sub>	3.73 <sup>+0.10</sup> <sub>-0.09</sub>	14.89 <sup>+1.09</sup> <sub>-0.71</sub>	3.40	—
13619	291.63402	-0.50408	18.54	17.98	16.11	14.97	15.74	12.97	12.34	12.06	4.56 <sup>+0.09</sup> <sub>-0.08</sub>	6.57 <sup>+0.05</sup> <sub>-0.08</sub>	3.78 <sup>+0.06</sup> <sub>-0.05</sub>	14.86 <sup>+1.11</sup> <sub>-0.90</sub>	4.59	—
13623	291.63538	-0.53109	16.83	16.51	14.84	13.81	14.57	12.07	11.52	11.26	4.59 <sup>+0.07</sup> <sub>-0.08</sub>	5.92 <sup>+0.06</sup> <sub>-0.07</sub>	3.77 <sup>+0.07</sup> <sub>-0.06</sub>	14.48 <sup>+0.92</sup> <sub>-1.00</sub>	2.42	—
13625	291.63658	-0.52122	16.40	16.18	14.58	13.61	14.25	12.00	11.50	11.29	4.62 <sup>+0.06</sup> <sub>-0.08</sub>	5.58 <sup>+0.04</sup> <sub>-0.05</sub>	3.69 <sup>+0.06</sup> <sub>-0.06</sub>	14.90 <sup>+0.77</sup> <sub>-0.96</sub>	3.75	—
13629	291.63815	-0.60530	20.38	18.89	16.05	14.38	15.59	11.12	10.11	9.57	4.55 <sup>+0.10</sup> <sub>-0.12</sub>	9.90 <sup>+0.06</sup> <sub>-0.13</sub>	3.96 <sup>+0.05</sup> <sub>-0.05</sub>	11.86 <sup>+1.26</sup> <sub>-1.28</sub>	1.33	—
13633	291.63874	-0.51169	17.03	16.72	15.11	14.13	14.73	12.48	11.95	11.68	4.54 <sup>+0.10</sup> <sub>-0.08</sub>	5.68 <sup>+0.09</sup> <sub>-0.10</sub>	3.74 <sup>+0.09</sup> <sub>-0.09</sub>	14.40 <sup>+1.25</sup> <sub>-0.96</sub>	1.97	—
13637	291.63967	-0.48499	19.11	18.28	16.11	14.82	15.70	12.54	11.89	11.53	4.59 <sup>+0.07</sup> <sub>-0.08</sub>	7.31 <sup>+0.05</sup> <sub>-0.06</sub>	3.68 <sup>+0.05</sup> <sub>-0.05</sub>	14.68 <sup>+0.94</sup> <sub>-0.99</sub>	2.80	—
13640	291.64012	-0.49535	19.84	18.97	16.77	15.45	16.38	13.16	12.42	12.04	4.58 <sup>+0.08</sup> <sub>-0.09</sub>	7.49 <sup>+0.06</sup> <sub>-0.08</sub>	3.74 <sup>+0.06</sup> <sub>-0.05</sub>	15.06 <sup>+1.03</sup> <sub>-1.07</sub>	2.56	—
13642	291.64018	-0.50203	19.67	18.98	16.94	15.72	16.56	13.60	12.90	12.55	4.57 <sup>+0.09</sup> <sub>-0.10</sub>	7.02 <sup>+0.07</sup> <sub>-0.10</sub>	3.78 <sup>+0.07</sup> <sub>-0.06</sub>	15.39 <sup>+1.14</sup> <sub>-1.14</sub>	1.76	—
13643	291.64081	-0.50365	16.31	15.76	13.81	12.62	13.38	10.60	9.98	9.60	4.62 <sup>+0.05</sup> <sub>-0.08</sub>	6.76 <sup>+0.05</sup> <sub>-0.05</sub>	3.78 <sup>+0.05</sup> <sub>-0.05</sub>	13.17 <sup>+0.73</sup> <sub>-0.93</sub>	3.51	—
13645	291.64112	-0.49692	19.93	19.27	17.33	16.17	16.94	14.12	13.45	13.15	4.51 <sup>+0.11</sup> <sub>-0.10</sub>	6.70 <sup>+0.09</sup> <sub>-0.12</sub>	3.79 <sup>+0.07</sup> <sub>-0.07</sub>	15.29 <sup>+1.27</sup> <sub>-1.05</sub>	1.76	—
13648	291.64161	-0.50244	18.74	18.08	16.08	14.87	15.70	12.78	12.15	11.83	4.59 <sup>+0.07</sup> <sub>-0.08</sub>	6.85 <sup>+0.07</sup> <sub>-0.07</sub>	3.71 <sup>+0.06</sup> <sub>-0.06</sub>	15.02 <sup>+0.94</sup> <sub>-1.00</sub>	2.66	—
13649	291.64232	-0.50134	17.79	17.31	15.48	14.36	15.10	12.44	11.87	11.54	4.59 <sup>+0.07</sup> <sub>-0.08</sub>	6.40 <sup>+0.07</sup> <sub>-0.07</sub>	3.76 <sup>+0.07</sup> <sub>-0.06</sub>	14.79 <sup>+0.87</sup> <sub>-0.97</sub>	2.30	—
13661	291.64460	-0.47546	20.18	19.67	17.77	16.65	16.95	14.53	13.94	13.48	4.53 <sup>+0.11</sup> <sub>-0.12</sub>	6.80 <sup>+0.14</sup> <sub>-0.16</sub>	4.00 <sup>+0.12</sup> <sub>-0.12</sub>	15.94 <sup>+1.38</sup> <sub>-1.27</sub>	1.31	SUB/EM
13662	291.64472	-0.52448	18.01	17.59	15.93	14.92	15.59	13.28	12.74	12.59	4.54 <sup>+0.10</sup> <sub>-0.08</sub>	5.61 <sup>+0.06</sup> <sub>-0.08</sub>	3.53 <sup>+0.06</sup> <sub>-0.06</sub>	15.27 <sup>+1.19</sup> <sub>-0.88</sub>	6.03	—
13663	291.64518	-0.43615	17.75	17.25	15.44	14.33	15.06	12.39	11.81	11.51	4.56 <sup>+0.09</sup> <sub>-0.08</sub>	6.38 <sup>+0.05</sup> <sub>-0.08</sub>	3.78 <sup>+0.06</sup> <sub>-0.06</sub>	14.32 <sup>+1.15</sup> <sub>-0.95</sub>	2.63	—
13664	291.64542	-0.66837	15.76	15.44	13.68	12.59	13.27	10.64	10.06	9.73	4.62 <sup>+0.05</sup> <sub>-0.07</sub>	6.40 <sup>+0.04</sup> <sub>-0.05</sub>	3.94 <sup>+0.06</sup> <sub>-0.05</sub>	13.28 <sup>+0.72</sup> <sub>-0.87</sub>	2.18	—
13665	291.64612	-0.49822	19.85	19.32	17.56	16.43	17.14	14.65	14.09	13.78	4.54 <sup>+0.11</sup> <sub>-0.11</sub>	6.12 <sup>+0.07</sup> <sub>-0.11</sub>	3.66 <sup>+0.07</sup> <sub>-0.07</sub>	16.46 <sup>+1.37</sup> <sub>-1.15</sub>	6.61	—
13666	291.64745	-0.47484	18.15	17.71	16.03	15.00	15.69	13.31	12.68	12.46	4.49 <sup>+0.10</sup> <sub>-0.07</sub>	5.84 <sup>+0.09</sup> <sub>-0.10</sub>	3.72 <sup>+0.07</sup> <sub>-0.07</sub>	14.49 <sup>+1.15</sup> <sub>-0.73</sub>	4.76	—
13667	291.64817	-0.51502	17.36	17.11	15.53	14.58	15.14	12.96	12.49	12.25	4.58 <sup>+0.08</sup> <sub>-0.08</sub>	5.52 <sup>+0.05</sup> <sub>-0.06</sub>	3.68 <sup>+0.07</sup> <sub>-0.06</sub>	15.39 <sup>+0.99</sup> <sub>-0.91</sub>	2.22	—
13674	291.65041	-0.46210	16.98	16.65	15.02	14.05	14.66	12.34	11.82	11.56	4.51 <sup>+0.10</sup> <sub>-0.07</sub>	5.71 <sup>+0.07</sup> <sub>-0.09</sub>	3.76 <sup>+0.07</sup> <sub>-0.07</sub>	13.87 <sup>+1.18</sup> <sub>-0.76</sub>	1.48	—
13676	291.65148	-0.51535	17.70	17.18	15.33	14.17	14.92	12.24	11.58	11.29	4.60 <sup>+0.07</sup> <sub>-0.09</sub>	6.54 <sup>+0.06</sup> <sub>-0.07</sub>	3.79 <sup>+0.06</sup> <sub>-0.06</sub>	14.53 <sup>+0.93</sup> <sub>-1.07</sub>	4.32	—

Continued on next page...

ID	$\ell$	$b$	u	g	r	i	H $\alpha$	J	H	K	$\log(T_{\text{eff}})$	$A_0$	$R_V$	$\mu$	$\chi^2$	Notes
13679	291.65269	-0.53159	16.43	16.06	14.39	13.37	14.03	11.75	11.20	10.98	4.59 <sup>+0.08</sup> <sub>-0.08</sub>	5.70 <sup>+0.05</sup> <sub>-0.07</sub>	3.58 <sup>+0.06</sup> <sub>-0.05</sub>	14.20 <sup>+0.98</sup> <sub>-0.97</sub>	4.50	—
13683	291.65303	-0.48777	18.05	17.65	15.99	14.97	15.60	13.31	12.75	12.56	4.54 <sup>+0.10</sup> <sub>-0.08</sub>	5.73 <sup>+0.07</sup> <sub>-0.08</sub>	3.63 <sup>+0.08</sup> <sub>-0.07</sub>	15.26 <sup>+1.26</sup> <sub>-0.92</sub>	3.89	—
13689	291.65598	-0.13386	19.97	19.88	18.31	17.39	17.91	15.89	15.21	14.92	4.59 <sup>+0.08</sup> <sub>-0.10</sub>	5.59 <sup>+0.10</sup> <sub>-0.11</sub>	3.88 <sup>+0.11</sup> <sub>-0.11</sub>	18.20 <sup>+1.01</sup> <sub>-1.16</sub>	3.52	—
13690	291.65643	-0.56202	16.85	16.29	14.25	13.00	13.79	10.58	9.77	9.32	4.59 <sup>+0.07</sup> <sub>-0.08</sub>	7.69 <sup>+0.05</sup> <sub>-0.06</sub>	4.25 <sup>+0.06</sup> <sub>-0.06</sub>	12.39 <sup>+0.93</sup> <sub>-0.90</sub>	1.87	—
13692	291.65685	-0.35440	14.14	14.16	12.91	12.16	12.59	11.01	10.68	10.52	4.54 <sup>+0.10</sup> <sub>-0.08</sub>	4.30 <sup>+0.06</sup> <sub>-0.08</sub>	3.48 <sup>+0.08</sup> <sub>-0.07</sub>	13.36 <sup>+1.18</sup> <sub>-0.87</sub>	1.51	—
13694	291.65783	-0.51084	15.27	15.05	13.43	12.45	13.01	10.83	10.37	10.06	4.61 <sup>+0.06</sup> <sub>-0.08</sub>	5.62 <sup>+0.04</sup> <sub>-0.05</sub>	3.70 <sup>+0.06</sup> <sub>-0.06</sub>	13.58 <sup>+0.81</sup> <sub>-0.93</sub>	3.37	—
13695	291.65801	-0.50644	18.07	17.58	15.78	14.70	15.42	12.91	12.37	12.07	4.56 <sup>+0.09</sup> <sub>-0.09</sub>	6.09 <sup>+0.08</sup> <sub>-0.09</sub>	3.63 <sup>+0.07</sup> <sub>-0.07</sub>	14.92 <sup>+1.17</sup> <sub>-1.02</sub>	2.29	—
13696	291.65823	-0.64955	18.24	17.81	15.96	14.85	15.59	12.84	12.22	11.88	4.60 <sup>+0.07</sup> <sub>-0.08</sub>	6.59 <sup>+0.05</sup> <sub>-0.06</sub>	3.90 <sup>+0.06</sup> <sub>-0.06</sub>	15.14 <sup>+0.91</sup> <sub>-0.99</sub>	1.16	—
13697	291.65835	-0.50782	18.09	17.67	15.91	14.86	15.58	13.10	12.56	12.33	4.60 <sup>+0.07</sup> <sub>-0.08</sub>	5.96 <sup>+0.05</sup> <sub>-0.06</sub>	3.61 <sup>+0.06</sup> <sub>-0.05</sub>	15.68 <sup>+0.89</sup> <sub>-0.99</sub>	3.40	—
13701	291.65877	-0.51396	19.85	19.28	17.49	16.35	17.04	14.40	13.76	13.51	4.53 <sup>+0.12</sup> <sub>-0.11</sub>	6.43 <sup>+0.08</sup> <sub>-0.13</sub>	3.82 <sup>+0.07</sup> <sub>-0.07</sub>	15.89 <sup>+1.45</sup> <sub>-1.18</sub>	6.65	—
13703	291.65934	-0.98644	15.55	15.46	14.03	13.20	13.70	11.84	11.40	11.21	4.57 <sup>+0.08</sup> <sub>-0.08</sub>	4.91 <sup>+0.05</sup> <sub>-0.07</sub>	3.60 <sup>+0.07</sup> <sub>-0.06</sub>	14.29 <sup>+1.06</sup> <sub>-0.93</sub>	1.34	—
13704	291.65958	-0.50541	19.46	18.82	16.89	15.73	16.54	13.78	13.22	12.90	4.56 <sup>+0.09</sup> <sub>-0.09</sub>	6.48 <sup>+0.06</sup> <sub>-0.08</sub>	3.61 <sup>+0.06</sup> <sub>-0.05</sub>	15.79 <sup>+1.11</sup> <sub>-1.01</sub>	2.77	—
13708	291.66120	-0.53148	18.22	17.83	16.17	15.14	15.62	13.42	12.83	12.56	4.50 <sup>+0.10</sup> <sub>-0.07</sub>	5.88 <sup>+0.09</sup> <sub>-0.10</sub>	3.78 <sup>+0.08</sup> <sub>-0.08</sub>	14.72 <sup>+1.23</sup> <sub>-0.76</sub>	2.55	EM
13710	291.66131	-0.53680	20.44	19.86	18.04	16.93	18.12	15.19	14.60	14.42	4.53 <sup>+0.12</sup> <sub>-0.12</sub>	6.05 <sup>+0.09</sup> <sub>-0.14</sub>	3.54 <sup>+0.08</sup> <sub>-0.08</sub>	16.85 <sup>+1.45</sup> <sub>-1.25</sub>	5.30	—
13717	291.66553	-0.50378	19.30	18.49	16.36	15.10	16.00	12.82	12.14	11.82	4.55 <sup>+0.09</sup> <sub>-0.08</sub>	7.28 <sup>+0.06</sup> <sub>-0.08</sub>	3.75 <sup>+0.06</sup> <sub>-0.05</sub>	14.45 <sup>+1.08</sup> <sub>-0.95</sub>	2.84	—
13721	291.66672	-0.49887	20.79	19.92	17.91	16.68	17.49	14.60	13.90	13.53	4.49 <sup>+0.13</sup> <sub>-0.15</sub>	6.90 <sup>+0.11</sup> <sub>-0.21</sub>	3.76 <sup>+0.08</sup> <sub>-0.08</sub>	15.51 <sup>+1.59</sup> <sub>-1.46</sub>	3.65	—
13722	291.66850	-0.49283	18.12	17.46	15.50	14.31	15.07	12.32	11.66	11.40	4.58 <sup>+0.08</sup> <sub>-0.09</sub>	6.66 <sup>+0.08</sup> <sub>-0.08</sub>	3.66 <sup>+0.07</sup> <sub>-0.06</sub>	14.38 <sup>+1.04</sup> <sub>-1.02</sub>	3.76	—
13725	291.67139	-0.66368	17.54	17.21	15.50	14.46	15.14	12.64	12.06	11.79	4.60 <sup>+0.07</sup> <sub>-0.08</sub>	6.10 <sup>+0.05</sup> <sub>-0.06</sub>	3.84 <sup>+0.06</sup> <sub>-0.06</sub>	15.07 <sup>+0.91</sup> <sub>-0.94</sub>	2.51	—
13726	291.67193	-0.66624	20.05	19.49	17.57	16.33	17.18	14.05	13.28	12.92	4.58 <sup>+0.08</sup> <sub>-0.10</sub>	7.31 <sup>+0.06</sup> <sub>-0.08</sub>	4.15 <sup>+0.07</sup> <sub>-0.07</sub>	15.89 <sup>+1.03</sup> <sub>-1.16</sub>	4.18	—
13728	291.67402	-0.46463	17.97	17.25	15.26	14.04	14.86	11.86	11.15	10.81	4.50 <sup>+0.11</sup> <sub>-0.08</sub>	7.04 <sup>+0.07</sup> <sub>-0.10</sub>	3.87 <sup>+0.06</sup> <sub>-0.06</sub>	12.90 <sup>+1.30</sup> <sub>-0.80</sub>	3.63	—
13731	291.67620	-0.47443	20.56	19.36	16.88	15.38	16.46	12.72	11.89	11.44	4.55 <sup>+0.09</sup> <sub>-0.12</sub>	8.44 <sup>+0.06</sup> <sub>-0.12</sub>	3.76 <sup>+0.05</sup> <sub>-0.05</sub>	13.98 <sup>+1.18</sup> <sub>-1.32</sub>	3.48	—
13736	291.68251	-1.62568	20.14	19.02	16.75	15.39	16.34	12.99	12.29	11.95	4.51 <sup>+0.12</sup> <sub>-0.12</sub>	7.58 <sup>+0.09</sup> <sub>-0.16</sub>	3.65 <sup>+0.06</sup> <sub>-0.05</sub>	14.07 <sup>+1.42</sup> <sub>-1.26</sub>	5.34	—
13738	291.68270	-1.00291	18.12	17.68	15.88	14.84	15.51	12.99	12.42	12.20	4.59 <sup>+0.07</sup> <sub>-0.08</sub>	6.13 <sup>+0.05</sup> <sub>-0.06</sub>	3.68 <sup>+0.06</sup> <sub>-0.05</sub>	15.42 <sup>+0.92</sup> <sub>-0.95</sub>	4.29	—
13739	291.68331	-0.53837	19.15	18.54	16.46	15.13	15.97	12.70	11.92	11.52	4.63 <sup>+0.05</sup> <sub>-0.08</sub>	7.73 <sup>+0.04</sup> <sub>-0.05</sub>	4.09 <sup>+0.06</sup> <sub>-0.06</sub>	15.02 <sup>+0.67</sup> <sub>-0.96</sub>	4.61	—
13740	291.68373	-0.50896	19.38	18.72	16.77	15.60	16.42	13.43	12.77	12.44	4.50 <sup>+0.10</sup> <sub>-0.08</sub>	6.89 <sup>+0.08</sup> <sub>-0.10</sub>	3.89 <sup>+0.07</sup> <sub>-0.06</sub>	14.46 <sup>+1.17</sup> <sub>-0.80</sub>	2.26	—
13743	291.68664	-0.66189	19.72	19.26	17.49	16.39	17.14	14.38	13.66	13.38	4.50 <sup>+0.13</sup> <sub>-0.11</sub>	6.57 <sup>+0.10</sup> <sub>-0.15</sub>	4.08 <sup>+0.09</sup> <sub>-0.09</sub>	15.41 <sup>+1.54</sup> <sub>-1.10</sub>	2.63	—
13744	291.68768	-0.69711	18.09	17.63	15.82	14.71	15.45	12.67	12.05	11.75	4.56 <sup>+0.09</sup> <sub>-0.08</sub>	6.57 <sup>+0.06</sup> <sub>-0.08</sub>	3.93 <sup>+0.06</sup> <sub>-0.06</sub>	14.54 <sup>+1.08</sup> <sub>-0.94</sub>	3.30	—
13746	291.69069	-0.45570	18.03	17.18	15.03	13.66	14.52	11.28	10.55	10.12	4.58 <sup>+0.08</sup> <sub>-0.09</sub>	7.67 <sup>+0.05</sup> <sub>-0.07</sub>	3.87 <sup>+0.05</sup> <sub>-0.05</sub>	13.07 <sup>+1.05</sup> <sub>-1.00</sub>	6.59	—
13761	291.70390	-0.53073	19.28	18.54	16.46	15.15	15.98	12.77	12.03	11.63	4.58 <sup>+0.08</sup> <sub>-0.10</sub>	7.57 <sup>+0.07</sup> <sub>-0.09</sub>	3.98 <sup>+0.06</sup> <sub>-0.06</sub>	14.52 <sup>+1.05</sup> <sub>-1.15</sub>	3.12	—
13765	291.70535	-0.56366	16.35	15.42	13.11	11.70	12.60	9.02	8.19	7.62	4.55 <sup>+0.09</sup> <sub>-0.08</sub>	8.41 <sup>+0.07</sup> <sub>-0.08</sub>	4.10 <sup>+0.06</sup> <sub>-0.05</sub>	10.10 <sup>+1.15</sup> <sub>-0.87</sub>	3.48	—
13770	291.70855	-0.61108	18.52	17.97	16.16	15.07	15.79	13.26	12.76	12.52	4.57 <sup>+0.09</sup> <sub>-0.10</sub>	6.04 <sup>+0.06</sup> <sub>-0.08</sub>	3.53 <sup>+0.06</sup> <sub>-0.06</sub>	15.47 <sup>+1.21</sup> <sub>-1.08</sub>	4.71	—
13777	291.71339	-1.34492	19.95	18.99	16.82	15.50	16.39	13.30	12.59	12.27	4.54 <sup>+0.11</sup> <sub>-0.12</sub>	7.26 <sup>+0.08</sup> <sub>-0.12</sub>	3.63 <sup>+0.06</sup> <sub>-0.06</sub>	14.73 <sup>+1.34</sup> <sub>-1.25</sub>	4.32	—
13779	291.71406	-0.59057	16.83	16.51	14.96	14.01	14.60	12.47	11.94	11.73	4.50 <sup>+0.11</sup> <sub>-0.07</sub>	5.39 <sup>+0.08</sup> <sub>-0.09</sub>	3.65 <sup>+0.07</sup> <sub>-0.07</sub>	13.95 <sup>+1.26</sup> <sub>-0.73</sub>	3.79	—

Continued on next page...

ID	$\ell$	$b$	u	g	r	i	H $\alpha$	J	H	K	$\log(T_{\text{eff}})$	$A_0$	$R_V$	$\mu$	$\chi^2$	Notes
13790	291.72205	-0.47429	18.19	17.56	15.69	14.56	15.31	12.69	12.15	11.88	4.55 <sup>+0.09</sup> <sub>-0.08</sub>	6.24 <sup>+0.06</sup> <sub>-0.08</sub>	3.54 <sup>+0.06</sup> <sub>-0.05</sub>	14.62 <sup>+1.16</sup> <sub>-0.94</sub>	3.90	—
13793	291.72479	-0.97913	19.02	18.22	16.09	14.87	15.70	12.83	12.15	11.86	4.59 <sup>+0.07</sup> <sub>-0.09</sub>	6.88 <sup>+0.05</sup> <sub>-0.07</sub>	3.54 <sup>+0.05</sup> <sub>-0.04</sub>	15.03 <sup>+0.97</sup> <sub>-1.06</sub>	2.94	—
13799	291.72912	-0.50153	18.74	18.06	16.16	15.02	15.79	13.15	12.59	12.29	4.49 <sup>+0.10</sup> <sub>-0.07</sub>	6.27 <sup>+0.08</sup> <sub>-0.09</sub>	3.55 <sup>+0.06</sup> <sub>-0.06</sub>	14.41 <sup>+1.16</sup> <sub>-0.75</sub>	2.29	—
13804	291.73847	-0.77952	19.72	18.88	16.82	15.59	16.42	13.33	12.69	12.37	4.49 <sup>+0.11</sup> <sub>-0.08</sub>	7.07 <sup>+0.09</sup> <sub>-0.11</sub>	3.74 <sup>+0.06</sup> <sub>-0.06</sub>	14.33 <sup>+1.26</sup> <sub>-0.85</sub>	5.32	—
13834	291.76419	-0.29297	16.78	16.66	15.22	14.35	14.89	12.94	12.56	12.35	4.58 <sup>+0.08</sup> <sub>-0.09</sub>	4.97 <sup>+0.06</sup> <sub>-0.07</sub>	3.58 <sup>+0.08</sup> <sub>-0.07</sub>	15.55 <sup>+1.06</sup> <sub>-1.00</sub>	2.62	—
13860	291.79601	-0.41104	18.47	17.53	15.23	13.84	14.77	11.26	10.49	10.11	4.59 <sup>+0.07</sup> <sub>-0.09</sub>	8.05 <sup>+0.05</sup> <sub>-0.07</sub>	3.87 <sup>+0.05</sup> <sub>-0.05</sub>	13.14 <sup>+0.95</sup> <sub>-1.04</sub>	5.67	—
13873	291.80996	-0.37289	18.26	18.13	16.57	15.61	16.30	14.02	13.51	13.27	4.63 <sup>+0.05</sup> <sub>-0.07</sub>	5.56 <sup>+0.04</sup> <sub>-0.05</sub>	3.79 <sup>+0.07</sup> <sub>-0.06</sub>	17.01 <sup>+0.67</sup> <sub>-0.85</sub>	2.71	—
13885	291.83013	-0.18090	15.94	15.73	14.24	13.36	13.89	11.85	11.44	11.19	4.51 <sup>+0.10</sup> <sub>-0.07</sub>	5.16 <sup>+0.07</sup> <sub>-0.09</sub>	3.66 <sup>+0.07</sup> <sub>-0.07</sub>	13.63 <sup>+1.21</sup> <sub>-0.79</sub>	1.55	—
13887	291.83089	-0.64396	19.56	19.08	17.28	16.19	16.92	14.26	13.63	13.30	4.54 <sup>+0.11</sup> <sub>-0.11</sub>	6.42 <sup>+0.07</sup> <sub>-0.06</sub>	3.88 <sup>+0.07</sup> <sub>-0.06</sub>	15.89 <sup>+1.41</sup> <sub>-1.15</sub>	1.46	—
13892	291.83661	-0.41833	16.29	16.19	14.79	13.95	14.47	12.59	12.17	12.01	4.56 <sup>+0.09</sup> <sub>-0.08</sub>	4.85 <sup>+0.05</sup> <sub>-0.07</sub>	3.58 <sup>+0.07</sup> <sub>-0.07</sub>	14.95 <sup>+1.14</sup> <sub>-0.87</sub>	2.82	—
13893	291.83694	-0.74031	20.11	19.32	17.28	16.04	16.86	13.85	13.31	12.95	4.53 <sup>+0.12</sup> <sub>-0.12</sub>	6.93 <sup>+0.09</sup> <sub>-0.15</sub>	3.68 <sup>+0.07</sup> <sub>-0.06</sub>	15.33 <sup>+1.52</sup> <sub>-1.30</sub>	5.61	—
13902	291.84503	-0.59058	17.45	16.43	14.20	12.80	13.69	10.47	9.75	9.35	4.55 <sup>+0.10</sup> <sub>-0.09</sub>	7.61 <sup>+0.06</sup> <sub>-0.10</sub>	3.67 <sup>+0.05</sup> <sub>-0.05</sub>	11.90 <sup>+1.27</sup> <sub>-1.00</sub>	7.30	—
13908	291.85377	-0.62944	18.29	17.53	15.61	14.46	15.22	12.61	12.05	11.81	4.49 <sup>+0.10</sup> <sub>-0.07</sub>	6.21 <sup>+0.08</sup> <sub>-0.10</sub>	3.44 <sup>+0.05</sup> <sub>-0.05</sub>	13.92 <sup>+1.14</sup> <sub>-0.78</sub>	5.40	—
13912	291.85548	-0.90367	18.53	17.71	15.55	14.32	15.15	12.16	11.46	11.13	4.55 <sup>+0.09</sup> <sub>-0.08</sub>	7.10 <sup>+0.07</sup> <sub>-0.09</sub>	3.64 <sup>+0.06</sup> <sub>-0.05</sub>	13.78 <sup>+1.12</sup> <sub>-0.92</sub>	1.18	—
13918	291.86299	-0.68141	16.91	16.47	14.59	13.46	14.09	11.36	10.78	10.34	4.60 <sup>+0.06</sup> <sub>-0.07</sub>	6.78 <sup>+0.05</sup> <sub>-0.06</sub>	3.97 <sup>+0.06</sup> <sub>-0.06</sub>	13.65 <sup>+0.84</sup> <sub>-0.89</sub>	3.54	EM
13931	291.87962	-0.50235	17.68	16.96	14.95	13.75	14.55	11.79	11.22	10.92	4.59 <sup>+0.08</sup> <sub>-0.08</sub>	6.57 <sup>+0.05</sup> <sub>-0.07</sub>	3.51 <sup>+0.05</sup> <sub>-0.04</sub>	14.11 <sup>+0.98</sup> <sub>-0.99</sub>	3.44	—
13933	291.88197	-0.06294	17.73	17.93	16.90	16.30	16.61	15.63	15.17	15.12	4.50 <sup>+0.09</sup> <sub>-0.07</sub>	3.44 <sup>+0.10</sup> <sub>-0.10</sub>	3.30 <sup>+0.12</sup> <sub>-0.12</sub>	17.59 <sup>+1.11</sup> <sub>-0.76</sub>	6.43	—
13934	291.88208	-0.89765	20.51	19.54	17.31	16.01	16.91	13.63	12.95	12.54	4.50 <sup>+0.13</sup> <sub>-0.12</sub>	7.50 <sup>+0.10</sup> <sub>-0.16</sub>	3.74 <sup>+0.06</sup> <sub>-0.06</sub>	14.55 <sup>+1.52</sup> <sub>-1.23</sub>	1.01	—
13937	291.88487	-0.93911	19.85	18.96	16.72	15.39	16.33	12.95	12.26	11.81	4.55 <sup>+0.09</sup> <sub>-0.10</sub>	7.70 <sup>+0.06</sup> <sub>-0.10</sub>	3.82 <sup>+0.06</sup> <sub>-0.05</sub>	14.45 <sup>+1.19</sup> <sub>-1.10</sub>	2.06	—
13939	291.88803	-0.91083	18.74	18.06	16.13	15.01	15.75	13.07	12.50	12.20	4.50 <sup>+0.09</sup> <sub>-0.07</sub>	6.38 <sup>+0.08</sup> <sub>-0.09</sub>	3.59 <sup>+0.06</sup> <sub>-0.06</sub>	14.38 <sup>+1.08</sup> <sub>-0.77</sub>	1.04	—
13942	291.88977	-0.92144	17.94	17.19	15.15	13.97	14.77	11.96	11.35	10.98	4.52 <sup>+0.10</sup> <sub>-0.07</sub>	6.70 <sup>+0.07</sup> <sub>-0.09</sub>	3.61 <sup>+0.05</sup> <sub>-0.05</sub>	13.31 <sup>+1.21</sup> <sub>-0.80</sub>	1.82	—
13945	291.89350	-0.94695	20.05	18.83	16.40	14.94	15.94	12.39	11.65	11.23	4.53 <sup>+0.11</sup> <sub>-0.09</sub>	8.09 <sup>+0.07</sup> <sub>-0.10</sub>	3.65 <sup>+0.05</sup> <sub>-0.05</sub>	13.50 <sup>+1.29</sup> <sub>-0.99</sub>	3.34	—
13946	291.89553	-1.00608	20.00	19.02	16.74	15.38	16.30	13.08	12.38	11.94	4.56 <sup>+0.10</sup> <sub>-0.11</sub>	7.56 <sup>+0.06</sup> <sub>-0.11</sub>	3.64 <sup>+0.06</sup> <sub>-0.05</sub>	14.64 <sup>+1.20</sup> <sub>-1.21</sub>	3.48	—
13948	291.89754	-1.73215	19.90	19.54	17.93	16.96	17.60	15.44	14.84	14.50	4.49 <sup>+0.11</sup> <sub>-0.09</sub>	5.54 <sup>+0.11</sup> <sub>-0.12</sub>	3.69 <sup>+0.09</sup> <sub>-0.09</sub>	16.71 <sup>+1.28</sup> <sub>-0.89</sub>	4.93	—
13952	291.90404	0.04145	20.61	19.93	17.86	16.61	17.48	14.27	13.37	13.03	4.52 <sup>+0.11</sup> <sub>-0.12</sub>	7.54 <sup>+0.09</sup> <sub>-0.15</sub>	4.07 <sup>+0.08</sup> <sub>-0.08</sub>	15.30 <sup>+1.41</sup> <sub>-1.25</sub>	0.67	—
13954	291.90934	-0.91501	17.84	16.83	14.44	13.04	13.93	10.61	9.92	9.48	4.62 <sup>+0.06</sup> <sub>-0.07</sub>	7.84 <sup>+0.04</sup> <sub>-0.05</sub>	3.63 <sup>+0.04</sup> <sub>-0.04</sub>	12.95 <sup>+0.73</sup> <sub>-0.89</sub>	2.84	—
13967	291.92761	-0.69628	19.74	19.37	17.70	16.63	17.33	14.77	14.22	13.89	4.55 <sup>+0.10</sup> <sub>-0.12</sub>	6.16 <sup>+0.08</sup> <sub>-0.12</sub>	3.93 <sup>+0.08</sup> <sub>-0.08</sub>	16.65 <sup>+1.24</sup> <sub>-1.27</sub>	4.83	—
13970	291.92927	0.01535	19.21	18.97	17.51	16.58	17.23	15.34	14.84	14.64	4.55 <sup>+0.10</sup> <sub>-0.09</sub>	4.89 <sup>+0.10</sup> <sub>-0.11</sub>	3.41 <sup>+0.10</sup> <sub>-0.09</sub>	17.52 <sup>+1.26</sup> <sub>-1.06</sub>	7.53	—
13974	291.93419	-0.61524	19.56	18.85	16.83	15.58	16.41	13.54	12.98	12.69	4.60 <sup>+0.07</sup> <sub>-0.11</sub>	6.74 <sup>+0.07</sup> <sub>-0.08</sub>	3.57 <sup>+0.07</sup> <sub>-0.07</sub>	15.95 <sup>+0.92</sup> <sub>-1.31</sub>	6.84	—
13985	291.94382	-0.51289	19.61	19.06	17.23	16.16	16.87	14.35	13.81	13.50	4.54 <sup>+0.10</sup> <sub>-0.10</sub>	6.11 <sup>+0.08</sup> <sub>-0.11</sub>	3.60 <sup>+0.07</sup> <sub>-0.07</sub>	16.13 <sup>+1.27</sup> <sub>-1.09</sub>	1.53	—
14009	291.96587	-0.37695	18.94	18.98	17.48	16.58	17.15	14.92	14.53	14.10	4.63 <sup>+0.05</sup> <sub>-0.07</sub>	5.58 <sup>+0.08</sup> <sub>-0.08</sub>	4.06 <sup>+0.10</sup> <sub>-0.10</sub>	17.92 <sup>+0.62</sup> <sub>-0.85</sub>	3.86	—
14016	291.97384	-0.77936	19.16	18.15	15.74	14.32	15.30	11.75	11.02	10.61	4.61 <sup>+0.06</sup> <sub>-0.09</sub>	8.09 <sup>+0.04</sup> <sub>-0.06</sub>	3.72 <sup>+0.05</sup> <sub>-0.05</sub>	13.92 <sup>+0.80</sup> <sub>-1.04</sub>	3.69	—
14024	291.98291	-0.27823	18.45	18.61	17.30	16.57	17.02	15.24	14.61	14.57	4.57 <sup>+0.08</sup> <sub>-0.08</sub>	4.95 <sup>+0.07</sup> <sub>-0.08</sub>	4.12 <sup>+0.11</sup> <sub>-0.10</sub>	17.53 <sup>+1.02</sup> <sub>-0.91</sub>	7.56	—

Continued on next page...

ID	$\ell$	$b$	u	g	r	i	H $\alpha$	J	H	K	$\log(T_{\text{eff}})$	$A_0$	$R_V$	$\mu$	$\chi^2$	Notes
14052	292.00673	-0.68706	18.51	18.08	16.37	15.33	15.99	13.51	13.00	12.71	4.54 <sup>+0.10</sup> <sub>-0.09</sub>	6.00 <sup>+0.07</sup> <sub>-0.10</sub>	3.74 <sup>+0.07</sup> <sub>-0.07</sub>	15.34 <sup>+1.26</sup> <sub>-1.00</sub>	2.79	—
14064	292.01688	-0.53942	16.18	15.98	14.51	13.63	14.19	12.17	11.73	11.52	4.51 <sup>+0.10</sup> <sub>-0.07</sub>	5.09 <sup>+0.07</sup> <sub>-0.09</sub>	3.64 <sup>+0.08</sup> <sub>-0.07</sub>	13.94 <sup>+1.14</sup> <sub>-0.77</sub>	1.94	—
14079	292.03130	-0.59555	16.39	16.22	14.77	13.89	14.41	12.41	11.96	11.64	4.49 <sup>+0.09</sup> <sub>-0.07</sub>	5.18 <sup>+0.09</sup> <sub>-0.10</sub>	3.79 <sup>+0.09</sup> <sub>-0.08</sub>	13.79 <sup>+1.07</sup> <sub>-0.70</sub>	1.74	—
14080	292.03263	-0.53819	15.75	15.75	14.49	13.73	14.19	12.47	12.12	11.88	4.48 <sup>+0.08</sup> <sub>-0.06</sub>	4.50 <sup>+0.08</sup> <sub>-0.09</sub>	3.70 <sup>+0.09</sup> <sub>-0.08</sub>	14.07 <sup>+0.97</sup> <sub>-0.66</sub>	1.75	—
14092	292.04152	-0.72793	17.27	16.57	14.55	13.37	14.14	11.13	10.47	10.14	4.52 <sup>+0.10</sup> <sub>-0.08</sub>	7.05 <sup>+0.07</sup> <sub>-0.09</sub>	3.85 <sup>+0.06</sup> <sub>-0.06</sub>	12.44 <sup>+1.24</sup> <sub>-0.84</sub>	2.75	—
14108	292.05200	-1.37972	15.14	14.55	12.78	11.69	12.36	9.92	9.41	9.13	4.49 <sup>+0.11</sup> <sub>-0.07</sub>	5.95 <sup>+0.08</sup> <sub>-0.10</sub>	3.56 <sup>+0.06</sup> <sub>-0.06</sub>	11.19 <sup>+1.23</sup> <sub>-0.74</sub>	4.50	—
14115	292.05839	-0.08164	19.96	19.22	17.26	16.06	16.89	14.06	13.35	13.08	4.52 <sup>+0.11</sup> <sub>-0.11</sub>	6.72 <sup>+0.08</sup> <sub>-0.13</sub>	3.70 <sup>+0.07</sup> <sub>-0.06</sub>	15.35 <sup>+1.35</sup> <sub>-1.11</sub>	5.09	—
14137	292.07375	-1.31566	14.16	14.20	12.96	12.19	12.64	11.04	10.73	10.58	4.58 <sup>+0.08</sup> <sub>-0.08</sub>	4.31 <sup>+0.05</sup> <sub>-0.07</sub>	3.46 <sup>+0.07</sup> <sub>-0.07</sub>	13.88 <sup>+1.07</sup> <sub>-0.74</sub>	3.25	—
14156	292.08584	-0.50917	17.32	17.02	15.40	14.44	15.01	12.73	12.23	12.00	4.55 <sup>+0.10</sup> <sub>-0.08</sub>	5.68 <sup>+0.07</sup> <sub>-0.08</sub>	3.74 <sup>+0.07</sup> <sub>-0.07</sub>	14.71 <sup>+1.20</sup> <sub>-0.88</sub>	2.09	—
14163	292.09035	0.33553	14.09	14.08	12.75	11.96	12.37	10.74	10.31	10.09	4.55 <sup>+0.09</sup> <sub>-0.08</sub>	4.64 <sup>+0.06</sup> <sub>-0.08</sub>	3.64 <sup>+0.08</sup> <sub>-0.07</sub>	13.02 <sup>+1.12</sup> <sub>-0.89</sub>	2.54	—
14167	292.09268	-0.57179	16.12	15.65	13.84	12.76	13.41	10.87	10.29	9.95	4.56 <sup>+0.09</sup> <sub>-0.08</sub>	6.31 <sup>+0.06</sup> <sub>-0.08</sub>	3.78 <sup>+0.06</sup> <sub>-0.06</sub>	12.79 <sup>+1.08</sup> <sub>-0.91</sub>	1.46	—
14172	292.09597	-0.34840	15.73	15.88	14.70	13.99	14.37	12.82	12.49	12.28	4.56 <sup>+0.09</sup> <sub>-0.08</sub>	4.31 <sup>+0.05</sup> <sub>-0.08</sub>	3.71 <sup>+0.09</sup> <sub>-0.08</sub>	15.32 <sup>+1.15</sup> <sub>-0.91</sub>	1.38	—
14182	292.10114	-0.17477	19.08	18.62	16.75	15.61	16.35	13.53	12.90	12.62	4.61 <sup>+0.06</sup> <sub>-0.08</sub>	6.70 <sup>+0.05</sup> <sub>-0.06</sub>	3.90 <sup>+0.06</sup> <sub>-0.06</sub>	15.93 <sup>+0.82</sup> <sub>-0.99</sub>	4.18	—
14183	292.10260	-0.54185	16.07	15.85	14.38	13.48	14.02	11.95	11.54	11.28	4.50 <sup>+0.10</sup> <sub>-0.07</sub>	5.19 <sup>+0.08</sup> <sub>-0.09</sub>	3.70 <sup>+0.08</sup> <sub>-0.07</sub>	13.52 <sup>+1.14</sup> <sub>-0.73</sub>	2.31	—
14187	292.10795	0.31766	15.52	15.34	13.87	13.03	13.52	11.62	11.21	10.99	4.51 <sup>+0.10</sup> <sub>-0.07</sub>	4.95 <sup>+0.07</sup> <sub>-0.09</sub>	3.57 <sup>+0.07</sup> <sub>-0.07</sub>	13.43 <sup>+1.21</sup> <sub>-0.76</sub>	0.49	—
14215	292.12775	-0.03638	19.58	18.97	16.94	15.70	16.53	13.52	12.83	12.45	4.60 <sup>+0.07</sup> <sub>-0.09</sub>	7.14 <sup>+0.06</sup> <sub>-0.07</sub>	3.87 <sup>+0.06</sup> <sub>-0.06</sub>	15.64 <sup>+0.91</sup> <sub>-1.04</sub>	2.11	—
14232	292.13654	-0.04185	16.86	16.43	14.70	13.61	14.28	11.69	11.08	10.85	4.56 <sup>+0.09</sup> <sub>-0.09</sub>	6.28 <sup>+0.06</sup> <sub>-0.08</sub>	3.86 <sup>+0.07</sup> <sub>-0.06</sub>	13.62 <sup>+1.17</sup> <sub>-1.01</sub>	5.72	—
14238	292.13888	-0.04047	17.10	16.76	15.07	14.06	14.71	12.25	11.65	11.37	4.53 <sup>+0.10</sup> <sub>-0.08</sub>	6.06 <sup>+0.08</sup> <sub>-0.09</sub>	3.91 <sup>+0.09</sup> <sub>-0.08</sub>	13.85 <sup>+1.29</sup> <sub>-0.87</sub>	0.88	—
14239	292.13979	-0.82736	14.82	14.67	13.20	12.35	12.86	10.88	10.46	10.23	4.54 <sup>+0.10</sup> <sub>-0.07</sub>	5.08 <sup>+0.06</sup> <sub>-0.08</sub>	3.66 <sup>+0.07</sup> <sub>-0.07</sub>	12.91 <sup>+1.19</sup> <sub>-0.80</sub>	0.67	—
14281	292.15965	-0.32478	14.92	14.69	13.13	12.18	12.69	10.54	10.03	9.66	4.55 <sup>+0.09</sup> <sub>-0.08</sub>	5.66 <sup>+0.06</sup> <sub>-0.08</sub>	3.86 <sup>+0.08</sup> <sub>-0.07</sub>	12.46 <sup>+1.17</sup> <sub>-0.90</sub>	3.35	—
14286	292.16485	-1.39803	16.29	15.83	14.04	13.01	13.65	11.11	10.60	10.29	4.53 <sup>+0.07</sup> <sub>-0.07</sub>	6.15 <sup>+0.06</sup> <sub>-0.08</sub>	3.74 <sup>+0.06</sup> <sub>-0.06</sub>	12.83 <sup>+1.10</sup> <sub>-0.80</sub>	1.52	—
14316	292.21123	-0.12231	20.00	18.99	16.71	15.35	16.30	12.78	12.04	11.68	4.54 <sup>+0.10</sup> <sub>-0.09</sub>	7.92 <sup>+0.06</sup> <sub>-0.10</sub>	3.82 <sup>+0.06</sup> <sub>-0.05</sub>	14.08 <sup>+1.28</sup> <sub>-1.02</sub>	6.67	—
14347	292.24607	0.49059	13.41	13.53	12.39	11.72	12.07	10.77	10.43	10.31	4.51 <sup>+0.09</sup> <sub>-0.07</sub>	3.87 <sup>+0.07</sup> <sub>-0.08</sub>	3.42 <sup>+0.08</sup> <sub>-0.08</sub>	12.86 <sup>+1.10</sup> <sub>-0.73</sub>	2.39	—
14359	292.25612	-0.29652	13.39	13.60	12.53	11.80	12.18	10.78	10.46	10.27	4.59 <sup>+0.08</sup> <sub>-0.08</sub>	4.06 <sup>+0.05</sup> <sub>-0.06</sub>	3.64 <sup>+0.09</sup> <sub>-0.08</sub>	13.69 <sup>+1.03</sup> <sub>-0.95</sub>	5.52	—
14365	292.26345	0.19358	12.65	13.23	12.57	12.12	12.31	11.59	11.40	11.20	4.51 <sup>+0.10</sup> <sub>-0.07</sub>	2.79 <sup>+0.07</sup> <sub>-0.08</sub>	3.73 <sup>+0.15</sup> <sub>-0.14</sub>	13.91 <sup>+1.23</sup> <sub>-0.74</sub>	6.27	—
14391	292.28560	-0.14512	15.05	14.86	13.36	12.50	13.04	11.01	10.53	10.27	4.49 <sup>+0.10</sup> <sub>-0.07</sub>	5.19 <sup>+0.08</sup> <sub>-0.09</sub>	3.73 <sup>+0.08</sup> <sub>-0.07</sub>	12.45 <sup>+1.21</sup> <sub>-0.69</sub>	0.75	—
14401	292.29574	0.04007	18.87	18.87	17.44	16.52	17.04	15.31	14.64	14.57	4.63 <sup>+0.05</sup> <sub>-0.07</sub>	5.06 <sup>+0.12</sup> <sub>-0.13</sub>	3.68 <sup>+0.12</sup> <sub>-0.12</sub>	18.38 <sup>+0.62</sup> <sub>-0.90</sub>	6.74	—
14405	292.29954	-0.18003	19.54	19.69	18.16	17.27	17.84	15.64	15.10	14.84	4.64 <sup>+0.04</sup> <sub>-0.06</sub>	5.61 <sup>+0.10</sup> <sub>-0.10</sub>	4.10 <sup>+0.12</sup> <sub>-0.12</sub>	18.65 <sup>+0.58</sup> <sub>-0.81</sub>	5.62	—
14415	292.31112	-0.67882	20.26	19.61	17.68	16.51	17.00	14.43	13.79	13.36	4.50 <sup>+0.11</sup> <sub>-0.08</sub>	6.79 <sup>+0.09</sup> <sub>-0.11</sub>	3.85 <sup>+0.07</sup> <sub>-0.07</sub>	15.49 <sup>+1.27</sup> <sub>-0.85</sub>	2.56	EM
14448	292.36524	-0.04512	16.40	16.79	15.94	15.36	15.70	14.68	14.26	14.08	4.51 <sup>+0.11</sup> <sub>-0.08</sub>	3.53 <sup>+0.19</sup> <sub>-0.19</sub>	3.89 <sup>+0.32</sup> <sub>-0.28</sub>	16.61 <sup>+1.41</sup> <sub>-0.90</sub>	3.41	—
14454	292.37157	-0.07212	19.55	18.67	16.44	15.12	16.01	12.83	12.19	11.83	4.59 <sup>+0.07</sup> <sub>-0.09</sub>	7.37 <sup>+0.05</sup> <sub>-0.07</sub>	3.60 <sup>+0.05</sup> <sub>-0.05</sub>	14.98 <sup>+0.89</sup> <sub>-1.06</sub>	3.12	—
14455	292.37295	-0.43848	20.27	19.98	18.34	17.35	18.01	15.63	15.05	14.80	4.55 <sup>+0.10</sup> <sub>-0.11</sub>	5.86 <sup>+0.10</sup> <sub>-0.11</sub>	3.86 <sup>+0.11</sup> <sub>-0.10</sub>	17.56 <sup>+1.26</sup> <sub>-1.17</sub>	3.04	—
14485	292.41451	-1.00395	17.54	16.90	14.99	13.85	14.62	11.80	11.21	10.89	4.52 <sup>+0.10</sup> <sub>-0.08</sub>	6.60 <sup>+0.07</sup> <sub>-0.09</sub>	3.74 <sup>+0.06</sup> <sub>-0.05</sub>	13.21 <sup>+1.19</sup> <sub>-0.83</sub>	2.54	—

Continued on next page...

ID	$\ell$	$b$	u	g	r	i	H $\alpha$	J	H	K	$\log(T_{\text{eff}})$	$A_0$	$R_V$	$\mu$	$\chi^2$	Notes
14488	292.42508	-1.02648	16.53	16.28	14.74	13.77	14.37	12.00	11.43	11.16	4.49 <sup>+0.09</sup> <sub>-0.07</sub>	5.82 <sup>+0.08</sup> <sub>-0.09</sub>	4.04 <sup>+0.08</sup> <sub>-0.08</sub>	13.22 <sup>+1.00</sup> <sub>-0.69</sub>	2.27	–
14502	292.43776	-0.23568	18.43	18.27	16.77	15.78	16.49	14.06	13.40	13.09	4.53 <sup>+0.10</sup> <sub>-0.08</sub>	5.91 <sup>+0.07</sup> <sub>-0.09</sub>	4.21 <sup>+0.09</sup> <sub>-0.09</sub>	15.57 <sup>+1.25</sup> <sub>-0.89</sub>	4.74	–
14534	292.46977	-0.84791	19.17	18.41	16.32	15.14	15.91	12.98	12.34	12.01	4.54 <sup>+0.10</sup> <sub>-0.09</sub>	6.94 <sup>+0.06</sup> <sub>-0.09</sub>	3.68 <sup>+0.06</sup> <sub>-0.06</sub>	14.52 <sup>+1.18</sup> <sub>-0.96</sub>	1.29	–
14539	292.47271	0.17059	20.37	19.70	17.65	16.39	17.22	14.34	13.68	13.32	4.59 <sup>+0.08</sup> <sub>-0.11</sub>	6.93 <sup>+0.07</sup> <sub>-0.09</sub>	3.66 <sup>+0.07</sup> <sub>-0.06</sub>	16.44 <sup>+1.03</sup> <sub>-1.28</sub>	4.52	–
14556	292.50032	0.49824	20.49	19.93	18.07	16.99	17.75	15.06	14.62	14.19	4.51 <sup>+0.13</sup> <sub>-0.12</sub>	6.24 <sup>+0.12</sup> <sub>-0.15</sub>	3.68 <sup>+0.10</sup> <sub>-0.09</sub>	16.51 <sup>+1.56</sup> <sub>-1.27</sub>	2.06	–
14565	292.50741	-1.02921	14.12	14.38	13.44	12.88	13.17	11.99	11.79	11.70	4.48 <sup>+0.09</sup> <sub>-0.07</sub>	3.39 <sup>+0.08</sup> <sub>-0.09</sub>	3.48 <sup>+0.10</sup> <sub>-0.10</sub>	13.94 <sup>+1.06</sup> <sub>-0.69</sub>	3.16	–
14572	292.50979	-1.01724	19.13	18.58	16.76	15.70	16.37	13.83	13.25	13.06	4.52 <sup>+0.10</sup> <sub>-0.08</sub>	6.14 <sup>+0.07</sup> <sub>-0.10</sub>	3.64 <sup>+0.06</sup> <sub>-0.06</sub>	15.36 <sup>+1.17</sup> <sub>-0.87</sub>	6.41	–
14605	292.56247	-0.56163	17.18	17.51	16.27	15.57	15.94	14.35	13.95	13.85	4.64 <sup>+0.04</sup> <sub>-0.06</sub>	4.46 <sup>+0.06</sup> <sub>-0.06</sub>	3.87 <sup>+0.09</sup> <sub>-0.08</sub>	17.83 <sup>+0.54</sup> <sub>-0.71</sub>	6.06	–
14619	292.58492	-0.16958	20.34	19.45	17.43	16.18	17.03	14.11	13.47	13.14	4.50 <sup>+0.13</sup> <sub>-0.12</sub>	6.82 <sup>+0.09</sup> <sub>-0.16</sub>	3.63 <sup>+0.06</sup> <sub>-0.06</sub>	15.21 <sup>+1.53</sup> <sub>-1.21</sub>	4.65	–
14652	292.63226	-0.79004	19.24	18.36	16.18	14.94	15.69	12.61	11.96	11.59	4.51 <sup>+0.10</sup> <sub>-0.08</sub>	7.30 <sup>+0.07</sup> <sub>-0.09</sub>	3.72 <sup>+0.06</sup> <sub>-0.05</sub>	13.77 <sup>+1.16</sup> <sub>-0.81</sub>	2.27	–
14689	292.69495	0.00351	18.22	17.79	16.16	15.17	15.81	13.63	13.18	12.99	4.50 <sup>+0.11</sup> <sub>-0.07</sub>	5.36 <sup>+0.09</sup> <sub>-0.10</sub>	3.43 <sup>+0.07</sup> <sub>-0.07</sub>	15.26 <sup>+1.26</sup> <sub>-0.76</sub>	4.15	–
14706	292.71718	0.15298	14.82	15.04	13.99	13.34	13.69	12.41	12.14	11.90	4.52 <sup>+0.10</sup> <sub>-0.07</sub>	3.80 <sup>+0.07</sup> <sub>-0.08</sub>	3.59 <sup>+0.11</sup> <sub>-0.10</sub>	14.57 <sup>+1.22</sup> <sub>-0.80</sub>	3.83	–
14717	292.73123	-2.00063	13.31	13.42	12.29	11.61	11.97	10.59	10.30	10.18	4.52 <sup>+0.09</sup> <sub>-0.07</sub>	3.92 <sup>+0.07</sup> <sub>-0.09</sub>	3.45 <sup>+0.09</sup> <sub>-0.08</sub>	12.78 <sup>+1.13</sup> <sub>-0.79</sub>	2.46	–
14732	292.75130	-1.93844	14.35	14.22	12.85	11.99	12.43	10.66	10.20	9.96	4.49 <sup>+0.10</sup> <sub>-0.07</sub>	4.88 <sup>+0.08</sup> <sub>-0.09</sub>	3.69 <sup>+0.08</sup> <sub>-0.08</sub>	12.21 <sup>+1.15</sup> <sub>-0.73</sub>	3.21	–
14765	292.79533	0.14057	14.31	14.60	13.63	13.07	13.37	12.22	12.03	11.86	4.50 <sup>+0.09</sup> <sub>-0.06</sub>	3.41 <sup>+0.07</sup> <sub>-0.08</sub>	3.46 <sup>+0.10</sup> <sub>-0.10</sub>	14.40 <sup>+1.03</sup> <sub>-0.69</sub>	2.10	–
14791	292.86367	-0.98272	20.50	19.10	16.42	14.91	15.92	11.99	11.14	10.65	4.49 <sup>+0.13</sup> <sub>-0.10</sub>	8.91 <sup>+0.09</sup> <sub>-0.14</sub>	3.78 <sup>+0.05</sup> <sub>-0.05</sub>	12.40 <sup>+1.51</sup> <sub>-1.03</sub>	0.97	–
14795	292.87455	0.69516	12.60	13.26	12.54	12.10	12.30	11.58	11.44	11.40	4.63 <sup>+0.05</sup> <sub>-0.07</sub>	2.67 <sup>+0.04</sup> <sub>-0.05</sub>	3.36 <sup>+0.10</sup> <sub>-0.10</sub>	15.46 <sup>+0.65</sup> <sub>-0.83</sub>	2.21	–
14812	292.90628	0.06930	18.12	18.41	17.29	16.70	16.98	15.91	15.33	15.06	4.56 <sup>+0.07</sup> <sub>-0.12</sub>	3.87 <sup>+0.13</sup> <sub>-0.12</sub>	3.62 <sup>+0.16</sup> <sub>-0.15</sub>	18.41 <sup>+0.96</sup> <sub>-0.91</sub>	5.49	–
14865	293.05290	-0.09041	19.67	19.29	17.55	16.60	17.07	15.15	14.56	14.60	4.58 <sup>+0.08</sup> <sub>-0.09</sub>	5.37 <sup>+0.08</sup> <sub>-0.09</sub>	3.33 <sup>+0.08</sup> <sub>-0.08</sub>	17.67 <sup>+1.00</sup> <sub>-1.05</sub>	5.99	–
14869	293.07914	-0.95492	20.29	19.45	17.35	16.07	16.89	13.62	12.85	12.51	4.50 <sup>+0.13</sup> <sub>-0.11</sub>	7.60 <sup>+0.09</sup> <sub>-0.14</sub>	4.01 <sup>+0.07</sup> <sub>-0.06</sub>	14.48 <sup>+1.51</sup> <sub>-1.11</sub>	4.98	–
14870	293.07989	-0.52894	13.06	13.60	12.86	12.57	12.68	12.39	12.31	12.28	4.57 <sup>+0.08</sup> <sub>-0.08</sub>	1.95 <sup>+0.05</sup> <sub>-0.06</sub>	2.53 <sup>+0.07</sup> <sub>-0.07</sub>	15.82 <sup>+1.00</sup> <sub>-0.93</sub>	6.34	–